7/1

NASA Tech Briefs

National
Aeronautics and
Space
Administration

NASl.29/31

Vol. 7, No. 1

Fall 1982

About the NASA Technology Utilization Program

The National Aeronautics and Space Act of 1958, which established NASA and the United States civilian space program, requires that "The Administration shall provide for the widest practicable and appropriate dissemination of information concerning its activities and the results thereof."

To help carry out this objective, NASA's Technology Utilization (TU) Program was established in 1962. Now, as an element of NASA's Technology Utilization and Industry Affairs Division, this program offers a variety of valuable services to help transfer aerospace technology to nonaerospace applications, thus assuring American taxpayers maximum return on their investment in space research; thousands of spinoffs of NASA research have already occurred in virtually every area of our economy.

The TU program has worked for engineers, scientists, technicians, and businessmen; and it can work for you.

NASA Tech Briefs

Tech Briefs is published quarterly and is free to engineers in U.S. industry and to other domestic technology transfer agents. It is both a current-awareness medium and a problem-solving tool. Potential products . . . industrial processes . .. basic and applied research . . . shop and lab techniques . . . computer software . . . new sources of technical data . . . concepts . . . can be found here. The short section on New Product Ideas highlights a few of the potential new products contained in this issue. The remainder of the volume is organized by technical category to help you quickly review new developments in your areas of interest. Finally, a subject index makes each issue a convenient reference file.

Further Information on Innovations

Although some new technology announcements are complete in themselves, most are backed up by Technical Support Packages (TSP's). TSP's are available without charge and may be ordered by simply completing a TSP Request Card found at the back of this volume. Further information on some innovations is available for a nominal fee from other sources, as indicated. In addition, Technology Utilization Officers at NASA Field Centers will often be able to lend necessary guidance and assistance.

Patent Licenses

Patents have been issued to NASA on some of the inventions described, and patent applications have been submitted on others. Each announcement indicates patent status and availability of patent licenses if applicable.

Other Technology Utilization Services

To assist engineers, industrial researchers, business executives, Government officials, and other potential users in applying space technology to their problems, NASA sponsors Industrial Applications Centers. Their services are described on page A7. In addition, an extensive library of computer programs is available through COSMIC, the Technology Utilization Program's outlet for NASA-developed software.

Applications Program

NASA conducts applications engineering projects to help solve public-sector problems in such areas as safety, health, transportation, and environmental protection. Two applications teams, staffed by professionals from a variety of disciplines, assist in this effort by working with Federal agencies and health organizations to identify critical problems amenable to solution by the application of existing NASA technology.

Reader Feedback

We hope you find the information in *NASA Tech Briefs* useful. A reader-feedback card has been included because we want your comments and suggestions on how we can further help you apply NASA innovations and technology to your needs. Please use it; or if you need more space, write to the Manager, Technology Transfer Division, P.O. Box 8757, Baltimore/Washington International Airport, Maryland 21240.

NASA Tech Briefs

National
Aeronautics and
Space
Administration

Fall 1982
Volume 7, Number 1

NEWARK PUBLIC LIBRARY
JAN 20 1983
U. S. GOVT. PUBS.
DEPOSITORY 376

Section	Page	Contents
NASA TU Services	A3	Technology Utilization services that can assist you in learning about and applying NASA technology.
New Product Ideas	A9	A summary of selected innovations of value to manufacturers for the development of new products.
Tech Briefs	1	**Electronic Components and Circuits**
	13	**Electronic Systems**
	23	**Physical Sciences**
	31	**Materials**
	45	**Life Sciences**
	49	**Mechanics**
	67	**Machinery**
	85	**Fabrication Technology**
	109	**Mathematics and Information Sciences**
Subject Index	117	Items in this issue are indexed by subject; a cumulative index will be published yearly.

COVERS: The photographs on the front and back covers illustrate developments by NASA and its contractors that have resulted in commercial and nonaerospace spinoffs. You can use the TSP Request Card at the back of this issue to learn more about the Wood Composite Structures [Circle 90] and Sewer-Monitoring System [Circle 91].

About This NASA Publication

NASA Tech Briefs, a quarterly publication, is distributed free to qualified U.S. citizens to encourage commercial application of U.S. space technology. For information on publications and services available through the NASA Technology Utilization Program, write to the Manager, Technology Transfer Division, P.O. Box 8757, Baltimore/Washington International Airport, Maryland 21240.

"The Administrator of National Aeronautics and Space Administration has determined that the publication of this periodical is necessary in the transaction of the public business required by law of this Agency. Use of funds for printing this periodical has been approved by the Director of the Office of Management and Budget."

Change of Address

If you wish to have NASA Tech Briefs forwarded to your new address, use the Subscription Card enclosed at the back of this volume of NASA Tech Briefs. Be sure to check the appropriate box indicating change of address, and also fill in your identification number (T number) in the space indicated.

Communications Concerning Editorial Matter

For editorial comments or general communications about NASA Tech Briefs, you may use the Feedback card in the back of NASA Tech Briefs, or write to: The Publications Manager, Technology Utilization Office (LGT-1), NASA Headquarters, Washington, DC 20546. Technical questions concerning specific articles should be directed to the Technology Utilization Officer of the sponsoring NASA Center (addresses listed on page A4).

Acknowledgements

NASA Tech Briefs is published quarterly by the National Aeronautics and Space Administration, Technology Transfer Division, Washington, DC: Administrator: **James E. Beggs;** Director, Technology Utilization and Industry Affairs Division: **Ronald J. Philips;** Publications Manager: **Leonard A. Ault.** Prepared for the National Aeronautics and Space Administration by **Logical Technical Services Corp.:** Editor-in-Chief: **Jay Kirschenbaum;** Art Director: **Ernest Gillespie;** Managing Editor: **Jerome Rosen;** Chief Copy Editor: **Oden Browne;** Staff Editors: **Donald Blattner, Larry Grunberger, Ted Selinsky, George Watson;** Graphics: **Luis Martinez, Janet McCrie, Huburn Profitt;** Editorial & Production: **Richard Johnson, Frank Ponce, Elizabeth Texeira, Vincent Susinno, Ernestine Walker.**

This document was prepared under the sponsorship of the National Aeronautics and Space Administration.. Neither the United States Government nor any person acting on behalf of the United States Government assumes any liability resulting from the use of the information contained in this document, or warrants that such use will be free from privately owned rights.

NASA
TU SERVICES

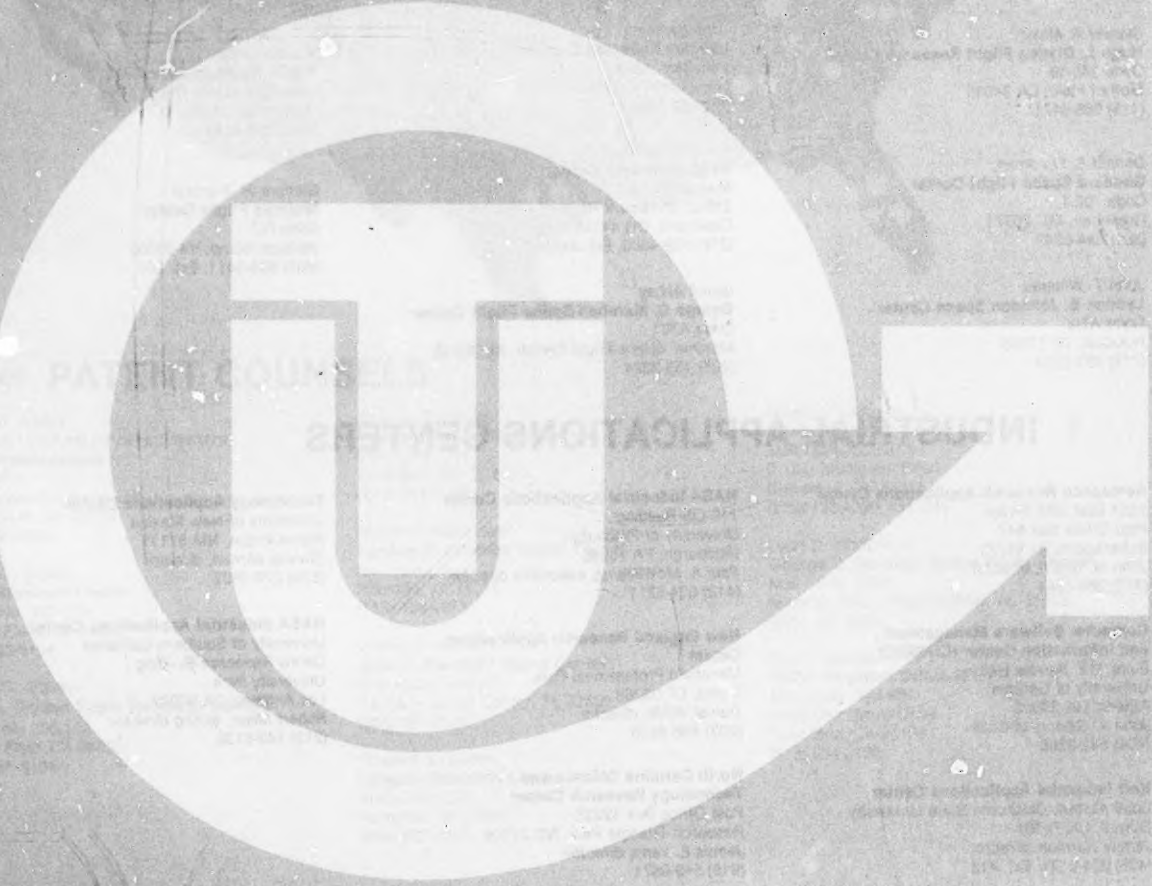

NASA TECHNOLOGY UTILIZATION NETWORK

★ TECHNOLOGY UTILIZATION OFFICERS

Stanley A. Miller
Ames Research Center
Code 240-10
Moffett Field, CA 94035
(415) 965-6471

Stanley A. Miller
Hugh L. Dryden Flight Research Center
Code 240-10
Moffett Field, CA 94035
(415) 965-6471

Donald S. Friedman
Goddard Space Flight Center
Code 702.1
Greenbelt, MD 20771
(301) 344-6242

John T. Wheeler
Lyndon B. Johnson Space Center
Code AT3
Houston, TX 77058
(713) 483-3809

U. Reed Barnett
John F. Kennedy Space Center
Code PT-SPD
Kennedy Space Center, FL 32899
(305) 867-3017

John Samos
Langley Research Center
Mail Stop 139A
Hampton, VA 23665
(804) 827-3281

Harrison Allen, Jr.
Lewis Research Center
Mail Code 7-3
21000 Brookpark Road
Cleveland, OH 44135
(216) 433-4000, Ext. 6422

Ismail Akbay
George C. Marshall Space Flight Center
Code AT01
Marshall Space Flight Center, AL 35812
(205) 453-2224

Leonard A. Ault
NASA Headquarters
Code ETD-6
Washington, DC 20546
(202) 755-2244

Aubrey Smith
NASA Resident Office-JPL
4800 Oak Grove Drive
Pasadena, CA 91103
(213) 354-4849

Gilmore H. Trafford
Wallops Flight Center
Code OD
Wallops Island, VA 23337
(804) 824-3411, Ext. 201

● INDUSTRIAL APPLICATIONS CENTERS

Aerospace Research Applications Center
1201 East 38th Street
Post Office Box 647
Indianapolis, IN 46223
John M. Ulrich, director
(317) 264-4644

Computer Software Management and Information Center (COSMIC)
Suite 112, Barrow Hall
University of Georgia
Athens, GA 30602
John A. Gibson, director
(404) 542-3265

Kerr Industrial Applications Center
Southeastern Oklahoma State University
Durant, OK 74701
James Harmon, director
(405) 924-0121, Ext. 413

NASA Industrial Applications Center
710 LIS Building
University of Pittsburgh
Pittsburgh, PA 15260
Paul A. McWilliams, executive director
(412) 624-5211

New England Research Applications Center
Mansfield Professional Park
Storrs, CT 06268
Daniel Wilde, director
(203) 486-4533

North Carolina Science and Technology Research Center
Post Office Box 12235
Research Triangle Park, NC 27709
James E. Vann, director
(919) 549-0671

Technology Applications Center
University of New Mexico
Albuquerque, NM 87131
Stanley Morain, director
(505) 277-3622

NASA Industrial Applications Center
University of Southern California
Denny Research Building
University Park
Los Angeles, CA 90007
Robert Mixer, acting director
(213) 743-6132

■ STATE TECHNOLOGY APPLICATIONS CENTERS

NASA/University of Florida
State Technology Applications Center
500 Weil Hall
University of Florida
Gainesville, FL 32611
J. Ronald Thornton, director

Gainesville:	(904) 392-6760
Boca Raton:	(305) 395-5100, Ext. 2292
Fort Lauderdale:	(305) 776-6645
Jacksonville:	(904) 646-2478
Orlando:	(305) 275-2706
Pensacola:	(904) 476-9500, Ext. 426
Tampa:	(813) 974-2499

NASA/University of Kentucky
State Technology Applications Program
109 Kinkead Hall
University of Kentucky
Lexington, KY 40506
William R. Strong, manager
(606) 258-4632

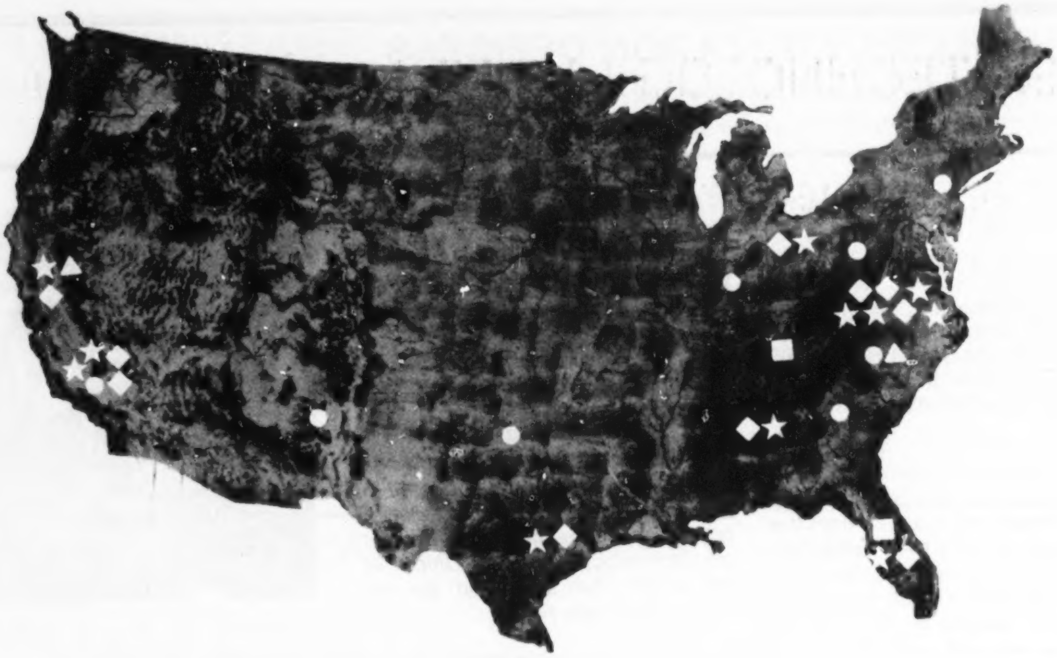

◆ PATENT COUNSELS

Robert F. Kempf
Asst. Gen. Counsel for patent matters
NASA Headquarters
Code GP-4
400 Maryland Avenue, SW.
Washington, DC 20546
(202) 755-3954

Darrell G. Brekke
Ames Research Center
Mail Code: 200-11A
Moffett Field, CA 94035
(415) 965-5104

Darrall G. Brekke
Hugh L. Dryden Flight Research Center
Mail Code: 200-11A
Moffett Field, CA 94035
(415) 965-5104

John O. Tresansky
Goddard Space Flight Center
Mail Code: 204
Greenbelt, MD 20771
(301) 344-7351

Marvin F. Matthews
Lyndon B. Johnson Space Center
Mail Code: AL-3
Houston, TX 77058
(713) 483-4871

James O. Harrell
John F. Kennedy Space Center
Mail Code: SA-PAT
Kennedy Space Center, FL 32899
(305) 867-2544

Howard J. Osborn
Langley Research Center
Mail Code: 279
Hampton, VA 23665
(804) 827-3725

Norman T. Musial
Lewis Research Center
Mail Code: 500-311
21000 Brookpark Road
Cleveland, OH 44135
(216) 433-4000, Ext. 346

Leon D. Wofford, Jr.
George C. Marshall Space Flight Center
Mail Code: CC01
Marshall Space Flight Center, AL 35812
(205) 453-0020

Paul F. McCaul
NASA Resident Office-JPL
Mail Code: 180-601
4800 Oak Grove Drive
Pasadena, CA 91103
(213) 354-2700

▲ APPLICATION TEAMS

Doris Rouse, director
Research Triangle Institute
Post Office Box 12194
Research Triangle Park, NC 27709
(919) 541-6980

James P. Wilhelm, director
SRI International
333 Ravenswood Avenue
Menlo Park, CA 94026
(415) 326-6200, Ext. 3520

TECHNOLOGY UTILIZATION OFFICERS

Technology transfer experts can help you apply the innovations in NASA Tech Briefs.

The Technology Utilization Officer at each NASA Field Center is an applications engineer who can help you make use of new technology developed at his center. He brings you NASA Tech Briefs and other special publications, sponsors conferences, and arranges for expert assistance in solving technical problems.

Technical assistance, in the form of further information about NASA innovations and technology, is one of the services available from the TUO. Together with NASA scientists and engineers, he can often help you find and implement NASA technology to meet your specific needs.

Technical Support Packages (TSP's) are prepared by the center TUO's. They provide further technical details for articles in NASA Tech Briefs. This additional material can help you evaluate and use NASA technology. You may receive most TSP's free of charge by using the TSP Request Card found at the back of this issue.

Technical questions about articles *in NASA Tech Briefs are answered in the TSP's. When no TSP is available, or you have further questions, contact the Technology Utilization Officer at the center that sponsored the research [see page A4].*

NASA INVENTIONS AVAILABLE FOR LICENSING

Over 3,500 NASA inventions are available for licensing in the United States — both exclusive and nonexclusive.

Nonexclusive licenses for commercial use of NASA inventions are encouraged to promote competition and to achieve the widest use of inventions. They must be used by a netotiated target date.

Exclusive licenses may be granted to encourage early commercial development of NASA inventions, especially when considerable private investment is required. These are generally for 5 to 10 years and usually require royalties based on sales or use.

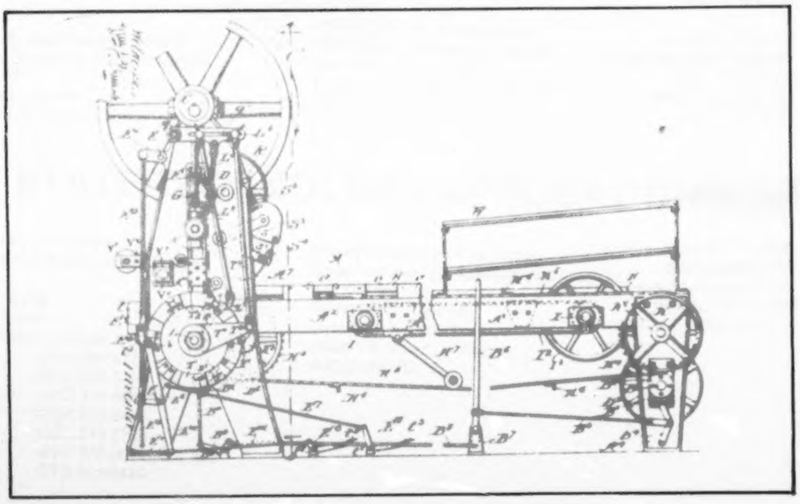

Additional licenses available include those of NASA-owned foreign patents. In addition to inventions described in NASA Tech Briefs, *"NASA Patent Abstract Bibliography"* (PAB), containing abstracts of all NASA inventions, can be purchased from National Technical Information Service, Springfield, VA 22161. The PAB is updated semiannually.

Patent licenses for Tech Briefs *are frequently available. Many of the inventions reported in NASA Tech Briefs are patented or are under consideration for a patent at the time they are published. The current patent status is described at the end of the article; otherwise, there is no statement about patents. If you want to know more about the patent program or are interested in licensing a particular invention, contact the Patent Counsel at the NASA Field Center that sponsored the research [see page A5]. Be sure to refer to the NASA reference number at the end of the Tech Brief.*

APPLICATION TEAMS

Technology-matching and problem-solving assistance to public-sector organizations

Application engineering projects are conducted by NASA to help solve public-sector problems in such areas as safety, health, transportation, and environmental protection. Some application teams specialize in biomedical disciplines; others, in engineering and scientific problems. Staffed by professionals from various disciplines, these teams work with other Federal agencies and health organizations to identify critical problems amenable to solution by the application of existing NASA technology.

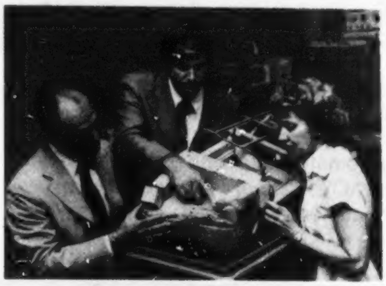

Public-sector organization *representatives can learn more about application teams by contacting a nearby NASA Field Center Technology Utilization Office [see page A4].*

INDUSTRIAL APPLICATIONS CENTERS

Computerized access to over 10 million documents worldwide

Computerized information retrieval from one of the world's largest banks of technical data is available from NASA's network of industrial Applications Centers (IAC's). The IAC's give you access to 1,800,000 technical reports in the NASA data base and to more than 10 times that many reports and articles found in nearly 200 other computerized data bases.

The major sources include:

- *750,000 NASA Technical Reports*
- *Selected Water Resources Abstracts*
- *NASA Scientific and Technical Aerospace Reports*
- *Air Pollution Technical Information Center*
- *NASA International Aerospace Abstracts*
- *Chem Abstracts Condensates*
- *Engineering Index*
- *Energy Research Abstracts*
- *NASA Tech Briefs*
- *Government Reports Announcements*

and many other specialized files on food technology, textile technology, metallurgy, medicine, business, economics, social sciences, and physical science.

The IAC services range from tailored literature searches through expert technical assistance:

- *Retrospective Searches:* Published or unpublished literature is screened, and documents are identified according to your interest profile. IAC engineers tailor results to your specific needs and furnish abstracts considered the most pertinent. Complete reports are available upon request.
- *Current-Awareness Searches:* IAC engineers will help design a program to suit your needs. You will receive selected monthly or quarterly abstracts on new developments in your area of interest.
- *Technical Assistance:* IAC engineers will help you evaluate the results of your literature searches. They can help find answers to your technical problems and put you in touch with scientists and engineers at appropriate NASA Field Centers.

Prospective clients *can obtain more information about these services by contacting the nearest IAC [see page A4]. User fees are charged for IAC information services.*

STATE TECHNOLOGY APPLICATIONS CENTERS

Technical information services for industry and state and local government agencies

Government and private industry
in Florida and Kentucky can utilize the services of NASA's State Technology Applications Centers (STAC's). The STAC's differ from the Industrial Applications Centers described on page A7, primarily in that they are integrated into existing state technical assistance programs and serve only the host state, whereas the IAC's serve multistate regions.

Many data bases,
including the NASA base and several commercial bases, are available for automatic data retrieval through the STAC's. Other services such as document retrieval and special searches are also provided. (Like the IAC's, the STAC's normally charge a fee for their services.)

To obtain information
about the services offered, write or call the STAC in your state [see page A4].

COSMIC®

An economical source of computer programs developed by NASA and other government agencies

A vast software library
is maintained by COSMIC — the Computer Software Management and Information Center. COSMIC gives you access to approximately 1,600 computer programs developed for NASA and the Department of Defense and selected programs for other government agencies. Programs and documentation are available at reasonable cost.

Available programs
range from management (PERT scheduling) to information science (retrieval systems) and computer operations (hardware and software). Hundreds of engineering programs perform such tasks as structural analysis, electronic circuit design, chemical analysis, and the design of fluid systems. Others determine building energy requirements and optimize mineral exploration.

NASTRAN
COSMIC
NASTRAN
NASA
STRUCTURAL ANALYSIS
Looking for the right computer program can sometimes feel like wandering through a maze.

COSMIC services
go beyond the collection and storage of software packages. Programs are checked for completeness; special announcements and an indexed software catalog are prepared; and programs are reproduced for distribution. Customers are helped to identify their software needs; and COSMIC follows up to determine the successes and problems and to provide updates and error corrections. In some cases, NASA engineers can offer guidance to users in installing or running a program.

Information about programs
described in NASA Tech Briefs articles can be obtained by completing the COSMIC Request Card at the back of this issue. Just circle the letters that correspond to the programs in which you are interested.

NEW PRODUCT IDEAS

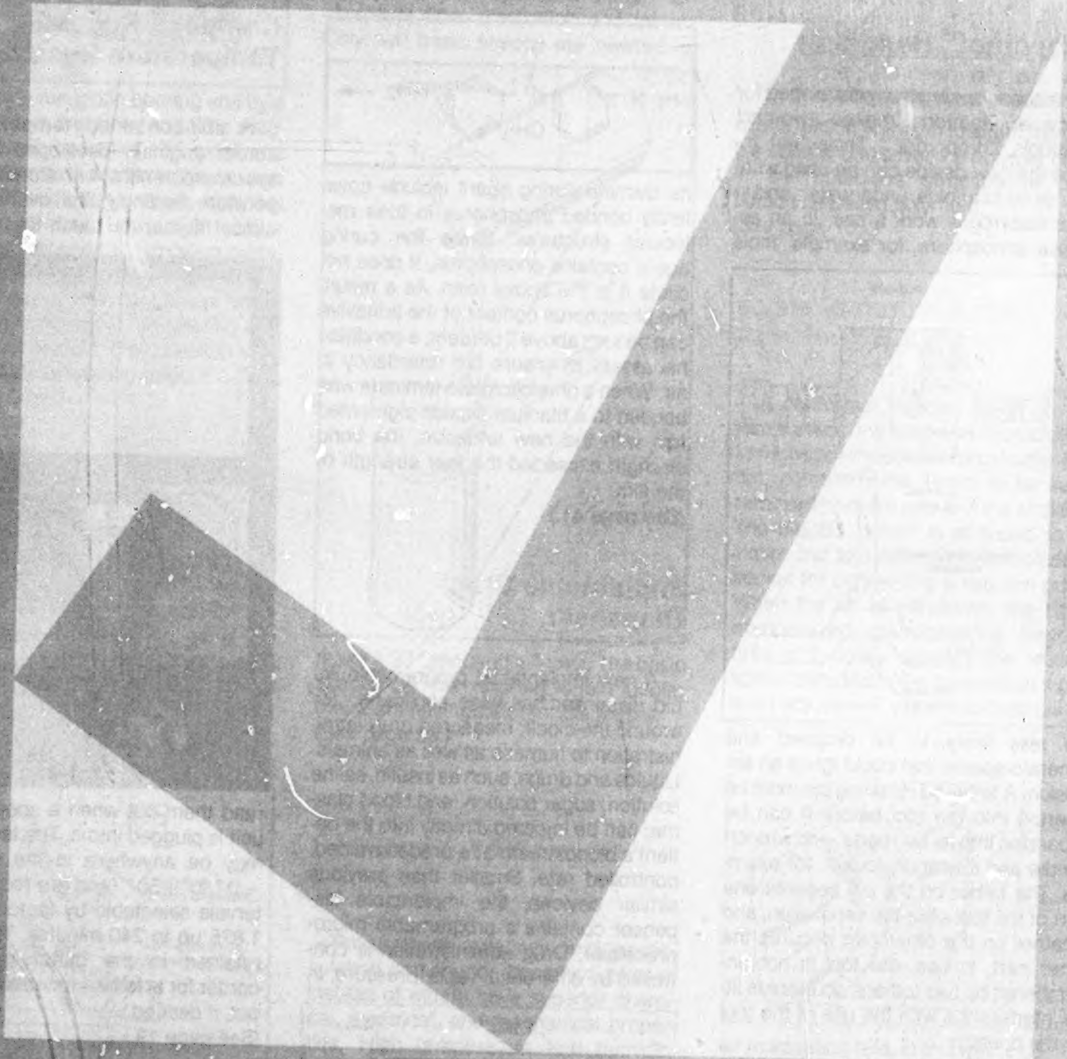

NEW PRODUCT IDEAS are just a few of the many innovations described in this issue of NASA Tech Briefs and having promising commercial applications. Each is discussed further on the referenced page in the appropriate section in this issue. If you are interested in developing a product from these or other NASA innovations, you can receive further technical information by requesting the TSP referenced at the end of the full-length article or by writing the Technology Utilization Office of the sponsoring NASA center (see page A4). NASA's patent-licensing program to encourage commercial development is described on page A6.

"Dropproof" Handtools

A mechanism originally developed for space applications makes two-part handtools "dropproof." Tools that include the new device can be used without risk on scaffolds, underwater, and in other hazardous work areas. In an explosive atmosphere, for example, tools are less likely to be dropped and generate sparks that could ignite an explosion. A tethered retaining pin must be inserted into the tool before it can be separated into its two parts — a wrench handle and a wrench socket, for example. The tether on the pin secures one part of the tool after the separation, and a tether on the other part secures the other part. In use, the tool is not encumbered by two tethers, so there is little interference with the use of the tool by the operator.
(See page 69.)

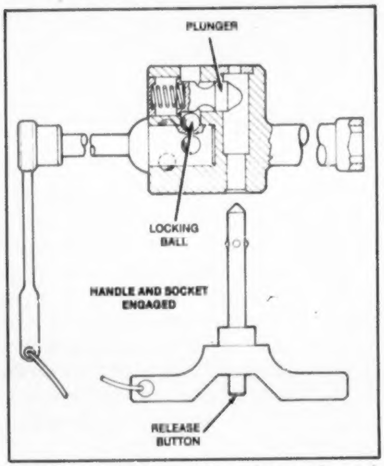

Fire-Retardant Epoxy Adhesives

A new phosphorus-containing epoxy is fire-retardant and translucent. Intended as an adhesive for laminated plastic sheets, the new material bonds well to titanium dioxide-filled plastic film, which ordinarily shows little surface interaction with adhesives. Both the epoxy resin and its diamine curing agent include covalently bonded phosphorus in their molecular structures. Since the curing agent contains phosphorus, it does not dilute it in the epoxy resin. As a result, the phosphorus content of the adhesive can be kept above 7 percent, a condition necessary to ensure fire retardancy in air. When a phenolic/glass laminate was bonded to a titanium dioxide-pigmented film with the new adhesive, the bond strength exceeded the tear strength of the film.
(See page 41.)

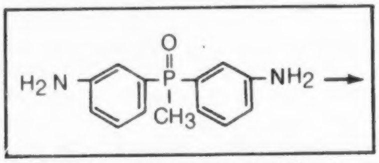

Implantable Drug Dispenser

A new implantable, programable liquid dispenser has wide application for around-the-clock, measured drug administration to humans as well as animals. Liquids and drugs, such as insulin, saline solution, sugar solution, and blood plasma, can be injected directly into the patient's bloodstream at a predetermined, controlled rate. Smaller than previous similar devices, the implantable dispenser contains a programable microprocessor. Drug administration is controlled by differential vapor pressure, in turn controlled by an integrated heating system. A 30-day drug supply can be applied at the rate of 1 cm^3 per day. The vapor can be a fluorocarbon or other volatile material sensitive to temperature changes.
(See page 48.)

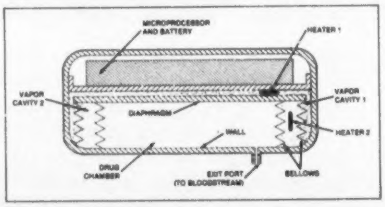

Compact, Rugged Temperature Recorder

A self-contained temperature recorder originally developed for use in space experiments can store 2,048 temperature readings taken over a period of almost a year (or much less) and then read them out when a special readout unit is plugged into it. The temperatures may be anywhere in the range from −0° to +50° and are recorded at intervals selectable by factors of 2 from 1.875 up to 240 minutes. The data are retained in the battery-operated recorder for at least 4 months before readout, if desired.
(See page 19.)

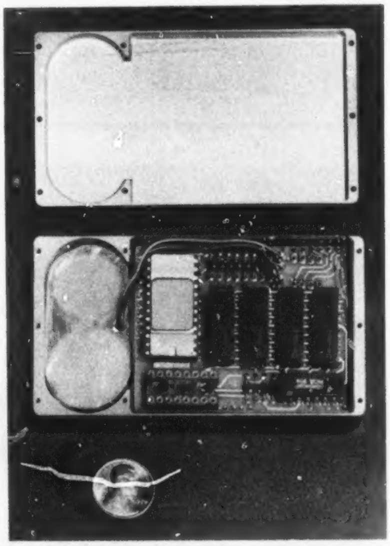

Magnetic Bearings Increase Pump Efficiency

Magnetic bearings compensate for rotor displacements and for asynchronous rotation of a counterrotating helical-screw gas compressor, making the two-element pump efficient enough for many applications. In the new design, each screw shaft is supported at

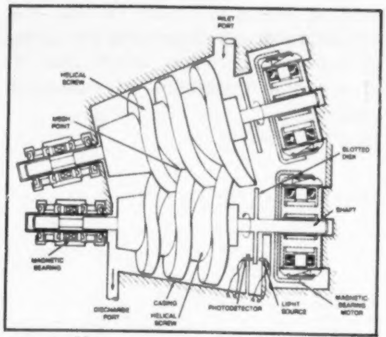

one end by a magnetic bearing and by a drive motor at the other end. The magnetic bearings balance the axial and radial forces that displace the screws from equilibrium. As a result, frictional losses are lowered, and a tight seal is maintained between the moving parts. The two-element pump could be used to compress gases in a mechanical refrigerator and in other counterrotating machinery; for example, in a pulverizer with a pair of counterrotating mills.
(See page 76.)

Miniature Two-Axis Joystick Controller

A movable-button-actuated self-centering controller uses optoelectronics to produce X and Y signals for aircraft control. In addition to being extremely small, the device is relatively immune to electrical noise. The combination of a new saddle-shaped button and positive centering gives a feel and breakout that have met with pilot approval. In the miniature controller, the motion of a spring-centered rocker varies the position of a lensed light-emitting diode (LED). These changes in the position are sensed by a two-axis photodetector. Other suitable applications for the joystick controller would include radar trackers/cursors, aircraft moving-map display controls, weapon pointing, and the like.
(See page 78.)

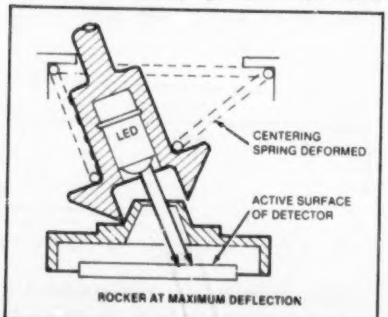
LED
CENTERING SPRING DEFORMED
ACTIVE SURFACE OF DETECTOR
ROCKER AT MAXIMUM DEFLECTION

Composite Tubular Connector

Joining composite tubular structural members with new connectors of the same composite materials can eliminate stress and weight problems encountered with metal connectors. Joint strengths can be optimized with proper choice of fiber orientation and fabric. Only two basic shapes are needed to make a 90° joint and a T-joint. The basic shapes can be modified to join tubular members having different diameters.
(See page 53.)

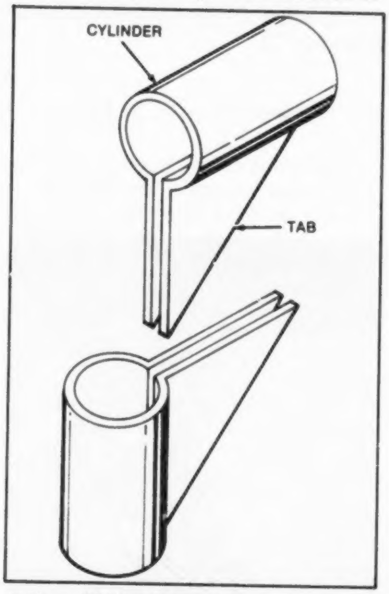

Stable Polyurethane Coatings for Electronic Circuits

Polyurethane coatings and encapsulation compounds based on alkanes instead of ethers have superior chemical, electrical, and mechanical properties. High temperature and humidity have little effect on the alkane-based polyurethanes, and water-vapor transmission rates through polyurethane film prepared from alkanes are low in comparison with those for ether-based materials. The alkane-based polyurethanes have major uses as connector potting materials and as conformal coatings for printed-circuit boards. In the alkane-based materials, a double bond is removed from the polymer chain by the hydrogenation of polyol. This process eliminates the point of attack for ozone, which is known to affect the double bond and to sever the polymer chain in the butadiene structure of polybutadiene-based polymers.
(See page 103.)

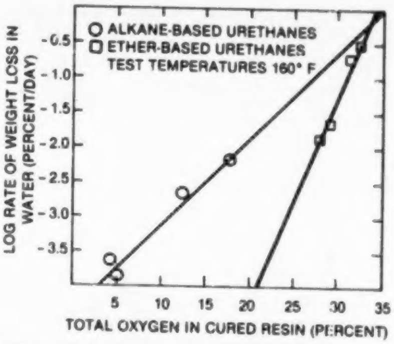

Spine Immobilizer for Accident Victims

A conformal bladder, made of resilient plastics and filled with microballons, immobilizes the spine of an accident victim, permitting the victim to be safely removed from the scene of the accident. The bladder, which is strapped to the victim and to a rescue chair, includes a socket for connecting a vacuum pump. When the air is withdrawn, the tightly compressed microballoons become firm and rigidly support the victim's spine. Included in the connection tubing is an adjustment valve that controls the air evacuation rate. In this way, a conformal blanket, formed by the bladder, can be reversibly softened and hardened so as best to fit the victim.
(See page 47.)

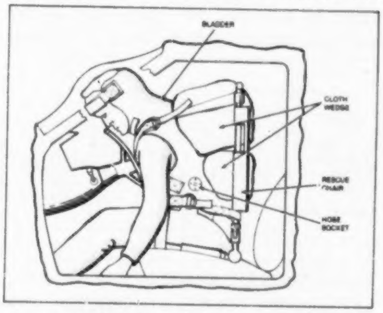

Dipole-Excited Ring Antenna

A dipole radiator drives a ring radiator in a new compact antenna. The antenna, which has been breadboarded and

tested, can be mounted flush with a surface. Compared with a horn or a parabolic dish with the same aperture, the new ring antenna has greater gain, lower side lobes, and narrower beamwidth. It can be used on vehicles requiring flush-mounted antennas with very-directive signals. For example, it could be used as a radar altimeter antenna for an aircraft. The new antenna exhibits a 2.5-dB improvement in gain over that of a waveguide horn antenna with the same aperture.
(See page 12.)

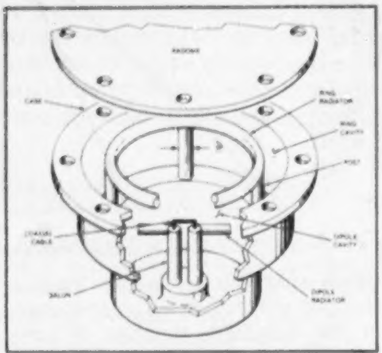

Mobile Air Sampler

A container mounted on a moving vehicle gathers air samples along highways and in tunnels. The air sampler consists of a hollow cylinder with spring-activated sealing caps at both ends held open by a thread. Air flows through the cylinder, which closes when a hot-wire cutter melts the plastic thread. Whereas conventional fixed air-collection systems usually require official approval, the mobile air samples can be used without government validation.
(See page 55.)

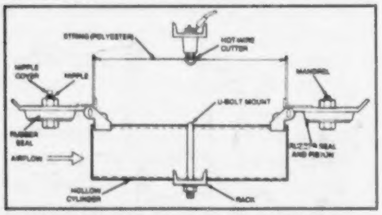

Clear Film Protects Against Ultraviolet Radiation

An acrylic film contains a screening agent that filters ultraviolet radiation up to 380 nanometers in wavelength but passes other components of Sunlight. The new film, which contains about 0.5 weight percent of an agent with a molecular weight of 60,000, absorbs substantially more ultraviolet radiation than commercial materials with similar properties. It can protect rubber and plastics that are degraded by ultraviolet light, solar cells, and outdoor sheets or pipes made of polyethylene or polypropylene. The film is applied to surfaces by solvent casting, coextrusion, or laminating. It may also be applied as a latex.
(See page 33.)

Cutter for Woven Material

A guillotine cutting tool makes it easy to produce accurate, square cuts in strips of woven or felted materials, such as high-temperature aramid fabric. The guillotine cutter can improve and increase production: It can cut faster than a scissors, papercutter, or knife with roller; and it gives the operator better control of the cut, resulting in sharper, better defined edges.
(See page 79.)

Spectrometer Analyzes Pollutants

A "real-time" mass spectrometer monitors and analyzes aerosol pollutant particles as small as 2 microns. The system can analyze changes in chemical composition to yield pollutant source information, which is particularly useful in coal-fired powerplants. Analytic capabilities include sulfur oxidation to sulfates, sodium sulfate and sodium sulfite ratios, lithium nitrate, and adipic and glutaric acids. By comparing each analysis with a reference aerosol, the spectrometer can determine the ratios of individual particles, which can indicate the presence of pollutant particles.
(See page 54.)

Portable I/V Tester

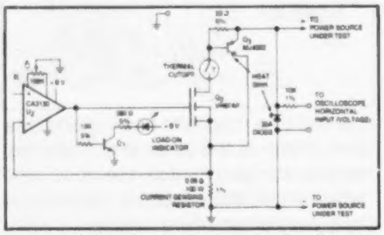
CA3130
U2
THERMAL CUTOFF
Q1
Q2
Q3
HEAT SINK
LOAD-ON INDICATOR
-9 V
DIODE
CURRENT SENSING RESISTOR
TO POWER SOURCE UNDER TEST
TO OSCILLOSCOPE HORIZONTAL INPUT (VOLTAGE)
TO POWER SOURCE UNDER TEST

A portable, battery-operated unit tests the current/voltage characteristics of dc power supplies and sources, such as photovoltaic cells. The I/V characteristic curve is displayed on an oscilloscope. The curve tester functions as a 60 Hz sawtooth signal generator and variable load for the dc power supply under test, and it also supplies drive signals to the horizontal (voltage) and vertical (current) inputs of the oscilloscope. A 9-volt transistor battery operates the tester.
(See page 9.)

Carbon Cloth Supports Catalytic Electrodes

New carbon-cloth-supported electrodes, originally developed for a sulfur-cycle hydrogen process, are more efficient, more stable, and require less catalyst. In the sulfur-cycle process, the carbon-cloth electrode is the anode or "electrolyzer." A comparison of a cell containing the new flexible anode and a conventional anode made of pressed carbon powder, catalyst, and binder demonstrated the better stability and efficiency of the carbon-cloth design. After 2-½ hours in sulfuric acid at a constant-current density, the cell voltage using the carbon-cloth electrode was 40 mV less than that of the conventional cell.
(See page 95.)

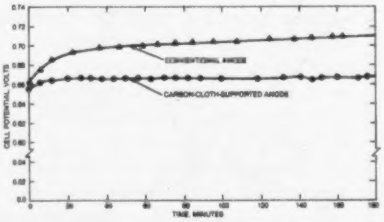

Electronic Components and Circuits

Hardware, Techniques, and Processes

3 Power-Factor Controller Avoids False Turnoff

4 Soft-Starting Power-Factor Motor Controller

5 Implementing Exclusive-OR Logic

6 Audio Distribution and Monitoring Circuit

7 500-Watt, 10-GHz Solid-State Amplifier

8 Integrated Submillimeter-Wave Mixer

9 Portable I/V-Curve Tester

10 Electronic Load Tests High-Voltage Solar Arrays

11 Flip-Chip Carrier Would Match Microwave FET Impedances

12 Dipole-Excited Ring Antenna

Power-Factor Controller Avoids False Turnoff

A phase-difference signal is utilized to ensure triggering each half cycle.

Marshall Space Flight Center, Alabama

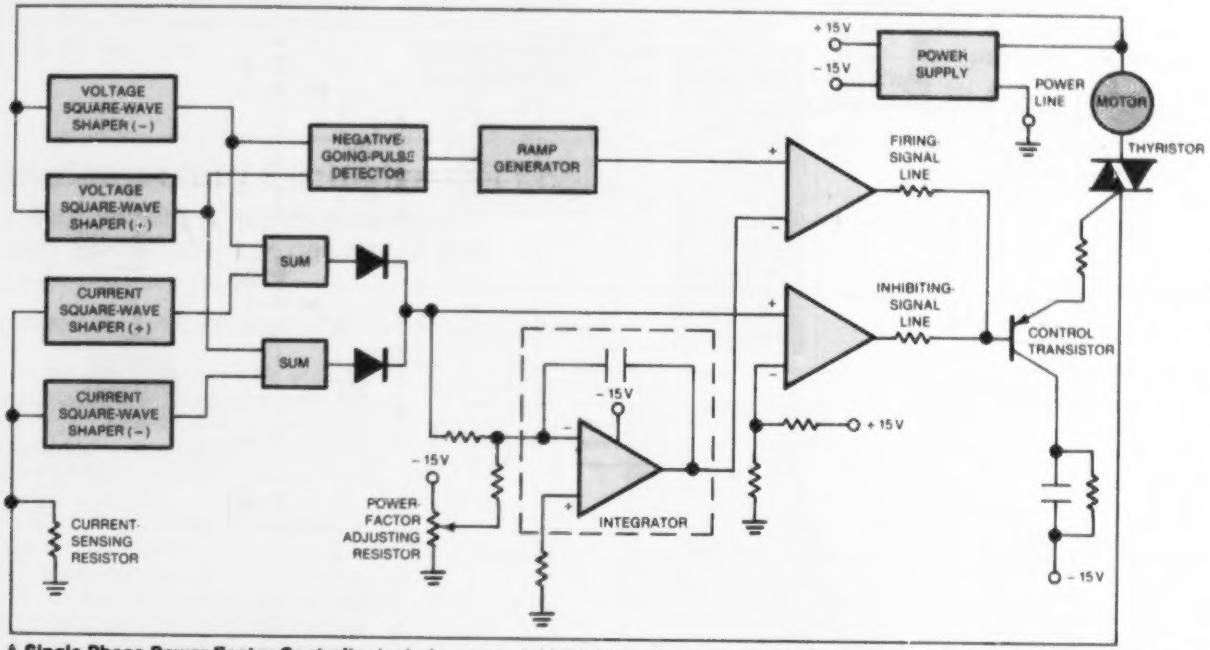
+15 V
−15 V
POWER SUPPLY
POWER LINE
MOTOR
THYRISTOR
VOLTAGE SQUARE-WAVE SHAPER (−)
NEGATIVE-GOING-PULSE DETECTOR
RAMP GENERATOR
FIRING-SIGNAL LINE
VOLTAGE SQUARE-WAVE SHAPER (+)
SUM
CURRENT SQUARE-WAVE SHAPER (+)
INHIBITING-SIGNAL LINE
CONTROL TRANSISTOR
SUM
CURRENT SQUARE-WAVE SHAPER (−)
−15 V
+15 V
−15 V
POWER-FACTOR ADJUSTING RESISTOR
INTEGRATOR
CURRENT-SENSING RESISTOR
−15 V

A Single-Phase Power-Factor Controller includes a special inhibiting circuit to avoid false turnoff. If the thyristor trigger signal occurs during the flow of current from the preceding half cycle, the inhibiting signal delays the application of the trigger pulse until the beginning of the next current half cycle.

An improved triggering circuit for power-factor motor controllers insures effective triggering at all current/voltage phase angles. The new circuit triggers the thyristor in the normal manner unless current from the preceding half cycle is flowing, but a signal already present in the power-factor controller is used to inhibit the transmission of the firing pulse to the thyristor gate until the current returns to zero.

A power-factor controller, used with inductive loads such as induction motors, samples line voltage and load current. A controller contains one or more thyristors that feed power to the load during a portion of the voltage cycle that depends on the phase difference between the sampled voltage and current.

In normal operation, the thyristor switches on when a trigger current pulse of a few microseconds is applied to the gate electrode and remains on until the anode current goes to zero. However, if the current phase lag is such that the trigger pulse occurs when current from the preceding half cycle is flowing, the thyristor will already be on. When the current goes to zero, the thyristor will go off and remain off during the following half cycle. The trigger pulse thus has no effect.

The new inhibiting circuit (see figure) establishes a reference time (namely, the moment the current goes to zero) for firing the thyristor based on the phase-difference signal and prevents generation of the firing pulse in advance of this reference time. An inhibiting pulse is generated if current is flowing from the preceding half cycle.

The base of the control transistor for the thyristor is connected to receive the signal from the inhibiting circuit and the signal from the thyristor firing-control circuit. The thyristor is connected so as to fire only when both signals are negative. If the firing signal occurs after the end of the inhibiting signal, it controls the transistor firing time; if it precedes the reference time, the transistor will not fire until the inhibiting signal is turned off. Thus, the trigger signal is delayed at least until the start of the next positive current half cycle and triggering of the thyristor is assured.

This work was done by Frank J. Nola of **Marshall Space Flight Center.** *For further information, Circle 1 on the TSP Request Card.*

Inquiries concerning rights for the commercial use of this invention should be addressed to the Patent Counsel, Marshall Space Flight Center [see page A5]. Refer to MFS-25616.

Soft-Starting Power-Factor Motor Controller

Starting current surges and motor
vibrations are suppressed.

Marshall Space Flight Center, Alabama

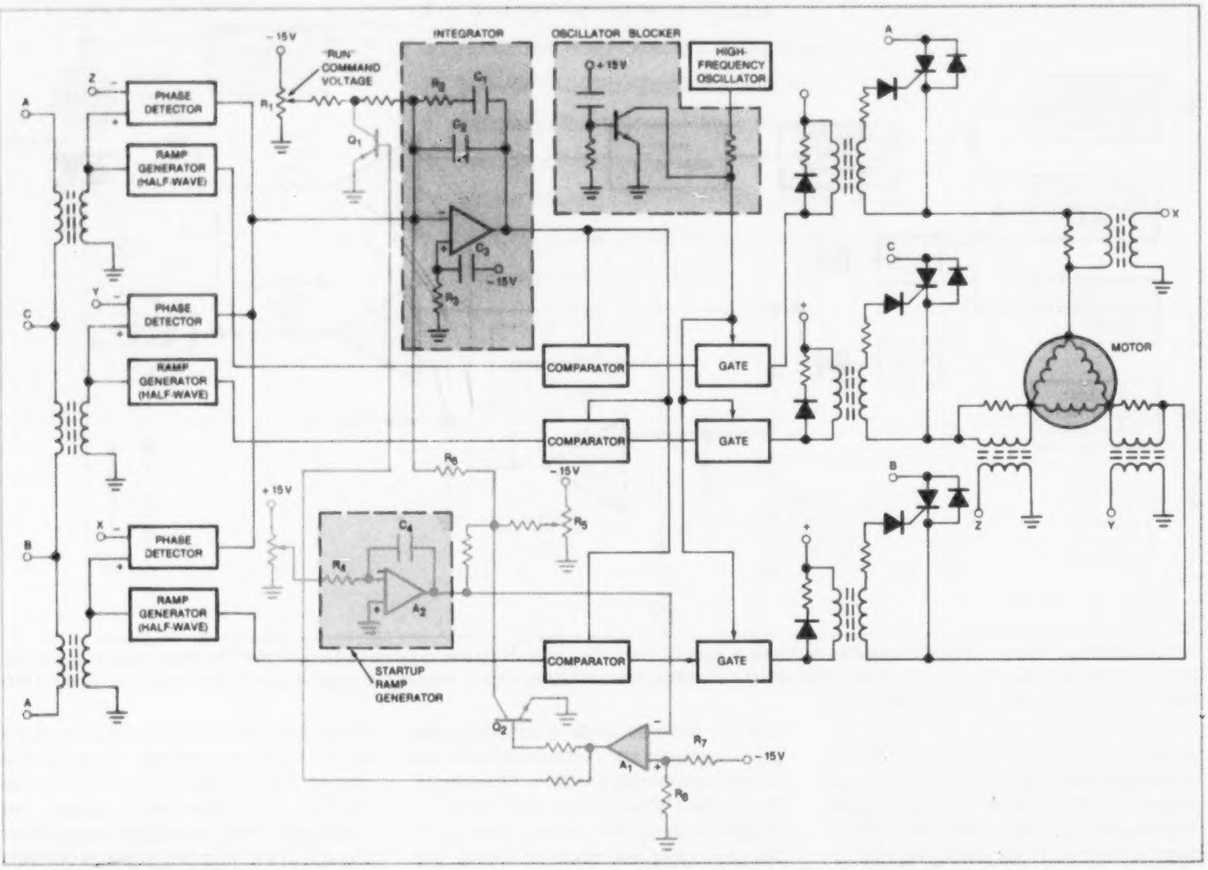
INTEGRATOR
OSCILLATOR BLOCKER
HIGH-FREQUENCY OSCILLATOR
– 15 V
"RUN" COMMAND VOLTAGE
R1
R2
C1
C2
Q1
C3
– 15 V
R3
+ 15 V
A
Z
PHASE DETECTOR
RAMP GENERATOR (HALF-WAVE)
C
Y
PHASE DETECTOR
RAMP GENERATOR (HALF-WAVE)
B
X
PHASE DETECTOR
RAMP GENERATOR (HALF-WAVE)
A
COMPARATOR
GATE
COMPARATOR
GATE
COMPARATOR
GATE
A
X
C
MOTOR
B
Z
Y
+ 15 V
C4
R4
A2
R6
– 15 V
R5
STARTUP RAMP GENERATOR
Q2
A1
R7
– 15 V
R8

The **Three-Phase Power-Factor Controller With Soft Start** is based on an earlier version that does not control starting transients. The additional components (color) serve to turn off the "run" command signal and to substitute a gradual startup command signal during a preset startup interval.

An improved three-phase power-factor controller reduces the large current surge that usually accompanies starting. Unlike circuits that apply power in discrete increments, the improved controller applies power smoothly, without causing motor vibrations.

The operation of the controller, after the decay of the starting transients, is described in "Three-Phase Power-Factor Controller," page 3, *NASA Tech Briefs*, Vol. 6, No. 1 (Spring 1981). In that version, a constant power-factor command voltage is applied at all times, with no provision for gradual turn-on.

In the improved version (see figure), the constant command voltage is disconnected during a startup interval of 5 to 30 seconds. During that interval, the constant command voltage is replaced by a ramp signal that is summed with the operating power-factor signal from the phase detectors to produce a starting control signal.

The combination of R_3 and C_3 applies a disabling voltage to the integrator during the first 100 or so milliseconds, to insure that no control signals are processed by the integrator until the substitute control signals are established. Similarly, the oscillator blocker grounds the oscillator output for the first 10 milliseconds until the integrator is fully disabled.

Transistor Q_1 is turned on during the entire startup time, so as to short the "run" command voltage from the R_1 cursor to ground. Transistor Q_2 is held in the "off" state during this period and is turned on at the end to short the startup command signal to ground, thus preventing the startup signal from being processed in the integrator with the other control signals during steady running.

The startup ramp signal is generated by the integrating circuit of R_4, C_4, and A_2. A negative-going ramp is produced, with a time constant determined by R_4 and C_4 selected so that the motor turns on at the desired rate. A positive bias from potentiometer R_5 is added to the ramp voltage, and this combined startup command signal is applied through R_6 to the integrator. The startup ramp is also applied to the inverting input of operational amplifier A_1. Acting as a comparator, A_1 switches Q_1 off and Q_2 on when the ramp voltage starts to go below the non-inverting-input bias voltage set by R_7 and R_8. This transition marks the end of the startup interval.

In all other respects, the circuit functions like the earlier version. The startup or "run" command signal is summed with the phase-detector outputs, and the resulting combined control signal is processed through the integrator and the remainder of the circuit. The modification extends the capability of the controller to reduce power consumption during starting as well as during full-speed operation and to provide a single control circuit for all stages of operation.

This work was done by Frank J. Nola of **Marshall Space Flight Center.** *For further information, Circle 2 on the TSP Request Card.*

This invention is owned by NASA, and a patent application has been filed. Inquiries concerning nonexclusive or exclusive license for its commercial development should be addressed to the Patent Counsel, Marshall Space Flight Center [see page A5]. Refer to MFS-25586.

Implementing Exclusive-OR Logic

A basic four-input XOR is assembled from one decoder and one NAND gate.

Lyndon B. Johnson Space Center, Houston, Texas

A BCD-to-decimal decoder and one four-input NAND gate can be wired as a four-input exclusive-OR (XOR) gate. Combining several of the basic two-IC arrangements allows XOR of any number of inputs.

The four-input version is shown in Figure 1. When the BCD input for 1, 2, 4, or 8 is applied, the corresponding decimal pin goes low; all other decimal pins stay high. Only the 1, 2, 4, and 8 decimal pins are connected to the NAND, and none of them would go low if two or more inputs went high or if no inputs went high. Thus the output from the NAND can go high only if just one of the four inputs is high.

Any number of inputs can be treated by expanding this basic concept. For example, a 16-input circuit is shown in Figure 2; the same function using standard logic elements would require more than 50 logic gates.

Not all complementary-symmetry metal-oxide-semiconductor (CMOS) decoders can be used for this application; some produce outputs with invalid inputs (BCD inputs above N = 9) and therefore are not acceptable. Many transistor-transistor-logic (TTL) BCD-to-decimal decoders are satisfactory.

This work was done by Monty E. Hough of Rockwell International Corp. for **Johnson Space Center.** *No further documentation is available.*
MSC-18458

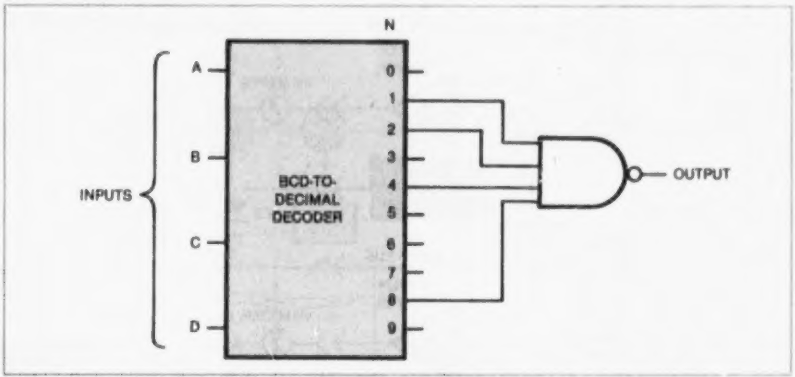

Figure 1. **Two Integrated Circuits,** a BCD-to-decimal decoder and a four-input NAND gate, form the basic four-input XOR circuit. Multiple-input exclusive-OR logic is implemented by combining several of the basic elements as shown in Figure 2.

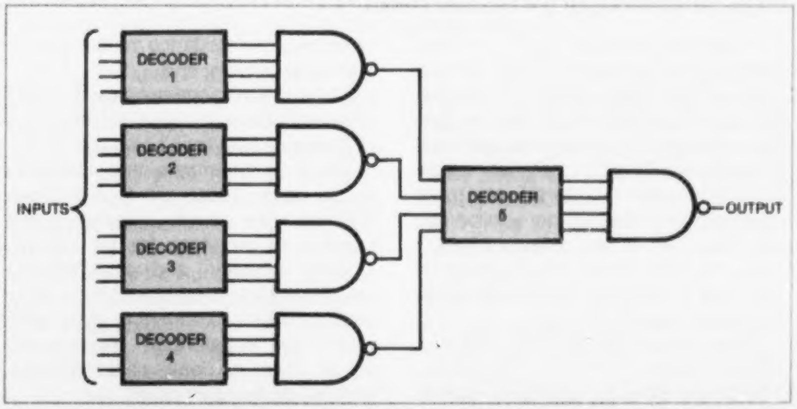

Figure 2. A **16-Input XOR Gate** is assembled from five NAND gates and five decoders. The same principle can be extended to handle more inputs.

Audio Distribution and Monitoring Circuit

A versatile circuit accepts and distributes TV audio signals.

Lyndon B. Johnson Space Center, Houston, Texas

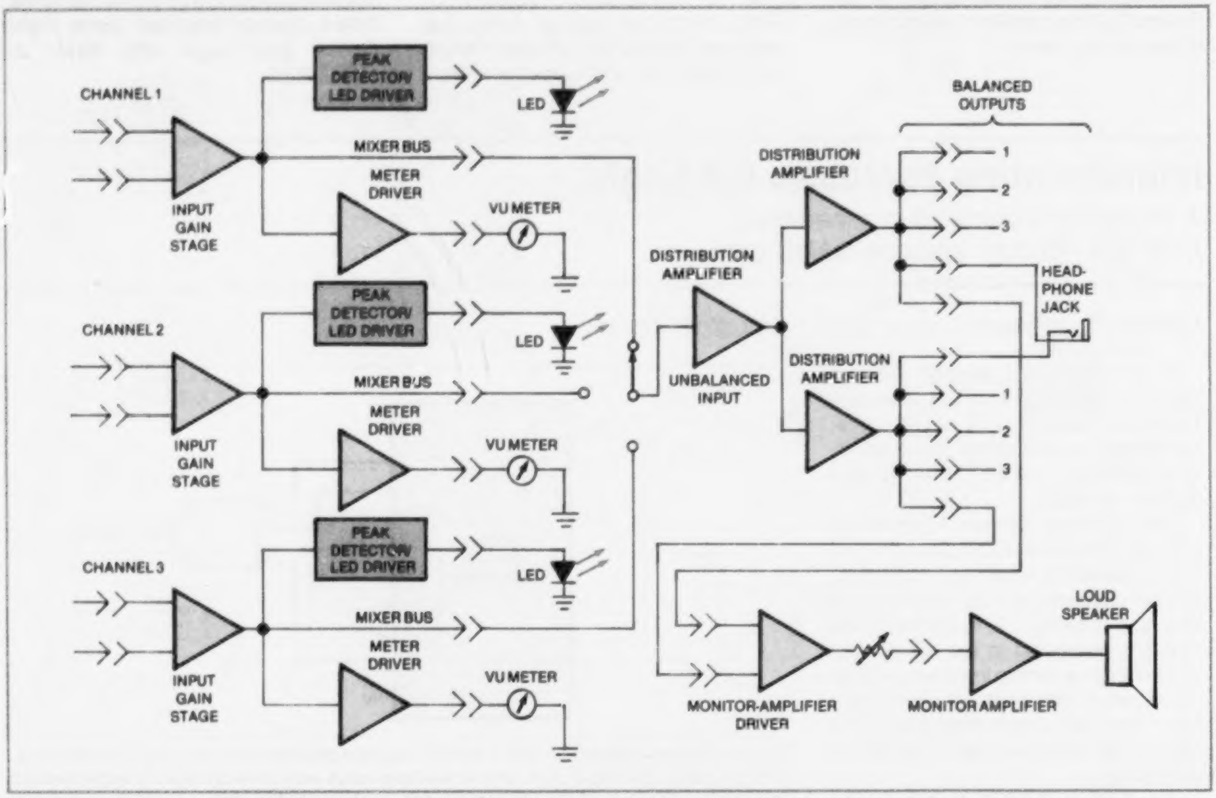
CHANNEL 1
PEAK DETECTOR/ LED DRIVER
LED
MIXER BUS
METER DRIVER
INPUT GAIN STAGE
VU METER
CHANNEL 2
PEAK DETECTOR/ LED DRIVER
LED
MIXER BUS
METER DRIVER
INPUT GAIN STAGE
VU METER
CHANNEL 3
PEAK DETECTOR/ LED DRIVER
LED
MIXER BUS
METER DRIVER
INPUT GAIN STAGE
VU METER
DISTRIBUTION AMPLIFIER
UNBALANCED INPUT
BALANCED OUTPUTS
DISTRIBUTION AMPLIFIER
1
2
3
HEAD-PHONE JACK
DISTRIBUTION AMPLIFIER
1
2
3
LOUD SPEAKER
MONITOR-AMPLIFIER DRIVER
MONITOR AMPLIFIER

The **Three-Meter Audio Distribution and Monitoring Circuit** provides flexibility in monitoring, mixing, and distributing audio inputs and outputs at various signal and impedance levels.

A distribution and monitoring unit has been built to handle the audio components of television signals at Johnson Space Center. The system includes mixing and drivers for various line levels and impedances. Program material may be simultaneously monitored on three channels. A single-channel version has also been built to monitor transmitted or received signal levels, drive a speaker, interface to building communications, and drive long-line circuits.

Other requirements met by the new circuit include:

- Sufficient drive for standard volume-unit (VU) indicators,
- Flexibility of VU reference levels so that meter indications reflect operating levels relative to those required for local or long-line circuits,
- One output stage to drive a monitor amplifier and/or a long line,
- Flexibility of impedance matching of inputs and outputs, and
- Input isolation to prevent more than 0.1 percent harmonic distortion from being introduced onto lines being monitored.

The three-meter version is illustrated in the figure. There are four program channels (the fourth channel is not used), a driver stage for an external monitor amplifier, and a distribution amplifier. Each program channel contains a balanced, bridging input gain stage, an unbalanced meter-driver stage, and a peak detector/light-emitting-diode (LED) driver.

The input stage provides input isolation and level correction for matching to any source and provides drive for a mixer bus if required. The meter driver isolates the meter from the mixer bus and allows independent calibration of each meter. The peak detector/LED driver gives a visual indication of peaks above a predetermined level that may be too fast to be indicated on a VU meter. The three inputs are normally terminated in the broadcast-standard 600 ohms, but can be left open for special applications.

Tests of the three-meter prototype yielded low noise (−80 dBm unweighted), low harmonic distortion (0.015 percent unweighted), excellent frequency response (−0.3 dB at 10 Hz, 1,000 Hz reference, −0.5 dB at 50 kHz), and low intermodulation distortion (0.007 percent).

This work was done by James M. Kirkland of Taft Broadcasting Corp. for **Johnson Space Center.** *For further information, Circle 3 on the TSP Request Card.*
MSC-20073

500-Watt, 10-GHz Solid-State Amplifier

X-band system amplifies low-duty-cycle pulses.

NASA's Jet Propulsion Laboratory, Pasadena, California

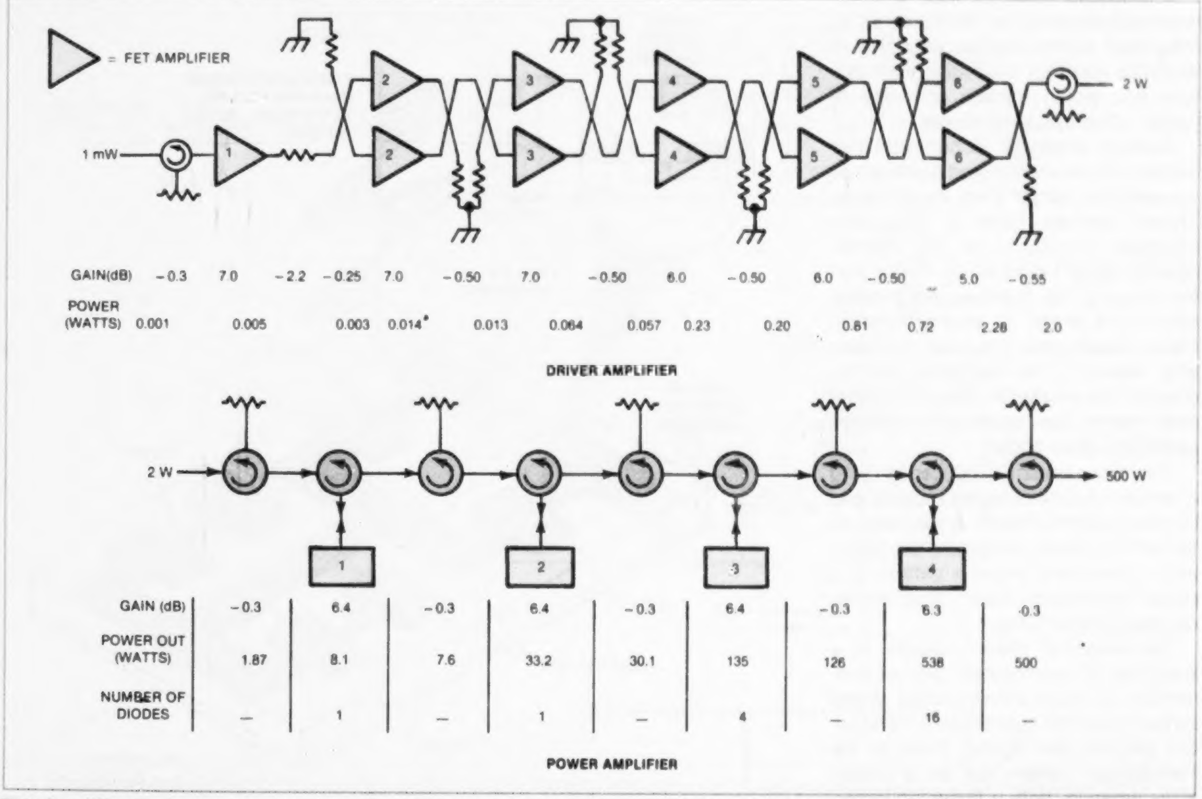
= FET AMPLIFIER
1 mW
1
2
2
3
3
4
4
5
5
6
6
2 W
GAIN(dB) -0.3 7.0 -2.2 -0.25 7.0 -0.50 7.0 -0.50 6.0 -0.50 6.0 -0.50 5.0 -0.55
POWER (WATTS) 0.001 0.005 0.003 0.014* 0.013 0.064 0.057 0.23 0.20 0.81 0.72 2.28 2.0
DRIVER AMPLIFIER
2 W
500 W
1
2
3
4
GAIN (dB) -0.3 6.4 -0.3 6.4 -0.3 6.4 -0.3 6.3 0.3
POWER OUT (WATTS) 1.87 8.1 7.6 33.2 30.1 135 126 538 500
NUMBER OF DIODES — 1 — 1 — 4 — 16 —
POWER AMPLIFIER

This **Amplifier Chain** consists of a driver-amplifier section (top), using GaAs FET's with hybrid couplers, and a power-amplifier section (bottom), using IMPATT diodes with circulators for input/output coupling and for isolation between stages.

A new, all-solid-state amplifier chain delivers a pulsed 10-GHz signal with peak power of 500 watts. The chain consists of two sections: A six-stage driver amplifier using gallium arsenide field-effect transistors (FET's) to boost milliwatt input pulses to 2 watts, and a four-stage power amplifier using impact-avalanche-and-transit-time (IMPATT) diodes to raise the 2-watt pulses to 500 watts. The duty cycle of the 10-GHz pulses is sometimes too low (duration 4 μs, repetition period 4 ms) to keep the IMPATT diodes at the temperature for proper operating impedance, so preheat bias pulses are applied to them by a bias-pulse modulator before RF output is to be produced. Likewise, for efficient, class A operation of the FET's, their biases are turned on before each RF pulse and turned off afterward.

As can be seen in the figure, the first stage of the driver is a single FET, and the next five stages use 3-dB quadrature hybrid power splitters/combiners to combine pairs of FET's in a balanced configuration. The balanced-pair power combining is essential for the 2-watt output from the sixth stage. In addition, the hybrids isolate the successive stages to improve the stability and phase linearity of the amplification. The driver has a certain inherent reliability in that it will continue to produce one-fourth of its normal output power if either device in a balanced pair should fail.

In the power-amplifier portion of the circuit, where two-terminal devices (i.e., diodes) are used for amplification, three-port circulators are used for input/output and for isolation between stages. The first two IMPATT stages are single-diode coaxial reflection amplifiers. The final two stages are cylindrical-resonant-cavity power combiners with 4 and 16 diodes, respectively.

The new solid-state X-band amplifier package constitutes a reliable, lightweight, compact, RF source. It can be used for many applications involving low- and variable-duty-cycle operation as well as fixed- and high-duty-cycle operation.

This work was done by Kenneth J. Russell and Octavius Pitzalis, Jr., of Hughes Aircraft Co. for **NASA's Jet Propulsion Laboratory.** *For further information, Circle 4 on the TSP Request Card.*
NPO-15022

Integrated Submillimeter-Wave Mixer

Planar construction would improve reliability and reduce noise.

NASA's Jet Propulsion Laboratory, Pasadena, California

A proposed mixer for submillimeter-wave signals would be fabricated as an integrated semiconductor structure. It would be made by molecular-beam epitaxy and would contain an array of planar Schottky-barrier diodes.

Gallium arsenide Schottky-barrier diodes are commonly used as mixers at wavelengths longer than about 1 mm. These devices have a fine wire ("whisker") contact for the low-frequency signal produced by mixing and for coupling the high-frequency radiation to the diode. At shorter submillimeter wavelengths, however, the parasitic losses in the semiconductor increase. The whisker is difficult to install and makes an unreliable contact, especially when cooled.

The losses would be reduced by using a semiconductor of higher mobility and by placing both contacts of the diode on the same surface. Integrating the diodes with a thin-metal antenna pattern in a planar technology would yield stable, repeatable structures.

The proposed mixer consists of a substrate of near-intrinsic gallium antimonide on which are deposited doped indium arsenide regions and a metalization pattern (see figure). Parts of the metalization pattern act as a phase-array antenna. With a dielectric superstrate on top of the pattern, it efficiently couples incident radiation from a signal source and from a local oscillator to the diodes. The undoped GaSb substrate is an insulator at submillimeter-wave frequencies. The InAs regions contain a highly-doped n+ part and a smaller moderately-doped n part. The n layer and the metal contact atop it form the active Schottky-barrier diode. The n+ layer provides a low-resistance path between the diode and the opposing metal contact.

The n layer must be precisely controlled in terms of doping (in the 10^{14}-to-10^{16}-cm^{-3} range) and thickness (0.2-to-2.0-μm range) to match the depletion-layer width of the Schottky barrier at the operating bias, otherwise parasitic resistance will be excessive. Furthermore, because of charge accumulation at an abrupt InAs/GaSb interface, a transition layer has to be implemented that avoids a short circuit along the edge of the lightly-doped InAs region. The nessary control over composition and doping on an atomic scale has recently become possible with molecular-beam epitaxy.

InAs was selected as the diode material in preference to indium antimonide because its lattice matches that of GaSb, which functions as a dielectric over a wider range of submillimeter wavelengths. InSb, in contrast, though giving slightly lower losses in the diode than InAs, would be useful as dielectric substrate only at the shortest wavelength of interest (0.15 mm).

This work was done by Joseph Maserjian, Udo Lieneweg, and Marvin Litrak of Caltech for **NASA's Jet Propulsion Laboratory.** *For further information, Circle 5 on the TSP Request Card.*
NPO-15238

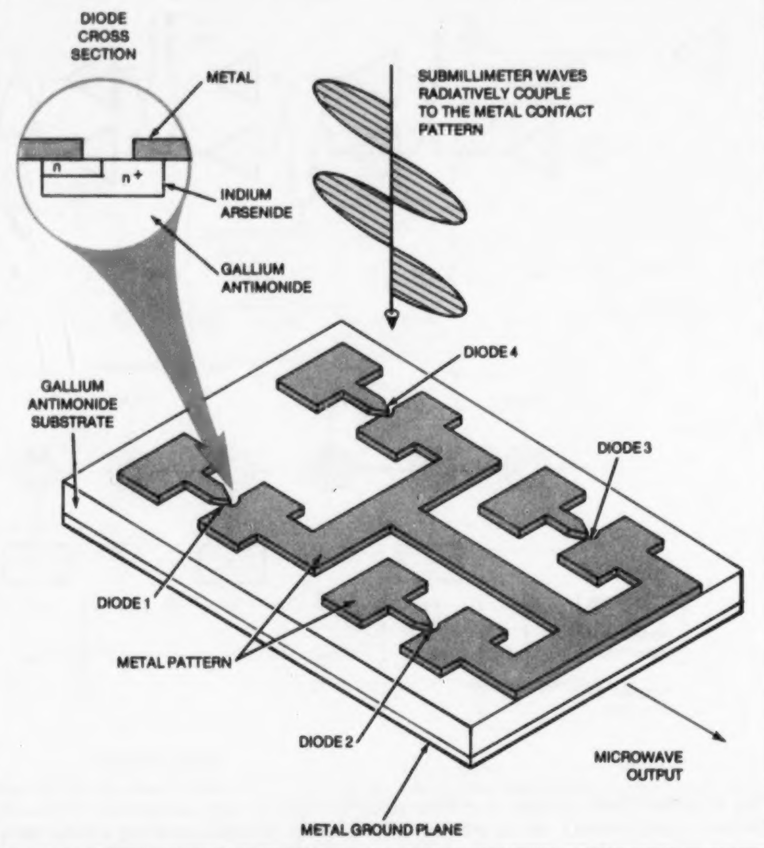

Indium Arsenide Schottky-Barrier Diodes in a gallium antimonide substrate mix submillimeter waves, producing a much lower frequency output. The integrated diode array has a relatively-high signal-to-noise ratio and wide frequency band. It operates at moderate cryogenic temperatures (100 K).

Portable I/V-Curve Tester

Battery-operated electronic load displays current/voltage characteristic on a portable oscilloscope.

NASA's Jet Propulsion Laboratory, Pasadena, California

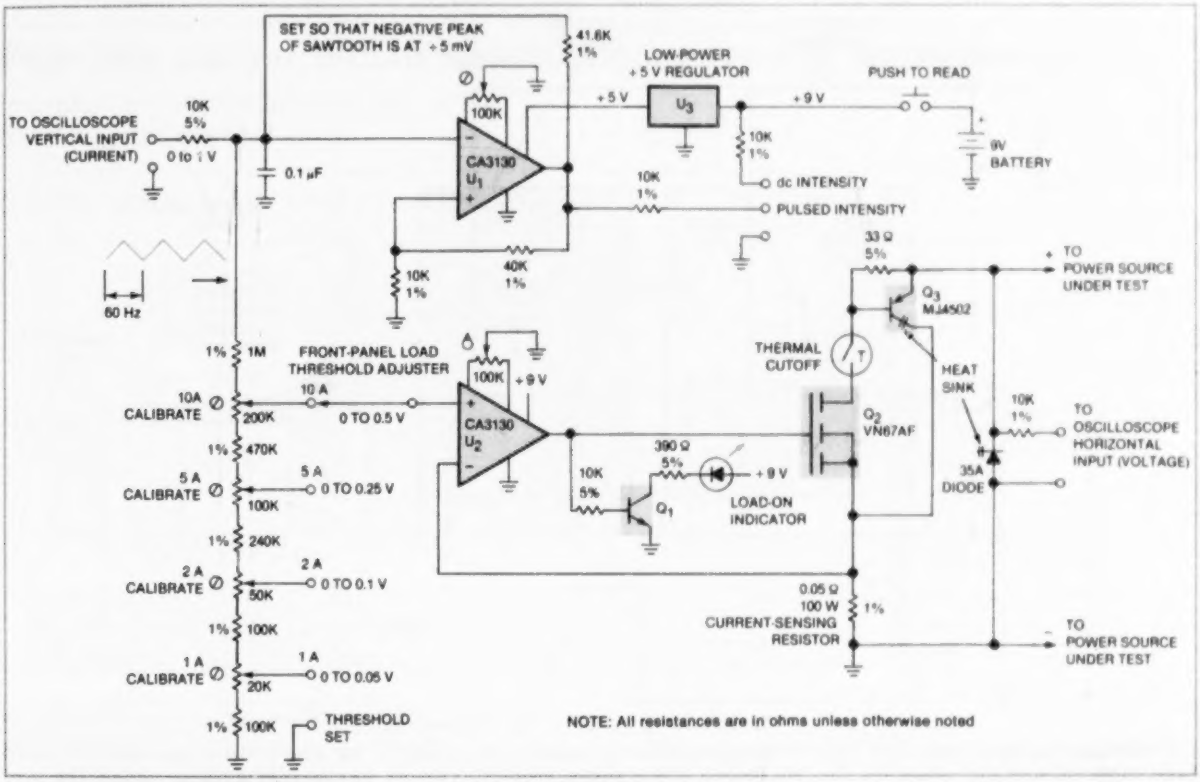

SET SO THAT NEGATIVE PEAK OF SAWTOOTH IS AT +5 mV
41.8K 1%
LOW-POWER +5 V REGULATOR
PUSH TO READ
TO OSCILLOSCOPE VERTICAL INPUT (CURRENT)
10K 5%
0 to 1 V
100K
+5 V
U3
+9 V
0.1 μF
CA3130 U1
10K 1%
9V BATTERY
dc INTENSITY
10K 1%
PULSED INTENSITY
60 Hz
10K 1%
40K 1%
33 Ω 5%
TO POWER SOURCE UNDER TEST
Q3 MJ4502
1% 1M
FRONT-PANEL LOAD THRESHOLD ADJUSTER
100K
+9 V
THERMAL CUTOFF
HEAT SINK
10A CALIBRATE
10 A
0 TO 0.5 V
200K
CA3130 U2
Q2 VN67AF
10K 1%
TO OSCILLOSCOPE HORIZONTAL INPUT (VOLTAGE)
1% 470K
390 Ω 5%
35A DIODE
5 A CALIBRATE
5 A
0 TO 0.25 V
100K
10K 5%
+9 V
Q1
LOAD-ON INDICATOR
1% 240K
2 A CALIBRATE
2 A
0 TO 0.1 V
50K
0.05 Ω 100 W CURRENT-SENSING RESISTOR
1%
1% 100K
TO POWER SOURCE UNDER TEST
1 A CALIBRATE
1 A
0 TO 0.05 V
20K
1% 100K
THRESHOLD SET
NOTE: All resistances are in ohms unless otherwise noted

An **Electronic Load Circuit** for displaying current/voltage characteristic curves of power sources uses low-cost low-power CMOS operational amplifiers to control load current flowing through power MOSFET Q_2 and main load transistor Q_3. A thermal cutoff device turns off transistor Q_3 in case of overload. To maximize battery life, the battery is connected via a "push-to-read" momentary-contact pushbutton switch.

A load-simulator circuit measures the current/voltage characteristics of photovoltaic solar-cell arrays. Since low-power complementary-metal-oxide-semiconductor integrated circuits are used, a 9-volt transistor-radio battery could power the circuit for field use.

The circuit is shown in the figure. Operational amplifier U_1 produces a 1-volt peak-to-peak sawtooth waveform. The sawtooth signal is proportional to, and is used to control, the current drawn from the power source being tested.

The sawtooth signal is also connected to the oscilloscope vertical input (current axis). The horizontal axis (voltage axis) is across the power source through a 10-kΩ resistor. The sawtooth energizes a voltage divider to provide a control signal for the servo loop controlling the main load transistor Q_3. A switch selects the tap corresponding to the desired current range, and a calibration adjustment potentiometer is provided for each tap.

Operational amplifier U_2 compares the sawtooth voltage to the voltage drop across the 0.05-Ω load-current sensing resistor. U_2 drives the gate of transistor Q_2, which in turn drives the base of the main load transistor Q_3. If the load current is lower than it should be at any moment, the voltage across the sensing resistor will be lower than the sawtooth voltage. This will cause the output of U_2 to go further positive, increasing the currents through Q_2 and Q_3 until the error is corrected.

An extra position on the range switch is used when adjusting the load threshold control so that the load current goes to zero when the sawtooth voltage goes to zero. The control is adjusted until the light-emitting diode "load-on" indicator goes out.

The circuit could be adapted for use with a slower display device, such as an X/Y recorder by increasing the value of the 0.1-μF integrating capacitor connected to the inverting input of U_1. The CA3130 operational amplifiers chosen for this circuit have good power-supply rejection so that they are well suited to portable battery operation. A regulator keeps the sawtooth amplitude constant.

This work was done by Steven W. Cole of Caltech for **NASA's Jet Propulsion Laboratory.** *For further information, Circle 6 on the TSP Request Card.* *NPO-15266*

Electronic Load Tests High-Voltage Solar Arrays

An adjustable load is provided by a combination of transistors and resistors.

NASA's Jet Propulsion Laboratory, Pasadena, California

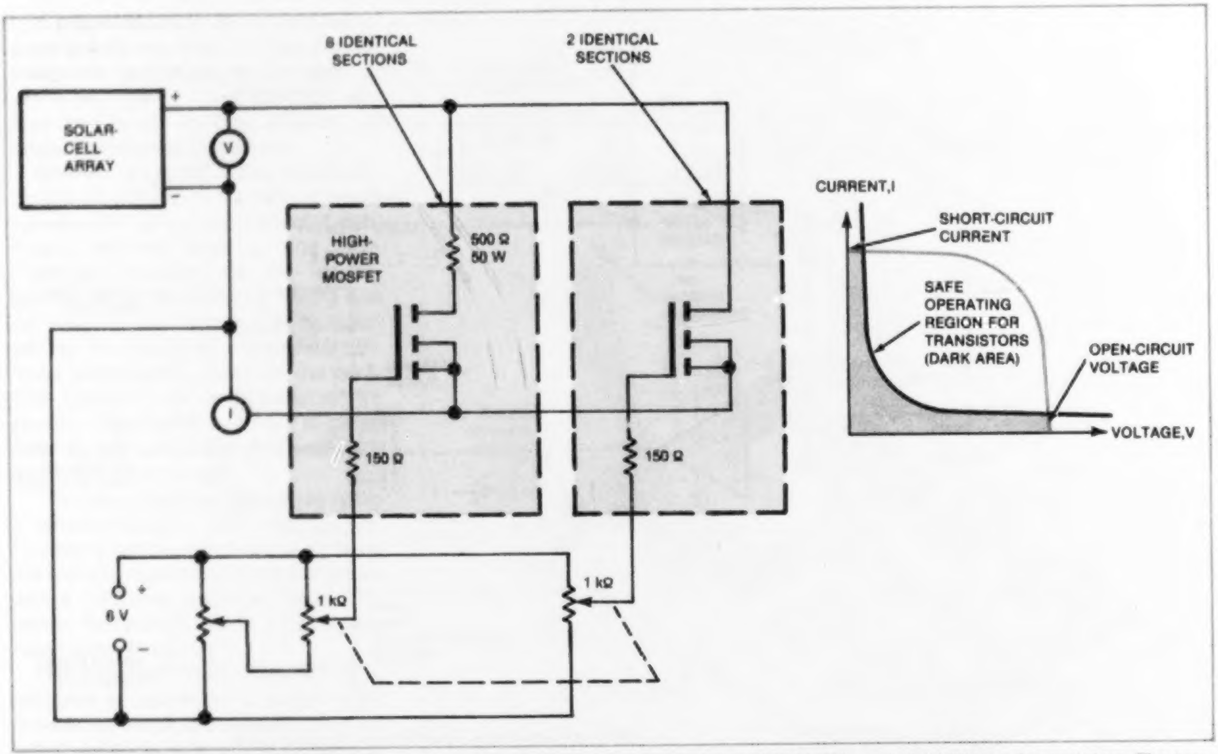

The **Adjustable Electronic Load** in the solar-cell-array test instrument uses ten power MOSFET's and eight 50-Ω series resistors. The two gate-control voltages that adjust the load are derived from a single, manually-operated, ganged potentiometer control. The third adjustable resistor adjusts the relative turn-on points of the two groups of transistors. A typical current/voltage curve for the solar array is shown at the right.

An electronic load instrument for field and laboratory measurement of photovoltaic power systems has digital displays of solar-cell-array output current and voltage. It also supplies analog signals for driving an x-y plotter. The instrument has been used to measure current/voltage characteristics of solar-cell arrays with open-circuit voltage of 350 volts and short-circuit current of 2.5 amperes.

Fixed resistors and high-voltage, high-power metal-oxide-semiconductor field-effect transistors (MOSFET's) are used in the circuit (see figure). A single control continuously adjusts the load from open circuit to short circuit. Unlike the bipolar power transistors used in conventional circuits, MOSFET's are immune to second breakdown (thermal runaway) and are thus easy to operate in parallel. The transistors are turned on at different points over the control range in a manner that operates each transistor within its power dissipation limit.

To avoid exceeding the power dissipation limit of the transistors, it is necessary to use current-limiting resistors in series with the transistors, except at lower voltages. In the circuit shown in the figure, a group of eight transistors is operated in this manner. (Alternatively, a larger number of transistors could have been used without the resistors.)

As the eight transistors are gradually turned on, the current/voltage curve of the solar-cell array is traced out from the open-circuit voltage point, past the knee of the curve where the power output is greatest, into the lower-voltage, constant-current region. Because of the series resistors, however, that part of the circuit cannot load the solar-cell array sufficiently to reach the short-circuit, zero-voltage point.

A second group of two transistors without series resistors gradually takes over the load from the first group in the low-voltage region to continue the current/voltage curve down to zero volts.

This type of electronic load is also suitable for testing other types of high-voltage power supplies. Since it is controlled by the voltage signals applied to the gates of the transistors, it could be controlled by electrical signals from other devices to present any sort of time-varying load that might be required. It can thus also be remotely controlled.

This work was done by Emmett L. Miller of Caltech for **NASA's Jet Propulsion Laboratory.** *For further information, Circle 7 on the TSP Request Card.*

Inquiries concerning rights for the commercial use of this invention should be addressed to the Patent Counsel, NASA Resident Office-JPL [see page A5]. Refer to NPO-15358.

Flip-Chip Carrier Would Match Microwave FET Impedances

Impedance transformers are part of the mounting and contact strips.

Goddard Space Flight Center, Greenbelt, Maryland

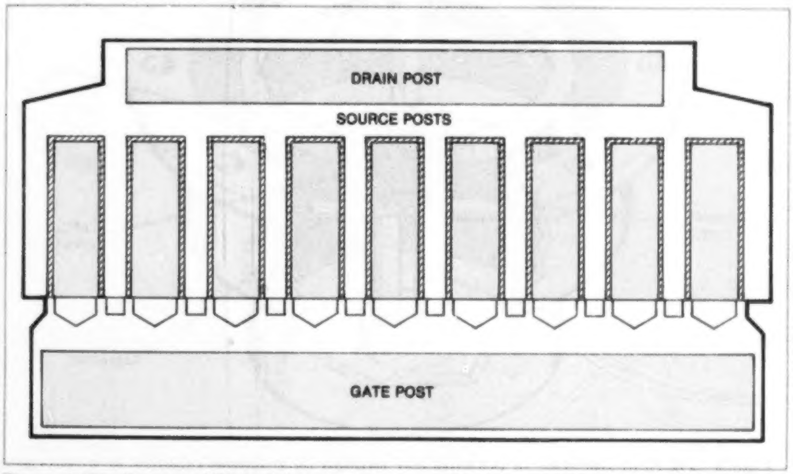

Figure 1. The **Proposed Field-Effect Transistor** would consist of three cells, such as the one shown here.

A proposed field-effect transistor (FET), roughly 2.5 mm long and 0.6 mm wide, would put out 3.5 watts at frequencies from 12 to 16 GHz. Posts plated onto the source, gate, and drain pads would allow flip-chip mounting to a special carrier. The gate and drain pads would be bonded directly to the carrier at metalized areas that are the proper width and length to serve as impedance-transformer sections of transmission line. Unwanted parasitic impedances are thus eliminated, and the bandwidth of the FET amplifier is greatly improved because the matching starts right at the terminal of the active channel.

Figure 1 shows a unit cell of the FET: Three such cells make up one complete FET pellet. A schematic of the three-cell FET, flip-chip mounted onto the carrier, is shown in Figure 2.

The gate pad width is 650 microns, which corresponds to a line impedance of about 15 ohms. The drain pad width is 500 microns, corresponding to a line impedance of 20 ohms. The input (gate) lines are paralleled after an electrical length of 40° at band center (14 GHz), and the output (drain) lines are paralleled after about 50°. These stub lengths and impedances for matching each cell were found by computer-aided design.

This work was done by Ho Chung Huang of RCA Corp. for **Goddard Space Flight Center.** *For further information, Circle 8 on the TSP Request Card.*

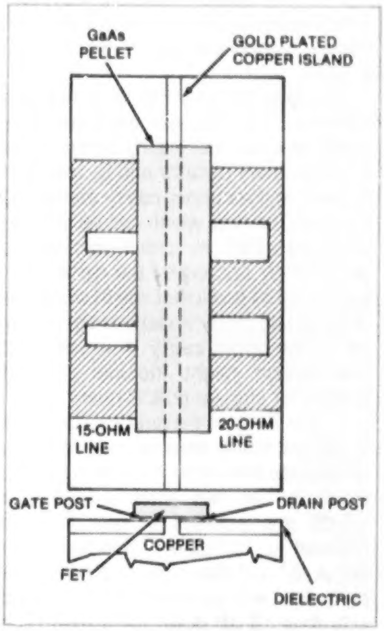

Figure 2. The **Pellet Is Flip-Chip Mounted** on a carrier, with the source grounded and the gate and drain posts connected directly to impedance-matching transmission-line segments.

This invention is owned by NASA, and a patent application has been filed. Inquiries concerning nonexclusive or exclusive license for its commercial development should be addressed to the Patent Counsel, Goddard Space Flight Center [see page A5]. Refer to GSC-12442.

Dipole-Excited Ring Antenna

Two-cavity antenna radiates low-side-lobe patterns.

Lyndon B. Johnson Space Center, Houston, Texas

A dipole radiator drives a ring radiator in a new compact C-band antenna. The antenna, which has been breadboarded and tested, can be mounted flush with a surface. Compared with a horn or a parabolic dish with the same aperture, the new ring antenna has greater gain, lower side lobes, and narrower beamwidth. It can be used on vehicles requiring flush-mounted antennas with very directive signals; for example, it could be used as a radar altimeter antenna for an aircraft.

The antenna (see Figure 1) has two cylindrical cavities, with the same symmetry axis: a lower cavity containing a dipole primary radiator and its feed and support and an upper cavity containing the ring. The ring, which can be circular or rectangular in cross section, is parasitically excited by the dipole. It is supported by posts that rise from the top of the dipole cavity. A radome covers the top of the upper cavity. A variation on this design might include crossed dipoles for circular polarization.

Figure 2 shows the gain improvement of the two-cavity antenna over that of a waveguide horn antenna with the same aperture. The new antenna exhibits a 2.5-dB improvement in gain. It also radiates a half-power beamwidth of about 40° and side lobes 18 dB down, as compared with a beamwidth of 60° and side lobe 13 dB down for a feed horn antenna. For comparison, the depth of the new antenna is about half a wavelength and the horn antenna more than a wavelength.

This work was done by Haynes Ellis, Jr., of Rockwell International Corp. for **Johnson Space Center.** *No further documentation is available.*
MSC-20201

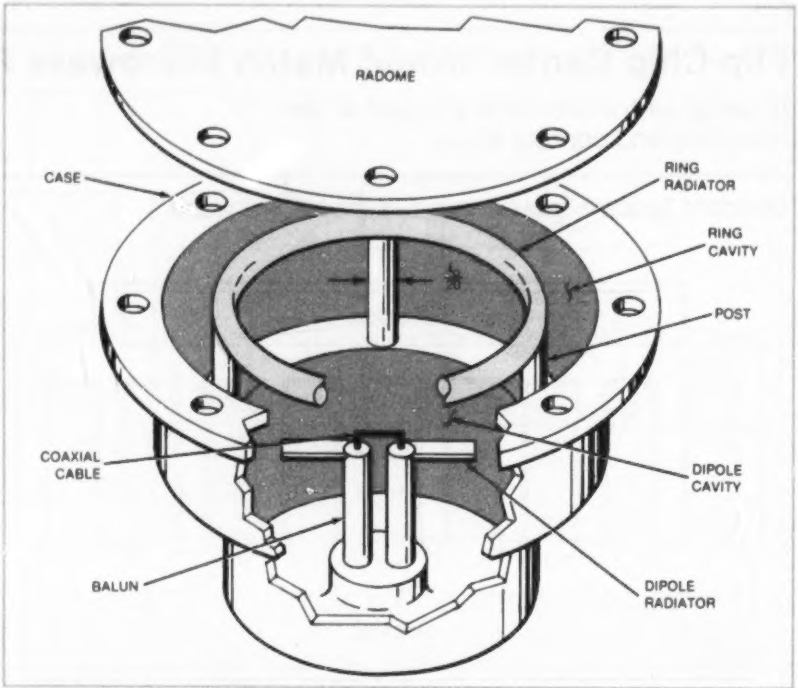

Figure 1. A **Ring Radiator** is parasitically excited by a dipole radiator in a two-cavity antenna. The lower cavity diameter is four thirds the wavelength of the center frequency (λ_0) and is $\lambda_0/4$ deep; the upper cavity is about $5\lambda_0/3$ in diameter and is also $\lambda_0/4$ deep.

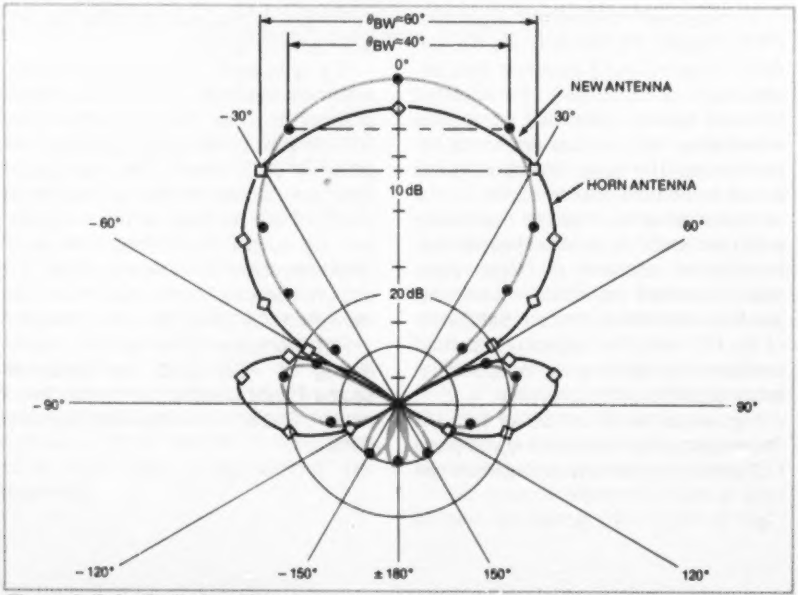

Figure 2. **Polar-Radiation Plots** show the gain improvement of the new antenna over a horn antenna.

Electronic Systems

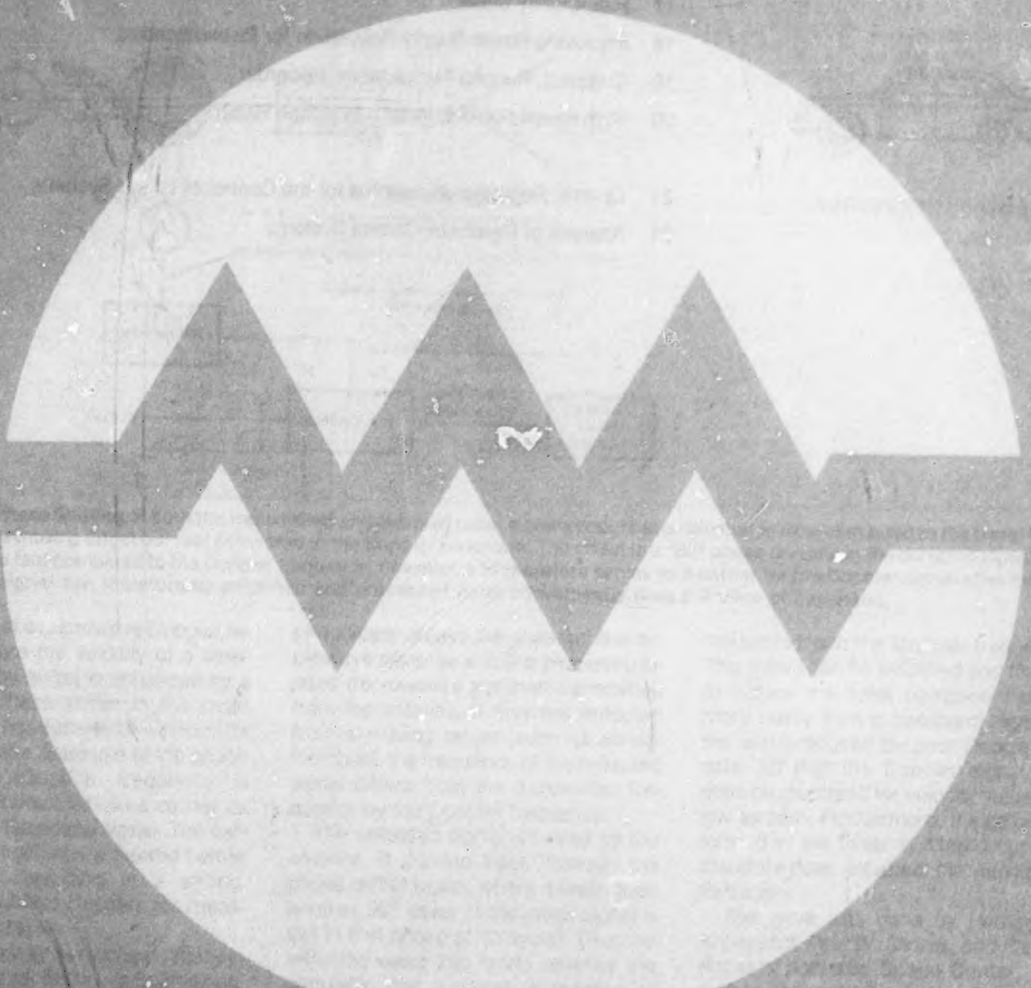

Hardware, Techniques, and Processes

15 Pulsed Phase Shifter Improves Doppler Radar
16 Converting Time Signals From BCD to IRIG-B
16 Sled Control and Safety System
17 Ride-Quality Meter
18 Improving Power-Supply Regulation for Pulsed Loads
19 Compact, Rugged Temperature Recorder
20 High-Resolution Subsurface-Interface Radar

Computer Programs

21 Optimal Regulator Algorithms for the Control of Linear Systems
21 Analysis of Feedback-Control Systems

Pulsed Phase Shifter Improves Doppler Radar

Periodic phase inversion puts Doppler signal on a carrier for easy amplification and processing.

Lyndon B. Johnson Space Center, Houston, Texas

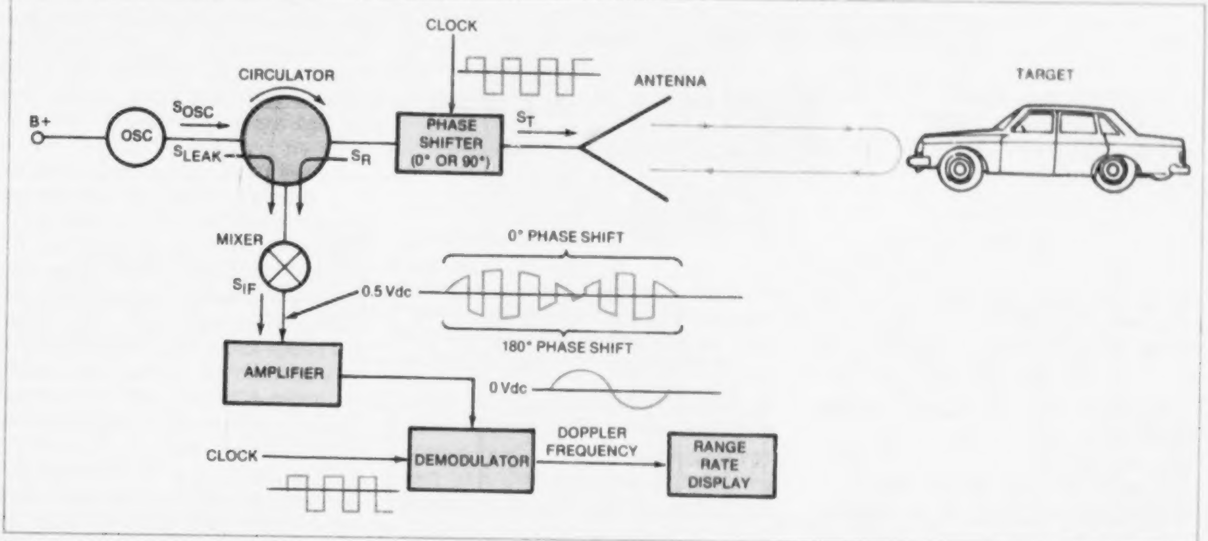

Periodic 90° Phase Shifting of both the transmitted and received radar signals occurs at a rate that is slow compared to the travel times to and from the moving target but fast compared to the Doppler waveform. The effect is a 180° phase reversal in the detected signal. The reversal rate is fast compared to the Doppler frequency, however, and therefore serves as a carrier for the Doppler signal after mixing. The Doppler signal can therefore be amplified and processed more conveniently than if it were at baseband.

The ability of a microwave Doppler radar to measure the velocity of a slow-moving nearby target is enhanced by a pulsed 90° phase shifter in the radar transmission line between the circulator and the antenna. Because of the phase shifting, the Doppler frequency is detected as modulation on a carrier instead of as a baseband signal. The carrier can be amplified and filtered before demodulation, resulting in a strong, clean demodulated Doppler for measurement and display.

The system is shown schematically in the figure. The oscillator is a Gunn diode, driven by a low-voltage dc source and generating a continuous-wave output at approximately 10 GHz. This microwave signal goes to a circulator, where some leaks to the detection port; most of it emerges from the transmit/receive port, however, and passes through the pulsed phase shifter to the antenna. The phase shifter is driven by a clock signal that periodically delays the phase of the microwave signal by $\pi/2$. The phase-modulated microwaves are then transmitted from the antenna. If they are reflected from a moving target (such as an automobile), the frequency of the reflected signal differs from the transmitted frequency by the Doppler frequency.

The reflected signal received by the antenna is carried back through the phase shifter again, where it undergoes another 90° delay (if the clock signal is still in that phase of its cycle). Thus the reflected wave that finally reaches the circulator has a phase modulation of 180°; the modulation frequency is the clock frequency.

The phase-delayed reflected signal emerges from the detector port of the circulator along with the leakage signal of the (unmodulated) oscillator frequency, and the two are heterodyned in a mixer. The resultant waveform is a carrier at the clock frequency, amplitude-modulated with the Doppler frequency. This signal can be amplified and filtered to reduce the noise component much more easily than a baseband signal of the sort produced by prior Doppler radars, so that the Doppler signal can even be displayed for velocity values as low as zero. Furthermore, the dc signal formed in the mixer is filtered out and therefore does not affect the velocity information.

This work was done by Herbert S. Kobayashi, Paul W. Shores, and Patrick Rozas of **Johnson Space Center.** *For further information, Circle 9 on the TSP Request Card.*

This invention is owned by NASA, and a patent application has been filed. Inquiries concerning nonexclusive or exclusive license for its commercial development should be addressed to the Patent Counsel, Johnson Space Center [see page A5]. Refer to MSC-18675.

Converting Time Signals From BCD to IRIG-B

Nine IC's convert parallel binary-coded-decimal time signals to serial IRIG standard time format B.

Lyndon B. Johnson Space Center, Houston, Texas

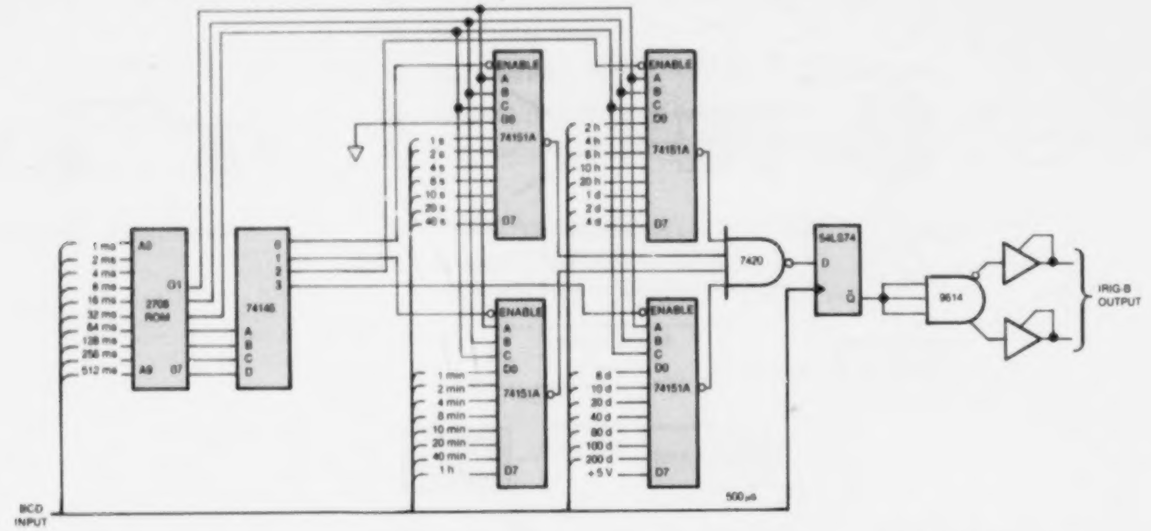

This **Time-Code Converter** converts time signals from BCD representation to IRIG-B representation so that it can be read on a standard time-code reader.

The coded representation of time signals — day, hour, minute, second — can be changed from the binary-coded decimal (BCD) to the IRIG standard time-code format B by a circuit that uses nine integrated circuits. The input to the code-converter circuit is parallel BCD pulses on a bus; the output is the serial pulses of IRIG-B on a single line.

As can be seen from the diagram of the code converter, the BCD representations of milliseconds, seconds, minutes, hours, and days are put to different uses. The milliseconds signals are used to address sequentially a read-only memory (ROM) that is loaded with a pattern corresponding to addresses in four multiplexers. The seconds, minutes, hours, and days BCD signals go directly to the multiplexers.

The contents of the 2708 ROM operate the four 74151A multiplexers, which in turn generate the IRIG-B signal. Thus the converter operates as a lookup table. The outputs from the four multiplexers are combined in the 7420 NAND gate to produce one signal, which is then filtered through a 7474 multivibrator and fed out through a 9614 line driver.

This circuit was developed to drive a display in a simulated cockpit. The IRIG-B generator is synchronized with the master timing-unit emulator.

This work was done by John B. Houston of Rockwell International Corp. for **Johnson Space Center.** *For further information, Circle 10 on the TSP Request Card.*
MSC-18963

Sled Control and Safety System

Microprocessor control keeps the velocity and acceleration within safe limits.

Lyndon B. Johnson Space Center, Houston, Texas

A computerized system for controlling the motion of a linear-track accelerator could be applied to other automated equipment, such as numerically-controlled machine tools and robot manipulators on assembly lines. The system supervises the motion and automatically shuts down if a safety hazard develops.

The original application was in generating drive signals for a "sled" used in tests with human subjects. The sled and subject move along a linear track in a sinusoidal motion of up to 1.5 meters amplitude. The frequency and amplitude are both variables in the tests. To insure the safety of the subject, the system shuts off automatically if the sled acceleration becomes too high, if there is a failure of the computer or other component, or if brake pressure falls.

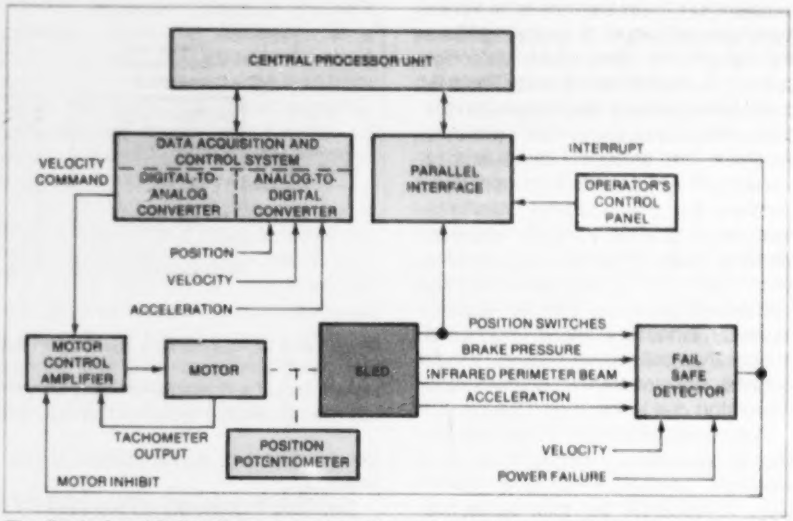

The **Control and Safety System** controls the motions of the sled with a sine-wave signal created digitally by the microprocessor. Dynamic parameters of the sled motion are monitored so that the sled may be stopped safely if a malfunction occurs. The sled is capable of sinusoidal accelerations up to 0.5 g with a 125-kg load.

The control paths between the major system components are shown in the figure. Test parameters, such as the frequency and amplitude of the sled motion, are entered from a control panel and fed to the central processing unit (CPU) through the parallel interface.

The CPU generates the required sine wave digitally; a digital-to-analog converter in the data acquisition and control subsystem (DACS) converts it to the analog form required by the motor controller. The CPU also monitors acceleration, velocity, and position signals from the motor controller; these are digitized in the DACS. In addition, the CPU monitors position-sensing switches located near the ends of the track.

The motor control amplifier maintains a motor speed proportional to the sine-wave signal from the CPU. The amplifier output is the drive current of the motor. The amplifier compares the commanded speed to the actual motor speed and adjusts the current as necessary to speed up or slow down the motor. Inhibiting inputs on the amplifier are used to prevent the amplifier from driving the sled on beyond limit switches near the ends of the track. In normal operation the sled does not quite reach these switches.

The fail-safe system checks for the various runaway and safety-hazard conditions and sends out the interruption and inhibition signals when trouble occurs. Automatic shutdown is accomplished by inhibiting the motor drive current and simultaneously applying the brake. In addition, the test operator may force an emergency shutdown via a single switch located on the control panel.

This work was done by Larry J. Forrest of Technology, Inc., for **Johnson Space Center.** *Further information may be found in NASA CR-167425 [N82-10061/NSP], "Operations and Maintenance Manual for the Linear Accelerator (Sled)" [$9.00]. A copy may be purchased [prepayment required] from the National Technical Information Service, Springfield, Virginia 22161. MSC-20082*

Ride-Quality Meter

Noise and vibration components are summed to produce an index of passenger discomfort.

Langley Research Center, Hampton, Virginia

A portable "ride-quality" meter measures passenger discomfort and the acceptability of vehicle interior noise and vibration. The meter is especially suited for determining vehicle comfort and design tradeoffs and for comparing the ride quality of vehicles.

The ride-meter output is in terms of "discomfort units," which directly relate to passenger subjective acceptance of the measured environment. It is derived from software implementation of psychophysical laws governing human response to combined noise and vibration. Complete recording, analysis, and transformation of measured data into subjective units are done on board the vehicle and in real time. The effects of multiple frequencies and multiple axes of vibration are automatically accounted for, as are the combined effects of noise and vibration (see figure).

Experimental studies utilizing approximately 2,200 test subjects have led to the development of an empirical model for predicting passenger discomfort. The ranges of noise and vibration amplitudes and frequencies used to derive the model include those known to influence passenger comfort most.

The ride-quality meter consists of the following components: sensing elements to measure vibration in five axes (vertical, lateral, longitudinal, roll, and pitch) and interior noise; analysis elements to weight and average the signals generated by the sensing elements; software elements to process the spectral data generated by the analysis elements in accordance with the specialized and detailed psychophysical relationships that define human response to noise and vibration; and readout elements that display all or selected components of subjective discomfort produced by the noise and vibration environment.

The electrical signal corresponding to the acoustical pressure fluctuations is applied to the input of an octave-band analyzer and filter, the output of which is applied as input to a noise-discomfort module that computes the subjective discomfort, D_N, due to the interior-noise environment. The electrical signals corresponding to each of the five vibration

(continued on next page)

acceleration levels are applied to the input of a set of frequency weighting filters that reflect the effect of vibration frequency on human discomfort. The outputs of the filters are then applied to rms detection circuits, which provide weighted rms levels for each axis of vibration. These weighted rms accelerations are then applied to the "comfort" modules, which transform the physical vibration characteristics into subjective discomfort units for each axis. The individual-axis discomfort units are applied to the combined-axis module and then to the duration-correction module, which outputs the total duration-corrected discomfort due to vibration, D_{vib}.

The noise component of discomfort, D_N, is algebraically summed with the vibration component of discomfort, D_{vib}, to generate the total subjective discomfort, D_{total}, attributable to the measured noise and vibration environment. The D_{total} signal is then applied to the visual-display module, which can also display selected values of discomfort produced at earlier stages of the process.

This work was done by Jack D. Leatherwood, Thomas K. Dempsey, Sherman A. Clevenson, and David G. Stephens of **Langley Research Center.** *For further information, Circle 11 on the TSP Request Card.*

This invention is owned by NASA, and a patent application has been filed. Inquiries concerning nonexclusive or exclusive license for its commercial development should be addressed to the Patent Counsel, Langley Research Center [see page A5]. Refer to LAR-12882.

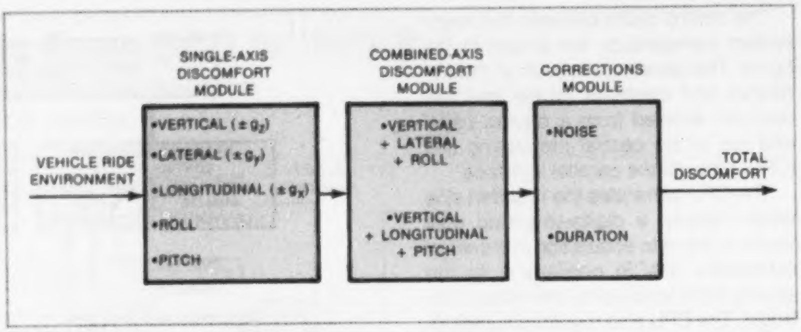
SINGLE-AXIS DISCOMFORT MODULE
COMBINED AXIS DISCOMFORT MODULE
CORRECTIONS MODULE
VEHICLE RIDE ENVIRONMENT
•VERTICAL ($\pm g_z$)
•LATERAL ($\pm g_y$)
•LONGITUDINAL ($\pm g_x$)
•ROLL
•PITCH
•VERTICAL + LATERAL + ROLL
•VERTICAL + LONGITUDINAL + PITCH
•NOISE
•DURATION
TOTAL DISCOMFORT

Single- and Combined-Axis Discomfort Are Corrected by the effects of noise and vibration to yield a measure of the total discomfort experienced by a rider. The three modules shown transform mathematically-weighted rms accelerations, which represent the physical vibration characteristics, into subjective discomfort units.

Improving Power-Supply Regulation for Pulsed Loads

A bypass circuit speeds up regulator response to turn-on transients.

Lyndon B. Johnson Space Center, Houston, Texas

A new power-supply voltage-regulator circuit speeds up the response to sudden load changes. As soon as the load increases, an additional feedback path is enabled. This path bypasses, and provides faster loop response than, the normal feedback path. Steady-state instability due to the faster loop response is avoided by progressively disabling the bypass loop and allowing the normal feedback path to take over.

A regulated power supply is supposed to maintain a constant voltage despite changes in the load current. If the current increases quickly, however, as in pulsed applications, the voltage may drop and then recover slowly.

To reduce these voltage changes, pulsed devices such as radar transmitter tubes use power supplies that have a fast-response feedback loop: Any drop in output voltage is sensed and fed to a correcting amplifier, which increases the supply voltage. High-voltage regulators with fast response, however, tend to be unstable under steady-state conditions.

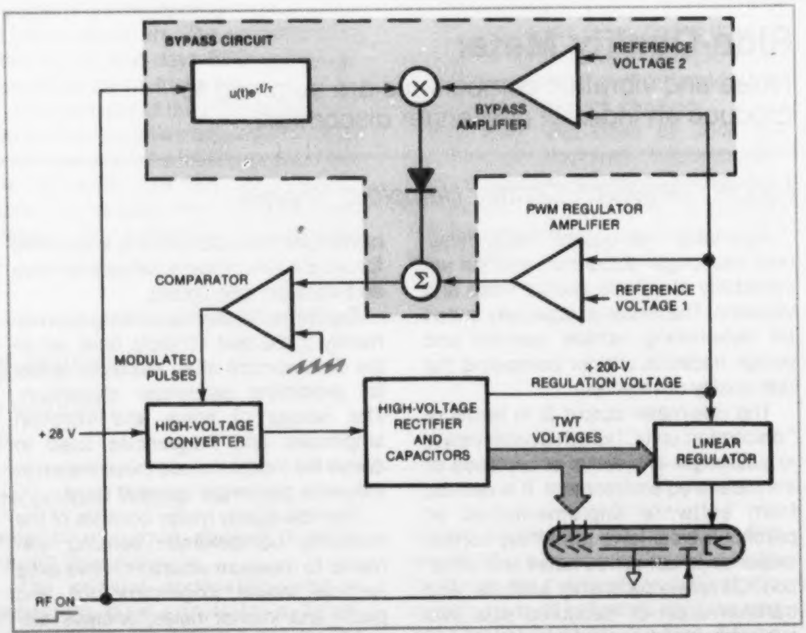
BYPASS CIRCUIT
$u(t)e^{-t/\tau}$
REFERENCE VOLTAGE 2
BYPASS AMPLIFIER
PWM REGULATOR AMPLIFIER
COMPARATOR
REFERENCE VOLTAGE 1
MODULATED PULSES
+ 200-V REGULATION VOLTAGE
+ 28 V
HIGH-VOLTAGE CONVERTER
HIGH-VOLTAGE RECTIFIER AND CAPACITORS
TWT VOLTAGES
LINEAR REGULATOR
RF ON

Fast-Response Regulation in this TWT power supply is enabled when the RF ON pulse suddenly increases the power load. The bypass circuit is activated to meet the sudden demand and then is progressively disabled.

The new bypass circuit was devised for a converter power supply that applies voltage to the collector in a pulsed traveling-wave tube (TWT). To minimize power-supply size and weight, the electron-beam collector in the TWT is operated at the lowest possible voltage. Any excessive decay of the collector voltage causes high TWT helix current, which can damage the fragile helix structure.

The power supply with bypass circuit is shown in the figure. During normal operation the bypass amplifier is disabled, and the pulse-width-modulated (PWM) regulator amplifier provides the feedback necessary to maintain the 200-volt regulation voltage on the TWT collector. When the application of a radio-frequency (RF) pulse to the input end of the TWT increases the load from 15 to 150 watts, the 200-V regulation voltage drops significantly, because of the slow response of the PWM regulator amplifier.

The fast-response bypass amplifier is enabled when the RF pulse is turned on. Reference voltage 2 is chosen so that the bypass amplifier will try to regulate the 200-V voltage at a predetermined fraction of its normal value. However, the output of the bypass amplifier is rectified so that it can raise, but not lower, the 200-V regulation voltage. This rectification and the fact that the bypass amplifier output is multiplied by the exponentially-decaying RF ON signal dampens potential oscillations.

The bypass signal is added to the output of the PWM regulator amplifier. Approximately 100 ms after TWT turn-on, the PWM regulator amplifier output is near its steady-state value, the rectifier becomes reverse-biased, and the bypass circuit no longer affects power-suppy operation.

This work was done by Charles R. Gulick and Ronnie B. Chan of Hughes Aircraft Co. for **Johnson Space Center.** *No further documentation is available.* *MSC-20016*

Compact, Rugged Temperature Recorder

Unattended solid-state unit stores 2,048 readings taken at intervals of 1.875 to 240 minutes.

Ames Research Center, Moffett Field, California

A small, light, self-contained temperature recorder that was originally developed for use in space experiments can store 2,048 temperature readings taken over a period of almost a year (or much less) and then read them out when a special readout unit is plugged into it. The temperatures may be anywhere in the range from −10° to +50° C and are recorded at intervals selectable by factors of 2 from 1.875 up to 240 minutes. The data can be retained in the recorder for at least 4 months before readout, if desired.

The battery-operated recorder has no moving parts — it is completely solid-state electronic (see figure). The temperature sensor is a linear integrated circuit that produces a current proportional to absolute temperature. Its output signals are converted to 8-bit digital data and stored in read/write memories. After the 2,048 readings have been taken at the predetermined intervals, the recorder switches to an ultra-low-power data-retention mode.

When the data are to be extracted, the recorder is connected to a unit that has analog, digital, and visual light-emitting-diode outputs. The unit also stores the data in semipermanent memories.

The basic recorder can be simplified to accommodate a variety of applications by such changes as the addition of extra memory to store more data, by

(continued on next page)

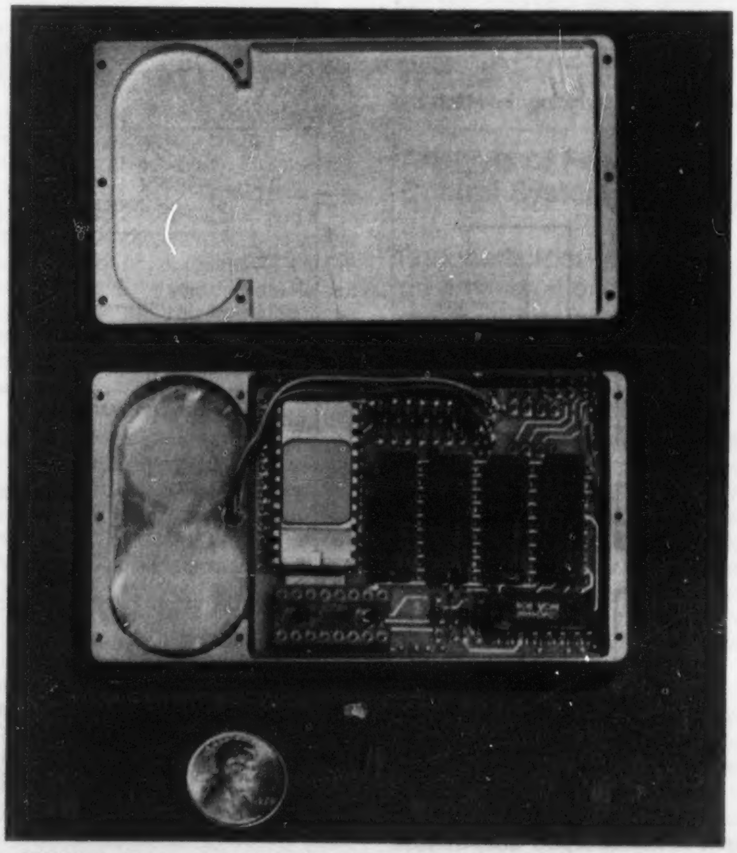

This **Solid-State Temperature Recorder,** shown here in its entirety with the cover removed, is compact, lightweight, and rugged. It can record 2,048 temperature readings over a period of up to nearly a year and retain them for at least another 4 months using just the batteries shown.

changing the front end to permit measurements other than temperature to be made, or by using different batteries to obtain different operating periods.

This work was done by Richard M. Westbrook, Lawrence D. Bennett, Robert A. Steinhauer, and Gordon J. Deboo of **Ames Research Center.** *Further information may be found in NASA TM-81267 [N81-23434/NSP], "A Solid-State Digital Temperature Recorder for Space Use" [$9]. A copy may be purchased [prepayment required] from the National Technical Information Service, Springfield, Virginia 22161.*
ARC-11304

High-Resolution Subsurface-Interface Radar

Mathematical technique yields more accurate information about depth of soil layers.

John F. Kennedy Space Center, Florida

Homomorphic deconvolution signal processing can enhance the information obtained in high-resolution soil-depth measurements by radar. The proposed technique is expected to increase the accuracy with which soil-layer depths are gaged.

The homomorphic deconvolution process involves the use of the inverse forward Fourier transform and complex forward and inverse natural logarithms (see Figure 1). The logarithmic processing forms a time-domain function, or cepstrum.

The intended use is with subsurface-interface radar sounding, in which the subsurface features of soils are mapped. An antenna placed near the ground is shock-excited by a capacitor discharge. The signal penetrates the soil, is reflected by subsurface discontinuities, and is received by the antenna. However, the return signal also contains unwanted multiple reflections created by the soil surface itself and by the mismatch in impedance of the antenna and the soil.

Homomorphic deconvolution aids in separating the unwanted returns. Slowly varying components of the return signal (which represent the transmitted signal) are discarded. Rapidly varying components, which yield information about the separation between soil layers, are preserved (Figure 2). Although homomorphic deconvolution demands considerable data processing beyond that ordinarily required for radar returns, it yields sharper resolution.

This work was done by William J. Steinway of the Georgia Institute of Technology for **Kennedy Space Center.** *For further information, Circle 12 on the TSP Request Card.*
KSC-11212

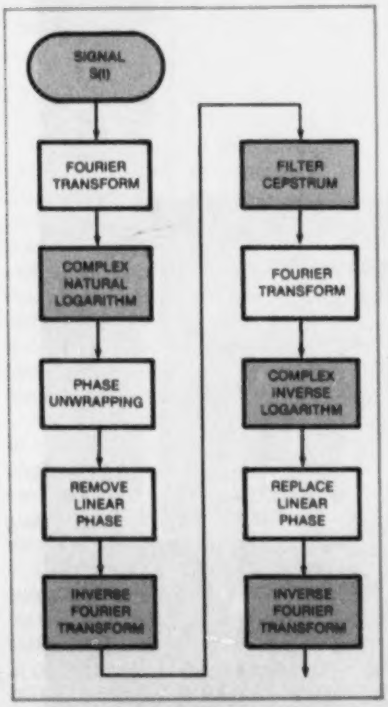

Figure 1. **Homomorphic Deconvolution** processes a time-varying signal S(t) and includes forward and inverse Fourier transform and complex logarithmic operations.

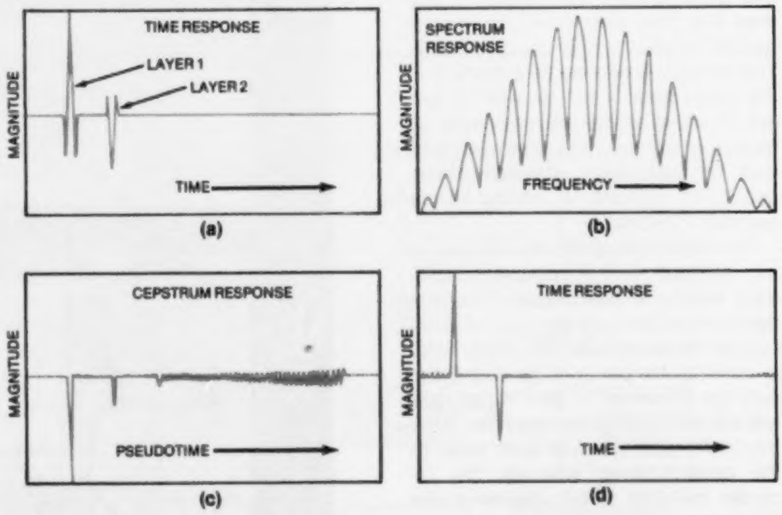

Figure 2. **Signal Processing Is Shown** for unequal signal returns from soil layers at two depths. The reflected pulses appear in (a). The spectrum of the composite returns appears in (b). The period of the rapidly varying component of the spectrum is inversely proportional to the separation of the layers. The high-pass portion of the cepstrum appears in (c). The deconvoluted return appears in (d). The time spread of each of the two returns is smaller in (d) than in (a), so that the resolution of the layer-depth measurement has been increased.

Computer Programs

These programs may be obtained at very reasonable cost from COSMIC, a facility sponsored by NASA to make new programs available to the public. For information on program price, size, and availability, circle the reference letter on the COSMIC Request Card in this issue.

Optimal Regulator Algorithms for the Control of Linear Systems

A rigorous tool for designing multi-input/multi-output control systems

A control-theory design package, called Optimal Regulator Algorithms for the Control of Linear Systems (ORACLS), aids in the design of controllers and optimal filters for systems that can be modeled by linear, time-invariant differential and difference equations. ORACLS is particularly attractive because it is a rigorous tool for dealing with multi-input and multi-output dynamic systems in both continuous and discrete forms.

Optimal linear quadratic regulator theory, currently referred to as the linear-quadratic-Gaussian (LQG) problem, has become the most widely accepted method of determining optimal control policy. Within this theory, the infinite-duration time-invariant problems, which lead to constant-gain feedback control laws and constant Kalman-Bucy filter gains for reconstruction of the system state, are highly tractable and potentially easy to implement. Various new and efficient methods in the field of numerical linear algebra have been combined in ORACLS, which solves time-invariant continuous or discrete LQG problems.

ORACLS is a collection of subroutines that can be used to formulate, manipulate, and solve various LQG design problems. By providing primary operations, an analysis of linear time-invariant systems, and control synthesis based on LQG methodology, ORACLS maintains considerable flexibility at each operational state. The input/output routines handle the reading and writing of numerical matrices, printing heading information, and accumulating output information. The basic vector-matrix operations include addition, subtraction, multiplication, equation, norm construction, tracing, transposition, scaling, juxtaposition, and the construction of null and identity matrices. The analysis routines provide for the following computations: the eigenvalues and eigenvectors of real matrices; the relative stability of a given matrix, matrix factorization; the solution of linear constant-coefficient vector-matrix algebraic equations; the controllability properties of a linear time-invariant system; the steady-state covariance matrix of an open-loop stable system forced by white noise; and the transient response of continuous linear time-invariant systems.

The control law design routines of ORACLS implement some of the more common techniques of time-invariant LQG methodology. For the finite-duration optimal linear regulator problem with noise-free measurements, continuous dynamics, and integral performance index, a routine is provided that implements the negative exponential method for finding both the transient and steady-state solutions to the matrix Riccati equation. For the discrete version of this problem, the method of backward differencing is applied to find the solutions to the discrete Riccati equation. A routine is also included to solve the steady-state Riccati equation by the Newton algorithms described by Klein for continuous problems and by Hewer for discrete problems.

Another routine calculates the prefilter gain to eliminate control-state cross-product terms in the quadratic performance index and the weighting matrices for the sampled-data optimal linear regulator problem. For cases with measurement noise, duality theory and optimal regulator algorithms are used to calculate solutions to the continuous and discrete Kalman-Bucy filter problems. Finally, routines are included to implement the continuous and discrete forms of the explicit (model-in-the-system) and implicit (model-in-the-performance-index) model following theory. These routines generate linear control laws that cause the output of a dynamic time-invariant system to track the output of a prescribed model.

In order to apply ORACLS, the user is required to write an executive (driver) program that inputs the problem coefficients, formulates and selects the routines to be used to solve the problem, and specifies the desired output. The ORACLS routines are written in FORTRAN IV for batch execution. Both CDC and IBM versions of the code are available. The CDC version has been implemented on a CDC 6000-series computer with a central memory requirement of approximately 13K (octal) of 60-bit words. The IBM version has been implemented on an IBM 370-series computer with a central memory requirement of approximately 300K of 8-bit bytes. The CDC version was developed in 1978, and the IBM version was generated in 1981.

This program was written by Ernest S. Armstrong of **Langley Research Center** *(CDC version) and by the Mechanical Engineering Department of Howard University (IBM version). For further information, Circle A on the COSMIC Request Card.*
LAR-12313 and LAR-12953

Analysis of Feedback-Control Systems

Reduced-order feedback-control equations are obtained for use in time- and frequency-domain analysis.

BLOCK IT implements an algorithm that obtains reduced-order feedback-control equations for use in both time- and frequency-domain analysis. In a more general context, BLOCK IT computes a real nonsingular similarity-transformation matrix that reduces a real nonsymmetric matrix to block-diagonal form, each block of which is a real quasi-upper triangular matrix.

The algorithm works with both defective and derogatory matrices. If the program should fail, the algorithm generates data output that can be used as a guide for reformulation of the mathematical equations that lead to the ill-conditioned matrix that could not be block-diagonalized.

(continued on next page)

Frequency response methods are of fundamental importance in the design and performance evaluation of feedback-control systems. Nearly all of the frequency response methods require that the user obtain transfer functions. For multivariable systems, a matrix of transfer functions must be obtained. BLOCK IT offers an automated procedure for obtaining transfer functions expressible as a partial fraction expansion that may be truncated via engineering judgment. Truncation decisions may be based upon gain coefficients that are real numbers formed by a direct multiplication of a modal observability coefficient and a modal controllability coefficient, along with system frequencies.

BLOCK IT utilizes an algorithm for computing reducing subspaces for block diagonalization. The program is tailored to meet the needs of the analyst requiring reduced-order dynamic models for feedback-control analysis. The algorithm is basically a continuation of the procedure used to compute eigenvalues. A sequence of similarity transformations is computed that keeps reducing the partially reduced matrix to successively simpler forms. This sequential procedure ends when the reduced form of the matrix is block-diagonal. The resultant similarity transformation is the accumulated product of the entire sequence of similarity transformations used in the reduction process.

BLOCK IT is written in FORTRAN IV for batch execution and has been implemented on an IBM 370-series computer with a central memory requirement of approximately 500K of 8-bit bytes. The program was developed in 1981.

This program was written by Harold P. Frisch of **Goddard Space Flight Center.**
For further information, Circle B on the COSMIC Request Card.
GSC-12723

Physical Sciences

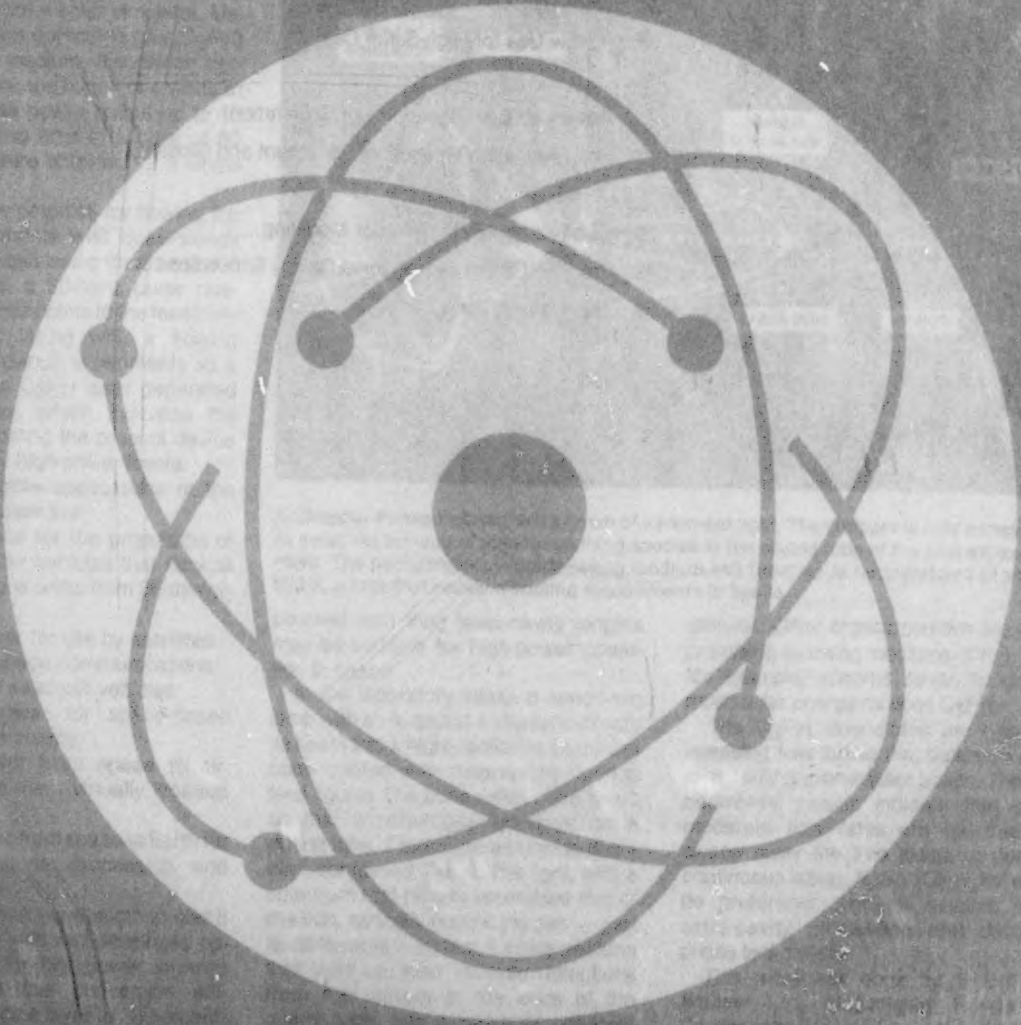

Hardware, Techniques, and Processes

25 Sunlight-Pumped Laser
26 Improved Heat-of-Fusion Energy Storage
26 Solar-Assisted Solution-Mining Concept
27 Mapping Ocean Winds by Radar
28 A New Use for High-Sulfur Coal

Books and Reports

28 Advanced Coal-Based Power Generation
29 Solar-Radiation Measuring Equipment and Glossary

Computer Programs

29 Cube-Corner Retroreflector Modeling
29 Two- and Three-Dimensional Galaxy Simulations
30 Star-Catalog Data Base

Sunlight-Pumped Laser

Organic iodide gas is stimulated by a portion of the Sun's spectrum to emit laser light.

Langley Research Center, Hampton, Virginia

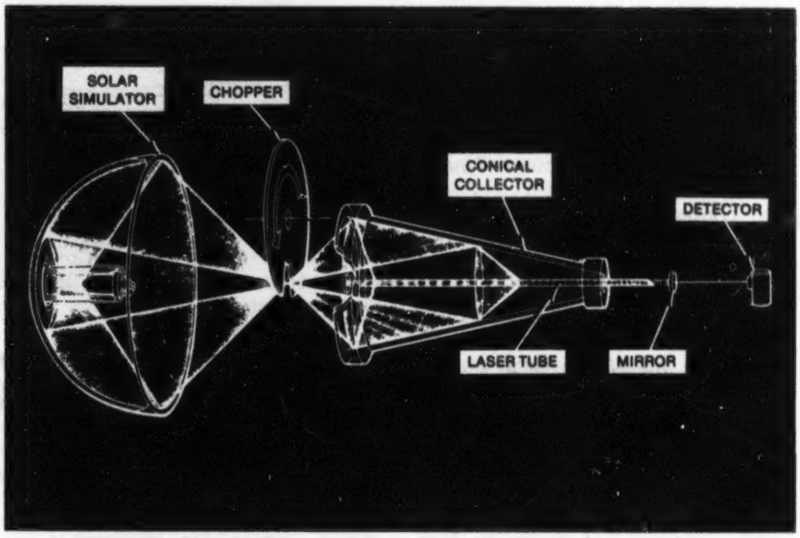

A Chopper Forms Pulses from a beam of xenon-arc light. The chopper is only necessary to avoid the buildup of laser-quenching species in the sealed tube of the present experiment. The perfluoropropyliodide lasing medium can function at temperatures of about 670 K, a fact that reduces cooling requirements in space.

A gas laser that is pumped by simulated Sunlight was tested in laboratory experiments with a solar simulator. Using a perfluoropropyliodide gas (C_3F_7I) as the lasing medium, the device produced a continuous output of 4 watts at 1.315 μm. Peak power output up to 10 watts and lasing time in excess of 60 milliseconds were obtained for a single static fill.

To verify the potential for flowing the lasant, experiments with quasi-steady gas flow produced lasing for almost 200 milliseconds at a 30-hertz pulse rate. This performance points to the feasibility of continuous lasing with a flowing medium. In previous experiments as a fusion driver, a C_3F_7I laser generated terawatt pulses, which indicates the potential for scaling the present device up to extremely high power levels.

Among possible applications of the solar-pumped laser are:

- Beaming power for the propulsion of orbiting transfer vehicles that service geosynchronous orbits from Shuttle orbits;
- Providing power for use by satellites;
- Beaming for space communications;
- Propulsion for solar-sail vehicles;
- Furnishing power for space-based scientific experiments;
- Beaming power from space to airplanes to give them virtually limitless range; and
- Beaming power from space to Earth for electricity, material processing, and fuel production.

The laser-output wavelength makes it suitable for use with well-developed optical materials for high-power infrared lasers. The internal conversion efficiency of the iodine laser is 20 percent. In the present experiment, the ratio to total power out of the laser to total power in is 0.1 percent. Enough Sunlight energy could be gathered by a modest-size solar collector, perhaps 2 meters in diameter for 4 watts output. Present research on laser power scaling indicates that relatively-simple, low-solar-concentration, troughlike collectors coupled with long laser-cavity lengths may be suitable for high-power operation in space.

In the laboratory setup, a xenon-arc lamp with an output of 4 kilowatts directs its beam into a highly-polished aluminum cone coated with magnesium fluoride (see figure). The cone reflects the beam so that it converges sideways on a quartz tube, 7 millimeters in inside diameter, containing C_3F_7I. The light, with a spectrum that closely resembles that of the Sun, optically pumps the gas — that is, stimulates it so that it emits photons that build up, after multiple reflections from the mirrors at the ends of the quartz tube, into a beam of coherent laser light at a fixed wavelength.

Only that portion of the Sunlight spectrum between 250 and 290 nanometers is effective in stimulating the gas. The laser utilizes about 1 percent of the incident solar energy. The transparency of the lasant to the solar visible and infrared results in a low waste-heat load and may require only a small thermal radiator. Other organic iodides are also promising as lasing mediums; $(CF_3)_2AsI$, for example, absorbs seven times as mush solar energy as does C_3F_7I.

The C_3F_7I dissociates as it lases, releasing free iodine that builds up and eventually prevents laser action. The experimental results indicate that only moderate flow rates are required to sweep away the free iodine to permit continuous lasing. Again, $(CF_3)_2AsI$ may be preferable, since it requires less extra-cavity processing and decomposes less readily.

This work was done by Willard R. Weaver, Jr., of **Langley Research Center** *and Ja H. Lee of Vanderbilt University. For further information, Circle 13 on the TSP Request Card.*

This invention is owned by NASA, and a patent application has been filed. Inquiries concerning nonexclusive or exclusive license for its commercial development should be addressed to the Patent Counsel, Langley Research Center [see page A5]. Refer to LAR-12870.

Improved Heat-of-Fusion Energy Storage

Alkali metal/alkali-halide mixtures are proposed for preventing solid buildup during energy recovery.

NASA's Jet Propulsion Laboratory, Pasadena, California

The heat-of-fusion method of storing energy may be made more practical by the use of some alkali metal/alkali-halide mixtures, such as Na/NaCl, for the phase-change materials. Solid material would not build up on the heat exchanger during energy recovery if such a mixture were used.

In conventional latent-heat energy storage, solidification during the energy-extraction period is likely to occur at the surface of the heat exchanger. The solid material degrades the thermal conduction and thus reduces heat transfer.

An alkali metal/alkali-halide phase-change material, at a temperature high enough to have two immiscible molten phases, would avoid this problem. For an Na/NaCl mixture at 795° C, a lighter, lower-melting-temperature, metal-rich phase exists above a salt-rich phase, which undergoes crystallization first upon cooling. Since the salt concentration in the metal-rich phase is very low, not much salt crystallizes in this phase. Immersing the heat-extraction component of the heat exchanger in the metal-rich phase, as shown in the figure, avoids the buildup of solids on the surface of the heat exchanger. Moreover, the salt crystals that form on the interface precipitate because of their greater density; hence, the interface is refreshed without agitation or forced circulation.

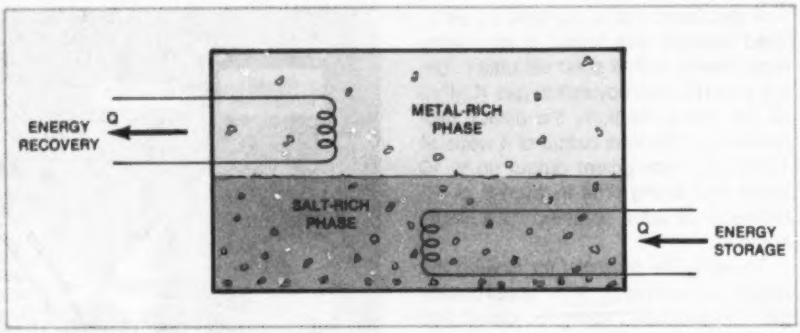

An **Alkali Metal/Alkali-Halide Latent-Heat System** for energy storage is illustrated schematically. When the mixture melts (by absorption of the heat of fusion), it forms two immiscible liquids. The salt-rich phase is heavier and has a higher melting/recrystallization temperature; so during energy recovery, salt crystallizes in this phase first. Since the heat exchanger for energy recovery is in the lighter metal-rich phase, solids do not form on it and there is no reduction of heat-recovery efficiency.

Besides avoiding buildup of solids on the heat exchanger, the alkali metal/alkali-halide mixtures have other advantages. By adding a small quantity of alkali metal, the energy-storage capacity is increased over that of the alkali-halide alone. The mixture also is more capable of releasing thermal stress so that the container and heat exchanger are less susceptible to stress damage.

This work was done by Kuo-Hung Chen and Ram Manvi of Caltech for **NASA's Jet Propulsion Laboratory.** *For further information, Circle 14 on the TSP Request Card.*
NPO-15318

Solar-Assisted Solution-Mining Concept

Brine heated in a solar pond would dissolve minerals from deposits.

NASA's Jet Propulsion Laboratory, Pasadena, California

A proposed solution-mining process would use solar energy to help dissolve minerals from layered deposits beneath the surface of a dry lake bed. Meeting the energy requirements of solution mining with fossil fuels is uneconomical; hence, no such process for mining dry-lake evaporite minerals is now in use.

The proposal envisions the mining of sodium carbonate (Na_2CO_3) from strata containing trona ($Na_2CO_3 \cdot NaHCO_3 \cdot 2H_2O$) located 35 m below the surface of Searles Lake, California. However, the same method could presumably be adapted for mining other minerals found in such sites.

In the proposed process (see figure), solar energy is collected within a brine in a thermal-gradient solar pond. Solar ponds can be excellent solar collectors, yet they are relatively inexpensive to construct. In such a pond a dense brine layer at the bottom efficiently absorbs solar energy while less-dense, cooler, brine and water layers float on top, preventing the bottom hot brine from naturally convecting to the surface. Thus, the upper layers reduce heat loss from the pond.

A brine that is sodium sulfate ($2Na_2SO_4 \cdot Na_2CO_3$) based would be heated in the pond. This hot brine would be pumped down a well to the mineral-bearing strata where Na_2CO_3 would be dissolved from the trona deposit. At the same time, sodium sulfate (Na_2SO_4) would crystallize out, physically replacing the Na_2CO_3, thereby reducing or preventing surface subsidence that would otherwise occur.

At one or more other wells the Na_2CO_3-enriched brine would be pumped back to the surface. Then solar energy would again be used, this time to concentrate the brine by evaporation in preparation for recovering the Na_2CO_3.

This work was done by Warren L. Dowler, Robert L. French, and John C. Becker, Jr., of Caltech and John Bills of Kerr McGee Corp. for **NASA's Jet Propulsion Laboratory.** *For further information, Circle 15 on the TSP Request Card.*
NPO-15343

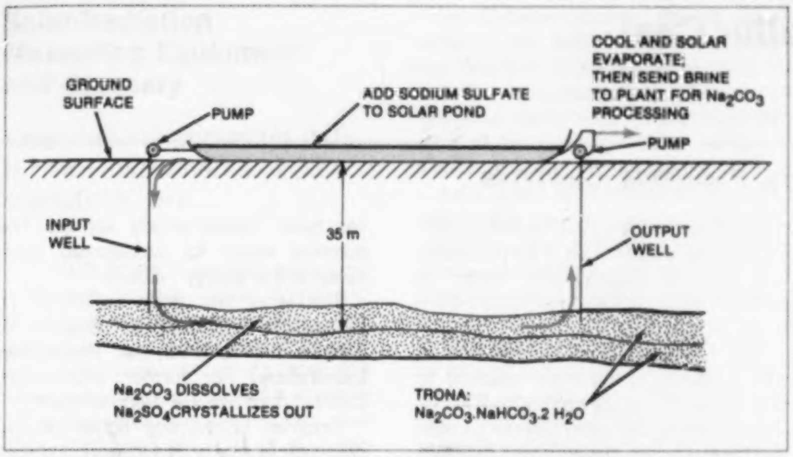
GROUND SURFACE
PUMP
ADD SODIUM SULFATE TO SOLAR POND
COOL AND SOLAR EVAPORATE; THEN SEND BRINE TO PLANT FOR Na_2CO_3 PROCESSING
PUMP
INPUT WELL
35 m
OUTPUT WELL
Na_2CO_3 DISSOLVES Na_2SO_4 CRYSTALLIZES OUT
TRONA: $Na_2CO_3 . NaHCO_3 . 2\,H_2O$

In the **Proposed Solution-Mining Process,** the hot brine could be pumped down one well and recovered at one or more other wells. The emerging brine is rich in the desired mineral (in this case, Na_2CO_3): This brine is evaporated in solar ponds to recover the mineral.

Mapping Ocean Winds by Radar

Algorithm recovers data on windspeed, wind direction, and wind patterns from radar returns.

NASA's Jet Propulsion Laboratory, Pasadena, California

Information about ocean weather can be extracted from radar returns with the aid of a special algorithm. Originally developed for use with data obtained by microwave radar on the Seasat satellite, the algorithm can determine windspeeds and wind directions at the ocean surface and from this information can locate low- and high-pressure centers, convergence regions, and zones of strong winds and wind shear associated with ocean weather-system fronts. Although the specific method for generating weather parameters is probably limited to processing weather-satellite data, the general techniques will be of interest to those involved in radar signal analysis in other applications.

The strength of radar signals reflected by capillary waves only a few centimeters long on the ocean surface is proportional to the capillary wave amplitude, which in turn is proportional to windspeed near the surface. Signal strength also varies with the wave orientation, which is determined by the wind direction. The radar reflections from the ocean surface therefore contain information about windspeed and wind direction, and a comparison of such information over large ocean areas reveals patterns of atmospheric pressure systems.

The satellite radar illuminates with two beams that form an X-shaped "footprint" on the ocean surface. Doppler filters subdivide the footprint electronically into resolution cells measuring approximately 50 by 15 km each over swaths of 200 to 700 km from the earth track of the satellite. The two fore and aft beams allow a given point on the surface to be examined from two different angles so that wind direction can be recovered from the returns.

The algorithm used to process the returns is an empirical model function that relates radar backscatter cross section to windspeed as a function of incidence angle (the lateral location in the swath), azimuth angle of the wind direction relative to beam direction, and polarization of the antenna beam. The algorithm recovers between one and four wind-vector solutions for each cell. The solutions are nearly equal in speed and vary systematically in direction. The multiple solutions are referred to as "aliases" of the true wind vector. When the algorithm produces two solutions, they are separated by nearly 180° in a direction parallel to one of the beam directions. Four solutions consist of two pairs separated by any angle up to 90°. Further processing is necessary to obtain the correct wind-direction solution.

During the Gulf of Alaska Seasat Experiment, data on the North Pacific produced by the algorithm were compared with surface measurements. Radar windspeed measurements were within ± 2 m/s of the surface measurements and wind direction measurements differed by about 16° on the average. Further refinement of the algorithm as larger data sets are analyzed is expected to reduce statistical biases and errors.

This work was done by James E. Overland (NOAA), Morton G. Wurtele (UCLA), and Peter M. Woiceshyn of Caltech for **NASA's Jet Propulsion Laboratory.** *For further information, Circle 16 on the TSP Request Card.*
NPO-15267

A New Use for High-Sulfur Coal

High-sulfur coal could be used without environmental liability.

NASA's Jet Propulsion Laboratory, Pasadena, California

A new process would recover some of the economic value of high-sulfur coal. Although high-sulfur content is undesirable in most coal-utilization schemes (such as simple burning), the proposed process prefers high-sulfur coal to produce electrical power or hydrogen.

In the proposed process, the coal is dissolved in H_2SO_4 at the boiling point of 330° C. The reaction between the coal and the acid produces sulfur dioxide, carbon dioxide, and water vapor. Ash remains dissolved in the acid. The CO_2 appears as a concentrated stream and can be sold for use in oil recovery. The SO_2 is reacted with water to produce hydrogen and reform concentrated acid.

The process could replace one in which H_2SO_4 is thermally cracked to SO_2, O_2, and H_2O by heating to 900° C. Since the new process requires a lower temperature, the containment problem for the acid is less severe.

Any kind of coal with a high-sulfur content can be used. The thermal cracking of H_2SO_4 to CO_2 and SO_2 with coal has been experimentally verified. The potential exists for widespread application in the energy industry.

This work was done by Daniel D. Lawson and Christopher England of Caltech for **NASA's Jet Propulsion Laboratory.** *For further information, Circle 17 on the TSP Request Card.*

Inquiries concerning rights for the commercial use of this invention should be addressed to the Patent Counsel, NASA Resident Office-JPL [see page A5]. Refer to NPO-15194.

Books and Reports

These reports, studies, and handbooks are available from NASA as Technical Support Packages (TSP's) when a Request Card number is cited; otherwise they are available from the National Technical Information Service.

Advanced Coal-Based Power Generation

An evaluation of promising technologies for large-scale power generation.

Advanced power-generation systems using coal-derived fuels are evaluated in a two-volume report. The report considers fuel cells, combined gas- and steam-turbine cycles, and magnetohydrodynamic (MHD) energy conversion. It presents the technological status of each type of system and analyzes the performance of each operating on medium-Btu fuel gas, either delivered via pipeline to the powerplant or generated by a coal-gasification process at the plantsite. The baseline technologies are those that could be commercially available in the late 1980's or the 1990's.

Combined-cycle gas- and steam-turbine systems are already commercially available. Only evolutionary improvements are needed to attain advanced-system performance. Such improvements are extensions of technology available in such systems as aircraft gas turbines.

The phosphoric acid fuel cell appears to be the next, most likely candidate for commercialization. An existing 4.5-MW demonstration plant is on a large enough scale to indicate operability in commercial power systems.

The molten-carbonate fuel cell is undergoing laboratory tests. MHD energy conversion has been demonstrated on a small laboratory scale, but technical problems remain — especially with regard to the containment of high-temperature fluids. Neither of these two systems is expected to become commercially viable before the 1990's.

The efficiencies of these advanced systems are attractive. For pipeline delivery, they range from 40.9 percent for the phosphoric acid fuel cell to 63 percent for the molten-carbonate fuel cell. In contrast, a conventional gas-fired steam station is 37 to 38 percent efficient.

For integrated powerplants, efficiencies range from 39 to 40 percent for the combined-cycle system to 46 to 47 percent for the molten-carbonate fuel cell. In contrast, the efficiency of a conventional coal-fired steam station (with flue-gas desulfurization to meet clean-air standards) is 33 to 35 percent.

This work was done by Fred L. Robson of United Technologies Research Center for **Marshall Space Flight Center.** *Further information may be found in NASA CR-161691 [N81-21538/NSP] and CR-161692 [N81-21539/NSP], "Final Study Report of an Applications Study of Advanced Power Generation Systems Utilizing Coal-Derived Fuels," Volumes I [\$6] and II [\$30]. Paper copies may be purchased [prepayment required] from the National Technical Information Service, Springfield, Virginia 22161. The reports are also available on microfiche at no charge. To obtain microfiche copies, Circle 18 on the TSP Request Card.*
MFS-25652.

Solar-Radiation Measuring Equipment and Glossary

Descriptions and other data for 145 instruments of 38 manufacturers.

A 1976 listing of commercially-available solar-radiation measuring equipment is presented in a 50-page report. Sensor type, response time, cost data, and comments concerning specifications and intended usage are listed for 145 instruments from 38 manufacturers. This is followed by a list of manufacturers' addresses.

An 83-term glossary defines solar-radiation and instrumentation terminology. Two short lists of reference works on radiation instrumentation, solar-energy data, and meteorology are also included. Most of the glossary entries contain a citation to one of the references.

Four types of instruments predominate in the listings: pyranometers, pyrgeometers, pyrheliometers, and radiometers. Calorimeters, photometers, Sunshine recorders, solar trackers, and calibration standards also appear.

The instrument data are given in tabular form in alphabetical order by manufacturer. A separate chart keyed to instrument type and price makes it easy to locate instruments of a given type and price range in the main listing. Price information provided by the manufacturers ranges from specific prices to price ranges to no indication of prices.

These data were collected in a mail survey of manufacturers in 1976. A copy of the survey form included in the report is recommended for adoption as a standard data sheet for describing solar-radiation measuring equipment. It could serve as a checklist when writing instrument purchase specifications.

This work was done by E. A. Carter, A. M. Patel, and S. A. Greenbaum of the University of Alabama in Huntsville for **Marshall Space Flight Center.** *To obtain a copy of the report, Circle 19 on the TSP Request Card.*
MFS-25770

Computer Programs

These programs may be obtained at very reasonable cost from COSMIC, a facility sponsored by NASA to make new programs available to the public. For information on program price, size, and availability, circle the reference letter on the COSMIC Request Card in this issue.

Cube-Corner Retroreflector Modeling

Programs compute impulse-response and interference effects of reflected pulses from optical cube corners.

A collection of computer programs analyzes arrays of optical cube corners used in laser ranging. The programs perform the computations required to construct the shape of a laser pulse (impulse response) after it has been retroreflected from a cube-corner array. The programs also calculate the interference-effects histogram and the far-field diffraction patterns. The programs model solid corner cubes with circular, unrecessed entrance faces and hollow cube corners made up of three mutually-perpendicular square mirrors.

An optical cube corner consists of three mutually-perpendicular reflecting surfaces. A laser beam entering the corner is returned toward the source regardless of the orientation of the cube corner, within the limitation of incidence angles interior to the reflecting surfaces.

The major calculations in the modeling of arrays of cube corners are the calculation of the exit-pupil area, gain, cross section for each cube corner, and strength of the return signal from the array. Impulse-response and interference-effects histograms are generated to display the characteristics of the retroreflected laser pulse.

The programs compute and display printer plots of range correction versus laser incidence beam angle, cross section versus laser incidence beam angle, cross section versus laser azimuthal angle, and return signal strength versus satellite zenith angle. They also compute and display the diffraction pattern of the cube-corner array for several laser-beam incidence angles. Separate stand-alone programs are included for computing the far-field diffraction patterns of individual solid or hollow cube corners.

Input consists of simple retroreflector descriptive parameters, incidence beam parameters, and output requests. Output may include both tabular and printer plot displays.

The programs are written in FORTRAN IV for batch execution and have been implemented on an IBM 360-series computer with a central memory requirement of approximately 550K of 8-bit bytes. The retroreflector modeling programs were developed in 1979.

This program was written by John G. Kirk, M. L. Regardie, P. N. Kumar, and J. Zimmerman of Computer Sciences Corp. for **Goddard Space Flight Center.** *For further information, Circle C on the COSMIC Request Card.*
GSC-12718

Two- and Three-Dimensional Galaxy Simulations

The dynamics of galaxies with up to 100,000 stars are simulated.

A real galaxy consists of stars and various forms of interstellar matter. Although electromagnetic and radiation effects do influence the evolution of galaxies, the large-scale structure of most systems is almost surely determined by gravitation. A set of computer programs available from COSMIC simulates the dynamics of isolated galaxies. In these computer models, a large number of simulation stars move in the combined gravitational field produced by the stars themselves (the self-consistent field) or by external matter (the fixed field).

The equations of motion for the stars are integrated by a "leap-frog"

(continued on next page)

scheme. The forces arising from the self-consistent portion of the gravitational field are derived from a gravitational potential, which is computed on a mesh by a discrete analog of Poisson's integral. This portion of the model employs a Fourier transform technique to model the galaxy as an isolated system. Programs are included for the simulation of both infinitesimally thin (two-dimensional) galaxies and fully three-dimensional galaxies. Typical simulations contain from 20,000 to 100,000 stars. The techniques employed in the galaxy simulations are very similar to those used in particle simulations in plasmas and may be adaptable to similar applications.

Input to the simulation program includes data concerning the initial conditions (such as the number of stars, initial radius, initial angular velocity, and initial velocity dispersion) and data concerning timespan of the simulation. Output consists of the positions and velocities of selected stars as well as the self-consistent forces acting on those stars at each time step in the simulation. Plots of the galaxy shapes at each time step may also be generated. A relocatable plot library is supplied with the program and can be adapted to almost any X-Y plotter.

The galaxy-simulation programs are written in FORTRAN IV and Assembler for batch execution and have been implemented on a CDC CYBER 170-series computer with the largest program having a central memory requirement of appproximately 200K (octal) of 60-bit words. The programs were developed in 1979.

This program was written by Frank Hohl of **Langley Research Center** *and Thomas A. Zang of the College of William and Mary. For further information, Circle D on the COSMIC Request Card.*
LAR-12907

Star-Catalog Data Base

System supports data on approximately 250,000 stars.

SKYMAP is a collection of computer programs and utility software for creating and maintaining a master star catalog and a hierarchical set of derivative star catalogs. It was developed to provide accurate stellar position and magnitude information for attitude-determination and analysis systems utilizing star sensor observations. The current master star catalog includes all documented stars with blue or visual magnitudes brighter than magnitude 9.0.

The principal sources for data on the approximately 250,000 stars in the SKYMAP master catalog are the Henry Draper Spectral Catalog and the Smithsonian Astrophysical Observatory Positional Catalog. The size of the master catalog precludes its use in most operations, so SKYMAP creates smaller, specialized catalogs including only those stars of interest for a particular application.

The SKYMAP system includes utility software for maintaining the master catalog and user-created catalogs. Software for integration into user programs to access the SKYMAP-generated catalogs is also included.

To provide complete and accurate star data at the user level with acceptable access time and storage requirements, SKYMAP furnishes a hierarchy of catalogs of decreasing size. As mentioned earlier, the master catalog contains data on approximately 250,000 stars. A much smaller mission catalog may be generated from the master catalog by excluding all parameters not required by a specific mission. This mission catalog may be reduced even more to generate a run catalog to meet the day-to-day needs of attitude-determination programs. The run catalog may be reduced to generate temporary core catalogs required for specialized rapid-access applications.

SKYMAP includes a collection of support and utility software for maintaining and implementing star catalogs. Programs are included for updating and modifying the master catalog and mission catalogs and for generating mission, run, and core catalogs from the master catalog or in hierarchial sequence.

The SKYMAP system also includes programs for computing statistical data describing the stars in a particular region of the sky to aid the user in developing star sensor utility criteria and selecting parameter exclusions for generating the reduced-size catalogs. SKYMAP also includes a collection of programs and routines developed since SKYMAP's inception to aid in the processing of stellar data and in the development of systems utilizing the SKYMAP-generated catalogs.

The SKYMAP distribution package consists of the SKYMAP system software and the complete, current master catalog. SKYMAP software is written in FORTRAN IV and Assembler for batch and interactive execution and has been implemented on an IBM 370-series computer. The largest program in SKYMAP has a central memory requirement of approximately 220K of 8-bit bytes. The SKYMAP system was originally developed in 1977 and was last updated in 1980.

This program was written by Dave Gotlieb and Steve McLaughlin of Computer Sciences Corp. for **Goddard Space Flight Center.** *For further information, Circle E on the COSMIC Request Card.*
GSC-12445

Materials

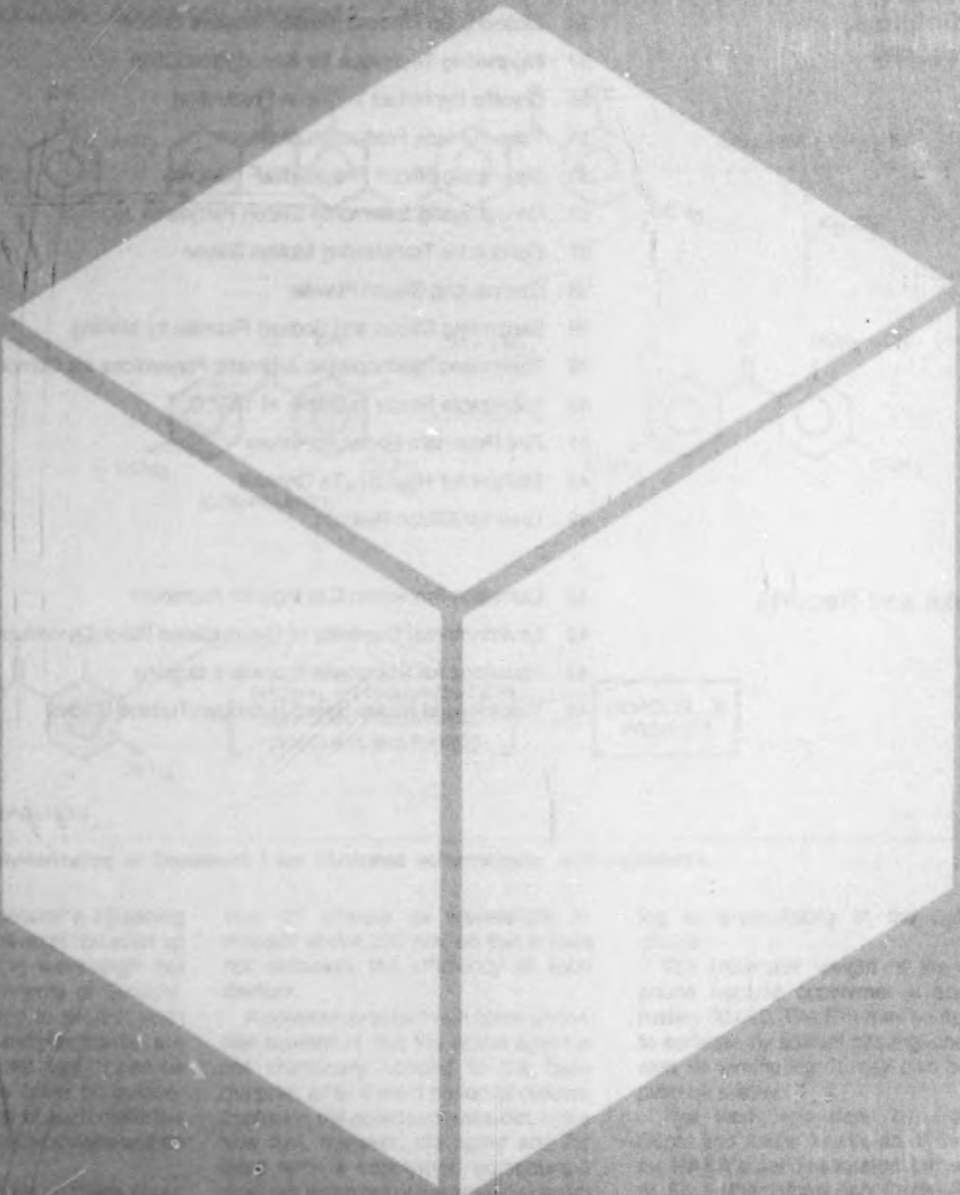

Hardware, Techniques, and Processes

33 Clear Film Protects Against Ultraviolet Radiation
34 Closed-Loop Process Yields Ultrapure Silicon
34 Bipulsating Technique for Sil[illegible]ction
35 Cryolite Byproduct in Silicon Production
36 Tube-Furnace Production of Silicon
36 Separating Silicon From Si/NaF Mixtures
37 Consolidating Submicron Silicon Particles
37 Conduit for Transferring Molten Silicon
38 Compacting Silicon Powder
39 Separating Silicon and Sodium Fluoride by Melting
39 Thermoset/Thermoplastic Aromatic Polyamides for Composites
40 Sterilizable Binder Is Stable at 135° C
41 Fire-Retardant Epoxy Adhesives
42 Etchant for $Hg_xCd_{1-x}Te$ Crystals
42 Liner for Silicon Reactor

Books and Reports

42 Corrosion-Protection Coatings for Aluminum
43 Environmental Durability of Electroplated Black Chromium
43 Equations for Composite-Propellant Burning
44 Properties of Nickel-Based Hydrogen-Turbine Blades

Clear Film Protects Against Ultraviolet Radiation

Weather-resistant material is a copolymer of a screening agent and an acrylic resin.

NASA's Jet Propulsion Laboratory, Pasadena, California

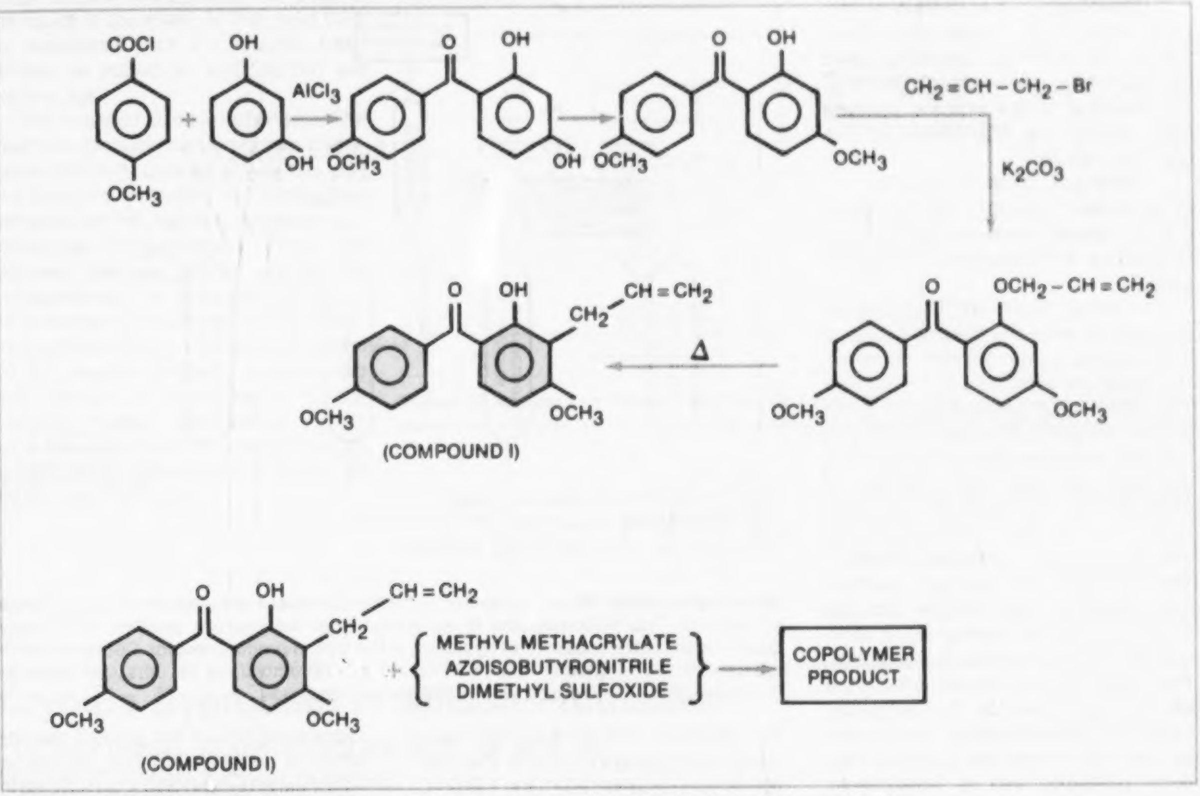

Synthesis and Copolymerization of Compound I are illustrated schematically, with ingredients.

An acrylic film contains a screening agent that filters ultraviolet radiation up to 380 nanometers in wavelength but passes other components of Sunlight. The film can be used to protect such materials as rubber and plastics that are degraded by ultraviolet light. It can be used as a protective cover on outdoor sheets or pipes made of such materials as polyethylene or polypropylene and on solar cells.

The new film, which contains about 0.5 percent by weight of 3-allyl-4,4′-dimethoxy-2-hydroxybenzophenone ("compound I") in copolymerization with the acrylic base (see figure), absorbs substantially more ultraviolet energy than typical commercial materials with similar properties. The new film is hard and dust-resistant. Its light absorption cuts off sharply as wavelength increases above 380 nm, so that it does not decrease the efficiency of solar devices.

A common problem with some ultraviolet screens is that the active agent is not chemically bonded to the base material; after a short period of outdoor exposure, the agent becomes lost. In the new film, however, the agent and the base form a copolymer; compound I does not leach out of the acrylic even after accelerated testing and long outdoor exposure. After long immersion in methanol, for example, the new film remained unchanged, but ordinary agents were extracted from the matrix. After accelerated tests in which mercury-arc light simulated Sunlight, the new film showed no signs of oxidation or of breaking or cross-linking of the polymer chains.

The molecular weight of the compound I-acrylic copolymer is approximately 60,000. The film may be applied to surfaces by solvent casting, coextrusion, or laminating. It may also be applied as a latex.

This work was done by Amitava Gupta and Andre Yavroulan of Caltech for **NASA's Jet Propulsion Laboratory.** *For further information, Circle 20 on the TSP Request Card.*

Inquiries concerning rights for the commercial use of this invention should be addressed to the Patent Counsel, NASA Resident Office-JPL [see page A5]. Refer to NPO-14971.

Closed-Loop Process Yields Ultrapure Silicon

Metallurgical-grade silicon is converted
into semiconductor-grade silicon.

NASA's Jet Propulsion Laboratory, Pasadena, California

A closed-loop process produces ultrapure silicon from metallurgical-grade silicon by forming, purifying, and hydropyrolizing tribromosilane ($HSiBr_3$). The essence of the process involves manipulating the equilibrium of the chemical reaction

$$HSiBr_3 + H_2 \rightleftharpoons Si + 3HBr$$

in a product reactor. The ultrapure granular silicon produced can be used to produce semiconductors and solar cells.

The only material that needs replenishing once the process begins is metallurgical-grade silicon; all other reactants are separated and recycled. The metallurgical-grade silicon, of about 90 percent purity or better, is fed to a fluid-bed hydrogenation reactor and a hydrogen bromide (HBr) reactor, at about 300° to 750° C, to produce a mixture of silicon tetrabromide, tribromosilane, and unreacted material. The hydrogen and hydrogen bromide are separated, and hydrogen bromide and part of the hydrogen are then recirculated to the reactors as feedstock. The balance of the hydrogen is fed to the silicon-product reactor. The remaining mixture of tribromosilane and silicon tetrabromide is then separated by fractional distillation into its constituents, and a vapor stream of tribromosilane is fed to the silicon-product reactor; the separated silicon tetrabromide is vaporized and then used as feedstock for the hydrogenation synthesis reactor.

The silicon-product fluid-bed reactor receives reactants in the molar ratio of from 5-to-1 to 26-to-1 hydrogen to tribromosilane and produces ultrapure silicon and hydrogen bromide. The reaction occurs between 900° and 1,200° C. At the bottom of the product reactor, the large silicon particles, which have grown to about 0.125 inch (0.327 cm) in diameter, are withdrawn. A fraction of the silicon withdrawn is ground to fine particles 50 to 500 microns in diameter, and returned to the reactor to serve as a deposition substrate. The overhead vapor stream from the product reactor, which is composed of HBr, unreacted $HSiBr_3$ and H_2, and $SiBr_4$, is recycled into the loop.

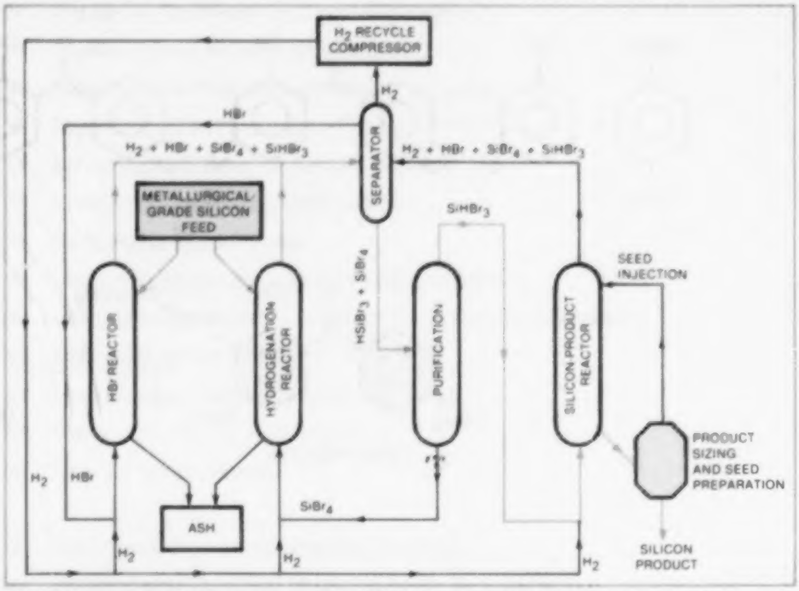

Metallurgical-Grade Silicon is transformed into tribromosilane by reacting it with process byproducts. The tribromosilane is separated from the mixture, purified, and finally decomposed in the presence of hydrogen in the silicon-product reactor. Conversion efficiencies of 30 to greater than 60 percent of tribromosilane to ultrapure granular polycrystalline silicon are typical in the product reactor.

This work was done by John C. Schumacher and Edward B. Moore of the J. C. Schumacher Co., for **NASA's Jet Propulsion Laboratory.** *For further information, Circle 21 on the TSP Request Card.*
NPO-15283

Bipulsating Technique for Silicon Production

Method controls reaction temperature and rate of
reaction of sodium and silicon tetrafluoride.

NASA's Jet Propulsion Laboratory, Pasadena, California

The reduction of silicon tetrafluoride by sodium, to produce high-purity silicon, is very fast and highly exothermic. It begins at temperatures around 150° to 200° C and the temperature can reach more than 2,000° C. A new proposal suggests that the temperature and rate of reaction can be regulated by alternately adding measured amounts of the reactants. This technique could be used in a large reactor, where heat dissipation becomes a serious problem, to control reactor temperatures. It would be a highly efficient method, which would utilize almost 100 percent of the raw materials.

A flow chart of the method is shown in the figure. A small amount of liquid sodium (Na) — for example, 1 gram — is "pulsed" into a nickel-lined reactor, which is held above the reaction temperature. A pulse of silicon tetrafluoride (SiF_4) then follows. As the reaction proceeds, the temperature rises, and the pressure of the SiF_4 drops. Additional pulses of SiF_4 follow periodically until, after a fresh SiF_4 pulse, no drop in pressure is observed. At that point SiF_4 is evacuated from the reactor, fresh sodium is pulsed in, and the process begins again.

The method has several benefits: The reaction products can be grown in columns, the only contact of which is with the base of the reactor, which simplifies removal of the reaction products and minimizes contamination. Since the process can be carried out at low temperatures, the impurities picked up from the reactor walls can be minimized. The process avoids premature reaction of the reaction products by delivering the sodium to the reactor under vacuum. It also avoids diffusion problems because the small drops of sodium splash on the bottom of the reactor to form a very thin layer.

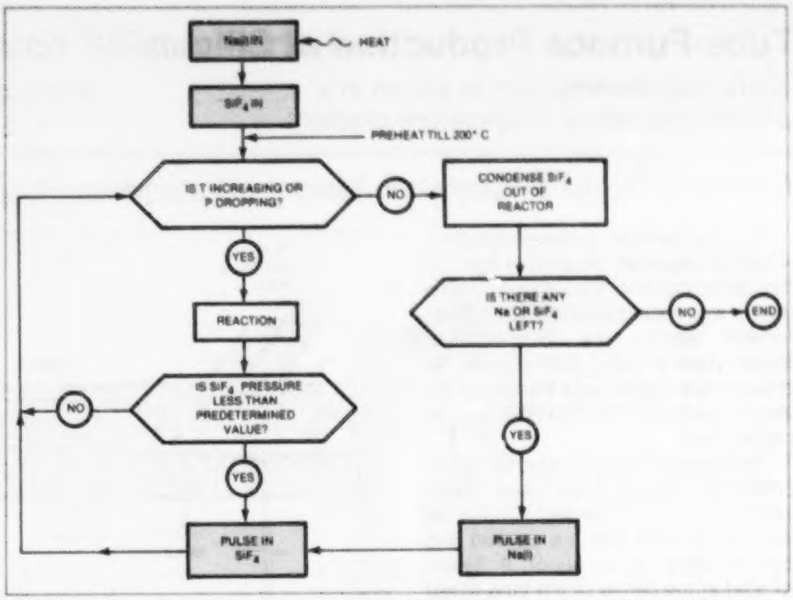
Na(l) IN
HEAT
SiF₄ IN
PREHEAT TILL 200° C
IS T INCREASING OR P DROPPING?
NO
CONDENSE SiF₄ OUT OF REACTOR
YES
REACTION
IS THERE ANY Na OR SiF₄ LEFT?
NO
END
IS SiF₄ PRESSURE LESS THAN PREDETERMINED VALUE?
NO
YES
YES
PULSE IN SiF₄
PULSE IN Na(l)

Pulses of Sodium and Silicon Tetrafluoride are added and the progress of the reaction monitored according to the flow scheme depicted. The pulses contain small amounts of the reactants.

This work was done by Angel Sanjurjo of SRI International for **NASA's Jet Propulsion Laboratory.** *For further information, Circle 22 on the TSP Request Card.*
NPO-15367

Cryolite Byproduct in Silicon Production

Process reacts alumina hydrate with HF and NaF from silicon-production process.

NASA's Jet Propulsion Laboratory, Pasadena, California

Cryolite (Na_3AlF_6), important as an electrolyte in aluminum refining, can be produced by adding a reaction step to a process that makes high-purity silicon from fluorosilicic acid (H_2SiF_6). The new extended process has been demonstrated in the laboratory and could be used in a commercial plant.

One of the silicon-production processes comprises the first three reactions listed in the figure. In addition to silicon, the H_2SiF_6 reactant contains another valuable element, fluorine, which is utilized in the cryolite-production reaction, shown as reaction (4) in the figure.

(1) $H_2SiF_6(aq) + 2NaF(s) \rightarrow Na_2SiF_6\downarrow + 2HF(aq)$

(2) $Na_2SiF_6 \xrightarrow{\Delta} SiF_4(g) + 2NaF(s)$

(3) $4Na(l) + SiF_4(g) \rightarrow Si(s/l) + 4NaF(l)$

(4) $\frac{1}{2}H_2SO_4(l) + 4NaF(s) + 2HF(aq) + \frac{1}{2}Al_2O_3(H_2O)_3(s) \rightarrow Na_3AlF_6\downarrow + \frac{1}{2}Na_2SO_4 + 3H_2O$

aq – Aqueous Solution
g – Gas
l – Liquid
s – Solid
↓ – Precipitate
Δ – Energy Added

High-Purity Silicon and Cryolite are produced in a four-reaction process starting from fluorosilicic acid. The form in which each reactant is used is indicated in parentheses.

In reaction (1), H_2SiF_6 is converted to Na_2SiF_6, leaving the byproduct hydrofluoric acid (HF). The Na_2SiF_6 from reaction (1) is thermally dissociated in reaction (2), producing silicon fluoride (SiF_4) and sodium fluoride (NaF), which is recycled back to reaction (1). In reaction (3), the SiF_4 is reduced with sodium to produce the product silicon and the byproduct NaF.

In the final reaction, the byproducts HF and NaF from the first three reactions react with alumina hydrate [$Al_2O_3(H_2O)_3$] to precipitate cryolite. This precipitation reaction requires an acid, such as the sulfuric acid (H_2SO_4) shown. Finally, the cryolite is separated from the waste liquor by filtration, then washed and dried.

This work was done by Robert W. Bartlett of SRI International for **NASA's Jet Propulsion Laboratory.** *For further information, Circle 23 on the TSP Request Card.*
NPO-15364

Tube-Furnace Production of Silicon

Silane gas decomposes to silicon in a packed bed with a temperature gradient.

NASA's Jet Propulsion Laboratory, Pasadena, California

Silicon of semiconductor-grade purity would be produced in particle form by the decomposition of ultrapure silane gas in a proposed packed-bed tubular furnace reactor. The decomposition temperature is about 700° C, and the product size depends on the size of the silicon particles that constitute the packed bed.

The tube-furnace technique for silicon production is shown in the figure. Silicon particles to form the packed bed are fed into the furnace and are packed and pushed along by an auger. A heater located at the center of the tube raises the temperature of the adjacent particles to approximately 1,000° C and creates a temperature gradient that is essential to the operation of the process.

The silane gas, fed into the packed bed of moving particles in the temperature-gradient region, decomposes to form more particles. This heterogeneous decomposition occurs without excessive formation of submicron fines.

The silicon particles fall out of the end of the furnace tube. Some are taken away for use in semiconductor manufacture, and some are returned to the furnace to form the packed bed for the continuing process. Whatever fines are produced are screened out and also reinserted into the furnace.

This work was done by Ernest G. Farrier, Joachim Rexer, and Paul J. Timmel of Union Carbide Corp. for **NASA's Jet Propulsion Laboratory.** *For further information, Circle 24 on the TSP Request Card.*
NPO-15274

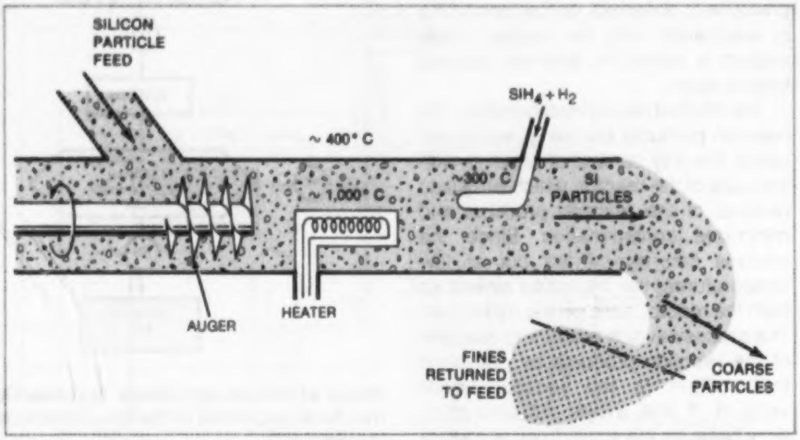

A **Packed-Bed Reactor** would produce silicon by decomposing ultrapure silane gas in a temperature gradient. On the basis of previous experiments with relatively low decomposition temperatures and with temperature gradients, it is expected that the heterogeneous decomposition will produce few fines.

Separating Silicon From Si/NaF Mixtures

A new method takes advantage of the lower melting point of NaF.

NASA's Jet Propulsion Laboratory, Pasadena, California

Silicon can be extracted from the mixture produced when silicon tetrafluoride is reduced by sodium, by taking advantage of the lower melting point of NaF. Previously, the finely interspersed mixture of NaF and silicon was separated by heating above the melting point of silicon (1,410° C). The new method is effective at temperatures up to 400° C below the melting point of Si. This results in energy and economic savings: simpler and smaller furnaces, less volatization loss, and a high percentage of separation.

In the new method, the Si/NaF mixture is heated in a graphite crucible to around 1,100° C, which is above the melting point of NaF but well below the melting point of silicon. The bottom of the graphite crucible has openings through which the NaF is discharged. At this temperature, a silicon sponge and part of the NaF remain in the crucible after discharging most of the molten NaF. The silicon sponge and very small amounts of NaF can be melted by raising the temperature to 1,450° C and the NaF traces removed by subsequent acid leaching.

An experiment showed that the NaF extracted by the process is uncontaminated with silicon particles. A 1-inch (2.54-cm) inner diameter, 3 inches (7.62 cm) high crucible with a 7/64-inch (0.28-cm) hole at the bottom, was loaded with a 10-gram Si/NaF mixture; the mixture was in the ratio of 1 part silicon to 4 parts NaF. At 1,100° C, it took 10 minutes to separate more than 80 percent of the NaF.

This work was done by Angel Sanjurjo and Leonard Nanis of SRI International for **NASA's Jet Propulsion Laboratory.** *For further information, Circle 25 on the TSP Request Card.*
NPO-15365

Consolidating Submicron Silicon Particles

Fine silicon powder melts and solidifies atop a silicon pedestal.

NASA's Jet Propulsion Laboratory, Pasadena, California

Two proposed techniques would use a molten pool of silicon at the top of a silicon pedestal to consolidate the submicron silicon particles produced by the silane process. The techniques avoid the contamination produced by casting containers. The consolidated material could be used directly to produce high-efficiency polycrystalline solar cells.

In one process, fine silicon powder is fed into the molten pool created by partially melting the top of a cylindrical silicon pedestal (see figure). The powder melts and becomes part of the pool. The second approach combines silane pyrolysis and silicon-powder consolidation by directly decomposing silane on the silicon pool. By controlled cooling of the bottom of the silicon pedestal with gas, it should be possible to form polysilicon material with grain boundaries predominantly parallel to the axis of the pedestal.

In both processes, the shape of the molten layer together with the surface tension of molten silicon stabilize the layer and control the diameter of the consolidated material. The molten layer is formed by surface induction heating, electron-beam bombardment, or other energy-efficient methods. After a stable molten layer forms, the silicon pedestal is lowered as the molten layer is fed with either silicon powder or droplets.

This work was done by Kazuo A. Yamakawa and Ralph Lutwack of Caltech for **NASA's Jet Propulsion Laboratory.** *For further information, Circle 26 on the TSP Request Card.*
NPO-15250

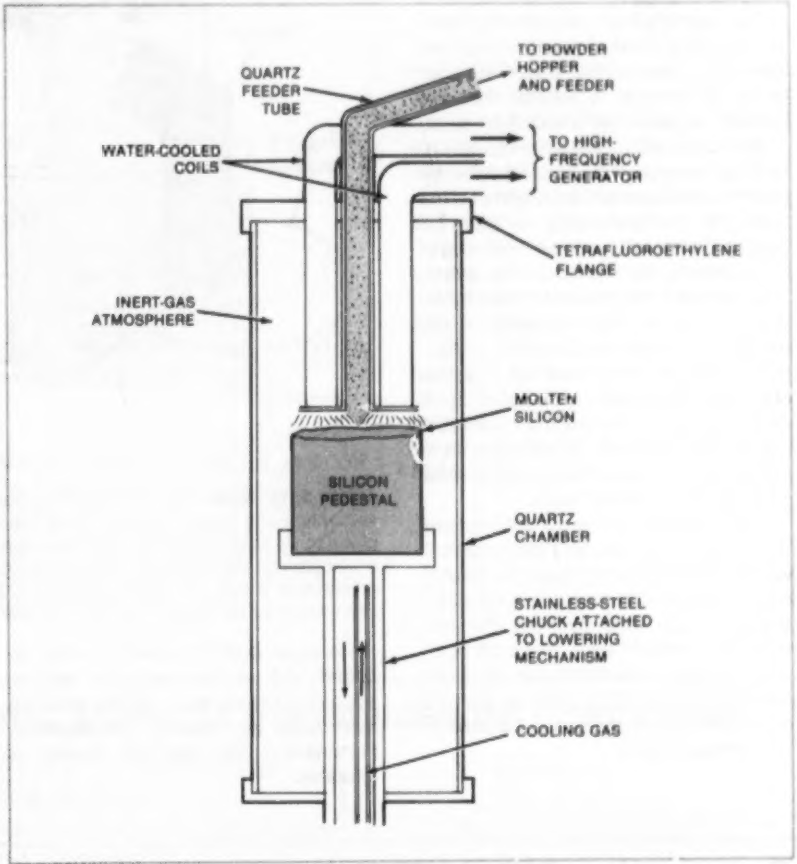
QUARTZ FEEDER TUBE
TO POWDER HOPPER AND FEEDER
WATER-COOLED COILS
TO HIGH-FREQUENCY GENERATOR
TETRAFLUOROETHYLENE FLANGE
INERT-GAS ATMOSPHERE
MOLTEN SILICON
SILICON PEDESTAL
QUARTZ CHAMBER
STAINLESS-STEEL CHUCK ATTACHED TO LOWERING MECHANISM
COOLING GAS

The **Molten-Silicon Pool** receives fine silicon powder and melts it. After a stable molten layer forms, the pedestal is lowered at a rate equal to the silicon-powder feed rate. If silane is directly decomposed on the silicon pool, the powder feeder is replaced by a jet of silane on the silicon surface, and the hydrogen produced in the decomposition of silane is pumped from the bottom end of the chamber.

Conduit for Transferring Molten Silicon

A proposed three-part conduit would transfer pure silicon between cruicibles.

NASA's Jet Propulsion Laboratory, Pasadena, California

Transferring molten silicon from one vessel to another without solidifying or contaminating it would be possible with a proposed conduit. Silicon oxide and other impurities would be removed by extracting molten silicon through the conduit and away from the slag that forms on the surface of the melt. The conduit could be used in a process for growing continuous crystal ribbon for solar cells, where there would be no size limitation on the finished product, because the crystallization crucible could be continuously replenished with pure silicon.

(continued on next page)

The conduit (see figure) is composed of three major parts: a transfer tube, a heater, and a multilayered thermally insulating and reinforcing structure. The molten silicon only comes in contact with the quartz transfer tube, with which it is compatible, while the outer insulating layers reinforce the quartz tube, which becomes somewhat soft at molten-silicon temperatures.

The heater is in contact with the transfer tube over most of its length. It consists of a series of four resistive strips, made of graphite sheeting, that are interconnected in pairs near their ends.

Several layers make up the insulation. Helically-wound silica tape followed by graphite sheet and another layer of silica tape are the inner core. A layer of graphite sheet followed by a heavy layer of graphite felt surround the inner layers. The graphite sheet prevents the graphite fibers in the felt from migrating to the heater and short-circuiting it. The insulation layer is completed by a dense outer shell of refractory material, such as solid graphite, that adds considerable rigidity and strength at elevated temperatures. The outer shell is split to allow passage of the heater leads.

Two methods can be used to transfer the molten silicon through the conduit: It can be siphoned, or a pressure regulator can be installed to maintain a constant pressure difference between the two crucible compartments. Since nitrogen and oxygen contaminate silicon, especially at high temperatures, an inert atmosphere of argon would be used in the compartments.

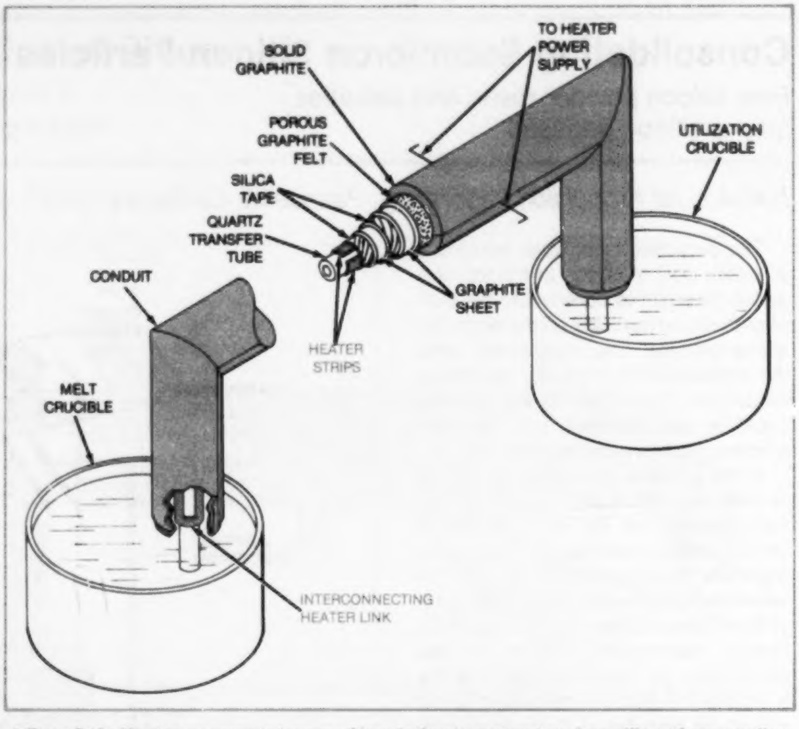

A **Four-Strip Heater** augments layers of insulation to prevent molten silicon from cooling and solidifying during transfer. Since the melt is maintained at a temperature relatively close to its fusion point, to minimize quartz erosion, even relatively-minor heat losses could precipitate solidification and terminate work in progress. Though only one pair of crucibles is shown, several crucibles may be fed through conduits from a central crucible. Each would be contained in its own compartment under an inert atmosphere.

Because quartz is fairly rapidly reduced and eroded away at molten-silicon temperatures, crucibles and conduits must be replaced occasionally. Fortunately, the rate of erosion is tolerable.

This work was done by George Fiegl and Walter Torbet of Siltec Corp. for **NASA's Jet Propulsion Laboratory.** *For further information, Circle 27 on the TSP Request Card.*
NPO-15109

Compacting Silicon Powder

Silicon powder is converted into flakes by passing it through a rolling mill.

NASA's Jet Propulsion Laboratory, Pasadena, California

When powdered silicon is produced by the free-space decomposition of silane gas, the average particle size of the silicon produced is typically low-micron to submicron, which makes the particles difficult to handle. To convert the silicon powder into flakes, making it easier to handle, the powder is passed through a rolling mill.

Silicon powder was compacted by sandwiching it between two flat sheets of metal and passing it through a horizontal rolling mill. This demonstrated the feasibility of the method. However, when the method is scaled up for production, the choice of metal making contact with the silicon will be important, if the high purity of the silicon is to be preserved.

The feasibility tests also showed that vacuum sintering the flakes at 1,350° C (60° C below the melting point of silicon) for 1 hour in a quartz crucible significantly increases their breaking strength.

This work was done by Ernest G. Farrier and Joachim Rexer of Union Carbide Corp. for **NASA's Jet Propulsion Laboratory.** *For further information, Circle 28 on the TSP Request Card.*
NPO-15271

Separating Silicon and Sodium Fluoride by Melting

Silicon is withdrawn from the bottom of a crucible after two immiscible liquids form.

NASA's Jet Propulsion Laboratory, Pasadena, California

A method for separating mixtures of silicon and salts of sodium and fluorine takes advantage of the immiscibility of the two components. The method may be used in conjunction with the reduction of SiF_4 gas by sodium to prepare large quantities of silicon for solar-cell fabrication and other uses. It could replace the method of multiple leachings to dissolve NaF and Na_2SiF_6 salts, which exposes the silicon to possible oxidation loss and contamination.

When heated in a graphite crucible to temperatures above the melting point of silicon (1,410° C) a powder mixture of NaF, Na_2SiF_6, and silicon rapidly separates into a molten-salt mixture and large drops of silicon that range in size from 1 to 10 mm in diameter. These drops combine and settle to the bottom of the crucible. Silicon can be continuously removed by tapping silicon from the crucible bottom (see figure) while feeding a fresh powder mixture through the top.

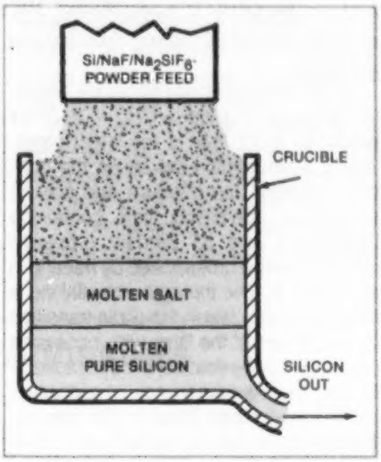

Silicon Is Withdrawn from the bottom of the crucible, once two immiscible liquid stages form, in this quasi-continuous method of separating silicon from other reaction products. The process would be periodically halted to remove the accumulated buildup of salts.

It is speculated that this separation occurs because the molten-salt phase coats the silicon and acts as a flux that aids in combining the smaller drops of silicon into larger drops that ultimately drop to the bottom of the crucible. The coating also prevents the silicon from wetting the graphite and producing a silicon carbide contaminant.

This work was done by Leonard Nanis and Vijay K. Kapur of SRI International for **NASA's Jet Propulsion Laboratory.** *For further information, Circle 29 on the TSP Request Card.*
NPO-15363

Thermoset/Thermoplastic Aromatic Polyamides for Composites

Pendent propargyl groups serve as latent cross-linking agents in a new series of polyamide resins.

Langley Research Center, Hampton, Virginia

New aromatic polyamides are processed at a relatively low temperature, then heat-treated to attain the high softening temperature required when the polyamides are used as matrix resins in structural composites. The new polyamides are compatible with the organic fibers (such as duPont Kevlar® aramid fibers, or equialent) often used as reinforcing agents in such composites.

The softening temperature of a thermoplastic matrix resin must be at least 50 K above its use temperature, so that the resin will have acceptable elastic modulus and stiffness. This problem is compounded when an organic fiber is the reinforcing agent in the composite, because the fiber has a characteristic temperature at which it begins to

(continued on next page)

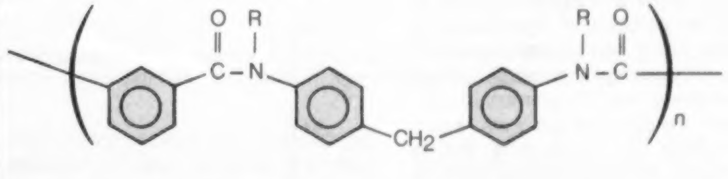

where n represents the repeating polymer unit and

R = $-CH_3$ and $-CH_2-C{\equiv}CH$ in varying ratios, ranging from $-CH_3$ at 99 percent and $-CH_2-C{\equiv}CH$ at 1 percent to $-CH_3$ at 0 percent and $-CH_2-C{\equiv}CH$ at 100 percent.

New Aromatic Polyamides contain pendent propargyl groups ($-CH_2-C{\equiv}CH$), which serve as latent cross-linking agents.

irreversibly lose its stiffness. This is generally due to a relaxation phenomenon occurring in a highly oriented fiber.

Aromatic polyamides with relaxation temperatures slightly below 573 K (300° C) are attractive as organic fibers for structural composites. In order to fabricate a structural laminate with this fiber reinforcement, a processing temperature of 553 K (280° C) should not be exceeded to ensure that the fiber stiffness is retained. This thermal restriction is in turn imposed on the resin or polymer, requiring that it be processable at a temperature below 553 K.

The new series of polyamides is processed no higher than 553 K. They are converted to a higher softening temperature due to a chemical reaction that occurs during this 553 K heat treatment. These thermoset/thermoplastic aromatic polyamides, suitable for fabricating structural composites, have the added advantage of being soluble before thermal processing but solvent-resistant after thermal processing.

The new process incorporates a propargyl cross-linking agent at various levels along the backbone of an aromatic polyamide, to produce a polymer of high molecular weight that softens at a relatively low temperature (427 K) and subsequently "sets up" when treated at a higher temperature (553 K). The sites of latent cross-linking do not enter into any chemical reactions during the fabrication of the thermoplastic component. However, on heating to the elevated temperature, the sites form cross-links that result in a polymer system with an increased softening temperature and an increased resistance to solvents.

In the new polyamide structure, shown in the figure, it is the $-CH_2-C{\equiv}CH$ or propargyl group that is the latent cross-linking agent, which increases the polymer softening temperature and solvent resistance. Polyamide films containing between 1 and 33 percent propargyl diamine can be cross-linked by heating in air at 553 K. The thermal cross-linking is evidenced by a rise in the glass-transition temperatures of the films with increasing propargyl concentration, a loss in solubility, and the disappearance of propargyl-related peaks from infrared film spectra. Thermal cross-linking occurs with only a slight loss in thermo-oxidative stability.

The propargyl-containing polyamides are attractive as matrices for polyamide fiber (for example, aramid fiber) composites. These materials are processable at advantageously low temperatures and thermally cross-linkable at temperatures below the relaxation temperature of the fiber. The compatibility of these resins with aromatic polyamide fibers gives them high potential for success as matrix resins for composites.

This work was done by Terry L. St. Clair, Anne K. St. Clair, and John D. Barrick of **Langley Research Center;** *James F. Wolfe of Virginia Polytechnic Institute and State University; and Thomas D. Greenwood of King College. Further information may be found in NASA TM-81918 [N81-14080/NSP], "Crosslinking of Aromatic Polyamides via Pendant Propargyl Groups" [$5]. A copy may be purchased [prepayment required] from the National Technical Information Service, Springfield, Virginia 22161.*

This invention is owned by NASA, and a patent application has been filed. Inquiries concerning nonexclusive or exclusive license for its commercial development should be addressed to the Patent Counsel, Langley Research Center [see page A5]. Refer to LAR-12723.

Sterilizable Binder Is Stable at 135° C

Material with few unsaturated double bonds has the needed stability.

NASA's Jet Propulsion Laboratory, Pasadena, California

A polyurethane binder for solid propellants that can endure heat sterilization without decomposition is based on an ester diol. The binder, which resists oxidation under prolonged exposure to 135° C temperature, is low enough in viscosity that it can be handled easily during processing and readily mixed with oxidizers, such as ammonium perchlorate. The polyurethane is also a suitable material for encapsulants, potting compounds, and coatings that must be sterilized.

Conventional polyurethanes, in contrast, quickly oxidize during sterilization because of their unsaturated double bonds. Attempts to improve their stability by hydrogenating the double bonds result in a viscous liquid that cannot carry the necessary high loading of propellant oxidizer.

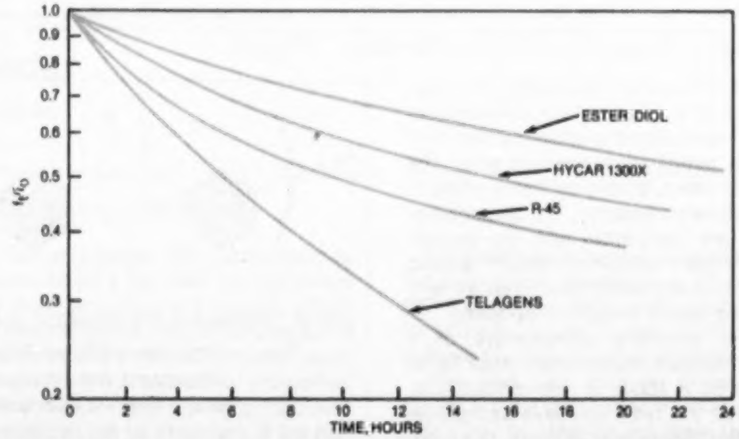

Stress Relaxation — a measure of resistance to degradation — is higher for ester-diol-based polyurethane than for other binders. In this plot, the horizontal axis represents the time of exposure to 135° C in nitrogen, and the vertical axis represents the ratio of stress after heat exposure to that before.

Polyurethanes are usually made from high-molecular-weight glycols or polyhydric alcohols and diisocyanates or triisocyanates. Such extenders or cross-linking agents as polyhydric alcohols or polyfunctional amines are added for further polymerization and cross-linking, to impart elasticity to the polymers.

The new polyurethane is based on a commercially-available dimerized fatty acid having high molecular weight (600) and low unsaturation and viscosity. Known as Empol 1010 dimer acid, the material is made from animal or vegetable fat by a proprietary dimerization process. The dimer acid is changed by esterification with a dihydric alcohol into an ester diol. Various molecular weights can be obtained by control of the ratio of dihydric alcohol to dimer acid. The product is converted to polyurethane by reaction with diisocyanates.

In stress-relaxation tests, the ester-diol-based polyurethane outperformed other major candidates for heat-sterilizable propellant binders (see figure). In other tests, cylindrical castings of the new binder, 3 inches (7.6 centimeters) in diameter, showed no change after four cycles of sterilization at 135° C, 55 hours per cycle, when they were subjected to X-ray inspection.

In an experimental procedure, the ester diol was synthesized by adding 500 grams of Empol 1010, 17.2 grams of p-toluene sulfonic acid, and 434 grams of 1.5 pentanediol to 1 liter of toluene. The solution was refluxed for a total of 13 hours to drive off water. The toluene solvent was then removed by evaporation under reduced pressure. The solution was then washed with deionized water in a separatory funnel. Finally, the product ester diol was dried for 2 hours at 100° C on a rotary evaporator under reduced pressure. A representative propellant composition is 9.93 grams ester diol with 3.03 grams isophorone diisocyanate, 3.04 grams castor oil, 67.80 grams ammonium perchlorate, and 16.00 grams aluminum.

This work was done by Sarkis H. Kalfayan and Andre H. Yavroulan of Caltech for **NASA's Jet Propulsion Laboratory.** *For further information, Circle 30 on the TSP Request Card.*
NPO-15020

Fire-Retardant Epoxy Adhesives

Phosphorus in both resin and curing-agent molecules prevents fire propagation.

Ames Research Center, Moffett Field, California

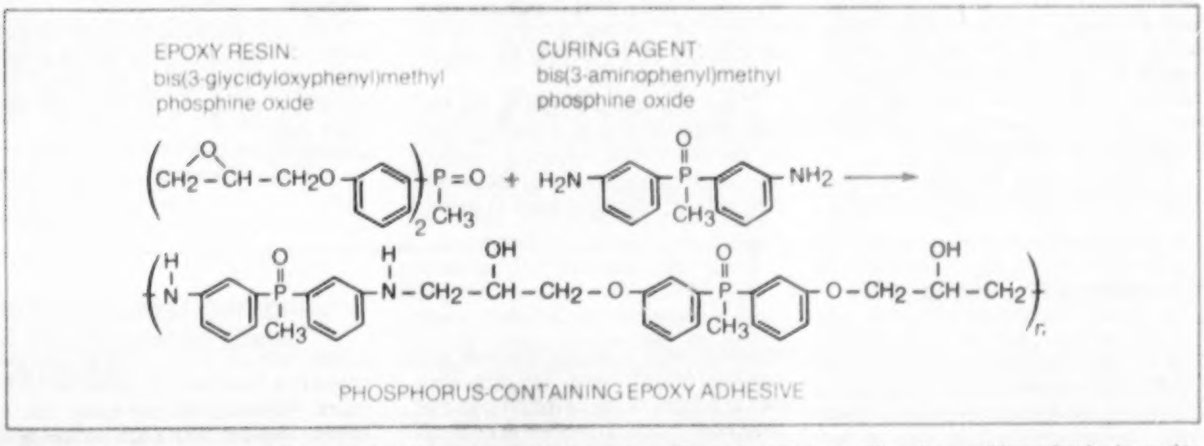
EPOXY RESIN:
bis(3-glycidyloxyphenyl)methyl phosphine oxide
CURING AGENT:
bis(3-aminophenyl)methyl phosphine oxide
CH2 – CH – CH2O
O
P = O
CH3
2
+
H2N
P
O
CH3
NH2
H
N
O
P
CH3
H
N – CH2 – CH – CH2 – O
OH
O
P
CH3
O – CH2 – CH – CH2
OH
n
PHOSPHORUS-CONTAINING EPOXY ADHESIVE

A Reaction for Representative Phosphorylated Components is shown here. The mole ratio is 1:1. When the resulting adhesive is used to bond phenolic/glass laminate to a titanium dioxide-pigmented film, the adhesive bond strength exceeded the tear strength of the film.

A new phosphorus-containing epoxy is fire-retardant and translucent. Intended as an adhesive for laminated plastic sheets, the new material bonds well to titanium dioxide-filled plastic film, which ordinarily shows little surface interaction with adhesives.

Both the epoxy resin and its diamine curing agent include covalently bonded phosphorus in their molecular structures (see figure). Since the curing agent contains phosphorus — unlike such typical curing agents as aminoethylpiperazine, it does not dilute the phosphorus in the epoxy resin. It is therefore possible to keep the phosphorus content of the adhesive above 7 percent, a condition necessary to ensure fire retardancy in air. For a phosphorus-containing epoxy mixed 1:1 on a molar basis with a phosphorus-containing diamine curing agent, for example, the net phosphorus content will be about 10 percent.

Tests have confirmed the desirable properties of the new adhesives. Of two experimental formulations, both adhered to a TiO_2-filled plastic film with a bond strength that exceeded the tear strength of the film. Fire retardancy has been demonstrated, and smoke density is low enough to avoid smoke obscuration.

This work was done by Norman Bilow and Thomas W. Giants of Hughes Aircraft Co. for **Ames Research Center.** *No further documentation is available.*
ARC-11430

Etchant for $Hg_xCd_{1-x}Te$ Crystals

A mixture of nitric and hydrochloric acids reveals crystal defects.

Marshall Space Flight Center, Alabama

A mixture of nitric and hydrochoric acids is a satisfactory etchant for $Hg_xCd_{1-x}Te$ crystals. Preferential etching by the acid solution reveals crystal-dislocation defects (type D) and impurity-dislocation defects (type S) in these crystals, which have optical and electrical applications.

The $Hg_xCd_{1-x}Te$ crystals are immersed in mixtures of nitric acid and hydrochloric acid. A crystal treated for 5 seconds with 0.25 HNO_3, 0.25 HCl, and 0.5 H_2O reveals both the S-type and D-type etch pits. The etching progresses more rapidly with added HNO_3 and progresses more slowly with more HCl and water, with more sensitivity shown to water.

This work was done by E. A. Irene of IBM Corp. for **Marshall Space Flight Center.** *No further documentation is available.*
MFS-25705

Liner for Silicon Reactor

A coating of sodium tetrafluoride minimizes contaminating high-purity silicon.

NASA's Jet Propulsion Laboratory, Pasadena, California

The production of high-purity silicon by the reaction of silicon tetrafluoride and sodium results in reaction products, sodium fluoride and silicon, that adhere to the reactor walls. The reaction, which begins at 150° C, can reach temperatures of 2,000° C. At these high temperatures, there exists the danger of the nickel reactor walls melting.

To avoid melting the nickel or contaminating the silicon, either by contact with the walls or by handtools needed to dislodge the NaF/Si, the reactor walls are coated with a layer of NaF. By using an NaF liner, the reaction products are removed by simply turning the reactor chamber upside down.

There are other benefits to the NaF liner. The liner acts as a seeding agent for the NaF formed during the reaction; thus, a clean segretation of silicon and NaF occurs, making it easy to extract the silicon. Also, the liner insulates the nickel walls from the hot reaction products.

This work was done by Angel Sanjurjo of SRI International for **NASA's Jet Propulsion Laboratory.** *For further information, Circle 89 on the TSP Request Card.*
NPO-15366

Books and Reports

These reports, studies, and handbooks are available from NASA as Technical Support Packages (TSP's) when a Request Card number is cited; otherwise they are available from the National Technical Information Service.

Corrosion-Protection Coatings for Aluminum

Study investigates 21 combinations of surface treatments, primers, and topcoats.

Test results show that outstanding protection can be afforded to 2219-T87 aluminum alloy in severe seacoast and seawater environments. The tests were part of a study of the developments that have been made on protective coatings for aluminum since early in the Space Shuttle program. The study considered several types of coatings, including primers, enamels, chlorinated rubbers, alkyds, epoxies, vinyls, polyurethanes, water-based paints, and antifouling paints; but many were eliminated from consideration because they were not expected to protect the Space Shuttle during launch and reentry. A 20-page report summarizes the study.

For the tests, sets of panels were primed and topcoated, subsequent to a surface treatment, using a conventional air-spray gun. Panels of 2219-T87 aluminum were prepared, primed, and coated with 21 different combinations, scribed with an 'X' on one side, and exposed to a 5-percent salt spray for 4,000 hours. Following the salt-spray test, a section was cut from each sample and exposed in a forced-air oven to determine resistance to high temperature [400° F (200° C)]. Application properties, adhesion, heat resistance, and corrosion protection were among the properties evaluated.

Results of these tests indicated four combinations with outstanding performance and four additional combinations with corrosion protection almost as good. These combinations are generally based on a chromated pretreatment, a chromate epoxy primer, and a polyurethane topcoat.

Of the outstanding samples, all had only very small blisters and light white corrosion products in the scribe marks after over 4,000 hours of salt-spray exposure; there was no undercutting of the paint at the scribe marks. In these tests, there was no discernible difference between the polyamide or amine cured epoxy primers, though primer choice must be compatible with the topcoats.

Because of the increasing demands to reduce the use of toxic materials, the survey included nonchromated inhibitors for use with aluminum alloys. The combinations without chromates, either in a conversion coating or the primer, failed along the scribe marks by blistering, undercutting the paint films, and losing adhesion. In general, it was found that these inhibitors are still in the development stage and are not satisfactory for severe corrosive environments.

The combination that afforded the least protection, with the exception of two zinc primers, used a wash primer pretreatment. The deterioration of two zinc-rich systems, phenoxy and epoxy polyamide, began almost immediately.

This work was done by R. H. Higgins of **Marshall Space Flight Center.** *Further information may be found in NASA TM-82402 [N81-19274/NSP], "Evaluation of Several Corrosion Protective Coating Systems on Aluminum" [$6]. A paper copy may be purchased [prepayment required] from the National Technical Information Service, Springfield, Virginia 22161. The report is also available on microfiche at no charge. To obtain a microfiche copy, Circle 31 on the TSP Request Card.*
MFS-25640

Environmental Durability of Electroplated Black Chromium

Coated aluminum solar panels were tested in rural, industrial, and seacoast environments.

A recent report describes tests of the durability of electroplated black-chromium coatings on solar-collector panels in rural, industrial, and seacoast environments for 60, 36, and 13 months, respectively. The black-chromium coating showed exceptionally-good optical durability in all three environments. As expected, the seacoast environment proved most severe. While optical degradation was not severe, considerable corrosion occurred.

Panels for collecting solar energy as heat are usually prepared from metals coated to increase the absorption of solar radiation (wavelengths in and near the visible region) without significantly increasing emissivity at the longer infrared (IR) wavelengths at which losses due to reradiation occur. Electroplated black chromium is one of several known coatings with suitable optical properties; namely, solar absorptance higher than 0.9 and infrared emittance around 0.1. Obtaining such optical selectivity requires the use of coatings so thin that their ability to protect the metal substrate from corrosive environments tends to be limited.

Commercial flat-sheet solar-collector panels made from 1100 aluminum were first plated with bright nickel 0.0005 inch (0.0127 mm) thick to improve corrosion resistance and then plated with a thin layer of black chromium to an unspecified thickness to obtain the desired absorptance/emittance ratio. The panels were 2 by 3 feet (0.6 by 0.9 m) and contained integral flow passages fabricated by the silk-screen/hot-roll process.

The panels were exposed bare to produce a "worst-case" condition. (In normal use, covers over the panels help to protect them from the environment.) A portable solar and infrared reflectometer was used to obtain the solar absorptance and IR emittance information shown in the figure.

The rural site at Marshall Space Flight Center near Huntsville, Alabama, is low in or essentially free of various corrosive pollutants. The industrial site was a highly industrialized area in North Birmingham, Alabama. At the seacoast site, Kennedy Space Center near Titusville, Florida, panels were tested at two locations, 120 feet (37 m) from the mean high-tide line and 1 mile (1.6 km) inland.

The panels were mounted at 45°, facing south except at the seacoast sites where the panels were mounted 30° from horizontal, facing east toward the ocean. At the rural site, corrosion was slight (some minute specks surrounded by small areas of discoloration), solar absorptance was unchanged, and IR emittance increased only slightly.

At the industrial site, corrosion resistance was considered good, but small brown spots 0.02 to 0.03 inch (0.05 to 0.08 cm) in diameter (apparently caused by cinder particles from a nearby metal furnace clinging to the panels and rusting) were scattered over the panels. Solar absorptance and IR emittance both increased slightly.

At the seacoast sites, corrosion was more severe with panels at both sites showing white corrosion spots 0.13 to 0.19 inch (0.32 to 0.48 cm) in size. Spots were more numerous at the beach site. Solar absorptance was essentially unchanged, but IR emittance increased slightly inland and moderately at the beach.

This work was done by James R. Lowery of **Marshall Space Flight Center.** *To obtain a copy of the report, Circle 32 on the TSP Request Card.*
MFS-25797

Equations for Composite-Propellant Burning

Progress is made toward a predictive model.

A reported study of composite-propellant burning summarizes recent advances in understanding the behavior of propellant formulations based on ammonium perchlorate (AP), binder, and aluminum in various proportions and particle size distributions. The approach presented in this report incorporates an adapted version of an earlier model for monopropellant AP. The objective is to predict the burning-rate characteristics of composite propellants at high pressure.

The report begins with a presentation of the revised model of AP monopropellant combustion. A trial surface temperature is selected and inserted into equations for mass flux, the fraction of AP reacted in the gas phase, the fraction of AP reacted in the condensed phase, heat content of the adiabatic flame, net surface heat, net heat release, flame standoff distance, and heat balance at the surface. The heat-balance equation yields a value of surface temperature that is then compared with the trial value and iterated until the two values converge.

An important concern is the allocation of AP/binder burning rates among particles of various sizes in multimodal propellants. As a first approximation, the finer particles are considered to burn more fuel rich than the coarser particles because of their greater surface area per unit mass. There is, however, some interaction among the various particle-size fractions: This is taken into account in deriving more realistic expressions for the oxygen/fuel ratios and burning rates as a function of the concentrations of particles of different sizes.

(continued on next page)

The diffusion-flame analysis generally follows that of the earlier model but with some changes to improve the continuity of the changing flame structure and to give more importance to the binder. The concept of flame interactions is discussed but is not incorporated into the model for a lack of data.

The effect of aluminum in bimodal and trimodal propellants is considered. It is concluded that aluminum agglomerates to a lesser extent with decreasing coarse AP size, increasing AP fine size, increasing fraction of fine AP, increasing pressure, and increasing aluminum size. It is further concluded that there is a coarse-aluminum regime in which agglomeration is independent of pressure. Formulas are given for the ignition and combustion distances of aluminum particles above the surface and for an effective aluminum flame height.

Surface-area and burning-rate equations are introduced. A new equation is derived for the burning rate of multimodal propellants, reflecting more closely than do earlier models the way propellants really burn.

The energy-balance equations for AP monopropellant are recited in a more sophisticated form for composite propellants. The new equations account for the heat feedback from the diffusion flame closing over the AP flame. A modified surface-temperature equation includes additional terms for the effects of the binder and the aluminum.

It is anticipated that the completed model will be applicable to many different propellants. Although the report does not discuss industrial applications, this work should stimulate further developments in combustion science and engineering.

This work was done by Leon D. Strand and Norman S. Cohen of Caltech for **NASA's Jet Propulsion Laboratory.** *To obtain a copy of the report, Circle 33 on the TSP Request Card.*
NPO-15324

Properties of Nickel-Based Hydrogen-Turbine Blades

Tests on alloys for hydrogen-burning engines of the future are described.

A 120-page report presents data on mechanical properties of cast nickel-based alloys for turbine blades operating in hydrogen and steam at high temperatures. In particular, the document deals with three alloys: single-crystal MAR-M-246 + Hf, single-crystal PWA 1480, and directionally-solidified MAR-M-246 + Hf. Properties were measured at 760° C and 871° C (1,400° F and 1,600° F). The alloys have been proposed for use in space propulsion systems operating on high-pressure hydrogen.

Described in the report are tensile properties (yield and ultimate strengths, elongation, reduction of area, and modulus of elasticity), creep-rupture properties (creep rate, rupture life, elongation, and reduction in area), low-cycle fatigue, and crack growth. Measurements were made on solid specimens exposed to gaseous hydrogen and hydrogen-enriched steam at a pressure of 5,000 lb/in.^{2} (34.5 MPa). Specimens were tested in both transverse and longitudinal orientations.

The report is arranged in sections covering: general results and conclusions; descriptions of materials, specimens, and tests and specific results and conclusions for each of the property tests. The report includes information from monthly progress reports previously issued in the test program and pertinent test results from previous contract work. In general, single-crystal PWA 1480 performed better than the other alloys, although there were some exceptions for low-cycle fatigue.

This work was done by D. P. Deluca, J. R. Warren, B. A. Cowles, D. P. Shoemaker, J. R. Teel, Jr., D. L. Pearson, C. G. Annis, Jr., D. A. Wilson, and B. J. Schwartz of United Technologies Pratt & Whitney Aircraft for **Marshall Space Flight Center.** *Further information may be found in NASA CR-14844 [N81-31192/NSP], "Mechanical Properties of Turbine Blade Alloys in Hydrogen at Elevated Temperatures" [$13.50]. A paper copy may be purchased [prepayment required] from the National Technical Information Service, Springfield, Virginia 22161. The report is also available on microfiche at no charge. To obtain a microfiche copy, Circle 34 on the TSP Request Card.*
MFS-25733

Life Sciences

Hardware, Techniques, and Processes

47 Spine Immobilizer for Accident Victims
48 Implantable Drug Dispenser

Spine Immobilizer for Accident Victims

A conformal bladder would safely blanket, immobilize, and restrain spine injury victims.

Ames Research Center, Moffett Field, California

In spite of advances in methods and appliances for the protection of the cord in spinal injuries, many victims who are able to move their extremities shortly after an accident receive irreparable damage to the spinal cord during transport from the scene of the accident to a hospital.

There are a number of techniques for the transport or removal of an accident victim suspected of having a spinal injury. In general, the techniques involve providing support for the body before any lifting takes place. Examples of this technique are the use of a spine board or an articulated chair to which the victim is strapped. Makeshift pads are placed between the victim and the board or chair. Unfortunately, the victim can be further injured while he is being fastened to the back support, and the pads often create undesirable pressure points on the victim.

A proposed conformal bladder, which is filled with tiny spheres called "microballoons," would enable the spine of an accident victim to be rapidly immobilized and restrained and permit the victim to be safely removed from the accident scene in an extremely short time after help arrives. The microballoons expand to form a rigid mass when the pressure within the bladder is less than ambient.

The bladder, which is made of resilient plastic, is strapped about the head and torso of the victim, as shown in the figure. The victim is secured with a pair of straps that cross one another over the chest, above the stomach region, and another pair of straps that engage a lower portion of the torso beneath the stomach region, so that the stomach region is kept free of any restraining forces. This is important because the stomach muscles are required in breathing under these circumstances, and any restraint on these muscles could be harmful.

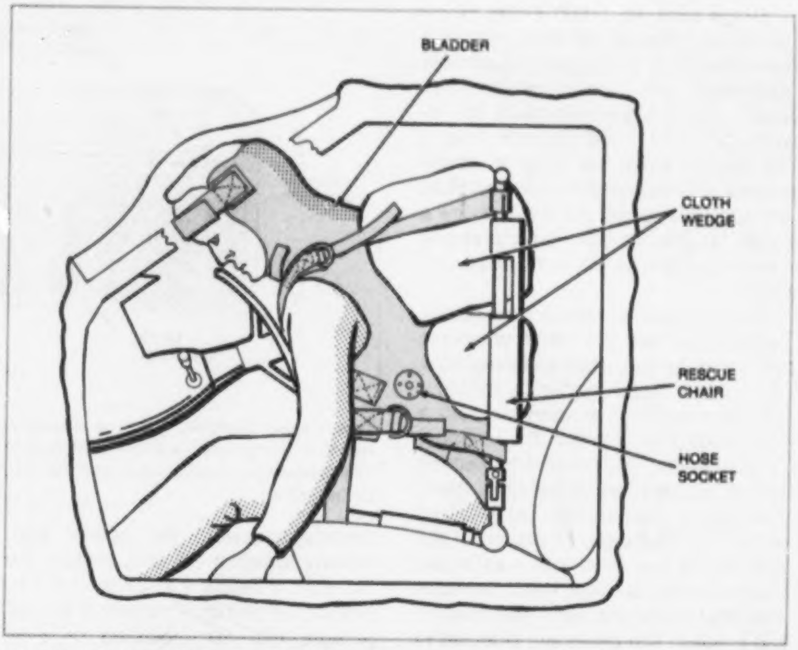

The **Spine Is Immobilized** by a bladder and support. The bladder, which is strapped to the victim (here behind the wheel of a car), is also strapped to a rescue chair. The void between bladder and chair is filled with cloth wedges.

Once the straps are adjusted, a hose is plugged into a socket on the bladder, and air is withdrawn by a pump. When the air is withdrawn, the tightly compressed microballoons that fill the bladder become as firm as concrete and rigidly support the victim's spine.

Included in the connection tubing is an adjustment valve that controls the air evacuation rate. In this way, a paramedic can reversibly soften and harden the microballoons and the conformal blanket formed by the bladder so as best to fit the victim. The rigidified bladder is then secured to a support, and the victim is transported from the accident scene by using the rigid support. When the victim has reached the hospital (or any other time that it is desired to soften the bladder) a valve is opened to admit air to the bladder.

In the flexible bladder is a filter for filtering air and for preventing the microballoons from escaping. The apparatus also includes an inlet/outlet coupling for connecting the interior of the bladder to a vacuum pump, and for securing the bladder in position on the patient and straps for assisting in securing the bladder to a rigid support for enabling the patient to be transported.

This work was done by Hubert C. Vykukal of **Ames Research Center** *and Kenneth Lampson of Kenneth Lampson & Associates. For further information, Circle 35 on the TSP Request Card.*

Inquiries concerning rights for the commercial use of this invention should be addressed to the Patent Counsel, Ames Research Center [see page A5]. Refer to ARC-11167.

Implantable Drug Dispenser

Differential vapor pressure allows fine control.

NASA's Jet Propulsion Laboratory, Pasadena, California

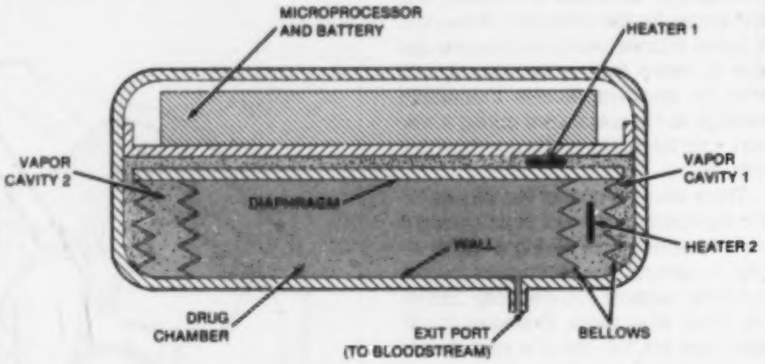

Two Vapor Cavities produce opposing forces on the drug-chamber diaphragm. Heaters in the cavities allow control of the direction and rate of motion of the bellows. The dispensing capsule can be fitted with a coil so that the batteries can be recharged by induction.

Drugs such as insulin would be injected as needed directly into the bloodstream by a compact implantable dispensing unit. The dispenser uses counteracting vapor pressures on opposite sides of a diaphragm to control the rate at which the drug is administered. Previous designs use liquids as the pressure media, but they require a larger volume than the vapor-pressure device to dispense the same amount of drug.

In the proposed device (see figure), heaters regulate the vapor pressures that force the drug into the bloodstream. The drug, in liquid solution, is held in a central chamber that connects with a tube leading to an artery. The chamber is surrounded by concentric bellows with a saturated vapor between them. The space outside the bellows and above the diaphragm at the top of the chamber is also filled with a saturated vapor that has a lower vapor pressure than that contained within the concentric bellows. The gases are selected to provide balanced forces at body temperature on the sides of the diaphragm. This stabilizes the diaphragm position without power input. The gases can be fluorocarbons or other material for which the vapor pressure varies widely with temperature and thus responds readily to heating.

Each of the vapor cavities defined by the concentric bellows contains an electric heater. A battery supplies power to the heaters under the control of a microprocessor. If heater 1 heats the vapor in cavity 1, the pressure in that cavity will increase and drive the diaphragm toward the bottom wall, thereby expelling the drug through the exit port. If heater 2 in cavity 2 is also heated, the rate of movement of the diaphragm can be regulated or even balanced so that it is held in a fixed position with respect to the wall.

When the programed amount of drug has been dispensed at the programed rate, current may be cut off from one or both heaters to establish a stable diaphragm position. No more drug is dispensed until a command is received from the microprocessor. Feedback can be provided to the microprocessor by temperature sensors in each cavity. The sensors would allow the microprocessor to monitor temperature and, indirectly, the rate and amount of dispensation.

When it is necessary to replenish the liquid in the drug chamber, heater 2 is energized while heater 1 is not. The diaphragm moves away from the wall, creating a negative pressure in the drug chamber that draws in a new supply of the drug from an external source. A dispensing device of implantable size could hold a 30-day supply of insulin to be dispensed at a rate of 1 cm^3 per day.

This work was done by Earl R. Collins, Jr., of Caltech for **NASA's Jet Propulsion Laboratory.** *For further information, Circle 36 on the TSP Request Card.*

Inquiries concerning rights for the commercial use of this invention should be addressed to the Patent Counsel, NASA Resident Office-JPL [see page A5]. Refer to NPO-15160.

Mechanics

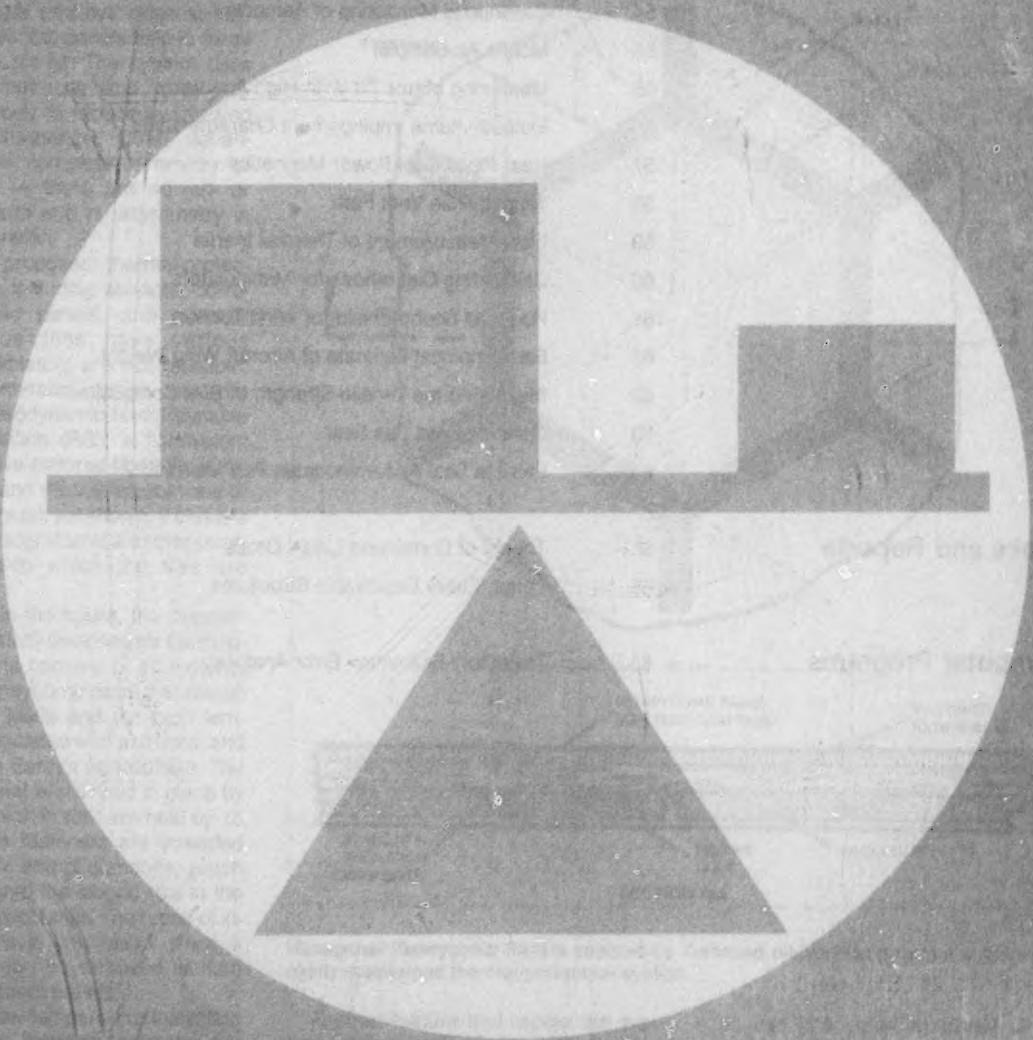

Hardware, Techniques, and Processes

51 Lightweight Thermal-Protection System
52 Pressure-Decay Measurements Improve Bubble-Point Test
53 Connector for Composite Tubes
54 Continuous Monitoring of Aerosols
55 Mobile Air Sampler
55 Measuring Mirror Tilt With High Accuracy
56 Exhaust-Plume Impingement Characteristics
57 Heat Pipes Cool Power Magnetics
59 Tapped-Hole Vent Path
59 Field Measurement of Thermal Inertia
60 Calculating Clearances for Manipulators
61 Rod-Wall Sound Shield for Wind Tunnels
62 Semiempirical Estimate of Aircraft Wing Weight
62 Measuring the Tensile Strength of B/Al Composites
63 Ceramic-Cord Gas Seal
64 Flexible Seal Accommodates Part Mismatch

Books and Reports

65 Theory of Compound Liquid Drops
65 Large, Easily Deployable Structures

Computer Programs

65 Trajectory-Estimation Error Analysis

Lightweight Thermal-Protection System

Hexagonal honeycomb panels are light, durable, and easy to maintain.

Langley Research Center, Hampton, Virginia

A thermal-protection system originally proposed for the exterior of Earth-to-orbit transports employs external hexagonal honeycomb panels held in place by Y-shaped plates. The system uses lightweight materials and novel assembly methods to reduce weight and simplify maintenance. Other advantages include complete symmetry of components — there are no left- or right-hand parts and no asymmetry in thermal expansion.

Previously-proposed thermal-protection systems, including ablators, corrugated metallic panels, and sintered silica fibrous tiles have various drawbacks: Ablators are not reusable. Corrugated metallic panels are not smooth for aerodynamic flow. Reusable surface insulation (RSI), a lightweight highly-insulative sintered-fiber tile, is relatively new; and the full implications of this system are not yet known. If tiles are used over an isogrid tank, a carrier panel is needed onto which the tiles are mounted.

As shown in the figure, the thermal-protection system designed for Earth-to-orbit transports consists of an external hexagonal honeycomb panel that resists aerodynamic loads and the high temperatures associated with exit from, and entry into, the Earth's atmosphere. The hexagonal panel is clamped in place by 6 Y-plates, which in turn are held by 18 fasteners. The fasteners are threaded into the female end of standoffs, which are screwed into the isogrid ribs in the vehicle propellant tanks. The repair of individual panels is very easy, since a single panel can be removed without removing adjacent panels.

High- and low-temperature insulation materials are installed beneath the panels. The thicknesses of the insulation are chosen to handle the local temperatures and heat loads.

For installation over an isogrid tank, this system is lighter than ceramic tile bonded to a carrier panel because the honeycomb panel serves as both carrier panel and outer thermal shield. Further, the lightweight flexible fibrous materials beneath the honeycomb serve as insulation instead of the heavier tile.

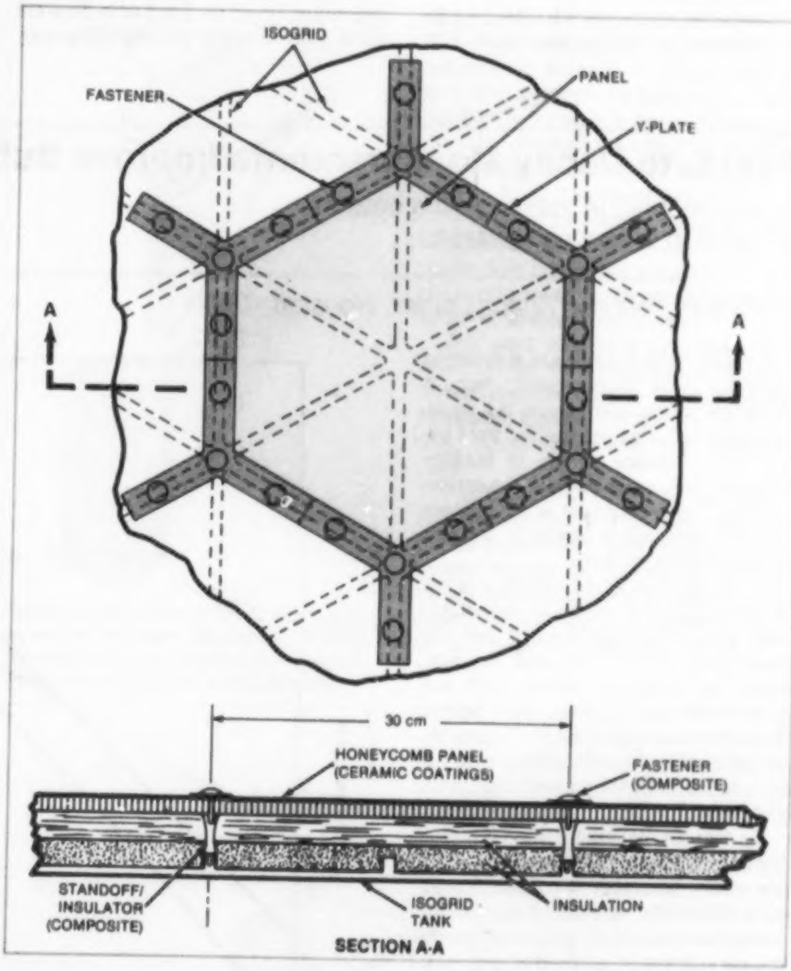

Hexagonal Honeycomb Panels secured by Y-shaped plates would form a lightweight, easily-maintained thermal-protection system.

Another feature that makes the system lightweight is component sharing. For example, the 6 fasteners shown at the corners of the hexagon are shared among 3 panels, while the 12 fasteners located on the legs of the Y-plate are shared by 2 panels. Therefore, out of 18 fasteners used for panel retention, the weight of only 8 is charged to any one panel. Also, each Y-plate is shared with three panels; therefore, the weight of only two Y-plates (6 divided by 3) is charged to any one panel.

In use, the outer facesheet of the panel becomes hot and radiates and conducts heat to the inner facesheet. As a result, there is very little difference between outer and inner facesheet temperatures and, therefore, almost no distortion of the panel. The hexagonal panel has the least perimeter for a given area of coverage, the second most attractive shape being a square panel and the third a rectangular panel. Also, it is advantageous to have the shortest continuous panel-edge length possible, to

(continued on next page)

discourage the flow of hot gases at the panel joints.

The honeycomb outer panel and fastener materials are selected to match the local heating rates. Typical materials could include composites, titanium, superalloys, and refractory metals.

An alternate configuration includes 120° flush-mounted fasteners. The Y-plates are countersunk by dimpling. In this design, the Y-plate thicknesses are increased to retain the honeycomb panels. In another configuration, an additional fastener could be placed at the center of the panel to provide additional support, since expansion due to temperature change is theoretically zero at the panel geometric center.

The system is flexible in that areas with different heating rates and flow properties could be fitted with different sandwich materials, all held in place by the Y-plates. The resulting surface would have a continuously low profile and would have improved aerodynamic surface characteristics.

This work was done by Ian O. MacConochie, Ashby G. Lawson, and Thomas C. Whiteman of **Langley Research Center** *and Evans P. Brien of Kentron International, Inc. For further information, Circle 37 on the TSP Request Card.*
LAR-12880

Pressure-Decay Measurements Improve Bubble-Point Test

A new technique improves the detection of flaws in wire-mesh screens.

Lyndon B. Johnson Space Center, Houston, Texas

Flaws in screen mesh are sometimes detected by a "bubble-point" test, in which the screen is immersed in a liquid, removed, and then pressurized from below until a steady stream of bubbles emerges from somewhere on the screen surface. The pressure at which bubbles are first observed is related to the size of flaws on the screen.

A new technique reduces by a factor of about 100 the minimum detectable flaw size in the bubble-point test. By measuring the rate of slow leakage, flaws as small as about 10^{-4} in.^{2} (0.06 mm^2) are detected (see figure). Since the technique does not require observation of the screen, tests can be run on screens already installed inside tanks and pipes.

To test an installed screen, its container is filled and then drained, leaving the screen saturated with liquid. A pressure differential is applied across the screen and increased until an abrupt decrease in pressure is noted on pressure-monitoring instruments. This pressure is the conventional bubble point.

To detect smaller flaws than those that determine the conventional bubble point, the screen is resaturated with liquid. This time, a pressure differential of about two-thirds to three-fourths of the bubble-point pressure is applied. There is no rapid drop in pressure this time. Instead, a slow leakage occurs, which is observed on the pressure gage.

Equations have been derived relating the leakage rate to the flaw size. The equations have been calibrated using screens with known flaw sizes. Tests show excellent agreement between the theoretical and measured pressure decays.

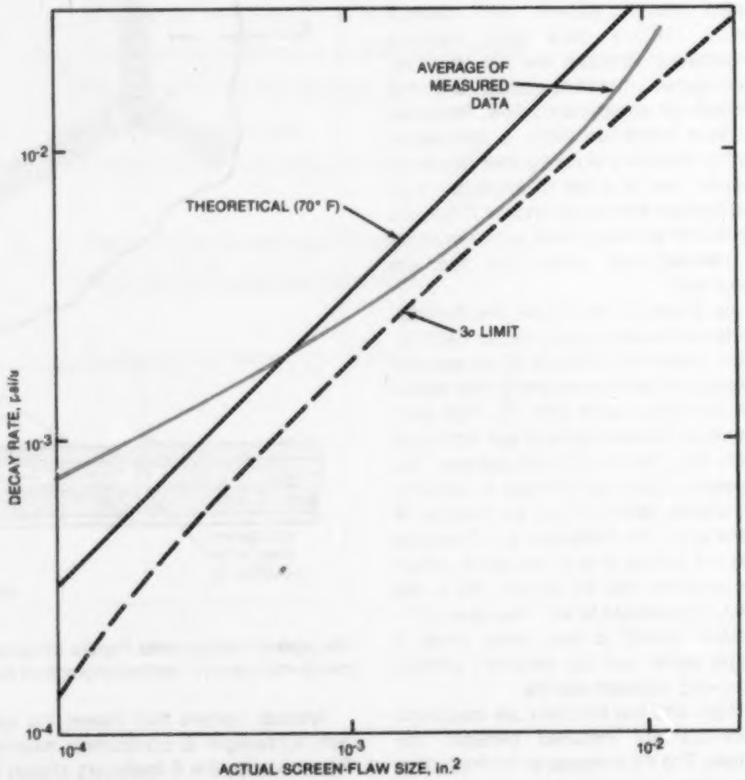

Predicted and Measured Pressure-Decay Rates for screens with known flaw sizes agree well enough to allow determinations of unknown flaw sizes from the measurement of decay rates. These data were obtained using a fluorocarbon gas and simulated screens for the Space Shuttle orbital-maneuver propellent system.

This work was done by Joseph S. Silkey and George F. Orton of McDonnell Douglas Corp. for **Johnson Space Center.** *For further information, Circle 38 on the TSP Request Card.*
MSC-18970

Connector for Composite Tubes

Elements made of composite join tubes at various angles.

Langley Research Center, Hampton, Virginia

Difficulties in joining tubular structural members made of composite materials are overcome by improved connectors. The connectors are made from the same composite as the structural shapes, eliminating the stress and weight problems experienced with metal connectors. The composites also allow the joint strength to be optimized by properly choosing the fiber orientation and the fabric. Only two basic shapes are required to make 90° and T-joints in a plane.

The shape of the basic joint element is a cylinder with a tab on each side of a longitudinal gap as shown in Figure 1. The inner surface of one tab lies in a plane through the centerline of the cylinder. The other tab is offset to leave a gap equal to the tab thickness. The inner diameter of the cylinder is 0.005 to 0.010 inch (0.0127 to 0.0254 cm) larger than the tube to be joined to allow for the adhesive thickness. To join tubes of different diameters, the cylinder diameter is changed, but the tab thickness and gap width are kept constant.

The basic element is made by placing fabric and resin over a mandrel, then vacuum bag molding and curing in an oven at the appropriate temperature. Eight connector elements are cut from a 12-inch (30.48-cm) piece, when sized for joining tubes in the diameter range of 0.75 to 1.25 inches (1.905 to 3.175 cm). The cuts are made perpendicular to the cylinder centerline. Then the tabs are trimmed to an angle required by the type of joint being made.

A right-angle joint is made by placing a connector element on each tube so that the inner surfaces of the tabs on the centerline face each other. Inserting one of these tabs into the gap of the other connector insures that the centerlines of the two tubes are in the same plane. The tabs may be trimmed along a 45° line as shown in Figure 1.

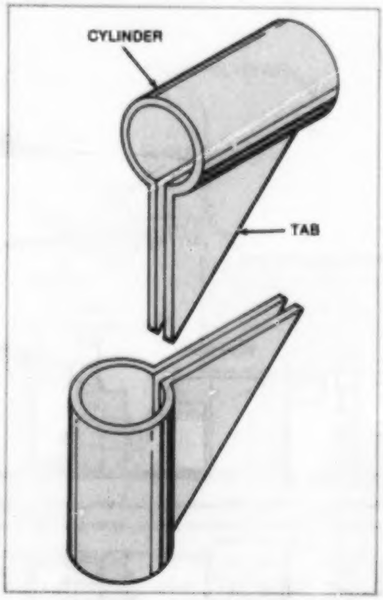

Figure 1. **A 90° Joint is made by combining two of the basic connector elements. The inner surface of one tab lies in a plane through the centerline of the cylinder.**

To make a T-joint, two of the basic connector elements are slid on the tube to each side of where the other tube is to join. Both basic elements are placed with their centerline tabs in the same plane. To complete the joint two different parts called web elements are used (see Figure 2). The tabs of each web element are one-half the thickness of the gap between the tabs of a basic element, so they will fit into the gap of the basic element. To keep the centerlines of the tubes in a plane, the tabs of the web elements are offset so that the outer surface of one lies on a plane through the centerline of the tube.

This technique can be applied to other regular-cross-section components made from composite materials. It can be used to assemble strong, lightweight, three-dimensional structures.

This work was done by Ernest Harrison, Jr., of the Mississippi Methodist Rehabilitation Center for **Langley Research Center.** *For further information, Circle 39 on the TSP Request Card.*

This invention is owned by NASA, and a patent application has been filed. Inquiries concerning nonexclusive or exclusive license for its commercial development should be addressed to the Patent Counsel, Langley Research Center [see page A5]. Refer to LAR-12744.

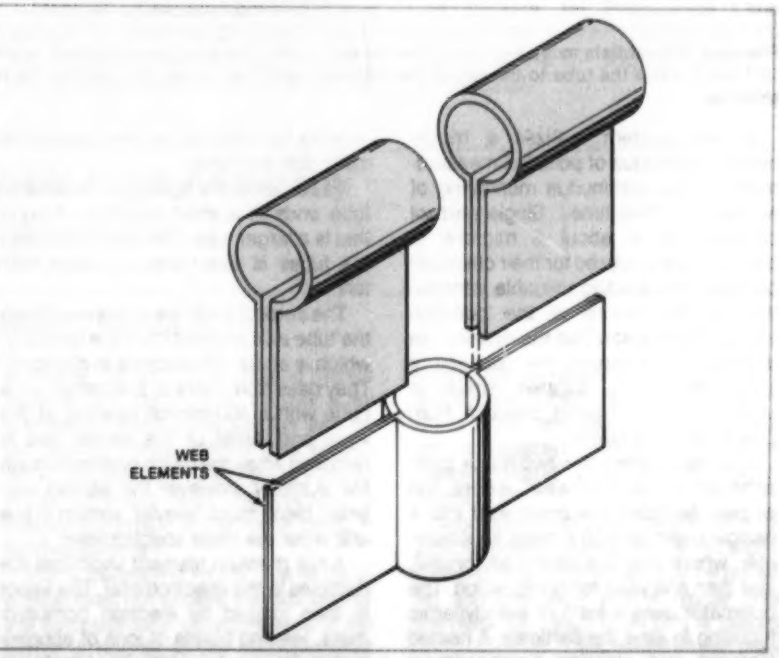

Figure 2. **Two Web Elements and Two Basic Elements are combined in a T-joint. The elements can also be designed to handle structural elements with noncircular cross sections.**

Continuous Monitoring of Aerosols

Online spectrometer monitors the composition of individual aerosol particles.

NASA's Jet Propulsion Laboratory, Pasadena, California

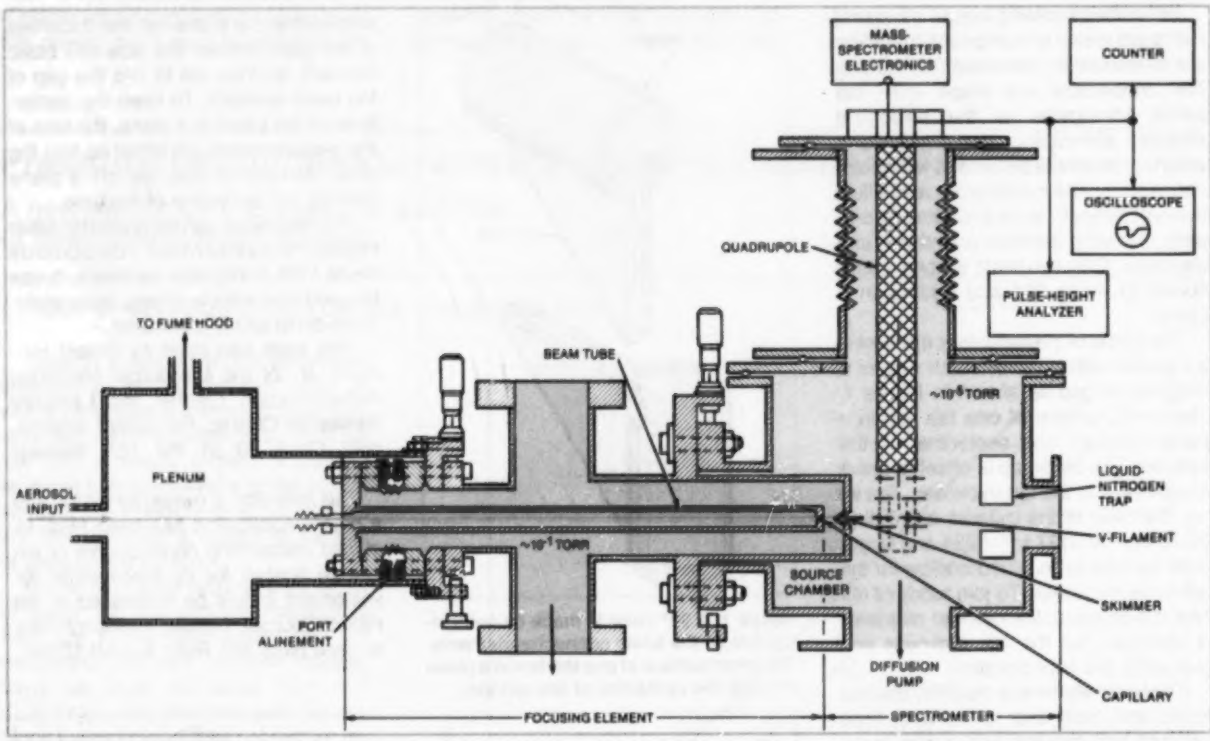

Pressure Differentials move and focus the aerosol beam. The pressure is highest in the innermost tube of the focusing element; it is 10^{-1} torr outside the tube to the left of the skimmer; and it is lowest (10^{-5} torr) in the mass-spectrometer chamber to the right of the skimmer.

A new system realizes a much-needed technique of pollution measurement — the continuous monitoring of aerosols in "real time." Single aerosol particles up to about 5 microns in diameter are analyzed for their chemical composition, yielding valuable information on the nature of the pollution source. Tests show that the system has promise for monitoring the oxidation of sulfur dioxide to sulfates, which is important in controlling pollution from coal-fired powerplants.

The new system has two major components: (1) a collimator, where the aerosol particles are channeled into a narrow beam and (2) a mass spectrometer, where they are vaporized, ionized, and then analyzed for composition. The collimator uses a form of aerodynamic focusing to aline the particles. A heated filament and electron bombardment convert the aerosol particles into ions suitable for analysis by the quadrupole mass spectrometer.

As shown in the figure, the collimator tube ends in a short capillary. Around that is a larger tube. The space between the tubes is evacuated to about 10^{-1} torr.

The aerosol particles are drawn down the tube axis and exit from the capillary, which is about 100 microns in diameter. They pass from there to a skimmer, — a cone with a 400-micron opening at the input end. Most of the carrier gas is removed when the beam passes through the skimmer; however the aerosol particles, being much heavier, remain in line and enter the mass spectrometer.

A hot rhenium filament vaporizes the particles in the spectrometer. The vapor is then ionized by electron bombardment, yielding bursts of ions of approximately 80-μs pulse width. The bursts are mass-analyzed by the quadrupole mass spectrometer.

Thus far, satisfactory analyses have been made of aerosols containing sodium sulfate and sulfite, ammonium sulfate, lithium nitrate, adipic and glutaric acids, dioctyl phthalate, and some of the amino acids. By comparing the analysis with that for a referance aerosol, it is possible to determine the sulfate-to-sulfite ratio of individual particles.

This work was done by Mahadeva P. Sinha, Charles E. Giffin, David D. Norris, and Sheldon K. Friedlander of Caltech for **NASA's Jet Propulsion Laboratory.** *For further information, Circle 40 on the TSP Request Card.*

Inquiries concerning rights for the commercial use of this invention should be addressed to the Patent Counsel, NASA Resident Office-JPL [see page A5]. Refer to NPO-15292.

Mobile Air Sampler

Vehicle-mounted sampler gathers specimens along highways and in tunnels.

NASA's Jet Propulsion Laboratory, Pasadena, California

A simple device for collecting air samples is used on a moving vehicle. It therefore provides realistic specimens for the analysis of air quality along highways and in tunnels. In contrast to fixed air-collection installations, the mobile sampler requires no official approval for its use on highways.

The device consists of an open tube 1.6 inches in diameter and 6 inches long (4.1 by 15.2 cm). However, size is not critical; the essential requirement is that the tube not restrict the flow of air through it. Sealing caps at both ends of the tube are spring-activated and are held open by a thread (see figure). When a wire loop around the thread is energized by an operator, it heats up and severs the plastic thread.

As soon as practial after a sample has been enclosed in the device, it is wired shut to prevent accidental opening of the end caps. When the collected sample is to be analyzed, a nipple on one of the end caps is uncovered, and tubing is connected to it. The tubing leads to a collection syringe or directly to a gas chromatograph or other instrument. The opposite end cap contains a mandrel-mounted seal that, when screwed to a pushrod, becomes a piston for expelling the sample.

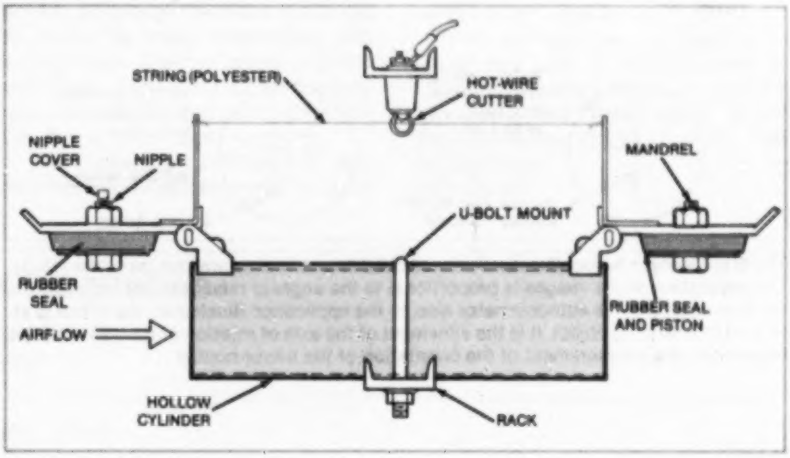

The Mobile Air-Sampling Device closes when the hot-wire cutter melts the plastic string.

After the sample has been removed from the container, the safety wire is removed from it, the nipple is covered, the piston seal is restored to its original position, and a new thread is installed. The sampler is then ready for reuse.

Many samplers can be installed on a vehicle. For example, 30 samplers were mounted on a frame on a pickup truck and used to sample air in one of the tunnels on the northbound Pasadena Freeway in southern California. The hot-wire cutters are operated either separately or in unison by switches in the truck cab.

This work was done by Curtis E. Tucker and Harold P. Holway of Caltech for **NASA's Jet Propulsion Laboratory.** *For further information, Circle 41 on the TSP Request Card.*
NPO-15220

Measuring Mirror Tilt With High Accuracy

Stroboscopic technique freezes mirror motion so that displacements can be measured.

Goddard Space Flight Center, Greenbelt, Maryland

An improved autocollimator accurately measures the angular tilt of plane mirrors in rotational or reciprocating motion. The device is a conventional autocollimator in which the steady light source is replaced by a stroboscope that can be synchronized with the mirror motion. It is accurate to 1 second of arc.

The stroboscopic autocollimator produces a collimated beam of light, the cross section of which is in the shape of a reticle pattern. The moving mirror reflects the light back to the autocollimator, which reimages the light on the source reticle pattern (see figure). When the autocollimator light is strobed in synchronism with the motion, it freezes the image of the mirror position for measurement.

For a translating mirror, the limits of motion must not exceed the diameter of the autocollimator objective lens. If the mirror is normal to the autocollimator beam, the reimaged pattern will match the source pattern precisely. However, if the mirror is tilted, the return image will be displaced. The displacements are measured and directly interpreted in terms of tilt.

Modification of the autocollimator for stroboscopic operation is straightforward. The original lamp is removed. An aperture plate with a typical hole diameter of 1 inch (2.54 cm) is placed

(continued on next page)

over the stroboscopic light source. The stroboscope is provided with a mounting that mates to instrument in the place of the lamp assembly.

The stroboscopic autocollimator can also be used for vibration analysis. For example, to measure the frequencies of vibration of a component, a mirror is attached to the component, and the autocollimator is alined with the mirror. The return image is viewed through the autocollimator while the strobe frequency is adjusted. The strobe frequency at which the return image is stationary is the vibration frequency of the component. The procedure is repeated to find other vibration frequencies of the component.

This work was done by Thomas J. Magner of **Goddard Space Flight Center.** *No further documentation is available.*

This is the invention of a NASA employee, and a patent application has been filed. Inquiries concerning license for its commercial development may be addressed to the inventor, Mr. Thomas J. Magner, Goddard Space Flight Center, Code 702.1, Greenbelt, MD 20771.
GSC-12701

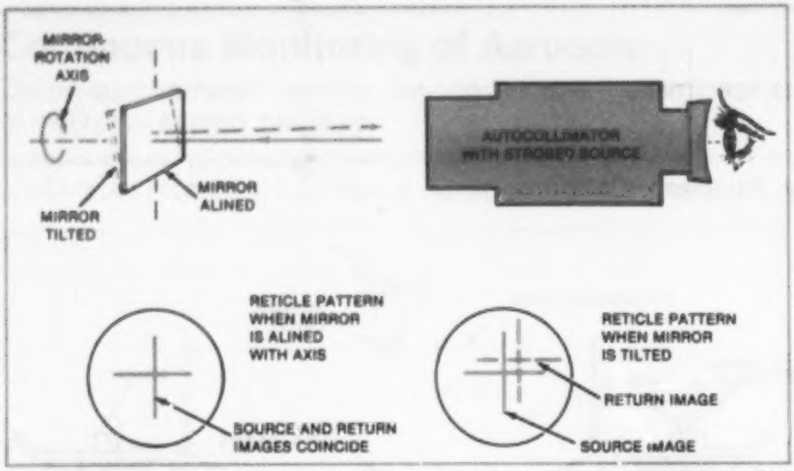
MIRROR-ROTATION AXIS
MIRROR TILTED
MIRROR ALINED
AUTOCOLLIMATOR WITH STROBED SOURCE
RETICLE PATTERN WHEN MIRROR IS ALINED WITH AXIS
SOURCE AND RETURN IMAGES COINCIDE
RETICLE PATTERN WHEN MIRROR IS TILTED
RETURN IMAGE
SOURCE IMAGE

The **Stroboscopic Autocollimator** forms strobed source and return images of the reticle. The separation of the images is proportional to the angle of misalinement between the mirror normal and the autocollimator axis. In the application illustrated, the mirror is attached to a rotating object. It is the alinement of the axis of rotation of the object that is checked by the measurement of the orientation of the mirror normal.

Exhaust-Plume Impingement Characteristics

Model estimates the effects on nearby objects.

Marshall Space Flight Center, Alabama

A new model for rocket-exhaust plumes calculates the effects of heat, pressure, and particle-impingement on nearby structures. The model compares well with experimental data. It is the result of theoretical and experimental studies of objects exposed to the plumes of rocket exhausts at low altitudes. The model has potential industrial applications in studies of the impingement of multiphase mixtures inside coal-gasification equipment and turbines.

Objects exposed to rocket exhaust are subjected to severe pressure and thermal loads. Furthermore, the exhaust from solid-fueled rockets can contain many solid and liquid particles, because aluminum or other metals is present in the propellant. A complete model must give both the gaseous and particulate contributions to the design loads.

At low altitudes, the exhaust-plume flow includes viscous effects that mix the exhaust gases with the air. The flow is further complicated by afterburning,

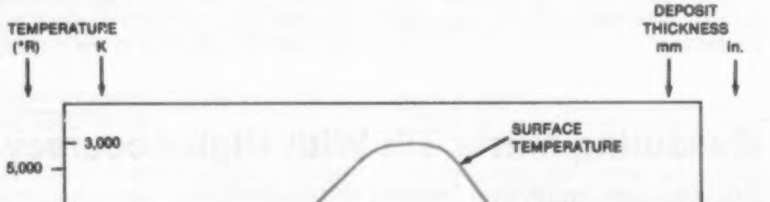

Thermal and Particle-Deposition Loads were calculated for the edge of the exhaust hole on the Space Shuttle Mobile Launch Platform. This represents the most severe condition expected to be encountered on the platform.

by shock waves developing ahead of solid objects in the plume, and by the effects of these shocks on the entrained particles. The model takes all the major contributing phenomena into account.

The nozzle/plume flow field is calculated according to an inviscid-flow computer code that considers the exchange of momentum and energy between the gas and particles. This code also handles equilibrium thermochemistry and takes into account the variations of specific-heat ratios.

Viscous and mixing effects are computed with a code that solves the boundary-layer form of the governing equations. Inputs to the code are the initial-jet and free-stream conditions (pressure, temperature, velocity, Prandtl number, Lewis number, and species distribution). A turbulent-kinetic-energy model relates the turbulent shear stress to a viscosity.

A plume-impingement flow-field calculation establishes the shock conditions ahead of the impinged body. The paths of typical particles in the flow field are traced through the shock to the wall to obtain the mass, momentum, and energy fluxes. The total pressure on the wall is calculated as the sum of the local gas pitot pressure and particle momentum flux at the surface.

The convective contribution to surface heating is relatively straightforward to calculate, but the particle contribution is somewhat more complex. Particle accumulation must be considered, along with the fraction of particle energy transferred to the wall and other effects.

Some final results of the complete model are shown in the figure. The temperature and particle-deposit thickness are plotted as a function of time for a point on a rocket-launching platform.

This work was done by Sheldon D. Smith and Carl J. Wojciehowski of Lockheed Missiles & Space Co., Inc., for **Marshall Space Flight Center.** *For further information, Circle 42 on the TSP Request Card.*
MFS-25489

Heat Pipes Cool Power Magnetics

Configurations originally developed for space use are effective in any orientation.

Lewis Research Center, Cleveland, Ohio

A high-frequency, high-power, low-weight transformer and inductor developed for space use were redesigned with heat-pipe cooling, which allows both a reduction in weight and a lower internal temperature rise. These particular magnetic devices are used in the power stage of a 3-kW ion-beam thrustor.

The use of heat pipes to cool power magnetics in a space environment is a practical solution in high-power designs, but imposes a severe problem when performing testing on Earth. The Earth's gravity field has an effect upon the heat-pipe wicking. If several heat pipes are required, as in modular designs, or if they are used in conjunction with a heat sink cooled by heat pipes, the packaging constraints of keeping all heat pipes horizontal for Earth test become so severe that their use becomes impractical. These newly-developed heat-pipe configurations overcome this limitation.

The high heat-transfer capability of these unique newly-developed, double-ended methanol/stainless-steel heat pipes (Figure 1) allows simultaneous reduction in both mass and internal temperature, which permits the 40-percent weight reduction of the transformer.

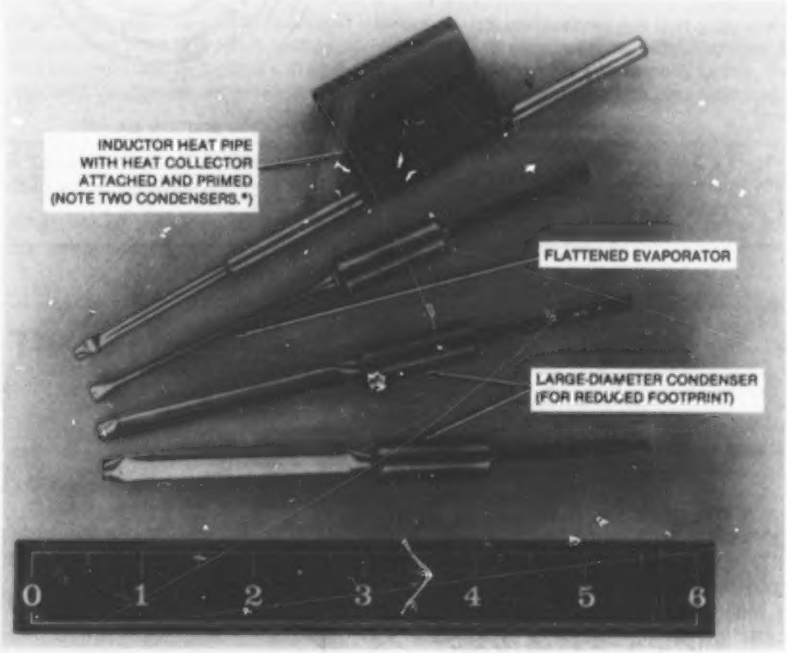

Figure 1. **Heat Pipes** integrated into high-power, high-frequency, high-voltage spaceflight magnetics reduce weight and improve reliability by lowering internal temperatures.

The heat pipe exploits the ability of the electrostatic shield to draw heat from the primary and secondary coils of the transformer. Figure 2 shows the electrostatic shield and heat-pipe assembly. Since the shield is physically located near the transformer hotspot and consists of a thin copper sheet, it forms a natural heat collector for the heat-pipe evaporator. There are two heat pipes per coil. The shield heat collector is formed as two separated sheets, one inside toward the primary and one outside toward the secondary. The two shields thus collect the heat generated in the coil winding wire. The shields are used to insure a smooth surface facing each

(continued on next page)

winding, thus controlling the voltage gradients and meeting the high-voltage corona requirements.

Weighing 1,200 grams, this transformer is one-third lighter than the 1,750 grams of the previous design. To maintain the desired reliability, while handling over 3,000 volt-amperes, the internal thermal rise was previously limited to 45° C. With the new design the temperature reaches a maximum of 25° C. Since the life of an insulation system doubles for each 10° C reduction in temperature, the expected life of this transformer has been quadrupled.

For space applications involving vacuum operation and total absence of convective cooling, this technology allows single-unit transformers to be built with ratings in excess of 10 kilowatts. The use of two condenser sections with a single evaporator allows the heat pipe to operate at maximum capability with any gravitational orientation. The pipe performs as if there were two short pipes end-to-end with a transport capability of over 50 watts. However, if the Earth's orientation places the pipe in a vertical position, the pipe must overcome the effects of gravity. In this position, while one condenser does not operate, the opposite condenser has 15 watts of transport capability, which is more than enough for the worst-case losses generated by the filter inductor.

Figure 3 depicts the heat flow from the inductor frame and heat-sink clamp. The incorporated heat pipe enabled a 40-percent weight reduction with a low (10° C) heat rise and a 5.5-watt loss increase at 12 A nominal operation.

This technology allows dramatic reductions in size and weight, while significantly improving reliability. In addition, the all-attitude design of the heat pipes allows operation of the heat pipes independent of local gravity forces.

This work was done by I. Hansen of **Lewis Research Center** *and M. Chester and E. Luedke of TRW, Inc. Further information, may be found in NASA CR-159659 [N80-13362/NSP], "Heat Pipe Cooled Power Magnetics" [$16.50]. A copy may be purchased [prepayment required] from the National Technical Information Service, Springfield, Virginia 22161.*
LEW-13507

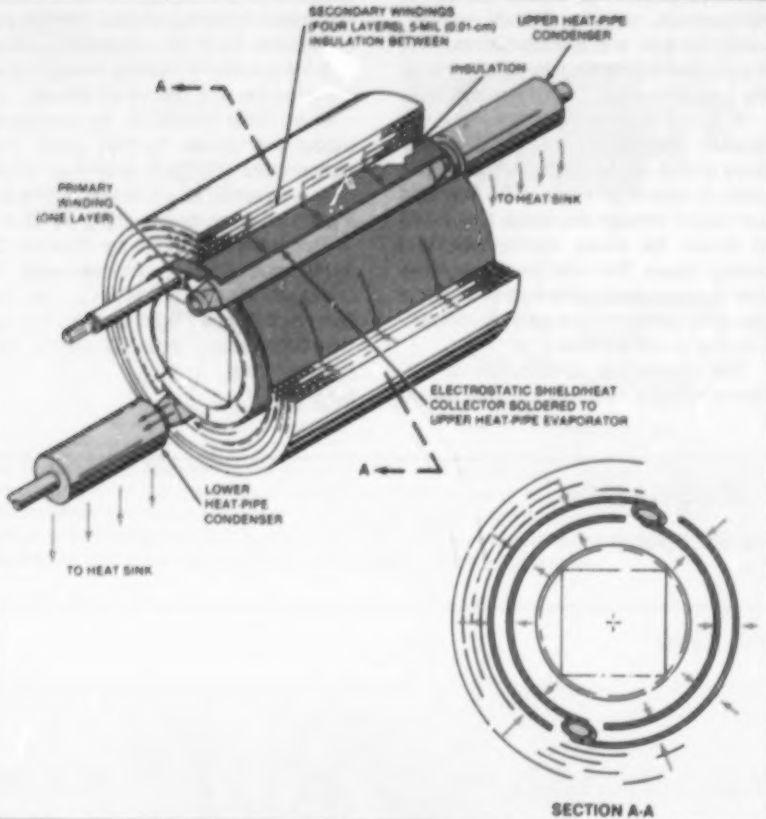
SECONDARY WINDINGS (FOUR LAYERS), 5-MIL (0.01-cm) INSULATION BETWEEN
UPPER HEAT-PIPE CONDENSER
INSULATION
A
PRIMARY WINDING (ONE LAYER)
TO HEAT SINK
ELECTROSTATIC SHIELD/HEAT COLLECTOR SOLDERED TO UPPER HEAT-PIPE EVAPORATOR
A
LOWER HEAT-PIPE CONDENSER
TO HEAT SINK
SECTION A-A

Figure 2. **Two Heat Pipes** integrated in the design of a power transformer cool the unit in any orientation. The electrostatic shield conducts heat from the windings to the heat-pipe evaporator.

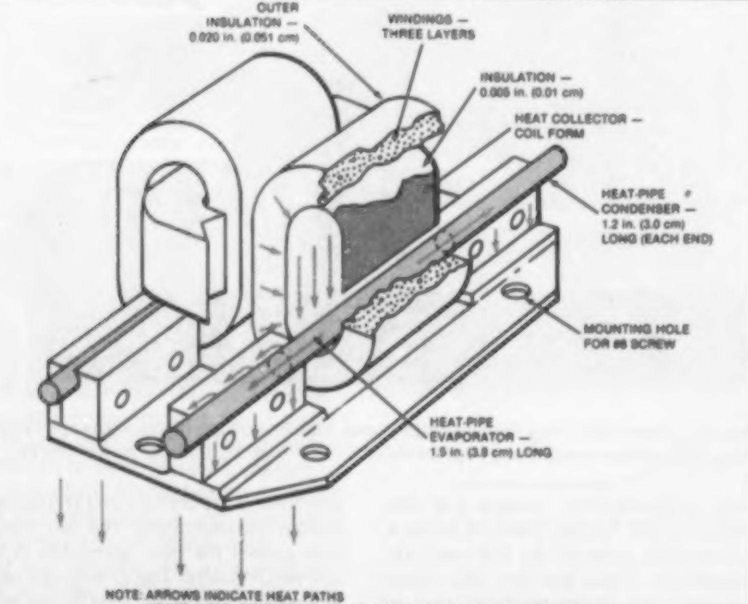
OUTER INSULATION — 0.020 in. (0.051 cm)
WINDINGS — THREE LAYERS
INSULATION — 0.005 in. (0.01 cm)
HEAT COLLECTOR — COIL FORM
HEAT-PIPE CONDENSER — 1.2 in. (3.0 cm) LONG (EACH END)
MOUNTING HOLE FOR #8 SCREW
HEAT-PIPE EVAPORATOR — 1.5 in. (3.8 cm) LONG

NOTE: ARROWS INDICATE HEAT PATHS
(LEADS, LEAD BRACKETS AND NEAR-SIDE HEAT PIPE CLAMPS NOT SHOWN)

Figure 3. **Double-Condenser Heat Pipes** cool these power inductors.

Tapped-Hole Vent Path

Meshing threads create a long vent path for hot, pressurized gas.

Lyndon B. Johnson Space Center, Houston, Texas

A long helical vent path safely releases hot gases from a pyrotechnically activated valve. Before it was fitted with the vent, the valve leaked pressurized pyrotechnic gases into a gas-sampler bottle, contaminating the sample and creating a potentially explosive mixture.

A schematic of the valve incorporating the vent is shown in the figure. The vent consists of a threaded hole and a mating stud. The gas vents slowly through the helical path between the threads of the hole and the stud. The outer diameter of the stud is slightly reduced to create a controlled cross-sectional area.

In the valve for which it was designed, the vent path was about 8 inches (20 cm) in length for a stud 0.62 inch (1.6 cm) long. The equivalent diameter of the threaded vent is about 0.020 inch (0.50 mm). In tests, the gases vented slowly over the long path so that they were cool enough to present no ignition hazard.

Other uses are possible for this vent. It could be used to meter the flow in refrigeration, pneumatic-control, and fluid-control systems by appropriately adjusting the size and length of the vent path.

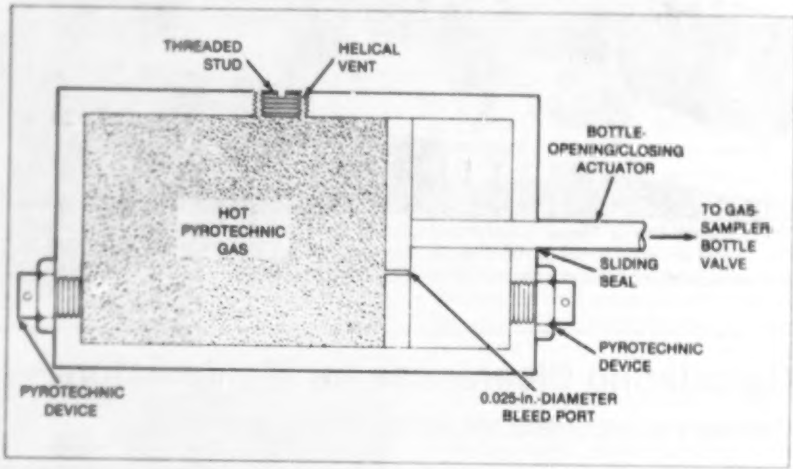

The Long Helical Vent Path cools and releases the hot pyrotechnic gas that exits along its spiraling threads. The current design uses 1/4-28 threads, with the outer diameter of the stud reduced by 0.025 in. (0.62 mm). To open or close the gas-sampler bottle, the pyrotechnic charges on either one side or the other of the valve cylinder are actuated.

This work was done by Joseph A. Chandler of ***Johnson Space Center.*** *No further documentation is available.*

Inquiries concerning rights for the commercial use of this invention should be addressed to the Patent Counsel, Johnson Space Center [see page A5]. Refer to MSC-20146.

Field Measurement of Thermal Inertia

Radiometric measurements determine thermal inertia for geologic materials.

NASA's Jet Propulsion Laboratory, Pasadena, California

A simple method and apparatus measure the thermal inertia of geologic materials in the field. Such measurements are correlated with data obtained by remote sensing, for discriminating varieties of rock encountered when exploring for minerals by aircraft or by satellites equipped with infrared scanners.

Thermal inertia (TI) is a derived property of a material; it incorporates the thermal conductivity (κ), density (ϱ), and specific heat (c) of the material and is expressed by

$$TI = \sqrt{\kappa \varrho c}$$

High values of thermal inertia indicate a high resistance to change in temperature.

The thermal-inertia meter measures the TI in situ by recording the surface-temperature rise of the materials. As can be seen from the photograph, a target and two standards are radiantly heated with calibrated quartz infrared heat lamps. Each lamp, three in all, pivots so that it can be quickly moved into position to heat the surface and removed to allow monitoring of the surface temperature. The lamps are mutually balanced by connecting them to voltage regulators.

The surface-temperature rise is monitored by an infrared radiometer. The detector head is mounted for rapid movement from reference standard to target. A portable digital voltmeter measures the voltage from the thermometer. The apparatus consists of three compartments, two for the standards and one for the target.

Comparison of the target-heating history with that of the two reference standards yields the target thermal inertia. The TI is calculated from a simple algebraic equation involving the measured quantities.

(continued on next page)

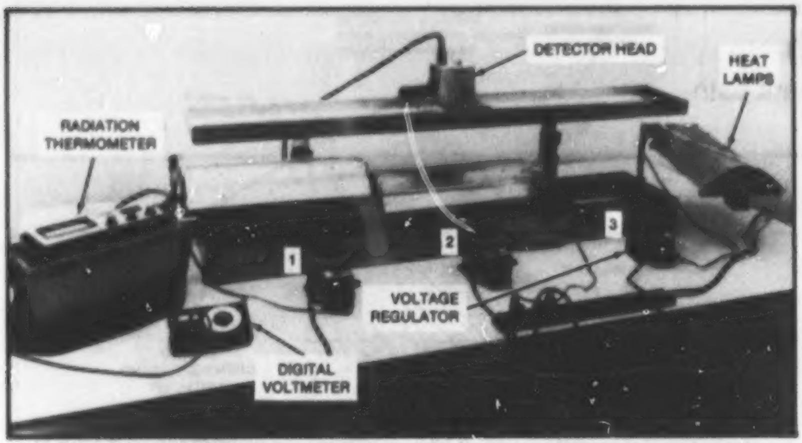

This **Thermal-Inertia Meter** apparatus includes three sample-measurement compartments that are open to the surface below. Compartments 1 and 3 contain the standards, and compartment 2 is left open to the surface to be measured.

The apparatus has been used to determine the TI of a variety of rock and soil types. The thermal-inertia reference standards chosen were geologic materials with high and low thermal-inertia values: dolomite (high) and 20/30-mesh Ottawa sand (low). The results indicate that fairly accurate values can be obtained in situ by this technique. In the field use of the TIM, such environmental conditions as wind and surface moisture must be taken into account.

This work was done by Anne B. Kahle, John P. Schieldge, and Stuart E. Marsh of Caltech for **NASA's Jet Propulsion Laboratory.** *For further information, Circle 43 on the TSP Request Card.*
NPO-15309

Calculating Clearances for Manipulators

Cylinders approximate structures and movements.

Lyndon B. Johnson Space Center, Houston, Texas

A set of algorithms rapidly calculates the minimum safe clearances for remote manipulators. Such calculations are used in the design of trajectories for manipulators to ensure that they do not accidentally strike surrounding objects — particularly important when the manipulator is sometimes out of view of its operator.

Earlier attempts to calculate manipulator clearances required excessive computer time and memory. These attempts employed accurate and detailed models of the manipulator geometry and motion. The new set of algorithms describes the manipulator and adjacent structures in terms of enclosing cylinders (see figure). The problem then becomes one of calculating the minimum clearance between finite cylinders in space.

The structural parts are considered as cylindrical shells having circular plane areas for ends. The possible kinds of contacts are then:

- Shell-to-shell
- Shell-to-circle
- Circle-to-plane
- Circle-to-circle

The algorithms exhaust the possibilities for such contacts through an executive logic scheme that can also be applied to general situations.

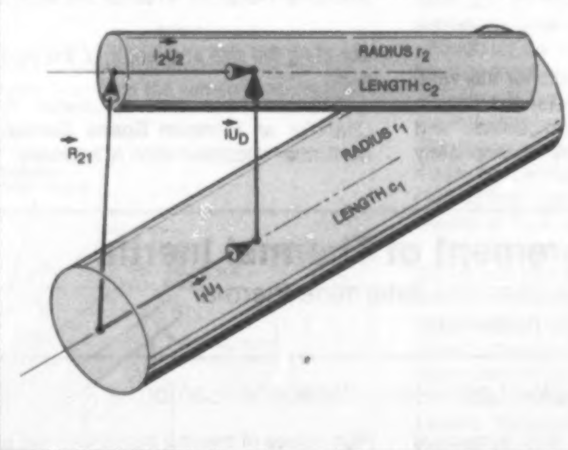
$l_2\overleftrightarrow{U_2}$
RADIUS r_2
LENGTH c_2
$l\overleftrightarrow{U_D}$
$\overleftrightarrow{R_{21}}$
RADIUS r_1
LENGTH c_1
$l_1\overleftrightarrow{U_1}$

ALGORITHMS

$\overleftrightarrow{U_D} = \text{UNIT}\,(\overleftrightarrow{U_1} \times \overleftrightarrow{U_2})$

$\overleftrightarrow{R_{21}} + l_2\overleftrightarrow{U_2} = l_1\overleftrightarrow{U_1} + l\overleftrightarrow{U_D}$

$\overleftrightarrow{U_1} \cdot \overleftrightarrow{U_D} = 0$

$\overleftrightarrow{U_2} \cdot \overleftrightarrow{U_D} = 0$

TO DETERMINE MINIMUM CLEARANCE

$d = l - r_1 - r_2$

$d > 0$

$0 < l_1 < c_1$

$0 < l_2 < c_2$

Structures Are Treated Mathematically as Cylinders for the purpose of calculating working clearances. The algorithm for the clearance between two skewed cylinders is shown here. This algorithm might be applied, for example, to find the clearance between two manipulator arms or between a crane and a tower.

Developed for the Space Shuttle remote-manipulation system, the clearance calculation method offers special benefits in industrial robotics, particularly in automated machining. Cutting tools can be described accurately as cylinders, and therefore the algorithms can predict interference efficiently. For more complex applications, surfaces of revolution may be used.

This work was done by Edward L. Copeland, John D. Peticolas, and Larry D. Ray of Lockheed Engineering and Management Services Co. for **Johnson Space Center.** *For further information, Circle 44 on the TSP Request Card.*
MSC-20208

Rod-Wall Sound Shield for Wind Tunnels

Test model is shielded from turbulence
radiated from wind-tunnel walls.

Langley Research Center, Hampton, Virginia

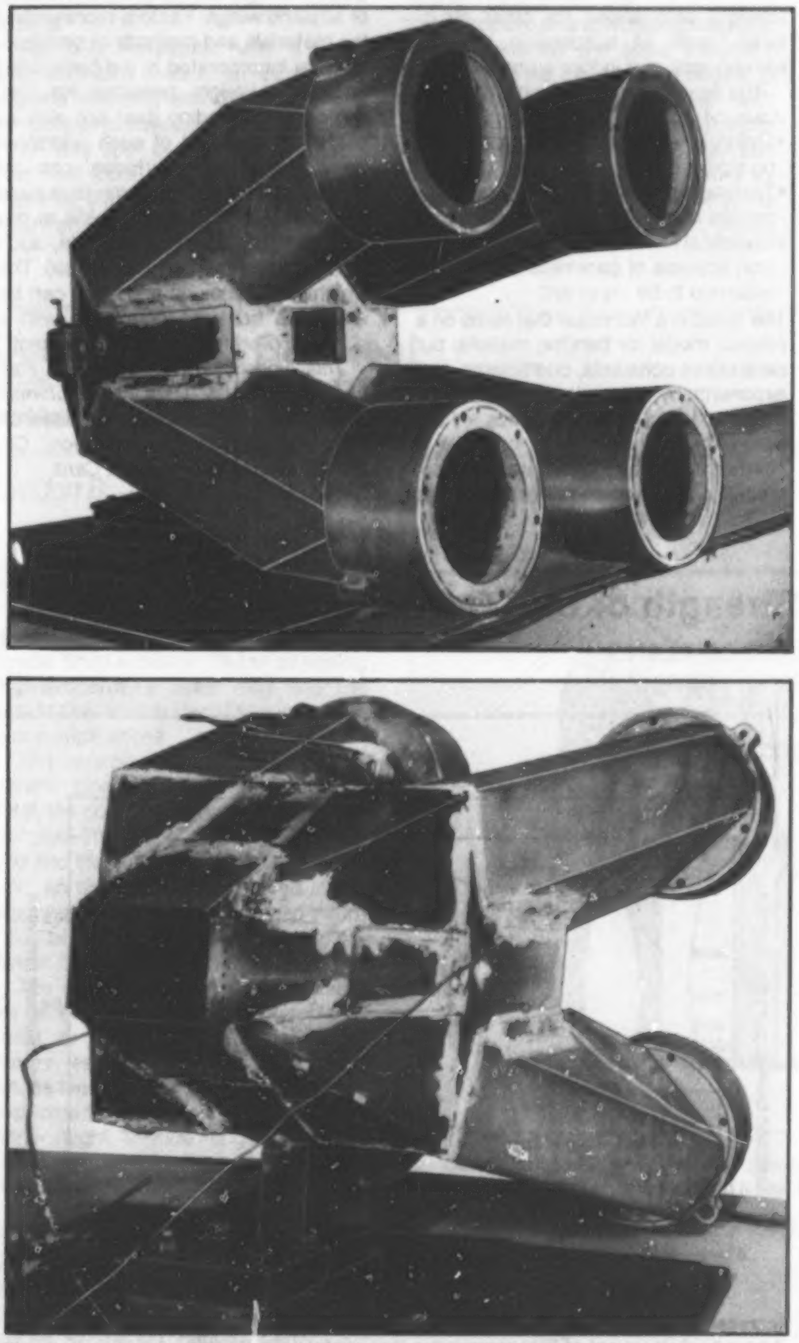

The Rectangular Rod-Wall Sound Shield shown in these two views protects models from noise radiated from wind-tunnel walls.

In supersonic and hypersonic wind tunnels, noise (pressure fluctuations) radiating from a turbulent boundary layer on the tunnel wall can cause premature transition of the model boundary layer. Two basic methods have previously been used to prevent or reduce the radiated noise. In the first, a laminar boundary layer is maintained on the tunnel wall by using longitudinal rods for the nozzle walls. Suction is applied between the rods to hold the boundary layer on the wall. The second method is to shield the model from the turbulent tunnel-wall boundary layer.

The rectangular structure shown in the figure shields an aircraft model from boundary-layer noise radiated from wind-tunnel walls. The shield is composed of four walls forming an open-ended box surrounded by a vacuum chamber. Each wall is composed of rods 0.25 inch (0.63 cm) in diameter spaced 0.040 inch (0.1 cm) apart. Vacuum pumping pulls the boundary layer around the rods, reducing the tendency of the layer to become turbulent.

The new shield overcomes problems caused by leading-edge configuration and leading-edge angle of inclination of previous designs. It has successfully maintained a laminar rather than turbulent boundary layer.

This work was done by Theodore R. Creel, Jr., and Ivan E. Beckwith of **Langley Research Center.** *Further information may be found in NASA TP-1672 [N80-26622/NSP], "Noise Reduction in a Mach 5 Wind Tunnel with a Rectangular Rod-Wall Sound Shield" [$9.50]. A copy may be purchased [prepayment required] from the National Technical Information Service, Springfield, Virginia 22161.*

This invention is owned by NASA, and a patent application has been filed. Inquiries concerning nonexclusive or exclusive license for its commercial development should be addressed to the Patent Counsel, Langley Research Center [see page A5]. Refer to LAR-12883.

Semiempirical Estimate of Aircraft Wing Weight

Method draws on theoretical equations and a data base to optimize estimates.

Ames Research Center, Moffett Field, California

A computational method estimates the weight of aircraft wings from theoretical relationships and empirical data. It permits the comparison of alternative materials, methods of construction, and design philosophies. The method can be used to make tradeoffs in preliminary design phases on the basis of simple input data and for more accurate calculations in later phases when more data are available. It eliminates the discontinuity inherent in comparing calculations made by different methods in different design phases.

The method is applicable to all types of fighter aircraft, commercial, general aviation, and others. Although developed expressly for aircraft wings, the principle can be adapted to weight and strength calculations for other structures, such as suspension bridges, warehouses, and indoor arenas.

The new method is a synthesis of previous methods:

- •Strictly theoretical techniques based on simple beam theory,
- •Techniques based on more elaborate models modified by experience, and
- •Statistical techniques based on regression analysis of parameters known or assumed to be important.

The result is a technique that relies on a rational model for bending material but determines constants, coefficients, and exponents by regression analysis to include nontheoretical influences on the box-beam weight.

The model draws on a data base representing the characteristics of 50 types of airplane wings. Factors representing the materials and methods of construction are incorporated in the basic wing equations. Weight penalties for fuel, engines, and landing gear are also included. The weight of such additional items as control surfaces can be estimated from values in the data base or from detailed data available at the final design stage (for example, such data as wing area and flap area). The weights of major components can be estimated from the data base with a standard deviation of only 8.6 percent.

This work was done by Peter York and Raymond W. Labell of Grumman Aerospace Corp. for **Ames Research Center.** *For further information, Circle 45 on the TSP Request Card.*
ARC-11435

Measuring the Tensile Strength of B/Al Composites

A proposed nondestructive technique correlates damping measurements with material strength.

Lewis Research Center, Cleveland, Ohio

The fabrication and maintenance of high-strength composite materials consisting of aluminum alloys reinforced by boron fibers are complicated by the fact that the strength of the fibers is significantly degraded by a boron/aluminum (B/Al) reaction at temperatures above 750° F (400° C). Composite material processing is often not fully documented due to unknown or complicated thermal fabrication histories. Thus, there exists a strong need to develop nondestructive test techniques for quantitatively evaluating the tensile strength of B/Al composite materials throughout the various stages of their structural lives.

Fundamental studies at Lewis Research Center have established that a principal source of the high-temperature strength degradation of B/Al composites is the diffusion of boron atoms into the aluminum matrix and the subsequent formation of a weak interfacial reaction

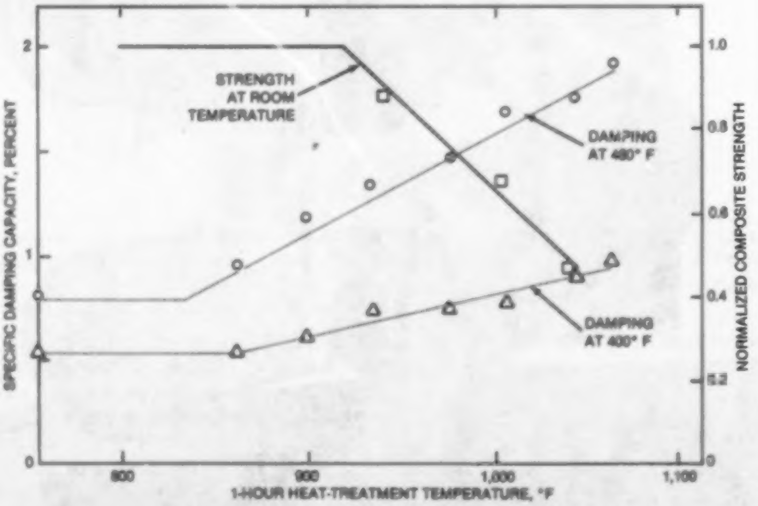

Increasing Axial Damping and Decreasing Axial Tensile Strength are observed after 1-hour heat treatment of B/Al composites that contain about 50 percent fiber. Damping was measured in a vacuum at frequencies near 2,000 Hz, and tensile strength was normalized by the maximum strength observed before thermally induced degradation.

phase on the fiber surface. Since the diffusion of small atoms such as boron is often accompanied by an increase in material damping, attempts were made to detect boron atoms within the aluminum by means of simple nondestructive damping measurements on B/Al composites that were heat-treated for 1 hour at temperatures above 750° F before testing.

For B/Al composites with a 6061-aluminum-alloy matrix, an increase in material damping was observed at test temperatures between 300° and 660° F (150° and 350° C) and stress frequencies near 2,000 Hz. As indicated in the figure by test data at 400° and 480° F (200° and 250° C), the B/6061-Al axial damping increased linearly with increasing heat-treatment temperature above 860° F (460° C). Also shown in the figure are room-temperatures results for B/6061-Al axial tensile strength after 1-hour heat treatment in the same temperature range.

Comparison of the damping and strength data shows that not only does the composite strength begin to degrade at approximately the same treatment temperature as the damping begins to increase but it also changes linearly with increasing temperature. Thus the degradation in composite tensile strength can be empirically correlated with the increase in composite damping. In terms of nondestructive evaluation, these results indicate that by developing damping-strength correlations for a B/6061-Al structure, one should be able to determine by periodic damping measurements not only the onset of thermally-induced strength degradation but also the quantitative magnitude of the structure's residual strength.

This work was done by James A. DiCarlo of **Lewis Research Center.** *Further information may be found in NASA TM-79080 [N79-16077/NSP], "High Temperature Dynamic Modulus and Damping of Aluminum and Titanium Matrix Composites" [$7.50]. A copy may be purchased [prepayment required] from the National Technical Information Service, Springfield, Virginia 22161.*
LEW-13807

Ceramic-Cord Gas Seal

High-temperature gasket material seals at temperatures above 1,100° C.

Lyndon B. Johnson Space Center, Houston, Texas

Braided cord made of ceramic fibers can form a low-pressure gas seal for temperatures up to 1,160° F (630° C). The alumina/boria/silica cord has been used as an exhaust-duct seal on the Space Shuttle orbiter. Those designing high-temperature seals may find the braided ceramic superior to asbestos in some applications.

The ceramic-cord seal between concentric pipes is shown in the figure. First, the cord is wrapped around the inner pipe. The wrapped inner pipe is then slid into the outer pipe. Following insertion, an expander tool is placed inside the inner pipe and used to expand the inner pipe, thus compressing the cord between the two pipes to form a seal.

The ceramic-fiber cord is adaptable for emergency repairs, quick replacement, or permanent installation. It requires less-stringent machining tolerances than are demanded by metal or elastomeric O-rings. Typical applications might include engine exhaust ducts or hot pipes passing through firewalls.

This work was done by Charles W. Etzel of Rockwell International Corp. for **Johnson Space Center.** *For further information, including a specification for preparing the braided ceramic cord, Circle 46 on the TSP Request Card.*
MSC-20200

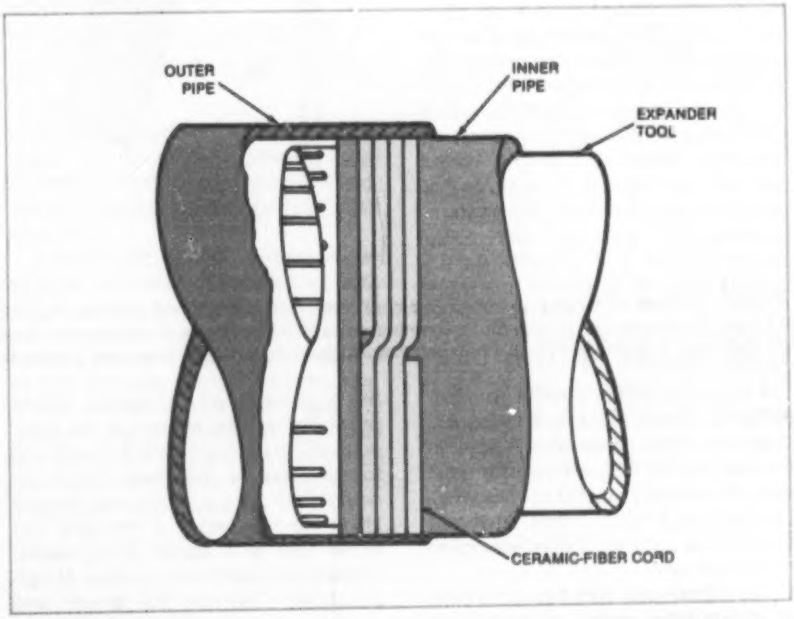

Concentric Exhaust Pipes are typical of applications in which ceramic-cord seals might be used. The cord is crushed to form a seal between the inner and outer pipes when the inner pipe is expanded into place.

Flexible Seal Accommodates Part Mismatch

Seal accommodates movement up to ½ inch as pressure is applied.

Marshall Space Flight Center, Alabama

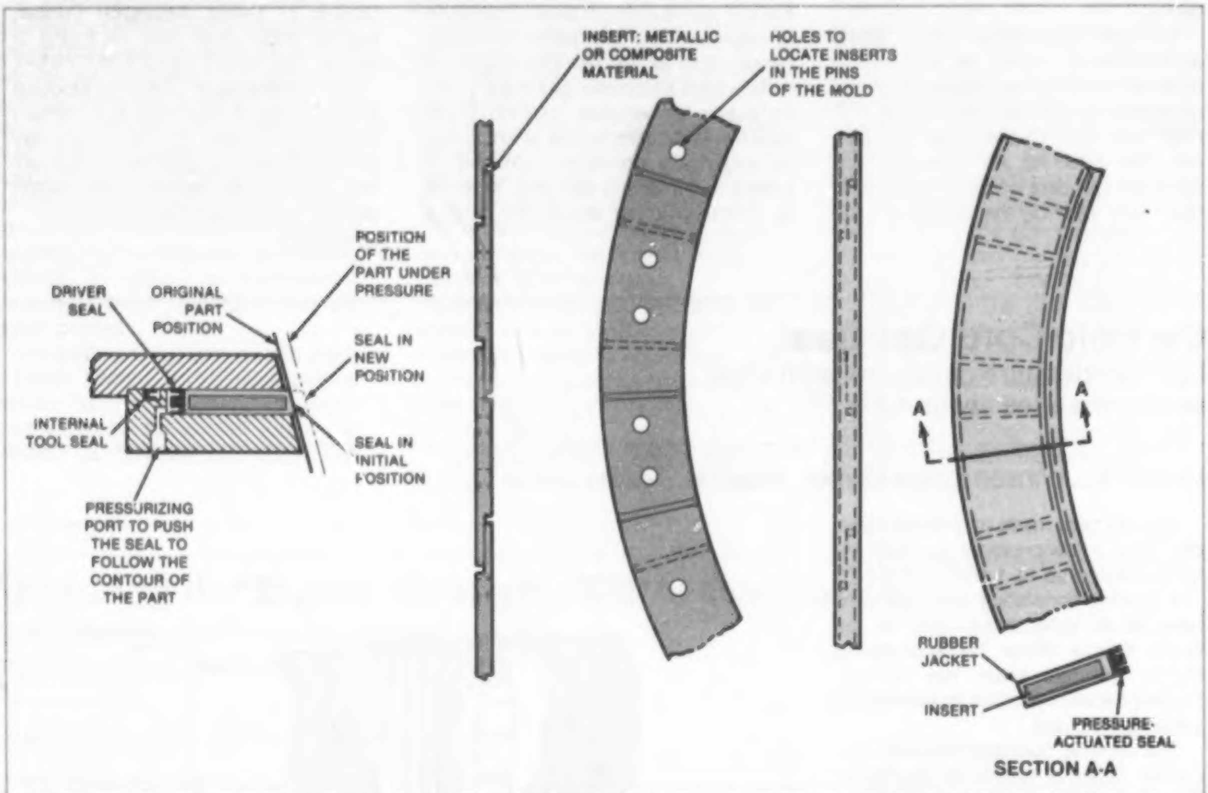
INSERT: METALLIC OR COMPOSITE MATERIAL
HOLES TO LOCATE INSERTS IN THE PINS OF THE MOLD
POSITION OF THE PART UNDER PRESSURE
DRIVER SEAL
ORIGINAL PART POSITION
SEAL IN NEW POSITION
INTERNAL TOOL SEAL
SEAL IN INITIAL POSITION
PRESSURIZING PORT TO PUSH THE SEAL TO FOLLOW THE CONTOUR OF THE PART
A
A
RUBBER JACKET
INSERT
PRESSURE-ACTUATED SEAL
SECTION A-A

A Chain of Plates embedded in the flexible seal enables it to withstand side loading of 2,300 psi (16 MPa) while sealing a gap of up to 0.5 inch (13 mm) between a cylindrical chamber wall and a test fixture. A pressure-actuated seal along the inner edge forces the seal into contact even though the cylinder wall becomes eccentric as cylinder pressure increases.

A new flexible seal deforms as needed during pressure testing of cylindrical chambers. Metal plates encapsulated in the seal enable it to withstand a pressure differential of 2,300 psi (16 MPa). Gaps up to 0.5 inch (13 mm) between a cylinder wall and a test fixture are closed by the new seal.

The primary seal (see figure) consists of overlapping metal or composite segments molded into a rubber jacket. The segments provide the rigidity needed to withstand side loads, and the rubber provides the sealing surface and the flexibility required to conform to the variable eccentric shape.

Since the primary seal must follow the constantly changing contour of the part being pressurized, a slightly higher pressure must be applied to the inner edge of the seal to enable it to seal and to withstand the side load. This is accomplished with a driver seal located along the inner edge of the seal. The driver seal is a double spring-loaded pressure-actuated configuration. At high pressures between the driver and primary seals, two split metal backup rings may be used to prevent flow of the driver seal into the rubber jacket of the primary seal.

The new seal should have many industrial applications, particularly where heat or pressure causes distortion of the chamber being sealed. This can occur when cylinder wall thickness is nonuniform or when parts of the chamber are at different temperatures. Multiple seals could be used to divide a chamber into regions of different pressures. The seal might also be used around the outside of a chamber so that external pressure could be applied.

This work was done by Imrich Bobb of Rockwell International Corp. for **Marshall Space Flight Center.** *For further information, Circle 47 on the TSP Request Card.*

Inquiries concerning rights for the commercial use of this invention should be addressed to the Patent Counsel, Marshall Space Flight Center [see page A5]. Refer to MFS-19710.

Books and Reports

These reports, studies, and handbooks are available from NASA as Technical Support Packages (TSP's) when a Request Card number is cited; otherwise they are available from the National Technical Information Service.

Theory of Compound Liquid Drops

Dynamic behavior is analyzed for a drop within a drop within an infinite fluid.

A report delves into the theory of the dynamics of compound liquid drops. Compound drops consist of three fluids: an infinitely-extending host fluid surrounding a second fluid in the form of a shell, which in turn surrounds a third, core fluid.

The report gives a theoretical basis for understanding the behavior of compound drops. It can aid in planning and interpreting experiments in the laboratory, in spacecraft, and in research aircraft. It also can provide insight into the fabrication of target pellets for nuclear fusion.

It considers the oscillations of a system when the two fluid interfaces are spherical and concentric. In particular, it examines the frequencies and relative displacement of the interfaces. The report notes that there are two types of oscillation: the "+" class, in which the two interfaces move in phase, and the "−" class, in which they move out of phase. As a core shrinks, the + modes produce oscillations of the core boundary alone, whereas the − modes produce oscillations of the outer boundary alone. It covers the equations of motion, linear approximation of the modes, the eigenvalue problem, and qualitative results.

It also contains development of the linear approximation and obtains exact solutions and linear approximations for the system velocity potential, energy, and angular momentum. It uses the energy solution to normalize the displacements and angular momentum.

The report presents numerical results for mode frequencies and interface displacements.

This work was done by Melvin M. Saffren, Daniel D. Elleman, and Won Kyu Rhim of Caltech for **NASA's Jet Propulsion Laboratory.** *To obtain a copy of the report, Circle 48 on the TSP Request Card.*
NPO-15389

Large, Easily Deployable Structures

Compactly folded structures are assembled quickly with relatively little effort.

A reported study of concepts for large space structures will interest those designing scaffolding, radio towers, rescue equipment, and prefabricated shelters.

A double-fold, double-cell module was selected for further design and for zero-gravity testing. The double-fold, double-cell concept is viable for deployment by humans outside a space vehicle as well as by a remotely operated manipulator. It was also found that rigid stops and supports should be built into the folded structure and that the members should have smooth faces so that they do not snag equipment or clothing.

The tests were carried out in a neutral-buoyancy simulator — a large, deep pool in which a weightless environment is simulated. Test operators wearing diving gear performed 15 separate tests. Test activities included unstowing (that is, releasing latches, holddowns, and other fasteners), deploying, transporting, and attaching the structural elements. In some tests, the objective was to restow the structural components from an already-assembled structure. A typical eight-step procedure for two divers was as follows:

1. Unstow first module.
2. Transport first module to aft mounting base.
3. Attach module to base at four corners.
4. Unfold first module.
5. Unstow second module.
6. Transport second module to end of previously installed module.
7. Attach second module to first module at four corners.
8. Unfold second module.

As an outgrowth of the work on manually deployable structures, there emerged a concept for self-deploying structures involving a double-fold, double-cell module system. Accessory arms are actuated to release all restraint cables around the folded structure. Cables driven by springs then open the structure and drive its elements into unfolded, locked positions. If the structure is to be self-refolding, a small 28-volt dc motor can be added to each deployment-cable reel.

This work was done by W. E. Agan of Vought Corp. for **Marshall Space Flight Center.** *To obtain a copy of the report, Circle 49 on the TSP Request Card.*
MFS-25647

Computer Programs

These programs may be obtained at very reasonable cost from COSMIC, a facility sponsored by NASA to make new programs available to the public. For information on program price, size, and availability, circle the reference letter on the COSMIC Request Card in this issue.

Trajectory-Estimation Error Analysis

Program computes errors caused by assumed values of unadjusted parameters.

The Orbital and Geodetic Parameter Estimation Error Analysis Program (ORAN) is a Bayesian least-squares simulation program for orbital trajectories. ORAN does not process data; rather, it computes the accuracy of the results of a data reduction if measurements are processed by a minimum-variance data-reduction program. Actual data may be used to provide the time when a given measurement was available and the estimated noise on

(continued on next page)

that measurement. ORAN considers a data-reduction process in which a number of satellite data periods are reduced simultaneously. If there is more than one satellite in a data period, satellite-to-satellite tracking may be analyzed.

The least-squares estimator in most orbital-determination programs assumes that measurements can be modeled by a nonlinear regression equation containing a function of assumed constant parameters and parameters to be estimated. The partitioning of parameters into those to be estimated (adjusted) and those assumed to be known (unadjusted) is somewhat arbitrary.

For any particular problem, the data will be insufficient to adjust all parameters subject to uncertainty, and some reasonable subset of these parameters is selected for estimation.

The final errors in the adjusted parameters may be decomposed into a component due to measurement noise and a component due to errors in the assumed values of the unadjusted parameters. Error statistics associated with the first component are generally evaluated in an orbital-determination program. ORAN simulates the orbital-determination processing and computes error statistics associated with the second component.

Satellite observations may be simulated with desired noise levels given in many forms, including range and range rate, altimeter height, right ascension and declination, direction cosines, X and Y angles, azimuth and elevation, and satellite-to-satellite range and range rate. The observation errors considered are bias, timing, transit time, tracking-station location, polar motion, solid-earth tidal displacement, ocean-loading displacement, tropospheric and ionospheric refraction, and space plasma. The force-model elements considered are Earth's potential, the gravitational constant, solid-earth tides, polar radiation pressure, Earth-reflected radiation, atmospheric drag, and thrust errors. The errors are propagated along the satellite orbital path.

ORAN is written in FORTRAN IV and Assembler for batch execution and has been implemented on an IBM 360-series computer with a central memory requirement of approximately 570K of 8-bit bytes. ORAN was developed in 1973 and was last updated in 1980.

This program was written by Barbara Putney of **Goddard Space Flight Center.** *For further information, Circle F on the COSMIC Request Card.*
GSC-12766

Machinery

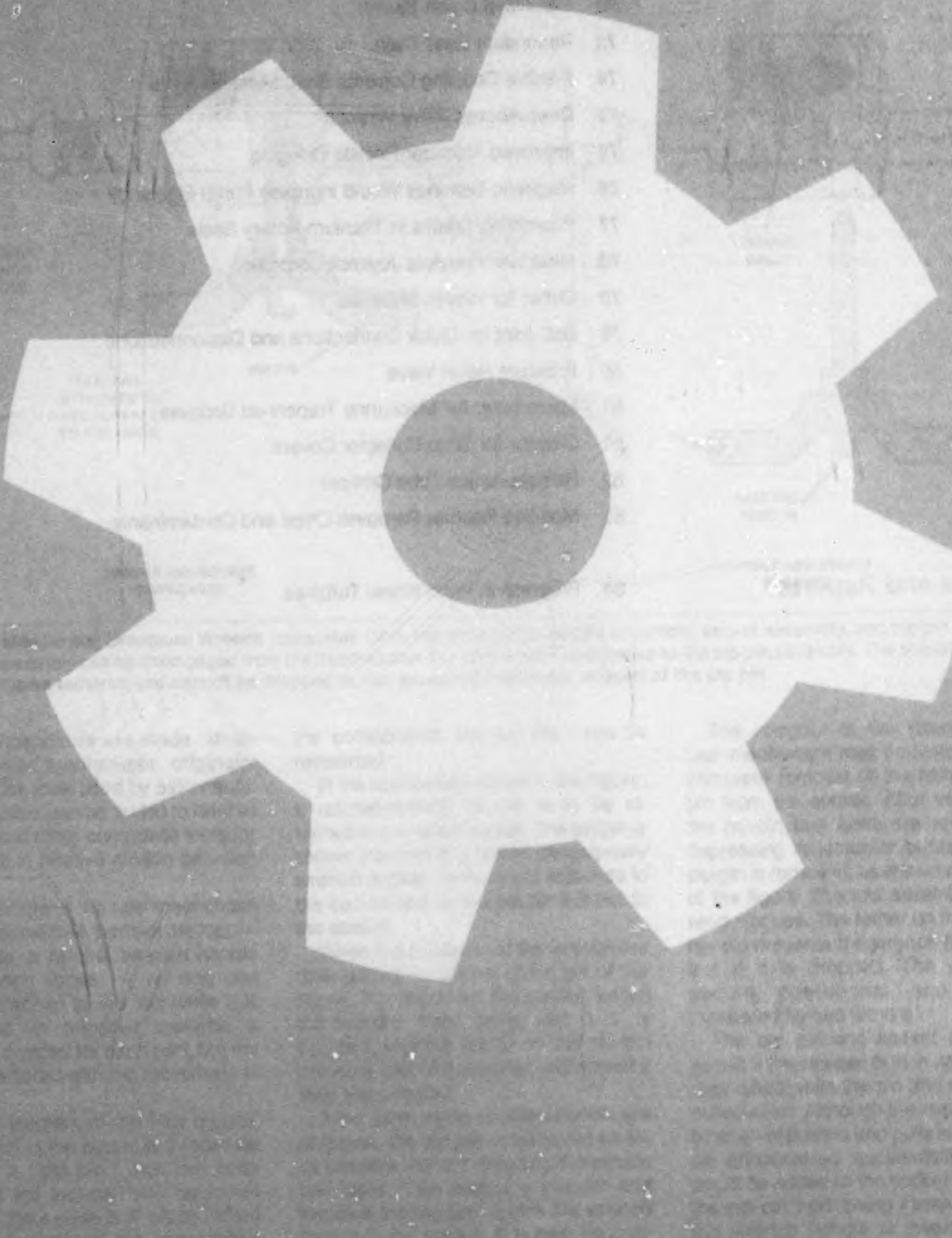

Hardware, Techniques, and Processes

69 Device Makes Handtools "Dropproof"
70 Quick-Connect, Self-Alining Latch
71 Screen Secures Detonator to Explosive Charge
72 Can-Filled Crash Barrier
73 Redundant Gear Train
74 Flexible Coupling Corrects Shaft Misalinements
75 Deep-Access Valve Wrench
76 Improved Atomizer Resists Clogging
76 Magnetic Bearings Would Increase Pump Efficiency
77 Preventing Cracks in Titanium Rotary Seals
78 Miniature Two-Axis Joystick Controller
79 Cutter for Woven Materials
79 Ball Joint for Quick Connections and Disconnections
80 Pressure Relief Valve
81 Micrometer for Measuring Trepanned Grooves
81 Cleaner for Solar-Collector Covers
82 Remote-Action Tube Crimper
83 Modified Reamer Removes Chips and Contaminants

Books and Reports

84 Progress in Wind-Wheel Turbines

Device Makes Handtools "Dropproof"

Wrench handle and socket cannot be separated unless both are tethered.

Lyndon B. Johnson Space Center, Houston, Texas

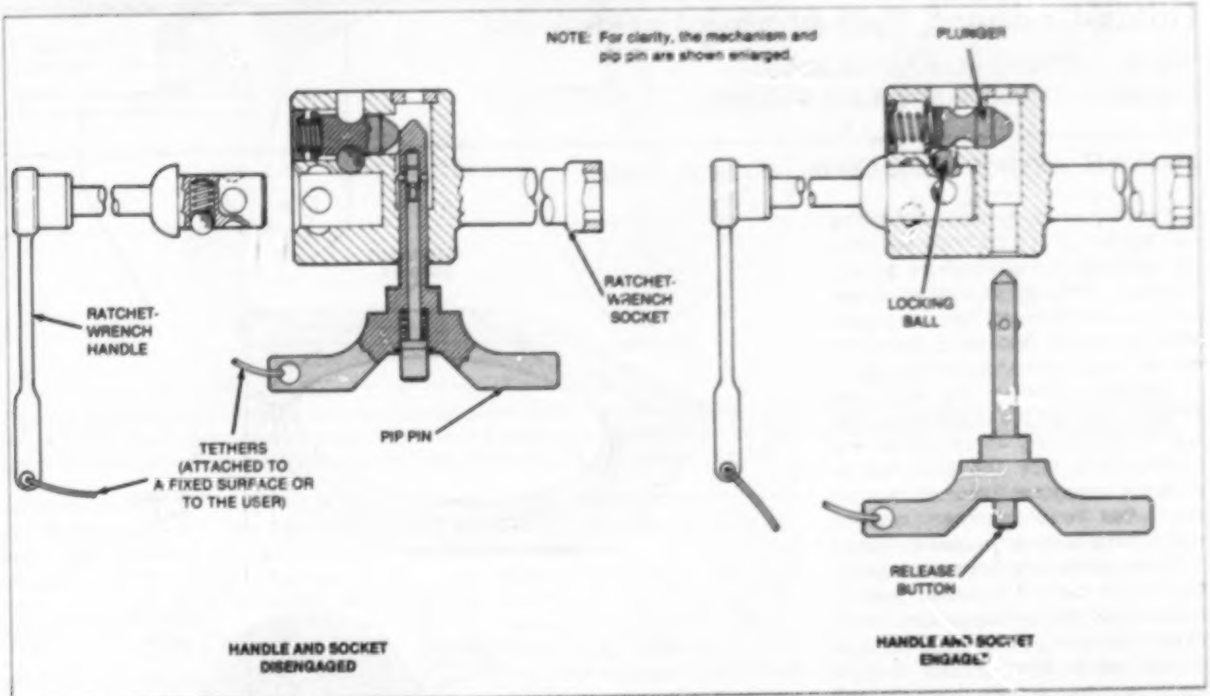
NOTE: For clarity, the mechanism and pip pin are shown enlarged.
PLUNGER
RATCHET-WRENCH HANDLE
RATCHET-WRENCH SOCKET
LOCKING BALL
PIP PIN
TETHERS (ATTACHED TO A FIXED SURFACE OR TO THE USER)
RELEASE BUTTON
HANDLE AND SOCKET DISENGAGED
HANDLE AND SOCKET ENGAGED

Interchangeable-Socket Dropproof Wrench comprises three essential parts: handle assembly, socket assembly, and pip-pin assembly. The socket assembly can be disengaged from the handle assembly only when it is engaged to the pip-pin assembly. The socket assembly therefore remains tethered and cannot be dropped or lost except by deliberate removal of the pip pin.

Two-part handtools are made "dropproof" by a mechanism originally developed for tools used by astronauts. The mechanism can be added to ratchet wrenches and other composite tools for which there is relative motion between the parts.

An advantage of the new mechanism is that it secures both parts of the tool — for example, a ratchet wrench handle and a wrench socket — yet only one tether is attached to the tool while it is being used. In previous systems, a tether was needed for each part, but the tethers interfered with the movement of the parts.

The key element of the new mechanism, shown in the figure, is a retaining pin called a "pip pin." The two components of the tool can only be joined together if the pip pin is in place. When the pip pin is removed, the components become locked together. To separate the components, the pip pin must be reinserted.

In the application shown in the figure, a ratchet-wrench handle is to be attached to a wrench socket. The pip pin is shown inserted in a drilled passageway wrench socket. Tethers are attached to the handle and to the pip pin but not to the socket.

When the two parts of the wrench are disengaged, as shown at the left of the figure, the tether on the handle keeps the handle from being lost if it is dropped; and the tether on the pip pin prevents loss of the pip pin and socket if they are dropped.

After both parts of the wrench are engaged, the pip pin is extracted as far as possible without releasing the pip-pin ball locks. This lowers a plunger and forces a locking ball to lock the wrench handle in the socket. It is then impossible to disengage the parts.

The integrity of the wrench-socket lock mechanism may be tested prior to complete removal of the tethering pip-pin from the socket. After verification, the pip-pin ball locks are released by depressing its actuator button and the pip-pin is removed, as shown at the right of the figure. The tool assembly is now ready for use. The tether on the wrench handle prevents the wrench from being lost if it is dropped. The wrench is secure, operational, and not encumbered by two tethers.

The pip pin and socket are disengaged if the release button on the pin is depressed while the pin and socket are pulled apart. Although the required combination of pushes and pulls is unlikely to be encountered accidentally, a pawl could be added to the socket to prevent the pip pin from being removed unless the wrench handle is inserted in the wrench socket.

(continued on next page)

The dropproof tool is useful wherever the loss of a component would be inconvenient or hazardous. It can be used by divers, for example, and by people working on scaffolds. The mechanism is easily operated by technicians wearing thick gloves, space suits, diving suits, or other protective attire.

This work was done by Bruce McCandless II of **Johnson Space Center.** *For further information, Circle 50 on the TSP Request Card.*

This invention is owned by NASA, and a patent application has been filed. Inquiries concerning nonexclusive or exclusive license for its commercial development should be addressed to the Patent Counsel, Johnson Space Center [see page A5]. Refer to MSC-20319.

Quick-Connect, Self-Alining Latch

Sturdy latch tolerates 10° of angular mismatch in joining structural elements.

Lyndon B. Johnson Space Center, Houston, Texas

A latch originally developed for joining two spacecraft in orbit holds securely, yet connects and disconnects quickly. The latch has possible uses as a pipe joint, as a connector for the parts of portable structures, and as a fitting for marine risers on offshore drilling rigs.

The passive half of the latch (see Figure 1) consists of a simple hexagonal frame containing three alinement grooves on its face. The active half includes a hexagonal frame on support struts that bears alinement keys to match the grooves in the passive frame.

Three slanting triangular plates guide the passive frame to its nested position in the active frame. The passive frame actuates proximity switches in the face of the active frame (Figure 2). The switches in turn actuate solenoids that release latches in the guide plates so that they capture the passive plate.

Once released, the latches are driven by springs to the "capture" position. Then the latch drive actuators pull the latch drive links down to engage the alinement keys and clamp the two frames together. Small motors retract the latches when it is necessary to release the passive frame. Dual solenoids, springs, and motors for each latch mechanism ensure that the latch operates even if one of a pair of components is defective.

Lateral and forward closing velocities between passive and active plates can be as much as 0.1 ft/s (3 cm/s). Pitch, roll, and yaw of 1° per second are acceptable. A lateral mismatch of 4 inches (10 cm) between passive and active plates can be accommodated, as can an angular mismatch of 10° in pitch, roll, and yaw. After mating, the angular mis-

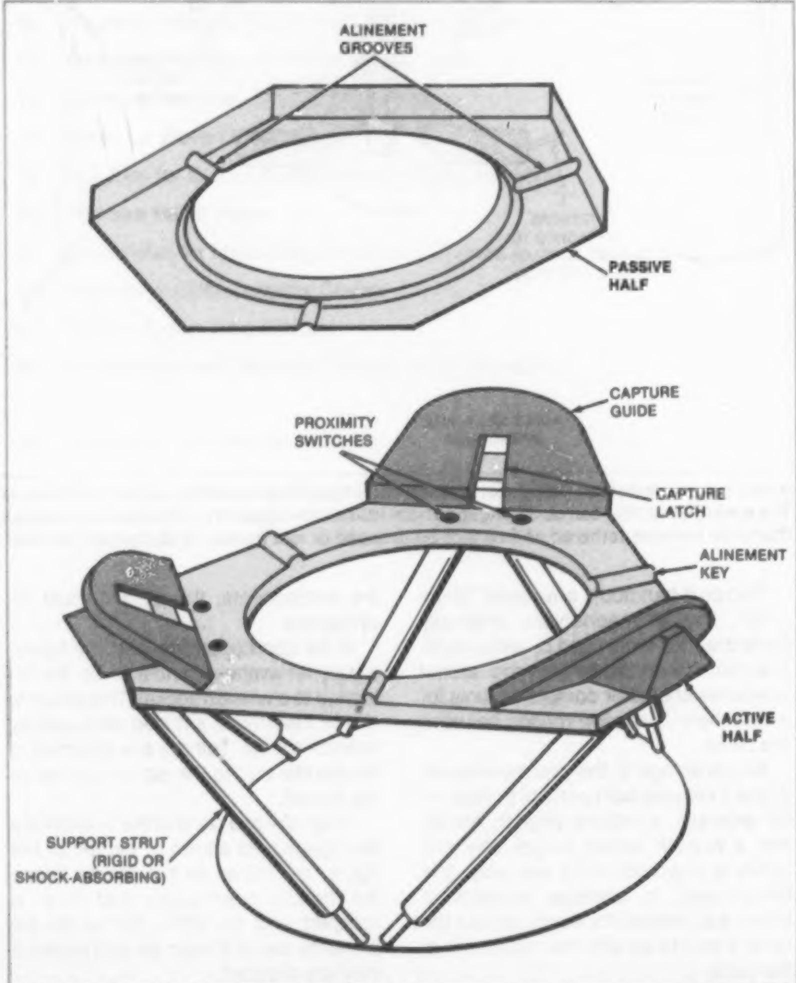

Figure 1. **Hexagonal Passive Plate Nests** in active plate, guided by capture plates and alinement keys and grooves. The center hole in both active and passive plates is 1 meter in diameter.

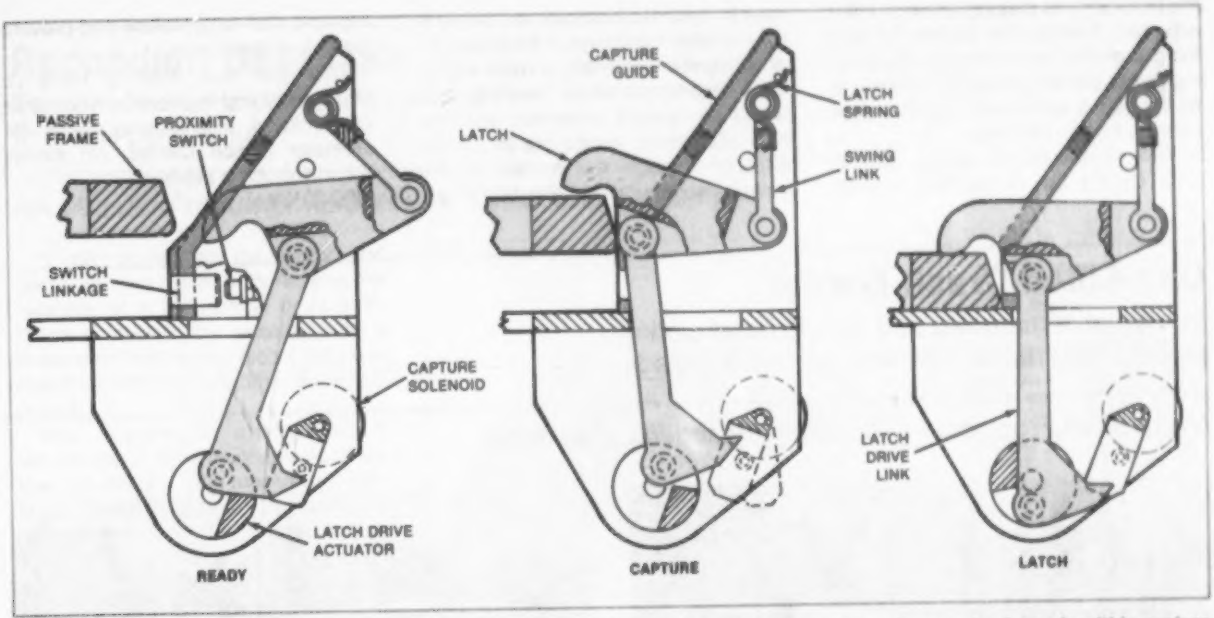

Figure 2. **In the Ready Position,** a latch is retracted below the surface of the capture guide. When the passive frame is within capture range, it actuates three or more of the six proximity switches on the active frame, causing the latches to move to the capture position. Latch drive actuators pull the latch drive link down, clamping the two frames together.

alinement in pitch, roll, and yaw is within ± 1.32 minutes of arc. After mating, the latch can withstand a thrust load of 20,000 lb (90,000 N) and moments in pitch, roll, and yaw of 16,000 lb-ft (22,000 m-N).

The active half of the latch operates on 28 to 33 volts dc. The peak power consumption during latching is 1,000 watts; no power is drawn before and after latching. In case of a power failure, the latch can be operated manually by means of a crank.

The weight of the active half, including controls, is less than 200 lb (91 kg). The weight of the passive half is less than 50 lb (23 kg). Switches on the active half control indicator lamps that show progressively that the latch is ready to berth, the capture is complete, and the latch mechanisms are secure.

The support struts on the active half are rigid. However, they can be replaced by shock mounts if energy absorption is required.

This work was done by Gene C. Burns and Edward J. Williams of McDonnell Douglas Corp. for **Johnson Space Center.** *No further documentation is available.*
MSC-20205

Screen Secures Detonator to Explosive Charge

The distance between cap and charge is easily controlled with a brass-screen sleeve.

Lyndon B. Johnson Space Center, Houston, Texas

A brass-screen sleeve (see figure) attaches a blasting cap to a fuse, shaped charge, detonating cord, or other formed explosive. The screen makes it easy to control the distance between the cap and the charge, because the user can see both parts, and to cool the cap by convection, making the use of low-cost blasting caps possible for some hot environments. Previously, a wooden spool was used to connect the parts.

To attach the cap to the charge, the brass-screen sleeve is positioned over

(continued on next page)

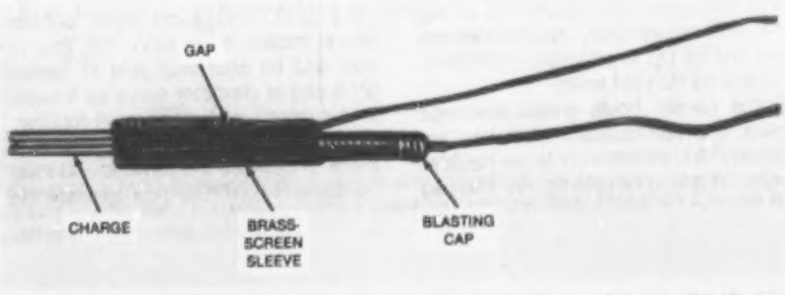

The **Brass-Screen Sleeve** allows the user to adjust visually the gap between the charge and the blasting cap.

the parts and the spacing between them adjusted. Twisting the screen tightens the grip on the cap and charge. By pouring glue or cement through the screen to fill the gap, a permanent cap-to-charge connection can be made.

With temperatures above 300° F (150° C), the use of standard blasting caps to detonate pyrotechnic charges is very unreliable because of the possibility of autoignition; normally, a more-expensive high-temperature blasting cap would be needed. However, with the new attachment, a cold gas jet can be directed through the screen at the charge/cap interface to maintain an acceptable cap temperature and prevent premature detonation.

This work was done by Harry D. Moshenrose and Raymond A. Kindsfather of Rockwell International Corp. for **Johnson Space Center.** *No further documentation is available.*
MSC-20138

Can-Filled Crash Barrier

Inexpensive materials and simple construction protect motorists at low and moderate speeds.

NASA's Jet Propulsion Laboratory, Pasadena, California

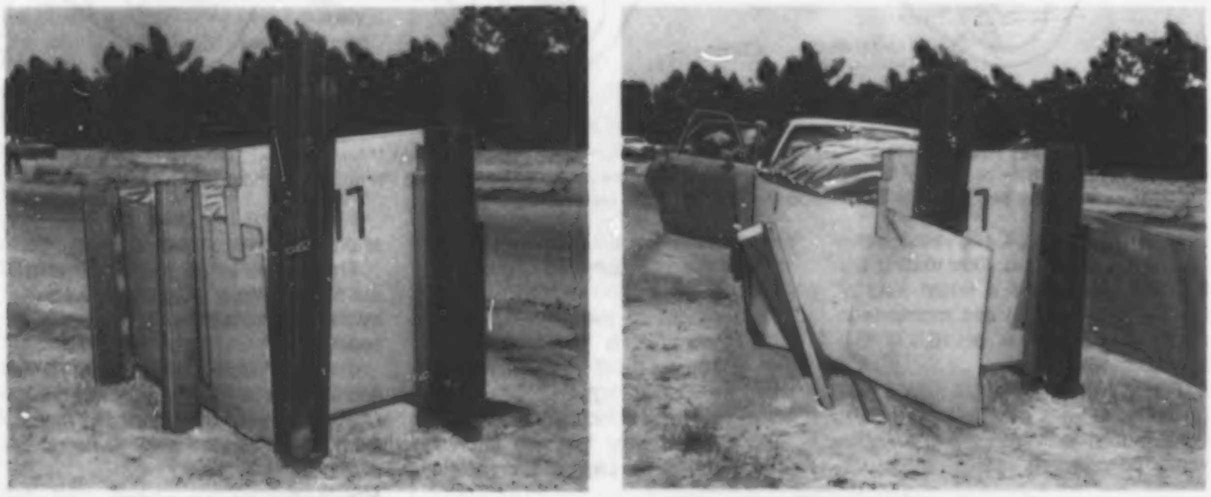

This **Collapsing Crash Barrier** is filled with empty beverage cans that collapse and thereby absorb the vehicle kinetic energy.

A crash barrier composed largely of used aluminum beverage cans protects the occupants of cars in collisions with poles or trees. Tested at NASA's Jet Propulsion Laboratory, the lightweight, can-filled barrier was very effective in softening the impact of an automobile in head-on and off-angle collisions. A professional test driver experienced only brief discomfort and no injuries during the tests. Preliminary results indicate that the barrier is effective in collisions up to a 40 mi/h (64 km/h).

The barrier holds empty beverage cans in a tear-resistant cloth bag encased in a collapsible container made of plywood and steel (see figure). The bag is flame-retardant and weather-resistant. Cans in the front part of the barrier bag are randomly oriented, and cans in the rear are oriented parallel to the direction of a head-on collision.

The barrier used in the tests is 6 ft (1.8 m) long, 3 ft (0.9 m) high, and 3½ ft (1.1 m) wide. Its side panels slide past its backstop as a car hits. Two 4-by-6-inch (10.2-by-15.2-cm) wood posts prevent lateral motion or rotation. The tree or pole and an additional pole 11 inches (27.9 cm) in diameter serve as a backstop support and further resist rotation.

When a car strikes the barrier, it starts to collapse the plywood-and-steel container, which in turn compresses the cans. The energy of the car is absorbed by the buckling metal of the cans and by air within the cans as it is compressed.

Accelerometers on the car frame and the driver's helmet measured acceleration during impact, and high-speed motion-picture cameras photographed the crashes. Impact against barriers of 55-gal (208-l) cans was harder than against the new collapsing barrier, according to both measured data and the driver's subjective experience.

This work was done by Abraham H. Wilson of Caltech for **NASA's Jet Propulsion Laboratory.** *For further information, Circle 51 on the TSP Request Card.*
NPO-15188

Redundant Gear Train

Tandem harmonic drives are immune to single-point failure.

NASA's Jet Propulsion Laboratory, Pasadena, California

Simply duplicating the motor and gears does not significantly improve the reliability of a mechanical drive train. There is always the possibility of a single-point failure, in which a failure in one drive path jams the other drive path as well.

Now, however, an arrangement of two harmonic drive mechanisms offers true redundancy. One mechanism continues transmitting power regardless of how the other fails. Besides being highly reliable, the dual harmonic drive is compact, occupying a smaller volume than a conventional gear train for the same power and speed reduction.

The harmonic drive is a simple compact gear system for achieving large speed reductions and large output torques. The "pancake" harmonic drive, used here, includes four main elements as shown in Figure 1. The wave generator is the input member, and either circular spline can serve as the output member. Speed reduction is achieved by engagement of a differential number of teeth on the flexible spline and stationary circular spline.

The redundant gear trains are shown schematically in Figure 2. Motor 1 drives spur gear No. 1 and an inner shaft. The inner shaft (to harmonic drive 1) passes through the center of a hollow outer shaft and continues through harmonic drive 2 without physical contact. The inner shaft is connected to the input of harmonic drive 1 through a cone clutch. The clutch is nonfunctional during normal operation. The clutch provides a redundant point of relative motion within the system 1 drive train and is required only when nonbackdrivable input gears are used.

When operation of system 2 is desired, the motor 2 drives spur gear 2, which rotates the input shaft to harmonic drive 2. That input shaft is located concentrically around the system 1 drive shaft. The input drive elements of system 1 and system 2 are totally separate and noncontacting. However, the operation of system 2 causes the entire

(continued on next page)

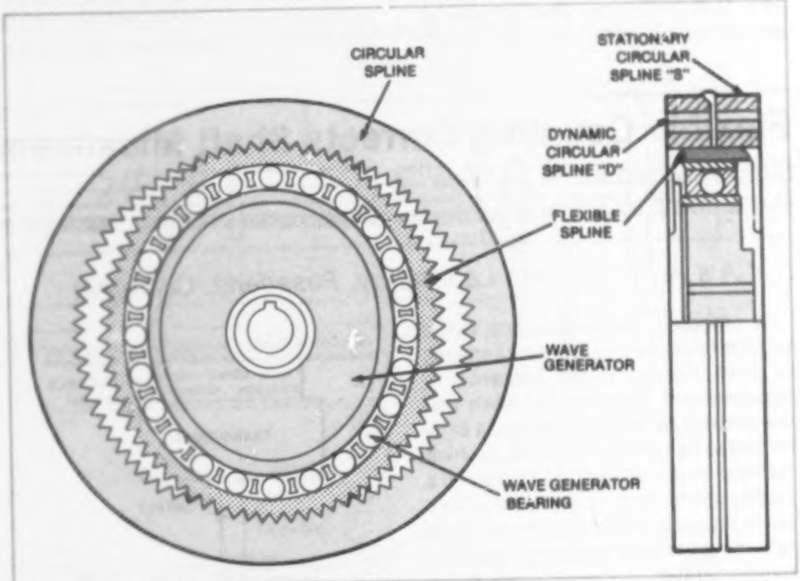
CIRCULAR SPLINE
STATIONARY CIRCULAR SPLINE "S"
DYNAMIC CIRCULAR SPLINE "D"
FLEXIBLE SPLINE
WAVE GENERATOR
WAVE GENERATOR BEARING

Figure 1. In a **Harmonic Drive Mechanism,** the combination of an elliptical wave generator and a tooth differential between the flexible spline and the circular spline produces a rotational speed reduction in a compact volume.

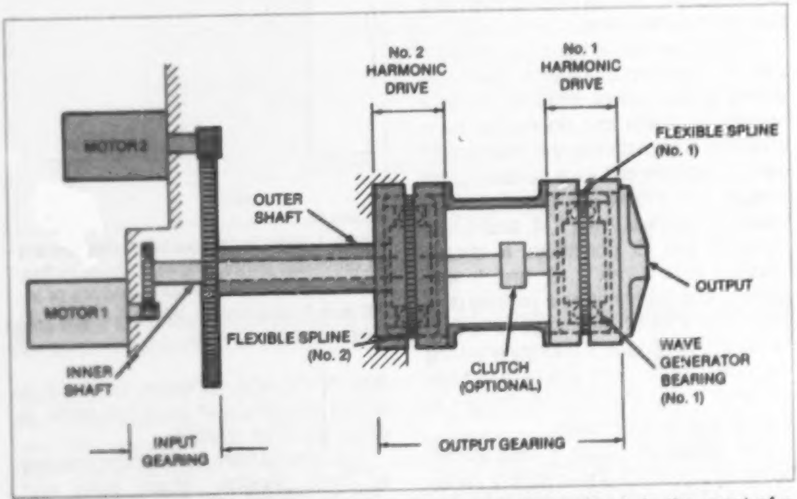
No. 2 HARMONIC DRIVE
No. 1 HARMONIC DRIVE
FLEXIBLE SPLINE (No. 1)
MOTOR 2
OUTER SHAFT
OUTPUT
MOTOR 1
FLEXIBLE SPLINE (No. 2)
CLUTCH (OPTIONAL)
WAVE GENERATOR BEARING (No. 1)
INNER SHAFT
INPUT GEARING
OUTPUT GEARING

Figure 2. A **Fully Redundant Drive** is normally operated by motor 1. In the event of a failure in drive train 1, however, motor 2 operates harmonic drive 2 via shaft 2, which is concentric with drive train 1.

system 1 harmonic drive to rotate as a single mass. The torque produced by system 2 is transmitted across harmonic drive 1 by the tooth mesh of flexible spline 1.

If motor 1 or any of the elements it drives should fail to rotate, motor 2 may be turned on, and the output shaft can still be rotated via the system 2 gear train. Both motors can also be operated simultaneously, and in that case the output rotational speed will be about twice that for single-motor operation. The output torque will be the same as for single-motor operation.

This drive train can also be designed to be "backdrivable." The term "backdriving" refers to the condition in which a torque applied at the output shaft of a nonoperating electromechanical drive will cause rotation of the unit input shaft and motor. The backdriving action does not damage either system, and in applications where torque limiting or manual override is required, a backdrivable configuration can satisfy those requirements.

This work was done by Douglas T. Packard of Caltech for NASA's **Jet Propulsion Laboratory.** *For further information, Circle 52 on the TSP Request Card.*
NPO-15317

Flexible Coupling Corrects Shaft Misalinements

Simple slotted tubes perform like a complex linkage.

NASA's Jet Propulsion Laboratory, Pasadena, California

A proposed flexible coupling would provide nearly error-free measurements of shaft rotation in the presence of misalinements between the shaft and the position-sensing transducer. It is intended to be used in situations in which the input or output shaft is mounted on a flexible joint. Its function is to insure equal input and output angular velocities by forcing the input and output shafts to remain parallel.

The coupling consists essentially of a concentric pair of cylinders that act as a flexible link between two shafts (Figure 1). The cylinders are machined and fastened together so that they function as a pair of universal joints.

The mechanism is based on Hooke's joint — the simple universal joint consisting of two yokes attached to their respective shafts and connected by a crossbar. Kinematically, the mechanism can be represented as a parallelogram linkage with Hooke's joints at its vertexes. In Figure 2, links 2, 4, and 5 with joints A and B constitute a double Hooke's joint. Links 2, 3, and 5 with joints C and D constitute a parallel double Hooke's joint. The linkage A, B, C, D forms a parallelogram, thereby ensuring that output shaft 5 remains parallel to input shaft 2 and that both shafts turn at the same angular velocity.

The linkage in Figure 1 uses slotted tubes to construct the Hooke's joints. Flexure at the slots corresponds to joint motion in the kinematic representation. The rods that join the inner and outer tubes keep the tube ends parallel, thus implementing the "rigid single links" seen in Figure 2. The concentric-tube construction is accurately concentric and parallel and is rigid in torsion. It is simple and, because of its few parts, is expected to be reliable.

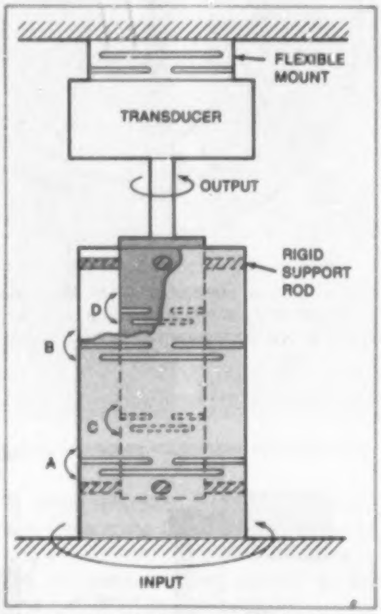

Figure 1. **Slots in Concentric Cylinders act as universal joints, allowing them to flex and compensate for misalinements of input and output shafts. Walls A-B and C-D always remain parallel.**

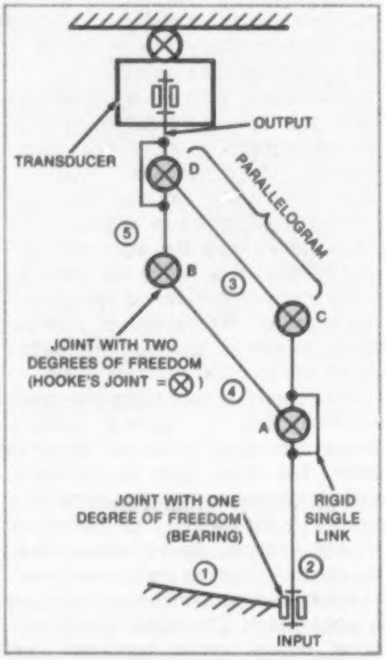
OUTPUT
TRANSDUCER
D
PARALLELOGRAM
⑤
B
③
C
JOINT WITH TWO DEGREES OF FREEDOM (HOOKE'S JOINT = ⊗)
④
A
JOINT WITH ONE DEGREE OF FREEDOM (BEARING)
RIGID SINGLE LINK
①
②
INPUT

Figure 2. **Linkage Composed of Universal Joints** (Hooke's joints) **ensures that opposite sides of the parallelogram ABDC remain parallel. The height of the parallelogram is exaggerated here; actually, the sides would be almost collinear.**

The mechanism can accommodate all three possible (small) input- and output-shaft misalinements — lateral, angular, and axial — in any combination. Moreover, any or all of these misalinements can vary in magnitude and direction.

The coupling concept was originally developed for antenna-position control systems. It may also find application in machinery having higher rates of rotation than the antenna.

This work was done by Robert A. Mayo of Caltech for **NASA's Jet Propulsion Laboratory.** *For further information, Circle 53 on the TSP Request Card.*
NPO-15393

Deep-Access Valve Wrench

A rod attached to an extension pipe holds the wrench jaw against the valve stem.

John F. Kennedy Space Center, Florida

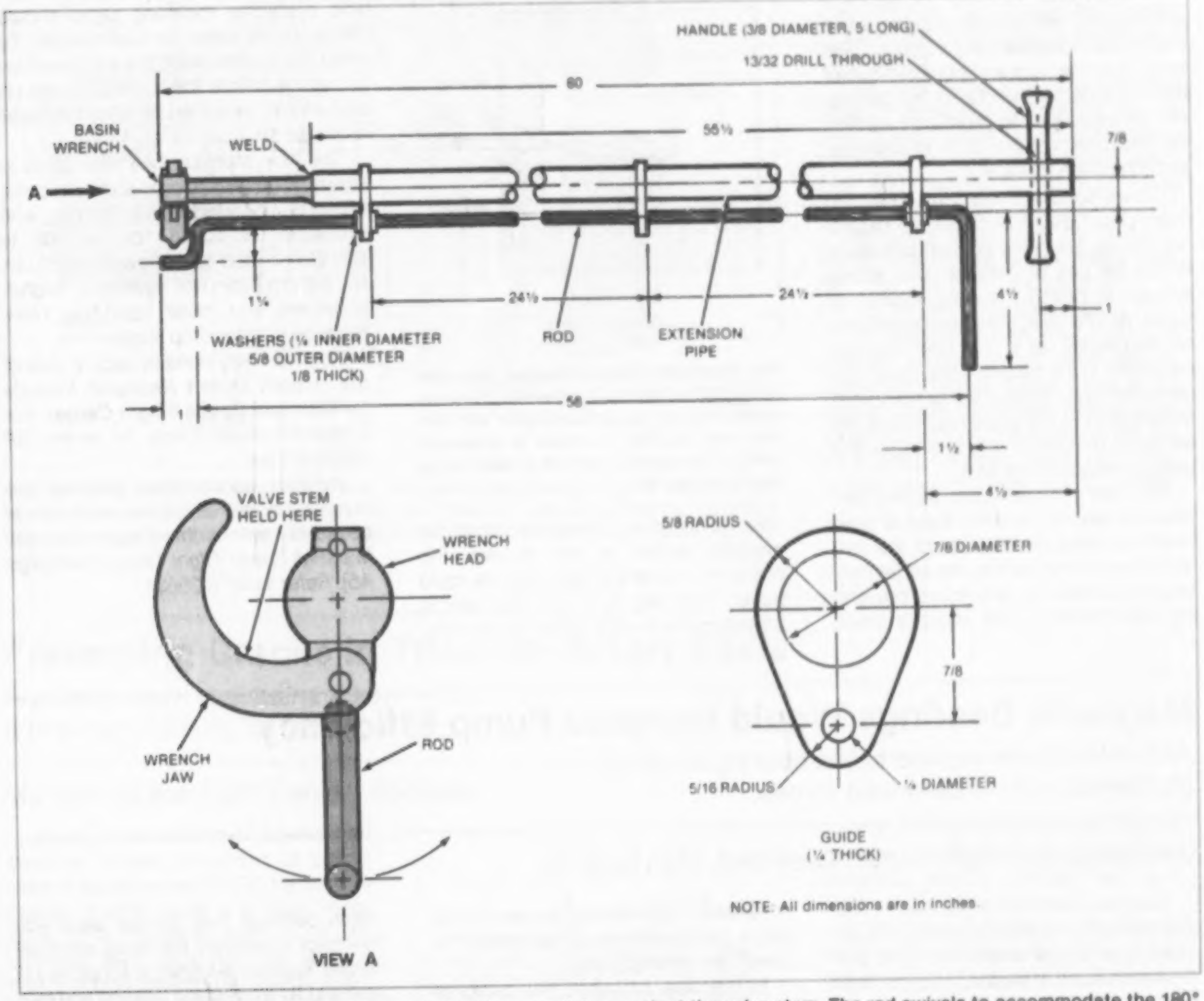
HANDLE (3/8 DIAMETER, 5 LONG)
13/32 DRILL THROUGH
60
BASIN WRENCH
WELD
56½
7/8
A
1¼
24½
24½
4½
1
WASHERS (¼ INNER DIAMETER 5/8 OUTER DIAMETER 1/8 THICK)
ROD
EXTENSION PIPE
1
58
1½
4½
VALVE STEM HELD HERE
WRENCH HEAD
WRENCH JAW
ROD
VIEW A
5/8 RADIUS
7/8 DIAMETER
7/8
5/16 RADIUS
¼ DIAMETER
GUIDE (¼ THICK)

NOTE: All dimensions are in inches.

The **Bent Rod on the Modified Basin Wrench** holds the wrench jaw against the valve stem. The rod swivels to accommodate the 180° rotation of the wrench jaw. Valves 5 feet (1.5 meters) underground can be operated with the tool.

A modified basin wrench makes it easier to open and close valves in deep valve boxes. Underground water valves, with broken or corroded handles can be operated with the tool.

The basin wrench is modified by a long handle and a rod for holding the wrench jaw against the valve stem (see figure). To extend the reach of the wrench, a 55-1/2 inch (1.4 m) length of 1/2-inch (1.3-cm) galvanized pipe is welded to its shaft. Welded to the pipe are three stainless-steel guides that hold the stainless-steel rod, 1/4 inch (0.64 cm) in diameter. Three stainless-steel washers are tack-welded to the rod, near the guides, to keep it from sliding away from the wrench jaw.

The rod swivels to hold the jaw of the wrench against the valve stem for both opening and closing the valve. At its bottom, the rod bends outward 1-1/4 inches (3.2 cm) and then turns down for 1 inch (2.5 cm) to form a surface that can butt against the wrench jaw; at its top, the rod bends outward 4-1/2 inches (11.4 cm) to provide a handle for maneuvering the bottom portion. A steel handle near the top of the pipe extension helps to turn the wrench.

This work was done by Harold E. Fleck of Boeing Services International, Inc., for **Kennedy Space Center.** *No further documentation is available.*
KSC-11229

Improved Atomizer Resists Clogging

A simple new design eliminates clogging.

Marshall Space Flight Center, Alabama

An improved atomizer produces a uniform mist with droplet concentration that remains substantially constant over time. The fine mist and constant-output make it especially useful for the generation of aerosols, cloud-physics studies, the production of thin uniform coatings, and inhalation therapy.

Conventional atomizers are subject to output fluctuations because the gas/liquid mixing passages contain spaces in which the gas or mixture flows slowly enough to permit the accumulation of liquid. At intervals, the accumulated liquid is caught up in the flow, causing variations in the output. If the liquid contains dissolved solids (for example, salt), evaporation of the liquid may cause the solids to deposit in the passages and possibly obstruct the flow.

The new atomizer (see figure) contains no spaces in which liquid or solid could accumulate. Because of the conical shape of the orifice, the air jet continually sweeps out any liquid, preventing accumulation. The liquid is channeled to the jet in a steady stream by the capillary action of the groove, the pressure drop in the flow, and the liquid pump. The regularity of the flow is limited mainly by that of the liquid pump, and a precise metering pump should therefore be used for best results. To keep the nozzle clear, the air should be turned on before the liquid is turned on and should be turned off after the liquid is turned off.

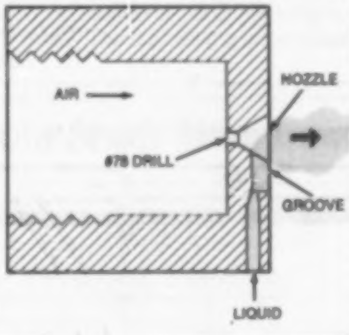

The Improved Constant-Output Atomizer has a conical orifice that permits the air to sweep out all liquid thoroughly and prevent any buildup of liquid or dissolved solids. The capillary groove guides the liquid to the gas jet.

The new atomizer has been used to make mists with micron-sized droplets. It can be operated in any position, with pressures of 10 to 100 psi (69 to 690 kN/m^2) and liquid-flow rates of 0.05 to 2.0 cm^3/min. In general, higher pressures and lower liquid-flow rates produce smaller drop sizes.

This work was done by Jack Y. Dea of the Nevada Desert Research Institute for **Marshall Space Flight Center.** *For further informatin, Circle 54 on the TSP Request Card.*

Inquiries concerning rights for the commercial use of this invention should be addressed to the Patent Counsel, Marshall Space Flight Center [see page A5]. Refer to MFS-25631.

Magnetic Bearings Would Increase Pump Efficiency

Active feedback applied to the bearing windings compensate for unbalanced forces.

Goddard Space Flight Center, Greenbelt, Maryland

Magnetic bearings would make a two-element rotary pump more efficient, according to a new proposal. In the concept developed at Goddard Space Flight Center, active feedback applied to the bearing windings would compensate for rotor displacements. The result would be lower friction and less backflow.

In the proposed compressor (see figure), counterrotating tapered screws force the gas through a tapered chamber, decreasing the gas volume until it discharges at higher pressure from the exit port. Ideally, the screws rotate without touching each other or the walls of the chamber and the motors are synchronized. Frictional losses are minimal, and a clearance seal is maintained between the moving parts.

In practice, however, the compression and transport of the gas create unbalanced radial and axial forces that displace the screws from their equilibrium positions. These forces tend to throw the drive motors out of synchronization. The result is higher frictional losses, gas leakage back toward the inlet port, and an overall lowering of efficiency.

Although conventional bearings cannot compensate for these effects, magnetic bearings are ideal for this configuration because they can be used with feedback to balance the radial and axial forces. Each screw shaft is supported at one end by a magnetic bearing and by a drive motor with radial control at the other end. Capacitive elements sense the axial and radial displacements of the shafts and develop error signals that are converted to changes in magnetic flux in the bearing and motor windings. The phases of these error signals are such that the flux changes tend to restore the shafts to their equilibrium positions.

Electro-optic devices keep the motors in synchronism. A slotted disk is mounted on each drive shaft, and an

LED and a photodetector are mounted adjacent to the disk. Each time a slot moves into the space between the light source and the detector, an electric pulse is generated. If the rotations are synchronized, the relative phase of the two pulse trains is constant. Phase changes are sensed by a phase-locked loop, which develops an error signal. The error signal is amplified and applied to the motor armatures to synchronize the rotations.

This pump could be used to compress fluids or gases in a mechanical refrigerator. Other types of counterrotating machinery may also use magnetic bearings and motors to maintain close clearance between rotating parts.

This work was done by Philip A. Studer of **Goddard Space Flight Center.** *For further information, Circle 55 on the TSP Request Card.*

This invention is owned by NASA, and a patent application has been filed. Inquiries concerning nonexclusive or exclusive license for its commercial development should be addressed to the Patent Counsel, Goddard Space Flight Center [see page A5]. Refer to GSC-12668.

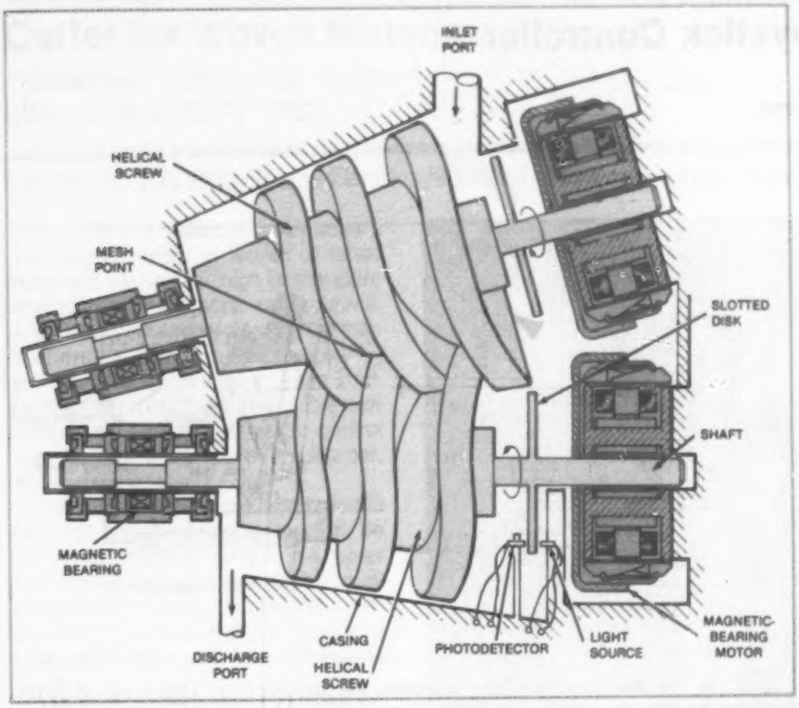

Helical-Screw Rotation compresses and transports gas charges, which subject the shafts to forces that tend to displace them from their equilibrium positions. Magnetic bearings would restore the shafts to equilibrium, lowering friction and increasing efficiency.

Preventing Cracks in Titanium Rotary Seals

A plastic insert maintains a seal while it prevents rubbing of metal parts.

Marshall Space Flight Center, Alabama

An improved rotating cryogenic joint employs a seal composed of polytrichlorofluorethylene (PTCFE) between titanium moving parts and other metal parts. In a cryogenic pump, a PTCFE labyrinth seal separates the housing from the titanium impeller (see figure).

Rotating seals that must operate at cryogenic temperatures present a particularly-difficult design problem. Often, titanium is selected as the material for at least one of the rubbing surfaces of a rotating seal for liquid hydrogen. However, titanium surfaces that rub against other metal surfaces are prone to cracking that eventually destroys the seal. Apparently, friction between the surfaces generates enough localized heat to initiate cracks in the titanium.

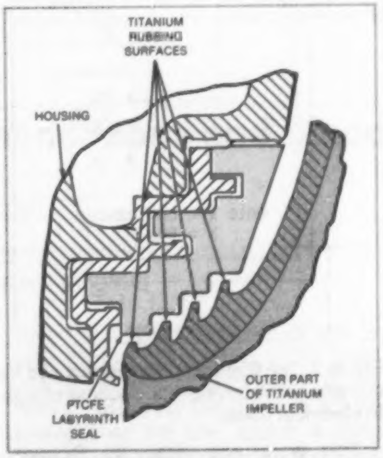

Titanium Rubs Against Plastic instead of metal in a new rotary seal for a cryogenic pump. Friction-induced cracks in titanium parts are thereby avoided.

In the improved joint, the titanium impeller rubs against plastic, not metal. As a result, localized heating of the titanium — and its subsequent cracking — is eliminated.

This work was done by James J. Ciana of Rockwell International Corp. for **Marshall Space Flight Center.** *No further documentation is available.*
MFS-19686

Miniature Two-Axis Joystick Controller

Pilots like the feel of a new device.

Ames Research Center, Moffett Field, California

A novel movable-button-actuated self-centering controller uses optoelectronics to produce X and Y signals for aircraft control. In addition to being extremely compact [1.0 in. (2.5 cm) in diameter by 1.3 in. (3.3 cm) tall, excluding the button], the device puts out voltages having a high signal-to-noise ratio, especially at the critical center position where in many controllers this ratio is poorest. The combination of a new saddle-shaped button and positive centering gives a "feel" and "breakout" (the pressure necessary to overcome the self-centering action) that have met with pilot approval.

As shown in Figure 1, a rocker, housing a lensed light-emitting diode (LED), is positioned over the truncated cone of a rocker plate and held there by pressure from a coil spring. The knife-edged rocker fits closely around the base of the cone, enabling the rocker to be tilted but not moved laterally. The spring exerts a downward force for self-centering and, additionally, when the rocker is tilted, a side force that prevents slippage away from the base of the cone.

Collimated light from the LED passes through a small aperture in the cone and forms a spot on the square photosensitive area of a commercially-available two-axis photodetector in a reduced-diameter case. When the spot is centered, the four output photocurrents are equal. When the rocker is tilted (see lower part of Figure 1), the spot is moved, and the ratio between the currents is varied. Operational amplifiers, within the controller, convert these currents to voltages as shown in Figure 2. Normalization, which is necessary for this type of device, and scaling are performed externally.

The new controller was developed for use in piloting flight-simulator vertical-takeoff-and-landing aircraft. It has not yet been flown. Other suitable applications would include radar trackers/cursors, aircraft moving-map display controls, weapon pointing, and others where size, weight, and ability to function in an electrically noisy environment are critical.

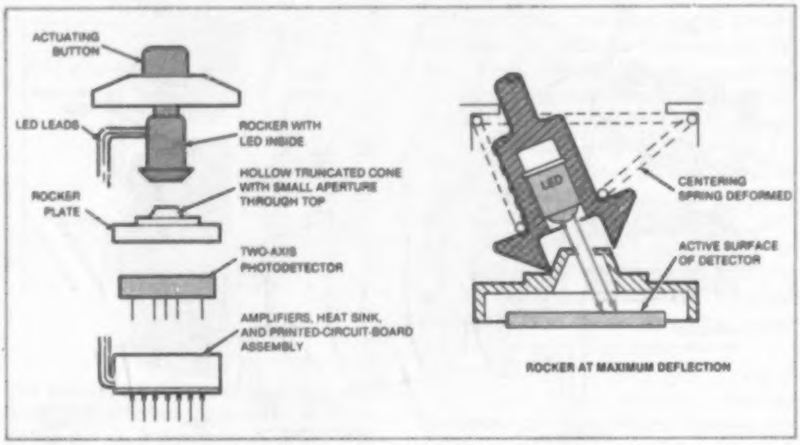
ACTUATING BUTTON
LED LEADS
ROCKER WITH LED INSIDE
HOLLOW TRUNCATED CONE WITH SMALL APERTURE THROUGH TOP
ROCKER PLATE
TWO-AXIS PHOTODETECTOR
AMPLIFIERS, HEAT SINK, AND PRINTED-CIRCUIT-BOARD ASSEMBLY
LED
CENTERING SPRING DEFORMED
ACTIVE SURFACE OF DETECTOR
ROCKER AT MAXIMUM DEFLECTION

Figure 1. In the **Miniature Two-Axis Controller**, the position of an LED is varied by the motion of a spring-centered rocker. The position is detected by a dual-axis photodetector.

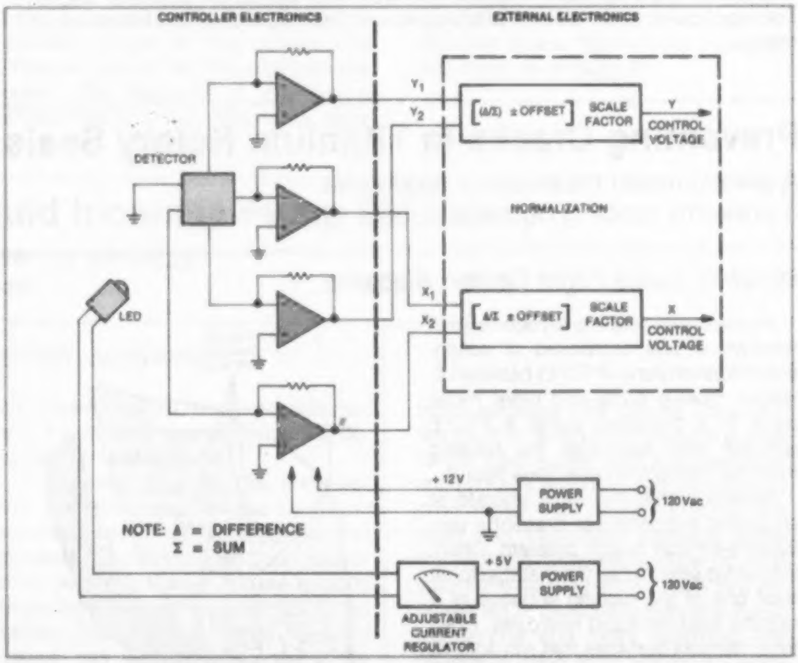
CONTROLLER ELECTRONICS
EXTERNAL ELECTRONICS
DETECTOR
LED
Y1
Y2
[(Δ/Σ) ± OFFSET] SCALE FACTOR
Y
CONTROL VOLTAGE
NORMALIZATION
X1
X2
[Δ/Σ ± OFFSET] SCALE FACTOR
X
CONTROL VOLTAGE
Σ
+12V
POWER SUPPLY
120 Vac
NOTE: Δ = DIFFERENCE
Σ = SUM
+5V
POWER SUPPLY
120 Vac
ADJUSTABLE CURRENT REGULATOR

Figure 2. The **Controller Electronics and External Electronics** convert the photodetector currents to control signals. Because of high signal levels, the system is relatively immune to electrical noise.

This work was done by Richard Hollow of Computer Sciences Corp. for **Ames Research Center.** *For further information, Circle 56 on the TSP Request Card.*

Inquiries concerning rights for the commercial use of this invention should be addressed to the Patent Counsel, Ames Research Center [see page A5]. Refer to ARC-11372

Cutter for Woven Materials

"Guillotine" cutting tool makes clean cuts in fabric strips.

Lyndon B. Johnson Space Center, Houston, Texas

A simple tool makes accurate square cuts through strips of woven or felted materials, such as high-temperature aramid fabric. Scissors, papercutters, and a knife with a roller were slower than the new "guillotine" cutter in preparing aramid fabric strips for the Space Shuttle thermal-protection system. The new cutter gave the operator better control over the cut and resulted in sharper, well-defined edges.

The cutter (see figure) has a slotted base for accepting the material to be cut. A razor blade is clamped in a holder that moves vertically in a bushed support bracket. A pivoted handle with a mechanical advantage of about 4 applies a downward force on the razor-blade holder.

The blade works against a slotted anvil of tough plastic. This reduces wear on the cutting edge and provides a clean cut. Two plastic blocks mounted on the base prevent rotation of the blade assembly, assuring a square cut.

This work was done by John M. Hammons and Andrew R. Keir of Rockwell International Corp. for **Johnson Space Center.** *For further information, Circle 57 on the TSP Request Card.*
MSC-20178

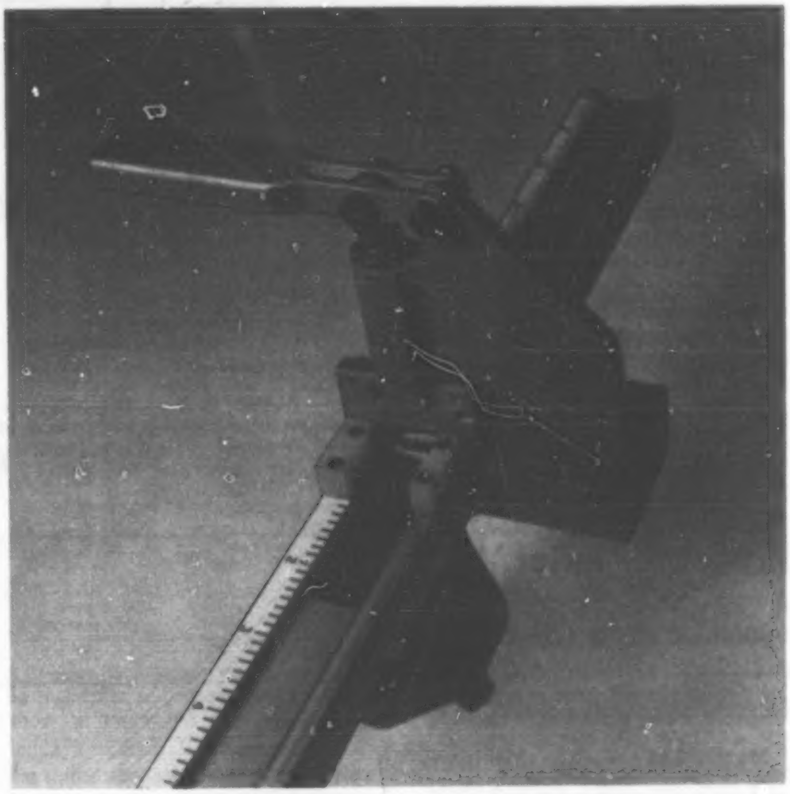

Pressing the handle on this Guillotine Cutter forces a razor blade through the strip of material in the slot, cutting the strip off squarely. The scale is for measuring the length of material to be cut. The cutter accepts strips 0.09 to 0.16 inch (2.3 to 4.1 mm) thick and 0.75 inch (19 mm) wide.

Ball Joint for Quick Connections and Disconnections

Joint is strong in shear and tension.

Langley Research Center, Hampton, Virginia

A proposed quick-connect/disconnect joint could be operated remotely, offers high strength in shear and tension, and allows rotational freedom. The joint consists essentially of an expandable collet that can be locked over a ball to form a ball-and-socket joint.

To attach the joint, the user depresses a button protruding from the center of a release tool handle and inserts the tool into a sleeve on the collet (see figure). Releasing the button allows locking balls in the tool shank to grip the sleeve when the user applies a lifting force. The lifting action allows fingers on the collet to expand.

With the collet fingers in the open position, the user can place the collet over a ball, which forms the fixed side of the joint, and then release the sleeve so that the collet fingers close over the ball. The quick-connect/disconnect joint is then secure. To disconnect the joint, the user inserts the release tool and raises the collet. The fingers open and free the ball.

(continued on next page)

The joint was proposed for possible use on the Space Shuttle for the attachment of heat-protection panels where deflection or thermally-induced moment loads are undesirable. It has a variety of other potential applications, for example:

- Quick attachment and detachment in hazardous, inaccessible, or blind locations;
- Linking parts of mechanisms (as a replacement for a spherical bearing, the joint would simplify assembly and design and allow easy replacement of bearing surfaces);
- Grasping spherical objects in robotic machines; and
- Coupling pneumatic tubes (besides quick connections and disconnections, the joint would allow flexure).

This work was done by Louis W. Palmer of Rockwell International Corp. for **Langley Research Center.** *For further information, Circle 58 on the TSP Request Card.*
LAR-12896

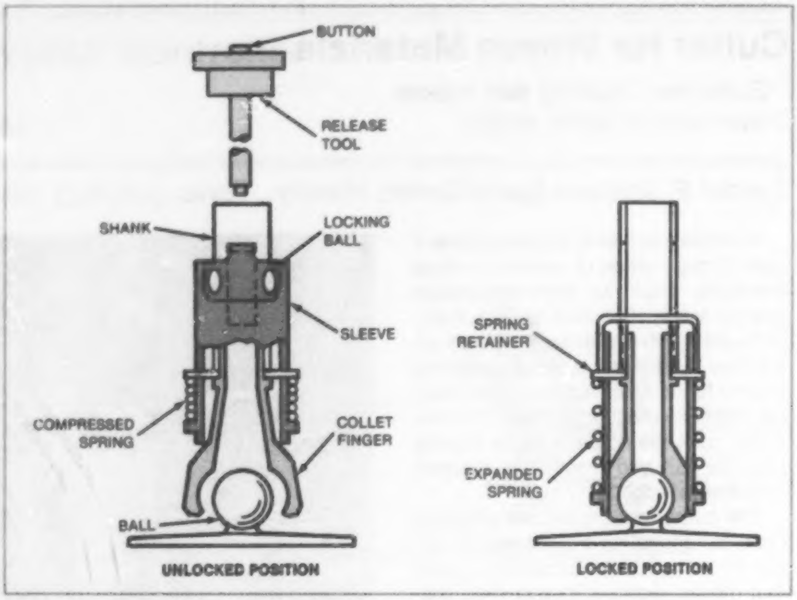

When a **Release Tool** is inserted into the sleeve of the joint, locking balls engage the sleeve and allow it to be pulled upward, compressing the spring and releasing the collet fingers. When the sleeve is released, the spring forces the sleeve and collet fingers over the ball on the fixed part of the joint.

Pressure Relief Valve

A cap with O-ring protects subatmospheric systems.

Lewis Research Center, Cleveland, Ohio

Many ordinary pressure relief valves used to protect subatmospheric instruments are very prone to leak, especially over extended periods of time. Some occasionaly fail to function after long periods of use.

A very simple design has been found to solve these problems. No failures have been seen after several years of test use. As shown in the figure, a body or housing is attached by a standard screw fitting to the piping circuit. The top surface of the housing has a machined groove in which is placed an O-ring. A simple cap with a pin made to fit very loosely in the housing simply rests on the O-ring. The undersurface of the cap is a machined surface. Thus, the weight of the cap presses the O-ring between two machined surfaces, effecting an adequate seal. The vacuum is fully maintained.

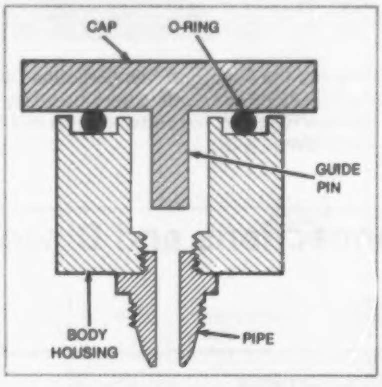

The **Valve Cap,** which is seated on an O-ring, lifts to relieve positive pressure. It is attached to the vacuum system by a screw-on housing.

If a system failure puts a positive pressure to the valve, the cap lifts to relieve the pressure. If there is a sudden severe change in pressure, the cap will pop off; but the stem prevents damage to the machined surface of the cap, making the cap reusable. Caps may be loosely tied to the pipe with twine or thin wire to make recovery simple. The weight of the cap and O-ring diameter can be sized to fit the desired overpressure limits.

This work was done by Theodore A. Brabbs of **Lewis Research Center.** *No further documentation is available.*
LEW-13800

Micrometer for Measuring Trepanned Grooves

Tool accurately measures groove diameter where standard calipers are not feasible.

Marshall Space Flight Center, Alabama

A special micrometer measures the diameter of a circular groove on the face of a large part, while the part is mounted in a lathe chuck. The tool has a curved frame (like that on an ordinary micrometer, but larger), so it can reach around an obstruction on the centerline of the part. At one end of the frame there is a blade/micrometer spindle for reaching into the groove to be measured; this type of spindle does not rotate when the micrometer thimble is turned in taking a measurement. The other end of the frame has a sliding foot with a blade.

The special tool was developed to permit measurements during the machining of a 26-inch (66 cm) groove on the flat face of an engine nozzle, which has a tolerance of 2 mils (0.005 cm). The groove and the obstacle to its measurement are seen at the top of the figure. The tool can also be used in other face-groove measurements where standard methods, such as vernier calipers, are not feasible.

As seen at the bottom of the figure, the large frame and blade/micrometer barrel that slides in and out without turning makes this tool very practical. The adjustable sliding foot at the anvil end of the frame allows the tool to measure a wide range of face-groove diameters, with accurate calibration in the 1-inch (2.54-cm) range of the blade/micrometer spindle.

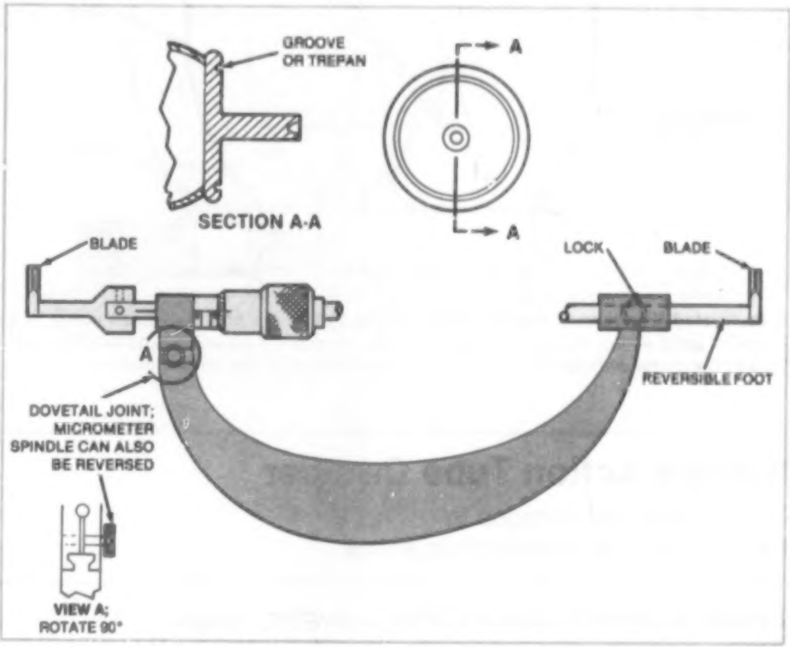

A Circular Face Groove (trepan groove), such as the one on the part shown at the top, can be measured accurately during the machining process with the special micrometer shown at the bottom. The large curved frame is not obstructed by the shaft projecting from the center of the part.

This work was done by Samuel K. Bird of Rockwell International Corp. for **Marshall Space Flight Center.** *No further documentation is available.*
MFS-19704

Cleaner for Solar-Collector Covers

A cleaning solution would be pumped over the collector cover.

NASA's Jet Propulsion Laboratory, Pasadena, California

A simple self-contained cleaning system has been proposed for solar collectors or solar-collector protective domes. Current cleaning methods are uneconomical because they are labor-intensive or because they require expensive machinery.

A thin transparent perforated polymeric film cap would be attached to the top of the dome (see figure). A small, low-pressure pump would pump a cleaning solution up under the cap. It would flow out through the perforated cap and then down over the surface of the dome, washing off any dirt. The cleaning fluid would be collected in a gutter around the bottom of the dome, filtered to remove particulate dirt, and then returned to a sump for reuse.

The pump could be controlled remotely or by a timer. The addition of fluid to

(continued on next page)

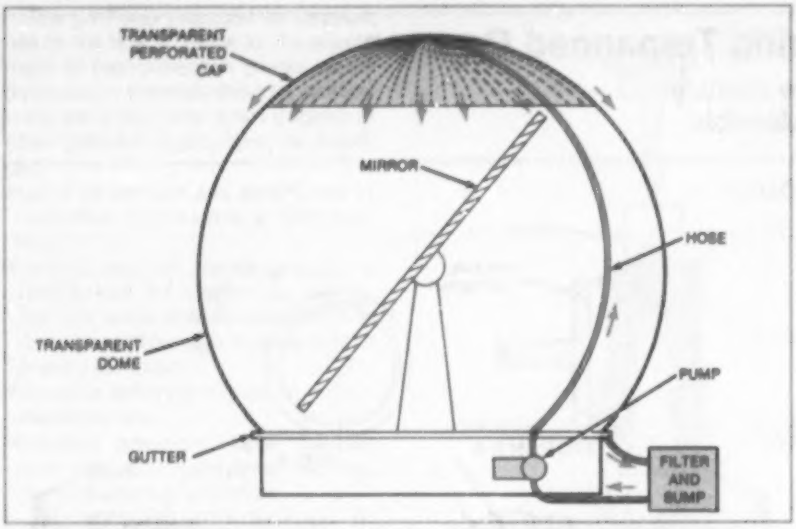
TRANSPARENT PERFORATED CAP
MIRROR
HOSE
TRANSPARENT DOME
PUMP
GUTTER
FILTER AND SUMP

A Perforated Transparent Plastic Cap attached to the top of a protective dome in a heliostat solar-energy collection system would distribute a cleaning fluid over the surface of the dome without blocking a significant fraction of the solar radiation.

replace evaporation losses would be controlled by a float switch. In a large multidome installation such as a heliostat field, a single centrally-located filtering and pumping system could be used.

The hardware required for the proposed cleaning system (including filters, sump, pump, timers, and float switch) is commercially available. The perforated-film technology required is similar to that used in permeable bleeder membranes developed in the aerospace reinforced-plastics industry. The system should be tested to verify that satisfactory cleaning is achieved with the relatively-gentle fluid flow proposed.

This work was done by Peter O. Frickland and Edward L. Cleland of Caltech for **NASA's Jet Propulsion Laboratory.** *For further information, Circle 59 on the TSP Request Card.*
NPO-15414

Remote-Action Tube Crimper

Tubing could be crimped in hard-to-reach and hazardous areas.

Lyndon B. Johnson Space Center, Houston, Texas

A proposed long-handled tube crimper could stop leaks or reduce fluid flow in hard-to-reach and hazardous areas. It is similar to tools for pinching off vacuum equipment and sealing it from its pumping source.

As shown in the figure, the tool includes a steel plunger, which is contained within a pipe, and long cam-action handles that open and close the crimping jaw. The movable jaw is wedge shaped and the stationary jaw is cylindrical. The length of the plunger and surrounding pipe can be varied from tool to tool to accommodate the reach required.

An adjustable stop in the handle avoids severing the tubing by stopping the handle closure at the proper distance for tube crimping. The stop is marked for various tube sizes so that the correct crimping pressure is applied.

This work was done by Richard L. Robbins and Shawn T. Harrison of Rockwell International Corp. for **Johnson Space Center.** *No further documentation is available.*
MSC-20197

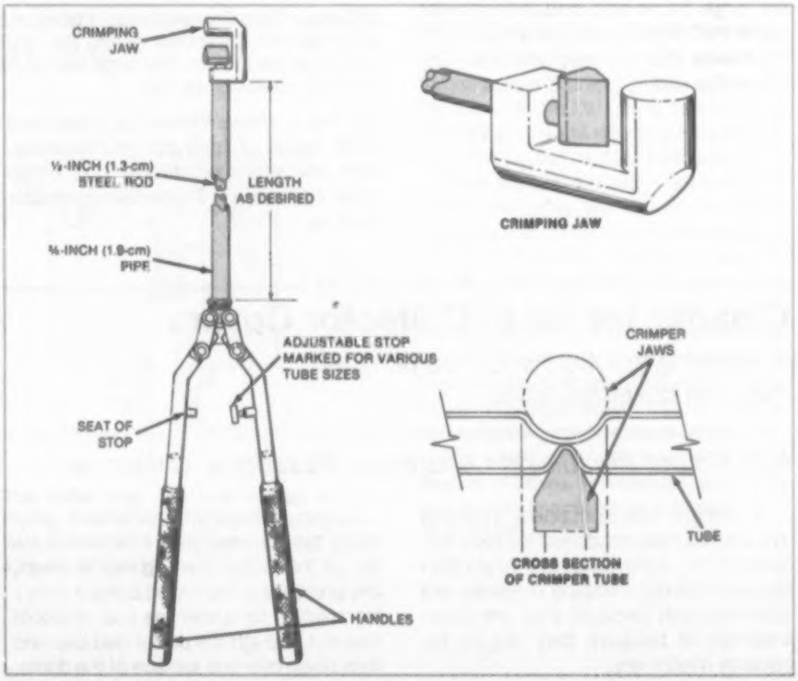
CRIMPING JAW
½-INCH (1.3-cm) STEEL ROD
LENGTH AS DESIRED
¾-INCH (1.9-cm) PIPE
ADJUSTABLE STOP MARKED FOR VARIOUS TUBE SIZES
SEAT OF STOP
HANDLES
CRIMPING JAW
CRIMPER JAWS
TUBE
CROSS SECTION OF CRIMPER TUBE

The Length of the Steel Rod and Surrounding Pipe determines the reach of the long-handled crimper. An enlarged view of the crimping jaw and a cross section of a crimped tube are also shown.

Modified Reamer Removes Chips and Contaminants

A proposed tool would prevent chips and lubricant from contaminating the cutting area.

Marshall Space Flight Center, Alabama

A proposed modification to a reamer would draw cutting chips and lubricant away from the cutting area. The tool would be especially useful when the surroundings must be kept free from contamination.

The modified reamer (see figure) has an internal passage connected to a vacuum source. Cuttings are drawn into the passage through holes in the reamer grooves. They exit the shaft through outlet holes that lead into a vacuum manifold, located near the machine chuck. The manifold collects the debris and passes it to a trap that protects the vacuum source. A positive pressure of 1 to 2 psi (7×10^3 to 14×10^3 N/m^2) inside the orifice helps to extract the chips.

Among the factors that need to be accounted for when modifying a reamer are the type of material being reamed and the size of the hole to be made. These factors will determine the size of the passage and the sizes of the inlet and outlet openings in the reamer shaft. Furthermore, the O-rings that maintain the vacuum seal on the manifold must be made of an elastomer that resists wear from the rotating reamer shaft.

This work was done by Larry L. Larson of Rockwell International Corp. for **Marshall Space Flight Center.** *No further documentation is available.*
MFS-19711

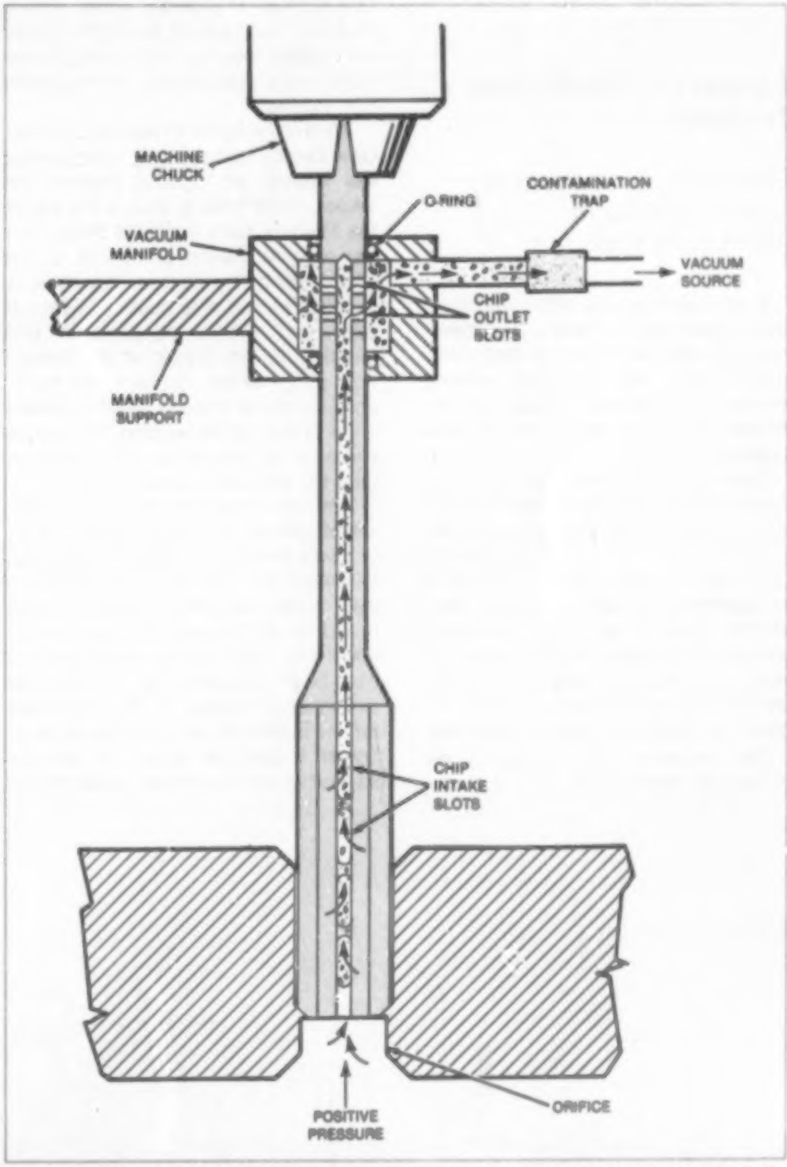

The **Reamer Shaft** is modified by a central passage and intake and outlet slots. To help draw away chips and lubricant and augment the vacuum, a positive pressure is applied inside the orifice of the part being reamed.

Books and Reports

These reports, studies, and handbooks are available from NASA as Technical Support Packages (TSP's) when a Request Card number is cited; otherwise they are available from the National Technical Information Service.

Progress in Wind-Wheel Turbines

Efficient turbine concept shows promise in preliminary tests.

A new wind turbine offers important advantages over conventional propeller wind tubines according to theoretical studies and tests of small working models. The project results are described in a final report that is now available.

Because of their simple construction, it seems likely that wind-wheel turbines will cost less to build and operate; at the same time, wind wheels are just as efficient as conventional wind machines in extracting energy from moving air. Wind wheels operate at lower rotational speeds and therefore are less subject to vibratory stress and fatigue. They also produce higher torque — useful for powering pumps and similar machines.

The improved wind wheel is described in "Wind-Wheel Electric Power Generator" (MFS-23515) on page 276 of *NASA Tech Briefs*, Vol. 3, No. 2. A streamlined version is described in "Aerodynamics Improve Wind Wheel" (MFS-25506) on page 78 of *NASA Tech Briefs*, Vol. 6, No. 1. The wind-wheel turbine consists of a bladed wheel, a main housing, two forward ducts (front concentrators), two side ducts (side concentrator and a base to support and elevate the housing.

Wind entering the forward ducts is accelerated by venturi tubes, which funnel the flowing air upward toward the blades. Wind flowing across the top of the forward ducts impinges directly on the exposed blades at the top of the wheel. Wind flowing over the sides is scooped by the side ducts into venturi tubes that reverse the airstream and direct it against blades at the bottom rear of the wheel. As the wheel turns, used air leaves through an exhaust vent at the bottom of the housing. The turbine pivots on its support so that it turns to face the wind like a weather vane.

Two sets of experiments on the wind-wheel concept have been carried out — one on a model composed of paper and cardboard and the other on a stainless-steel model. A simplified analytical model based on four blades has been developed, and performance characteristics have been computed from it. A detailed performance analysis of the wind-wheel turbine is difficult since the device does not fit a classical pattern. It behaves somewhat like a simple water-paddle wheel and somewhat like an impulse gas turbine. A complete performance analysis should include the interaction between the inlet flow, the wheel-blade flow, and the outlet flow.

A practical version of the wind wheel will probably require more than four blades. The final wheel design will be a result of blade size, shape, and quantity. Variable-pitch stator blades may be added to control wheel speed, maintaining constant rotational frequency so that constant-frequency electric power is produced.

The wind-wheel turbine bearings present a much-simpler design problem than the bearings for a propeller-type wind turbine. The forces on the blades exert only a torque on the wheel, which in itself produces no load on the bearings. There is little side or thrust load on the bearings since the transverse airflow forces are balanced.

Sufficient information is available for a final design of a functional turbine using off-the-shelf parts and components. This design can now avoid special engineering-design and development tasks, which are unnecessary and costly. However, final performance of the system can only be determined by field testing a prototype unit.

This work was done by Walter Frost and Philip A. Kessel of FWG Associates, Inc., for **Marshall Space Flight Center.** *To obtain a copy of the report, Circle 60 on the TSP Request Card.*
MFS-25796

Fabrication Technology

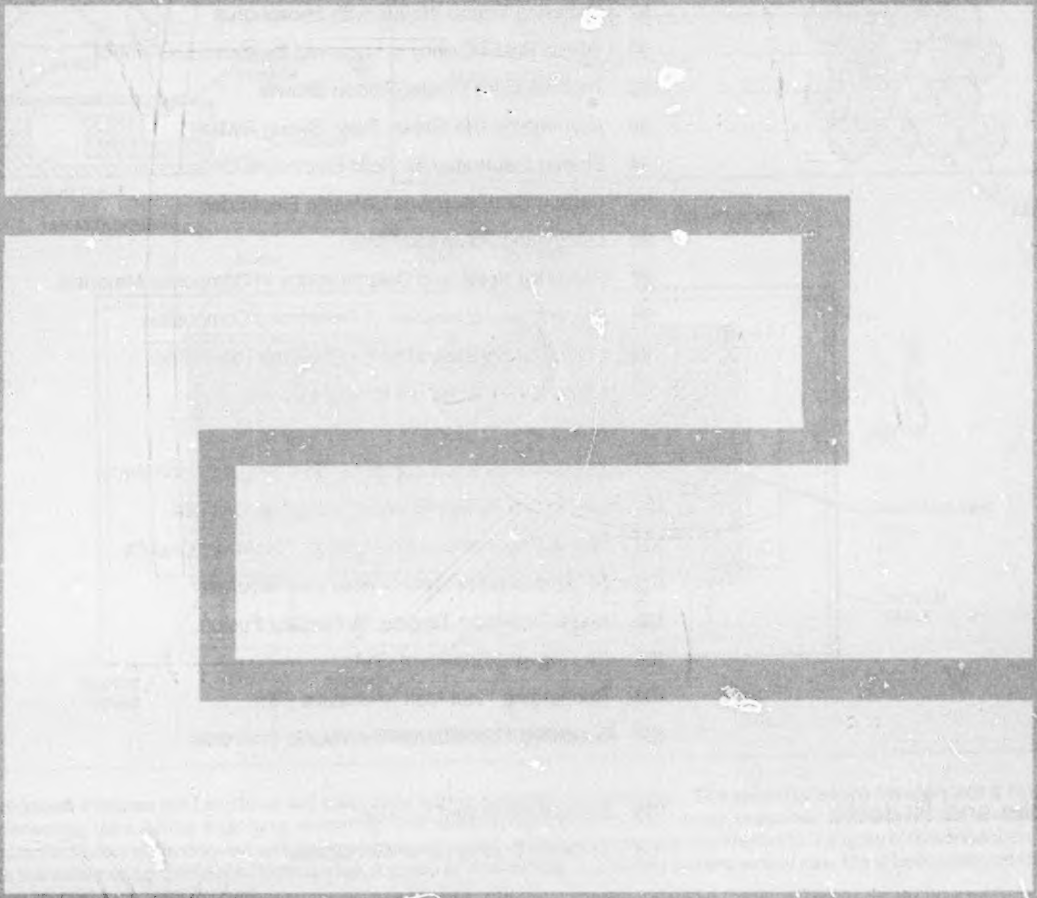

Hardware, Techniques, and Processes

87 Assembly of Photovoltaic Arrays
88 Pellet Feed for Dendritic-Web Growth
89 Barrier for Continuous-Crystal-Growth Crucible
90 Modified Silicon Furnace Lowers Crystal Cost
91 Controlling Thermal Gradients During Silicon Web Growth
92 Gettering Silicon Wafers with Phosphorus
92 Silicon Sheet Quality is Improved By Meniscus Control
93 Technique for Crystal-Ribbon Growth
94 Asymmetric Die Grows Purer Silicon Ribbon
94 Striped Electrodes for Solid-Electrolyte Cells
95 Carbon Cloth Supports Catalytic Electrodes
96 Laminating Polyimide Films
97 Repairing Voids and Delaminations in Composite Materials
98 Solventless Fabrication of Reinforced Composites
99 Solar-Cell Encapsulation by One-Step Lamination
99 Improved Photosensor for Light Valves
100 Ampoule With Integral Feedthroughs
101 Fabricating a Microcomputer on a Single Silicon Wafer
102 Electrolyte Reservoir Would Lengthen Cell Life
103 Stable Polyurethane Coatings for Electronic Circuits
104 RF Sputtering of Gold Contacts on Niobium
105 Mass Producing Targets for Nuclear Fusion
105 Etching and Growth of GaAs
106 Recharging "Hot-Melt" Adhesive Film
107 Simplified Heat-Source/Thermionic Converter

Books and Reports

108 Etching Integrated Circuits
108 Tests on Double-Layer Metalization

Assembly of Photovoltaic Arrays

Heat lamps on a trolley
melt preapplied solder.

NASA's Jet Propulsion Laboratory, Pasadena, California

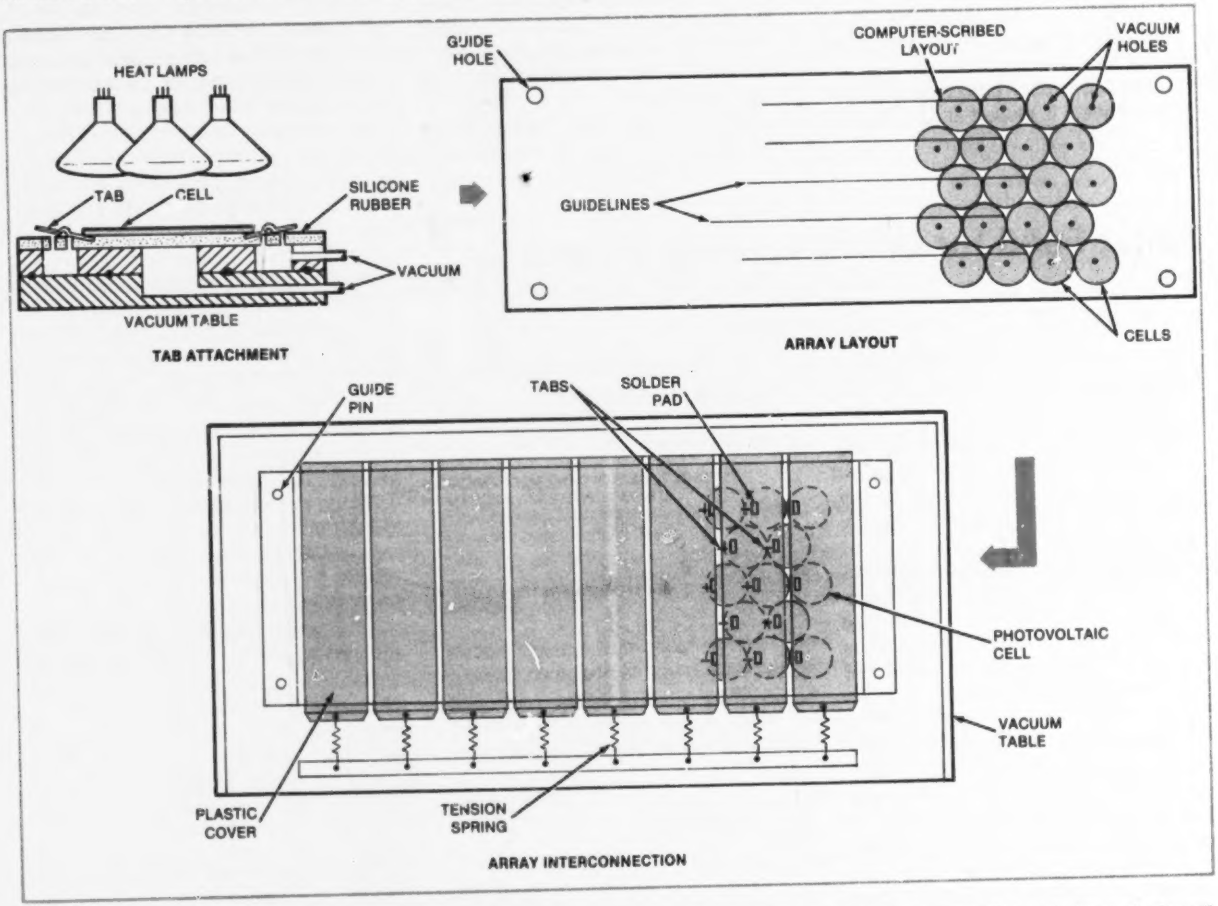
HEAT LAMPS
TAB
CELL
SILICONE RUBBER
VACUUM
VACUUM TABLE
TAB ATTACHMENT
GUIDE HOLE
COMPUTER-SCRIBED LAYOUT
VACUUM HOLES
GUIDELINES
CELLS
ARRAY LAYOUT
GUIDE PIN
TABS
SOLDER PAD
PHOTOVOLTAIC CELL
VACUUM TABLE
PLASTIC COVER
TENSION SPRING
ARRAY INTERCONNECTION

Vacuum Holddown Fixtures hold photovoltaic solar cells during assembly into an array. The tab-attachment fixture holds a single cell and interconnecting tabs during heat-lamp soldering. The array-layout fixture has a computer-scribed layout template and holds the cells (with attached tabs) while they are being placed in position and while they are being transferred to the array-interconnection fixture, which holds the cells during the final soldering step. A group of heat lamps on a trolley passes slowly over the interconnection fixture to heat the cells to soldering temperature.

In a new system for assembling photovoltaic arrays, solder and flux are applied to pads on the individual cells by a screen process and then heated to soldering temperature by heat lamps during final assembly. Fixtures with vacuum holddowns keep the cells and interconnecting tabs in proper alinement. [A description of the interconnection geometry is given in "Parallel Connections Would Improve Array Reliability" (NPO-15310) in *NASA Tech Briefs*, Vol. 6, No. 4, Spring/Summer 1982, page 375. The radiant-heat soldering technique is described in "Heat Lamps Solder Solar Array Quickly" (NPO-14866) in *NASA Tech Briefs*, Vol. 6, No. 1, Spring 1981, page 101.]

The steps of the new assembly process (see figure) are as follows:

- Flux and solder are applied at solder pads on the front and back of the individual solar cells.
- Two types of interconnecting tabs (contact strips) with crimps for strain relief are prepared. Tabs for connecting from the front of one cell to the back of another have a Z-shaped crimp; those for connecting between solder pads on the same surface of two cells have a U-shaped hump in the middle.
- The first vacuum holddown fixture holds a single solar cell and tabs while infrared lamps heat the cell to solder the tabs to the cell.
- The cells (with attached tabs) are then arranged by hand on the second vacuum holddown fixture. This layout fixture has a computer-scribed template to guide the operator in placing the cells. The vacuum holddown holds the cells

(continued on next page)

securely (see next step), yet loosely enough that they can be adjusted in position.

- With vacuum still applied, the second fixture is turned over and placed face down on a third fixture. Locating pins ensure proper registration. Vacuum is then applied to the third fixture and released from the second, transferring the cells to the third fixture while maintaining cell alinement. The second fixture is then removed.
- A series of narrow transparent-plastic cover sheets is placed across the fixture, over the cells, and held tautly in place by springs. The covers hold the exposed interconnecting tabs against the cells during soldering. (A one-piece cover sheet proved unsatisfactory because creeping of the sheet as the heat lamps passed over the array caused the tabs to shift.)
- The heat-lamp carriage passes over the array at 1 ft/min (0.3 m/min), raising the cells to soldering temperature and completing the interconnection of the cells into an array.

During the final soldering step all the soldering points are under compression by essentially flat surfaces (between cover and cells or between cells and fixture). Thus the solder joints tend to come out flat without solder lumps. In methods used previously, such lumps caused the cells to be unduly vulnerable to breakage in later handling.

This work was done by Peter J. Coyle, Angelo G. Lazzery, and Marvin S. Crouthamel of RCA Corp. for **NASA's Jet Propulsion Laboratory.** *For further information, Circle 61 on the TSP Request Card.*
NPO-15311

Pellet Feed for Dendritic-Web Growth

Silicon pellets automatically added to the crucible would sustain crystal growth for days.

NASA's Jet Propulsion Laboratory, Pasadena, California

A technique for replenishing the silicon melt during the growth of a continuous dendritic web would permit uninterrupted crystal growth for several days or longer.

In dendritic-web growth, a crystal ribbon is formed by freezing a liquid supported on each edge by a needlelike dendritic crystal. The growth is thus shaped by crystallographic forces and surface tension rather than by dies (see figure).

The technique for melt replenishment uses a compartmented crucible. It has a large compartment from which web is grown, and a smaller compartment into which silicon pellets are fed as needed to maintain the desired melt level. The barrier that separates the two compartments prevents unmelted pellets from floating to the growing web and interfering with growth. It also prevents ripples, caused by pellets falling into the melt, from moving across the melt surface and disturbing the growth. The barrier has an opening below the surface of the melt, which permits continuous equalization of the melt levels in the two compartments. Pellets as large as 4 millimeters in diameter have been used successfully.

The remainder of the system consists of a pellet reservoir, a mechanism for feeding pellets one at a time, a feed tube, and suitable penetrations through the susceptor lid and shields into the crucible.

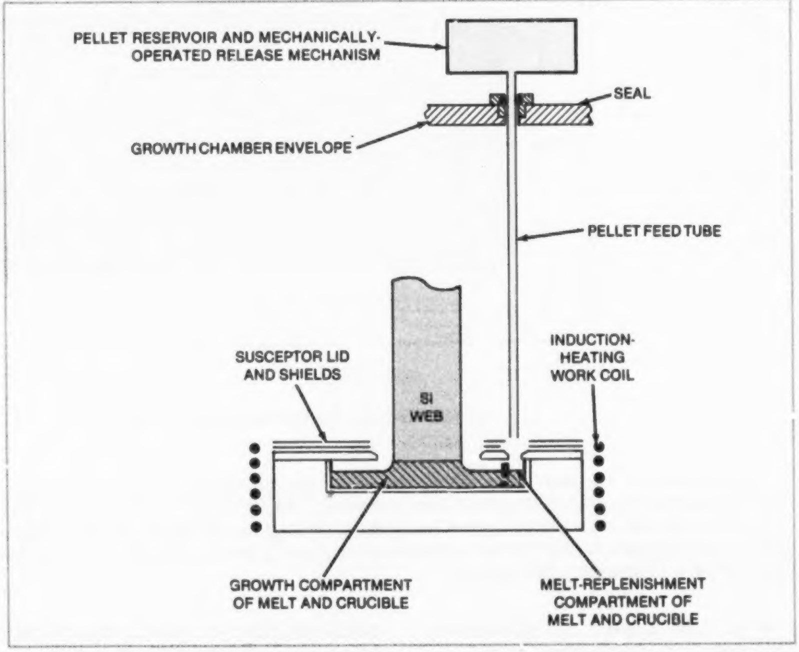
PELLET RESERVOIR AND MECHANICALLY-OPERATED RELEASE MECHANISM
SEAL
GROWTH CHAMBER ENVELOPE
PELLET FEED TUBE
SUSCEPTOR LID AND SHIELDS
Si WEB
INDUCTION-HEATING WORK COIL
GROWTH COMPARTMENT OF MELT AND CRUCIBLE
MELT-REPLENISHMENT COMPARTMENT OF MELT AND CRUCIBLE

This **Melt Replenishment** system would sustain the continuous growth of silicon dendritic web for several days. It thus substantially increases the size of a batch, which would then be limited mainly by the level of impurities and the life of the crucible.

This work was done by Charles S. Duncan, Marie E. Skutch, and James P. McHugh of Westinghouse Electric Corp. for **NASA's Jet Propulsion Laboratory.** *For further information, Circle 62 on the TSP Request Card.*
NPO-15198

Barrier for Continuous-Crystal-Growth Crucible

Properly designed openings permit free flow of melt while restraining pellets.

NASA's Jet Propulsion Laboratory, Pasadena, California

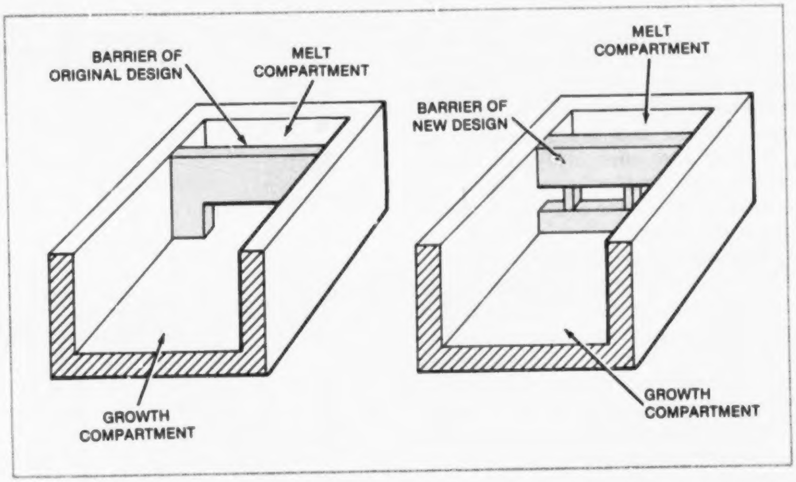

The **Old and New Designs** for the barrier between the feed compartment and the crystal-growth compartment in a heated crucible for continuous growth of silicon web are shown here. The old design (left) had a gap at the bottom to let melted silicon flow between compartments. The new design (right) has a low wall along the bottom and a gap above the low wall.

A redesigned partition between the growth region and the melt-replenishment region of a crystal-growth crucible makes it less likely that the crucible will run out of feed material in the middle of a cycle. Melt replenishement makes possible the continuous growth of silicon web and thus is an important factor in low-cost production of quality solar cells. The supply of molten silicon is maintained by the addition of silicon pellets to a compartment at one end of the heated crucible, and a partition or barrier is required to hold the pellets while allowing the melted silicon to flow from the compartment.

The original barrier design is shown at the left of the figure. To allow more-flexible thermal conditions and prevent emptying of the replenishment compartment, the barrier shown at the right of the figure was developed. This new design includes a low wall along the bottom of the crucible, preventing liquid flow between compartments until a substantial fraction of the silicon has melted.

Above the low bottom barrier is a gap that allows the flow of melted silicon from the feed compartment into the growth compartment. Above the gap is the rest of the barrier, which keeps the silicon pellets from floating into the growth compartment and also keeps gas from carrying stray particles of silicon over from the space above the feed compartment to the crystal-growth compartment.

This work was done by Marie E. Skutch and Paul A. Piotrowski of Westinghouse Electric Corp. for **NASA's Jet Propulsion Laboratory.** *For further information, Circle 63 on the TSP Request Card.*
NPO-15338

Closed-Loop Process Yields Ultrapure Silicon

A closed-loop process produces ultrapure silicon from metallurgical-grade silicon by forming, purifying, and hydropyrolizing tribromosilane (HSiBr$_3$). The ultrapure granular silicon obtained can be used to produce semiconductors and solar cells. The only material that needs replenishing once the process begins is metallurgical-grade silicon; all other reactants are separated and recycled. The metallugrical-grade silicon is transformed into tribromosilane by reacting it with process byproducts. The tribromosilane is separated from the mixture, purified, and finally decomposed in the presence of hydrogen in a silicon-product reactor.
(See page 34.)

Bipulsating Technique for Silicon Production

The reduction of silicon tetrafluoride by sodium, to produce high-purity silicon, is very fast and highly exothermic. A method is proposed that controls the temperature and rate of reaction by alternately adding measured amounts of reactants. This technique could be used in a large reactor, where heat dissipation becomes a serious problem, to control reactor temperatures. It would be a highly efficient method that would utilize almost 100 percent of the raw materials. One of the benefits of the method is that the reaction products can be grown in columns, the only contact being with the base of the reactor.
(See page 34.)

Cutter for Woven Materials

A simple tool makes accurate square cuts through strips of woven or felted materials, such as high-temperature aramid fabric. Scissors, papercutters, and a knife with a roller were slower than the new "guillotine" cutter in preparing aramid fabric strips for the Space Shuttle thermal-protection system. The new cutter gave the operator better control over the cut and resulted in sharper, well-defined edges. The cutter has a slotted base for accepting strips 0.09 to 0.16 inch thick and 0.75 inch wide. A razor blade is clamped in a holder that moves vertically in a support bracket.
(See page 79.)

Modified Silicon Furnace Lowers Crystal Cost

Functional changes reduce cycle time and prolong crucible life.

NASA's Jet Propulsion Laboratory, Pasadena, California

A modified Czochralski setup grows several large crystals in succession from one crucible. Previously, the crucible would be destroyed by thermal-contraction differences during the cool-down phase and would have to be replaced after each crystal was completed. The modified apparatus is expected to reduce the cost per crystal by about 50 percent.

The redesign allows the crucible to be kept hot, the hot zone of the furnace to be always under vacuum or low argon pressure, crystals to be removed from the furnace without the admission of air, and polysilicon feedstock to be added safely and reliably to the hot crucible. The key features are: an isolation valve between the growth and pulling chambers, an enlarged pulling chamber, and a recharging mechanism. These features are seen in the figure.

The water-cooled vacuum-tight isolation valve is closed when a completed crystal is being removed from the pull chamber or new feedstock is being introduced. While a crystal is growing, the feedstock is suspended on a cable at the side of the pull chamber. After the crystal has been grown and removed, the recharge material is moved forward and lowered into the crucible. The material is lowered slowly as it melts and continually weighed so that the correct amount is added to the crucible. When the recharge material is retracted, reseeding proceeds immediately without opening of the furnace chamber.

Operation of the modified furnace has demonstrated that high-quality crystals can be grown from at least three successive melts in the same crucible and that the crucible can be filled to a capacity, in excess of cold filling techniques.

This work was done by Richard L. Lane of Kayex Corp. for **NASA's Jet Propulsion Laboratory.** *For further information, Circle 64 on the TSP Request Card.*
NPO-15041

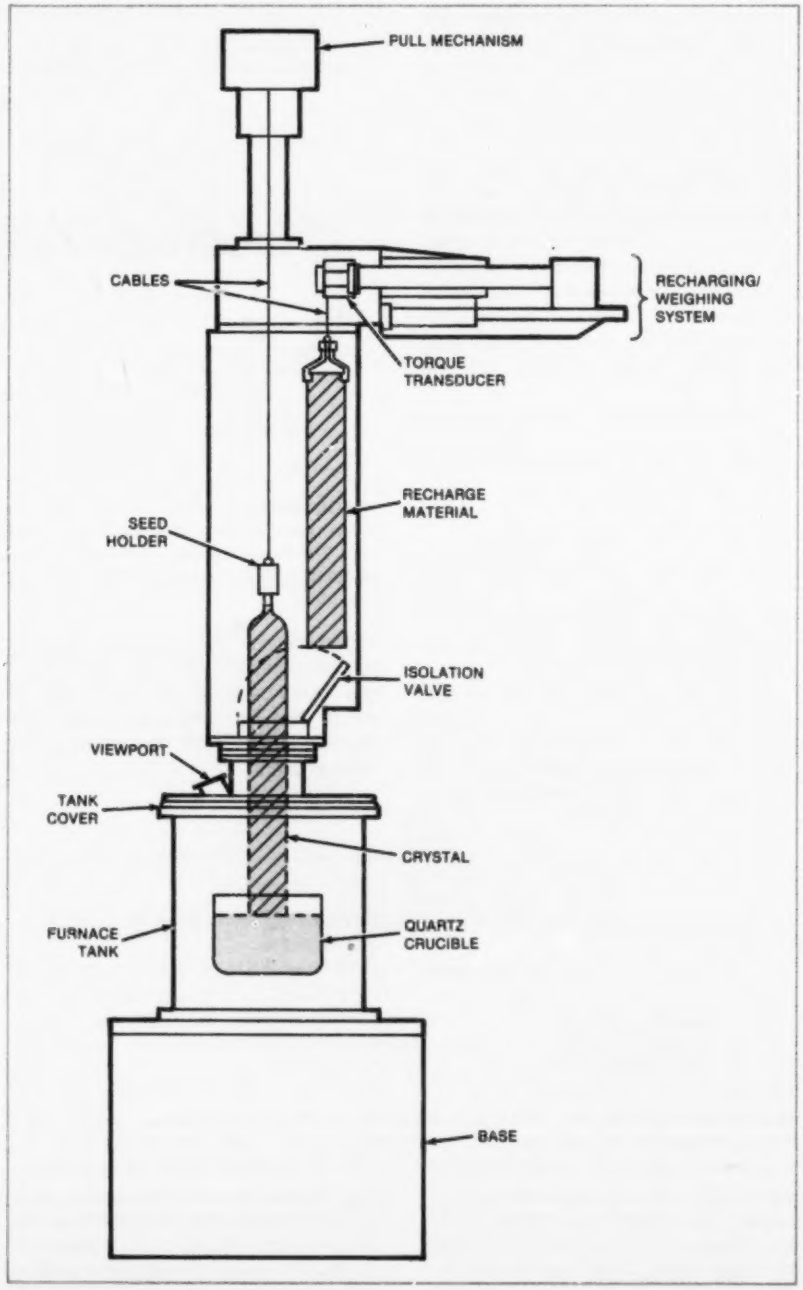

Czochralski Growth Facility, modified for continuous operation, is shown in the crystal-growth mode. The recharge material at the right will be moved in position over the crucible after the crystal has been grown and removed. An isolation valve keeps the air from contacting the hot crucible when the crystal is removed.

Controlling Thermal Gradients During Silicon Web Growth

A slotted susceptor helps keep the melt-replenishment region hot.

NASA's Jet Propulsion Laboratory, Pasadena, California

A strategically placed slot helps to control critical thermal gradients in a crucible for silicon web growth. The slot thermally isolates the feed region of the crucible from the growth region, so that the region where pellets are added stays hot.

Silicon ribbons for solar cells are grown continuously from a crucible inside an inductively heated susceptor [see "Crucible Grows Wide Silicon Ribbon" (NPO-14859) and "Improved Facility for Producing Silicon Web" (NPO-14860) in *NASA Tech Briefs*, Vol. 6, No. 1, Spring 1981, pages 91 and 93, respectively]. To maintain the supply of melted silicon in the crucible, pellets of silicon are fed in at one end. Unfortunately, the heat absorbed by the pellets during melting causes a thermal unbalance that can upset the growth conditions.

The slot is machined in the susceptor underneath the crucible, between the melt-replenishment and the growth compartments of the crucible. It does not extend all the way to the walls of the susceptor (see figure), so the inductive-heating currents are not interrupted; only the thermal conduction mode of heat transfer is interrupted. The slot size depends on the amount of temperature difference desired. Increased shielding at the melt-replenishment compartment requires a larger (i.e., wider or deeper) slot to keep the gradients essentially flat and symmetrical in the growth region.

Use of the slotted susceptor in several crystal-growth runs has confirmed the improved thermal geometry. This method of temperature-gradient control should be applicable to other types of crystal growth from the melt; for example, the Czochralski method.

This work was done by Charles S. Duncan, James P. McHugh, Marie E. Skutch, and Paul A. Piotrowski of Westinghouse Electric Corp. for **NASA's Jet Propulsion Laboratory.** *For further information, Circle 65 on the TSP Request Card.*
NPO-15337

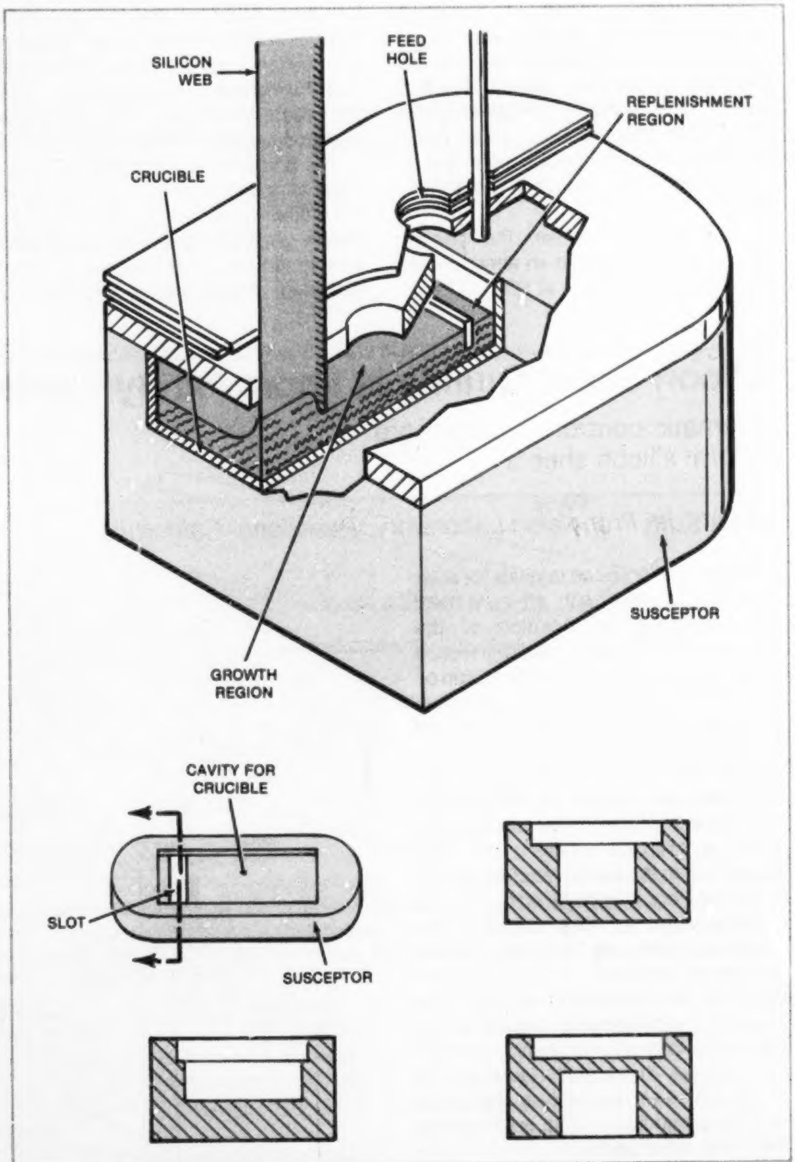

Cutaway Views show various shapes that the thermal-isolation slot may have in the susceptor. The slot permits inductive heating of both regions of the susceptor, but prevents thermal conduction between them.

Gettering Silicon Wafers with Phosphorus

Phosphorus absorbs impurities to improve the efficiency of solar cells.

NASA's Jet Propulsion Laboratory, Pasadena, California

Silicon wafers subjected to gettering in a phosphorus atmosphere have longer diffusion lengths and higher solar-cell efficiencies than untreated wafers. The gettering treatment improves the properties of solar cells manufactured from impure silicon and is compatible with standard solar-cell processing.

To remove impurities, the silicon wafers are immersed in an atmosphere containing phosphorus at 900° C for a half hour. After immersion, the surface layer containing the phosphorus dopant is removed from the wafers in the normal etching step that follows saw cutting the wafers from ingots. The wafers then are processed into solar cells.

The phosphorus treatment, when applied to solar-grade wafers, increases the minority-carrier diffusion length. Before gettering, typical values of diffusion length are 70 to 100 microns; after gettering, these values increase to about 120 to 150 microns. The corresponding solar-cell efficiencies for the two cases are 11.5 percent without the phosphorus treatment and 13.2 percent with the treatment.

This work was done by Robert V. D'Aiello of RCA Corp. for **NASA's Jet Propulsion Laboratory.** *For further information, Circle 66 on the TSP Request Card.*
NPO-15357

Silicon Sheet Quality is Improved By Meniscus Control

Automatic control ensures more uniform silicon sheets.

NASA's Jet Propulsion Laboratory, Pasadena, California

Better-quality silicon crystals for solar cells are possible with an instrument that monitors the position of the meniscus as a sheet of solid silicon is drawn from a melt. Using information on the meniscus height, the instrument generates a feedback signal to control the melt temperature.

The instrument is intended for use with the edge-defined film-fed growth technique in which molten silicon rises inside a graphite capillary die (see figure). When the silicon reaches the top of the capillary, it cools, solidifies, and is pulled away as a continuous sheet. The instrument observes the position of the meniscus between the silicon liquid/solid interface and the die edge. The height of the meniscus is determined by the pulling speed and the temperature of the melt at the growth interface. A change in height indicates a change in operating conditions that could affect the sheet cross section.

The position of the liquid/solid interface is sensed through the contrast in radiation reflected from the liquid and solid phases, the solid phase being more strongly reflective. A lens forms an image of the liquid/solid interface with a magnification of about 2. Located at the

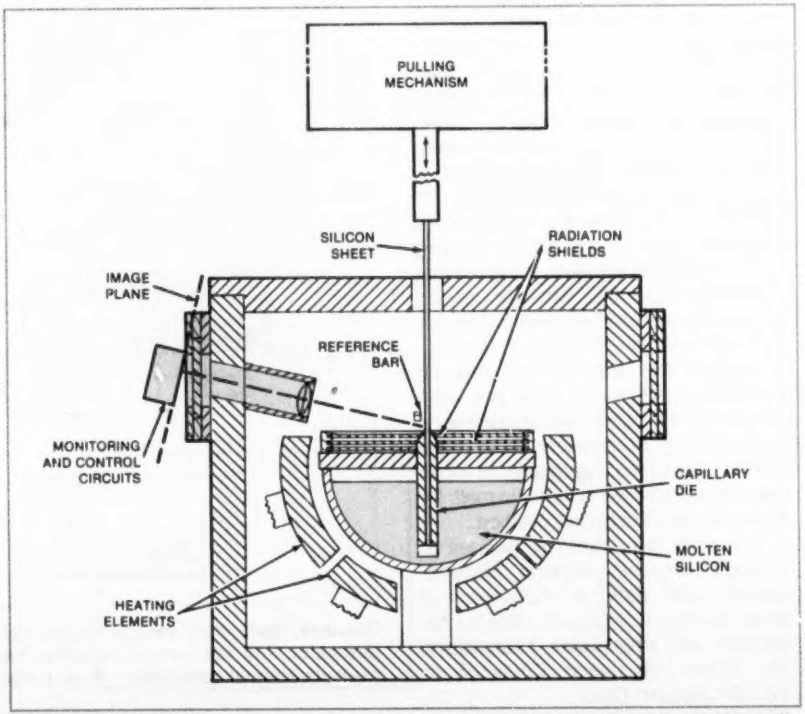

A Sheet of Solid Silicon is pulled at a constant rate from a capillary die as the melt temperature is adjusted by the monitoring and control unit. The adjustment maintains a nearly constant position of the liquid/solid interface at the top of the capillary.

image plane of the lens is a vertical linear array of light detectors sensitive to radiation at 0.5 micrometer, a wavelength at which silicon reflects strongly. The electrical output of each detector in the array is proportional to the intensity of the light impinging on it. The position of the detector having the greatest output therefore indicates the position of the solid side of the liquid/solid interface.

The monitoring and control unit adjacent to the detector array contains an analog shift register for storing the output values of the individual detectors. The register periodically releases its stored values to a comparator, which compares them with reference values that define the ideal position of the liquid/solid interface. If the interface is above or below its ideal position, the control unit increases or decreases the voltage to the heating elements, thereby raising or lowering the melt temperature and restoring the interface to its proper position.

The reference bar shown in the figure eliminates convection-current jitter — shifts in the image on the sensors caused by variations in the index of refraction of the hot vapor surrounding the liquid/solid interface. Any shift of the image of the interface caused by convection currents will produce an equal shift in the image of the edge of the reference bar. The control unit recognizes such simultaneous shifts as spurious and discounts them.

This work was done by Douglas A. Yates, Arthur E. Hatch, and Jeff M. Goldsmith of Mobil Tyco Solar Energy Corp. for **NASA's Jet Propulsion Laboratory.** *For further information, Circle 67 on the TSP Request Card.*
NPO-15384

Technique for Crystal-Ribbon Growth

Ribbon is formed by pulling nearly horizontally from a shallow melt.

NASA's Jet Propulsion Laboratory, Pasadena, California

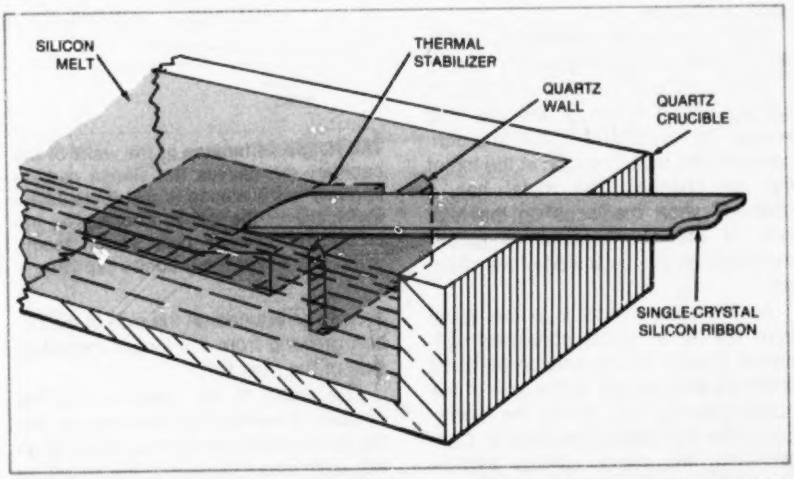

Single-Crystal Ribbon of silicon or other material can be grown from the melt by placing a seed crystal on the surface and then pulling it away at a slight angle from the horizontal. The bottom configuration in the crucible establishes temperature gradients that determine the shape of the ribbon.

In a proposal originated at NASA's Jet Propulsion Laboratory, a single-crystal ribbon of silicon or other material would be grown by pulling it at a low angle from a shallow melt. The thin monocrystalline ribbon would then be scored and broken into shapes required for the manufacture of such devices as solar cells. By pulling the crystal at a small angle, the technique prevents the overflow problem experienced with horizontal growth. It also creates a meniscus that minimizes growth defects in the main portion of the ribbon. The use of a shallow pool, prevents convection problems.

As the figure shows, there is a thermal stabilizer beneath the surface of the silicon melt to shape the temperature gradients in the melt, and there is a quartz wall with its top just flush with the surface of the melt. The temperature is adjusted so that a seed crystal placed on the surface of the liquid causes the surface liquid to solidify. The seed is then pulled at a slight angle over the edge of the wall, producing a raised meniscus behind the wall and between the ribbon and the surface of the molten silicon.

The shape of the ribbon is determined by the temperature gradients introduced by the stabilizer. The leading edge, where the crystal forms, is arc shaped; this shape directs imperfections toward the side edges. The thickness of the ribbon, like the width, is determined by the temperature gradients; but the thickness can also be varied slightly by varying the pulling speed.

This growth technique can be used to form ribbons of materials other than semiconductors. For example, sapphire ribbon for windows may be formed with this procedure and so can such bubble-memory materials as gallium, gadolinium, and garnet.

This work was done by David N. Jewett and Herbert E. Bates of Energy Materials Corp. for **NASA's Jet Propulsion Laboratory.** *For further information, Circle 68 on the TSP Request Card.*

Inquiries concerning rights for the commercial use of this invention should be addressed to the Patent Counsel, NASA Resident Office-JPL [see page A5]. Refer to NPO-15177.

Asymmetric Die Grows Purer Silicon Ribbon

Graphite die distributes silicon carbide impurities asymmetrically.

NASA's Jet Propulsion Laboratory, Pasadena, California

The concentration of carbide impurities in silicon ribbon is reduced by growing the crystalline ribbon with a die that has one wall higher than the other. The height difference controls the shape of the meniscus at the liquid/crystal interface and concentrates the silicon carbide impurity near one of the broad faces. The opposite face is left with above-average purity. This significantly improves the efficiency of solar cells made from the ribbon.

The new die has several vertical capillaries that feed the molten silicon into a top channel. The top of the channel is beveled and cut back on one side (see figure), so that its two sides are of unequal heights.

The top of the die is heated to 10° to 30° C above the melting point of silicon. A seed crystal is lowered and kept in contact with the top of the die long enough for its bottom to melt and connect with the molten silicon at the top of the die channel. The metal has a relatively short meniscus on the high side of the channel and a longer meniscus on the lower side of the channel.

As the seed crystal is pulled away from the die at a rate consistent with crystal growth, silicon carbide particles preferentially migrate to the side of the ribbon growing from above the meniscus on the high side of the channel. Consequently, the silicon carbide particle density is reduced on the side of the ribbon growing from the longer meniscus side of the melt film.

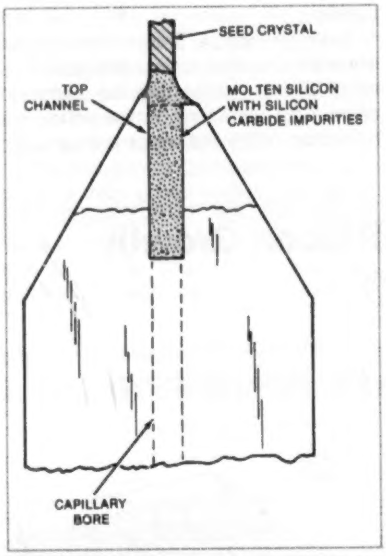

The **Height Difference** of the walls of the capillary die causes the silicon carbide impurity in the silicon to distribute asymmetrically in the grown ribbon. The impurities form when pure silicon reacts with the walls of the graphite capillary.

The width of the channel and the amount of vertical displacement of the top surfaces of the channel depend on the width and thickness of the crystal to be grown. To sustain the growth of silicon ribbons with widths up to 7.5 cm and thicknesses between 0.01 and 0.05 cm, the top surfaces of the die are displaced preferably by no more than 0.012 cm.

Ribbons made from the new capillary die have a substantial concentration of silicon carbide (1 to 10 particles per cm^2) on one side, while the opposite ribbon surface is virtually free of such particles and smooth in appearance. Solar cells made with the purer side as the junction side have efficiencies of between 9 and 10.6 percent. In contrast, solar cells made from the opposite side of the ribbon have efficiencies of less than 5 percent.

The same principle of displaced die-channel tops can be used in growing other crystalline materials where dissolved die materials precipitate in the grown crystal; for example, sapphire ribbons using molybdenum dies. Dies with displaced top surfaces also can be used for growing undoped silicon ribbon of other cross sections. Still another possible application of the die is for intentionally distributing impurities asymmetrically in the crystal.

This work was done by Juris P. Kalejs, Bruce Chalmers, and Thomas Surek of Mobil Tyco Solar Energy Corp. for **NASA's Jet Propulsion Laboratory.** *For further information, Circle 69 on the TSP Request Card.*
NPO-15385

Striped Electrodes for Solid-Electrolyte Cells

Gas flows freely between contact stripes.

NASA's Jet Propulsion Laboratory, Pasadena, California

Striped electrodes have been tested as a way of improving solid-electrolyte cell performance. The spaces between the contact stripes facilitate the flow of gases into and out of the electrolyte. [A wire-mesh electrode based on the same principle is described in "Integrated Solid-Electrolyte Construction" (NPO-15471), page 227, *NASA Tech Briefs*, Vol. 6, No. 2, Summer 1981.]

A striped electrode pattern is shown in the figure. The electrodes are made of platinum that is deposited as a thick film of ink or paste on the electrolyte surface and then fired. Typical solid electrolytes include sintered stabilized zirconia, doped alumina, or other ion conductors.

In previous designs, the platinum was deposited in a thin layer over the entire contact surface. The layer had to be sufficiently porous to allow gases to pass through. In practice, it has been difficult to achieve the required porosity, and the obstruction to gas flow by the platinum layer is responsible for most of the electrical resistance of the cell.

In cells with striped electrodes, the platinum is too thick to be porous. However, the spaces between the contact stripes remove the barrier to gas

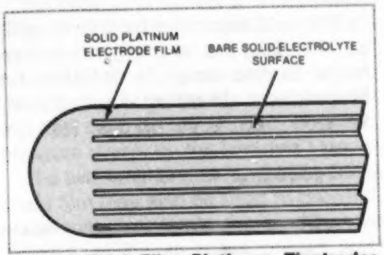

Striped Thick-Film Platinum Electrodes help to insure lower overall cell resistance by permitting the free flow of gases in the gaps between the stripes. The thick-film stripes are also easier to fabricate than porous thin-film electrodes that cover the entire surface.

flow across the electrolyte/atmosphere interface. The failure to cover the entire surface with electrode material does not significantly degrade cell performance as long as the electrode gaps do not exceed the ion conduction thickness of about 1 mm.

The additional electrode thickness also lowers the electrical resistance of the electrodes themselves, which contribute a large part of the total cell resistance. Possible applications for the improved cells include oxygen production from carbon dioxide, the extraction of oxygen from air, small fluidic pumping, sewage treatment, and fuel cells.

This work was done by Robert Richter of Caltech for **NASA's Jet Propulsion Laboratory.** *For further information, Circle 70 on the TSP Request Card.*

This invention has been patented by NASA [U.S. Patent No. 4,331,742]. Inquiries concerning nonexclusive or exclusive license for its commercial development should be addressed to the Patent Counsel, NASA Resident Office-JPL [see page A5]. Refer to NPO-15269.

Carbon Cloth Supports Catalytic Electrodes

New design requires less catalyst.

NASA's Jet Propulsion Laboratory, Pasadena, California

Carbon cloth is the starting material for promising new catalytic electrodes. Originally developed for a sulfur-cycle hydrogen process, the carbon-cloth electrodes are more efficient than the sintered-carbon configuration previously used. They are also chemically stable and require less catalyst — an important economic advantage when the catalyst is a noble metal such as platinum.

In the sulfur-cycle process, the carbon-cloth-supported electrode is the anode, or "electrolyzer." Sulfur dioxide is oxidized electrochemically in water, producing sulfuric acid at the anode. Hydrogen gas is removed at the cathode. The sulfuric acid is continuously drawn off and concentrated, then catalytically reduced at 870° C to produce water, sulfur dioxide, and oxygen. The sulfur dioxide is recycled into the hydrogen-generating reaction.

A comparison of a cell containing a carbon-cloth-supported anode with a conventional one (that is, one composed of pressed carbon powder, catalyst, and binder) demonstrated the better stability and efficiency of the new electrode. The voltage of the conventional cell rose steadily, while that of the carbon-cloth-supported cell remained nearly constant (see figure).

Other tests showed that the catalyst content is not critical. For example, an electrode containing about 7 mg/cm^2 of platinum performs just as well as one containing 12 mg/cm^2.

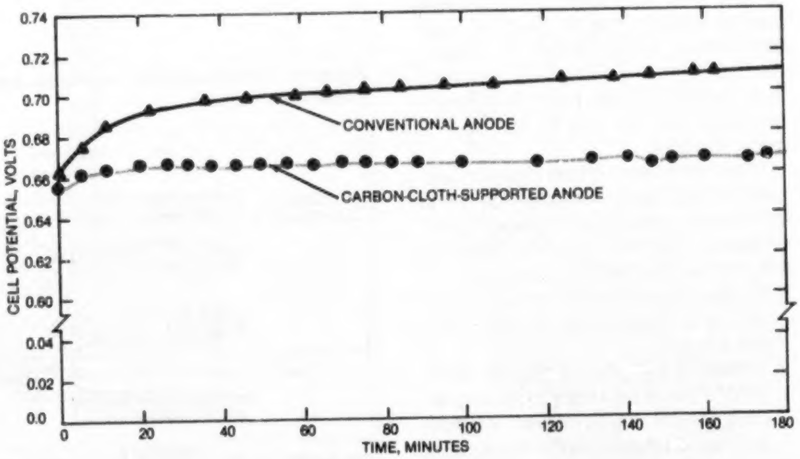

These **Two Curves** are for electrolyzers operated at a constant current density of 100 mA/cm^2 in 50 weight percent sulfuric acid. After 2½ hours, the cell voltage of the more-efficient carbon-cloth-electrode cell is 40 mV less than that of the conventional cell.

The first step in the fabrication of an electrode is degreasing in acetone a piece of commercial carbon cloth measuring 5 by 5 cm and cleaning it ultrasonically in distilled water. The cloth is 0.08 cm thick and has a flexural strength of 330 MPa.

Next, 0.55 g of platinum-catalyzed carbon powder is mixed with 20 ml of distilled water. The catalyzed carbon contains 10 percent by weight of platinum particles, 80 percent of which are smaller than 80 μm. To the carbon suspension is added a binder solution composed of 60 weight percent of polytetrafluoroethylene (PTFE) in distilled water.

The carbon cloth, while it is still wet, is placed on a perforated stainless-steel plate. Supported in a special fixture, the underside of the perforated plate is exposed to a cavity connected to a vacuum pump. The carbon/PTFE suspension is spread over the cloth and allowed to filter through it as the vacuum pump provides a pressure differential of about 1 mm of mercury. Meanwhile the cloth and its newly-applied carbon layer are heated by an infrared lamp for about an hour.

(continued on next page)

Compression and sintering are the final fabrication steps. The carbon-impregnated carbon cloth is transferred to a die where it is pressed between Teflon (or equivalent) sheets at a pressure of 15 to 30 MPa. The cloth is sintered at 320° C for 2 hours in a hydrogen atmosphere. (Oxides such as platinum oxide can also be used as the catalyst, but must be sintered in a nitrogen atmosphere.)

The product is a flexible electrode having a 0.03- to 0.05-cm layer of catalyzed carbon on the cloth substrate. It contains 20 to 23 weight percent of PTFE binder and about 2 mg/cm^2 of platinum.

This work was done by Wen-Tong P. Lu and Robert L. Ammon of Westinghouse Electric Corp. for **NASA's Jet Propulsion Laboratory.** *For further information, Circle 71 on the TSP Request Card.*
NPO-15268

Laminating Polyimide Films

New processes yield void-free flexible laminates.

Langley Research Center, Hampton, Virginia

A new process for laminating large areas of high-temperature polyimide film has applications in vehicle construction and in preparing flexible printed circuits. Linear polyimides are excellent candidates for such applications because of their high thermal stability at temperatures between 477 K (400° F) and 589 K (600° F), their flexibility, and their light weight. The objectives of the process are to improve the bonding of high-temperature polyimide film, to prepare flexible, large-area, void-free laminates from polyimide film, and to laminate polyimide film not only to itself but to metal surfaces.

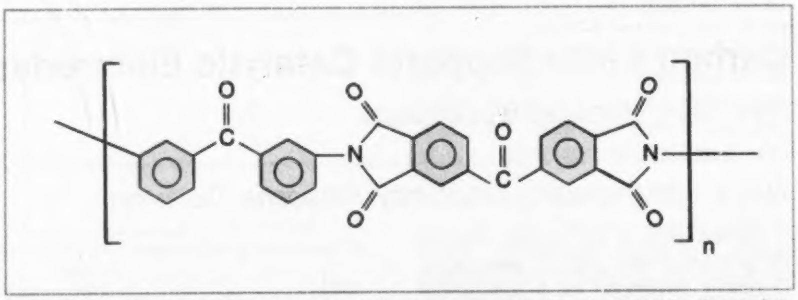

Figure 1. A **Thermoplastic Polyimide Adhesive** is used to bond polyimide sheets into flexible laminates.

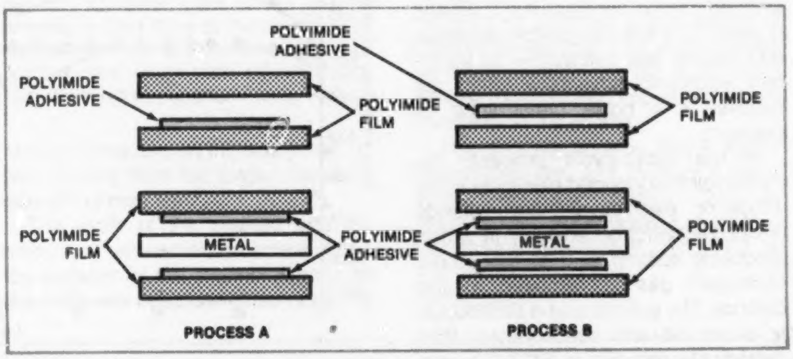

Figure 2. **Processes for Laminating Polyimide Films** with each other or with metal are shown here. In process A, the films are first primed with polyimide adhesive, then bonded together under heat and pressure. The adhesive is cast on a separate surface in process B, then sandwiched between the polyimide and/or metal films for final assembly.

Polyimide adhesive (see Figure 1) was used to bond Kapton® H polyimide film to itself and to metal sheets in two process variations. The first variation (Figure 2, left) involves the following four steps:

1. Priming one polyimide film with a thin coat of a linear polyamic acid adhesive solution,
2. B-staging the primed film to 493 K (428° F) in air for 1 hour to remove excess solvent and to convert the polyamic acid adhesive to the more stable polyimide,
3. Thermoplastically bonding the B-staged film to another sheet of primed or unprimed film in a steel mold at 616 K (650° F) for 5 minutes under 50 to 300 psi (3 to 20 MPa) pressure, and
4. Cooling the polyimide film laminate under pressure before removing from the mold.

The resulting laminate is clear yellow, extremely flexible, and 100 percent void-free. Attempts at peeling the laminate cause the film itself to fail.

The second variation (Figure 2, right) involves the following five steps:

1. Fabricating a thin film of the polyamic acid adhesive by casting the solution on a flat surface,
2. Thermally imidizing the polyamic acid adhesive film to the polyimide by heating in air to 493 K (428° F) for an hour,
3. Stripping the adhesive film from the casting surface and placing it between two sheets of polyimide film,
4. Placing the sandwich in a steel mold and thermoplastically laminating as before, and
5. Cooling under pressure.

Ultimate success in obtaining a void-free laminate depends on the complete removal of excess solvent and the thermal conversion of the polyamic acid adhesive to the polyimide prior to laminating. Bumping (the release of pressure followed by a reapplication of the same pressure), often used to allow the escape of excess volatiles in lamination, proved to be unnecessary in this process for the preparation of void-free laminates. Preheated platens were used for successful laminations at pressures of 50 psi, 150 psi, and 300 psi.

Success in obtaining a well-consolidated laminate depends on attaining an even distribution of pressure. The use of several layers of release cloth or woven glass fabric between the laminate and the steel mold did much to distribute the pressure evenly on the laminate.

The two variations for laminating polyimide film may also be used to prepare metal-containing laminates, as shown in Figure 2. Aluminum, brass, copper, and stainless steel have been successfully laminated to polyimide film using this process. Other metals or metal-coated film may also be used; the metals need only to be degreased with a solvent, such as ethanol or methylethylketone, prior to laminating, although a more-strenuous surface preparation may be used if desired.
(Kapton ® is a registered trademark of E. I. du Pont de Nemours & Co., Inc.)

This work was done by Anne K. St. Clair, Terry L. St. Clair, and Philip D. Robinson of **Langley Research Center.** *For further information, Circle 72 on the TSP Request Card.*

Inquiries concerning rights for the commercial use of this invention should be addressed to the Patent Counsel, Langley Research Center [see page A5]. Refer to LAR-12742.

Repairing Voids and Delaminations in Composite Materials

Proposed tool forces adhesive into cracks.

Lyndon B. Johnson Space Center, Houston, Texas

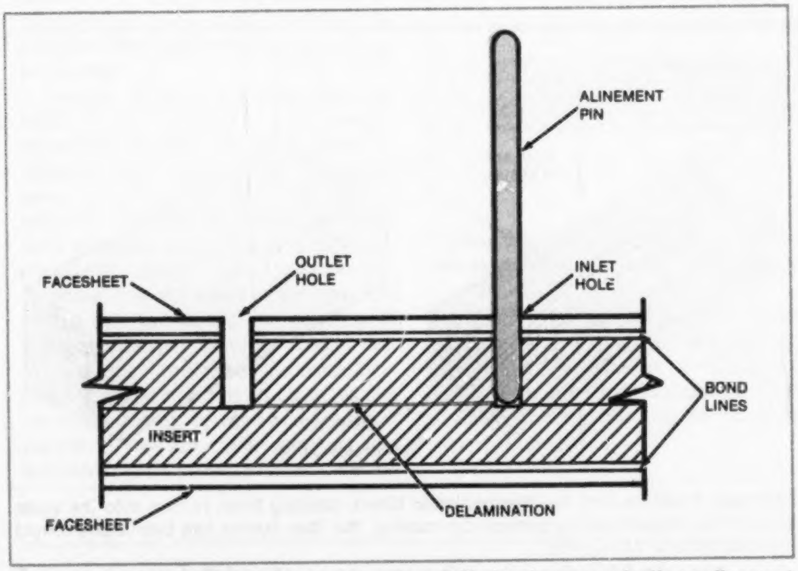

Figure 1. After **Inlet and Outlet Holes Have Been Drilled** to the proper depth, an alinement pin is inserted in the inlet hole.

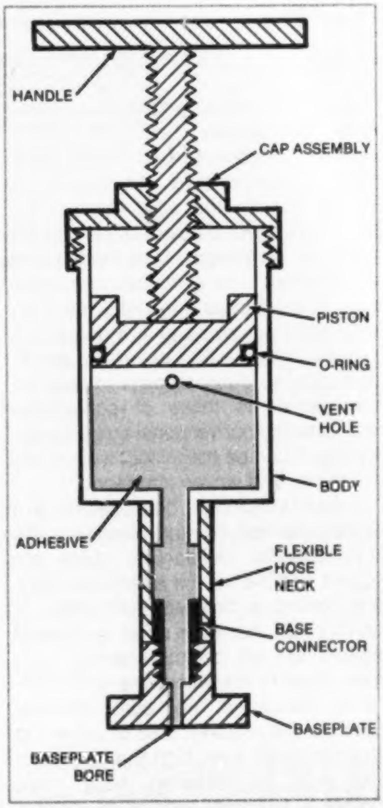

Figure 2. The **Injection Repair Tool** consists of three main sections: baseplate, body, and piston/handle/cap assembly. The sections are separable.

A proposed method for repairing voids and delaminations in graphite/epoxy composite materials is based on the injection of an adhesive under pressure. A hole is drilled in the material to the depth of the void or delamination, and adhesive is forced through the hole into the material. The adhesive fills a void (a gap resulting from the absence of bonding material) or is forced into a delamination (a crack between unbonded layers of laminate), expanding the delamination slightly to ensure full penetration.

Previously, a syringe was used to inject adhesive. However, the poor seal between the syringe needle and the laminate prevented pressure from building up enough to ensure full penetration. A vacuum line has been attached to the outlet hole to aid adhesive penetration: This procedure has been moderately successful in filling voids but self-defeating with delaminations since the vacuum tends to force unbonded surfaces together and thus impedes penetration.

In the new method, the location of the void or delamination is first determined from X-ray photographs. Two No. 50 holes are drilled into the discontinuity at its extremities. When air can be passed from one hole to the other, the holes have been drilled to the proper depth. An alinement pin is inserted in one of the

(continued on next page)

holes (Figure 1). Contact cement is applied to the facesheet of the laminate around the alinement pin and to the bottom surface of an injection repair tool (Figure 2). The baseplate is slipped over the pin and pressed against the facesheet so that the plate and sheet adhere, and then the pin is removed. (The alinement pin prevents contact cement from entering the injection hole and ensures that the baseplate bore and injection hole are alined.)

The body of the injection tool, less the piston, handle, and cap assembly, is threaded onto the baseplate; and the body is filled with adhesive up to its vent-hole. The piston, handle, and cap assembly are then attached to the body. The handle is turned so that it forces the piston downward and displaces air from the body through the vent. As the handle is rotated farther, it forces adhesive through the baseplate, into the delamination or void, and out the outlet hole. The repair is then complete.

The tool is removed and cleaned with solvent so that it is ready for reuse. The baseplate is pried away from the facesheet with a putty knife.

The proposed repair method is not limited to graphite/epoxy composites. It has potential applications in the repair of fiber-reinforced plastic structures, such as aircraft components, boats, storage tanks, and some automobile bodies.

This work was done by David D. Ott of McDonnell Douglas Corp. for **Johnson Space Center.** *For further information, Circle 73 on the TSP Request Card.*

Inquiries concerning rights for the commercial use of this invention should be addressed to the Patent Counsel, Johnson Space Center [see page A5]. Refer to MSC-20131.

Solventless Fabrication of Reinforced Composites

Heat and pressure convert a fiber bundle into a fiber-reinforced composite.

Langley Research Center, Hampton, Virginia

A new processing technique developed at Langley Research Center creates fiber-reinforced composites from solvent-resistant thermoplastics. In the new method, solid fibers of the thermoplastic and fibers of reinforcing agent are intimately mixed, heated, and compressed. The combination of pressure and temperature melts the thermoplastic, causing it to flow and fill the spaces between the reinforcing fibers. After cooling, the composite has properties similar to those of composites fabricated by conventional solvent processing. It can be machined, wound into filaments, and woven into fabric.

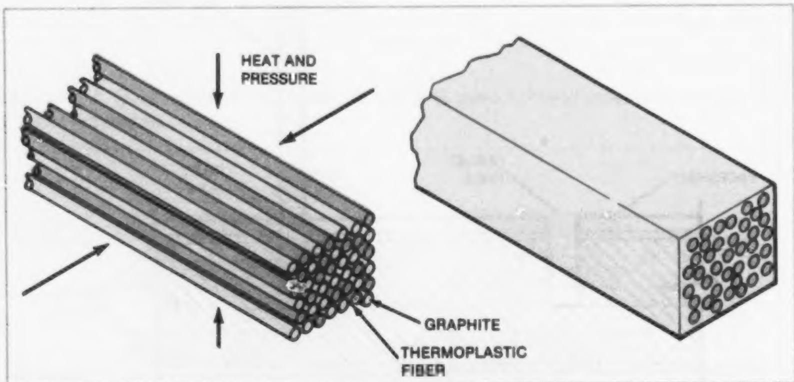

Heat and Pressure melt the thermoplastic fibers, causing them to flow into the voids around the graphite reinforcement. On cooling, the fiber bundle has been transformed into a structural composite.

Fiber-reinforced composites are usually formed by first dissolving the thermoplastic. Reinforcing fibers are added, and the solvent is removed, leaving behind a finished composite. In some cases, however, small residues of solvent are left behind, creating voids and possible delaminations in the finished composite. For some thermoplastics, the required ratio of solvent to thermoplastic is so high that the process must be repeated many times before a sufficient amount of thermoplastic accumulates around the fiber reinforcement. Other thermoplastics are very solvent-resistant and cannot be processed at all.

The figure shows the new process schematically. Fibers of thermoplastic are mixed with fibers of reinforcing fiber (typically graphite). The two fibers have approximately the same diameter. Heat and pressure are applied simultaneously, causing the thermoplastic fiber to melt. Upon cooling, the fibers fuse into a continuous matrix. The required temperature and pressure depend on the properties of the particular thermoplastic used.

This work was done by Robert M. Baucom of **Langley Research Center.** *No further documentation is available.*
LAR-12856

Solar-Cell Encapsulation by One-Step Lamination

Prefabricated covers are brought together with interconnected solar cells and cured in a single step.

NASA's Jet Propulsion Laboratory, Pasadena, California

A simple method of potting solar cells reduces encapsulating the cells to a one-step lamination process. The simplified process should save time and expense.

Two arrangements for solar-cell encapsulation are shown in the figure. In either arrangement, the interconnected solar cells are attached to one of the covers, either top or bottom, by an adhesive. In the one-step lamination process, potting material is applied over the solar cells and over the opposite cover. The two prefabricated components then are brought together, and the laminated assembly is cured in a single step.

Several different materials can be used for the assembly components depending on which cover receives the adhesive that initially holds the solar cells. Among the choices for potting material are polyvinyl butyral, ethylene vinyl acetate copolymers, and ethylene propylene rubbers. If the bottom cover receives the adhesive, then the top cover can be Korad (or equivalent) stabilized acrylic films or Tedlar (or equivalent) stabilized fluorocarbon polymers, and the bottom cover would be wood, metal, or reinforced-cement panels. If the top cover receives the adhesive (transparent), examples of materials for the bottom cover include stabilized acrylic/steel foil/stabilized acrylic, polyester/steel foil/stabilized acrylic, and polyvinyl chloride/aluminum foil/polyvinyl chloride; and the top cover would be glass.

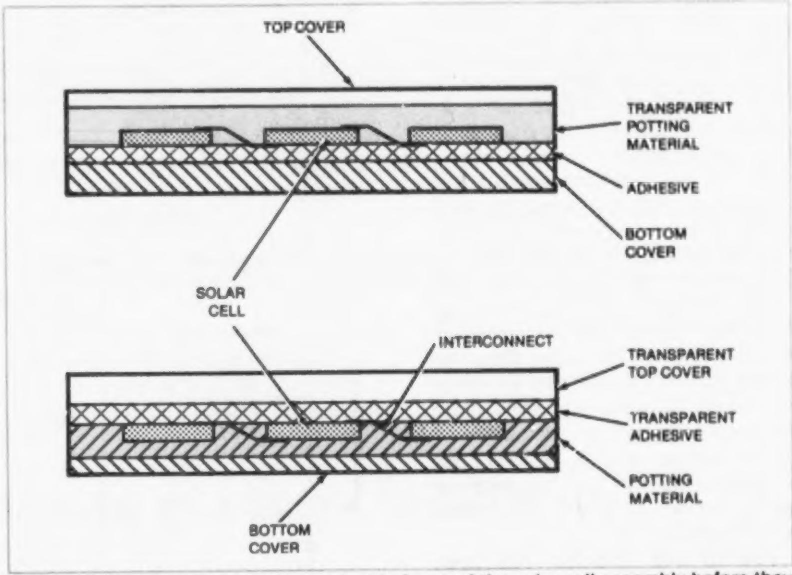

Potting Material is added to the two inside faces of the solar-cell assembly before they are sandwiched and cured. Two different assembly configurations are shown.

This work was done by Mohammad N. Sarbolouki of Caltech for **NASA's Jet Propulsion Laboratory.** *For further information, Circle 74 on the TSP Request Card.*
NPO-15222

Improved Photosensor for Light Valves

Innovations in processing optimize the CdS layer for good sensitivity and low negative memory.

Lyndon B. Johnson Space Center, Houston, Texas

Processing changes have improved the performance of a liquid-crystal light valve for displaying projection TV images. Before the changes were made, the display had an undershoot when it changed from high intensity to low (see figure). The effect occurred because a negative form of the previous image was superimposed on the new image for awhile; this negative memory phenomenon is associated with the cadmium sulfide (CdS) photosensor layer in the light valve. (The recombination rate of trapped holes exceeded the detrapping rate of electrons from shallow energy levels.)

It was discovered empirically that the negative memory in the light valve could be reduced to an acceptable level by

(continued on next page)

nitrogen doping of the CdS during sputter deposition, controlling the substrate temperature carefully during deposition, and annealing the deposited film in an argon atmosphere.

The approach taken was to monitor the performance of the finished light valves for given changes in the CdS process and experimentally to optimize the process for good sensitivity and low negative memory. The measure of sensitivity was the ratio of current amplitudes for various light inputs, relative to the dark signal. For 100 μW/cm^2 imaging light input, this ratio is typically somewhat greater than 2.0.

To hold the negative memory below 10 seconds and the sensitivity ratio above 2.5, the nitrogen doping had to be about 40 percent and the substrate level held at 140° C during deposition. Without the N_2 doping, the temperature had to be 150° C or higher to achieve a sensitivity ratio of 2. The doped films had such a dramatic increase of sensitivity with annealing, however, that the lower deposition temperature was feasible.

This work was done by N. John Koda of Hughes Aircraft Co. for **Johnson Space Center.** *No further documentation is available.*

Title to this invention has been waived under the provisions of the National Aeronautics and Space Act [42 U.S.C. 2457(f)], to the Hughes Aircraft Company, P.O. Box 90515, Los Angeles, CA 90009.

MSC-20036

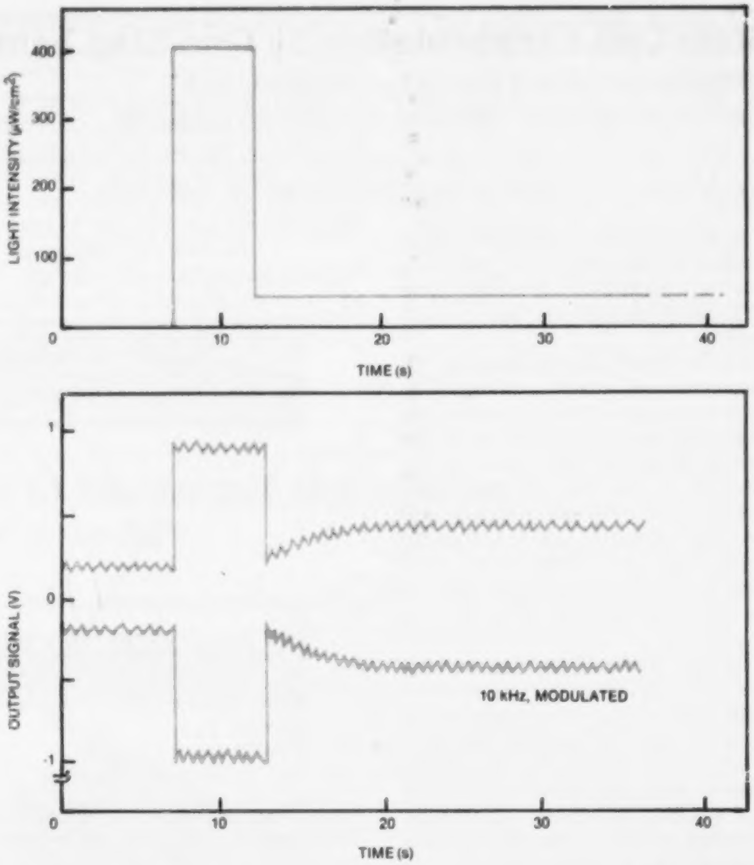

Negative Memory in a light valve is an undershoot of the output-signal envelope when the light level decreases abruptly.

Ampoule With Integral Feedthroughs

A vacuum-tight ampoule is used for crystal growth by the Bridgman method.

Langley Research Center, Hampton, Virginia

The key feature of a new crystal-growth ampoule is a molybdenum-to-quartz vacuum feedthrough that can be assembled in the laboratory. One feedthrough is attached to each end of the cylindrical ampoule, used for crystal growth by the Bridgman method, allowing interface demarcation by passing periodic current pulses through the sample during growth. The new ampoule is also vacuum-tight, so that it protects exposed areas of the furnace from corrosive vapors emanating from the sample and at the same time prevents changes in composition of the melt due to preferential vaporization of one of its components.

To form the molybdenum/quartz feedthrough (see figure), a quartz tube is sealed to a quartz capillary. As gas flows through the capillary, the walls of the quartz tube are thickened, making sure that there is still room in the thickened region for a molybdenum foil to be inserted and that the diameter of the rest of the tube is large enough for another piece of capillary to be placed inside.

A piece of molybdenum foil with a wire spot-welded to each end is inserted into the tube such that the wire feeds through each capillary up to the spot weld and the foil is surrounded by the thickened quartz wall. A seal is made at the open end of the quartz tube. This assembly is then mounted on a lathe and is attached to a vacuum system, which pumps through the capillary.

The quartz tube is collapsed onto the foil from the center out to the spot weld on each end. Another seal is made along the length of the capillary, and the excess tubing is cut off and discarded.

One feedthrough is sealed under vacuum in the end of the quartz ampoule. A press fit is made between the wire and either a piece of oriented semiconductor (for seeded growth) or a piece of graphite with a cone cut in the end toward the semiconductor melt.

Another feedthrough with a conical piece of graphite attached to the wire is mounted in the vacuum system so that it can be lowered and positioned in the ampoule. The ampoule is then mounted on the vacuum system and evacuated. The feedthrough is lowered until it makes contact with the semiconductor material, and the final vacuum seal is made.

The ampoule is mounted in the furnace, and connections are made to the wires to apply current pulses. The system is then ready for the Bridgman growth to proceed.

Crystals have been grown in the ampoule with the hot zone temperature as high as 1,150° C, the temperature gradient along the sample as high as 240° C/cm, and current pulses up to 40 A/cm^2. The configuration has been temperature-cycled from 25° to 1,000° C up to three times without the loss of vacuum or of electrical continuity.

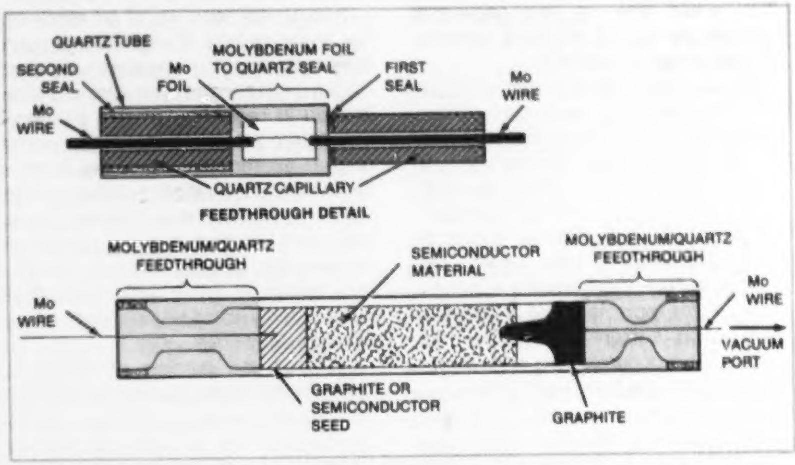

Bridgman-Growth Ampoule has molybdenum-to-quartz feedthroughs at both ends. The detail shows the feedthrough structure before the quartz tube has been collapsed onto the foil.

This work was done by Roger K. Crouch and W. J. Debnam of **Langley Research Center** *and R. Ryan of BOMCO, Inc. For further information, Circle 75 on the TSP Request Card.*
LAR-12899

Fabricating a Microcomputer on a Single Silicon Wafer

Proposed fabrication would reduce microcomputer packaging costs.

NASA's Jet Propulsion Laboratory, Pasadena, California

A concept for a "microcomputer on a slice" would reduce microcomputer costs by eliminating the scribing, wiring, and packaging of individual circuit chips. All components for a microcomputer — central processing unit, input/output circuitry, read-only memory, and random-access memory (CPU, I/O, ROM, and RAM) — would be placed on a single silicon wafer. The components would be interconnected by metal paths according to instructions from a computer. The slice would then be encapsulated as a single package of modest size.

Current practice, in contrast, is to build microcomputer circuits out of separately-packaged integrated circuits, or chips. One package contains the CPU, one the I/O, another the ROM, and others the RAM. The packages are interconnected externally on a printed-circuit board. Some commercial CPU chips do include a small amount of "scratch-pad" RAM and some ROM, however, these devices require additional memory to assemble a complete microcomputer.

Element	Unit Space	Number Required	Yield	Number Deposited	Total Spaces
CPU	2	1	20%	5	10
I/O	1	1	40%	3	3
ROM	1	2	40%	5	5
RAM	1	190	40%	475	475
					493

A **Low-Cost Microcomputer on a Silicon Slice** would contain redundant components. If the area of a RAM (of which about 510 can be placed on a 100-mm-diameter wafer) is regarded as a unit, the quantities shown in the table could be deposited. Each RAM has a storage capacity of 16,384 bits; thus at expected yield, the microcomputer would have a data capacity of 3,112,960 bits.

In manufacture of conventional integrated circuits, an entire slice of silicon is usually devoted to multiple replicas of a single component — all CPU's or all RAM's, for example. After the circuits have been deposited on a slice, they are scribed and broken into individual chips, which are wired to external leads and packaged.

In the new concept, microcomputers would be smaller because external wiring on circuit boards is unnecessary.

(continued on next page)

They would also be less expensive because the cost of individual handling of chips would be avoided.

Extra circuits of each component type would be deposited on the microcomputer slice to allow for possible defective circuits. For example, a slice might contain 5 CPU's, 3 I/O's, 5 ROM's, and 475 RAM's, even though only 1 CPU and I/O, 2 ROM's, and 190 RAM's are needed for the microcomputer (see table). The number of redundant circuits would be based on the expected yield of good circuits, which is largely a function of the area a circuit occupies on a chip. Larger circuits generally have lower yields.

Interconnections would be made by the usual method of exposure through masks. So that an excessive number of masks is not needed, elements would be located in regular geometric patterns. The interconnection computer would call up appropriate submasks from a library and automatically place them in position, and the entire interconnection network would be built up by a series of masking and deposition steps. The circuits would be tested and circuits that fail their tests would be isolated by blowing out fusible links.

Although the number of RAM's is large, connections to them and interconnections among them do not present a particularly difficult problem. A common data bus could be used, since the RAM's are addressable memories. As each RAM is tested, it is either disconnected or left connected, according to the test results. Once an adequate number of good RAM's has been found, the remainder may be disconnected whether they are good or bad to reduce power consumption.

This work was done by Vincent L. Evanchuk of Caltech for **NASA's Jet Propulsion Laboratory.** *For further information, Circle 76 on the TSP Request Card.*
NPO-15053

Electrolyte Reservoir Would Lengthen Cell Life

A proposed controlled-capillary sump would extend the life of sealed cells that depend on gas recombination.

Lewis Research Center, Cleveland, Ohio

Certain electrochemical cell types depend on the recombination of gases within them in order to insure long operating lives in the sealed condition without undue pressure buildup. Nickel/cadmium cells, in particular, depend on the recombination of oxygen that is generated on the nickel electrode during charge with cadmium metal in the presence of the potassium hydroxide electrolyte. This is generally accomplished by using separator materials (typically nonwoven nylon felts) that permit gases to cross from one electrode to the other and yet remain wetted with electrolyte so as to maintain good ionic conductivity between the electrodes. This property results from having the proper binodal pore size distribution within the wettable felt; that is, it contains some fine pores and some large pores. Due to the effects of cell aging or just the random aspects associated with the electrodes and separator materials going into any one cell, some electrodes can be kept with more than the desired amount of electrolyte while others can have too little.

It is suggested here that an electrolyte sump be placed within these cells below the assembly of anodes and cathodes to supply the proper amount of electrolyte during the course of operation. This sump cannot be simply free

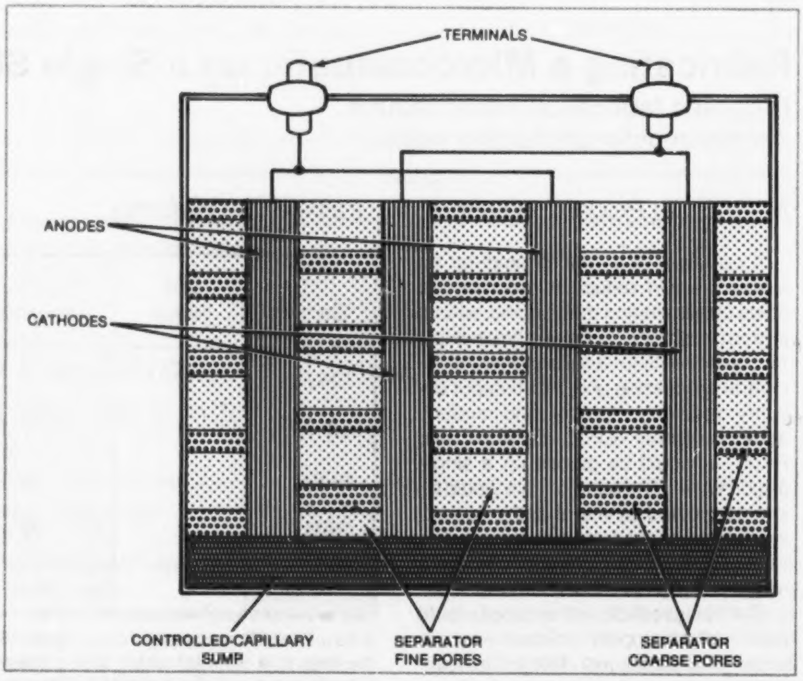

The **Controlled-Capillary Sump,** below the anode and cathode assembly, supplies the proper amount of electrolyte during cell operation. It releases the electrolyte to compensate for the electrolyte that empties from the electrodes and separators.

volume but must be of a capillarity intermediate between that of the fine pore portion of the separator and the coarse pore portion of the separator (see figure). In that way, as the fine pore portion of the separator or the pores of the electrodes begin to empty, the electrolyte within the controlled capillary sump would supply this amount and yet would not flood the large pore portion of the separator.

In cells where gaseous recombination is employed, fully flooded conditions are not desired since this would prohibit the free passage of oxygen gas from the nickel to the cadmium electrode. The term "starved" usually implies that there is a deficiency of electrolyte within the cell when the sums of all the porosities of all the cell components are considered. A certain free volume, devoid of electrolyte solution, is desired between the closely spaced electrodes. The fact that this portion of the cell that is devoid of electrolyte is in the separator results from a careful consideration of the pore size, capillarity, range of pore-size, etc. of each of the cell components.

The term "capillarity" is used to describe a component's tendency to retain electrolyte. When the capillarity of component A (C_A) is greater than that of component B (C_B), then the pores of component A will fill in preference to those of component B. Only when the pores of component A are filled will the pores of B begin to fill.

In a typical starved cell, the capillarity of the electrodes and of the separator need to be considered. Four capillarities can be considered. The separator has two separate capillarities: one for the small pores of the wettable filaments of the material used to make the felt and one for the large pores located between the bundles of filaments. In general, the capillarity for the fine pores of the separator should be greater than that of the two electrodes, and the capillarity of the two electrodes in turn should be greater than that of the large pore portion of the separator felt.

In this way, a cell can be loaded with electrolyte such that the pores of both electrodes, as well as the fine pore portion of the separator, are filled with electrolyte whereas the coarse pores of the separator are devoid of electrolyte and thus are permeable to gas. The ionic conduction between the electrodes thus permits electrochemical processes to proceed whereas the empty spaces within the large pores of the separator permit chemical recombination processes to take place.

A certain degree of electrolyte volume tolerance is displayed with this construction since the capillarity of the separator (highest) assures that there will be an electrolyte connection across the separator. Likewise, slight excesses are taken up in some of the large pores of the separator. The changes that occur within the electrodes during cycle life are such that there is a gradual tendency to require more electrolyte as the active material is repeatedly cycled. This process can slowly remove the electrolyte from the fine pores of the separator if the capillarity values are close to one another or the electrodes slowly become devoid of solution if this extra volume cannot be supplied by the separator. The life of certain cells of this type can be shortened if there is no way to provide for the increased demand for electrolyte volume.

This work was done by L. H. Thaller of **Lewis Research Center.** *No further documentation is available.*

Inquiries concerning rights for the commercial use of this invention should be addressed to the Patent Counsel, Lewis Research Center [see page A5]. Refer to LEW-13788.

Stable Polyurethane Coatings for Electronic Circuits

Alkane-based polyurethanes resist deterioration
while maintaining good dielectric properties.

Marshall Space Flight Center, Alabama

Polyurethane coatings and encapsulation compounds based on alkanes instead of ethers have superior chemical, electrical, and mechanical properties. High temperature and humidity have little effect on the alkane-based polyurethanes. Water-vapor transmission rates through polyurethane film prepared from alkanes are low in comparison with those for ether-based material.

The alkane-based materials absorb little or no water when immersed in water at 160° F (71.1° C) and lose little weight when dried after immersion, whereas ether-based polyurethanes absorb water and swell in hot water and weigh significantly less than their original weight after drying (see figure).

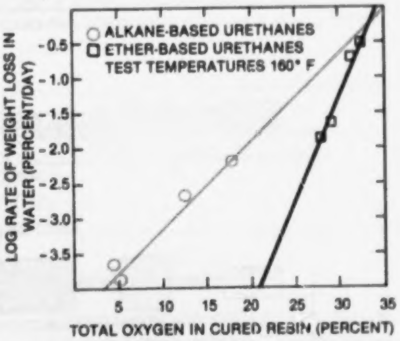

Weight Loss After Prolonged Immersion in hot water is far less for alkane-based polyurethanes than for the more-common ether-based polyurethanes, at any given oxygen content.

The alkane-based polyurethanes are prepared from polybutadiene polyols (which are sometimes used in place of ethers as a starting material in commercial resins). These types of polyurethanes were previously known to have excellent dielectric properties and to be hydrolytically stable. However, when polybutadiene-based polyurethanes are exposed to ozone under stress, they deteriorate because ozone attacks the double bond in the butadiene structure and severes the polymer chain. In alkane-based polyurethanes the double bond is removed from the polymer chain by hydrogenation of the polyol, and there is therefore no point of

(continued on next page)

attack for ozone. These urethanes are thus oxidatively stable as well as hydrolytically stable.

Major uses of polyurethanes are as connector potting materials and as conformal coatings for printed-circuit boards. An important requirement for such applications is good dielectric properties — in particular, low dielectric constant and dissipation factor. MSFC-SPEC-515, a specification for urethane molding and potting material, requires a dielectric constant of 5.0 or less and a maximum dissipation factor of 0.09. The dielectric properties of alkane-based polyurethanes are well within the specification and remain so after temperature, humidity, ozone, and immersion tests.

This work was done by Donald E. Morris of **Marshall Space Flight Center.** *For further information, Circle 77 on the TSP Request Card.*
MFS-25663

RF Sputtering of Gold Contacts on Niobium

Low-resistance contacts are stable down to 4.2 K.

NASA's Jet Propulsion Laboratory, Pasadena, California

Reliable gold contacts are deposited on niobium by a combination of RF sputtering and photolithography. The process results in structures that have gold only where desired for electrical contact. The contacts are stable under repeated cycling from room temperature to 4.2 K. They show a room-temperature contact resistance as much as 40 percent below that of indium contacts made by thermal-compression bonding.

The process consists of photolithography, gold sputtering, and metal lift-off. In the first step of the process (see figure), photoresist is applied to the niobium on the insulating substrate. Photolithography then opens windows in the photoresist, exposing the niobium to which contact is to be made. Next, the metal is RF sputtered to etch about 200 Å of the niobium surface. After this, the RF is applied to the gold target to sputter a 1,000-Å layer of gold over the niobium substrate.

Finally, the gold-coated structure is removed from the sputtering chamber and placed in a solvent for the photoresist. This removes the photoresist and lifts off the gold situated above it, leaving behind gold sputtered onto the niobium only in the regions where windows were originally opened in the photoresist.

This work was done by Daniel W. Barr of the University of Virginia for **NASA's Jet Propulsion Laboratory.** *For further information, Circle 78 on the TSP Request Card.*
NPO-15624

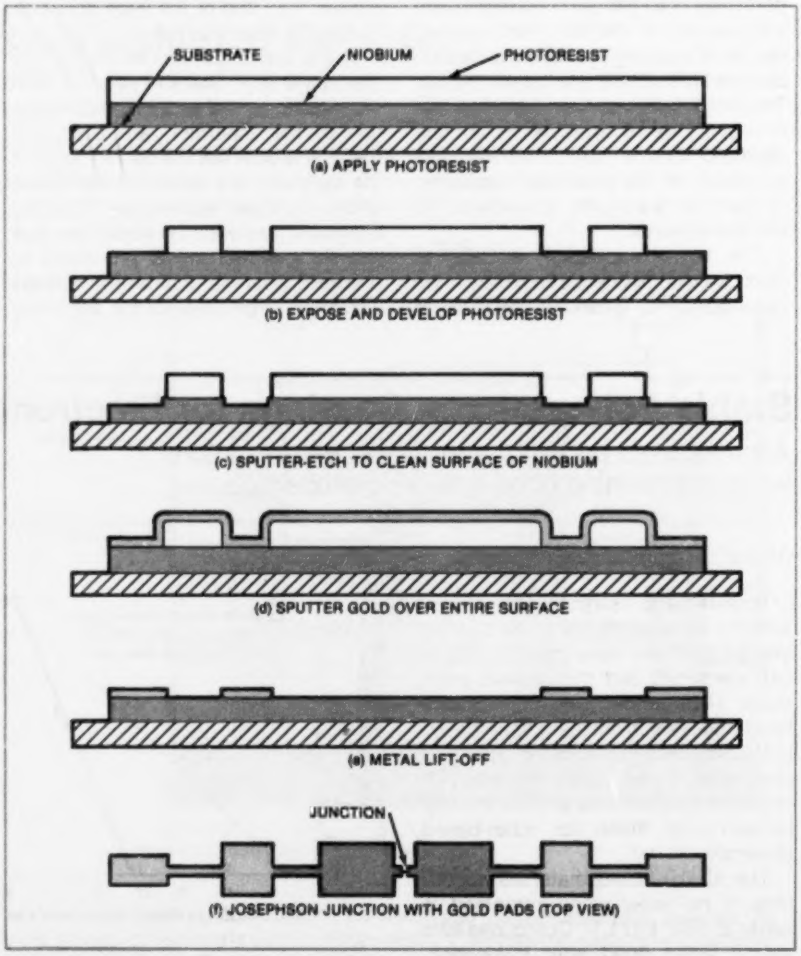
SUBSTRATE
NIOBIUM
PHOTORESIST
(a) APPLY PHOTORESIST
(b) EXPOSE AND DEVELOP PHOTORESIST
(c) SPUTTER-ETCH TO CLEAN SURFACE OF NIOBIUM
(d) SPUTTER GOLD OVER ENTIRE SURFACE
(e) METAL LIFT-OFF
JUNCTION
(f) JOSEPHSON JUNCTION WITH GOLD PADS (TOP VIEW)

Gold Is Sputtered (d) over the entire surface after etching the unmasked niobium surface (c). The process was used to make contacts to a Josephson junction (f).

Mass Producing Targets for Nuclear Fusion

A metal-encapsulation technique would advance the prospects of controlling nuclear fusion.

NASA's Jet Propulsion Laboratory, Pasadena, California

A process tested in the laboratory could mass-produce targets for controlled nuclear fusion. Spherical capsules — the targets — are formed from molten metal and simultaneously filled with heavy isotopes of hydrogen that would serve as the nuclear fuel. Rapid solidification of the molten metal takes place while the targets are in free fall, promoting a spherical form.

Inertial-confinement fusion is one of the promising technologies for power generation in the future. A target, placed within a reactor, is imploded by an intense, focused burst of laser energy. The fuel is compressed to the high temperature and pressure needed for fusion to occur, releasing a large amount of energy. For power generation the process would be conducted with a high-repetition rate. Targets now undergoing testing are formed of glass, but newer designs employ metal shells. These are currently produced individually by the very costly method of micromachining.

In the new process, molten metal — tin, gold, or lead, for example — is forced through an axisymmetric nozzle that contains a center tube providing a flow of fill gas, which could be the fuel. The resultant hollow liquid jet spontaneously pinches off uniform lengths of the gas jet, encapsulating the fill gas. These quickly separate under free fall and become spherical before they completely freeze.

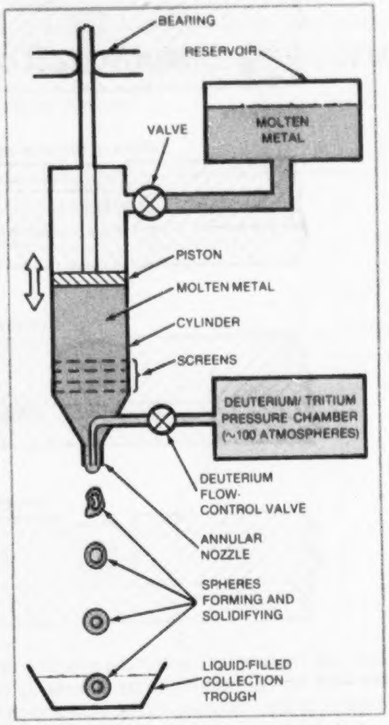
BEARING
RESERVOIR
VALVE
MOLTEN METAL
PISTON
MOLTEN METAL
CYLINDER
SCREENS
DEUTERIUM/ TRITIUM PRESSURE CHAMBER (~100 ATMOSPHERES)
DEUTERIUM FLOW-CONTROL VALVE
ANNULAR NOZZLE
SPHERES FORMING AND SOLIDIFYING
LIQUID-FILLED COLLECTION TROUGH

Prefilled Fusion Targets are formed at a nozzle as molten metal such as tin flows through its outer channel and pressurized deuterium/tritium gas flows through its inner channel. The molten metal completely encloses a gas charge as it drops off the nozzle.

The process is shown schematically in the figure. A piston forces the liquid metal through the annular orifice in a batch mode. The flow of fill gas is initiated simultaneously with the piston motion and proceeds at a rate commensurate with that of the liquid. The process of forming hollow shells is then continuous during the batch, with shells being formed at a rate of a few tens to a few thousands per second, depending upon the size being produced. In tests at atmospheric pressure, shells ranging between 0.7 and 7.0 mm in diameter have been produced. By placing the apparatus within a pressure vessel, it would be possible to produce targets filled to an internal pressure exceeding 2,000 lb/in.^{2} (1.4 × 10^7 N/m^2).

This work was done by Taylor G. Wang, Daniel D. Elleman, and James M. Kendall, Jr., of Caltech for **NASA's Jet Propulsion Laboratory.** *For further information, Circle 79 on the TSP Request Card.*

This invention has been patented by NASA [U.S. Patent No. 4,279,632]. Inquiries concerning nonexclusive or exclusive license for its commercial development should be addressed to the Patent Counsel, NASA Resident Office-JPL [see page A5]. Refer to NPO-15455.

Etching and Growth of GaAs

Precise temperature control adjusts melt composition before each etch.

NASA's Jet Propulsion Laboratory, Pasadena, California

A simple arrangement for etching away a surface layer of a gallium arsenide crystal before an epitaxial layer is deposited on it prevents an unwanted high-resistivity interface from forming. The etching and deposition setup is expected to simplify processing and improve the characteristics of gallium arsenide lasers, high-frequency amplifiers, and advanced integrated circuits.

Etching and deposition are carried out in a standard gallium arsenide liquid-phase epitaxial reactor. The arsenic source crystal and the gallium arsenide substrate crystal are held in separate slots in a graphite slider, under a graphite boat holding the etch melt and the growth melt (see figure).

The first step is to saturate the etch melt with arsenic at a temperature below the growth-melt saturation temperature. The slider is moved so that the source crystal is positioned under the etch melt at a temperature of 745° C for 1 hour — long enough to saturate the bottom of the gallium etch melt with arsenic.

Next, the slider is moved so that both the substrate and the source crystal are removed from the melts. The tem-

(continued on next page)

perature is raised 5° C, to 750° C, the growth-melt saturation temperature.

The substrate and source crystal are moved quickly under the etch melt so that only the source crystal is positioned under the growth melt. The source crystal saturates the growth melt with arsenic.

The furnace temperature is reduced to 748° C, but the etch melt is still 3° C above the temperature at which it was exposed to the arsenic source crystal and is therefore undersaturated by a precisely known amount. The substrate is moved under the undersaturated etch melt, which removes material from the substrate surface. The length of time the substrate is under the melt determines the depth of etch.

At the end of the etching period, the substrate is quickly moved under the growth melt. This melt, which was saturated by the source crystal at 750° C, is now supersaturated by 2° C and therefore deposits gallium arsenide on the substrate.

This work was done by Alan C. Seabaugh and Robert J. Mattauch of the University of Virginia for **NASA's Jet Propulsion Laboratory.** *For further information, Circle 80 on the TSP Request Card.*
NPO-15625

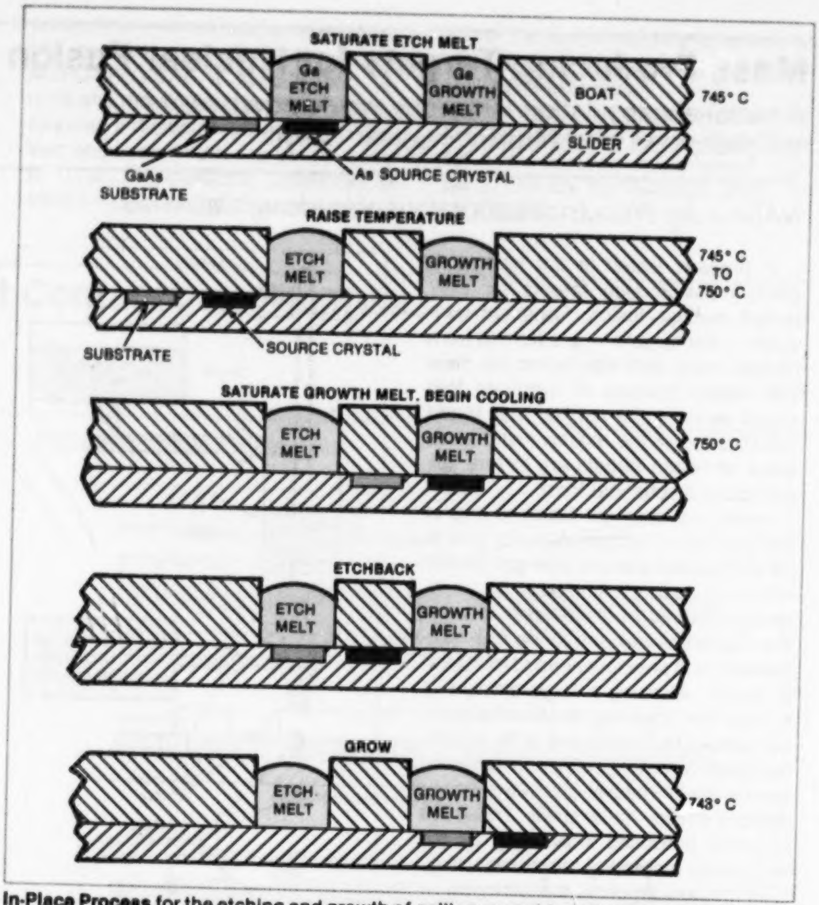

In-Place Process for the etching and growth of gallium arsenide calls for presaturation of the etch and growth melts by an arsenic source crystal. The procedure allows precise control of the thickness of the etch and of the newly grown layer on the substrate.

Recharging "Hot-Melt" Adhesive Film

Hot-melt adhesive charge is held in place by a one-sided tape.

Langley Research Center, Hampton, Virginia

A technique for recharging a surface with a "hot-melt" adhesive film makes use of a one-sided, high-temperature, pressure-sensitive adhesive tape. The technique was originally developed for use in space, where the absence of gravity can cause the adhesive charge to "float" away, due to the lack of tack.

The primary purpose of the one-sided tape is to hold the hot-melt charge in place until it is fused to the surface. After the adhesive has fused to the surface and has been cooled, the tape is removed, leaving the adhesive on the surface.

The technique will be used to recharge the surface-attachment assembly (SAA) pads of the work-restraint unit (WRU) of the Shuttle orbiter. The SAA pads utilize a high-temperature hot-melt adhesive for attachment to the surface-insulation tiles of the orbiter.

Since the adhesive is depleted from the surface of the pads after successive attachments and detachments, a way of recharging the adhesive is needed. The one-sided-tape technique satisfies this need, allowing an astronaut to recharge the adhesive on the pads and increasing the number of possible pad attachments and detachments.

The hot-melt film is sandwiched between the pressure-sensitive tape and a thin release film. Tabs are provided for removing the tape and the film.

The release film is first stripped from the hot-melt charge and the tape. While still on the tape, the charge is precisely positioned over the designated area on the pad. The adhesive tape is then pressed down on the rim and glass cloth of the pad.

To transfer the adhesive, the pad is heated to the melt temperature of the charge, in this case approximately 163° C (325° F), and is held at that temperature for a short time. The pad is then cooled to a lower temperature, in this case approximately 66° C (150° F). The adhesive tape is then stripped from the pad, leaving the pad recharged with the hot melt adhesive and ready for use.

This technique could be used on Earth where certain constraints, such as fixed inverted position of the surface to be recharged, would limit the use of other methods for applying a hot-melt adhesive film.

This work was done by Donald J. Progar of **Langley Research Center.** *For further information, Circle 81 on the TSP Request Card.*

This invention is owned by NASA, and a patent application has been filed. Inquiries concerning nonexclusive or exclusive license for its commercial development should be addressed to the Patent Counsel, Langley Research Center [see page A5]. Refer to LAR-12881.

Simplified Heat-Source/Thermionic Converter

Heat is transferred by radiation across a vacuum gap.

NASA's Jet Propulsion Laboratory, Pasadena, California

A new design for a nuclear-powered electric generator simplifies its assembly and reduces its size and weight. Intended to supply 120 kW for propulsion of a spacecraft, the generator uses a nuclear reactor to produce heat, which is then transformed into electricity by an array of thermionic converters. The new design concept would be also applicable to terrestrial and nonnuclear thermionic power supplies.

As can be seen in the figure, heat is extracted from the reactor by heat pipes, which form a heat-radiating cylindrical wall outside of the reactor. A vacuum gap separates this inner (heat-source) cylindrical wall from an outer (converter) cylindrical wall formed by an array of heat-receiving surfaces fastened to the thermionic converters. The outside of the converter cylinder radiates any excess heat.

In this design, heat crosses the vacuum gap as thermal radiation. An earlier design had a ceramic instead of the vacuum between the reactor heat pipes and the thermionic converters and had additional heat pipes for cooling the collectors of the thermionic converters. Ceramic was used because the wall had to be electrically nonconducting to permit a series connection of thermionic converters on a common heat pipe. Elimination of the ceramic makes the entire structure shorter, narrower, and lighter and also avoids the difficult problem of generator assembly and of finding a material that is electrically insulating at the high temperature (about 1,650 K) of operation.

This work was done by Katsunori Shimada of Caltech for **NASA's Jet Propulsion Laboratory.** *For further information, Circle 82 on the TSP Request Card.*
NPO-15278

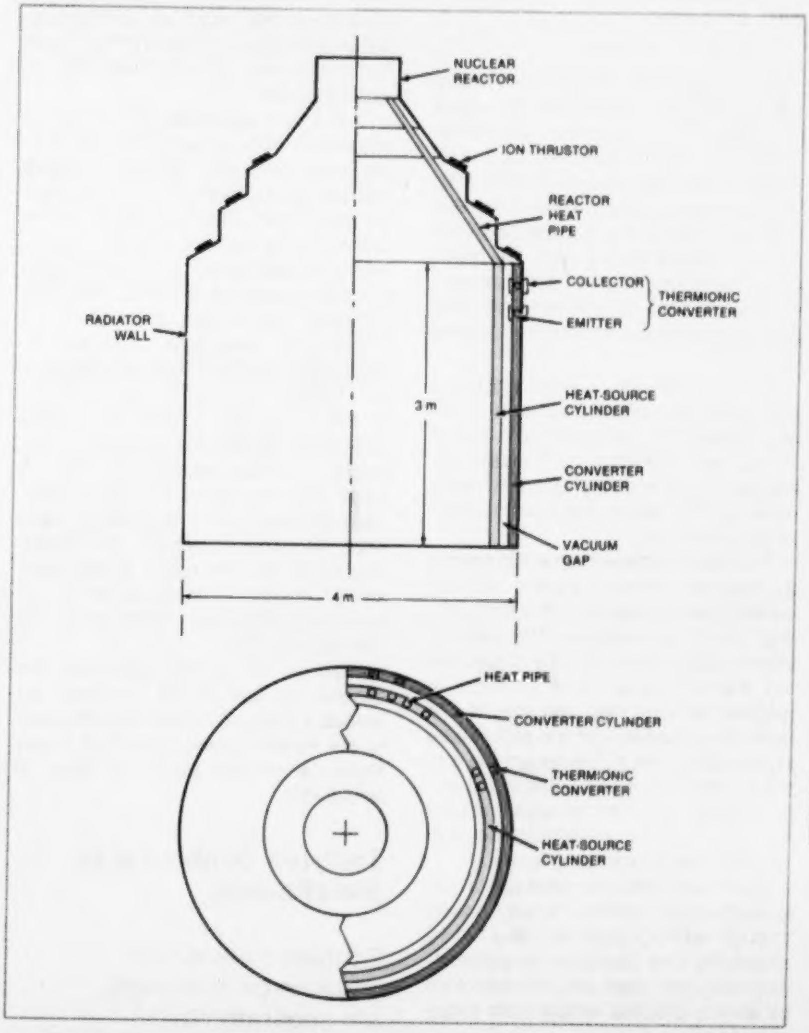

Radiation Coupling of the heat from the heat-source cylinder to the converter cylinder through the vacuum gap eliminates the need for high-temperature electrical insulators between the reactor heat pipes and the thermionic converters. In addition, no radiator heat pipe is necessary because the collectors of the thermionic converters from which excess heat must be removed radiate directly to space.

Books and Reports

These reports, studies, and handbooks are available from NASA as Technical Support Packages (TSP's) when a Request Card number is cited; otherwise they are available from the National Technical Information Service.

Etching Integrated Circuits

Report reviews manual and automatic methods, both wet and dry.

A 20-page report reviews the methods available for etching specific layers on wafers and discusses automation techniques and the features of one particular automated system. It compares the two major etching methods, chemical (wet) and plasma (dry), and discusses the areas in need of development. The methods covered include the "dip-and-dunk" manual method of chemical etching, automated chemical etching, and plasma etching.

About 85 percent of wafer etching is performed manually. The operator transfers baskets of wafers in and out of strong acid solutions to remove unwanted materials left exposed after masking. The wafers are then rinsed to remove the acids.

The mechanized equipment presently available for chemical etching includes walking-beam systems, in-line sprayers, and centrifugal sprayers. The walking-beam system mechanically duplicates the manual dip-and-dunk method: A mechanical arm lifts and lowers the wafer-filled baskets into the appropriate etching tank, with movement of the arm being controlled by an automatic timer. The disadvantage of the walking-beam system is that the entire machine must be protected against acid fumes.

Eliminating this disadvantage, in-line spray/etching systems convey wafers through etching, cleaning, and drying chambers. One machine can automatically etch and rinse and will eventually be able to process wafers from a cassette to a tray.

The batch and in-line chemical processes offer high production rates. The chemicals can etch deeply into any material, and etch rates are generally faster than with plasma etching. However, the procurement, storage, handling, and disposal of chemicals are expensive, troublesome, and hazardous; and chemical purity is a constant concern.

In the dry technique of plasma etching, highly-energized plasma particles react with the substrate to be etched, and the volatile products of the reaction are removed from the chamber by the vacuum pump. Plasma etching is commonly used to pattern such materials as silicon dioxide, silicon nitride, silicon, tantalum, tantalum nitride, tantalum oxide, molybdenum, and tungsten. Many of the previous problems associated with plasma etching, such as overheating, wafer damage, and overetching, have been alleviated by improvements in reactor design.

The report concludes with a list of specifications for an automatic processing system for semiconductor wafers and with the features of the rinser/dryer for the system. The illustrations in the report include the sequence for an automated etching system and photographs of the automatic wafer etcher, its carrier transport, and its rinser and dryer.

This work was done by Bobby W. Kennedy of **Marshall Space Flight Center.** *Further information may be found in NASA TM-82411 [N81-74978/NSP], "Chemical Etching for Automatic Processing of Integrated Circuits" [$6]. A paper copy may be purchased [prepayment required] from the National Technical Information Service, Springfield, Virginia 22161. The report is also available on microfiche at no charge. To obtain a microfiche copy, Circle 83 on the TSP Request Card.*

Inquiries concerning rights for the commercial use of the invention described in the report should be addressed to the Patent Counsel, Marshall Space Flight Center [see page A5]. Refer to MFS-25661.

Tests on Double-Layer Metalization

Sputtered aluminum patterns on two levels are separated by an insulating oxide.

A 28-page report describes experiments in the fabrication of integrated circuits with double-layer metalization. The double-layer metalization requires much less silicon "real estate" and allows more flexibility in the placement of circuit elements than does single-layer metalization.

The integrated circuit chosen for the demonstration is a complementary metal-oxide-semiconductor/silicon-on-sapphire (CMOS/SOS) solar-cell controller. Up to the metalization stage, the circuit is fabricated in the standard way: Silicon is deposited on a sapphire substrate; transistors, diodes, capacitors, and resistors are formed in the silicon by ion implantation; an oxide layer is formed over the circuit surface; and contact holes are opened in the oxide.

Then the metalization is applied. The first layer is a 0.8-μm-thick pattern of aluminum containing 2 percent silicon, deposited by sputtering. On the first layer is grown a 0.6-μm-thick insulating layer of silane oxide. Through holes 7.6 μm square are etched in the insulating layer so that the second metalization layer can make contact where needed with the first layer and with the circuit elements. Next, the second layer, a 1.2-μm-thick pattern of pure aluminum, is evaporated from a filament or sputtered on the insulating layer. Finally, a 0.6-μm-thick protective oxide film is grown over the surface.

Optical and scanning electron microscope measurements show that the first-layer metal is very smooth — an essential condition for reducing the incidence of short circuits between the two metal layers. The second-layer metal is continuous over steps in the first layer.

The probe yield of good IC chips on two wafers, each containing about 850 chips, was about 12 percent. Of the 132 chips that were encapsulated in dual-in-line packages, 95 passed final tests. Of these, 25 chips with leakage current less than 100 μA were selected for burn-in life tests consisting of three bias cycles: 168 hours at 125° C, 72 hours at 150° C, and 168 hours at 150° C. Only three chips failed the burn-in tests, probably because of a short between the metal layers through the insulating layer. The remaining 22 chips functioned well, and 18 of them maintained leakage current below 100 μA.

This work was done by D. S. Woo of RCA Corp. for **Marshall Space Flight Center.** *To obtain a copy of the report, Circle 84 on the TSP Request Card. MFS-25688*

Mathematics and Information Sciences

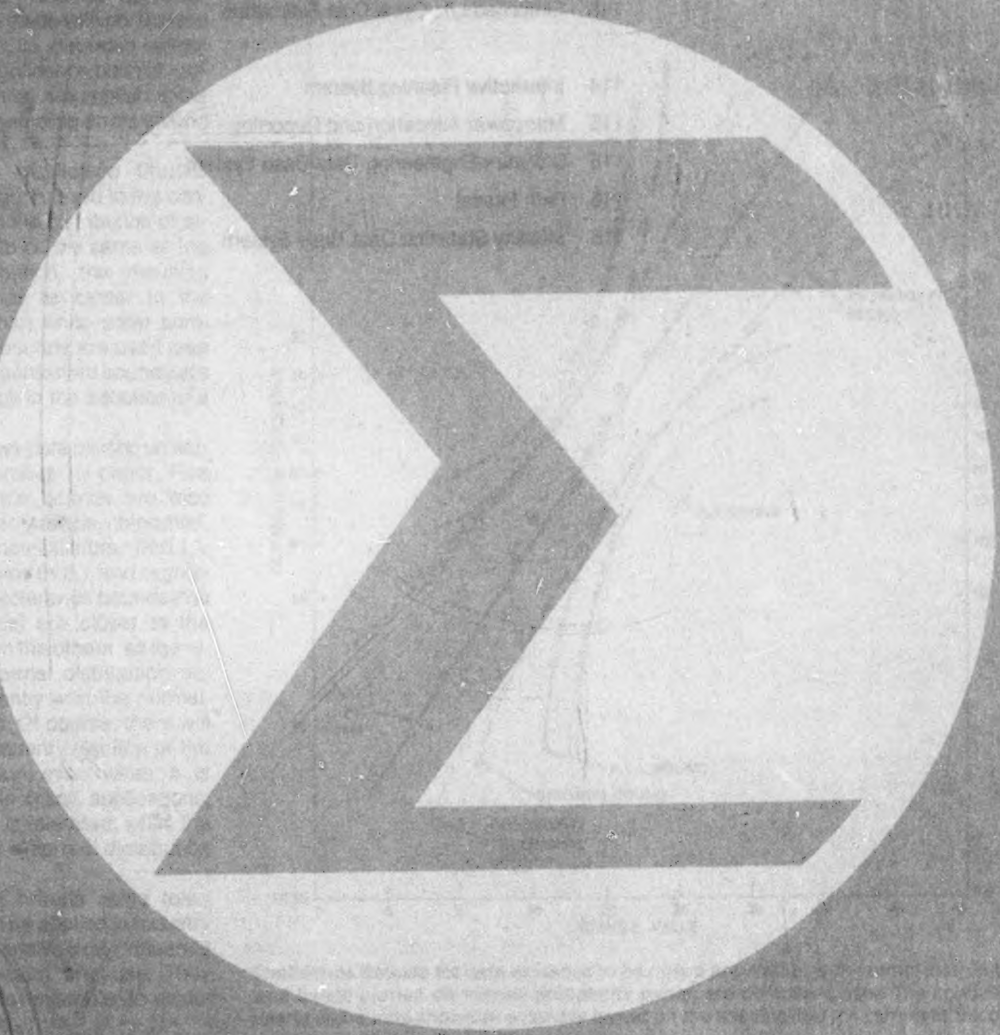

Hardware, Techniques, and Processes

111 Consistent Tolerance Bounds for Statistical Distributions
112 Computing Graphical Confidence Bounds
113 Formulas for Precise Transverse Mercator Projection
113 Simplified Life-Cycle Cost Estimation

Computer Programs

114 Interactive Planning System
115 Manpower Allocation and Reporting
115 Software-Engineering Data-Base System
115 Path Pascal
116 Stability Statistics Data Base System

Consistent Tolerance Bounds for Statistical Distributions

False hypotheses are screened by using consistent tolerance bounds.

Lyndon B. Johnson Space Center, Houston, Texas

The assumption that a sample comes from a population with a particular distribution can be made with confidence C if the data all lie between certain bounds. These "confidence bounds" depend on C and on an assumption about the distribution of sampling errors around the regression line.

The analysis of Space Shuttle surface-tile strength has led to the conclusion that when the distribution of errors is assumed to be the same as the population distribution, the resulting confidence bounds lie closer to the regression line than when other common confidence bounds are used (see figure). Thus, the consistent bounds are least likely to result in the adoption of a false hypothesis.

The figure shows data plotted on normal (Gaussian) probability paper. Five sets of confidence bounds are also shown: normal-tolerance, binomial, Kilmogorov-Smirnov-Lilliefors (K.S.L.), Kilmogorov-Smirnov (K.S.), and regression. The normal-tolerance bounds (the consistent bounds) are closer to the "best-fit" line than the others, so the rejection of the normal distribution occurs more frequently with the normal-tolerance bounds. Of course, there will also be more frequent rejection of the normal distribution even when it is valid; however, in many applications, this type of error is tolerated, while the acceptance of an incorrect distribution is not.

Graphical test criteria using tolerance bounds can be applied in industry where statistical analysis can influence product development and use. They can be applied, for example, to evaluate equipment life.

This work was done by Michael A. Mezzacappa of Rockwell International Corp. for **Johnson Space Center.** *For further information, Circle 85 on the TSP Request Card.*
MSC-20090

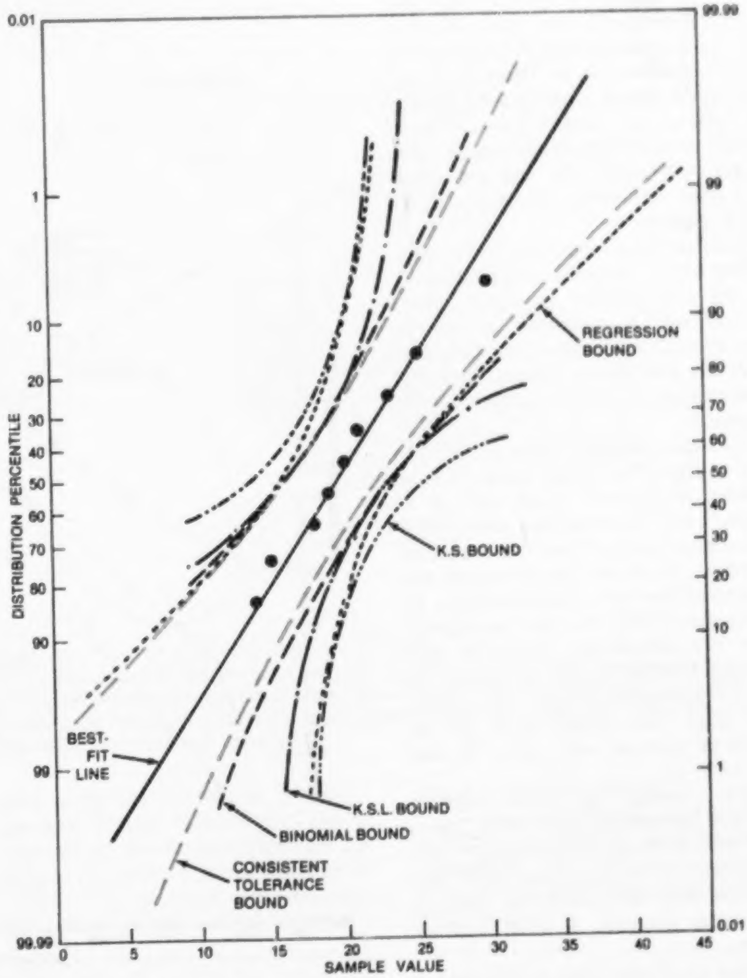

Confidence Bounds for data assumed to be from a population with normal distribution (and hence plotted on normal probability paper) are compared here. The consistent tolerance bounds shown in color are based on the assumption that errors in the data also have a normal distribution.

Computing Graphical Confidence Bounds

An approximation formula is easily computed on a programable calculator.

Lyndon B. Johnson Space Center, Houston, Texas

A new approximation for graphical confidence bounds is simple enough to run on a programable calculator. The approximation can be used in lieu of numerical tables, which are not always available, and exact calculations, which often require rather sizable computer resources. The approximation has been verified for a collection of up to 50 data points.

Confidence bounds define the limits within which a data set can be assumed to fit a particular statistical distribution — for example, a normal distribution. If any data point falls outside the confidence bounds, then the assumption of distribution normality is rejected.

The figure shows 10 data points plotted on lognormal graph paper. A true normal distribution would plot as a straight line; however, the data points are scattered about the line because of sampling variability. Also shown are the 5- and 95-percent confidence bounds, calculated using the new approximation. For comparison, the exact confidence bounds are also indicated. Excellent agreement is seen over the entire scale. The agreement is just as good for samples with up to 50 data points.

This method has been used to analyze tile-strength data on the Space Shuttle thermal-protection system. The efficiency of the approximation can reduce labor and computer costs of statistical analyses in other applications.

This work was done by Michael A. Mezzacappa of Rockwell International Corp. for ***Johnson Space Center.*** *For further information, Circle 86 on the TSP Request Card.*
MSC-18908

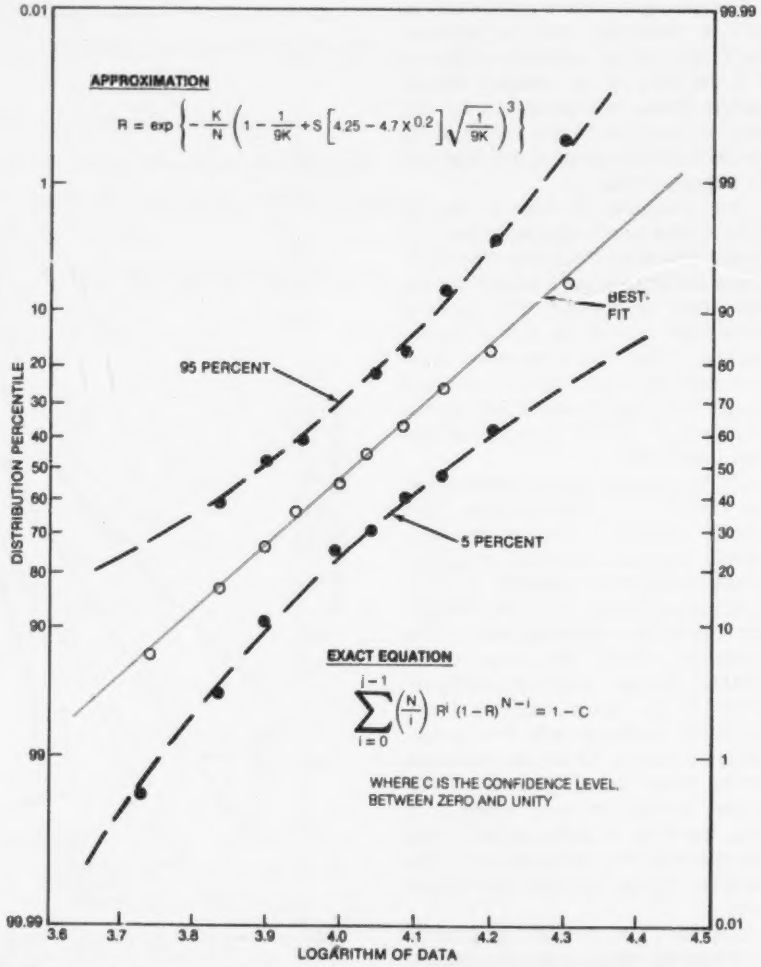

Confidence Bounds, calculated approximately, are shown as plotted points and, calculated exactly, as dashed lines. The sample data are shown in color. In the confidence-ranking approximation formula, the parameters X, S, and K are determined exactly before starting the calculation. The exact formula is solved by iteration on a computer.

Implementing Exclusive-OR Logic

A BCD-to-decimal decoder and one four-input NAND gate can be wired as a four-input exclusive-OR (XOR) gate. Combining several of the basic two-IC arrangements allows XOR of any number of inputs.

(See page 5.)

Calculating Safe Clearances for Manipulators

A method rapidly calculates the minimum safe clearances for remote manipulators. The method offers special benefits in industrial robotics, particularly in industrial machining.

(See page 60.)

Mapping Ocean Winds by Radar

Data on windspeed, wind direction, and wind patterns at the ocean surface are extracted from radar signals, using a special algorithm. From this information other weather parameters can be derived.

(See page 27.)

Formulas for Precise Transverse Mercator Projection

A new method yields precise geodetic maps.

NASA's Jet Propulsion Laboratory, Pasadena, California

A new method for producing geodetic maps is not only easier to use than older methods but is also more precise.

The new technique is a simplified method for computing the transverse Mercator projection. In this projection, points on the surface of Earth are projected conformally onto a cylinder (see figure) that is tangent at a principal meridian (including both poles). The cylinder is then cut and flattened to form a planar map.

The new method makes use of a set of formulas that connect coordinates of points on an oblate-spheroid-shaped Earth to rectangular map coordinates. The formulas are a new generalization of the previously known formulas for a spherical Earth.

The formulas are in the form of conjugate harmonic series in odd powers of the spheroidal latitudinal eigenfunction and odd harmonics of the sine and cosine of the longitude. The coefficients of the series are rational-coefficient polynomials in the spheroidal eccentricity of Earth or other body to be mapped. These coefficients may be precomputed. The leading terms of the harmonic series are actually those of the conventional polar stereographic projection.

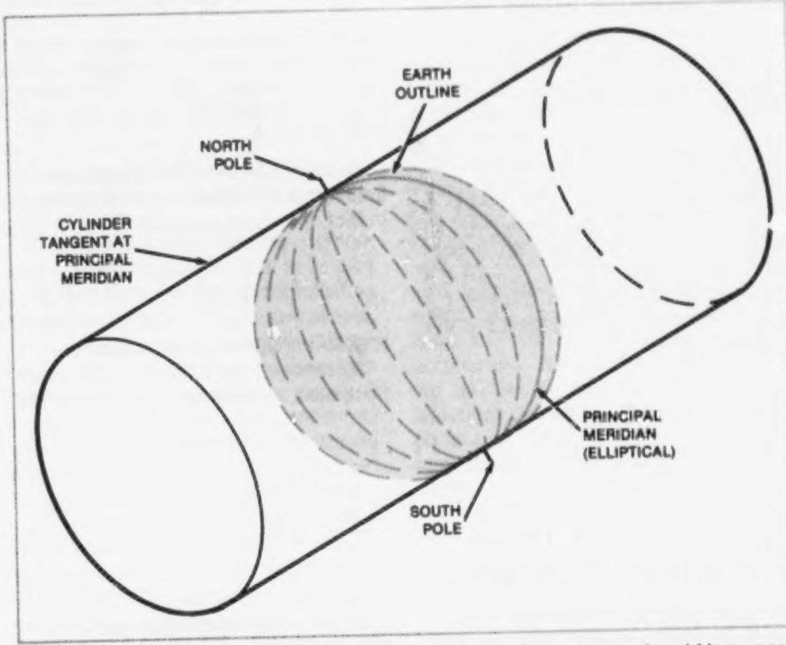
EARTH OUTLINE
NORTH POLE
CYLINDER TANGENT AT PRINCIPAL MERIDIAN
PRINCIPAL MERIDIAN (ELLIPTICAL)
SOUTH POLE

In the **Transverse Mercator Projection,** the surface of Earth or other spheroid is mapped onto a cylinder that is tangent at a meridian of longitude. The new method performs the mapping by means of a mathematical series in which the higher order terms correct for the deviation from exact sphericity.

Tables of the calculus of the spheroidal latitudinal eigenfunction and related functions, and power series for these functions have been developed. The argument of the eigenfunction may be expressed either in distance from the pole along the meridional arc or in geodetic latitude. Besides their use in mapmaking, the functions can be applied to the design of streamlined structures — for example, when distance along an ellipsoidal surface requires a simple analytic expression.

This work was done by David E. Wallis of Caltech for **NASA's Jet Propulsion Laboratory.** *For further information, Circle 87 on the TSP Request Card.*
NPO-15409

Simplified Life-Cycle Cost Estimation

A formula using a single parameter gives accurate results.

NASA's Jet Propulsion Laboratory, Pasadena, California

A simple method for life-cycle cost (LCC) estimation avoids the pitfalls inherent in formulations requiring separate estimates of inflation and interest rates. The method depends for its validity on the observation that interest and inflation rates closely track each other.

The LCC of a project is the lump sum of money that would have to be set aside at one time (usually at the beginning of the project) to cover all expenditures during the entire life cycle of the project. In estimating LCC the "time value of money" is taken into account. The amount of money that must be set aside to cover a future expenditure is affected by both interest and inflation rates. Interest may be earned on the money set aside, but inflation will increase the amount of the final expenditure. Thus the effects of interest and inflation rates

(continued on next page)

tend to offset each other and the net effect on LCC is essentially due to the difference in these rates.

With an annual inflation rate j, an expenditure that costs C at time t_0 will at a later time t cost

$$C(1 + j)^{t-t_0}$$

With annual interest rate i, the discounted value of this cost at time t_0 is:

$$C(1 + j)^{t-t_0}(1 + i)^{-(t-t_0)}$$

This can be reexpressed as

$$CV^{t-t_0}$$

where $V = (1 + j)/(1 + i)$. Thus LCC can be calculated by specifying an assumed value for V rather than for both i and j. Specifically, if $C_1, \ldots, C_n$ are the assumed yearly costs in present (t_0) dollars, then the LCC (evaluated at the present) is given by

$$LCC = \sum_{k=1}^{n} C_k V^k$$

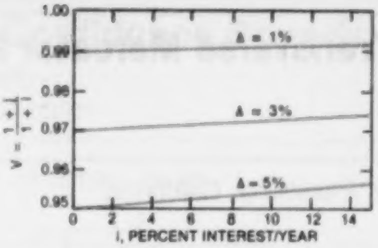

The Parameter V is shown as a function of interest rate i for various fixed differences between interest and inflation rates, Δ = i − j. At low interest rates, V is nearly equal to 1 − Δ.

As the figure shows, V is essentially a function of the difference of rates, i − j. In fact, the approximation

$$V = 1 - \frac{i - j}{1 + i} \approx 1 - (i - j)$$

is good enough for most purposes.

Historically, the difference i − j has fluctuated considerably less than i and j themselves, with the difference usually being about 2 to 3 percent. A modeling study has been done using actual interest and inflation rates for the period 1950 to 1976 in LCC calculations for projects of 5- to 20-year duration and starting dates from 1950 to 1972. A choice of V = 0.983 gave good results over the entire period.

The study shows that inflation and discounting largely cancel each other and that it is essentially only the difference between them that affects LCC. Furthermore, fluctuations in the rates tend to cancel out over project lifetimes. As a consequence, a single parameter V can be chosen to estimate the net effect of future discount and inflation rates with a reasonable degree of confidence.

This work was done by Donald S. Remer, Gary Lorden, and Isidore Eisenberger of Caltech for **NASA's Jet Propulsion Laboratory.** *For further information, Circle 88 on the TSP Request Card.*
NPO-15228

Computer Programs

These programs may be obtained at very reasonable cost from COSMIC, a facility sponsored by NASA to make new programs available to the public. For information on program price, size, and availability, circle the reference letter on the COSMIC Request Card in this issue.

Interactive Planning System

System helps managers plan projects within time, budget, and manpower constraints.

The NASA Interactive Planning System (NIPS) supports resources analysis and tracking and long-range resources planning. NIPS is based on a hierarchical-tree data-base structure and remote graphics terminal input and output. It assists the program-planning groups at NASA Headquarters in developing long-range plans for the total space effort. These functions involve meeting goals and objectives within time, budget, and manpower constraints. Although NIPS is oriented toward NASA planning, it is a general tool that could be adapted to any resource-management and allocation problem.

NIPS aids financial planners in monitoring resource expenditures (i.e., dollars and manpower) for ongoing projects as well as in preparing long-range plans. The NIPS data base centralizes resources data and maintains a history of data evolution. NIPS is fully interactive, enabling the analyst to enter, modify, or delete data rapidly.

Large amounts of graphical and textual data can be generated rapidly by NIPS for analysis or manager review. Upon analysis, changes can be made in minutes to respond to "what if" questions, with complete new graphical and tabular displays generated showing the impact of any changes. NIPS should find applications in any situation where resources monitoring is important and rapid evaluation of alternative resource-allocation plans is desirable.

NIPS consists of four subsystems:

- NIPS-RTOP (Research and Technology Operating Plan),
- NIPS-PCS (Project Control System),
- NIPS-PMR (Program Management Report), and
- NIPS-LRP/POP (Long Range Planning/Program Operating Plan).

NIPS-RTOP tracks the resources status of individual RTOP efforts. It is primarily an inquiry system that allows the user to obtain the status of any RTOP or groups of RTOP's quickly.

NIPS-PCS is a tool for project resource analysts. It tracks actual performance, both technical milestones and resources, against a project plan.

NIPS-PMR is oriented to the needs for resources management of programs and projects. The basic function of the system is to assist in the tracking of actual cost against planned cost over a 12-month (fiscal-year) operating period. The data base for NIPS-PMR consists of planned and actual figures for both obligations and costs and actual figures for commitments.

NIPS-LRP/POP is oriented to the needs for building, modifying, and analyzing plans composed of activities for a long period of time. The data base consists of planning data (costs, manpower, and schedules) as they are forecast for a lifetime of an activity. This subsystem can be used for Program Operating Plan (POP) planning exercises.

NIPS is written in FORTRAN and COMPASS for the RUN compiler and has been implemented on a CDC 6000-series computer using the SCOPE operating system. The largest NIPS subsystem has a central memory requirement of 52K (octal) 60-bit words. NIPS can be accessed interactively or executed from batch. For interactive processing, a Tektronix 4014-1 terminal and supporting vendor software are required.

This program was written by David A. Nippert, T. H. Beerman, and Jerry L. Pittenger of Battelle Memorial Institute for **NASA Headquarters.** *For further information, Circle G on the COSMIC Request Card.*
HQN-10920

Manpower Allocation and Reporting

Interactive program handles data for up to 75 projects and allocations for up to 60 months.

The interactive Manpower Allocation and Reporting System (MARS) helps planners make manpower allocation decisions. MARS includes provisions to enter overall constraints for projects and persons, to assign individuals to projects, to compute automatically the overhead category, to report on deviations from constraints, and to generate manpower resource allocation reports.

The MARS data base may contain data for up to 75 projects, 75 people, and manpower allocations for 60 months. For each project, data stored include a unique project number, project name, manpower constraints, manpower totals, and manpower data pointers. For each person, data stored include their name, section number, skill code, employee code, manpower available, manpower totals, and manpower data pointers. Manpower allocation data are stored in terms of the portion of a man-month allocated for each person for each project by month.

MARS is an interactive menu-driven program consisting of an executive routine and three major components. The input/modify component allows the user to enter new data or to modify existing data in the data base. The report-generator component allows the user to look at data that are in the data base.

Three basic types of reports may be generated: A manpower report consists of either a display of persons versus time for a specific project, of projects versus time for a specific person, or of projects versus time for a specific organization. A person or project list report consists of a list of all the persons or projects in the data base. Constraint reports consist of displays of projects over constraint, projects under constraint, persons over constraint, and persons under constraint. The user has the option to see detailed constraint reports for particular persons or projects.

The interactive-scheduling component of MARS allows the user to employ a trial-and-error method of rescheduling manpower for both projects and people. The user requests the display of manpower reports and then interactively changes any of the manpower values. If a change causes manpower constraints to be exceeded, informative messages are displayed to aid the user in the formulation of further rescheduling trials.

MARS is written in FORTRAN IV Plus and Assembler for interactive execution and has been implemented on a DEC PDP-11/70 computer under RSX-11M with a central memory requirement of approximately 33K of 16-bit words. MARS was developed in 1977 and updated in 1978.

This program was written by Phillip D. Merwarth of **Goddard Space Flight Center.** *For further information, Circle H on the COSMIC Request Card.*
GSC-12708

Software-Engineering Data-Base System

System collects and maintains data for software-development efforts.

The Software Engineering Laboratory Data Base Maintenance System (SEL/DBAM) collects and maintains a data base for evaluating software-development methodologies. SEL/DBAM provides interactive facilities for the management of data collected by the Software Engineering Laboratory at Goddard Space Flight Center.

SEL/DBAM is organized into four component functions: create, archive, restore, and update. The interactive update programs may be classed into four groups based on the type of files processed and the program organization. These four classes consist of data-base summary and header files, complex data files, simple data files, and special data files. The update activities are divided into three modes: add new records, change existing records, and delete existing records. These modes allow the user to add to or modify files interactively in the data base as part of the regular data-collection procedure or in response to requests for changes by reviewers.

The create component of SEL/DBAM initializes required header records and creates new data-base files. It operates in an interactive mode and prompts the user for all information needed to add new data-base files. A tape copy of the entire data base or of a list of user-specified files is made by the archive component. This utility is useful in backing up files to tape for security and historical purposes. The restore component of SEL/DBAM recovers files from tapes generated with the archive utility.

SEL/DBAM is written in FORTRAN IV and Assembler for interactive execution. It has been implemented on a DEC PDP-11/70 computer with RSX-11M V3.1 and has a central memory requirement of approximately 64K of 8-bit bytes. SEL/DBAM was developed in 1980.

This program was written by David N. Card of Computer Sciences Corp. for **Goddard Space Flight Center.** *For further information, Circle J on the COSMIC Request Card.*
GSC-12669

Path Pascal

Pascal is extended to treat real-time concurrent systems.

Path Pascal is a high-level experimental programing language based on Pascal, which incorporates extensions for systems and real-time programing. Developed to investigate the benefits and problems that arise when path expressions are combined with a high-level language to provide a system programing tool, Path Pascal includes objects for information encapsulation,

(continued on next page)

path expressions for synchronization of processes that execute independently, and provisions for coding interrupt processes to deal with I/O devices. The language also includes abstract data and protection features. Instead of altering Pascal extensively, a few features were added such that standard P4 Pascal programs would still compile and execute, as long as the programs did not use Path Pascal reserved words as identifiers. Path Pascal can aid in investigating the problems of programing real-time concurrent systems.

The general Path Pascal system consists of a Path Pascal Compiler, a Path Pascal Interpreter, and a Path Pascal Linker. The Path Pascal Compiler accepts programs written in Path Pascal as input and generates P-code output. The Path Pascal Interpreter accepts P-code as input, which it interprets and executes based upon an extended version of the P4 interpreter virtual computer. The Path Pascal Linker combines two or more P-code files without having to recompile all of the source code.

Path Pascal is based on the P4 subset of Pascal. This subset was augmented with an encapsulation mechanism, open path expressions, and a process mechanism. Open paths are integrated with the encapsulation mechanism to enforce a strict discipline upon the programer to describe shared-information objects. All access to the encapsulated object is performed by operations synchronized by open paths. A routine invoking such operations may execute the operation only if permitted by the open path expressions associated with the shared-data object.

The Path Pascal Compiler, Interpreter, and Linker are written in the P4 subset of Pascal. The Path Pascal system has been implemented on a number of systems with the current base system for the version distributed by COSMIC being a CDC CYBER 170-series computer. The knowledgeable user should be able to implement Path Pascal on any system supporting the P4 subset of Pascal. The Path Pascal system was developed in 1979.

This program was written by Roy H. Campbell, Robert B. Kolstad, Daniel F. Holle, Thomas J. Miller, Philip Krause, Kurt Horton, and Tom Macke of the University of Illinois at Urbana-Champaign for **Langley Research Center.** *For further information, Circle K on the COSMIC Request Card.*
LAR-12854

Stability Statistics Data Base System

Four FORTRAN modules implement edit, sort, report-generation, and other functions.

The Stability Statistics Data Base System is written entirely in FORTRAN and does not require the use of outside data-management routines. It is used with a directly-accessible data base containing simple card images.

Although currently used with a data base containing data for the computation of computer hardware/software stability statistics, the Stability Statistics Data Base System could be adapted to numerous other data-base applications. With smaller data bases (approximately 15,000 records or less), the fast-response time of the report generator module makes it suitable for running in the demand mode. For larger amounts of data, the module may be run in the batch mode.

The Stability Statistics Data Base System consists of four functional modules. These are the stability data-base preprocessor (DRNEW), the data-base sort program (SORTNEW), the data-base transformation program (TRANSF10), and the data-base report generator (NEWNSTATS).

DRNEW edits raw input data, merges update records with the data-base records, and generates daily and summary time line reports. SORTNEW sorts the card image records via UNIVAC system sort package, CLINK$.

TRANSF10 transforms the sequential data base into a direct-access data base via the DEFINE FILE method. The direct-access data base generated by TRANSF10 is used by the report generator program NEWNSTATS. NEWNSTATS allows the user to perform ad hoc inquiries and report generation.

A "skip-sequential" search algorithm is implemented in NEWNSTATS to provide fast response. This module currently responds to inquiries and generates reports concerning the computer hardware/software stability statistics as mean time to failure, mean time to repair, mean time between failures, and numerous other statistics on computer system stability.

The Stability Statistics Data Base System is written in FORTRAN V for execution in the batch and demand modes and has been implemented on a UNIVAC 1108 computer with a central memory requirement of approximately 20K of 36-bit words for the largest functional module. The system was developed in 1980.

This program was written by Gee-Yin Kwok and Adrian Domingues of Computer Sciences Corp. for **Johnson Space Center.** *For further information, Circle L on the COSMIC Request Card.*
MSC-20014

SUBJECT INDEX

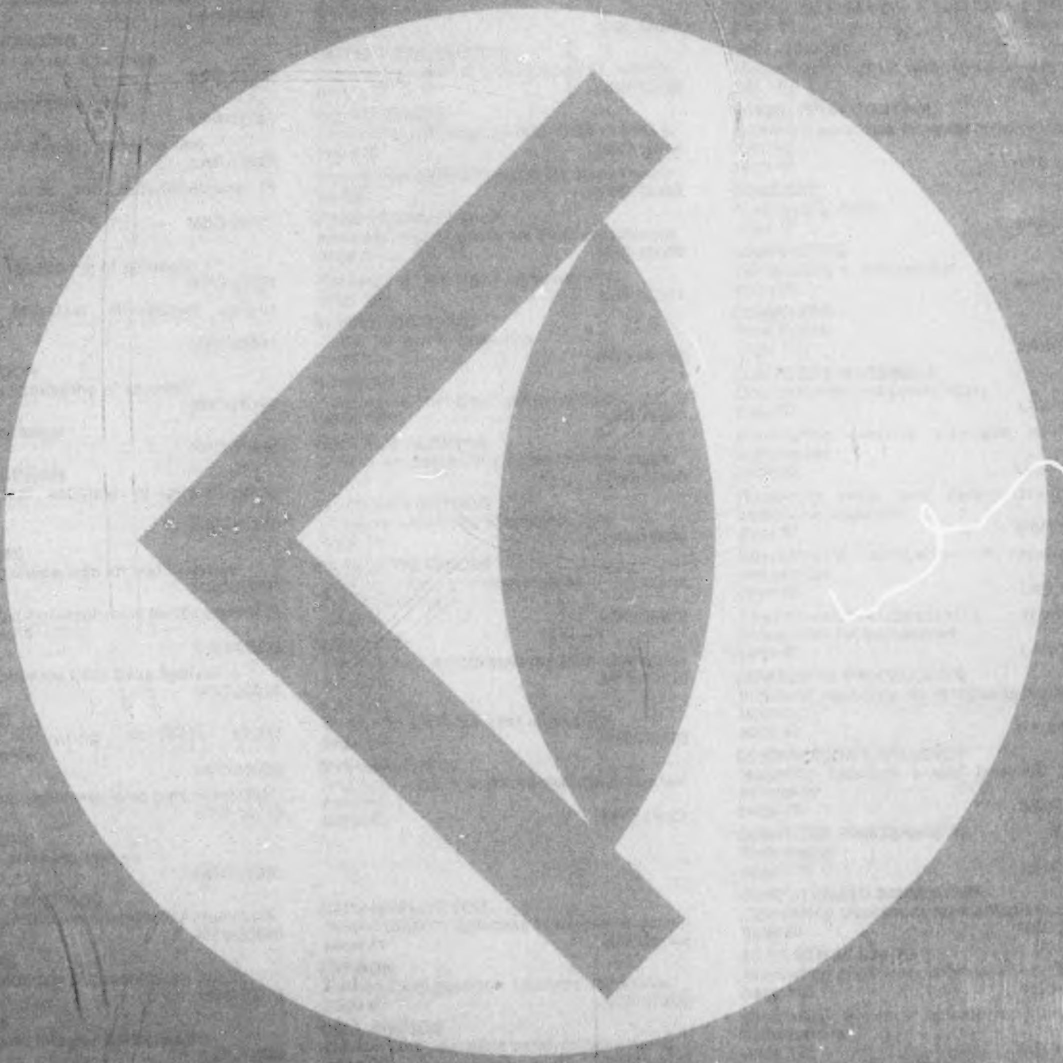

ACCIDENT PREVENTION
Can-filled crash barrier
page 72 NPO-15188
Sled control and safety system
page 16 MSC-20082
Spine immobilizer for accident victims
page 47 ARC-11167
ACRYLIC RESINS
Clear film protects against ultraviolet radiation
page 33 NPO-14971
ADHESION
Corrosion protection coatings for aluminum
page 42 MFS-25640
Recharging "hot-melt" adhesive film
page 106 LAR-12881
ADHESIVE BONDING
Fire-retardant epoxy adhesives
page 41 ARC-11430
Laminating polyimide films
page 96 LAR-12742
Recharging "hot-melt" adhesive film
page 106 LAR-12881
Repairing voids and delaminations in composite materials
page 97 MSC-20131
AEROSOLS
Continuous monitoring of aerosols
page 54 NPO-15292
Improved atomizer minimizes output fluctuations
page 76 MFS-25631
AIR POLLUTION
Continuous monitoring of aerosols
page 54 NPO-15292
Mobile air sampler
page 55 NPO-15220
AIRCRAFT DESIGN
Semi-empirical estimate of aircraft wing weight
page 62 ARC-11435
ALGORITHMS
Calculating clearances for manipulators
page 60 MSC-20208
Optimal regulator algorithms for the control of linear systems
page 21 LAR-12313
Stability Statistics Data Base System
page 116 MSC-20014
ALIGNMENT
Flexible coupling corrects shaft misalinements
page 74 NPO-15393
Flexible seal accommodates part mismatch
page 64 MFS-19710
ALLOCATIONS
Interactive planning system
page 114 HQN-10920
ALUMINUM COATINGS
Corrosion protection coatings for aluminum
page 42 MFS-25640
AMPLIFIERS
Audio distribution and monitoring circuit
page 6 MSC-20073
AMPOULES
Ampoule with integral feedthroughs
page 100 LAR-12899
ANTENNAS
Parasitically-excited ring antenna
page 12 MSC-20201
ANTIFRICTION-BEARINGS
Magnetic bearings would increase pump efficiency
page 76 GSC-12668
ASTRONOMICAL MODELS
Two- and three-dimensional galaxy simulations
page 29 LAR-12907
ATOMIZERS
Improved atomizer minimizes output fluctuations
page 76 MFS-25631
AUDIO EQUIPMENT
Audio distribution and monitoring circuit
page 6 MSC-20073
AUTOMOBILE ACCIDENTS
Can-filled crash barrier
page 72 NPO-15188

BALLS
Ball joint for quick connections and disconnections
page 79 LAR-12896
BATTERY SEPARATORS
Electrolyte reservoir would lengthen cell life
page 102 LEW-13788
BINARY CODES
Converting time signals from BCD to IRIG-B
page 16 MSC-18963
Simple exclusive-OR circuit for many inputs
page 5 MSC-18458
BINDERS (MATERIALS)
Heat-sterilizable binder for solid propellants
page 40 NPO-15020
Recharging "hot-melt" adhesive film
page 106 LAR-12881
BLADES (CUTTERS)
Cutter for woven materials
page 79 MSC-20178
BONDING
Recharging "hot-melt" adhesive film
page 106 LAR-12881
BOOLEAN ALGEBRA
Simple exclusive-OR circuit for many inputs
page 5 MSC-18458
BRIDGMAN METHOD
Ampoule with integral feedthroughs
page 100 LAR-12899
BUBBLE TECHNIQUE
Pressure-decay measurements improve bubble-point test
page 52 MSC-18970
BUCKLING
Flexible seal accommodates part mismatch
page 64 MFS-19710
BUDGETING
Simplified life-cycle cost estimation
page 113 NPO-15228
BURNING RATE
Improved equations for composite-propellant burning
page 43 NPO-15324

CAPS (EXPLOSIVES)
Screen secures detonator to explosive charge
page 71 MSC-20138
CARBON
Carbon cloth supports catalytic electrodes
page 95 NPO-15268
CELL ANODES
Carbon cloth supports catalytic electrodes
page 95 NPO-15268
CHEMICAL REACTORS
Liner for silicon reactor
page 42 NPO-15366
CHROMIUM
Environmental durability of electroplated black chromium
page 43 MFS-25797
CIRCUIT BOARDS
Stable polyurethane coatings for electronic circuits
page 103 MFS-25663
CLAMPS
Remote-action tube crimper
page 82 MSC-20197
CLUTCHES
Redundant gear train
page 73 NPO-15317
COAL UTILIZATION
A new use for high-sulfur coal
page 28 NPO-15194
Advanced coal-based power generation
page 84 MFS-25652
COATINGS
Corrosion protection coatings for aluminum
page 42 MFS-25640
CODING
Converting time signals from BCD to IRIG-B
page 16 MSC-18963
COLLIMATORS
Measuring mirror tilt with high accuracy
page 55 GSC-12701
COMBUSTION CONTROL
Improved equations for composite-propellant burning
page 43 NPO-15324
COMFORT
Ride-quality meter
page 17 LAR-12882
COMPACTING
Compacting silicon powder
page 38 NPO-15271
COMPILERS
Path Pascal
page 115 LAR-12854
COMPOSITE MATERIALS
Connector for composite tubes
page 53 LAR-12744
Measuring tensile strength of B/Al composites
page 62 LEW-13807
Repairing voids and delaminations in composite materials
page 97 MSC-20131
Solventless fabrication of reinforced composites
page 98 LAR-12856
Thermoset/thermoplastic aromatic polyamides for composites
page 39 LAR-12723
COMPOSITE PROPELLANTS
Improved equations for composite-propellant burning
page 43 NPO-15324
COMPRESSOR EFFICIENCY
Magnetic bearings would increase pump efficiency
page 76 GSC-12668
COMPUTER PROGRAMMING
Path Pascal
page 115 LAR-12854
COMPUTERIZED SIMULATION
Calculating clearances for manipulators
page 60 MSC-20208
CONFIDENCE LIMITS
Computing graphical confidence bounds
page 112 MSC-18908
Consistent tolerance bounds for statistical distributions
page 111 MSC-20090
CONNECTORS
Connector for composite tubes
page 53 LAR-12744
Screen secures detonator to explosive charge
page 71 MSC-20138
CONSOLIDATION
Consolidation of submicron silicon particles
page 37 NPO-15250
CONTROL SIMULATION
Calculating clearances for manipulators
page 60 MSC-20208

CONTROL THEORY
Optimal regulator algorithms for the control of linear systems
page 21 LAR-12313

COOLING
Heat pipes cool power magnetics
page 57 LEW-13507

CORROSION PREVENTION
Corrosion protection coatings for aluminum
page 42 MFS-25640

COST ANALYSIS
Simplified life-cycle cost estimation
page 113 NPO-15228

COUPLINGS
Ball joint for quick connections and disconnections
page 79 LAR-12896
Connector for composite tubes
page 53 LAR-12744
Flexible coupling corrects shaft misalinements
page 74 NPO-15393
Screen secures detonator to explosive charge
page 71 MSC-20138

CRACK INITIATION
Preventing cracks in titanium rotary seals
page 77 MFS-19686

CRASH INJURIES
Can-filled crash barrier
page 72 NPO-15188
Spine immobilizer for accident victims
page 47 ARC-11167

CRUCIBLES
Controlling thermal gradients during silicon web growth
page 91 NPO-15337
Improved barrier for continuous-crystal-growth crucible
page 89 NPO-15338
Modified silicon furnace lowers crystal cost
page 90 NPO-15041
Technique for crystal-ribbon growth
page 93 NPO-15177

CRYOLITE
Cryolite byproduct in silicon production
page 35 NPO-15364

CRYSTAL GROWTH
Improved barrier for continuous-crystal-growth crucible
page 89 NPO-15338
Modified die yields purer silicon ribbon
page 94 NPO-15385
Modified silicon furnace lowers crystal cost
page 90 NPO-15041
Pellet feed for dendritic-web growth
page 88 NPO-15198
Silicon sheet quality is improved by meniscus control
page 92 NPO-15384
Technique for crystal-ribbon growth
page 93 NPO-15177
Controlling thermal gradients during silicon web growth
page 91 NPO-15337

CUTTERS
Cutter for woven materials
page 79 MSC-20178

CZOCHRALSKI METHOD
Controlling thermal gradients during silicon web growth
page 91 NPO-15337
Modified silicon furnace lowers crystal cost
page 90 NPO-15041
Pellet feed for dendritic-web growth
page 88 NPO-15198
Technique for crystal-ribbon growth
page 93 NPO-15177

DAMPING
Measuring tensile strength of B/Al composites
page 62 LEW-13807

DATA BASES
Stability Statistics Data Base System
page 116 MSC-20014

DATA CONVERTERS
Converting time signals from BCD to IRIG-B
page 16 MSC-18963

DATA MANAGEMENT
Interactive planning system
page 114 HQN-10920
Manpower allocation and reporting
page 115 GSC-12708
Software-engineering data-base system
page 115 GSC-12669

DENSIFICATION
Consolidation of submicron silicon particles
page 37 NPO-15250

DEPOSITION
RF sputtering of gold contacts on niobium
page 104 NPO-15624

DETONATORS
Screen secures detonator to explosive charge
page 71 MSC-20138

DEUTERIUM PLASMA
Mass producing targets for nuclear fusion
page 105 NPO-15455

DIRECT CURRENT
Portable I/V-curve tester
page 9 NPO-15266

DIRECTIONAL ANTENNAS
Parasitically-excited ring antenna
page 12 MSC-20201

DISCONNECT DEVICES
Ball joint for quick connections and disconnections
page 79 LAR-12896
Quick-connect, self-alining latch
page 70 MSC-20205

DISPENSERS
Implantable drug dispenser
page 48 NPO-15160

DISPLAY DEVICES
Improved photosensor for light valves
page 99 MSC-20036

DISTRIBUTION
Audio distribution and monitoring circuit
page 6 MSC-20073

DOMES (STRUCTURAL FORMS)
Cleaning system for solar-collector covers
page 81 NPO-15414

DOSAGE
Implantable drug dispenser
page 48 NPO-15160

DROPS (LIQUIDS)
Theory of compound liquid drops
page 65 NPO-15389

DRUGS
Implantable drug dispenser
page 48 NPO-15160

DUCTS
Ceramic-cord gas seal
page 63 MSC-20200

DYNAMIC RESPONSE
Analysis of feedback-control systems
page 21 GSC-12723

ELECTRIC CONTACTS
RF sputtering of gold contacts on niobium
page 104 NPO-15624

ELECTRIC GENERATORS
Advanced coal-based power generation
page 84 MFS-25652

ELECTRIC MOTORS
Power-factor controller avoids false turnoff
page 7 LAR-22313
Soft-starting power-factor motor controller
page 4 MFS-25586

ELECTRIC POWER PLANTS
Advanced coal-based power generation
page 84 MFS-25652

ELECTROCHEMICAL CELL
Electrolyte reservoir would lengthen cell life
page 102 LEW-13788

ELECTRODE FILM BARRIERS
Striped electrodes for solid-electrolyte cells
page 94 NPO-15269

ELECTROLYTIC CELLS
Carbon cloth supports catalytic electrodes
page 95 NPO-15268
Striped electrodes for solid-electrolyte cells
page 94 NPO-15269

ELECTRONIC CONTROL
Soft-starting power-factor motor controller
page 4 MFS-25586

ELECTRONIC PACKAGING
Fabricating a microcomputer on a single silicon wafer
page 101 NPO-15053

ELECTROPLATING
Environmental durability of electroplated black chromium
page 43 MFS-25797

ENCAPSULATING
Solar-cell encapsulation by one-step lamination
page 99 NPO-15222
Stable polyurethane coatings for electronic circuits
page 103 MFS-25663

EPOXY RESINS
Fire-retardant epoxy adhesives
page 41 ARC-11430

ERROR ANALYSIS
Computing graphical confidence bounds
page 112 MSC-18908
Consistent tolerance bounds for statistical distributions
page 111 MSC-20090
Trajectory-estimation error analysis
page 66 GSC-12766

ETCHING
Controlled-saturation etching of gallium arsenide
page 105 NPO-15625
Etching integrated circuits
page 108 MFS-25661

EXHAUST SYSTEMS
Ceramic-cord gas seal
page 63 MSC-20200

EXPLOSIVES
Screen secures detonator to explosive charge
page 71 MSC-20138
Tapped-hole vent path
page 59 MSC-20146

EXTRACTION
Cryolite byproduct in silicon production
page 35 NPO-15364
Liner for silicon reactor
page 42 NPO-15366
Separating silicon and sodium fluoride by melting
page 39 NPO-15363
Separating silicon from Si/NaF mixtures
page 36 NPO-15365

FABRICS
Cutter for woven materials
page 79 MSC-20178

FASTENERS
Ball joint for quick connections and disconnections
page 79 LAR-12896

Recharging "hot-melt" adhesive film
page 106 LAR-12881
FEEDBACK CONTROL
Analysis of feedback-control systems
page 21 GSC-12723
FIELD EFFECT TRANSISTORS
Flip-chip carrier would match microwave FET impedances
page 11 GSC-12442
FILE MAINTENANCE (COMPUTERS)
Software-engineering data-base system
page 115 GSC-12669
FILLERS
Repairing voids and delaminations in composite materials
page 97 MSC-20131
FINANCIAL MANAGEMENT
Simplified life-cycle cost estimation
page 113 NPO-15228
FLAKING
Compacting silicon powder
page 38 NPO-15271
FLAME RETARDANTS
Fire-retardant epoxy adhesives
page 41 ARC-11430
FLOW MEASUREMENT
Tapped-hole vent path
page 59 MSC-20146
FLUID BOUNDARIES
Theory of compound liquid drops
page 65 NPO-15389
FLUIDIZED BED PROCESSORS
Closed-loop process yields ultrapure silicon
page 34 NPO-15283
FOLDING STRUCTURES
Large, easily deployable structures
page 65 MFS-25647
FREQUENCY ANALYZERS
Analysis of feedback-control systems
page 21 GSC-12723
FUEL CAPSULES
Mass producing targets for nuclear fusion
page 105 NPO-15455
FUEL CELLS
Advanced coal-based power generation
page 84 MFS-25652
FUSES (ORDNANCE)
Screen secures detonator to explosive charge
page 71 MSC-20138

GALAXIES
Two- and three-dimensional galaxy simulations
page 29 LAR-12907
GALLIUM ARSENIDE
Controlled-saturation etching of gallium arsenide
page 105 NPO-15625
GAS FLOW
Tapped-hole vent path
page 59 MSC-20146
GAS LASERS
Sunlight-pumped laser
page 25 LAR-12870
GAS TURBINE ENGINES
Properties of nickel-based hydrogen-turbine blades
page 44 MFS-25733
GASKETS
Ceramic-cord gas seal
page 63 MSC-20200
GEARS
Redundant gear train
page 73 NPO-15317
GEODETIC SURVEYS
Formulas for precise transverse Mercator projection
page 113 NPO-15409
GEOLOGICAL SURVEYS
Field measurement of thermal inertia
page 59 NPO-15309
GETTERS
Gettering silicon wafers to remove impurities
page 92 NPO-15357
GLASS FIBER REINFORCED PLASTICS
Solventless fabrication of reinforced composites
page 98 LAR-12856
GOLD COATINGS
RF sputtering of gold contacts on niobium
page 104 NPO-15624
GRAVITATIONAL FIELDS
Two- and three-dimensional galaxy simulations
page 29 LAR-12907

HARDWARE
Device makes handtools "dropproof"
page 69 MSC-20319
HEAT SHIELDING
Lightweight thermal-protection system
page 51 LAR-12880
HEAT TRANSFER
Heat pipes cool power magnetics
page 57 LEW-13507
HERMETIC SEALS
Ceramic-cord gas seal
page 63 MSC-20200
HIGH FREQUENCIES
500-watt, 10-GHz solid-state amplifier
page 7 NPO-15022
HIGH TEMPERATURE NUCLEAR REACTORS
Simplified heat-source/thermionic converter
page 107 NPO-15278
HIGH VOLTAGES
Electronic load tests high-voltage solar arrays
page 10 NPO-15358
HONEYCOMB STRUCTURES
Lightweight thermal-protection system
page 51 LAR-12880
HUMAN FACTORS ENGINEERING
Ride-quality meter
page 17 LAR-12882
HYDROGEN FUELS
Properties of nickel-based hydrogen-turbine blades
page 44 MFS-25733

IMAGERY
Improved photosensor for light valves
page 99 MSC-20036
IMMOBILIZATION
Spine immobilizer for accident victims
page 47 ARC-11167
IMPEDANCE MATCHING
Audio distribution and monitoring circuit
page 6 MSC-20073
Flip-chip carrier would match microwave FET impedances
page 11 GSC-12442
IMPLANTATION
Implantable drug dispenser
page 48 NPO-15160
IMPURITIES
Modified die yields purer silicon ribbon
page 94 NPO-15385
INDUCTION MOTORS
Power-factor controller avoids false turnoff
page 3 MFS-25616
INDUSTRIAL SAFETY
Sled control and safety system
page 16 MSC-20082
INHIBITORS
Corrosion protection coatings for aluminum
page 42 MFS-25640
INITIATORS (EXPLOSIVES)
Screen secures detonator to explosive charge
page 71 MSC-20138
INSULIN
Implantable drug dispenser
page 48 NPO-15160
ION ENGINES
Simplified heat-source/thermionic converter
page 107 NPO-15278

JOINTS (JUNCTIONS)
Ball joint for quick connections and disconnections
page 79 LAR-12896
Connector for composite tubes
page 53 LAR-12744
Flexible coupling corrects shaft misalinements
page 74 NPO-15393
Quick-connect, self-alining latch
page 70 MSC-20205
JUNCTION DIODES
Integrated submillimeter-wave mixer
page 8 NPO-15238

LAMINATES
Fire-retardant epoxy adhesives
page 41 ARC-11430
Laminating polyimide films
page 96 LAR-12742
Repairing voids and delaminations in composite materials
page 97 MSC-20131
Solar-cell encapsulation by one-step lamination
page 99 NPO-15222
LASERS
Cube-corner retroreflector modeling
page 29 GSC-12718
Sunlight-pumped laser
page 25 LAR-12870
LATCHES
Quick-connect, self-alining latch
page 70 MSC-20205
LINEAR SYSTEMS
Optimal regulator algorithms for the control of linear systems
page 21 LAR-12313
LININGS
Liner for silicon reactor
page 42 NPO-15366
LINKAGES
Flexible coupling corrects shaft misalinements
page 74 NPO-15393
Quick-connect, self-alining latch
page 70 MSC-20205
LIQUID HYDROGEN
Preventing cracks in titanium rotary seals
page 77 MFS-19686
LIQUID SURFACES
Theory of compound liquid drops
page 65 NPO-15389

MACHINE TOOLS
Sled control and safety system
page 16 MSC-20082
MAINTENANCE
Remote-action tube crimper
page 82 MSC-20197
MANIPULATORS
Calculating clearances for manipulators
page 60 MSC-20208

MANPOWER
Interactive planning system
page 114 HQN-10920
Manpower allocation and reporting
page 115 GSC-12706
MAPS
Formulas for precise transverse Mercator projection
page 113 NPO-15409
MATERIALS HANDLING
Vacuum reamer
page 83 MFS-19711
MATRIX ANALYSIS
Analysis of feedback-control systems
page 21 GSC-12723
MEASURING INSTRUMENTS
Audio distribution and monitoring circuit
page 6 MSC-20073
MECHANICAL DRIVES
Redundant gear train
page 73 NPO-15317
MEMBRANE STRUCTURES
Cleaning system for solar-collector covers
page 81 NPO-15414
MENISCI
Modified die yields purer silicon ribbon
page 94 NPO-15385
Silicon sheet quality is improved by meniscus control
page 92 NPO-15384
MERCATOR PROJECTION
Formulas for precise transverse Mercator projection
page 113 NPO-15409
METAL BONDING
Laminating polyimide films
page 96 LAR-12742
METAL CUTTING
Vacuum reamer
page 83 MFS-19711
METEOROLOGICAL CHARTS
Mapping ocean winds by radar
page 27 NPO-15267
METEOROLOGICAL INSTRUMENTS
Solar-radiation measuring equipment and glossary
page 28 MFS-25770
MICROWAVE AMPLIFIERS
500-watt, 10-GHz solid-state amplifier
page 7 NPO-15022
MICROWAVE TRANSMISSION
Flip-chip carrier would match microwave FET impedances
page 11 GSC-12442
MICROWAVE TUBES
Improving power-supply regulation for pulsed loads
page 18 MSC-20016
MINERAL DEPOSITS
Solar-assisted solution-mining concept
page 26 NPO-15343
MINERAL EXPLORATION
Field measurement of thermal inertia
page 59 NPO-15309
MINIATURE ELECTRONIC EQUIPMENT
Miniature two-axis joystick/controller
page 99 ARC-11372
MINING
Solar-assisted solution-mining concept
page 26 NPO-15343
MIRRORS
Measuring mirror tilt with high accuracy
page 55 GSC-12701
MIXING CIRCUITS
Audio distribution and monitoring circuit
page 6 MSC-20073
Integrated submillimeter-wave mixer
page 8 NPO-15238
MODE TRANSFORMERS
Flip-chip carrier would match microwave FET impedances
page 11 GSC-12442

NICKEL ALLOYS
Properties of nickel-based hydrogen-turbine blades
page 44 MFS-25733
NICKEL CADMIUM BATTERIES
Electrolyte reservoir would lengthen cell life
page 102 LEW-13788
NIOBIUM
RF sputtering of gold contacts on niobium
page 104 NPO-15624
NOISE (SOUND)
Ride-quality meter
page 17 LAR-12882
Rod-wall sound shield for wind tunnels
page 61 LAR-12883
NONDESTRUCTIVE TESTS
Measuring tensile strength of B/Al composites
page 62 LEW-13807
Pressure-decay measurements improve bubble-point test
page 52 MSC-18970
NUCLEAR FUELS
Mass producing targets for nuclear fusion
page 105 NPO-15455
NUMERICAL CONTROL
Sled control and safety system
page 16 MSC-20082

O RINGS
Pressure relief valve
page 80 LEW-13800
OBLATE SPHEROIDS
Formulas for precise transverse Mercator projection
page 113 NPO-15409
OCEAN SURFACE
Mapping ocean winds by radar
page 27 NPO-15267
OPTICAL EQUIPMENT
Cube-corner retroreflector modeling
page 29 GSC-12718
Measuring mirror tilt with high accuracy
page 55 GSC-12701
ORGANIC LASERS
Sunlight-pumped laser
page 25 LAR-12870

PANELS
Lightweight thermal-protection system
page 51 LAR-12880
PASSENGERS
Ride-quality meter
page 17 LAR-12882
PELLETS
Pellet feed for dendritic-web growth
page 88 NPO-15198
PHOSPHOROUS
Gettering silicon wafers to remove impurities
page 92 NPO-15357
PHOTOSENITIVITY
Improved photosensor for light valves
page 99 MSC-20036
PHOTOVOLTAIC CELLS
Assembly of photovoltaic arrays
page 87 NPO-15311
Electronic load tests high-voltage solar arrays
page 10 NPO-15358
PIPE (TUBES)
Connector for composite tubes
page 53 LAR-12744
Remote-action tube crimper
page 82 MSC-20197
PNEUMATIC EQUIPMENT
Tapped-hole vent path
page 59 MSC-20146
POLLUTION CONTROL
Continuous monitoring of aerosols
page 54 NPO-15292
Mobile air sampler
page 55 NPO-15220
POLYAMIDE RESINS
Thermoset/thermoplastic aromatic polyamides for composites
page 39 LAR-12723
POLYMERS
Laminating polyimide films
page 96 LAR-12742
POTTING COMPOUNDS
Solar-cell encapsulation by one-step lamination
page 99 NPO-15222
Stable polyurethane coatings for electronic circuits
page 103 MFS-25663
POWDER (PARTICLES)
Compacting silicon powder
page 38 NPO-15271
Consolidation of submicron silicon particles
page 37 NPO-15250
POWER AMPLIFIERS
500-watt, 10-GHz solid-state amplifier
page 7 NPO-15022
POWER SUPPLIES
Electronic load tests high-voltage solar arrays
page 10 NPO-15358
Improving power-supply regulation for pulsed loads
page 18 MSC-20016
Portable I/V-curve tester
page 9 NPO-15266
POWER TRANSMISSION
Redundant gear train
page 73 NPO-15317
PRESSURE CHAMBERS
Flexible seal accommodates part mismatch
page 64 MFS-19710
PRESSURE MEASUREMENTS
Pressure-decay measurements improve bubble-point test
page 52 MSC-18970
PRESSURE REGULATORS
Pressure relief valve
page 80 LEW-13800
PRIMERS (COATINGS)
Corrosion protection coatings for aluminum
page 42 MFS-25640
PRINTED CIRCUITS
Etching integrated circuits
page 108 MFS-25661
Stable polyurethane coatings for electronic circuits
page 103 MFS-25663
PROGRAMMING LANGUAGES
Path Pascal
page 115 LAR-12854
PROJECT PLANNING
Interactive planning system
page 114 HQN-10920
Simplified life-cycle cost estimation
page 113 NPO-15228

PROPELLANT COMBUSTION
Improved equations for composite-propellant burning
page 43 NPO-15324

PROTECTIVE COATINGS
Clear film protects against ultraviolet radiation
page 33 NPO-14971

PSYCHOLOGICAL EFFECTS
Ride-quality meter
page 17 LAR-12882

PUMPS
Magnetic bearings would increase pump efficiency
page 76 GSC-12668
Preventing cracks in titanium rotary seals
page 77 MFS-19686

PURIFICATION
Bipulsating technique for silicon production
page 34 NPO-15367
Cryolite byproduct in silicon production
page 35 NPO-15364
Gettering silicon wafers to remove impurities
page 92 NPO-15357
Separating silicon and sodium fluoride by melting
page 39 NPO-15363

PYRANOMETERS
Solar-radiation measuring equipment and glossary
page 28 MFS-25770

RADAR ANTENNAS
Parasitically-excited ring antenna
page 12 MSC-20201

RADAR MEASUREMENTS
High-resolution subsurface-interface radar
page 20 KSC-11212

RADIATION MEASURING INSTRUMENTS
Solar-radiation measuring equipment and glossary
page 28 MFS-25770

RADIOMETERS
Solar-radiation measuring equipment and glossary
page 28 MFS-25770

RECORDING INSTRUMENTS
Compact, rugged temperature recorder
page 28 ARC-11304

REFLECTANCE
Cube-corner retroreflector modeling
page 29 GSC-12718

REFRACTORY MATERIALS
Ceramic-cord gas seal
page 63 MSC-20200
Lightweight thermal-protection system
page 51 LAR-12880

REFRIGERATING MACHINERY
Magnetic bearings would increase pump efficiency
page 76 GSC-12668

REGRESSION ANALYSIS
Computing graphical confidence bounds
page 112 MSC-18908
Consistent tolerance bounds for statistical distributions
page 111 MSC-20090

REINFORCING FIBERS
Thermoset/thermoplastic aromatic polyamides for composites
page 39 LAR-12723

RELIEF VALVES
Pressure relief valve
page 80 LEW-13800

REMOTE CONTROL
Calculating clearances for manipulators
page 60 MSC-20208
Miniature two-axis joystick/controller
page 99 ARC-11372

REMOTE HANDLING
Calculating clearances for manipulators
page 60 MSC-20208

REPORTS
Manpower allocation and reporting
page 115 GSC-12706

RESOURCE ALLOCATION
Interactive planning system
page 114 HQN-10920
Manpower allocation and reporting
page 115 GSC-12706

RETROREFLECTION
Cube-corner retroreflector modeling
page 29 GSC-12718

ROCKS
Field measurement of thermal inertia
page 59 NPO-15309

ROTATING BODIES
Preventing cracks in titanium rotary seals
page 77 MFS-19686

ROTATING SHAFTS
Flexible coupling corrects shaft misalinements
page 74 NPO-15393

SAFETY DEVICES
Can-filled crash barrier
page 72 NPO-15188
Sled control and safety system
page 16 MSC-20082

SALT SPRAY TESTS
Corrosion protection coatings for aluminum
page 42 MFS-25640

SANDWICH STRUCTURES
Lightweight thermal-protection system
page 51 LAR-12880

SCRAP
Vacuum reamer
page 83 MFS-19711

SEALS (STOPPERS)
Ceramic-cord gas seal
page 63 MSC-20200
Flexible seal accommodates part mismatch
page 64 MFS-19710

SELF-ERECTING DEVICES
Large, easily deployable structures
page 65 MFS-25647

SERVOCONTROL
Miniature two-axis joystick/controller
page 99 ARC-11372

SHAFTS (MACHINE ELEMENTS)
Redundant gear train
page 73 NPO-15317

SHOTTKY DIODES
Integrated submillimeter-wave mixer
page 8 NPO-15238

SIDELOBE REDUCTION
Parasitically-excited ring antenna
page 12 MSC-20201

SILANES
Closed-loop process yields ultrapure silicon
page 34 NPO-15283
Tube-furnace production of silicon
page 36 NPO-15274

SILICON
Bipulsating technique for silicon production
page 34 NPO-15367
Closed-loop process yields ultrapure silicon
page 34 NPO-15283
Compacting silicon powder
page 38 NPO-15271
Consolidation of submicron silicon particles
page 37 NPO-15250
Controlling thermal gradients during silicon web growth
page 91 NPO-15337
Cryolite byproduct in silicon production
page 35 NPO-15364
Gettering silicon wafers to remove impurities
page 92 NPO-15357
Improved barrier for continuous-crystal-growth crucible
page 89 NPO-15338
Liner for silicon reactor
page 42 NPO-15366
Modified die yields purer silicon ribbon
page 94 NPO-15385
Modified silicon furnace lowers crystal cost
page 90 NPO-15041
Pellet feed for dendritic-web growth
page 88 NPO-15198
Separating silicon and sodium fluoride by melting
page 39 NPO-15363
Separating silicon from Si/NaF mixtures
page 36 NPO-15365
Silicon sheet quality is improved by meniscus control
page 92 NPO-15384
Technique for crystal-ribbon growth
page 93 NPO-15177
Tube-furnace production of silicon
page 36 NPO-15274

SMOKE
Continuous monitoring of aerosols
page 54 NPO-15292

SOIL MAPPING
High-resolution subsurface-interface radar
page 20 KSC-11212

SOLAR CELLS
Assembly of photovoltaic arrays
page 87 NPO-15311
Clear film protects against ultraviolet radiation
page 33 NPO-14971
Electronic load tests high-voltage solar arrays
page 10 NPO-15356
Gettering silicon wafers to remove impurities
page 92 NPO-15357
Modified die yields purer silicon ribbon
page 94 NPO-15385
Portable I/V-curve tester
page 9 NPO-15266
Silicon sheet quality is improved by meniscus control
page 92 NPO-15384
Solar-cell encapsulation by one-step lamination
page 99 NPO-15222
Technique for crystal-ribbon growth
page 93 NPO-15177

SOLAR COLLECTORS
Cleaning system for solar-collector covers
page 81 NPO-15414
Environmental durability of electroplated black chromium
page 43 MFS-25797

SOLAR ENERGY
Solar-assisted solution-mining concept
page 26 NPO-15343
Solar-radiation measuring equipment and glossary
page 28 MFS-25770
Sunlight-pumped laser
page 25 LAR-12870

SOLIDIFICATION
Consolidation of submicron silicon particles
page 37 NPO-15250

SPECTROHELIOGRAPHS
Solar-radiation measuring equipment and glossary
page 28 MFS-25770

SPECTROMETERS
Continuous monitoring of aerosols
page 54 NPO-15292

SPEED CONTROL
Sled control and safety system
page 16 MSC-20082

SPINAL CORD
Spine immobilizer for accident victims
page 47 ARC-11167

SPRAY NOZZLES
Improved atomizer minimizes output fluctuations
page 76 MFS-25631

SPUTTERING
RF sputtering of gold contacts on niobium
page 104 NPO-15624

STARS
Two- and three-dimensional galaxy simulations
page 29 LAR-12907

STATISTICAL ANALYSIS
Stability Statistics Data Base System
page 116 MSC-20014

STROBOSCOPES
Measuring mirror tilt with high accuracy
page 55 GSC-12701

STRUCTURAL MEMBERS
Large, easily deployable structures
page 65 MFS-25647

SUBMILLIMETER WAVES
Integrated submillimeter-wave mixer
page 8 NPO-15238

SUCTION
Vacuum reamer
page 83 MFS-19711

SUNLIGHT
Sunlight-pumped laser
page 25 LAR-12870

SWITCHING CIRCUITS
Power-factor controller avoids false turnoff
page 3 MFS-25616

Soft-starting power-factor motor controller
page 4 MFS-25586

SWIVELS
Ball joint for quick connections and disconnections
page 79 LAR-12896

SYNTHETIC FIBERS
Thermoset/thermoplastic aromatic polyamides for composites
page 39 LAR-12723

TARGETS
Mass producing targets for nuclear fusion
page 105 NPO-15455

TEMPERATURE CONTROL
Heat pipes cool power magnetics
page 57 LEW-13507

TEMPERATURE MEASURING INSTRUMENTS
Compact, rugged temperature recorder
page 28 ARC-11304

TENSILE STRENGTH
Measuring tensile strength of B/Al composites
page 62 LEW-13807

TERRAIN ANALYSIS
High-resolution subsurface-interface radar
page 20 KSC-11212

TEST STANDS
Exhaust-plume impingement characteristics
page 56 MFS-25489

THERMAL DISSOCIATION
A new use for high-sulfur coal
page 28 NPO-15194

THERMAL INSULATION
Conduit for transferring molten silicon
page 37 NPO-15109

THERMAL MAPPING
Field measurement of thermal inertia
page 59 NPO-15309

THERMAL PROTECTION
Lightweight thermal-protection system
page 51 LAR-12880

THERMIONIC CONVERTERS
Simplified heat-source/thermionic converter
page 107 NPO-15278

THERMOSETTING RESINS
Thermoset/thermoplastic aromatic polyamides for composites
page 39 LAR-12723

THICK FILMS
Striped electrodes for solid-electrolyte cells
page 94 NPO-15269

THIN FILMS
RF sputtering of gold contacts on niobium
page 104 NPO-15624

TIME SIGNALS
Converting time signals from BCD to IRIG-B
page 16 MSC-18963

TITANIUM
Preventing cracks in titanium rotary seals
page 77 MFS-19686

TOOLS
Cutter for woven materials
page 79 MSC-20178

Deep-access valve wrench
page 75 KSC-11229

Device makes handtools "dropproof"
page 69 MSC-20319

Remote-action tube crimper
page 82 MSC-20197

TRAJECTORY ANALYSIS
Trajectory-estimation error analysis
page 66 GSC-12766

TRANSMISSION LINES
Flip-chip carrier would match microwave FET impedances
page 11 GSC-12442

TRAVELING WAVE TUBES
Improving power-supply regulation for pulsed loads
page 18 MSC-20016

TRIGGER CIRCUITS
Power-factor controller avoids false turnoff
page 3 MFS-25616

TURBINE BLADES
Properties of nickel-based hydrogen-turbine blades
page 44 MFS-25733

TURBINES
Progress in wind-wheel turbines
page 84 MFS-25796

TURBULENT BOUNDARY LAYERS
Rod-wall sound shield for wind tunnels
page 61 LAR-12883

ULTRAVIOLET FILTERS
Clear film protects against ultraviolet radiation
page 33 NPO-14971

VACUUM SYSTEMS
Ampoule with integral feedthroughs
page 100 LAR-12899

Pressure relief valve
page 80 LEW-13800

VALVES
Deep-access valve wrench
page 75 KSC-11229

VIBRATION MEASUREMENT
Measuring mirror tilt with high accuracy
page 55 GSC-12701

Ride-quality meter
page 17 LAR-12882

VOLT-AMPERE CHARACTERISTICS
Portable I/V-curve tester
page 9 NPO-15266

VOLTAGE REGULATORS
Improving power-supply regulation for pulsed loads
page 18 MSC-20016

WAFERS
Etching integrated circuits
page 106 MFS-25661

Fabricating a microcomputer on a single silicon wafer
page 101 NPO-15053

WASHERS (CLEANERS)
Cleaning system for solar-collector covers
page 81 NPO-15414

WASTE DISPOSAL
Vacuum reamer
page 83 MFS-19711

WIND (METEOROLOGY)
Mapping ocean winds by radar
page 27 NPO-15267

WIND TUNNELS
Rod-wall sound shield for wind tunnels
page 61 LAR-12883

WINDMILLS (WINDPOWERED MACHINES)
Progress in wind-wheel turbines
page 84 MFS-25796

WINGS
Semi-empirical estimate of aircraft wing weight
page 62 ARC-11435

WIRE CLOTH
Pressure-decay measurements improve bubble-point test
page 52 MSC-18970

WRENCHES
Deep-access valve wrench
page 75 KSC-11229

Device makes handtools "dropproof"
page 69 MSC-20319

National Aeronautics and
Space Administration
Washington, D.C.
20546

Official Business
Penalty for Private Use $300

NO POSTAGE
NECESSARY
IF MAILED
IN THE
UNITED STATES

BUSINESS REPLY MAIL

FIRST CLASS PERMIT NO. 12028 WASHINGTON, D.C.

POSTAGE WILL BE PAID BY NASA

Manager, Technology Transfer Division
P.O. Box 8757
Baltimore/Washington International Airport, MD 21240

NASA

National Aeronautics and
Space Administration
Washington, D.C.
20546

Official Business
Penalty for Private Use $300

NO POSTAGE
NECESSARY
IF MAILED
IN THE
UNITED STATES

BUSINESS REPLY MAIL

FIRST CLASS PERMIT NO. 12028 WASHINGTON, D.C.

POSTAGE WILL BE PAID BY NASA

Manager, Technology Transfer Division
P.O. Box 8757
Baltimore/Washington International Airport, MD 21240

NASA

National Aeronautics and
Space Administration
Washington, D.C.
20546

Official Business
Penalty for Private Use $300

NO POSTAGE
NECESSARY
IF MAILED
IN THE
UNITED STATES

BUSINESS REPLY MAIL

FIRST CLASS PERMIT NO. 12028 WASHINGTON, D.C.

POSTAGE WILL BE PAID BY NASA

Manager, Technology Transfer Division
P.O. Box 8757
Baltimore/Washington International Airport, MD 21240

NASA

TECH BRIEFS SUBSCRIPTIONS

FALL
1982

☐ Please place me on the subscription list for NASA Tech Briefs (issued quarterly).

☐ I wish to change the delivery address for my current subscription. The identification number at the top right of my current mailing label is T__________.

1. Please check any of the following that describe your organization:
   - ☐ Federal Government
   - ☐ State Government
   - ☐ Municipal Government
   - ☐ University/College
   - ☐ Secondary School
   - ☐ Trade/Vocational School
   - ☐ Manufacturing
   - ☐ Sales
   - ☐ Research
   - ☐ Consulting
   - ☐ Medicine
   - ☐ Professional Society
   - ☐ News Media
   - ☐ Information Sciences/Library
2. Please check the number of employees in your organization: ☐ Under 25 ☐ 25-100 ☐ 100-500 ☐ Over 500
3. Please indicate if your position is one of the following: ☐ Owner or Chief Executive Officer ☐ Administrator/Manager ☐ Scientist ☐ Engineer ☐ Other __________

[PLEASE PRINT]

NAME __________ TITLE __________

COMPANY & STREET ADDRESS __________ PHONE __________

CITY __________ STATE ________ ZIP ________

TECH BRIEFS SUBSCRIPTIONS

FALL
1982

☐ Please place me on the subscription list for NASA Tech Briefs (issued quarterly).

☐ I wish to change the delivery address for my current subscription. The identification number at the top right of my current mailing label is T__________.

1. Please check any of the following that describe your organization:
   - ☐ Federal Government
   - ☐ State Government
   - ☐ Municipal Government
   - ☐ University/College
   - ☐ Secondary School
   - ☐ Trade/Vocational School
   - ☐ Manufacturing
   - ☐ Sales
   - ☐ Research
   - ☐ Consulting
   - ☐ Medicine
   - ☐ Professional Society
   - ☐ News Media
   - ☐ Information Sciences/Library
2. Please check the number of employees in your organization: ☐ Under 25 ☐ 25-100 ☐ 100-500 ☐ Over 500
3. Please indicate if your position is one of the following: ☐ Owner or Chief Executive Officer ☐ Administrator/Manager ☐ Scientist ☐ Engineer ☐ Other __________

[PLEASE PRINT]

NAME __________ TITLE __________

COMPANY & STREET ADDRESS __________ PHONE __________

CITY __________ STATE ________ ZIP ________

FEEDBACK — YOUR COMMENTS

FALL
1982

WE NEED YOUR HELP!

Our ultimate goal is to provide you with solutions to your day-to-day technical problems. Are we meeting that goal? Tell us how Tech Briefs has helped you, or how it can be made more useful. We are especially interested in brief descriptions of specific instances where Tech Briefs has either helped you solve a problem or been applied to your product line.

____

____

____

____

If you need more space, write us a letter at the address on the front of this card.

[PLEASE PRINT]

NAME __________ TITLE __________

COMPANY & STREET ADDRESS __________ PHONE __________

CITY __________ STATE ________ ZIP ________

TSP REQUESTS

Please send me the Technical Support Package (TSP)
for the Tech Brief articles circled below:

FALL
1982

☐ I would like information about NASA's Industrial Applications Centers and other NASA TU services.

I am requesting these TSP's for:

☐ Current Awareness
☐ Product Development
☐ Other __________
☐ Process Improvement
☐ Problem Solving

Approximately how many TSP's have you requested from NASA in the last five years?

☐ 0 to 10 ☐ 11 to 25 ☐ over 25

[PLEASE PRINT]

NAME __________

TITLE __________

COMPANY __________ PHONE __________
&
STREET ADDRESS __________

CITY __________ STATE ______ ZIP ______

1	2	3	4	5	6	7	8	9	10	11	12	13	14	15
16	17	18	19	20	21	22	23	24	25	26	27	28	29	30
31	32	33	34	35	36	37	38	39	40	41	42	43	44	45
46	47	48	49	50	51	52	53	54	55	56	57	58	59	60
61	62	63	64	65	66	67	68	69	70	71	72	73	74	75
76	77	78	79	80	81	82	83	84	85	86	87	88	89	90
91														

TSP REQUESTS

Please send me the Technical Support Package (TSP)
for the Tech Brief articles circled below:

FALL
1982

☐ I would like information about NASA's Industrial Applications Centers and other NASA TU services.

I am requesting these TSP's for:

☐ Current Awareness
☐ Product Development
☐ Other __________
☐ Process Improvement
☐ Problem Solving

Approximately how many TSP's have you requested from NASA in the last five years?

☐ 0 to 10 ☐ 11 to 25 ☐ over 25

[PLEASE PRINT]

NAME __________

TITLE __________

COMPANY __________ PHONE __________
&
STREET ADDRESS __________

CITY __________ STATE ______ ZIP ______

1	2	3	4	5	6	7	8	9	10	11	12	13	14	15
16	17	18	19	20	21	22	23	24	25	26	27	28	29	30
31	32	33	34	35	36	37	38	39	40	41	42	43	44	45
46	47	48	49	50	51	52	53	54	55	56	57	58	59	60
61	62	63	64	65	66	67	68	69	70	71	72	73	74	75
76	77	78	79	80	81	82	83	84	85	86	87	88	89	90
91														

COSMIC REQUESTS

I would like price and availability information about the computer program(s) circled below.

FALL
1982

A B C D E F G H J K L

[PLEASE PRINT]

NAME __________

TITLE __________

COMPANY __________
&
STREET ADDRESS __________

CITY __________ STATE ______ ZIP ______

Please send me further information about software and services available from COSMIC. I am particularly interested in programs in the following areas:

____

____

____

____

National Aeronautics and
Space Administration

Washington, D.C.
20546

Official Business
Penalty for Private Use $300

NO POSTAGE
NECESSARY
IF MAILED
IN THE
UNITED STATES

BUSINESS REPLY MAIL

FIRST CLASS PERMIT NO. 12028 WASHINGTON, D.C.

POSTAGE WILL BE PAID BY NASA

Manager, Technology Transfer Division
P.O. Box 8757
Baltimore/Washington International Airport, MD 21240

National Aeronautics and
Space Administration

Washington, D.C.
20546

Official Business
Penalty for Private Use $300

NO POSTAGE
NECESSARY
IF MAILED
IN THE
UNITED STATES

BUSINESS REPLY MAIL

FIRST CLASS PERMIT NO. 12028 WASHINGTON, D.C.

POSTAGE WILL BE PAID BY NASA

Manager, Technology Transfer Division
P.O. Box 8757
Baltimore/Washington International Airport, MD 21240

National Aeronautics and
Space Administration

Washington, D.C.
20546

Official Business
Penalty for Private Use $300

NO POSTAGE
NECESSARY
IF MAILED
IN THE
UNITED STATES

BUSINESS REPLY MAIL

FIRST CLASS PERMIT NO. 12028 WASHINGTON, D.C.

POSTAGE WILL BE PAID BY NASA

COSMIC
Computer Software Management and Information Center
Suite 112, Barrow Hall
Athens, GA 30602

National Aeronautics and
Space Administration

Washington, D.C.
20546

Official Business
Penalty for Private Use $300

THIRD-CLASS BULK

THIRD-CLASS BULK RATE
POSTAGE & FEES PAID
NASA
WASHINGTON, D.C.
PERMIT No. G27

Workers prepare to install an ultrasonic sewer monitor, one of several distributed in the Washington, D.C., system to check water depths and flow rates. NASA sensor technology and circuit design techniques are combined in the monitor, which helps city engineers in sewer planning and management. [See the bottom of page A1.]

7/2

NASA Tech Briefs

National
Aeronautics and
Space
Administration

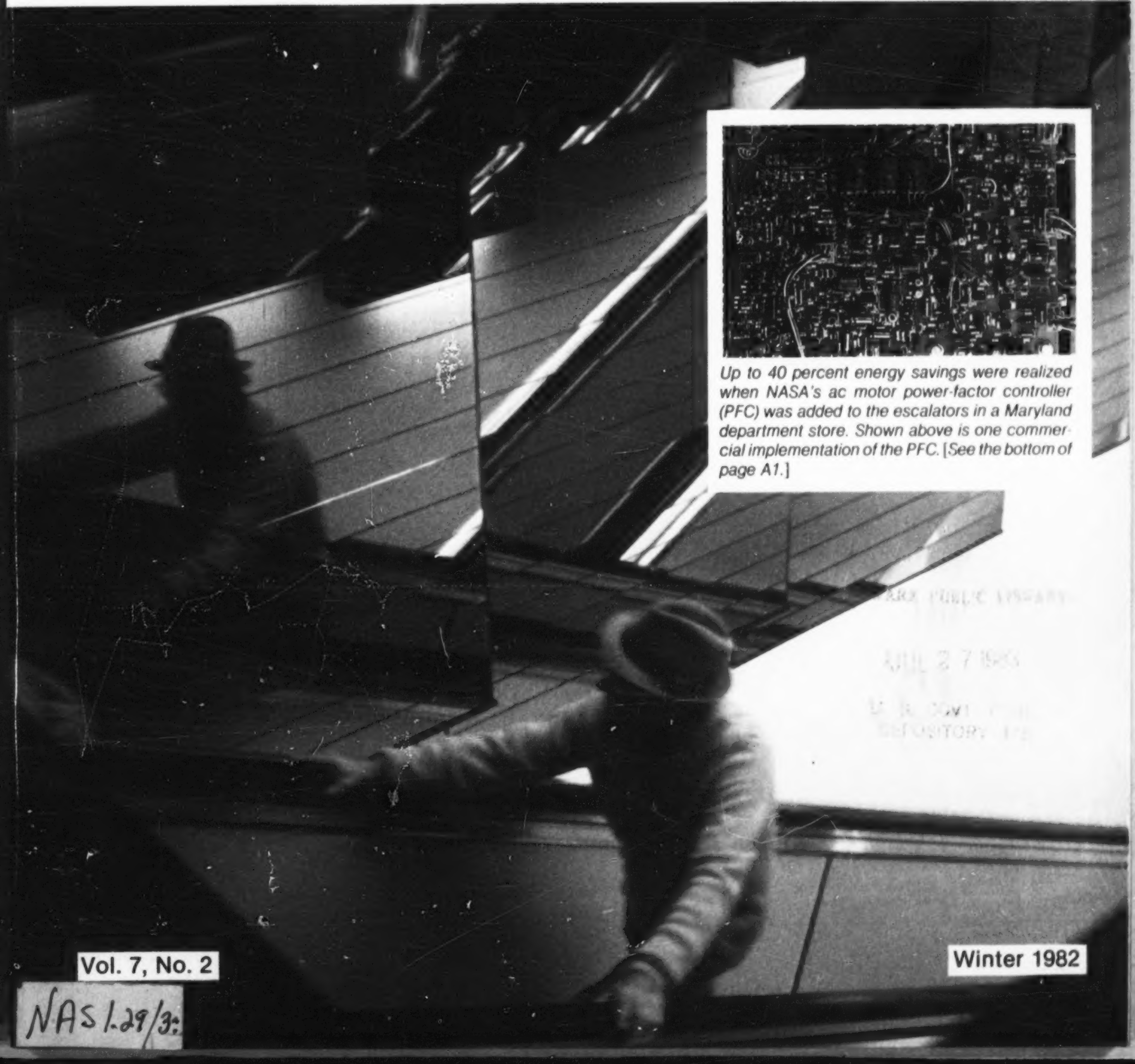

Up to 40 percent energy savings were realized when NASA's ac motor power-factor controller (PFC) was added to the escalators in a Maryland department store. Shown above is one commercial implementation of the PFC. [See the bottom of page A1.]

ARK PUBLIC LIBRARY
JUL 2 7 1983
U. S. GOVT [illegible]
DEPOSITORY [illegible]

Vol. 7, No. 2

Winter 1982

NAS 1.29/3:

About the NASA Technology Utilization Program

The National Aeronautics and Space Act of 1958, which established NASA and the United States civilian space program, requires that "The Administration shall provide for the widest practicable and appropriate dissemination of information concerning its activities and the results thereof."

To help carry out this objective, NASA's Technology Utilization (TU) Program was established in 1962. Now, as an element of NASA's Technology Utilization and Industry Affairs Division, this program offers a variety of valuable services to help transfer aerospace technology to nonaerospace applications, thus assuring American taxpayers maximum return on their investment in space research; thousands of spinoffs of NASA research have already occurred in virtually every area of our economy.

The TU program has worked for engineers, scientists, technicians, and businessmen; and it can work for you.

NASA Tech Briefs

Tech Briefs is published quarterly and is free to engineers in U.S. industry and to other domestic technology transfer agents. It is both a current-awareness medium and a problem-solving tool. Potential products . . . industrial processes . . . basic and applied research . . . shop and lab techniques . . . computer software . . . new sources of technical data . . . concepts . . . can be found here. The short section on New Product Ideas highlights a few of the potential new products contained in this issue. The remainder of the volume is organized by technical category to help you quickly review new developments in your areas of interest. Finally, a subject index makes each issue a convenient reference file.

Further Information on Innovations

Although some new technology announcements are complete in themselves, most are backed up by Technical Support Packages (TSP's). TSP's are available without charge and may be ordered by simply completing a TSP Request Card found at the back of this volume. Further information on some innovations is available for a nominal fee from other sources, as indicated. In addition, Technology Utilization Officers at NASA Field Centers will often be able to lend necessary guidance and assistance.

Patent Licenses

Patents have been issued to NASA on some of the inventions described, and patent applications have been submitted on others. Each announcement indicates patent status and availability of patent licenses if applicable.

Other Technology Utilization Services

To assist engineers, industrial researchers, business executives, Government officials, and other potential users in applying space technology to their problems, NASA sponsors Industrial Applications Centers. Their services are described on page A7. In addition, an extensive library of computer programs is available through COSMIC, the Technology Utilization Program's outlet for NASA-developed software.

Applications Program

NASA conducts applications engineering projects to help solve public-sector problems in such areas as safety, health, transportation, and environmental protection. Two applications teams, staffed by professionals from a variety of disciplines, assist in this effort by working with Federal agencies and health organizations to identify critical problems amenable to solution by the application of existing NASA technology.

Reader Feedback

We hope you find the information in *NASA Tech Briefs* useful. A reader-feedback card has been included because we want your comments and suggestions on how we can further help you apply NASA innovations and technology to your needs. Please use it; or if you need more space, write to the Manager, Technology Transfer Division, P.O. Box 8757, Baltimore/Washington International Airport, Maryland 21240.

NASA Tech Briefs

National
Aeronautics and
Space
Administration

Winter 1982
Volume 7, Number 2

NASA TU Services	A3	Technology Utilization services that can assist you in learning about and applying NASA technology.
New Product Ideas	A9	A summary of selected innovations of value to manufacturers for the development of new products.
Tech Briefs	125	**Electronic Components and Circuits**
	135	**Electronic Systems**
	143	**Physical Sciences**
	153	**Materials**
	169	**Life Sciences**
	173	**Mechanics**
	187	**Machinery**
	201	**Fabrication Technology**
	225	**Mathematics and Information Sciences**
Subject Index	231	Items in this issue are indexed by subject; a cumulative index will be published yearly.

COVERS: The photographs on the front and back covers illustrate developments by NASA and its contractors that have resulted in commercial and nonaerospace spinoffs. You can use the TSP Request Card at the back of this issue to learn more about the Power-Factor Controller [Circle 66] and High-Intensity Xenon Lamps [Circle 67]

About This NASA Publication

NASA Tech Briefs, a quarterly publication, is distributed free to qualified U.S. citizens to encourage commercial application of U.S. space technology. For information on publications and services available through the NASA Technology Utilization Program, write to the Manager, Technology Transfer Division, P.O. Box 8757, Baltimore/Washington International Airport, Maryland 21240.

"The Administrator of National Aeronautics and Space Administration has determined that the publication of this periodical is necessary in the transaction of the public business required by law of this Agency. Use of funds for printing this periodical has been approved by the Director of the Office of Management and Budget."

Change of Address

If you wish to have NASA Tech Briefs forwarded to your new address, use the Subscription Card enclosed at the back of this volume of NASA Tech Briefs. Be sure to check the appropriate box indicating change of address, and also fill in your identification number (T number) in the space indicated.

Communications Concerning Editorial Matter

For editorial comments or general communications about NASA Tech Briefs, you may use the Feedback card in the back of NASA Tech Briefs, or write to: The Publications Manager, Technology Utilization Office (LGT-1), NASA Headquarters, Washington, DC 20546. Technical questions concerning specific articles should be directed to the Technology Utilization Officer of the sponsoring NASA Center (addresses listed on page A4).

Acknowledgements

NASA Tech Briefs is published quarterly by the National Aeronautics and Space Administration, Technology Transfer Division, Washington, DC: Administrator: **James M. Beggs;** Director, Technology Utilization and Industry Affairs Division: **Ronald J. Philips;** Publications Manager: **Leonard A. Ault.** Prepared for the National Aeronautics and Space Administration by **Logical Technical Services Corp.:** Editor-in-Chief: **Jay Kirschenbaum;** Art Director: **Ernest Gillespie;** Managing Editor: **Jerome Rosen;** Chief Copy Editor: **Oden Browne;** Staff Editors: **Donald Blattner, Larry Grunberger, Jordan Randjelovich, Ted Selinsky, George Watson, Fred Wetzler;** Graphics: **Luis Martinez, Janet McCrie, Huburn Profitt;** Editorial & Production: **Richard Johnson, Leslie Iwaskow, Frank Ponce, Elizabeth Texeira, Vincent Susinno, Ernestine Walker.**

This document was prepared under the sponsorship of the National Aeronautics and Space Administration. Neither the United States Government nor any person acting on behalf of the United States Government assumes any liability resulting from the use of the information contained in this document, or warrants that such use will be free from privately owned rights.

NASA
TU SERVICES

NASA TECHNOLOGY UTILIZATION NETWORK

★ TECHNOLOGY UTILIZATION OFFICERS

Stanley A. Miller
Ames Research Center
Code 240-10
Moffett Field, CA 94035
(415) 965-6471

Stanley A. Miller
Hugh L. Dryden Flight Research Center
Code 240-10
Moffett Field, CA 94035
(415) 965-6471

Donald S. Friedman
Goddard Space Flight Center
Code 702.1
Greenbelt, MD 20771
(301) 344-6242

John T. Wheeler
Lyndon B. Johnson Space Center
Code AT-3
Houston, TX 77058
(713) 483-3809

U. Reed Barnett
John F. Kennedy Space Center
Code PT-SPD
Kennedy Space Center, FL 32899
(305) 867-3017

John Samos
Langley Research Center
Mail Stop 139A
Hampton, VA 23665
(804) 865-3281

Harrison Allen, Jr.
Lewis Research Center
Mail Code 7-3
21000 Brookpark Road
Cleveland, OH 44135
(216) 433-4000, Ext. 6422

Ismail Akbay
George C. Marshall Space Flight Center
Code AT01
Marshall Space Flight Center, AL 35812
(205) 453-2224

Leonard A. Ault
NASA Headquarters
Code ETD-6
Washington, DC 20546
(202) 755-2244

Aubrey Smith
NASA Resident Office-JPL
4800 Oak Grove Drive
Pasadena, CA 91103
(213) 354-4849

Gilmore H. Trafford
Wallops Flight Center
Code OD
Wallops Island, VA 23337
(804) 824-3411, Ext. 201

● INDUSTRIAL APPLICATIONS CENTERS

Aerospace Research Applications Center
1201 East 38th Street
Post Office Box 647
Indianapolis, IN 46223
John M. Ulrich, director
(317) 264-4644

Computer Software Management and Information Center (COSMIC)
Suite 112, Barrow Hall
University of Georgia
Athens, GA 30602
John A. Gibson, director
(404) 542-3265

Kerr Industrial Applications Center
Southeastern Oklahoma State University
Durant, OK 74701
James Harmon, director
(405) 924-0121, Ext. 413

NASA Industrial Applications Center
710 LIS Building
University of Pittsburgh
Pittsburgh, PA 15260
Paul A. McWilliams, executive director
(412) 624-5211

New England Research Applications Center
Mansfield Professional Park
Storrs, CT 06268
Daniel Wilde, director
(203) 486-4533

North Carolina Science and Technology Research Center
Post Office Box 12235
Research Triangle Park, NC 27709
James E. Vann, director
(919) 549-0671

Technology Applications Center
University of New Mexico
Albuquerque, NM 87131
Stanley Morain, director
(505) 277-3622

NASA Industrial Applications Center
University of Southern California
Denny Research Building
University Park
Los Angeles, CA 90007
Robert Mixer, acting director
(213) 743-6132

■ STATE TECHNOLOGY APPLICATIONS CENTERS

NASA/University of Florida
State Technology Applications Center
500 Weil Hall
University of Florida
Gainesville, FL 32611
J. Ronald Thornton, director

Gainesville:	(904) 392-6760
Boca Raton:	(305) 395-5100, Ext. 2292
Fort Lauderdale:	(305) 776-6645
Jacksonville:	(904) 646-2478
Orlando:	(305) 275-2706
Pensacola:	(904) 476-9500, Ext. 426
Tampa:	(813) 974-2499

NASA/University of Kentucky
State Technology Applications Program
109 Kinkead Hall
University of Kentucky
Lexington, KY 40506
William R. Strong, manager
(606) 258-4632

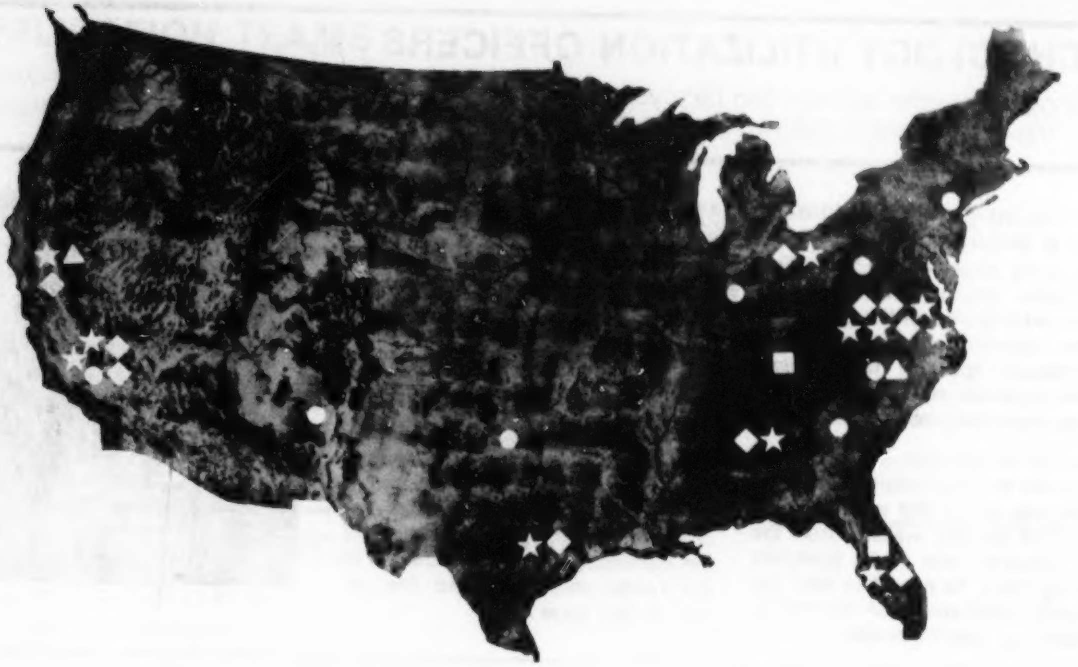

◆ PATENT COUNSELS

Robert F. Kempf
Asst. Gen. Counsel for patent matters
NASA Headquarters
Code GP-4
400 Maryland Avenue, SW.
Washington, DC 20546
(202) 755-3954

Darrell G. Brekke
Ames Research Center
Mail Code: 200-11A
Moffett Field, CA 94035
(415) 965-5104

Darrell G. Brekke
Hugh L. Dryden Flight Research Center
Mail Code: 200-11A
Moffett Field, CA 94035
(415) 965-5104

John O. Tresansky
Goddard Space Flight Center
Mail Code: 204
Greenbelt, MD 20771
(301) 344-7351

Marvin F. Matthews
Lyndon B. Johnson Space Center
Mail Code: AL-3
Houston, TX 77058
(713) 483-4871

James O. Harrell
John F. Kennedy Space Center
Mail Code: SA-PAT
Kennedy Space Center, FL 32899
(305) 867-2544

Howard J. Osborn
Langley Research Center
Mail Code: 279
Hampton, VA 23665
(804) 827-3725

Norman T. Musial
Lewis Research Center
Mail Code: 500-311
21000 Brookpark Road
Cleveland, OH 44135
(216) 433-4000, Ext. 346

Leon D. Wofford, Jr.
George C. Marshall Space Flight Center
Mail Code: CC01
Marshall Space Flight Center, AL 35812
(205) 453-0020

Paul F. McCaul
NASA Resident Office-JPL
Mail Code: 180-601
4800 Oak Grove Drive
Pasadena, CA 91103
(213) 354-2700

▲ APPLICATION TEAMS

Doris Rouse, director
Research Triangle Institute
Post Office Box 12194
Research Triangle Park, NC 27709
(919) 541-6980

James P. Wilhelm, director
SRI International
333 Ravenswood Avenue
Menlo Park, CA 94026
(415) 326-6200, Ext. 3520

TECHNOLOGY UTILIZATION OFFICERS

Technology transfer experts can help you apply the innovations in NASA Tech Briefs.

The Technology Utilization Officer at each NASA Field Center is an applications engineer who can help you make use of new technology developed at his center. He brings you NASA Tech Briefs and other special publications, sponsors conferences, and arranges for expert assistance in solving technical problems.

Technical assistance, in the form of further information about NASA innovations and technology, is one of the services available from the TUO. Together with NASA scientists and engineers, he can often help you find and implement NASA technology to meet your specific needs.

Technical Support Packages (TSP's) are prepared by the center TUO's. They provide further technical details for articles in NASA Tech Briefs. This additional material can help you evaluate and use NASA technology. You may receive most TSP's free of charge by using the TSP Request Card found at the back of this issue.

Technical questions about articles *in NASA Tech Briefs are answered in the TSP's. When no TSP is available, or you have further questions, contact the Technology Utilization Officer at the center that sponsored the research [see page A4].*

NASA INVENTIONS AVAILABLE FOR LICENSING

Over 3,500 NASA inventions are available for licensing in the United States — both exclusive and nonexclusive.

Nonexclusive licenses for commercial use of NASA inventions are encouraged to promote competition and to achieve the widest use of inventions. They must be used by a netotiated target date.

Exclusive licenses may be granted to encourage early commercial development of NASA inventions, especially when considerable private investment is required. These are generally for 5 to 10 years and usually require royalties based on sales or use.

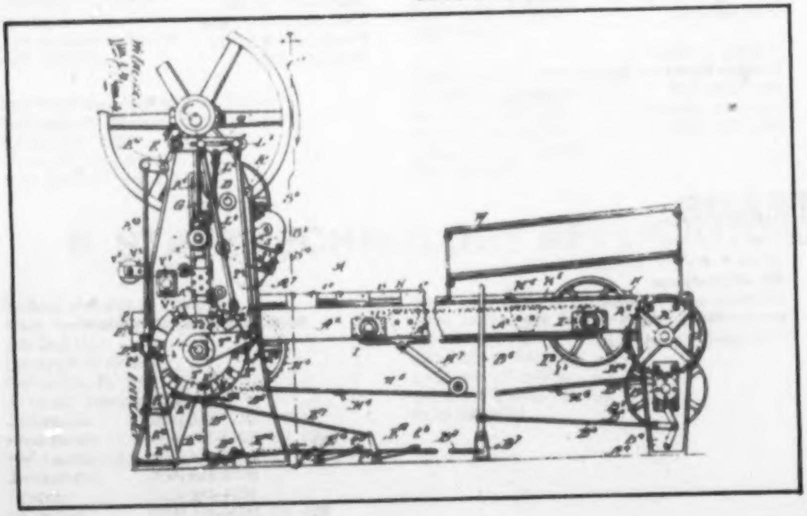

Additional licenses available include those of NASA-owned foreign patents. In addition to inventions described in NASA Tech Briefs, *"NASA Patent Abstract Bibliography"* (PAB), containing abstracts of all NASA inventions, can be purchased from National Technical Information Service, Springfield, VA 22161. The PAB is updated semiannually.

Patent licenses for Tech Briefs *are frequently available. Many of the inventions reported in NASA Tech Briefs are patented or are under consideration for a patent at the time they are published. The current patent status is described at the end of the article; otherwise, there is no statement about patents. If you want to know more about the patent program or are interested in licensing a particular invention, contact the Patent Counsel at the NASA Field Center that sponsored the research [see page A5]. Be sure to refer to the NASA reference number at the end of the Tech Brief.*

APPLICATION TEAMS

Technology-matching and problem-solving assistance to public-sector organizations

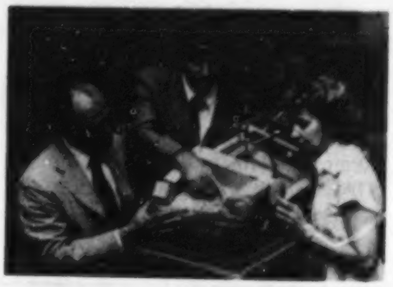

Application engineering projects are conducted by NASA to help solve public-sector problems in such areas as safety, health, transportation, and environmental protection. Some application teams specialize in biomedical disciplines; others, in engineering and scientific problems. Staffed by professionals from various disciplines, these teams work with other Federal agencies and health organizations to identify critical problems amenable to solution by the application of existing NASA technology.

Public-sector organization *representatives can learn more about application teams by contacting a nearby NASA Field Center Technology Utilization Office [see page A4].*

INDUSTRIAL APPLICATIONS CENTERS

Computerized access to over 10 million documents worldwide

Computerized information retrieval from one of the world's largest banks of technical data is available from NASA's network of Industrial Applications Centers (IAC's). The IAC's give you access to 1,800,000 technical reports in the NASA data base and to more than 10 times that many reports and articles found in nearly 200 other computerized data bases.

The major sources include:

- *750,000 NASA Technical Reports*
- *Selected Water Resources Abstracts*
- *NASA Scientific and Technical Aerospace Reports*
- *Air Pollution Technical Information Center*
- *NASA International Aerospace Abstracts*
- *Chem Abstracts Condensates*
- *Engineering Index*
- *Energy Research Abstracts*
- *NASA Tech Briefs*
- *Government Reports Announcements*

and many other specialized files on food technology, textile technology, metallurgy, medicine, business, economics, social sciences, and physical science.

The IAC services range from tailored literature searches through expert technical assistance:

- *Retrospective Searches:* Published or unpublished literature is screened, and documents are identified according to your interest profile. IAC engineers tailor results to your specific needs and furnish abstracts considered the most pertinent. Complete reports are available upon request.
- *Current-Awareness Searches:* IAC engineers will help design a program to suit your needs. You will receive selected monthly or quarterly abstracts on new developments in your area of interest.
- *Technical Assistance:* IAC engineers will help you evaluate the results of your literature searches. They can help find answers to your technical problems and put you in touch with scientists and engineers at appropriate NASA Field Centers.

Prospective clients *can obtain more information about these services by contacting the nearest IAC [see page A4]. User fees are charged for IAC information services.*

STATE TECHNOLOGY APPLICATIONS CENTERS

Technical information services for industry and state and local government agencies

Government and private industry in Florida and Kentucky can utilize the services of NASA's State Technology Applications Centers (STAC's). The STAC's differ from the Industrial Applications Centers described on page A7, primarily in that they are integrated into existing state technical assistance programs and serve only the host state, whereas the IAC's serve multistate regions.

Many data bases, including the NASA base and several commercial bases, are available for automatic data retrieval through the STAC's. Other services such as document retrieval and special searches are also provided. (Like the IAC's, the STAC's normally charge a fee for their services.)

To obtain information *about the services offered, write or call the STAC in your state [see page A4].*

COSMIC®

An economical source of computer programs developed by NASA and other government agencies

A vast software library is maintained by COSMIC — the Computer Software Management and Information Center. COSMIC gives you access to approximately 1,600 computer programs developed for NASA and the Department of Defense and selected programs for other government agencies. Programs and documentation are available at reasonable cost.

Available programs range from management (PERT scheduling) to information science (retrieval systems) and computer operations (hardware and software). Hundreds of engineering programs perform such tasks as structural analysis, electronic circuit design, chemical analysis, and the design of fluid systems. Others determine building energy requirements and optimize mineral exploration.

NASTRAN
COSMIC
NASTRAN
NASA STRUCTURAL ANALYZER
Looking for the right computer programs can sometimes feel like wandering through a maze.

COSMIC services go beyond the collection and storage of software packages. Programs are checked for completeness; special announcements and an indexed software catalog are prepared; and programs are reproduced for distribution. Customers are helped to identify their software needs; and COSMIC follows up to determine the successes and problems and to provide updates and error corrections. In some cases, NASA engineers can offer guidance to users in installing or running a program.

Information about programs *described in NASA Tech Briefs articles can be obtained by completing the COSMIC Request Card at the back of this issue. Just circle the letters that correspond to the programs in which you are interested.*

NEW PRODUCT IDEAS

NEW PRODUCT IDEAS are just a few of the many innovations described in this issue of NASA Tech Briefs and having promising commercial applications. Each is discussed further on the referenced page in the appropriate section in this issue. If you are interested in developing a product from these or other NASA innovations, you can receive further technical information by requesting the TSP referenced at the end of the full-length article or by writing the Technology Utilization Office of the sponsoring NASA center (see page A4). NASA's patent-licensing program to encourage commercial development is described on page A6.

Quick-Disconnect Fastener

A proposed quick-disconnect fastener for two or more parts resists shear loads and torque. It would center the parts to be joined, clamp them, and then tighten them into a single unit. The fastener consists of a spring-loaded hexagonal actuating pin, six springy collet fingers, and a hexagonal-nut locking collar. An adjustable locking collar compensates for component assemblies of different thicknesses. Potential applications for the removable fastener include holding parts for welding, brazing, soldering, riveting, and gluing. Other possible uses would be for attaching removable panels and panels with poor access on one side and for plugging leaks in pressure vessels.
(See page 190.)

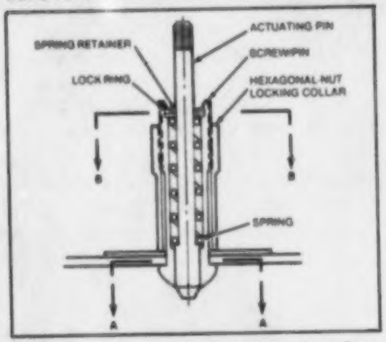

Ball Bearings Are Lubricated Automatically

Inserts on the ball-separator ring of ball bearings could provide a steady flow of lubricant to the ball surfaces. Developed for hard-to-lubricate turbopumps for cryogenic liquids, the self-lubricating bearings could be utilized on equipment for which maintenance is difficult and the lubrication interval is uncertain, such as household appliances, automobiles, and boat engines. The small inserts are made of a material rich in molybdenum disulfide and PTFE. The material can be machined or molded. In operation, the balls rub against the inserts as they turn, picking up a film of lubricant, which is transferred to the bearing races.
(See page 196.)

INCHES
1
2
CENTIMETERS
5

Improved Gloves for Firefighters

New firefighter's gloves are more flexible and more comfortable than previous designs. There are two versions of the new glove, one made of composite material and the other dip-coated. An aramid fabric was selected as the material for the outer shell of the composite glove because it is strong and resistant to flame and heat. For the liner, aramid felt was selected because it is puncture resistant and thermally insulating. For the dip-coated glove, the shell is coated with a yellow, flame-retardant neoprene layer. A friction layer on the palm side improves the wearer's grip. The new gloves may also find uses in foundries, steel mills, and other plants where they can be substituted for asbestos gloves.
(See page 211.)

Fiber-Optics Temperature Sensor

A new instrument uses an optical sensor to measure temperature. A small gap in the sensor widens as the temperature rises, increasing the number of spectral bands passed to a receiver. A count of the received bands is translated into temperature changes. The instrument has digital output.
(See page 177.)

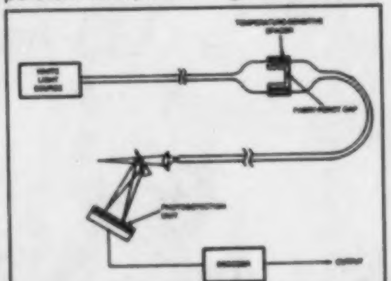

Acoustic Ground-Impedance Meter

A portable instrument uses a Helmholtz resonator to measure the acoustic impedance of the ground or other surfaces. The meter can be used in conjunction with other acoustic measurements in predicting the effects of aircraft noise. The sound pressure generated by a cam-driven piston in the chamber is measured near the ground surface by a microphone mounted flush

with the wall of the chamber. Using a five-lobed cam, sound vibrations up to 300 Hz are excited and measured. This range is extended to nearly 1,000 Hz by a 15-lobed cam.
(See page 181.)

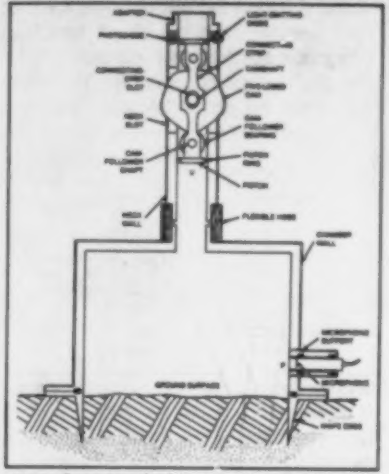

High-Performance PMR Polyimides

Highly-cross-linked PMR polyimides are formed at 600° F (315° C) from the in situ thermopolymerization of four monomer reactants. A variety of compositions are formed by adding 4 to 20 mole percent PN to the standard PMR-15 composition. These modified resins, intended for use in advanced composites, adhesives, and neat resin articles, show better processability and elevated-temperature stability than state-of-the-art PMR-15 polymers.
(See page 159.)

Metering Fluid Container

A hand-held container accepts, stores, and discharges a preset amount of fluid from a pressurized supply. The supply pressure drives a spring-loaded piston that stores enough mechanical energy to discharge the measured liquid into another container. The container attaches to a fluid supply through a quick-disconnect fitting. The desired amount of fluid is selected by turning a collar that controls the length of the piston travel. Possible applications include the dispensing of toxic fluids or metering liquids for household, commercial, or laboratory uses.
(See page 189.)

Regulating Oxygen Pressure Safely

A pressure regulator for oxygen allows gas flow to be shut off on its low-pressure side rather than its high-pressure side. The initial rush of oxygen occurs in the second stage rather than in the first stage of pressure reduction. The regulator thus avoids the fire hazard associated with the rapid pressurization and consequent adiabatic heating of oxygen on the input side when the regulator is turned on. The new regulator can reduce the danger of fire in aircraft and in systems that supply oxygen for medical emergencies.
(See page 194.)

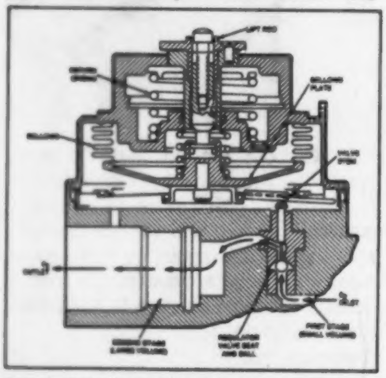

Fasteners for Solar Panels

A simple articulating linkage secures solar panels into a supporting framework. The five-element linkage collapses into a W-shape for easy placement into the framework, then expands to form a rectangle of the same dimensions as those of the panel. The result is a large retaining ring around the outer edges of the panel. Removal of the linkage is simply by the reverse of installation. The fastener could also be used on removable wall panels, photographs, and signs.
(See page 182.)

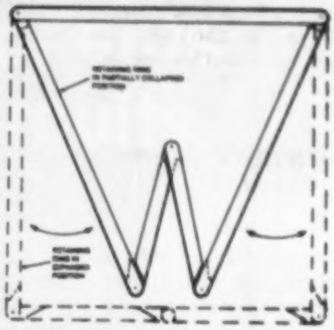

Microwaves Detect Icing on Aircraft Surfaces

A new instrument can be used in aircraft to warn pilots of the onset of dangerous ice buildup. It also has potential as a research tool in cloud studies and in investigations of icing phenomena. The instrument employs microwave waveguides implanted just below the surface to be monitored. A change in the resonant frequency of the waveguides, caused by ice buildup, is measured by a microprocessor and converted to a dc voltage that is proportional to the ice thickness. A microprocessor also computes the change in ice thickness with respect to time to obtain the ice-accretion rate. The ice thickness and accretion rates are displayed digitally.
(See page 178.)

Hydraulic Tubing Cutter

A hydraulically powered tool cuts tubing and cable in areas of limited accessibility. Mounted on one end of a flexible "gooseneck" extension, the cutter jaws are closed by a hydraulic piston when the operator squeezes the handle grip. The jaws are released by flipping an on/off lever. The hydraulic cutter was originally designed to deactivate aircraft ejection seats in rescue operations by

severing the pressure supply lines to the ejector. It can also be useful in automobile and fire rescue work.
(See page 199.)

Solvent-Resistant Polymer

A new thermoplastic polymer incorporates the best properties of polyimides and polysulfones. It can be used as a molding resin, as an adhesive, and as a matrix resin for fiber-reinforced composites. The new structure is obtained by incorporating an aromatic sulfone moiety in the backbone of an aromatic linear polyimide to yield an aromatic poly(imidesulfone) prepared in bis(2-methoxyethyl) ether solvent. This polymer system results in a thermoplastic with better processability than the base polyimide. The incorporation of an imide segment into the base polysulfone results in a polymer that is insoluble in common solvents.
(See page 159.)

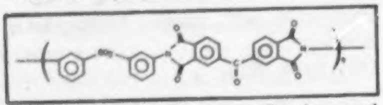

Easy-Change Terminal Strip

A laminated copper and polyimide terminal strip makes it easy to modify a printed-circuit board, after the board has been fabricated. The "easy-change" strip is composed of two parallel rows of pins on an insulating base. It is epoxied over conductors or an insulating portion of the PC board. Copper conductors, attached to the pins, serve as bonding pads for integrated-circuit leads. The strip can be bonded to a board directly over existing conductor patterns, making it unnecessary to remove unused portions of the circuit pattern.
(See page 134.)

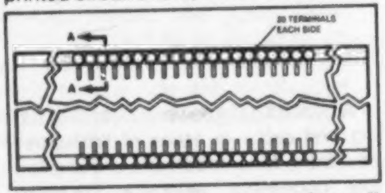

Portable Pipe Wrapper

A new tool applies fragile layered insulation to cryogenic tubing. It has been used routinely to apply two layers of fiberglass and one layer of aluminum foil on pipe used as the inner line in vacuum-jacketed cryogenic plumbing. The new pipe wrapper has three freely revolving drums that hold the wrapping material. It controls both tension and the wrap angle. The wrapper is easy to use and is made from inexpensive, readily available parts. It could prove useful in applying thermal insulation to hot-water pipes and refrigerant-distribution lines. A similar tool could be used to wrap electrical insulation.
(See page 198.)

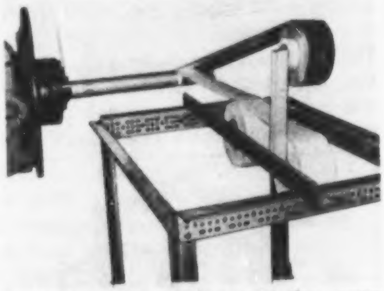

Ferrofluid Would Seal a Linear-Motion Valve

A proposed valve would employ a ferrofluid to make a tight seal against vacuum and pressure. The seal would require no precisely machined parts, and hand lapping of valve seats would be unnecessary. The valve consists of a hollow shaft with magnetically soft sheaths that slide through a ring magnet with annular pole pieces. A ferrofluid (magnetic fluid) is held in place around the shaft by the ring magnet. The ferrofluid seals the space between the shaft and the pole piece in the chamber wall. If more than one ferrofluid seal is used on a shaft, the valve could be used as a switching valve in a plumbing system.
(See page 197.)

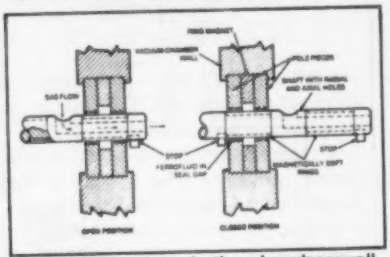

Multipanel Trough Solar Concentrator

A cylindrical solar concentrator composed of many flat-plate mirrors is efficient even when pointing away from the Sun by as much as 5°. The concentrator is designed to backlight an array of photovoltaic cells. However, unlike ordinary backlit concentrators, the multiple-flat-plate reflector does not lose very much efficiency if it is slightly out of alinement with the Sun. The design is economical and easy to fabricate.
(See page 206.)

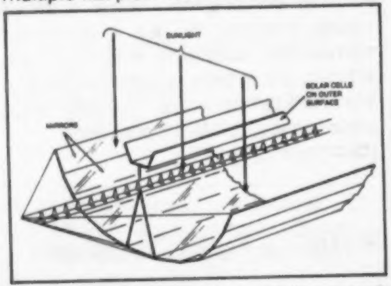

Electronic Components and Circuits

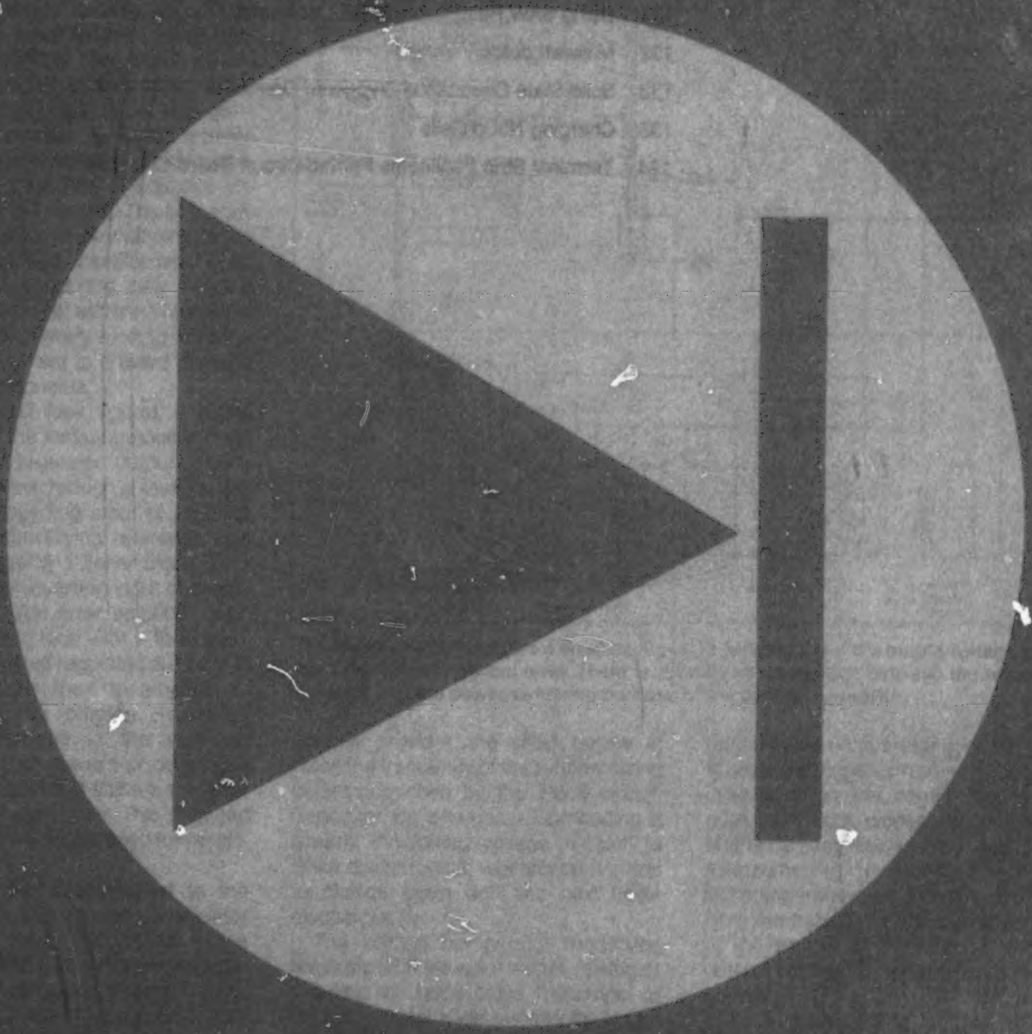

Hardware, Techniques, and Processes

127 Voltage Regulator for a dc-to-dc Converter
128 Microprogramed Sequencer for Tunable RF Oscillator
129 Tangleproof Rotary Electrical Coupling
130 VLSI Reed-Solomon Encoder
131 Using SAW Resonators in RF Oscillators
132 Milliwatt dc/dc Inverter
133 Solid-State Circuits for Cryogenic Operation
133 Charging Ni/Cd Cells
134 Terminal Strip Facilitates Printed-Circuit Board Changes

Voltage Regulator for a dc-to-dc Converter

An extra transformer winding eliminates the need for isolation components.

NASA's Jet Propulsion Laboratory, Pasadena, California

A voltage regulator for a dc-to-dc converter momentarily short-circuits the secondary winding on its drive transformer. The short circuit temporarily turns off the drive to the output transistors. In effect, the short circuit changes the width of the drive pulses, thereby regulating the output voltage.

The new voltage regulator isolates signals from the power-switching converter without the use of complex circuitry or optical couplers. The only addition is an extra secondary winding on the existing interstage transformer. Error signals short-circuit the new winding and inhibit converter action. A resistor in series with the primary winding limits the short-circuit current to prevent damage to circuit components.

In the circuit (see figure), a signal representing the instantaneous voltage at the 12-volt regulated output is sampled and applied through a resistor network to the inverting input of an error amplifier. A nonvarying reference voltage established by a Zener diode is applied to the noninverting input of the error amplifier. The error amplifier operates in a closed loop with a fixed gain. When the sampled regulated output is at precisely 12 volts, the error amplifier dc output does not change. However, microvolt changes in the sampled voltage — either upward or downward — produce significant shifts in the error amplifier dc output level. This changed output is the error signal used for regulation.

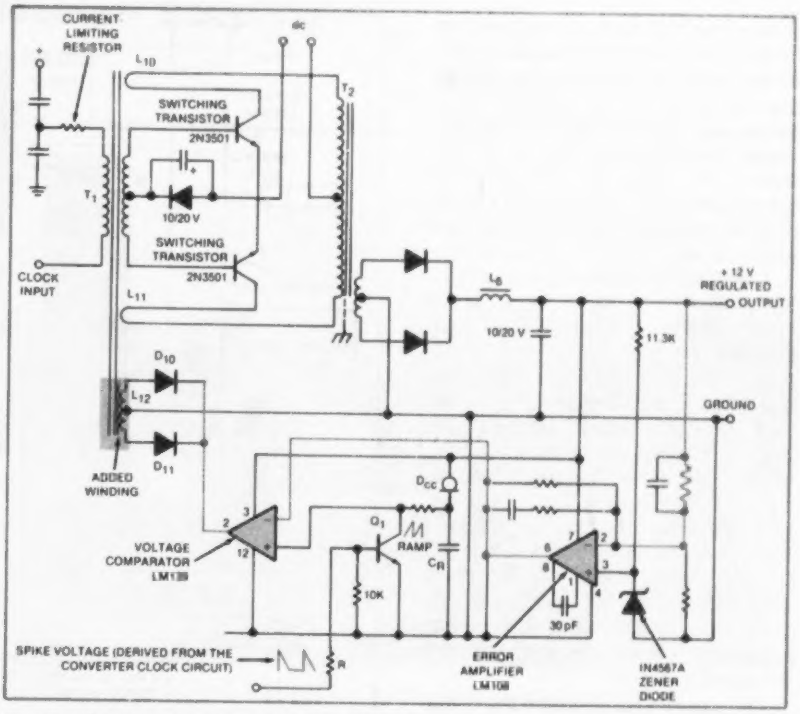

The **Feedback Path** applies a shorting signal to winding L_{12} if the output voltage strays from the 12-volt nominal level. There is virtually no interaction between the regulation voltages and the power-switching portions of the dc-to-dc converter.

The error signal is applied to the inverting input of a voltage comparator and a ramp voltage is applied to the noninverting input. The ramp-voltage input to the comparator is generated in the following way: A constant current is supplied to the capacitor C_R by the constant-current diode D_{CC}. The discharge of the capacitor is controlled by a positive-going spike applied to the base of transistor Q_1. A diode-bridge doubler provides the spike pulses at twice the frequency of the synchronizing pulses furnished by the clock circuit. Capacitor C_R charges — producing a linearly increasing voltage — until a spike discharges it, whereupon it starts to charge again until the next spike discharges it.

The voltage comparator modulates the ramp with the error signal, raising or lowering the ramp peak. The output of the comparator short-circuits the output of the interstage current-limiting transformer through diodes D_{10} and D_{11} of the center-tapped secondary winding L_{12} — the extra winding added to the interstage transformer. When the output of the comparator goes high, L_{12} is essentially open circuited. During the interval when the comparator output goes low, both diodes go to ground, short-circuiting the winding and therefore removing drive current from the switching transistors. The output pulses from the transistors are thus shortened by the amount of this interval, and the output voltage is proportionately reduced.

This work was done by Colonel W. T. McLyman of Caltech for **NASA's Jet Propulsion Laboratory.** *For further information, Circle 1 on the TSP Request Card.*
NPO-15208

Microprogramed Sequencer for Tunable RF Oscillator

Standard IC chips and digitally tuned oscillator are combined.

Langley Research Center, Hampton, Virginia

A circuit originally designed to "dither" the transmitter frequency of a K-band radar at high rates may find application in such other areas as automated test equipment or computer-controlled receiver tuning. The circuit consists of a PROM-based microprogramed control sequencer, which drives a group of diode switches to select one of eight tuning capacitors in an L-C oscillator.

A synchronizing pulse is used to clock the various mode-control inputs and a "next address" into the 74LS377 latch shown in the circuit diagram. The outputs of the latch then become an address for the PROM, and the PROM outputs $DO_5 - DO_7$ form a 3-bit code to determine the desired frequency for the oscillator. The 3-bit code is further decoded in the 74S138 1-of-8 decoder. Only one output from the 74S138 is active at a time, and the active output provides a current sink for the PIN diode switch connected to it. All other diodes in the array are cut off, and only one tuning capacitor is active at a time, except for parasitic effects.

The control inputs perform the following functions:

- The WIDE/NARROW switch selects either a wideband sweep (i.e., large separation between frequencies) or a narrowband sweep (i.e., small deviations close to the undeviated carrier).
- The MANUAL/AUTO switch allows an operator to take control of the system and select any one of the eight frequencies using the thumbwheel switch.
- The DEFAULT/NORMAL input is provided to allow removal of the control switches and thumbwheel switch by disconnecting a connector. The connector provides a return to ground for the A_8 input to the PROM. When disconnected from the control switches, the circuit defaults to an automatic wideband sweep mode.

The contents of the TBP18S42 PROM are determined by the desired sequence of frequencies. Bits $DO_1 - DO_3$ form the memory address of the next desired frequency. Bits $DO_5 - DO_7$ are an encoded version of the current desired frequency. The sequence is arbitrary.

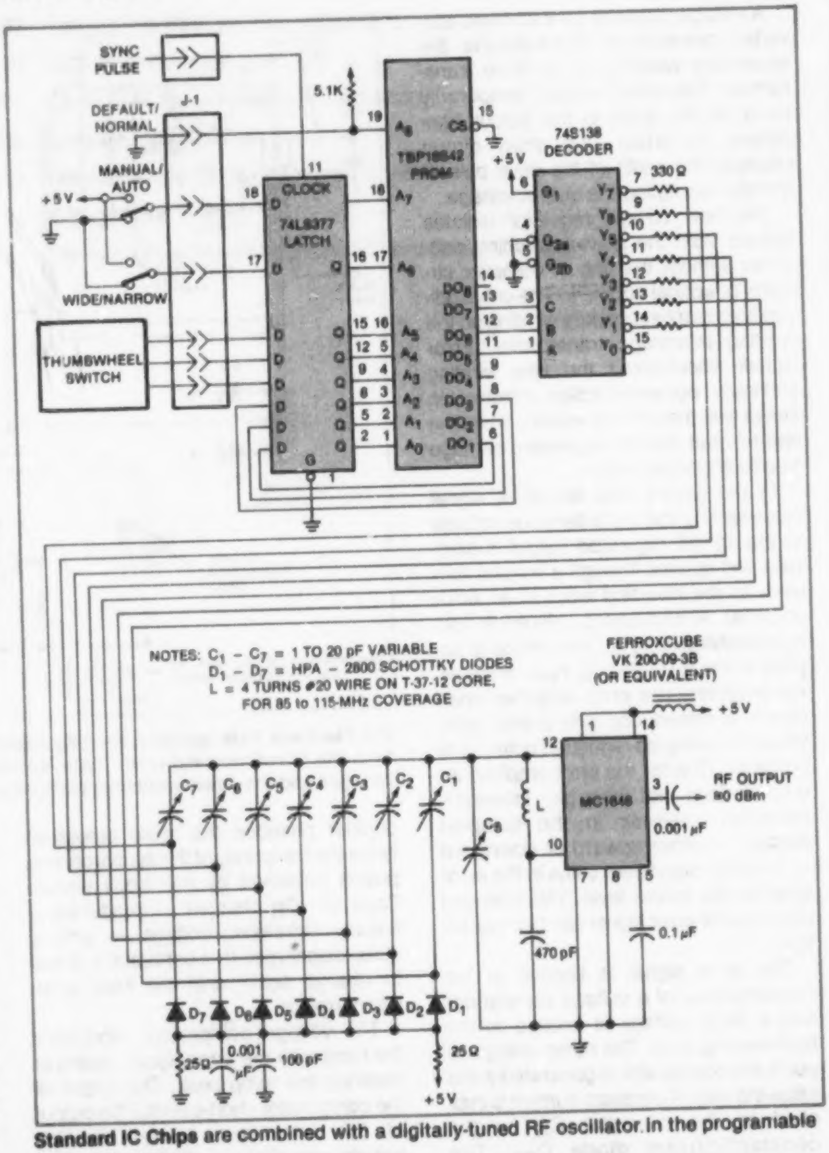
SYNC PULSE
DEFAULT/ NORMAL
J-1
MANUAL/ AUTO
+5V
WIDE/NARROW
THUMBWHEEL SWITCH
5.1K
CLOCK
74LS377 LATCH
D
Q
G
TBP18S42 PROM
A_8
A_7
A_6
A_5
A_4
A_3
A_2
A_1
A_0
CS
DO_8
DO_7
DO_6
DO_5
DO_4
DO_3
DO_2
DO_1
74S138 DECODER
G_1
G_{2A}
G_{2B}
C
B
A
Y_7
Y_6
Y_5
Y_4
Y_3
Y_2
Y_1
Y_0
330 Ω
FERROXCUBE VK 200-09-3B (OR EQUIVALENT)
+5V
MC1648
RF OUTPUT ≈0 dBm
0.001 μF
0.1 μF
470 pF
L
C_1
C_2
C_3
C_4
C_5
C_6
C_7
C_8
D_1
D_2
D_3
D_4
D_5
D_6
D_7
25Ω
0.001 μF
100 pF
25 Ω
+5V

NOTES: $C_1 - C_7$ = 1 TO 20 pF VARIABLE
$D_1 - D_7$ = HPA – 2800 SCHOTTKY DIODES
L = 4 TURNS #20 WIRE ON T-37-12 CORE, FOR 85 to 115-MHz COVERAGE

Standard IC Chips are combined with a digitally-tuned RF oscillator in the programable frequency source.

The oscillator is required to provide a near-sinusoidal signal, the frequency of which is controlled by the tuning capacitance and the amplitude of which is constant with changing frequency. This system utilizes an emitter-coupled-pair circuit in the form of an MC1648. The tuning system is actually a "delta" tune approach, in which the highest frequency is determined by the main tuning capacitor, C_8, and frequency deltas are produced by shunting appropriate trimmer capacitors to ground via a PIN diode. This approach, as opposed to using separate tuning capacitors, results in less interaction between tuning adjustments, potentially better stability, and faster switching since a small capacitance is involved.

The procedure for setting the frequency is to start with the highest frequency and progress down to the lowest frequency. There is a slight interaction because of the residual shunt capacitance of the diodes in the "off" state, making it necessary to perform this procedure twice to achieve precise adjustments of all eight frequencies.

This work was done by Richard H. Couch, Chase P. Hearn, and James B. Williams of **Langley Research Center.** *No further documentation is available.*
LAR-12903

Tangleproof Rotary Electrical Coupling

Electrical cables are carefully dressed to permit 320° rotation.

Marshall Space Flight Center, Alabama

A new rotary coupling connects a large number of elecrical cables to a turntable without stressing the cables or tangling them. The device accommodates 246 cables containing a total of 758 conductors and allows the turntable to rotate through an arc of 320° (see figure). At the extremes of rotation (± 160°), the cables are loose enough that they are not pulled taut and overstressed. At the halfway point (0°), the cables are not so loose that they become entangled.

The cables are held in a hollow shaft 5 inches (12.7 cm) in diameter and 18 inches (45.7 cm) long. At the rotating end of the shaft, the cables are distributed among five large circular holes around the periphery of a disk. At the ends of the shaft, the cables are bunched together and embedded in a resilient potting compound. The cables thus form a shape reminiscent of a truncated cone with the narrow portion at the fixed end of the coupling. The conical configuration prevents undue slackness or tension.

The rotary connector was developed to carry electrical signals to and from a telescope platform on a satellite without a complex and electrically noisy set of slip rings. The principle is also suitable to rotary actuators.

This work was done by Franz Keller of American Science & Engineering, Inc., for **Marshall Space Flight Center.** *No further documentation is available.*
MFS-25174

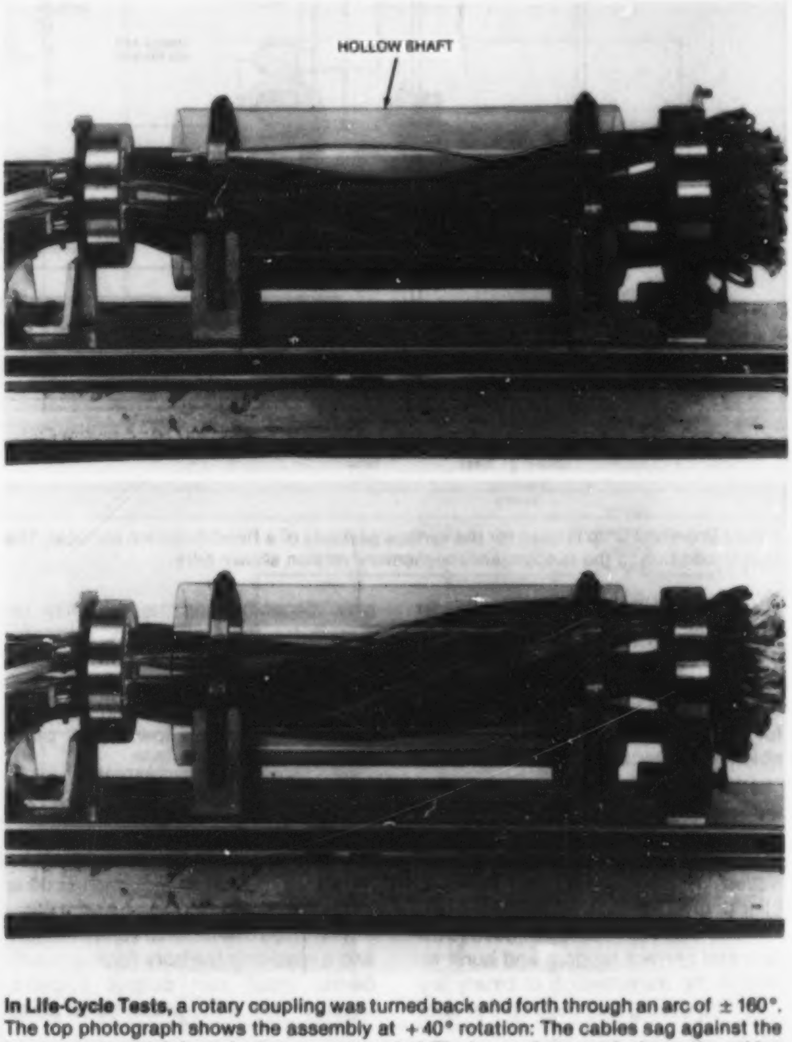

In Life-Cycle Tests, a rotary coupling was turned back and forth through an arc of ± 160°. The top photograph shows the assembly at + 40° rotation: The cables sag against the transparent containing tube but are not tangled. The lower photograph shows the cables at − 140° rotation: They are not tight and will not become tight at − 160°.

VLSI Reed-Solomon Encoder

Very-large-scale integrated chips are cascaded to yield the desired level of reliability.

NASA's Jet Propulsion Laboratory, Pasadena, California

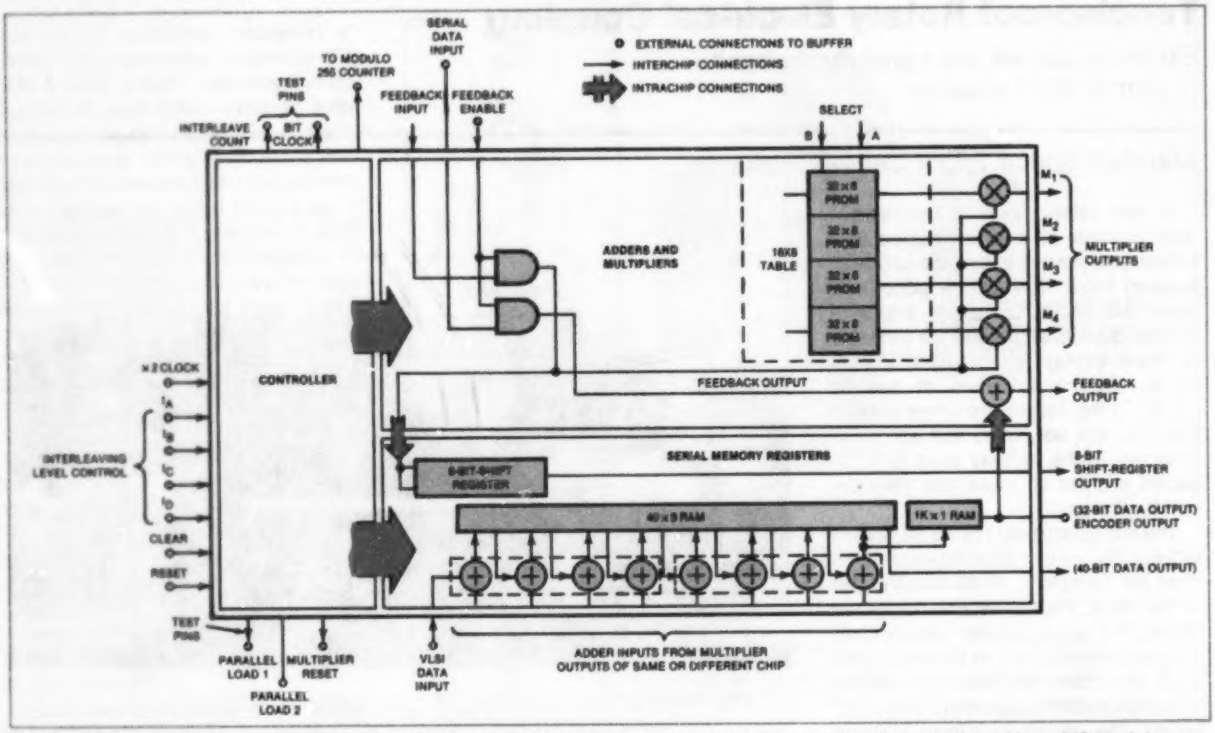
SERIAL DATA INPUT
EXTERNAL CONNECTIONS TO BUFFER
INTERCHIP CONNECTIONS
INTRACHIP CONNECTIONS
TO MODULO 256 COUNTER
TEST PINS
INTERLEAVE COUNT
BIT CLOCK
FEEDBACK INPUT
FEEDBACK ENABLE
SELECT
B
A
ADDERS AND MULTIPLIERS
16X8 TABLE
32 x 8 PROM
32 x 8 PROM
32 x 8 PROM
32 x 8 PROM
M1
M2
M3
M4
MULTIPLIER OUTPUTS
x 2 CLOCK
CONTROLLER
FEEDBACK OUTPUT
FEEDBACK OUTPUT
I A
I B
I C
I D
INTERLEAVING LEVEL CONTROL
SERIAL MEMORY REGISTERS
8-BIT-SHIFT REGISTER
8-BIT SHIFT-REGISTER OUTPUT
40 x 8 RAM
1K x 1 RAM
(32-BIT DATA OUTPUT) ENCODER OUTPUT
CLEAR
RESET
(40-BIT DATA OUTPUT)
TEST PINS
PARALLEL LOAD 1
MULTIPLIER RESET
PARALLEL LOAD 2
VLSI DATA INPUT
ADDER INPUTS FROM MULTIPLIER OUTPUTS OF SAME OR DIFFERENT CHIP

A VLSI Universal Chip is used for the various portions of a Reed-Solomon encoder. The chip has been designed in a shift-register version in addition to the random-access-memory version shown here.

A modular Reed-Solomon encoder uses identical custom VLSI chips called "symbol slices." By cascading and properly interconnecting a group of these chips, an encoder can be made for any desired error-correcting capability and interleaving level.

Two versions of the symbol-slice chip have been designed: One uses shift registers as the internal serial memory while the other uses a random-access memory (see figure). The multiplier configuration is the same in both.

Reed-Solomon codes are used to detect and correct random and burst errors in the transmission of binary signals. The coding may be simple or complex, depending on the reliability required for the application. Concatenated (interlinked) coding systems using Reed-Solomon codes have been suggested for space-communication channels requiring low error probabilities.

The new VLSI chips are utilized in an encoder in which the Reed-Solomon code is concatenated with a Viterbi convolutional code in five-level interleaving. (The Reed-Solomon code is the outer code.)

The chips use internal serial memory and a read-only memory (lookup table). Serial input and output circuits, together with a two-phase serial parallel finite-field multiplication circuit, and on-chip clock control circuits keep the number of input and output pins to a minimum. To minimize the number of multipliers required, a generator polynomial that yields symmetrical coefficients is used in a special interchip-connection technique. The resulting VLSI encoder requires only one-tenth the number of chips required by a conventional Reed-Solomon circuit implemented with discrete IC's.

This work was done by Kuang Y. Liu of Caltech for **NASA's Jet Propulsion Laboratory.** *For further information, Circle 2 on the TSP Request Card. NPO-15470*

Using SAW Resonators in RF Oscillators

Two circuits illustrate the potential of surface-acoustic-wave resonators.

Ames Research Center, Moffett Field, California

Surface-acoustic-wave (SAW) resonators are used as the frequency-determining elements in radio-frequency oscillator circuits at NASA's Ames Research Center. The oscillators can be frequency-modulated, phase-modulated, or pulse-modulated. Two such circuits are described here.

The SAW resonators are especially applicable to low-power subminiature applications, such as biotelemetry and wind-tunnel instrumentation, where they can advantageously replace crystals. The resonators are smaller than crystals and very thin — an advantage where small package size is important. They are fabricated with integrated-circuit techniques, so their use in place of crystals gives promise of totally-integrated telemetry systems in the future. SAW oscillators can be directly modulated without the need for the multiplying stages often required with crystals, which simplifies the circuitry and further reduces size.

The transistor used as the amplifying element in the oscillator has three connections, and the two-port SAW resonator has four. Therefore numerous circuit configurations are possible. Figure 1 shows a single-pole two-port SAW resonator used as the frequency-controlling element in a Colpitts-type oscillator operating at 150 MHz. The SAW device uses an ST-cut quartz substrate to achieve a higher temperature stability than can be obtained with other substrates, such as lithium niobate or lithium tantalate. However, since the ST-cut quartz has a higher insertion loss than the other substrates, the voltage is fed back directly from the collector rather than from a capacitor tap as is usual with this type of oscillator. The variable capacitor is adjusted for resonance at the operating frequency. This version of the oscillator can be used with supplies ranging from 1 to 6 volts, and current drains as low as 0.4 mA can be achieved by increasing the values of the bias resistors.

(continued on next page)

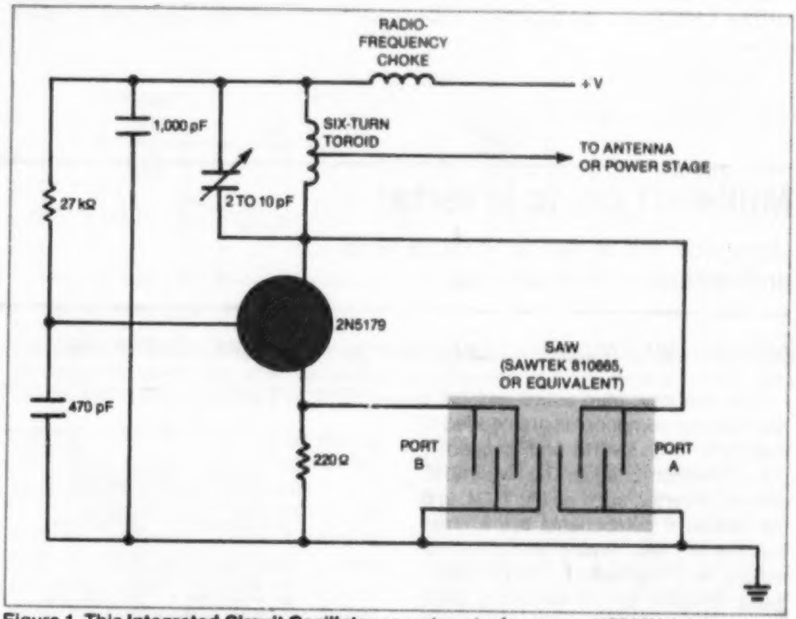
RADIO-FREQUENCY CHOKE
+V
1,000 pF
SIX-TURN TOROID
TO ANTENNA OR POWER STAGE
27 kΩ
2 TO 10 pF
2N5179
SAW (SAWTEK 810665, OR EQUIVALENT)
470 pF
PORT B
220 Ω
PORT A

Figure 1. This **Integrated-Circuit Oscillator** operates at a frequency (150 MHz) determined by the surface-acoustic-wave resonator.

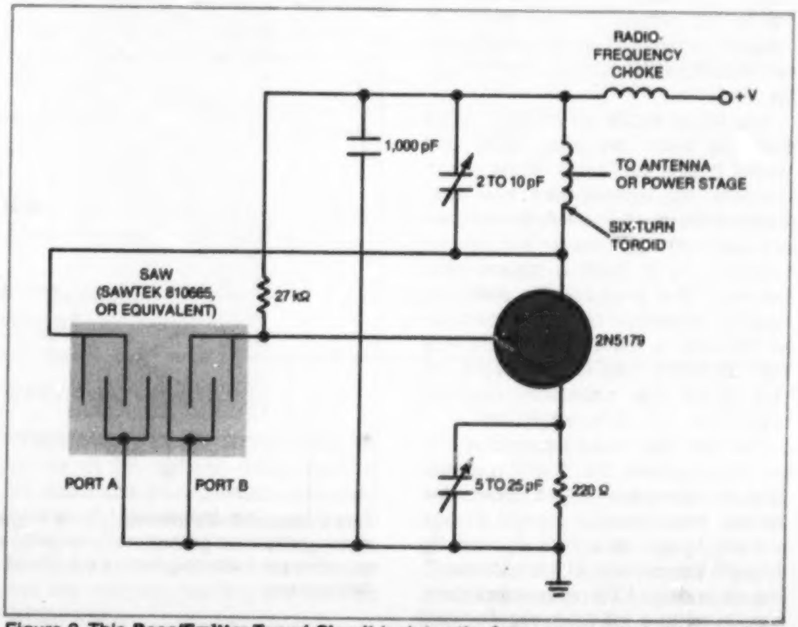
RADIO-FREQUENCY CHOKE
+V
1,000 pF
2 TO 10 pF
TO ANTENNA OR POWER STAGE
SIX-TURN TOROID
SAW (SAWTEK 810665, OR EQUIVALENT)
27 kΩ
2N5179
PORT A
PORT B
5 TO 25 pF
220 Ω

Figure 2. This **Base/Emitter-Tuned Circuit** isolates the frequency-control elements from the output circuit; but, unlike the circuit in Figure 1, a separate tuning is needed for the collector and base/emitter circuits.

Frequency trimming or modulation is accomplished with the mechanically variable or voltage-variable capacitor between the SAW resonator and the emitter of the transistor; deviations of up to 100 kHz are possible without the loss of frequency stability. For pulse modulation, the 27-kilohm bias resistor is connected to a control voltage source that swings from ground to the positive supply level.

A second circuit that uses the SAW device is shown in Figure 2. This circuit is base/emitter-tuned, with the voltage fed back from the collector. Again, frequency trimming is accomplished with a variable capacitor at the emitter of the transistor, while the collector capacitor can be used to peak the power output. Pulse modulation is accomplished in the same manner as in the circuit of Figure 1.

Of the two circuits, the first is easier to frequency-modulate and only requires a single adjustment for peaking output power. However, the second circuit isolates the frequency-control elements from the output circuit, providing better frequency stability when the output is loaded than does the first circuit.

This work was done by Richard M. Westbrook and Gordon J. Deboo of **Ames Research Center.** *No further documentation is available.*
ARC-11390

Milliwatt dc/dc Inverter

Compact unit shifts dc voltage level and isolates it from the input.

NASA's Jet Propulsion Laboratory, Pasadena, California

Only one integrated circuit and just a few external components are needed to make a dc-to-dc inverter with isolated input and output voltages. The required IC is a hex inverter, such as the 7404, and the outboard components are a small transformer, two diodes, and a few resistors and capacitors. The inverter gates function as the switching oscillator and the driver amplifier for the circuit. If the IC is a transistor-transistor-logic (TTL) module, the inverter delivers 100 to 150 milliwatts; if only microwatt power is required, a CMOS (complementary metal-oxide semiconductor) IC may be used.

The figure shows an inverter circuit that has been designed, built, and tested. It uses the CMOS 74C04, which contains six independent inverters. Three of the inverters — A, B, and C — are used with resistors R_1 and R_2 and capicitor C_1 to form a square-wave generator that produces the switching required for voltage inversion. Operation at 100 kHz is feasible. This relatively high operating frequency reduces the size of the filter capacitors required, resulting in a small packaged unit.

The oscillator output power is amplified by inverters D, E, and F in parallel. Their square-wave output allows the 10-Vdc local power source to charge and discharge capacitors C_2 and C_3 through the primary of transformer T. The secondary of T is center-tapped and connected to a full-wave rectifier (two 1N916 diodes) to charge a 0.1-microfarad capacitor to the new, isolated, output voltage level.

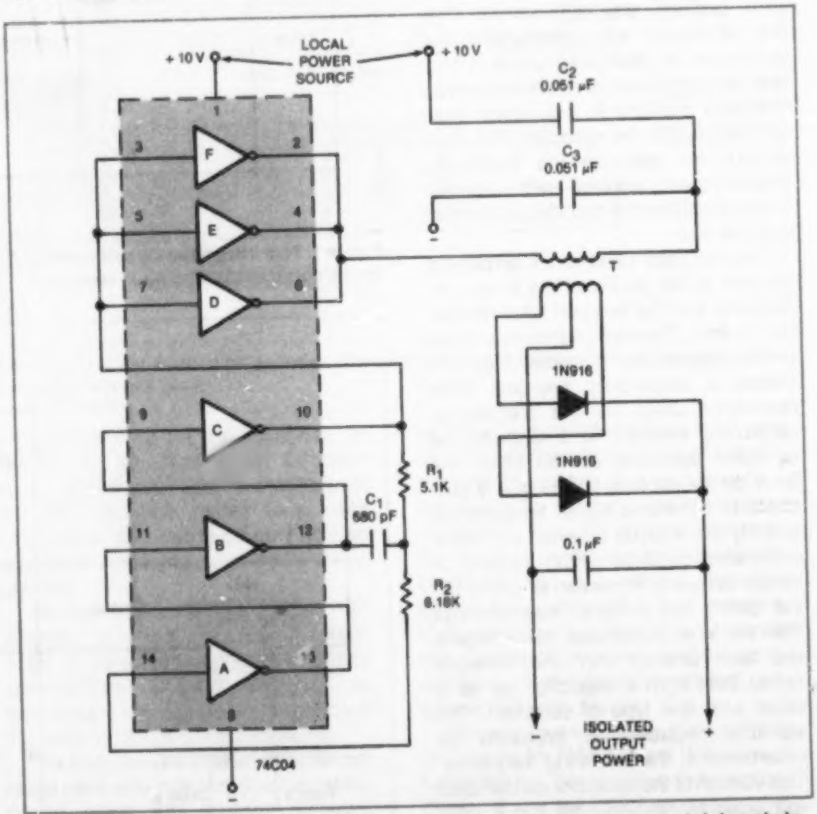

This Compact dc/dc Inverter uses a single integrated-circuit package containing six inverter gates that generate and amplify a 100-kHz square-wave switching signal. The square-wave switching inverts the 10-volt local power to an isolated voltage at another desired level.

This work was done by Colonel W. T. McLyman of Caltech for **NASA's Jet Propulsion Laboratory.** *For further information, Circle 3 on the TSP Request Card.*
NPO-15157

Solid-State Circuits for Cryogenic Operation

Selected commercially available components perform satisfactorily at 1.25 K.

NASA's Jet Propulsion Laboratory, Pasadena, California

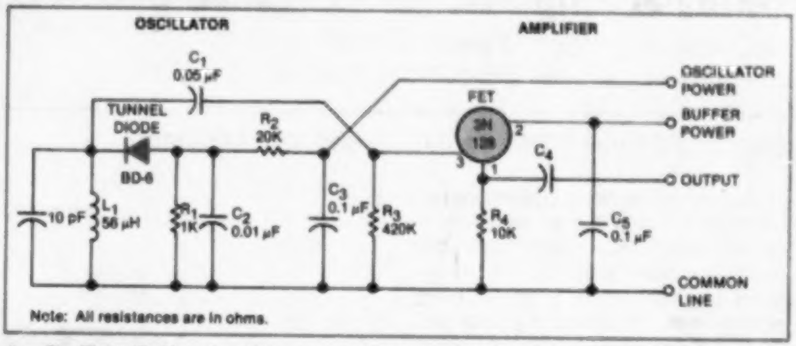

Note: All resistances are in ohms.

An **Oscillator/Buffer Amplifier** circuit that operates reliably at both normal and cryogenic temperatures, after repeated cycling between the two, uses a tunnel diode for the 4-MHz oscillator and a MOSFET source follower for the amplifier.

Tests at NASA's Jet Propulsion Laboratory confirm the operation of five commercial semiconductor devices at cryogenic temperatures. The five devices — one tunnnel diode, one field-effect transistor, and three CMOS integrated circuits — all perform well in circuits immersed in a liquid-helium bath. For some of the tests, the bath temperature was reduced to 1.25 K by pumping.

While intrinsic semiconductors such as pure silicon and pure germanium turn into insulators at cryogenic temperatures, some extrinsic materials, such as InSb and GaAs, retain free charge carriers and are candidates for low-temperature semiconductor devices. In addition, devices that produce free carriers by field effect, rather than by thermal excitation, and devices dependent on carrier tunneling are also possibilities for cryogenic operation. Circuit properties vary from batch to batch, however, and each unit has to be tested to verify its performance in a cryogenic environment.

The transistor tested for the NASA work is a low-current 3N128 MOSFET. It was used in a buffer amplifier operating at supply voltages between 2.3 and 7 volts dc. Low-current, low-power operation is important for cryogenic operation since large power dissipation would rapidly boil off the liquid helium. Power consumption for the transistor was about 1 milliwatt.

The figure shows the amplifier circuit and a tunnel-diode oscillator circuit, both of which performed well at temperatures below 4.2 K. The BD-6 tunnel diode has been used previously for low-temperature work; however, designers may be interested in the specific circuit configuration shown here. Metal-film resistors are used since the resistance of carbon increases substantially at low temperature.

A multiplexer circuit for signals from 133 liquid-level sensors was assembled using CD4051 CMOS multiplexers, a CD4028 BCD-to-decimal decoder, and a CD4049 buffer/level converter. Drivers for the circuit were located outside the cryostat, but the main circuit elements were operated in liquid helium. The liquid-level sensors were short lengths of constantan-alloy wire covered by a superconducting alloy with a transition temperature of 2.9 K.

This work was done by Dusan Petrac and Robert L. Spencer of Caltech for **NASA's Jet Propulsion Laboratory.** *For further information, Circle* ***4*** *on the TSP Request Card.*
NPO-15255

Charging Ni/Cd Cells

Procedure is faster, reduces heating, and yields a higher end-of-charge voltage.

Goddard Space Flight Center, Greenbelt, Maryland

A new procedure for recharging nickel/cadmium batteries is fast and eliminates overcharging. The method charges "dead" cells using current increments rather than continuous, constant current.

Formerly, Ni/Cd cells removed from storage were activated by a C/20 charging current (i.e., an amperage equal to one-twentieth of the ampere-hour capacity of the battery) maintained for 48 hours. This practice involved an overcharge of 100 percent, which evolved a great deal of heat. The end-of-charge voltage was relatively low because of the low charging rate and the elevated temperature.

The new procedure starts with a low charging rate (C/20) for 6 hours to remove some of the passive material that adds to the impedance of the electrochemical cell. Then the charging rate is maintained at C/10 for another 6 hours. Next, the cell is charged at C/5 until 1.435 volts per cell are reached. Charging is continued at this fixed voltage until

(continued on next page)

the current has tapered down to the C/10 to C/20 rate.

The time required for the procedure is approximately 18 hours, and the correspondingly reduced overcharging reduces the generation of heat. A further advantage is that the cells are more electrochemically active than after the 48 hours of charging by the old method.

This work was done by Gerald Halpert and C. Michael Tasevoli of **Goddard Space Flight Center.** *No further documentation is available.*
GSC-12779

Terminal Strip Facilitates Printed-Circuit Board Changes

Strip can be bonded to board directly over used or unused conductor patterns.

Goddard Space Flight Center, Greenbelt, Maryland

A laminated copper and polyimide terminal strip makes it easy to modify a printed-circuit (PC) board, after the board has been fabricated. When epoxied over conductors or an insulating portion of the PC board, the strip provides a series of solder-coated copper conductor pads to which integrated-circuit leads can be soldered for functional changes. The terminal strips can accommodate the leads on a dual, in-line IC package or as staggered single or multiple leads on planar mounted flatpacks.

The conductors are laminated to a polyimide base (see figure) with each conductor brazed to a copper pin. Wires soldered to the pins connect the integrated circuit to other components on the circuit board.

The terminal strip is bonded to a circuit board with an epoxy adhesive. It can be attached over any existing metallization. The strip-insulating base of polyimide makes it unnecessary to remove unwanted patterns on the board. It is usually unnecessary to disconnect unwanted patterns in other layers of a multilayer board by drilling out plated-through holes. However, plated-through holes can be used when needed to connect strip-soldered leads of integrated circuits on opposite sides of a board.

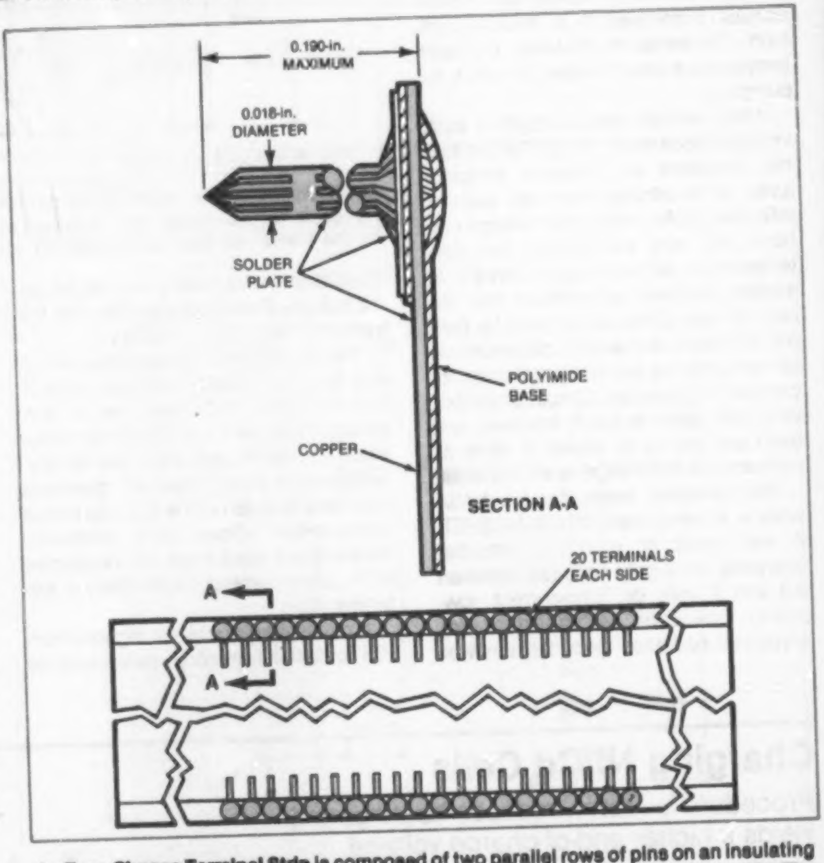

An **Easy-Change Terminal Strip** is composed of two parallel rows of pins on an insulating base. As the cross-sectional view shows, copper conductors are attached to the pins. The conductors are bonding pads for integrated-circuit leads. The length and width of the terminal strip can be chosen by the manufacturer; usually a strip contains 20 pairs of pins. The shape of the pins is optional; they can be rounded instead of pointed, for example.

With the new terminal strip, changes can be made at any stage of circuit-board population, up until the installation of the board in the final product. Besides serving as a soldering pad for integrated-circuit leads, the terminal strip can perform the same function for the circuit-board connector inputs and outputs when their links with board components must be changed.

This work was done by E. A. Pinto and C. E. McOsker of General Electric Co. for **Goddard Space Flight Center.** *For further information, Circle 5 on the TSP Request Card.*
GSC-12748

Electronic Systems

Hardware, Techniques, and Processes

137 Video Target Tracking and Ranging System
138 Transport Control for High-Density Digital Recorder
139 Phase-Sensing Guidance for Wire-Following Vehicles
140 Hardware Fault Simulator for Microprocessors
141 Control System Damps Vibrations

Books and Reports

141 Space-Platform Technology

Computer Programs

142 Shuttle Communications Blackout Study

Video Target Tracking and Ranging System

A microcomputer-controlled two-camera TV system would track a moving object and determine its range and range rate.

Lyndon B. Johnson Space Center, Houston, Texas

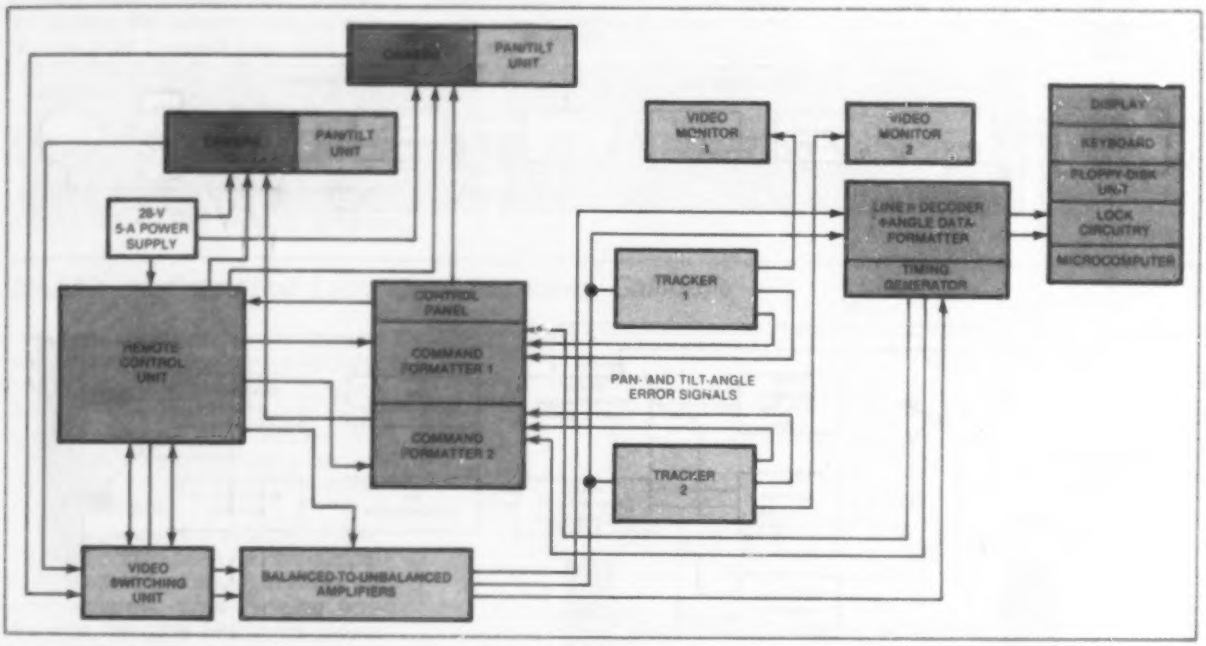
CAMERA
PAN/TILT UNIT
CAMERA
PAN/TILT UNIT
28-V 5-A POWER SUPPLY
REMOTE CONTROL UNIT
CONTROL PANEL
COMMAND FORMATTER 1
COMMAND FORMATTER 2
VIDEO MONITOR 1
VIDEO MONITOR 2
TRACKER 1
TRACKER 2
PAN- AND TILT-ANGLE ERROR SIGNALS
LINE n DECODER &ANGLE DATA FORMATTER
TIMING GENERATOR
DISPLAY
KEYBOARD
FLOPPY-DISK UNIT
LOCK CIRCUITRY
MICROCOMPUTER
VIDEO SWITCHING UNIT
BALANCED-TO-UNBALANCED AMPLIFIERS

A proposed **Target Tracking and Ranging System** uses two automatic video target trackers to keep two TV cameras trained on the object being tracked. A microcomputer calculates range and range-rate information by triangulation. The input data for this calculation are the position coordinates of the two cameras and the pan and tilt aiming angles of the two cameras.

A proposed microcomputer-controlled system computes the range and range rate of a moving object being tracked by two TV cameras. The pan and tilt (azimuth and elevation) angles of each camera are controlled by correction signals derived from the camera video signals. The range and range rate of the object are computed by triangulation from pan- and tilt-angle data and known camera coordinates.

The system could be useful for target ranging at distances up to about 1,000 feet (300 m) in such applications as vehicle collison avoidance, traffic monitoring, and surveillance. It might also substitute for short-range radar in situations where the radar signal could not be tolerated.

The figure shows a block diagram of one proposed configuration. The two TV cameras are aimed at the object being tracked. They are mounted on pan and tilt units that are controlled by the remote-control unit. Camera aiming might be controlled manually in some applications; but in the configuration shown, a closed feedback loop that keeps the cameras aimed at the moving object. Each camera digitally encodes its current angle settings into one TV frame line.

The two TV signals are fed to TV monitors and to video target trackers by the video switching unit and the remote-control unit. The balanced-to-unbalanced amplifiers convert the video into the standard unbalanced format required by the trackers.

The trackers do two things: They insert cursors into the video signals to mark the camera aim points on the monitor screens, and they develop analog error-signal voltages that indicate the direction and magnitude of aiming errors in both the horizontal and vertical directions. The error signals go to zero when the target edge being tracked coincides with the cursor location. The command formatter converts the analog error signals into digital commands for the pan and tilt units to aim the cameras directly at the object.

The line n decoder retrieves the pan- and tilt-angle data from the TV signals and feeds them to the microcomputer system in which the triangulation calculations are performed. The range and range-rate results are displayed, either on the video monitors or else on separate readout units. The range data could also be used to control directly other automatic-response systems.

This work was done by Larry A. Freedman of RCA Corp. for **Johnson Space Center.** *For further information, Circle 6 on the TSP Request Card. MSC-20098*

Transport Control for High-Density Digital Recorder

New servo feedback technique controls tape transport by monitoring deskew buffers.

Goddard Space Flight Center, Greenbelt, Maryland

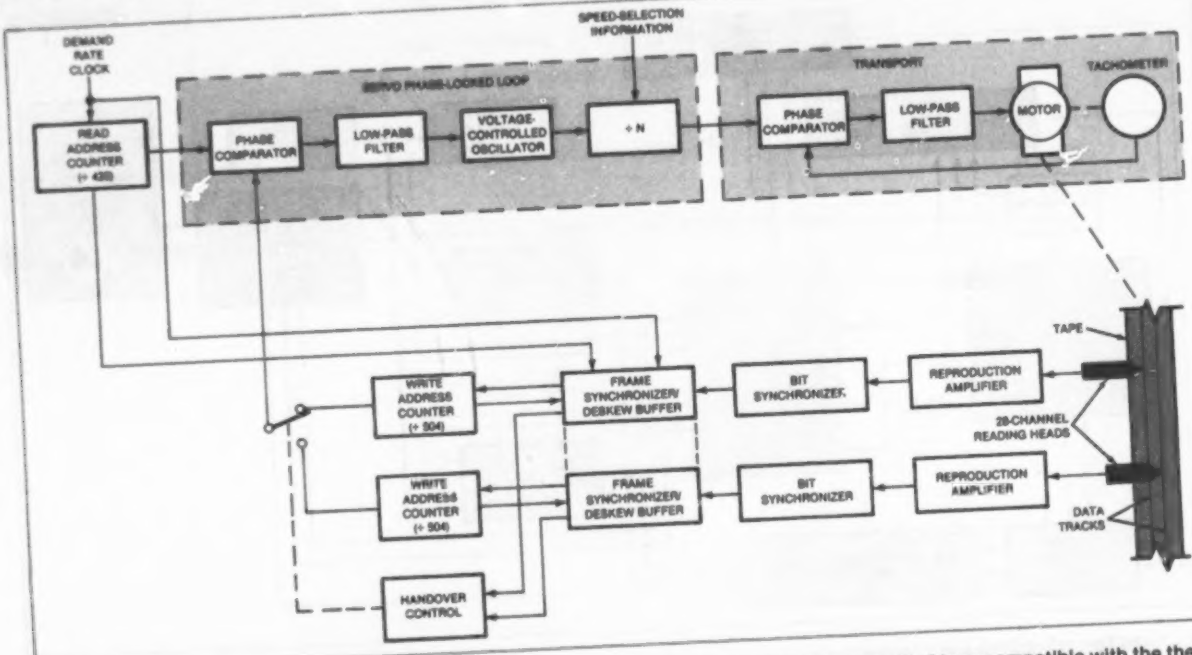
DEMAND RATE CLOCK
SPEED-SELECTION INFORMATION
SERVO PHASE-LOCKED LOOP
TRANSPORT
TACHOMETER
READ ADDRESS COUNTER (÷ 420)
PHASE COMPARATOR
LOW-PASS FILTER
VOLTAGE-CONTROLLED OSCILLATOR
÷ N
PHASE COMPARATOR
LOW-PASS FILTER
MOTOR
TAPE
WRITE ADDRESS COUNTER (÷ 504)
FRAME SYNCHRONIZER/ DESKEW BUFFER
BIT SYNCHRONIZER
REPRODUCTION AMPLIFIER
28-CHANNEL READING HEADS
WRITE ADDRESS COUNTER (÷ 504)
FRAME SYNCHRONIZER/ DESKEW BUFFER
BIT SYNCHRONIZER
REPRODUCTION AMPLIFIER
DATA TRACKS
HANDOVER CONTROL

The Tape Capstan Drive Motor speed is controlled by a phase-locked loop to keep the data rate off of tape compatible with the the demand clock rate, thus preventing deskew-buffer overflow or underflow. Immunity to speed perturbations caused by data dropouts is obtained by switching to a different data-channel reference signal whenever a dropout is detected by the frame synchronizer in the channel currently in use. The desired tape speed is selected by changing the frequency of the demand rate clock and changing the divisor N in the programable divider.

At data densities above 33 kbit/in. (13 kbit/cm), conventional servocontrol techniques proved to be inadequate for controlling tape movement in a ground-support recorder for a NASA satellite. Tachometer feedback did not have the required resolution; conventional tape feedback lacked stability (particularly at low speeds) and was sensitive to tape dropouts. A new system has the necessary resolution and is less sensitive to dropouts than are other tape feedback systems. It is also stable at low speeds.

In the new system the servo feedback signal is derived from the data track signals, so that no separate servo track is required. The system can be adapted to any recorder that uses deskew buffers. It requires no overhead information beyond the synchronizing words already required for data deskewing.

At high bit densities a skew occurs between the data read from different tracks; that is corresponding data bits on different tracks arrive at slightly different times. To correct skew error, sync words are recorded periodically in each track. During reproduction, the data read from different tracks are resynchronized using the sync words for framing reference. Frame synchronization is achieved by storing the data bits from each track in a separate deskew buffer memory as they are read from the tape and then clocking out corresponding bits from all the deskew buffers simultaneously.

The figure shows the signal paths of the servo loop. A phase-locked-loop circuit compares the phase of a signal derived from the demand rate clock to that of a signal derived from one of the data tracks being written. The phase error between these two signals is directly proportional to the level of data in the deskew buffer. Depending on the sign and magnitude of the detected phase error, the reference frequency of the tape-transport servo is raised or lowered slightly to reduce the phase error toward zero, thus maintaining a constant net level of data in the buffer.

The tape transport is also phase-locked using a motor/tachometer feedback signal. This allows the transport to have constant gain (20 dB) out to about 700 Hz. Since the bit sync circuit also has constant gain (0 dB) to about 500 Hz, it is possible to control the entire system response with the servo phase-locked loop. By keeping the servo bandwidth very small (2 Hz at the lowest tape speed), total system stability is ensured.

In effect, the servo phase-locked loop monitors the level of data in one of the deskew buffers and adjusts the speed of the transport accordingly. By regulating the speed of the transport, it controls the rate at which data are written into the buffer, thereby preventing buffer overflow and underflow. It also maintains the optimum level of fullness, which provides maximum deskew capability.

Dropouts in the data channel providing the feedback signal cause a phase error in that signal, which, if uncorrected, would cause bit errors. A dropout tends to reveal itself, however, by causing the following sync word to turn up at an incorrect separation. The frame synchronizer detects this and signals the handover control to switch to a second data channel that is still properly phased, before erroneous information gets to the phase detector. Thus, phase lock is maintained in spite of data dropouts. In applications where frequent data dropouts can be tolerated, this makes it possible to use cheaper tape.

This work was done by Mark D. Matlin and Arthur M. York of Martin Marietta Corp. for **Goddard Space Flight Center.** *For further information, Circle 7 on the TSP Request Card.*

This invention is owned by NASA, and a patent application has been filed. Inquiries concerning nonexclusive or exclusive license for its commercial development should be addressed to the Patent Counsel, Goddard Space Flight Center [see page A5]. Refer to GSC-12727.

Phase-Sensing Guidance for Wire-Following Vehicles

An array of coils senses phase changes that occur when the wire is crossed.

NASA's Jet Propulsion Laboratory, Pasadena, California

A guidance system for wire-following vehicles has been tested successfully at speeds exceeding 50 mi/h (80 km/h) on a difficult 1-mile (1.6-km) course. Unlike previous sensors that compare the amplitudes of signals picked up from the guide wire, the new system compares the signal phases.

In the new system, an array of coils, mounted in a line along the front bumper of the vehicle (see figure) monitors the electromagnetic signal radiating from the wire. The guide wire on the ground beneath the vehicle carries a 6- to 7-kHz alternating current.

The phase-sensing system is less sensitive to electromagnetic noise than was the amplitude-sensing system. In addition, the system "remembers" the last position of the wire and validates a new position only if it falls immediately on either side of the previous position. The remembered position is also used during brief periods of lost signal.

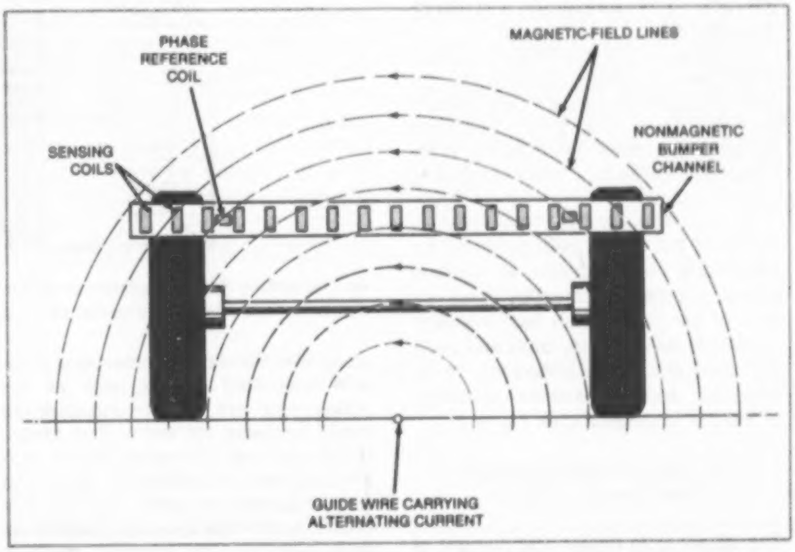
PHASE REFERENCE COIL
MAGNETIC-FIELD LINES
SENSING COILS
NONMAGNETIC BUMPER CHANNEL
GUIDE WIRE CARRYING ALTERNATING CURRENT

The **Phase-Sensitive Guidance Sensor** uses a series of vertical-axis coils and two horizontal-axis coils to detect an alternating-current signal from the guide wire. The arrows indicate the direction of the magnetic field at one moment. The signals from the horizontal coils serve as a phase reference for the electronics. Signals from the vertical coils to the left of the wire are 180° out of phase with the signals from the coils to the right of the wire. The phase-transition point indicates the position of the guide-wire.

The signals picked up by the two coils mounted horizontally serve as a phase reference. The vertically mounted coils are sensitive only to the vertical component of the guide-wire magnetic field which changes sign from one side of the wire to the other. As the vehicle moves to one side with respect to the wire, one coil after another undergoes a phase reversal, indicating the change in the position of the vehicle.

The amplitude of the signal varies somewhat from coil to coil due to the differing distances from the wire and to the variation in angle between the coils and the magnetic field. Before the phase comparisons are done, the signals are amplified and clipped to constant amplitude. The phase state of each coil is stored in a flip-flop. Only a coil passing directly over the wire should undergo a phase reversal; any other reversal is considered spurious — indicating noise interference or other undesirable effects. Spurious reversals of each flip-flop are prevented by controlling the set and reset inputs with signals from the two adjacent flip-flops. If those two flip-flops have identical output polarity, change is inhibited. (The inhibition logic could be extended to as many adjacent flip-flops as desired.)

The flip-flop outputs can encode numerical values of wire position for telemetry, data processing, and control. The deviation in position with respect to the wire can be expressed as a number proportional to the tracking error. This error signal can be used to control the vehicle-steering motors.

This work was done by George R. Hansen of Caltech for **NASA's Jet Propulsion Laboratory.** *For further information, Circle 8 on the TSP Request Card.*
NPO-15341

Hardware Fault Simulator for Microprocessors

A breadboarded circuit is faster and more thorough than a software simulator.

NASA's Jet Propulsion Laboratory, Pasadena, California

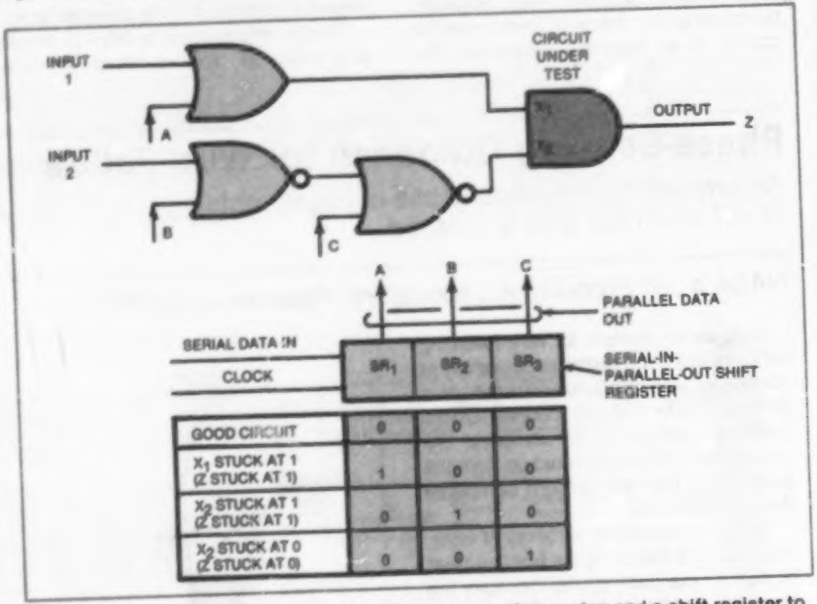

GOOD CIRCUIT	0	0	0
X_1 STUCK AT 1 (Z STUCK AT 1)	1	0	0
X_2 STUCK AT 1 (Z STUCK AT 1)	0	1	0
X_2 STUCK AT 0 (Z STUCK AT 0)	0	0	1

An Elementary Fault Simulator for an AND Gate uses three gates and a shift register to simulate stuck-at-one or stuck-at-zero conditions at the inputs and output.

A fault simulator built in hardware for a commercially available microprocessor operates twice as fast as a comparable simulator implemented in software. According to tests at NASA's Jet Propulsion Laboratory, a microprocessor circuit can be tested for "stuck" faults more quickly and more efficiently by using the fault-simulator circuit. Designers of fault-test circuits should consider a hardware approach where speed is more important than cost of parts and where there are facilities available for breadboarding and testing the circuits.

In CMOS (complementary metal-oxide semiconductor) technology, the most probable faults are those where a gate is stuck at either 1 or 0. Therefore the stuck-fault detection efficiency is the parameter measured when evaluating test procedures.

A fault simulator may be a software model of the circuit, with provision for simulating malfunctions at various points; or it may be a breadboarded version of the circuit, with fault injectors added. In either case, proposed tests are tried out on a deliberately faulty simulator, and the detection efficiency of the test is measured as the ratio:

$$\frac{\text{Number of Faults Detected}}{\text{Total Number of Faults}}$$

The object is to detect 100 percent of possible malfunctions. An optimum set of tests should detect all malfunctions with a minimum number of tests.

To test the new hardware simulator concept, an 1802 microprocessor was first duplicated in breadboard form by about 200 standard commercially available integrated circuits, with all the nodes that are usually inaccessible made available for entry. The breadboard was then converted into a fault simulator by the addition of gates and serial-in/parallel-out shift registers (for example, see figure), which function as fault injectors. The injectors made it possible to select and simulate single or multiple stuck faults.

Experimental results showed that the hardware fault simulator for the microprocessor gave faster results than a software simulator, by two orders of magnitude, with one test being applied every 4 microseconds.

The testing of all large-scale and very-large-scale integrated-circuits for stuck-high and stuck-low faults can benefit from this type of hardware fault simulator. More recently, it was found that with proper initialization and sorting of the list of test vectors, stuck-open faults can also be identified.

This work was done by Lawrence M. Hess and Constantin C. Timoc of Caltech for **NASA's Jet Propulsion Laboratory.** *For further information, Circle 9 on the TSP Request Card.*
NPO-15080

Microprogramed Sequencer for Tunable RF Oscillator

A programable frequency synthesizer originally designed to test K-band radar transmitters is applicable to automated test equipment and computer-controlled receiver tuning. The circuit consists of a PROM-based control sequencer driving a group of diode switches, which select one of eight tuning capacitors in an L-C oscillator.

(See page 128.)

Tangleproof Rotary Electrical Coupling

A new rotary coupling connects up to 246 cables containing a total of 758 conductors to a turntable without overstressing or tangling the cables. The device permits turntable rotation through 320°. At the rotation extremes (±160°), cables maintain enough slack to eliminate overstressing and enough stress to prevent cable entanglement at the midpoint (0°).

(See page 129.)

Using SAW Resonators in RF Oscillators

Surface-acoustic-wave (SAW) resonators are direct replacements for crystals as frequency-determining elements in RF oscillators. Because SAW's are fabricated using integrated-circuit technology, they are much smaller than crystals and are especially applicable in low-power, subminiature instrumentation, such as in biotelemetry devices.

(See page 131.)

Control System Damps Vibrations

An electromechanical control system compensates for the natural vibrational modes of a structure.

NASA's Jet Propulsion Laboratory, Pasadena, California

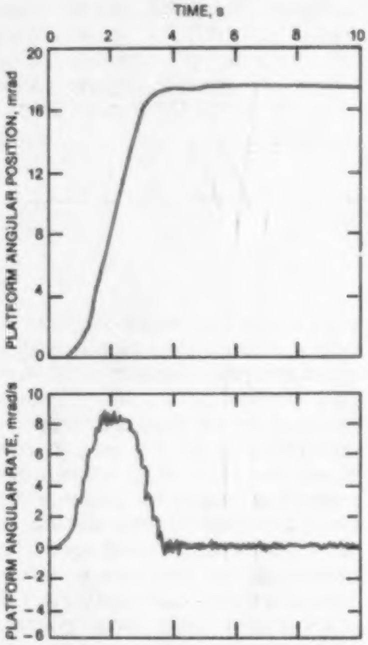

The Motion Of A Torque-Motor-Driven Camera platform is shown by position and rate curves. Structural vibrations excited by the motion are seen in the rate curve, but are effectively damped by the torque-command signals generated in the phase-locked-loop compensation system.

A new control system damps vibrations in rotating equipment with the help of phase-locked-loop techniques. Vibrational modes are controlled by applying suitable currents to the drive motor. The control signals are derived from sensors mounted on the equipment.

This system was developed for stabilizing the stator section of the Galileo spacecraft. The stator has four elastic modes below 10 Hz. One phase-locked loop (PLL) captures the resonance signal for each mode.

In a PLL, a local signal is generated with a variable-frequency oscillator. This signal is fed as a reference into a phase detector, where it is compared to the input to develop an error signal that is proportional to the phase angle between the input and reference signals. The error signal corrects the oscillator phase and frequency. This signal is then used to generate a compensating element of the torque-command signal. The PLL is easily implemented in either hardware or software: For Galileo it is all software, with oscillator signals generated by integrating rate equations.

In one example of compensation performance, the gyro moved a camera to take a series of 1-second exposures for a photo mosaic. The PLL compensated for a 5.5-Hz vibration. The angular position and rate of the camera platform are shown as functions of time in the figure. Structural vibrations at 5.5 Hz were excited by the motion. However, the vibrations are damped in less than 2 seconds.

This work was done by Edward H. Kopf, Jr., Thomas K. Brown, and Elbert L. Marsh of Caltech for **NASA's Jet Propulsion Laboratory.** *For further information, Circle 10 on the TSP Request Card.*
NPO-15002

Books and Reports

These reports, studies, and handbooks are available from NASA as Technical Support Packages (TSP's) when a Request Card number is cited; otherwise they are available from the National Technical Information Service.

Space-Platform Technology

Future needs and technology are projected.

A study has examined the possibility of using a few large platforms in space instead of many small satellites to provide communications and other services. The study was based in large measure on a user survey. A list of 31 potential services was presented to leading telecommunications firms (including carriers, programers, users, and manufacturers). Both favorable and antagonistic viewpoints were solicited. The result was a wealth of information on individual satellite system requirements of the future.

The study produced information on a variety of subjects, including:

- Best locations for geostationary platforms,
- Potential missions and their characteristics,
- Interface requirements between a geostationary platform and equipment for specific services,
- A compendium of payload characteristics, and
- Comparative antenna characteristics.

Platforms will be transported to low Earth orbit by Space Shuttle in one or more launches. Sections of the platform will be assembled and partially tested in low orbit. Upper-stage vehicles, such as the Centaur rocket, will carry the platform to geostationary orbit. The basic platform will provide electric power, telemetry, stationkeeping, coarse pointing, and heat control for the individual services, which may include voice and data telecommunications, television and

(continued on next page)

radio broadcasting, data collection, intersatellite links, navigation, maritime and aircraft communications, and many others.

One of the major conclusions of the study was that additional work is needed on multibeam antennas using wide scan angles. The shape of the individual beams from such antennas varies over the area to be covered (the shape is not a simple hexagon as is often assumed), and interference from side lobes can be considerable. However, the study found that if the area to be covered is broken into different parts (for example, if a country is divided into several regional markets covered by various independent reflectors), the scan angle can be reduced so that the beam pattern is more sharply defined and side-lobe levels are reduced.

A platform will be required to generate about 20 kilowatts of power and to dissipate about 16 kilowatts as heat. In many cases, it will have to maintain attitude within ±0.1°, with subplatforms providing additional pointing accuracy where required.

This work was done by the COMSAT Laboratories of Communications Satellite Corp. for **Marshall Space Flight Center.** *Further information may be found in NASA CR-161807, [N81-26164/NSP] and CR-161808 [N81-26165/NSP], "Final Report Geostationary Platforms Mission and Payload Requirements Study," Volume I [$10.50] and Volume II [$15]. Paper copies may be purchased [prepayment required] from the National Technical Information Service, Springfield, Virginia 22161. The reports are also available on microfiche at no charge. To obtain microfiche copies, Circle 11 on the TSP Request Card.*
MFS-25704

Computer Programs

These programs may be obtained at very reasonable cost from COSMIC, a facility sponsored by NASA to make new programs available to the public. For information on program price, size, and availability, circle the reference letter on the COSMIC Request Card in this issue.

Shuttle Communications Blackout Study

The RF power loss through a three-dimensional plasma sheath is computed.

The atmospheric reentry and landing of the Space Shuttle orbiter require precise targeting control from the deorbit point to ground touchdown. Radio communications with the orbiter during this time period are critical to provide accurate state vector updates for vehicle guidance programs. The Space Shuttle Orbiter Entry Communications Blackout Study computer program models, investigates, and predicts communication blackout envelopes based on mission entry trajectory and associated data from tracking stations. It should be of interest to those designing and using communications systems susceptible to blackout.

When the orbiter reenters the Earth's atmosphere during a typical deorbit-to-landing trajectory, it initially travels at hypersonic speeds. Shock-heated air envelops the entire orbiter in a layer of dissociated and ionized air molecules termed the "plasma sheath." This plasma sheath is electrically conducting, and electromagnetic interaction with the free electrons in the plasma can significantly impair radio-frequency transmissions. In addition to the signal attenuation due to propagation in the plasma, the reflections and refractions at the plasma interface can also represent a significant power loss to the overall communications link with the orbiter.

The Orbiter Entry Communications Blackout Study program determines the three-dimensional shock shape of the orbiter, used to define the plasma properties and plasma sheath aerodynamically, from the real shape of the vehicle flow field and the associated boundary-layer displacement. The program computes the electromagnetic-radiation power loss through the plasma sheath based on the vehicle antenna characteristics and the actual line-of-sight vector determined by the receiver station relative to the flightpath and the attitude of the vehicle in space. The program can be readily adapted to predict the entry communications blackout for any nonablative entry vehicle.

This program is written in FORTRAN IV for batch execution and has been implemented on a CDC 6000-series computer with a central memory requirement of approximately 163K (octal) of 60-bit words. The program was developed in 1980.

This program was written by Robert L. Haben and Robert J. Budica of Rockwell International Corp. for **Johnson Space Center.** *For further information, Circle M on the COSMIC Request Card.*
MSC-20141

Physical Sciences

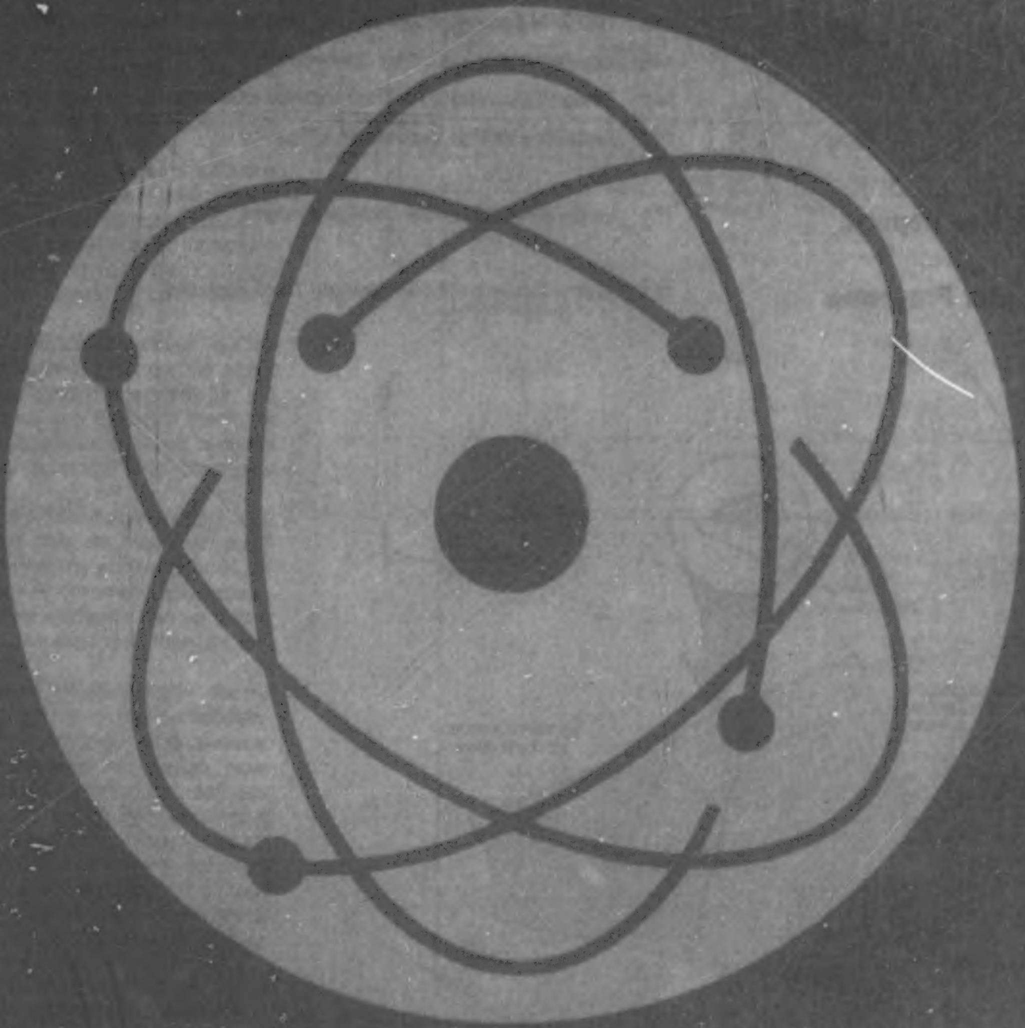

Hardware, Techniques, and Processes

145 Curved-Surface Beam Splitter
146 Optical Sensor for Robotics
147 Holographic Microscopy System
148 TRISCAN Antenna-Positioning Algorithm
148 Ion Mass/Velocity/Charge Spectrometer
149 Design Calculations for Thermoelectric Generators
150 Evaluating Energy Conversion Efficiency

Books and Reports

151 Large Electrochemical Storage Systems

Computer Programs

151 Estimating Insolation Incident on Tilted Surfaces

Curved-Surface Beam Splitter

Spherical entrance and exit surfaces minimize optical aberrations.

Goddard Space Flight Center, Greenbelt, Maryland

A beam splitter with curved entrance and exit surfaces introduces less chromatic aberration and Seidel aberrations in some optical systems than traditional plate or block beam splitters. The new design is used in pupil-concentric systems, such as the Schmidt-type mirror objective shown in the figure.

Many optical applications require one objective to form images at several focal planes. Examples include color-TV cameras with three vidicon tubes and cameras used to separate a color image into separate colors for color printing presses.

In pupil-concentric systems, all the optical elements are concentric about the aperture stop; the system has no preferred axis, and therefore there are no off-axis aberrations. Such systems exhibit only spherical and chromatic aberrations.

The introduction of a block beam splitter destroys the symmetry of pupil-concentric systems and introduces severe Seidel and chromatic aberrations. Compensating elements can be added but only at the expense of weight and compactness.

The proposed beam splitter — like the block beam splitter — has an optically-flat, partially-reflecting interior surface. Unlike the conventional design, however, the beam entrance and exit surfaces are spherical and concentric about the aperture stop. Thus the beam splitter surfaces generate only spherical and chromatic aberrations. While these aberrations may be larger than without the beam splitter, no new types of aberration are introduced.

The interior reflecting surface can be metallic for wavelength-independent beam splitting or dichroic (showing different color in different directions) to split the beam into different wavelength bands. Since the lens power and spherical aberration of the proposed beam splitter are quite low, systems with a very large wavelength range are possible without resorting to additional optical

(continued on next page)

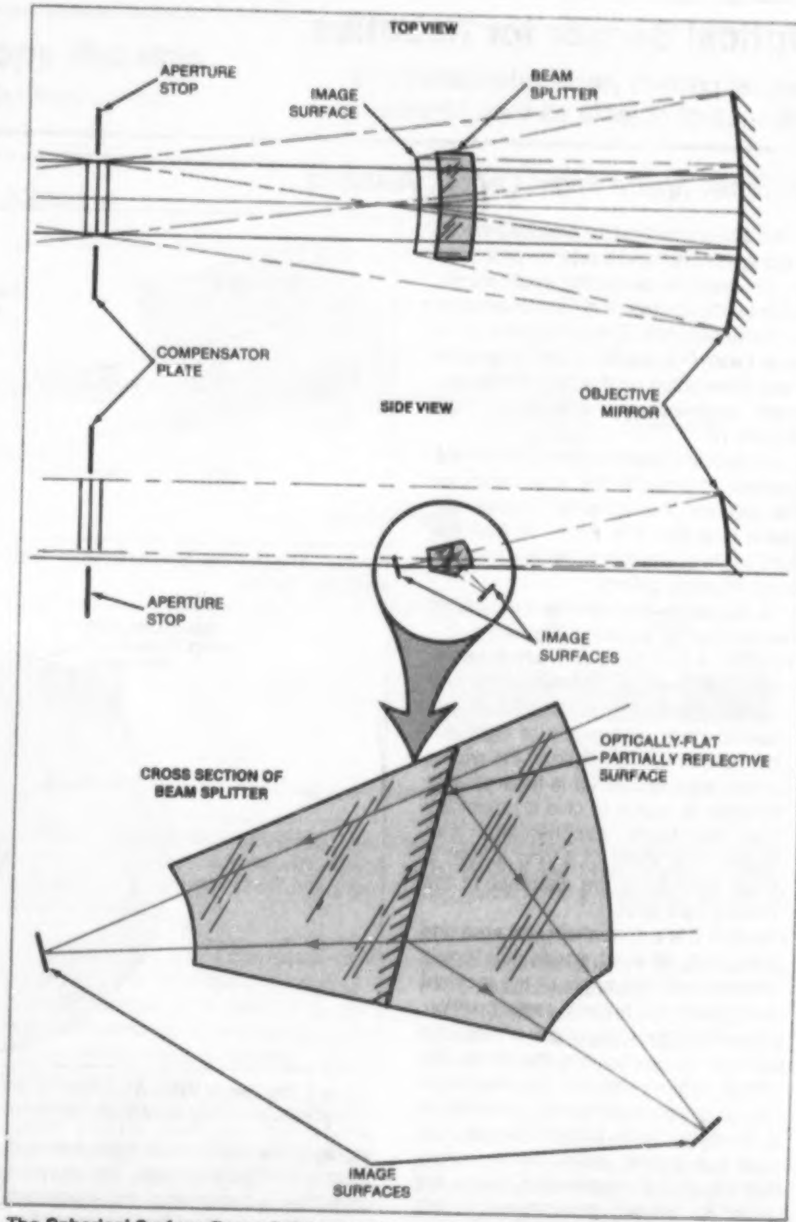

The Spherical-Surface Beam Splitter can be used in a Schmidt-type mirror objective to split the converging image-forming beam so that two images are formed. The small aberrations introduced can be corrected by a compensator plate located at or near the aperture stop.

components for the compensation of chromatic aberration.

The scheme can be extended to more than two images. The number of splits is limited only by energy absorption in the splitter and by available space.

This work was done by Peter O. Minott of **Goddard Space Flight Center.** *For further information, Circle 12 on the TSP Request Card.*

This invention is owned by NASA, and a patent application has been filed. Inquiries concerning nonexclusive or exclusive license for its commercial development should be addressed to the Patent Counsel, Goddard Space Flight Center [see page A5]. Refer to GSC-12683.

Optical Sensor for Robotics

Optical pattern yields orientation and distance of objects as they approach.

Marshall Space Flight Center, Alabama

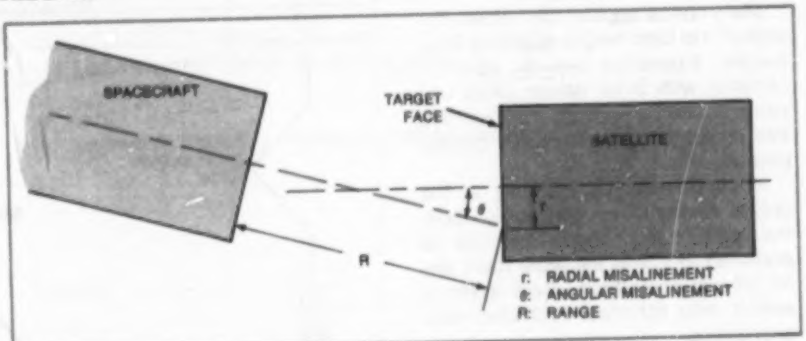

Figure 1. **The Docking Sensor System** determines radial misalinement, angular misalinement, and range.

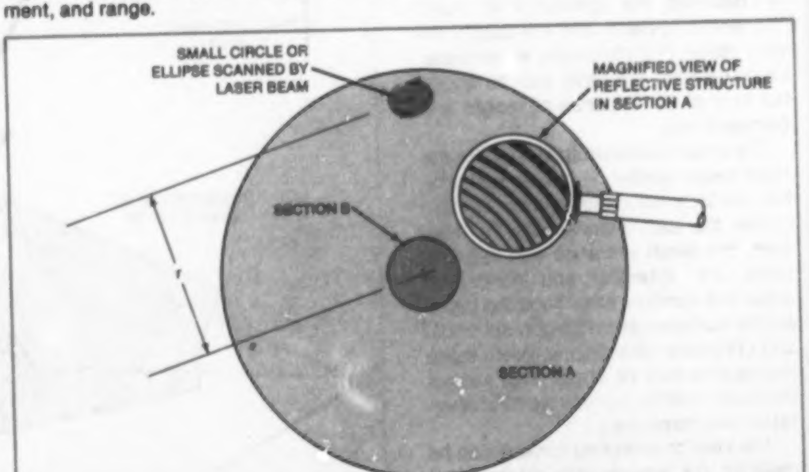
SMALL CIRCLE OR ELLIPSE SCANNED BY LASER BEAM
MAGNIFIED VIEW OF REFLECTIVE STRUCTURE IN SECTION A
SECTION B
r
SECTION A

Figure 2. **The Target Pattern** consists of rings of alternating high and low reflectivity and a central section where reflectivity varies with the angle of incidence but not with position.

An optical method for precisely docking a spacecraft and a satellite promises to be useful in terrestrial applications, such as the control of robot movements in manufacturing. The reflections of a laser beam from patterns on the satellite yield information on the radial misalinement, angle between axes, and range (Figure 1).

An optical transmitter/receiver on the spacecraft projects the laser beam on the satellite. A mechanism moves the beam direction in a cone, so that the light beam scans the target in a circular or an elliptical pattern.

A target on the satellite consists of two concentric sections (Figure 2):

- Section A is an annulus in which reflectivity decreases with distance from the center of the target. It consists of concentric rings, alternately of high and low reflectivity. The ratio of the widths of two adjacent zones is tapered as a function of radius to give a reflectivity that decreases exponentially with radius. The width of a ring is only a small fraction of the diameter of the moving light spot.
- Section B is a central circular area, the reflectivity of which varies in a known manner with the angle of the incident laser beam but not with radial position.

To determine the range, or distance between the sensor and the target, the optical system adjusts the scanning-cone angle so that the ratio of maximum to minimum power from the target rings equals a preset value. As a consequence of the exponential taper, the range is inversely proportional to this scanning-cone angle. (When there is angular misalinement, the range heading may be slightly in error on account of the consequent elliptical shape of the scan.)

The direction of the radial misalinement is derived from the beam-scan angles at the moments of maximum and minimum reflected power. The required correction is a rotation of the spacecraft in the plane defined by the scanning-beam positions at maximum and minimum reflection, toward the position of maximum reflection from section A. A sequence of such corrections will cause the center of the cone to approach the center of the target.

As the radial misalinement is reduced to a small value, the beam illuminates more and more of the central circular area of the target, section B. The low reflectivity of section B produces increasingly long dips at the output of the light sensor, signaling the approaching end of the radial correction phase. That phase is ended when the entire conical scan falls into section B.

The amount of angular misalinement is indicated by the ratio of maximum to minimum power reflected from section B. As the angular misalinement decreases, the fluctuations in reflected power decrease until reflected power remains at a constant level. The required correction for angular misalinement is rotation of the spacecraft about an axis in the plane of the target perpendicular to the plane defined by the scanning beam at the points of maximum and minimum reflection from section B.

This work was done by Fredrick Weindling of United Aircraft Corp. for **Marshall Space Flight Center.** *For further information, Circle 13 on the TSP Request Card.*
MFS-25713

Holographic Microscopy System

System achieves 2-μm resolution throughout a 100-cm^3 sample volume.

Marshall Space Flight Center, Alabama

A holographic system originally developed for testing theories of two-liquid systems could be used for measurements of aerosols, particles in a transparent medium, or microscopic biological specimens. The holograms are recorded in 3- to 5-millisecond exposures on high-resolution holographic film using the system shown in the figure.

In the playback system, the developed holograms are illuminated with the same type of laser used in the construction system. After passing through the hologram, the beam is incident upon the vidicon tube of a television camera, producing a real image of the test cell and its contents.

A commercial automated feature-analysis system measures the size distribution of the particles in the test cell by analyzing the video signal from the TV camera. The analysis system includes a TV monitor, particle-sizing electronics, and a computer (with video monitor, keyboard, and printer).

The portion of the test cell that can be viewed in sharp focus at one time is about 0.1 mm thick. By moving the hologram nearer or farther from the TV camera, any portion of the cell can be observed. Depending on the relative positions of the spatial filter, hologram, and TV camera, the reconstruction system can achieve magnifications ranging from 1X to 1,200X even though no magnifying lenses are used.

For the experiments on phase separation of immiscible liquids, an isothermal test cell maintains a fixed temperature within ±0.001 K. A temperature bath surrounding the test cell is monitored with a thermistor connected in an ac Wheatstone-bridge circuit. The bridge is in balance at the preset temperature, and the bridge error signal controls power to a heater wire in the temperature bath.

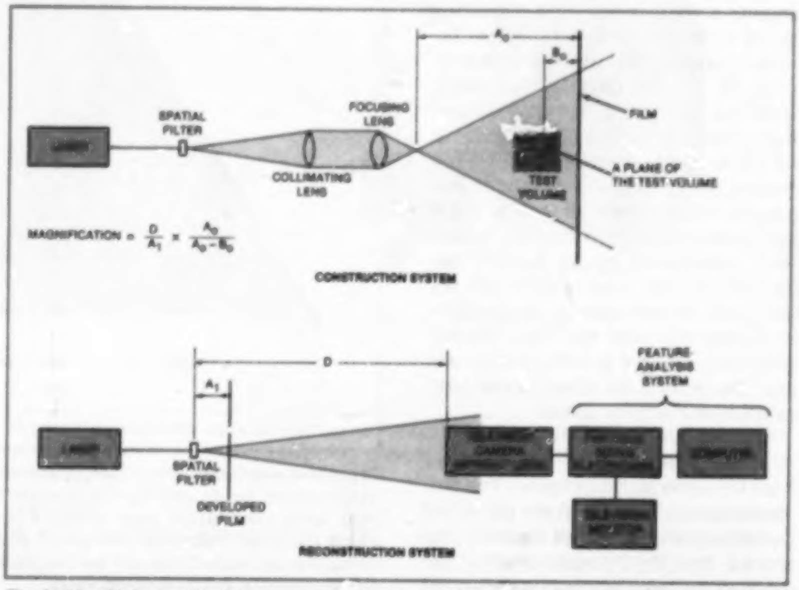

The **In-Line Holographic Microscopy System** includes a construction or recording system and a reconstruction or playback system. Both systems use 1-watt argon-ion lasers operating at a wavelength of 514.5 nm, TEM$_{00}$ mode, with a coherence length of approximately 1 m.

Liquids analyzed thus far with the system include diethylene glycol and ethyl salicylate. A thin test-sample cell (0.1 mm thick along the optical axis) was used because high particle densities (10^5 to 10^7 particles/cm^3) were predicted by theory. Particle size and growth rate were monitored over a 1/2-hour period. By comparing holograms taken at different times, particle motion was also studied.

This work was done by William K. Witherow of **Marshall Space Flight Center.** *Further information may be found in NASA TM-82437 [N81-30212/NSP], "Holographic Microscopy Studies of Emulsions" [$9]. A paper copy may be purchased [prepayment required] from the National Technical Information Service, Springfield, Virginia 22161. The report is also available on microfiche at no charge. To obtain a microfiche copy, Circle 14 on the TSP Request Card.*
MFS-25673

TRISCAN Antenna-Positioning Algorithm

A method developed expressly for digital positioning improves accuracy and sensitivity.

NASA's Jet Propulsion Laboratory, Pasadena, California

TRISCAN is a scanning algorithm that improves the alinement between the boresight of a radar antenna and a target. The algorithm was originally developed for digitally pointed antennas in the deep-space network; however, it could possibly be used in locating radio sources on Earth.

TRISCAN (the acronym stands for triangular scan) estimates the coordinate errors in hour angle and declination between the predicted and the true locations of a radio source. For stars, TRISCAN employs a set of measurements made by a noise-adding radiometer. This device yields a temperature reading proportional to the system background noise power plus any noise power emanating from the star; the latter is attenuated by an amount that depends on the antenna boresight offset. When the background temperature is subtracted from the total reading while the boresight is in the vicinity of a star, the result is the effective star temperature at the given offset.

The algorithm uses the measurement of three effective star temperatures from the same star (see figure). The first measurement is made at the predicted or best-known location of the star. The second and third measurements are made at the base points of a known triangle. The ratios T_0/T_1 and T_0/T_2 are used to calculate offset parameters, using the general relationship between relative temperature reading and boresight offset. The offset parameters are then used in trigonometric calculations to estimate the offset from the predirected point to the star. A typical TRISCAN star scan takes about 5 minutes. For applications where the signal source changes direction rapidly, the process would have to be automated to speed up the analysis.

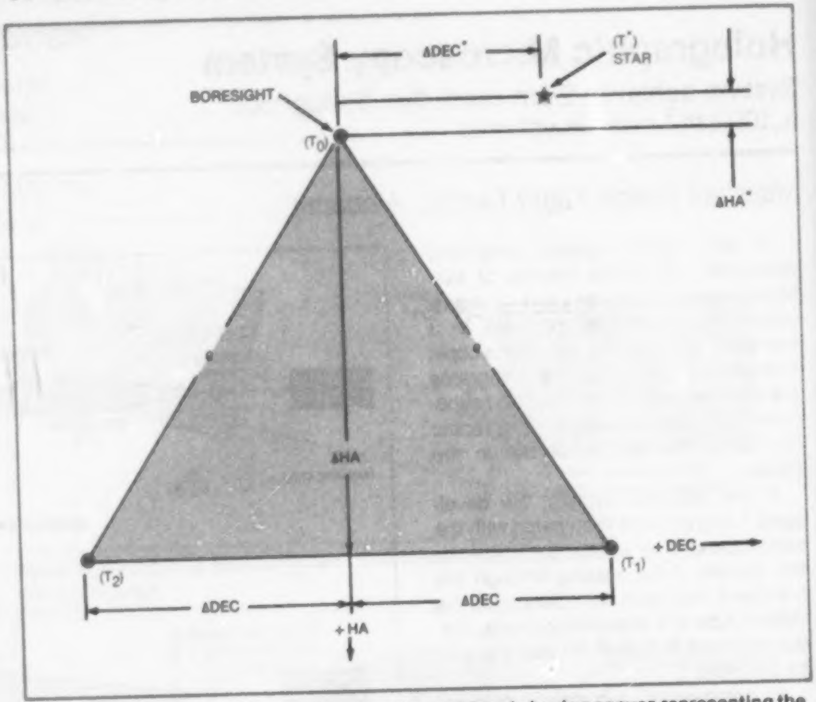

Three Measurements of Star Temperature form a triangle having apexes representing the temperatures T_0, T_1, and T_2. The triangle height is a downward excursion in hour angle (HA), while the triangle base consists of sideways excursion in declination (± DEC). Using the three measured star temperatures and the triangle geometry, an algorithm calculates estimated offsets from the predicted point to the star, indicated as ΔHA* and ΔDEC*, for final antenna positioning.

This work was done by Robert C. Bunce of Bendix Field Engineering Corp. for ***NASA's Jet Propulsion Laboratory.*** *For further information, Circle 15 on the TSP Request Card.*
NPO-15577

Ion Mass/Velocity/Charge Spectrometer

m/q is resolved to 1 part in 40.

NASA's Jet Propulsion Laboratory, Pasadena, California

An ion spectrometer, originally developed for spacecraft analysis of the solar wind and cometary ions, distributes ions two-dimensionally and measures three characteristics of the incident-ion beam: (1) mass/charge distribution, (2) ion velocity distribution, and (3) the direction of incidence. It could also be useful for diagnosis in experimental plasma physics in the collisionless regime.

Ions that enter from directions within the field of view are reflected by a charged-grid electrostatic mirror into the accelerator grids (see figure). The voltage on the accelerator grids is modulated to scan a wide range of incident-ion speeds, v, and to bring those speeds within the narrower acceptance range of the magnetic analyzer. The azimuth angle, ϕ, of incoming-ion velocities is scanned by spacecraft rotation or by stepping the electrostatic mirror in azimuth.

The magnetic analyzer serves as a momentum/charge (mv/q) filter with an angular acceptance of ±(0.5° to 0.9°) in ϕ and ±30° in the elevation angle, θ. The ions selected by the magnetic analyzer are dispersed two-dimensionally by the electrostatic deflector according to mass/charge (m/q) and θ.

The two-dimensional sensors in the electrostatic-deflector section include 2,500-volt accelerating grids followed by microchannel-plate (MCP) electron multipliers. The MCP output at each point is collected by 1 of 40 conductive anode strips that run along the m/q axis, each strip receiving ions with θ values in a ±3.75° range. The location of the incident-ion beam, and therefore the m/q value, is deduced by sensing the pulses on the strip. The data are manipulated by a microprocessor before transmission.

In tests, a model of the spectrometer resolved m/q to 1 part in 40 (with m/q measured in atomic mass units per elementary electric charge). Some other performance figures include:

- m/q ranges, 1 to 4, 12 to 24, and 28 to 56;
- Ion-energy range, 0 to $8[1 + 1/(m/q)]$ keV; and
- Energy resolution (digitization), ±7.8 eV.

This work was done by Marcia M. Neugebauer, Douglas R. Clay, and Bruce E. Goldstein of Caltech for **NASA's Jet Propulsion Laboratory.** *For further information, Circle 16 on the TSP Request Card.*
NPO-15423

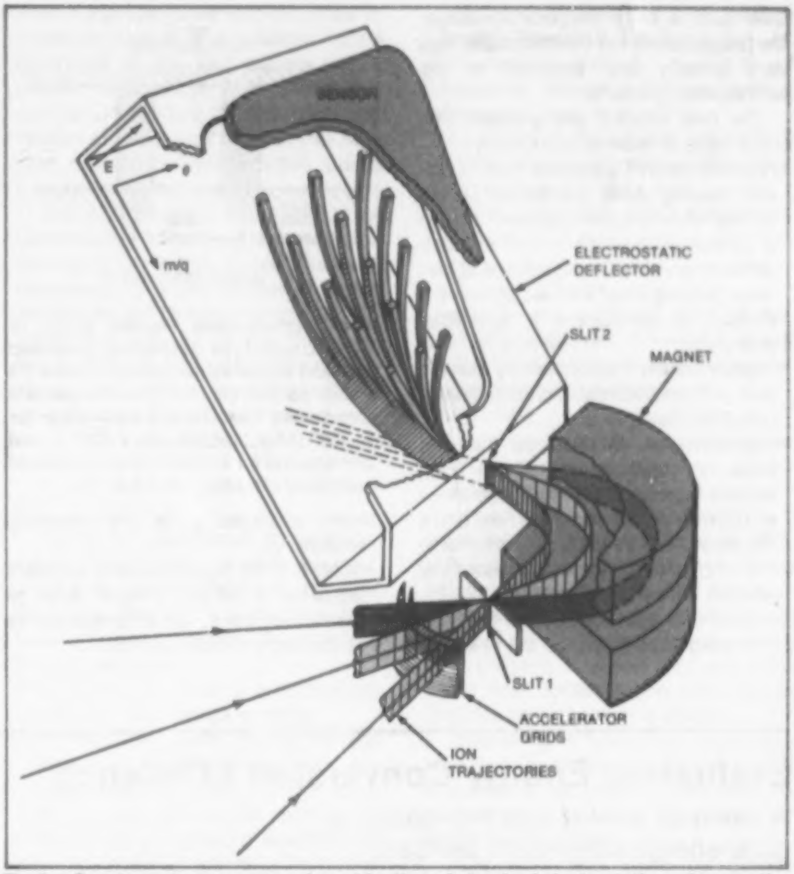

The Ion Spectrometer uses a novel combination of standard electrostatic and magnetic deflection techniques to sort incident ions according to speed, the direction of incidence, and mass/charge ratio.

Design Calculations for Thermoelectric Generators

Heat rate, power delivered to load, and thermodynamic efficiency can be calculated with high accuracy.

NASA's Jet Propulsion Laboratory, Pasadena, California

Nine simplified analytic models based on average properties accurately predict heat rates for silicon/germanium thermoelectric generators. Solutions from these simplified models were compared with those obtained using sophisticated numerical analysis. The maximum errors in calculated heat rate range from about 4 percent to about 0.2 percent. The models may also be used to calculate power delivered to a load and thermodynamic efficiency.

Even with modern computers, the differential equations that describe steady power generation in semiconductor thermocouples are difficult to solve. The reason is that such devices experience sizable temperature differences, and the properties of the silicon/germanium vary widely and nonlinearly with temperature.

A silicon/germanium thermoelectric generator (shown schematically in the figure) may be operated between thermocouple hot-junction temperatures as high as 850°C and cold-junction temperatures below 200°C.

(continued on next page)

Over such a large temperature range, the properties of the thermocouple legs vary greatly with position in the temperature gradient.

The new models are grouped into three types in order of complexity:

- Approximation I assumes that Thomson heating (heat generated or absorbed when a current passes through a conductor in which there is a temperature gradient) is negligible and that Joule heating (heat evolved by current through a resistance) is uniformly distributed.
- Approximation II assumes only that the sum of Thomson heat and Joule heat is uniformly distributed.
- Approximation III assumes that the local net heat generated per unit volume is made of two components — a uniformly distributed Joule heat and a Thomson heat, which is proportional to the product of the thermal conductivity and the temperature gradient.

Each type of approximation in turn has three subgroups based on the three different averages $\hat{\rho}$ for the electrical resistivity ρ:

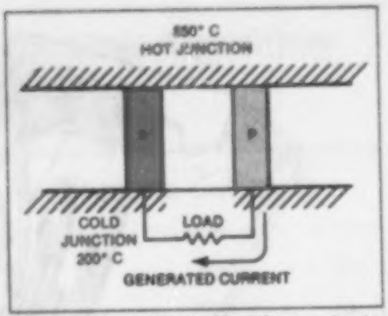

New Mathematical Models apply to thermocouple-type generators composed of n- and p-type semiconductor alloys (78 atomic percent silicon, 22 atomic percent germanium). Calculations were made for an 850° C hot junction and a 200° C cold junction and for a ratio of load to internal resistance ranging from 0.8 to 1.5.

- Subgroup (a) regards $\hat{\rho}$ as a constant equal to a simple integral average taken over the range of temperatures of the hot and cold junctions.
- Subgroup (b) regards $\hat{\rho}$ as equal to an integral average obtained by using the thermal conductivity as a weighting function over the range of temperatures of the hot and cold junctions.
- Subgroup (c) expresses $\hat{\rho}$ as a spatial integral average over all positions within the device between cold and hot junctions.

Approximation I, subgroup (b) introduces the greatest error (4.2 percent) in heat rate. Approximation III, subgroup (b), introduces the least error, (less than 0.2 percent.

The models can be selected according to the accuracy needed. Similar average-property models can be used to refine the accuracy of lumped-parameter approximations for electrical transmission lines, flow through chemical reactors, and limit-stressed structural members.

This work was done by Burton Zeldin of Caltech for **NASA's Jet Propulsion Laboratory.** *For further information, Circle 17 on the TSP Request Card.*
NPO-15286

Evaluating Energy Conversion Efficiency

A family of curves aids in evaluatiing solar-energy conversion devices.

Langley Research Center, Hampton, Virginia

Devices that convert solar radiation directly into storable chemical or electrical energy, such as photovoltaic, biological photosynthetic, photochemical, and photoelectrochemical, have a characteristic energy absorption spectrum; specifically, each of these devices has an energy threshold. The conversion efficiency of a generalized system that encompasses all threshold devices has been analyzed, resulting in a family of curves for devices of various threshold energies operating at different temperatures.

The system consists of a blackbody source at 6,000 K and a radiant energy converter having a threshold energy E_0 operating in contact with a reservoir at a fixed temperature T_R. The analysis is based on the first and second laws of thermodynamics and leads to a determination of the limiting or ultimate efficiency for any conversion system having a characterestic threshold energy (such as the band gap of a solar cell) and an operating temperature.

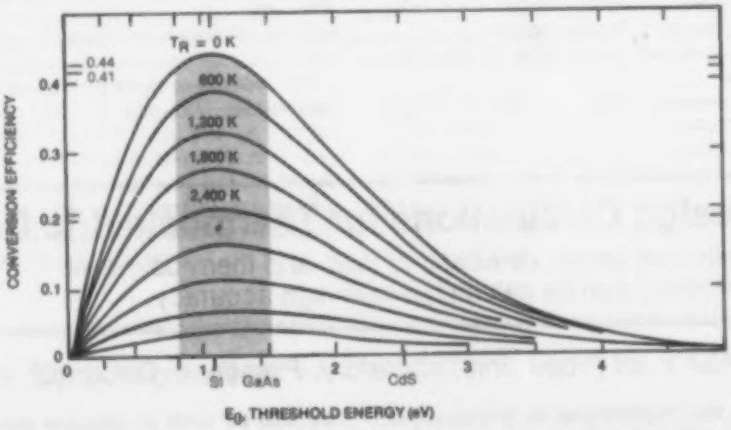

Conversion Efficiency Limits vs. threshold energies of various photosensitive devices can be compared with the aid of a family of characteristic curves. The maximum efficiency is 44 percent for silicon. The highest solar-energy conversion efficiencies correspond to threshold energy levels between 0.75 and 1.5 eV for all operating temperatures.

The curves shown give the maximum possible conversion efficiency for any device having a threshold energy. The maximum efficiency of 44 percent requires an operating temperature of 0 K and a threshold energy of 1.1 eV. This threshold energy coincides with the energy band gap for silicon. For comparison, the limiting efficiency for a gallium arsenide device is 41 percent and for a cadmium sulfide device is 22 percent at this same temperature.

As the operating temperature of a threshold device increases, its limiting solar conversion efficiency decreases. The curves indicate that the highest solar conversion efficiencies will be for devices with threshold energies between 0.75 and 1.5 eV for all temperatures. Limiting efficiencies decrease rapidly for threshold energies greater than 1.5 eV or less than 0.75 eV for practical operating temperatures.

Although the efficiency curves refer specifically to the conversion of solar radiation, they can also be used to find the limits to the conversion efficiency for threshold devices and radiation from a blackbody at any temperature with a simple modification. In addition, they can be used to find the maximum conversion efficiency for devices that have both a threshold and a cutoff energy (i.e., an absorption band.)

The analysis gives the limits to the conversion efficiency of any threshold device, given only its temperature and threshold energy and the temperature of the blackbody radiator. It does not include any specific device characteristics. The inclusion of specific characteristics will result in conversion efficiencies less than the limits indicated.

This work was done by C. E. Byvik of **Langley Research Center** *and A. M. Buoncristiani and B. T. Smith of Christopher Newport College. Further information, may be found in:*

NASA TM-83230 [N82-18696/NSP], "The Ultimate Efficiency of Photosensitive Systems" [$6.], and

NASA TM-83228 [N82-18697/NSP], "Thermodynamic Limits to the Efficiency of Solar Energy Conversion by Quantum Devices" [$6].

Copies of these reports may be purchased [prepayment required] from the National Technical Information Service, Springfield, Virginia 22161.

LAR-12948

Books and Reports

These reports, studies, and handbooks are available from NASA as Technical Support Packages (TSP's) when a Request Card number is cited; otherwise they are available from the National Technical Information Service.

Large Electrochemical Storage Systems

Batteries are evaluated that can deliver megawatts for hours.

A study released in 1979 assesses the status of electrochemical energy storage for powerplants that utilize the Sun's heat to drive electric generators. Electrochemical energy storage is also applicable to photovoltaic arrays, wind turbines, and similar variable and intermittent sources of electricity.

The study considered the stage of development, cost, and performance of existing storage systems and projected their cost, performance, and availability as advanced systems. It addressed three broad areas:

- The electrochemical, or battery, component of the storage system;
- The remaining parts of the storage system, including inverter or converter; and
- The overall solar-thermal plant.

The study produced a tabulation of the costs of delivered energy from complete plants with 16 different advanced electrochemical systems, ranking the systems in order of economic attractiveness. Manufacturers and developers were consulted during the assessment.

A major conclusion was that the familiar lead/acid battery is the only existing cell that can meet the needs for near-term demonstration programs. Lead/acid batteries are expensive, however, costing from $170 to $220 (1979 dollars) per kilowatt hour. These values apply to batteries that can operate for 2,000 cycles at 80 percent depth of discharge and efficiency of 70 to 85 percent. Between 1985 and 1990, lower cost batteries are expected to become commercially available.

Inverter and converter equipment was found to consitute a sizable part of system cost exclusive of cell cost. Inverter/converter costs are lower for higher bus voltages.

This work was done by Stanley Krauthamer and Harvey A. Frank of Caltech for **NASA's Jet Propulsion Laboratory.** *Further information may be found in JPL Publication 79-95, Revision 1, [N80-29658/NSP], "Electrochemical Energy Storage Systems for Solar Thermal Applications" [$12]. A copy may be purchased [prepayment required] from the National Technical Information Service, Springfield, Virginia 22161.*

NPO-15185

Computer Programs

These programs may be obtained at very reasonable cost from COSMIC, a facility sponsored by NASA to make new programs available to the public. For information on program price, size, and availability, circle the reference letter on the COSMIC Request Card in this issue.

Estimating Insolation Incident on Tilted Surfaces

Solar radiation on several types of solar collectors is calculated from ASHRAE relationships.

In designing or analyzing a solar-energy system, the principal question is how much energy the system can deliver to meet load demands. One of the main parameters determining the amount of energy the system delivers is the amount of solar energy available (energy incident on the surface of the collector array) to the system. The ASHMET computer program estimates the amount of solar insolation incident on the surfaces of several types of solar collectors, including fixed-position flat-plate, monthly-tilt-adjusted flat-plate, beam-tracking, and fixed-azimuth-tracker.

(continued on next page)

The basic methodology employed in ASHMET is to use ASHRAE relationships to obtain the clear-day total daily insolation incident on the collector surface for a representative day of each month of the year. The clear-day total daily insolation is then multiplied by a clearness index to obtain the typical or average daily insolation. Climatological data for determining this clearness index for 248 U.S. cities are included with the ASHMET program. The breakout of direct and diffuse insolation may be selected as either the ASHRAE relationships or the correlation of Liu and Jordan.

ASHMET is an interactive program and prompts the user for all required data. These data include the latitude of the desired location, the collector slope measured from the horizontal, the azimuth of the collector surface, the type of collector, the ground reflectance (if desired), and the city to be used for cloud-cover calculations. Output consists of an echo of the input data, the hourly clear-day incident insolation, the total clear-day insolation, and the typical daily insolation for each month. Also output are the maximum yearly insolation and the probable yearly insolation.

The ASHMET program is written in FORTRAN IV-Plus for interactive execution and has been implemented on a DEC PDP-11/70 computer with a central memory requirement of approximately 48K of 16-bit words. ASHMET was developed in 1980.

This program was written by Robert E. Elkin and Ronald G. Toelle of **Marshall Space Flight Center.** *For further information, Circle A on the COSMIC Request Card.*
MFS-25501

Materials

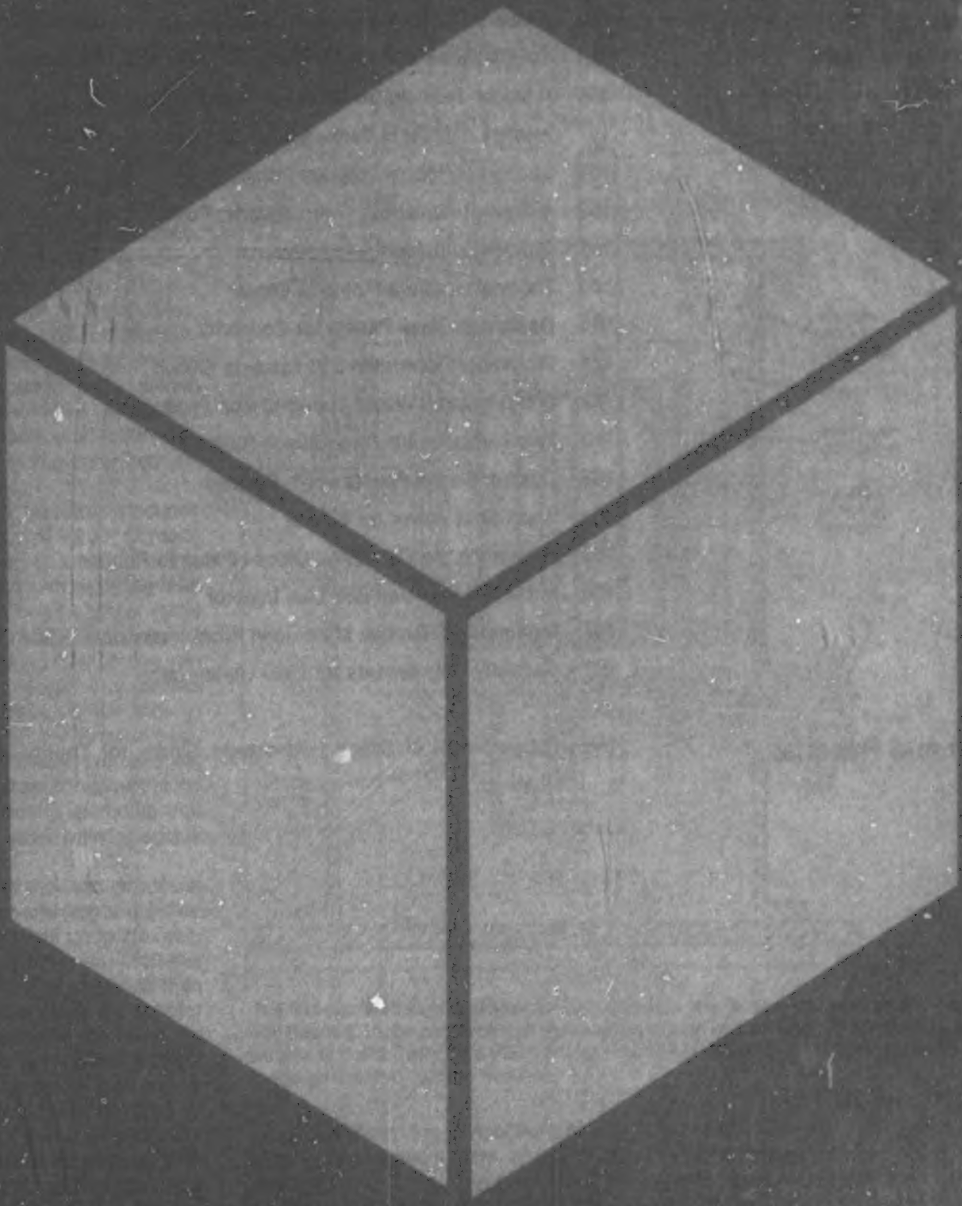

Hardware, Techniques, and Processes

155 Efficient Silicon Reactor
156 Silicon-Delivery Tube
156 A Milder Solution for Stress-Corrosion Tests
157 Heated Aluminum Tanks Resist Corrosion
158 Vacuum Ampoule Isolates Corrosive Materials
159 A Solvent-Resistant, Thermoplastic Poly(imidesulfone)
159 High-Performance Matrix Resins
160 Thermal-Gradient Fining of Glass
161 Designing Glass Panels for Economy and Reliability
161 Processor Generates and Extracts Silicon
162 Sodium Spray Would Speed Silicon Production
163 Two-Temperature-Zone Silicon Reactor
163 Casting Silicon Pellets From Powder
164 Short Shot Tower for Silicon
165 Estimating the Degree of Cross-Linking in Rubber
166 Improved Fluidized-Bed Gas Injector
167 Membranes Remove Metal Ions From Industrial Liquids
167 Viscosity Depressants for Coal Liquefaction

Books and Reports

168 Development of Silane Hydrolysate Binder for Thermal-Control Coatings

Efficient Silicon Reactor

Narrow temperature excursions and large surface area minimize heat expenditure and processing time.

NASA's Jet Propulsion Laboratory, Pasadena, California

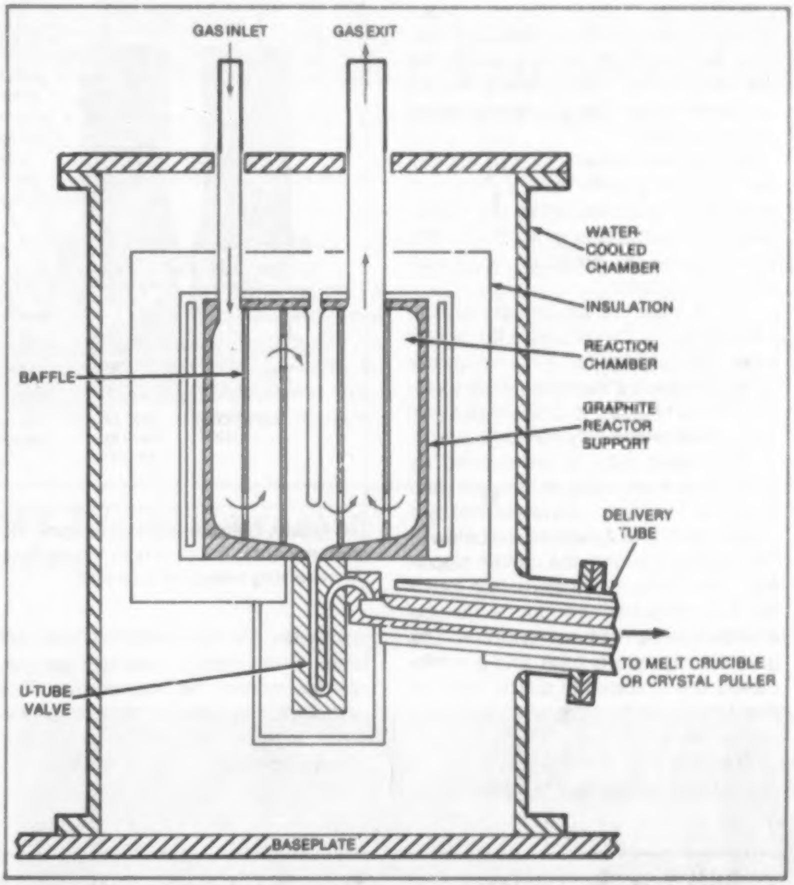

The **Reactor Walls and Baffles** combine to create a large surface area onto which silicon can deposit. In the two cycles of the reactor, silicon is first deposited and then removed. Details of the delivery tube that transfers the silicon from the reactor to a crucible appear in the article that follows this one.

High-purity silicon can be efficiently produced and transferred by a continuous two-cycle reactor. The new reactor operates in a relatively-narrow temperature range, 1,200° to 1,450° C, and uses a large surface area to minimize heat expenditure and processing time in producing silicon by the hydrogen reduction of trichlorosilane. Conventional methods of silicon production, by the hydrogen reduction of trichlorosilane, produce solid silicon units and require shutdown, setup, and startup between each production run, which requires a much greater heat expenditure.

The new quartz reactor produces silicon and deposits it at 1,200° C, melts and feeds the silicon to a melt crucible or crystal puller, and then seals the feed tube at 1,200° C to begin another cycle of silicon production. The large internal surface area is created by inserting vertical baffles (see figure). The baffles create gas turbulence, which aids in mixing the reactants, and provide heat-transfer area that speeds the reaction. Heat loss from the reactor is minimized by covering the heating elements that surround the reactor with adequate insulation.

The two cycles of the reactor consist of silicon production and removal. Initially, the reactor is brought up to the reaction temperature under an inert-gas flow. A small amount of silicon is then melted in the U-tube below the reactor vessel to form a positive seal, and the U-tube temperature is dropped to about 1,200° C to seal itself; the tube has its own separate heating element and insulation and a vent that prevents complete drainage of its lower section. With the tube sealed, the reactant-gas flow begins and continues until the desired amount of silicon is deposited.

At that point the reactant gases are flushed out of the reactor with argon to begin the silicon-removal cycle. Keeping the U-tube at 1,200° C, the reactor is raised to about 1,450° C to melt the deposited silicon, and the gas pressure between the reactor and delivery tube is equalized. Next, the temperature of the U-tube and delivery tube is raised to about 1,415° C, causing the silicon to drain, under gravity, from the reactor. When drained, the reactor is returned to reaction temperature, and the U-tube and delivery tube are returned to 1,200° C. Finally, the reactant gases are readmitted to the reactor to start another silicon-production cycle.

To prevent the reaction vessel from sagging when the silicon melts from it, a pressure equalizer maintains a slight positive pressure inside the vessel. The same pressure equalizer also prevents any larger pressure buildup that would rupture the vessel.

This work was done by Herbert E. Bates, David M. Hill, and David N. Jewett of Energy Materials Corp. for **NASA's Jet Propulsion Laboratory.** *For further information, Circle 18 on the TSP Request Card.*
NPO-15636

Silicon-Delivery Tube

Heated quartz tube transfers molten silicon.

NASA's Jet Propulsion Laboratory, Pasadena, California

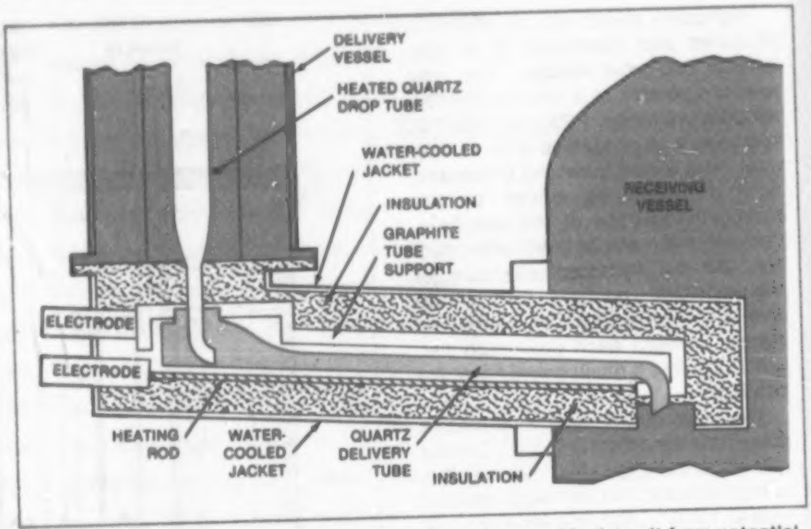

The **Quartz Delivery Tube** transports the molten silicon and isolates it from potential contaminants. The tube is sealed to the bottom of the delivery vessel by a flange and to the receiving vessel by a gasket.

A delivery tube transfers molten silicon between high-temperature vessels. The transport tube is sealed to the delivery vessel and receiving vessel and is slanted so that gravity moves the molten silicon.

The delivery vessel could be the output end of a growth reactor, in which pure silicon is produced by the reduction of trichlorosilane at 1,200° C. The receiving vessel could be a crystal-growing crucible.

The only part of the delivery tube to contact the molten silicon is the quartz inner tube (see figure). A heated quartz drop tube feeds it from the delivery vessel. Contamination is prevented since the molten silicon only contacts quartz.

The quartz tube is surrounded by layers that heat, support, insulate, and isolate it. The inner tube is kept hot by a resistively-heated graphite rod below it. The heater prevents the molten silicon from solidifying and interrupting transfer. A graphite casing supports the tube and completes the heating circuit. The graphite rod, quartz tube, and graphite casing are wrapped in quartz tape for isolation from the graphite-felt insulation surrounding them.

The insulation is encased in a water-cooled steel jacket. The insulation distributes the heat uniformly over the tube. Strategically placed thermocouples monitor the temperature. The tube is flanged to the bottom of the delivery vessel and gasketed into the receiving vessel.

This work was done by Herbert E. Bates, David M. Hill, and David M. Jewett of Energy Materials Corp. for **NASA's Jet Propulsion Laboratory.** *For further information, Circle 19 on the TSP Request Card.*
NPO-15637

A Milder Solution for Stress-Corrosion Tests

Excessive pitting is eliminated.

Marshall Space Flight Center, Alabama

A solution of 2.86 percent NaCl and 0.52 percent $MgCl_2$ in H_2O is suitable for stress-corrosion testing of aluminum alloys. It gives test results similar to those obtained with synthetic seawater, but is less expensive to prepare.

In a stress-corrosion-cracking (SCC) test, the alloy sample is strained in a coated aluminum stressing jig, then alternately immersed in the corrosive solution until failure or until the end of the test period (typically, 3 months). The test solution should be just corrosive enough to enable discrimination among metals of low, intermediate, and high SCC resistance.

If the solution causes extensive pitting, it is too corrosive for sensitive testing: The tensile stresses at the apexes of the pits are difficult or impossible to calculate, and the net section stress is greater than the original applied stress. As a result, the SCC effects are masked by pitting effects.

In the search for a mild corrosive, 14 different salt solutions were screened in alternate-immersion tests on 3 aluminum alloys. The most-widely-used solution of 3.5 percent NaCl in H_2O was too corrosive when prepared with pure salt and pure water. The best results were obtained with the NaCl/$MgCl_2$ solution and with the synthetic seawater (which contains nearly the same proportions of NaCl and $MgCl_2$ along with precise, minute amounts of eight other salts).

Material		Stress		$NaCl/MgCl_2$		Synthetic Seawater		Saltwater	
Alloy	Raw Form**	MPa	kpsi	Ratio***	Days to Failure	Ratio***	Days to Failure	Ratio***	Days to Failure
2024-T4	Plate	140	20	5/5	2, 2, 5, 5, 6	5/5	2(4), 5		
2024-T6	Plate	310	45	0/4		3/6	30*, 36*, 34*	3/3	47, 48, 61
7075-T651	Plate	205	30	5/5	2(4), 12	5/5	2, 2, 5, 15*, 20*		
7075-T651	Bar	275	40	4/5	12*, 28*, 33*, 43*	4/5	12, 15*, 15*, 40*	5/5	2(4), 16
7075-T7651	Plate	240	35	3/5	2, 5, 6	4/5	5, 7, 18*, 18*	4/5	2, 2, 3, 5

*Failed at edge or under coating

**Machined to round tensile specimens that were exposed by alternate immersion to the indicated solutions until failure or a maximum of 90 days

***(Number of specimens that failed)/(Number of specimens tested)

Stress-Corrosion-Cracking Tests were performed on aluminum alloys to assess the $NaCl/MgCl_2$ and synthetic-seawater solutions. The highly corrosive saltwater was included for comparison.

The table summarizes SCC tests performed with the $NaCl/MgCl_2$, "seawater," and saltwater solutions. The results with the first two solutions are generally consistent with the previously-known corrosion resistances of the alloys. Because the $NaCl/MgCl_2$ solution is less expensive than the artificial seawater, it will probably be preferred for future SCC testing.

This work was done by T. S. Humphries and J. E. Coston of **Marshall Space Flight Center.** *Further information may be found in NASA TM-82452 [N82-13216/NSP], "An Improved Stress Corrosion Test Medium for Aluminum Alloys" [$6]. A paper copy may be purchased [prepayment required] from the National Technical Information Service, Springfield, Virginia 22161. The report is also available on* *microfiche* *at no charge. To obtain a microfiche copy, Circle 20 on the TSP Request Card.*
MFS-25792

Heated Aluminum Tanks Resist Corrosion

Keeping a tank warm prevents moisture from condensing on it.

Marshall Space Flight Center, Alabama

The simple expedient of heating foam-insulated aluminum alloy tanks prevents them from being corroded by salt-laden moisture. A relatively-small temperature difference between such a tank and the surrounding air will ensure that the life of the tank is extended by many years.

Aluminum is corrosion-resistant in air containing water vapor alone because of the protective oxide film that forms on its surface. However, the aluminum can corrode near seawater. The salt in the air breaks down the protective film and causes pitting.

Water vapor penetrates the foam insulation from its warm exterior surface to the cool surface of the aluminum tanks. The vapor from seawater, condensing on the cool tank, thus initiates corrosion. However, heating the interior of the tank to a temperature above that of the ambient air reverses the vapor-permeation trend and prevents moisture from condensing on the aluminum.

(continued on next page)

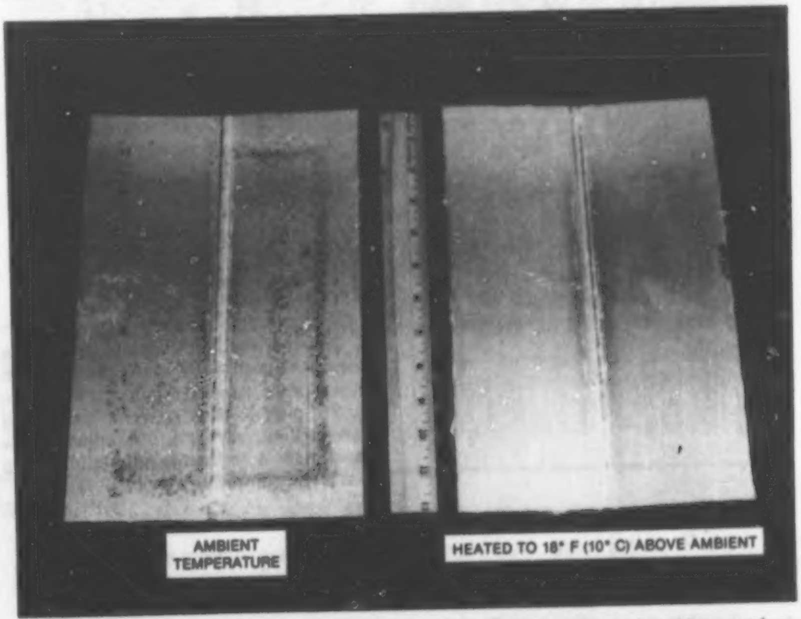

The **Pitted Aluminum Specimen** at the left was not heated above the ambient temperature in the salt-spray chamber. The completely uncorroded specimen at right was heated to 112° F (44° C) by a small light bulb in a box behind the specimen.

Corrosion tests were conducted on foamed aluminum panels in a 5-percent-salt fog. One panel was heated from the back to a temperature 18° F (10° C) above the 94° F (34° C) air temperature in the test chamber. After 11 days exposure, the panels were removed from the test chamber, and the foam was stripped from them. The heated panel showed no corrosion, but the unheated panel was pitted (see figure). Interestingly, the foam was much more easily removed from the unheated panel. Apparently moisture not only corrodes the aluminum but also decreases the adhesion of the foam.

The 18° F temperature difference on the heated panel was selected arbitrarily. The corrosion of aluminum tanks occurs most rapidly when the outside temperature and humidity are both high [on a warm day, the outside of the foam can reach 114° F (46° C) while the aluminum is 8°F (4° C) less]. On cool days or on days when the humidity is low, water-vapor permeation is negligible. Thus, the heating of tank interiors would not be required at all times; it would be needed more in the warm and humid summer months than in the cooler and dryer months.

Further study is needed to determine precisely the minimum temperature difference that will prevent corrosion under various atmospheric conditions. Further study will also determine the types of heaters, heating capacity, and heat circulation necessary to maintain tank interiors at the requisite temperature.

This work was done by Lyle E. Johnson of Martin Marietta Corp. for **Marshall Space Flight Center.** *For further information, Circle 21 on the TSP Request Card.*
MFS-25780

Vacuum Ampoule Isolates Corrosive Materials

A quartz vacuum container assures reliable thermophysical measurements of molten materials.

Langley Research Center, Hampton, Virginia

A quartz vacuum ampoule provides a measurement window and sample containment isolation for determining the thermophysical properties of semiconductor materials in a molten state. The quartz ampoule permits reliable measurement of the melt properties of a material such as lead/tin/telluride (PbSnTe). Confinement of the sample in a vacuum prevents contamination of the measurement system by hot corrosive vapors and any interference by preferential evaporation of the melt.

The sample is contained in a quartz tube between two quartz plugs polished on both ends. One plug is inserted into the quartz tube and sealed with a torch (the bottom plug in the figure). After this seal cools, a PbSnTe wafer with parallel faces and known thickness is placed in the tube. The PbSnTe wafer is sized to allow for thermal expansion and an expansion in volume when the phase change occurs at the melting temperature.

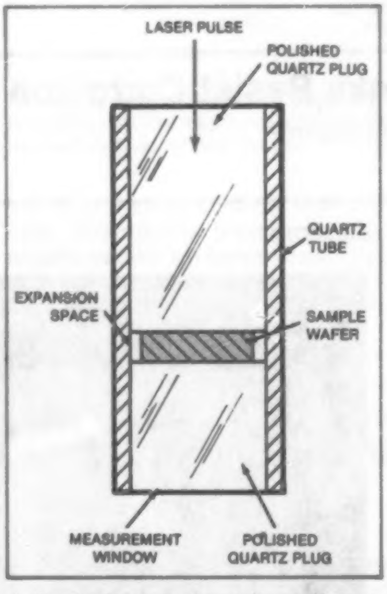

A **Quartz Vacuum Ampoule** confines a corrosive sample wafer between two quartz plugs inserted in a quartz tube. One quartz plug is a window for measuring sample thermodynamic properties while a laser pulse entering the other quartz plug heats the sample to a molten state.

The tube is then mounted on a special attachment to the vacuum system, and the second (top) quartz plug is inserted flush with the top of the PbSnTe wafer. A vacuum seal is made between the top quartz plug and the tube.

Thermal diffusivity measurements are made using the laser flash technique with one of the polished quartz plugs serving as the window to the sample. In addition to its use with PbSnTe, this technique could be applied to other semiconductor materials, such as germanium and mercury/cadmium/telluride.

This work was done by Roger K. Crouch and William J. Debnam of **Langley Research Center** *and Ray Taylor of CINDAS. For further information, Circle 22 on the TSP Request Card.*

This invention is owned by NASA, and a patent application has been filed. Inquiries concerning nonexclusive or exclusive license for its commercial development should be addressed to the Patent Counsel, Langley Research Center [see page A5]. Refer to LAR-12898.

A Solvent-Resistant, Thermoplastic Poly(imidesulfone)

Polymer incorporates the desirable properties of polyimides and polysulfones.

Langley Research Center, Hampton, Virginia

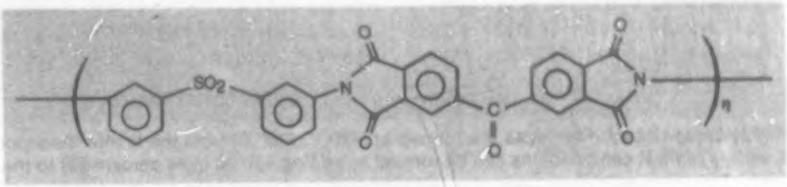

The Solvent-Resistant Thermoplastic Poly(imidesulfone) has the structure shown here. The parameter η represents several hundred repeated units.

A process for preparing a thermoplastic poly(imidesulfone) results in a material that has the excellent thermoplastic properties generally associated with polysulfones and the excellent solvent resistance generally associated with polyimides. The new thermoplastic, solvent-resistant polymer can be used as a molding resin, as an adhesive, and as a matrix resin for fiber-reinforced composites. The process for thermoplastically forming this resin can be used to produce moldings, adhesive bonds, and fiber-reinforced composites.

Aromatic polysulfones, a class of thermoplastic polymers, are soluble in such solvents as chloroform, methylene chloride, cyclohexanone, cresol, and hydraulic fluids. Since components fabricated from these polysulfones are susceptible to damage by these solvents, this polymer system cannot be used in many applications where the solvents are present. Aromatic polyimides, on the other hand, are a class of polymers that are exceptionally resistant to solvents but that are generally considered not readily processable by thermoplastic techniques. Both polymer systems have good thermal stabilities.

The desired poly(imidesulfone) is obtained through the incorporation of an aromatic sulfone moiety in the backbone of an aromatic linear polyimide to yield an aromatic poly(imidesulfone) prepared in bis(2-methoxyethyl) ether solvent. This polymer system results in a thermoplastic with better processability than the base polyimide. Conversely, the incorporation of an imide segment into the base polysulfone results in a solvent-resistant polymer that was previously soluble in common solvents. The structure of the polymer is shown in the figure. In the structure shown, it is the 3,3′-disubstituted diphenylsulfone segment of the polymer that causes it to be thermoplastic.

Thin films of the poly(imidesulfone) placed in various solvents were not affected. After removal from the solvents, the films had the same softening temperatures as before exposure. Even slight solvation of the polymer would cause a considerable lowering of the softening temperature.

Adhesive lap-shear samples prepared with the poly(imidesulfone) had exceptionally high strengths when tested at ambient temperature, at 177° C, and at 232° C, both before and after aging for 1,000 hours at 232° C in a flowing-air oven. Unfilled moldings prepared from the poly(imidesulfone) were clear and had properties that are reasonable for a linear thermoplastic. Graphite-fiber-reinforced moldings (composites) were successfully prepared using unidirectional high-tensile-strength fibers in the resin.

This poly(imidesulfone) can be thermoplastically processed in the 250°-to-350° C range to yield high-quality tough moldings, strong high-temperature-resistant adhesive bonds, and well-formed structural composites. The poly(imidesulfone) should be an excellent candidate for further development as a high-temperature adhesive and molding compound for aerospace applications.

This work was done by Terry L. St. Clair of **Langley Research Center** *and David Yamaki of the Massachusetts Institute of Technology. For further information, Circle 23 on the TSP Request Card.*

This invention is owned by NASA, and a patent application has been filed. Inquiries concerning nonexclusive or exclusive license for its commercial development should be addressed to the Patent Counsel, Langley Research Center [see page A5]. Refer to LAR-12858.

High-Performance Matrix Resins

Modified PMR polyimides have better processability and thermo-oxidative stability.

Lewis Research Center, Cleveland, Ohio

State-of-the-art PMR polyimides (in situ polymerization of monomer reactants) provide good strength and light weight in a wide variety of critical applications. However, improved processability and elevated-temperature thermo-oxidative stability are desired in such polyimide systems. A series of improved polymer resins was developed at Lewis Research Center. These high-performance matrix resins, intended for use in advanced composites, adhesives, and neat resin articles, show improvements in both processability and elevated-temperature stability over the state-of-the-art PMR-15 polymers.

(continued on next page)

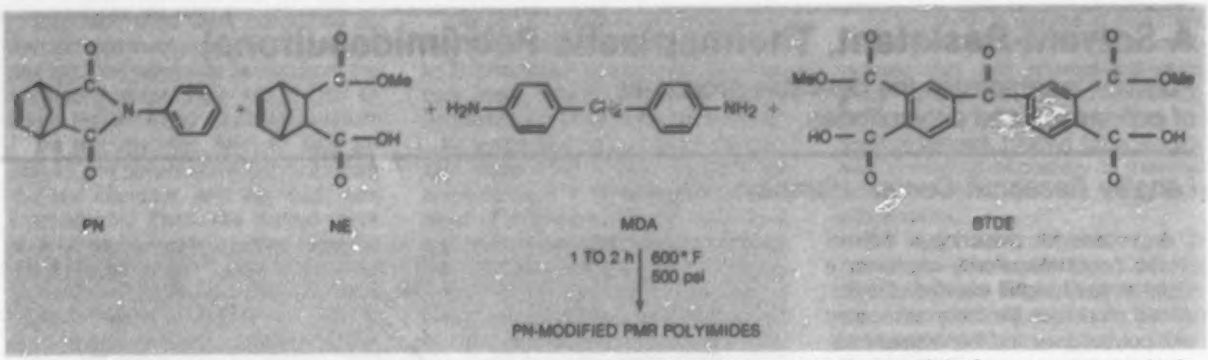

Highly-Cross-Linked Polyimides are formed at 600° F (315° C) from the in situ thermopolymerization of the four monomer reactants. A variety of PMR compositions can be formed by adding 4 to 20 mole percent PN to the standard PMR-15 composition.

The improved modification of the PMR-15 system results from the addition of N-phenylnadimide (PN) to the basic three-monomer reactant system. The basic three monomers are monomethyl ester of 5-norbornene-2, 3-dicarboxylic acid (NE), dimethyl ester of 3,3', 4,4'-benzophenonetetracarboxylic acid (BTDE), and 4,4'-methylenedianiline (MDA) and are present in their standard concentrations. A varity of modified-PMR compositions are formulated by adding 4 to 20 mole percent PN to the standard PMR-15 composition. As shown in the figure, highly-cross-linked polyimides are formed at 600° F (315° C) from in situ thermopolymerization of the four monomer reactants.

A 50 weight percent solid solution is prepared by dissolving the four monomer reactants of known composition in annydrous methanol at room temperature. The solution is applied to fibers, fabrics, or chopped fibers and then molded into composite articles by curing at 600° F (315° C) and 500 psi (3.45×10^6 N/m^2) pressure for 1 to 2 hours. It can also be applied to surfaces of adherents for bonding composites, metals, or other materials. The solventless powders can be molded into neat resin objects having various shapes and forms.

Of the five modified polymers evaluated, PMR-P1 and PMR-P2, which contain 4 and 9 mole percent PN, respectively, are unique in that they exhibited simultaneously-improved resin-flow properties and thermo-oxidative stability over PMR-15. These materials are low-cost, similar to PMR-15, while having superior processing and elevated-temperature performance compared to PMR-15.

This work was done by Ruth H. Pater of **Lewis Research Center.** *Further information may be found in NASA TM-82733 [N82-11117/NSP], "Novel Improved PMR Polyimides" [$6.00]. A copy may be purchased [prepayment required] from the National Technical Information Service, Springfield, Virginia 22161.*

Inquiries concerning rights for the commercial use of this invention should be addressed to the Patent Counsel, Lewis Research Center [see page A5]. Refer to LEW-13864.

Thermal-Gradient Fining of Glass

Temperature gradients may drive off bubbles in a gravity-free environment.

Marshall Space Flight Center, Alabama

Molten glass could be fined (cleared of bubbles) by heating with a suitable temperature gradient, according to preliminary experiments. Although thermal-gradient fining has been studied by NASA as one of several material-processing methods for use in low-gravity manufacturing, the technique could also be of value in terrestrial glass processing.

A temperature gradient produces a force on gas bubbles trapped in molten glass pushing the bubbles to a higher temperature region where they can be collected. The concept has been demonstrated in experiments on Earth and on a rocket.

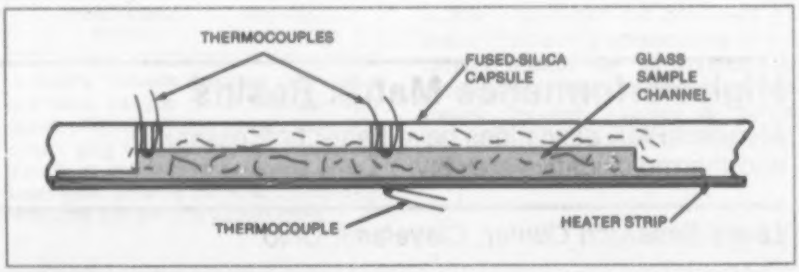

A **Sample of Sodium Borate Glass** is encapsulated by fused silica and a strip heater. The sample channel dimensions are 0.5 by 1 by 10 mm.

In a NASA experiment, a glass sample was packaged in a test cell consisting of a silica glass capsule, a platinum/rhodium strip heater, and thermocouples (see figure). Housed in an automatic test payload, the cell was launched on a Spar rocket, and the sample was heated during the 4 minutes of zero gravity before the payload returned to Earth. The sample was a sodium borate glass, which has a negative temperature coefficient of surface tension.

During the zero-gravity period, a camera in the payload took 246 photographs of the molten glass sample at 1-second intervals. At the same time, temperature data from the thermocouples embedded in the glass and welded to the heating strip were telemetered back to Earth. A signal proportional to the current drawn by the camera film-advance motor was also telemetered as a time indicator for the film sequence.

The photographic record shows that many of the bubbles in the glass were rapidly swept out by the high temperature gradient as it heated up to about 913° C. Since there was also a strong transverse gradient, bubbles migrated not only longitudinally along the sample-capsule channel but also transversely to the strip heater. Once they contact the strip, bubbles move slowly if at all. As the experiment progressed, bubbles that were in cooler regions were slowly drawn to the center of the channel.

This work was done by W. R. Wilcox of Westinghouse R&D Center for **Marshall Space Flight Center.** *For further information, Circle 24 on the TSP Request Card.*
MFS-25757

Designing Glass Panels for Economy and Reliability

Method considers such factors as glass temper and load duration.

NASA's Jet Propulsion Laboratory, Pasadena, California

An analytical method determines the probability of failure of rectangular glass plates subjected to uniformly distributed loads such as those from wind, Earthquake, snow, and deadweight. Although developed as an aid in the design of protective glass covers for solar-cell arrays and solar collectors, the method should also be useful in estimating the reliability of large windows in buildings exposed to high winds and can be adapted to nonlinear stress analysis of simply supported plates of any elastic material.

For economy, glass plates should have the minimum thickness consistent with a reasonably low risk of failure. In the past, the minimum allowable thickness has been determined from design curves published by glass manufacturers, but such curves have certain shortcomings: They are sometimes derived from tests on only a few samples and therefore do not have a strong statistical base. Usually the curves do not take load history into account, even though the breaking strength of glass depends strongly on load duration. Snow and deadweight ordinarily are not important in vertical windows; but because solar-collector panels are tilted, such loads last longer than windloads and may cause failure at lower stress.

The new method allows the designer to select the glass thickness that will sustain given normal pressure loads at a specified failure rate. There are two key elements of the method: First, design curves were developed that permit the user to estimate the stress in the glass caused by the given applied loads. Second, statistical analysis was used to produce curves that give the breaking strength of the glass as a function of failure rate, glass temper, load duration, and panel area. A satisfactory design is attained when the estimated applied stress is slightly less than the estimated breaking strength corresponding to the accceptable failure rate.

This work was done by Donald M. Moore of Caltech for **NASA's Jet Propulsion Laboratory.** *For further information, Circle 25 on the TSP Request Card.*
NPO-15252

Processor Generates and Extracts Silicon

An impinging jet/funnel system separates the silicon and salt formed in the reduction of silicon tetrachloride by sodium.

NASA's Jet Propulsion Laboratory, Pasadena, California

A processor now under development would continuously generate pure silicon and separate it from reaction byproducts. In a laboratory prototype, the reduction of silicon tetrachloride by sodium is the key reaction and the byproduct is NaCl, although other silicon halides could probably be substituted for the tetrachloride.

In the processor (see figure), vapors or fine liquid sprays of sodium and silicon tetrachloride react to form gaseous NaCl and liquid droplets of silicon. To prevent condensation of the salt vapor or solidification of the silicon, the reactor temperature is held above 1,415° C, 5° C above the melting point of silicon. The reactor pressure is about 0.25 atm ($2.5x10^4$ N/m^2).

The products exit through an orifice at the bottom of the reactor into a volume

(continued on next page)

kept at less than half the reactor pressure. The pressure difference creates a jet of gaseous NaCl that carries the silicon droplets.

A separator/collector surface, placed across the jet in the low-pressure region, intercepts the impinging jet. The silicon hits the surface, which is held near 1,412° C, and collects on it. The salt flows away to cooler surfaces in regions of even lower pressures. These cooler surfaces rapidly condense the salt vapor, eliminating the need for vacuum pumps.

The separator/collector surface is a pedestal in the center of a crucible. The silicon, separated from the salt, flows down the funnel-shaped walls of the separator/collector into a much larger collector, where it rapidly solidifies. The collector is isolated from the reactor and separator in the process vessel by a vacuum lock. The filled collector is periodically removed and replaced by an empty one.

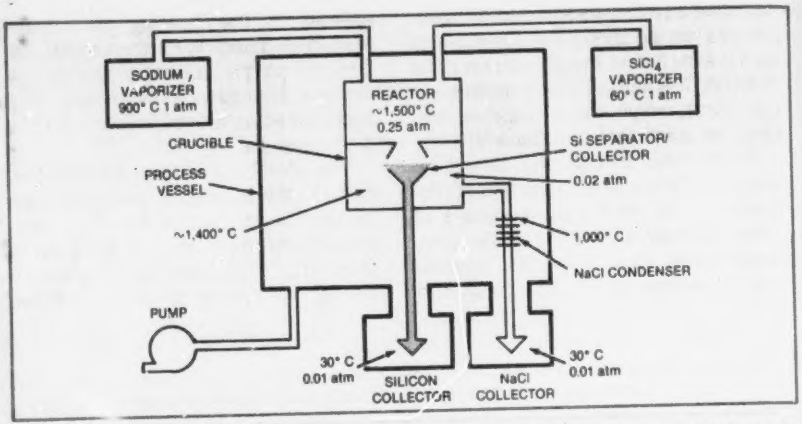

The **Silicon Separator/Collector** intercepts an impinging jet of reaction products and selectively funnels the silicon into a larger collector. The salt byproduct is removed by a tubular condenser, which is held at 1,000° C, and then flows into a collector, where it solidifies. Vacuum locks permit periodic salt removal without disturbing continuous operation.

This work was done by Robert K. Gould and Charles P. Dickson of AeroChem Research Laboratories, Inc., for **NASA's Jet Propulsion Laboratory.**

For further information, Circle 26 on the TSP Request Card.
NPO-15582

Sodium Spray Would Speed Silicon Production

The production rate of solar-grade silicon in a sodium/silicon tetrafluoride reactor would be increased by a spray feed.

NASA's Jet Propulsion Laboratory, Pasadena, California

Liquid sodium would be sprayed into a sodium/silicon tetrafluoride reactor according to a new proposal for increasing the production rate of solar-grade silicon. The large surface-to-volume ratio of the sprayed sodium droplets would make the reaction proceed faster than if the liquid sodium was poured into the reactor.

In the proposal, the liquid sodium at about 100° C is sprayed (see figure) into the silicon tetrafluoride gas and reacts with it only at the bottom of the reactor, where the temperature is 400° to 900° C. The rest of the reactor temperature is low enough to avoid excessively vaporizing the sodium, so that the reaction products form only on the reactor bottom. Also, to insure that the sodium spray does not clog the reactor, by hitting the walls, the angle of the spray cone is sufficiently narrow, and a baffle is installed.

When the reactor is full, the sodium and silicon tetrafluoride flows stop. The silicon and sodium fluoride products in the reactor are then separated.

This method could be applied to similar processes where electropositive metals reduce halides. Halides that can be reduced this way include $TiCl_4$, ZrF_4, and HfF_4; and the metals used include sodium, magnesium, and zirconium.

This work was done by K. M. Sancier of SRI International for **NASA's Jet Propulsion Laboratory.** *For further information, Circle 27 on the TSP Request Card.*
NPO-15246

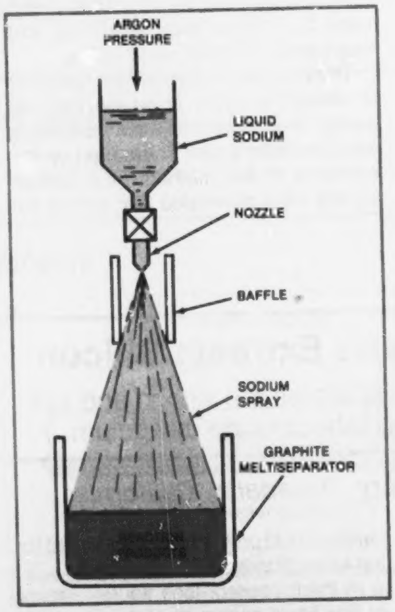

The Liquid-Sodium Droplet Size is controlled by the pressure of argon gas and by the nozzle design. The baffle helps to prevent the reactor opening from becoming clogged by reaction products.

Two-Temperature-Zone Silicon Reactor

Temperature profile confines SiF_4 reduction by sodium to the reactor bottom.

NASA's Jet Propulsion Laboratory, Pasadena, California

When high purity silicon is synthesized by the reduction of silicon tetrafluoride by sodium, a very-fast highly exothermic reaction takes place. A controlled reaction has been proposed in which a SiF_4-pressurized vertical reactor operates with two temperature zones (see figure). The lower part of the reactor is kept at a temperature higher than 300° C, and the upper part is kept at 110° C. Liquid sodium feeds from a nozzle at the top of the reactor without reacting with the SiF_4. When the sodium reaches the higher temperature region at the bottom, the reaction takes place immediately.

Some of the advantages that this technique has over previous batch techniques are:

- A constant pressure can be used, simplifying the SiF_4 feeding system;
- The temperature of the reaction can be controlled easily by changing the feeding rate of Na and the pressure of SiF_4, resulting in more-homogeneous reaction products;
- The efficiency of material consumption is almost 100 percent;
- The impurity pickup from the reactor walls is minimized; and
- The reaction products only contact the reactor walls at the base, making it easier to remove them from the reactor.

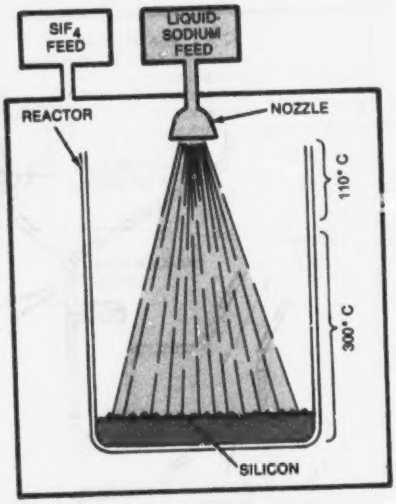

Small Droplets of Sodium sprayed from a nozzle flatten and react when they hit the bottom of a reactor. This technique creates a large reaction area over a narrow depth.

Reaction parameters for a two-temperature-zone reactor have yet to be worked out. These parameters include the size of the sodium droplets, the rate of sodium delivery, and the reactor temperature.

This work was done by Angel Sanjurjo, Leonard Nanis, Vijay K. Kapur, and Robert D. Weaver of SRI International for **NASA's Jet Propulsion Laboratory.** *For further information, Circle 28 on the TSP Request Card.*
NPO-15368

Casting Silicon Pellets From Powder

Fine silicon powder melts in a thin quartz bubble that breaks upon cooling.

NASA's Jet Propulsion Laboratory, Pasadena, California

A new technique converts finely powdered silicon into solid pellets. The pellets are used in spark-source mass-spectroscopic analysis of the silicon and in electrical-resistivity measurements for detecting low-level contaminants.

Powdered silicon is produced when silane is cracked in a free-space reactor. It must be converted to pellet form to perform the impurity testing.

A previous method for casting the powder using silica containers sometimes caused the solid pellets to crack because of the difference in thermal expansion between the melt and the mold. The new technique uses a thin-walled quartz mold. Although the quartz fractures on cooling, the solid silicon remains crack-free.

The pellets are fabricated in a thin-walled bubble blown in the end of a quartz tube. In a test, the tube was 24 mm in diameter, and the bubble wall was about 0.1 mm in thickness. With silicon powder packed into the bubble, the tube is heated in a vacuum furnace. Upon cooling, the bubble shatters, leaving behind a crack-free pellet of silicon.

This work was done by Ernest G. Farrier and Joachim Rexer of Union Carbide Corp. for **NASA's Jet Propulsion Laboratory.** *For further information, Circle 29 on the TSP Request Card.*
NPO-15272

Short Shot Tower for Silicon

Passage through a cold liquid reduces the drop length for shot formation.

NASA's Jet Propulsion Laboratory, Pasadena, California

The drop length necessary to convert molten silicon to shot is expected to be reduced by a proposed new process. In addition to falling through a gas, the droplets of molten silicon fall through a cold liquid. Both the heat-transfer coefficient and the temperature difference between the hot silicon and the cold surrounding liquid are greater than they would be for a gas. Therefore the heat of the silicon droplets is transferred more quickly, and they become hard spheres within a shorter drop distance.

The conversion of silicon from powder or chunks to shot often simplifies processing. Shot is more easily handled in most processing equipment — in furnaces, for example.

The silicon droplets are ejected from a nozzle into gaseous argon, through which they fall into liquid methanol (see figure). In the methanol, the silicon cools and solidifies, falling as shot to the bottom of the tower, where it can be collected. The methanol liquid collected with the shot is recycled.

The argon flowing above the liquid methanol prevents methanol vapor from entering the upper part of the tower and the nozzle. What methanol vapor does arise is carried off through the argon vent pipe and recycled.

This work was done by Herbert E. Bates, David M. Hill, and David N. Jewett of Energy Materials Corp. for **NASA's Jet Propulsion Laboratory.** *For further information, Circle 30 on the TSP Request Card.*
NPO-15607

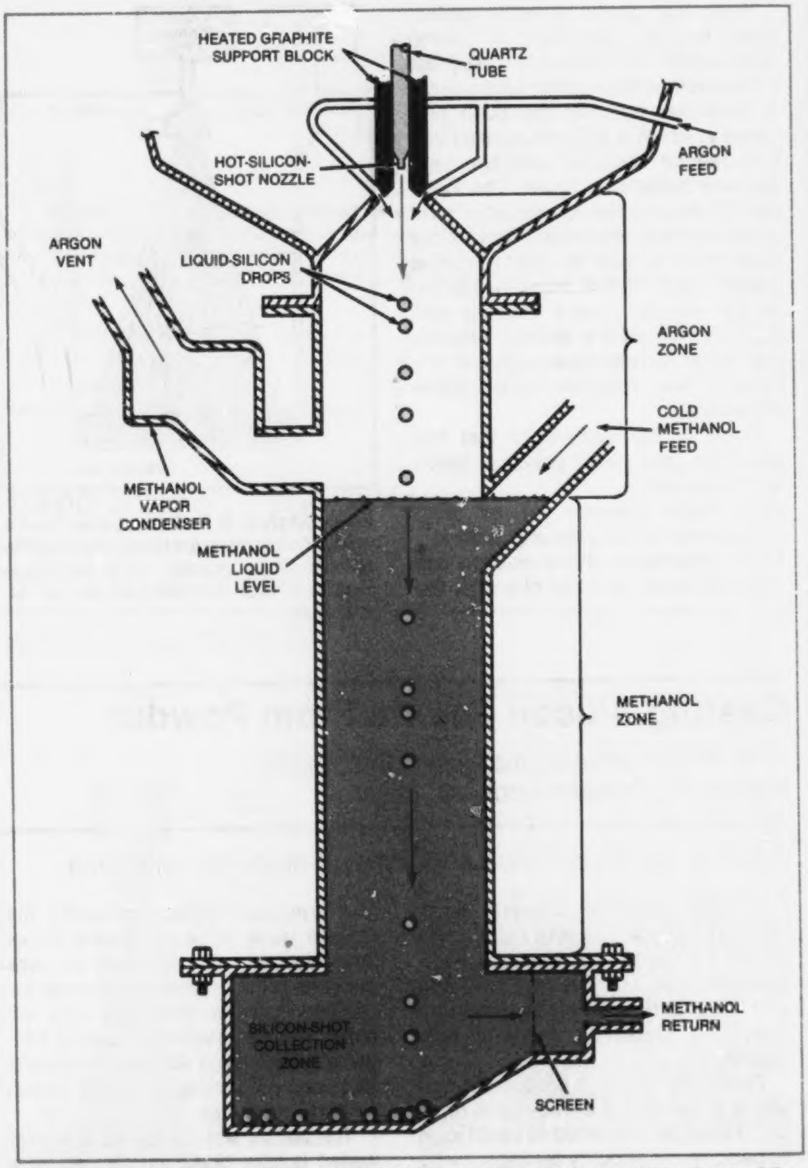
HEATED GRAPHITE SUPPORT BLOCK
QUARTZ TUBE
ARGON FEED
HOT-SILICON-SHOT NOZZLE
ARGON VENT
LIQUID-SILICON DROPS
ARGON ZONE
COLD METHANOL FEED
METHANOL VAPOR CONDENSER
METHANOL LIQUID LEVEL
METHANOL ZONE
METHANOL RETURN
SILICON-SHOT COLLECTION ZONE
SCREEN

Drops of Liquid Silicon fall through a protective cloud of argon, then through a rapidly cooling bath of methanol, where they quickly turn into solid shot.

Estimating the Degree of Cross-Linking in Rubber

A new analysis of both the extension and
retraction may give better estimates.

NASA's Jet Propulsion Laboratory, Pasadena, California

The degree of cross-linking or network chain concentration of rubber is estimated with the aid of a new method. The quantity is needed in studies of the mechanical behavior of rubber. The new method is based on the finding that rubber follows different stress/strain relationships in extension and retraction.

Previously, chain concentration was estimated by measuring the uniaxial stress/strain response in extension and using the measurements in an equation having the chain concentration as one of its terms. One deficiency of this method is that rubber is basically viscoelastic, and therefore equilibrium or time-independent data are difficult to obtain. However, it has recently been found that while the stress/strain response in extension invariably follows equation (1) in the figure, the subsequent stress/strain response in the same specimen in retraction almost invariably obeys equation (2) provided that elongation is not close to the elongation at which stress was reversed and that the maximum elongation is relatively large.

Tests were performed on ring specimens in a standard stress/strain testing machine. When the maximum extension was reached, the test machine was reversed so that retraction occurred at the same constant rate as in extension. The strain for both extension and retraction was calculated on the basis of the original dimensions of the specimen — that is, no account was taken of permanent set, which was quite small.

The network chain concentration in the samples was estimated by this method to be 122×10^{-6} mole/cm^3, which agrees well with the value of 110×10^{-6} mole/cm^3 found by an independent technique. However, if one were to use the data from extension alone, the value would be much lower: 73×10^{-6} mole/cm^3.

It is suggested that a gum vulcanizate is composed of two interdependent networks. One network is composed of those chains attached at each end to chemically cross-linked units and known as permanent network chains. The other network consists of entangled but not cross-linked chains; it is referred to as the transient network.

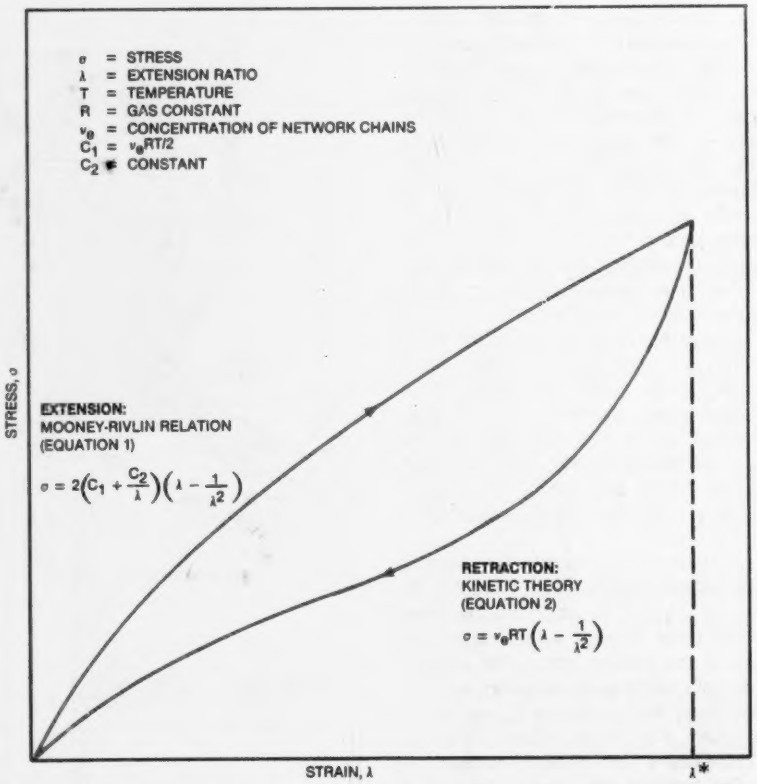

When a Rubber Specimen is stretched to a given extension ratio λ and then released, its stress-vs.-strain curve follows two paths: one for extension and another for retraction.

When the combined networks are subjected to a load, the permanent chains respond almost immediately, but the chains in the transient network move more slowly from their initial position to a final position, which is reached after the entanglements have gone through their maximum travel. The transient-network chains then function as if they formed a permanent network and continue to do so until the load is reduced to near zero; then relatively slow rearrangements occur, and the entanglements move back to a stress-free position.

For rubber containing a filler material, there is the additional effect of dewetting or separation of the rubber from the surface of the filler particles under load. The modulus of filled rubber is given by two contributions: (1) that from the network chain concentration of the rubber itself and (2) that from the presence of filler. This latter contribution is proportional to the fraction of surface area of filler in contact with the rubber. The higher the elongation, the lower will be the modulus because some fraction of the surface area of the filler will have separated from the rubber. As the load is reduced in the retraction portion of the load cycle, rewetting does not occur instantly, and therefore the response is equivalent to that of a sample with a lower filler level. When the load is reduced to zero, the rubber rewets the particles, and eventually the properties of the original unstressed sample are restored.

This work was done by Robert F. Fedors of Caltech for **NASA's Jet Propulsion Laboratory.** *For further information, Circle 31 on the TSP Request Card.*
NPO-15590

Improved Fluidized-Bed Gas Injector

Annular gas flow would cool and protect the injector cone.

NASA's Jet Propulsion Laboratory, Pasadena, California

A new single-cone gas injector has been proposed for fluidized-bed particle-coating systems (see figure). The injector would use a protective annular stream of high-velocity gas to cool the cone and to reduce or eliminate abrasion by circulating particles. This diluent/fluidization gas would enter at several places around the base of the injector cone or through a continuous annulus. It would then flow toward the apex of the cone, carrying particles into the highly-agitated reaction zone.

A very highly agitated region is required to coat particles with such materials as silicon or carbon in a fluidized-bed system. Simple gas-injection cones are often abraded by particles that strike the base of the cone. Simple cones also cause the bed to surge or slug, resulting in some stagnation of the bed.

In the improved injector, the reaction gas that decomposes to provide the silicon or carbon to coat the particles would enter through a tube along the axis of the injector cone. For carbon, thermally decomposable gases, such as methane (CH_4) or ethane (C_2H_6), could be used. For silicon, silane (SiH_4) or trichlorosilane ($SiHCl_3$) could be used.

The reaction gas decomposes as it comes in contact with the hot particles. If necessary to prevent premature decomposition, the reaction gas could be cooled right up to the moment it enters the fluidized bed.

The seed particles would enter through a piston valve at one side of the bed and flow quickly down the side, up the cone, and into the reaction zone. Coated particles would be drawn off through a similar valve on the other side. Depending on purity requirements, injector components could be constructed from such materials as quartz, carbon, or metal.

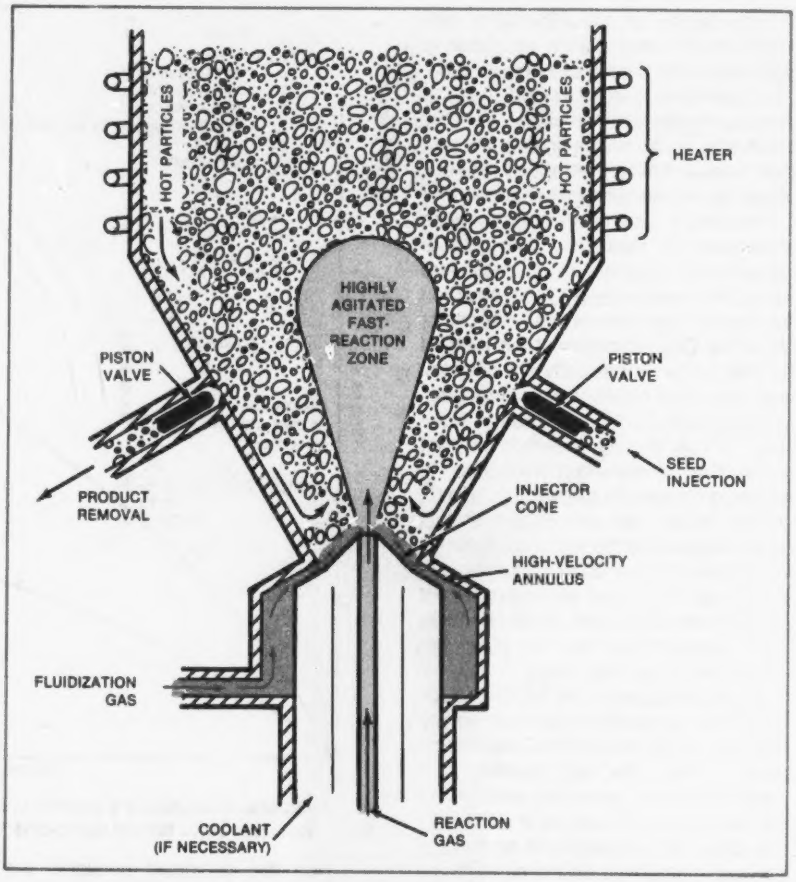

The **Gas-Injection Cone** in a fluidized-bed reactor for coating particles with silicon or carbon could be cooled and protected from abrasion by a stream of gas flowing over the surface of the cone. Hot particles entering the reaction zone would be coated with silicon or carbon supplied by thermal decomposition of a suitable gas injected into the reaction zone.

This work was done by Richard A. Hogle of Caltech for **NASA's Jet Propulsion Laboratory.** *For further information, Circle 32 on the TSP Request Card.*
NPO-15572

Membranes Remove Metal Ions From Industrial Liquids

The low-cost membranes are simply suspended in metal-ion/liquid solutions to remove impurities.

Lewis Research Center, Cleveland, Ohio

Disposing of contaminated liquids is an increasing problem in today's industrial society. Metal cations (positively charged atoms) are present as contaminants or impurities in many industrial liquids. Liquids with these impurities are either enviromental pollutants or possible sources of recoverable materials. In either case it is desirable to remove these metal ions efficiently. Current systems employ cation-exchange resins as powders, beads, or granules for use in metal-removal filtration systems. In terms of energy requirements and capital equipment costs, however, these systems are not optimized since they are expensive and not necessarily cost-effective. These systems require pumping a liquid through a filtration system that is subject to both clogging and resin fouling.

A method has been developed at Lewis Research Center that is a major improvement in metal-ion removal. It eliminates the need for costly pumping and filtration equipment in specific applications. This technique enables the cation-exchange resin to be fabricated into a more efficient form, that of a thin membrane film of various sizes. Membranes of this type may be simply suspended in metal-ion/liquid solutions to remove the impurities. This removal system does not require pumping, filtration equipment, or constant movement of the solution. The unique quality of these membrane films is that they are nonfouling and have outstanding high-absorption capacity.

The use of these membrane films affords a convenient and economical alternative for removing and recovering metal cations present in low concentrations from large quantities of liquid solutions. Possible applications of these membrane films include use in analytical chemistry for the determination of small amounts of toxic metallic impurities in lakes, streams, and municipal effluents. It is also possible that this type of ion-exchange membrane may be suitable for use as an absorber of certain pollutant gases and odors present in confined areas.

These membrane films comprise a cross-linked copolymer of polyacrylic acid (the active ion exchanger) and polyvinyl alcohol (the antifouling agent). An aqueous solution of these constituents is cast (poured) onto a smooth surface and dried. The dried film is removed and formed into any desired shape. It is then exposed to ionizing radiation that causes copolymerization and crosslinking. Treatment with aqueous calcium hydroxide converts the polyacid and has a wide variety of applications.

This work was done by W. Philipp, L. Hsu, and C. May of **Lewis Research Center.** *Further information may be found in:*

NASA TM-81670 [N81-16123/NSP], "New Ion Exchange Membranes" [$6], and

NASA TP-1407 [N79-21120/NSP], "Three Methods for In Situ Crosslinking of Polyvinyl Alcohol Films for Application as Ion Conducting Membranes in Potassium Hydroxide Electrolyte" [$12].

Copies of these reports may be purchased [prepayment required] from the National Technical Information Service, Springfield, Virginia 22161.

Inquiries concerning rights for the commercial use of this invention should be addressed to the Patent Counsel, Lewis Research Center [see page A5]. Refer to LEW-13853.

Viscosity Depressants for Coal Liquefaction

Certain unsaturated hydrocarbons would prevent coal from solidifying during liquefaction.

NASA's Jet Propulsion Laboratory, Pasadena, California

A proposed process modification would incorporate viscosity depressants to prevent coal from solidifying during liquefaction. The depressants would reduce the amount of heat needed to liquefy coal.

While the coal is processed, unsaturated hydrocarbons containing eight or more carbon atoms would be put into the liquid medium to act as viscosity depressants. Among possible depressants are metallic soaps, such as lead stearate, and amides, such as stearamide and dimer acid amides. Other possibilities are such epoxylated fatty acids as epoxylated linseed oil, epoxylated olive oil, and epoxylated linolenic acid, and waxes, such as beeswax, carnauba wax, and paraffin wax. Any of these compounds would be satisfactory viscosity depressants for coal, but the epoxylated fatty acids are preferred when used in an amount of less than 0.1 weight percent, based on the amount of coal used.

This work was done by Sarkis H. Kalfayan of Caltech for **NASA's Jet Propulsion Laboratory.** *For further information, Circle 33 on the TSP Request Card.*
NPO-15174

Books and Reports

These reports, studies, and handbooks are available from NASA as Technical Support Packages (TSP's) when a Request Card number is cited; otherwise they are available from the National Technical Information Service.

Development of Silane Hydrolysate Binder for Thermal-Control Coatings

Tough coating requires a cure temperature of only 66° C.

A technical report describes the theoretical and experimental development of a methyltriethoxysilane (MTES) hydrolysate binder for white, titanium dioxide-pigmented thermal-control coatings such as are often needed on satellites. The new coating is tougher and more abrasion-resistant than the conventional coating, S-13G, which comprises zinc oxide in a hydroxyl-terminated dimethylsiloxane binder. For an earlier article on methyl trialkoxysilane hydrolysates, see "Binders for Thermal-Control Coatings," in *NASA Tech Briefs*, Vol. 6, No. 3 (Fall/Winter 1981), page 287 (MFS-25620).

Ultraviolet absorptance on both the old and new coatings held at about 0.2 during a 930-h exposure in a solar-radiation simulator. (Longer tests would be required to assess any difference between the two coatings in ultraviolet resistance.) In an outgassing test of the new coating run at 10^{-6} torr and temperatures up to 212° F (100° C), weight loss was less than 0.2 percent per hour, which is considered acceptable for coating materials in space. In a thermal-cycling test — five cycles, -150° to 150° F (-101° to 66° C), bend tests on cycled samples of the new coating showed no significant increase in tendency to craze or crack.

In the optimum formulation, MTES monomer is polymerized by hydrolysis with water in the mole-equivalent ratio 10/3.25 (MTES/H_2O) and mixed with TiO_2 (previously ball-milled in ethanol) in a weight ratio 12/26 (TiO_2/binder). The formulation is then sprayed on an aluminum substrate and cured for 24 h at 75° F (24° C) followed by 3 days at 150° F. Cured thickness is 2 to 2.5 mils (0.05 to 0.06 mm).

In arriving at this formulation, a series of tests was run to determine the parameters of pigment/binder ratio, ethanol content, pigment particle size, coating thickness, and cure conditions. The effect of elevated temperature on the hydrolysis rate was striking and undesirable: At 120° F (50° C), some gelation and precipitation of insoluble polymer occurred.

This work was done by W. J. Patterson of **Marshall Space Flight Center.** *Further information may be found in NASA Technical Paper 1900 [N81-31365/NSP], "Development of a Silane-Hydrolysate Binder for UV-Resistant Thermal Control Coatings" [$6]. A paper copy may be purchased [prepayment required] from the National Technical Information Service, Springfield, Virginia 22161. The report is also available on microfiche at no charge. To obtain a microfiche copy, Circle 34 on the TSP Request Card.*
MFS-25749

Life Sciences

Hardware, Techniques, and Processes

171 Tissue-Culture Method of Cloning Rubber Plants

Computer Programs

171 Life Sciences MIS

Tissue-Culture Method of Cloning Rubber Plants

By adjusting the culture medium, an excised shoot tip can produce up to 50 identical guayule plants.

NASA's Jet Propulsion Laboratory, Pasadena, California

The guayule plant, a high-yield rubber plant, can be cloned by a tissue-culture method to produce multiple new plants that mature quickly. With this method many clones can be bred from a single parent, and each clone can then be rooted and transplanted to soil where it will grow and mature. The method preserves a desired genetic identity (genotype), so that the clones should produce as prolifically as their parents if planted in the same environment.

The guayule plant, *Parthenium argentatum*, forms many lateral buds, the majority of which can be removed without affecting the growth of the parent plant. The small shoot tips, the most regenerative parts of the plant, are removed by microscalpels and placed on slants of sterilized tissue-culture medium. The culture medium contains water, agar, minerals, sucrose, thiamin hydrochloride, and the cytokinin benzylaminopurine (BAP).

By varying the concentration of the cytokinin, a single excised tip can produce either 1 or several (up to 50) new plants. In a medium with a 0.1-mg/l concentration of BAP, the tips respond quickly and produce new leaves, which does not occur with shoot tips grown in a culture medium that lacks BAP. Higher concentrations of the cytokinin accelerate these developments.

The figure shows plantlets grown in cultures with different concentrations of BAP. After a month of growth, the cultures can be either transferred intact or separated into individual shoots and placed in a rooting medium containing 3 percent B-indolybutyric acid and no cytokinin, which inhibits root growth.

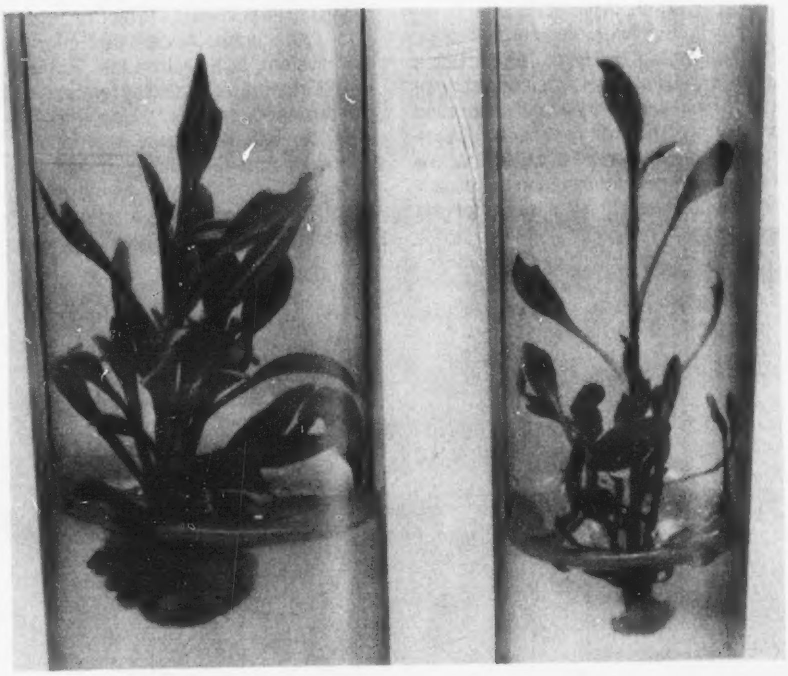

The **Numerous Shoots of the Clone Plantlets** grown in cultures containing 1 mg/l of BAP were short and thick-stemmed (left). Plantlets from media containing 0.1 mg/l BAP were slender (right). However, within 30 days after removal from the culture medium, both plantlets produced numerous roots.

To compare the growth of the clones with that of seeded plants, potted clone plantlets were grown in full Sunlight for 13 months along with equal-aged seedlings. During the first 6 months, a few of the plantlets flowered, a sign of a mature plant, but only one seedling did so; most of the seedlings continued vegetative growth without flowering. A check of the chromosome count of the plantlets and seedlings showed they were both the same, 36 — the normal number for sexually-reproducing guayule plants.

This work was done by Ernest A. Ball of The Regents of the University of California for **NASA's Jet Propulsion Laboratory.** *For further information, Circle 35 on the TSP Request Card.*
NPO-15756

Computer Programs

These programs may be obtained at very reasonable cost from COSMIC, a facility sponsored by NASA to make new programs available to the public. For information on program price, size, and availability, circle the reference letter on the COSMIC Request Card in this issue.

Life Sciences MIS

An interactive system utilizing "form-fillout" capability

The Management Information System, MIS, provides the Life Sciences Projects Division at Johnson Space Center with an automated system for project management. MIS development objectives included:

a. A simple system that allows for the rapid and accurate update and review of the status of any active task within the project,

b. The ability to store and update desired

(continued on next page)

management-level data and to manipulate the data for display,

c. The ability to display the information to conduct status meetings with a large number of participants,

d. To provide a network among remote users enabling them to exchange and review information, and

e. To provide an access-limiting security system around the data base.

The Life Sciences commitment to the Shuttle Program will ultimately include a series of multiple payloads consisting of from 5 to 50 experiments and supporting equipment. This committment necessitated the development of MIS to handle the management information necessary to keep abreast of all aspects of the program.

NASA has found that a disciplined "goal-oriented" program is the only effective approach in meeting launch dates with confidence. In building a data base to support a goal-oriented program, the project schedule becomes the focal point around which all other information revolves; i.e., cost, open items, problems, and narrative status. MIS provides the Life Sciences Projects Division with just a schedule-centered information system. MIS utilizes the Tektronix 4027 color graphics display terminal and its form-fillout capability. User interface with the MIS data base is through a series of forms including: a technical assessement form, an event-planning form, a milestone schedule form with 6-month, 1-, 2-, or 4- year schedule displays, a project cost/funding status form, a cost-trend chart form, and a miscellaneous form for maintaining information in the data base that is not covered by one of the other forms.

MIS is written in VAX COBOL and FORTRAN for interactive execution on the DEC VAX-11/780 through the Tektronix 4027 terminal. MIS was developed in 1981.

This program was written by Robert A. Dittman of **Johnson Space Center** *and Victor Marks of MATSCO. For further information, Circle B on the COSMIC Request Card.*
MSC-20238

Mechanics

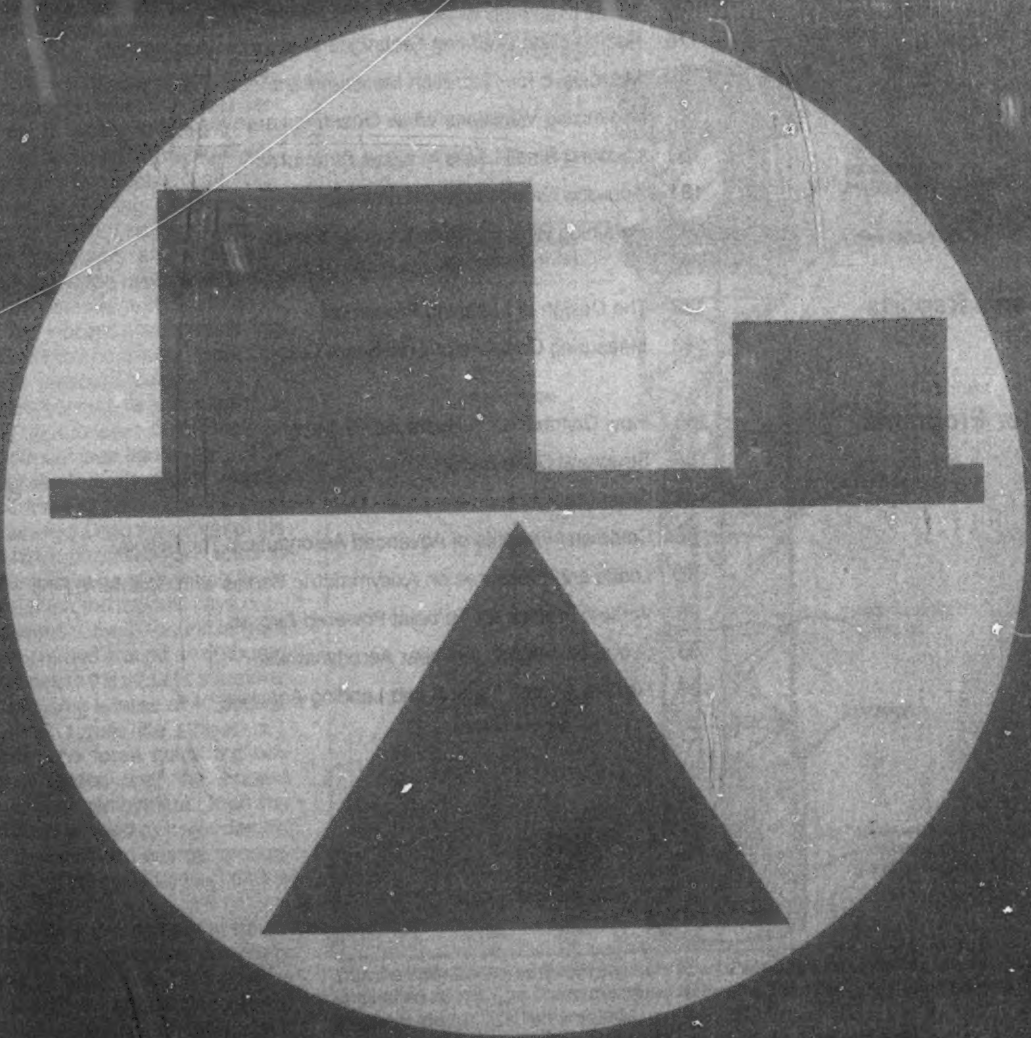

Hardware, Techniques, and Processes

175 Boom Deploys With Controlled Energy Release
176 Eliminating Wind-Tunnel Flow Breakdown
176 Vibration Analysis Reduces Computer Time
177 Optical Temperature Sensor Has Digital Output
178 Radionuclide Counting Technique Measures Wind Velocity
178 Microwave Ice-Accretion Measurement Instrument (MIAMI)
179 Minimizing Vibrations While Orienting Large Structures
180 Locating Small Leaks in Large Structures
181 Acoustic Ground-Impedance Meter
182 Retaining Ring Fastener for Solar Panels

Books and Reports

182 The Design of Lightning Protection
183 Measuring Contours of Coal-Seam Cuts

Computer Programs

183 Flow Distribution in Hydraulic Systems
184 Structural Optimization
184 Structural-Vibration-Response Data Analysis
185 Costs and Benefits of Advanced Aeronautical Technology
185 Loads and Pressures on Axisymmetric Bodies with Cruciform Fins
185 Vertical Profiles for Turbojet-Powered Aircraft
186 Supersonic-Wind Nonlinear Aerodynamics
186 Flexible Aircraft Takeoff and Landing Analysis

Boom Deploys With Controlled Energy Release

A lanyard and a spring-mounted viscous damper regulate rate of stored-energy expenditure.

NASA's Jet Propulsion Laboratory, Pasadena, California

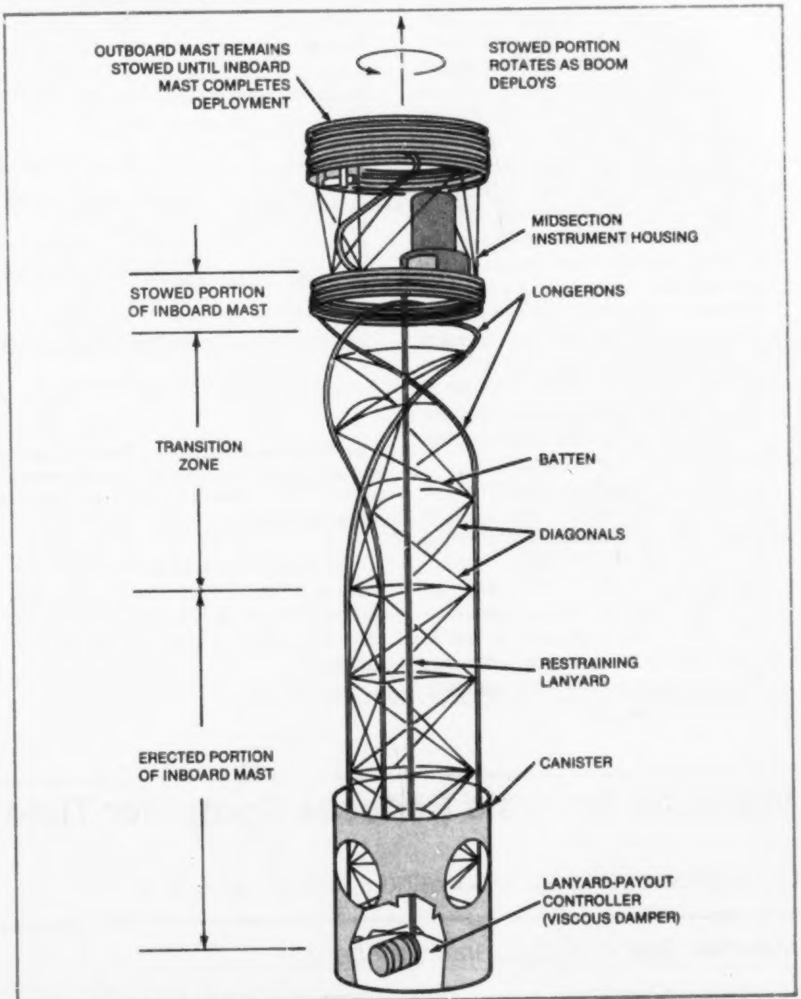
OUTBOARD MAST REMAINS STOWED UNTIL INBOARD MAST COMPLETES DEPLOYMENT
STOWED PORTION ROTATES AS BOOM DEPLOYS
MIDSECTION INSTRUMENT HOUSING
STOWED PORTION OF INBOARD MAST
LONGERONS
TRANSITION ZONE
BATTEN
DIAGONALS
RESTRAINING LANYARD
ERECTED PORTION OF INBOARD MAST
CANISTER
LANYARD-PAYOUT CONTROLLER (VISCOUS DAMPER)

This **Partially Deployed Boom** consists of an erect base, an uncoiling transition zone, and still-coiled zones. The boom members form a lattice structure that is shear-stiffened by diagonal elements when erected.

A collapsible boom is deployed in a controlled fashion, yet has no electric or commandable elements. In effect, the structure consists of many fiberglass "springs" that are forcibly coiled during initial stowage in a canister. A considerable amount of energy stored in the structure is released during deployment.

The boom has two sections: an "outboard" mast, containing electronic instrumentation or other hardware that is carried by the boom, and "inboard" mast, which holds the canister in which the collapsed boom is stored before it is deployed. The inboard mast unfolds first during the deployment sequence, followed by the outboard mast.

The deployment rate is controlled by a viscous damper located at the base of the inboard mast (see figure). As the inboard mast deploys, its elastic energy produces a force of 20 pounds (89 newtons) on a lanyard along the center of the mast. The lanyard transmits the force to a rotary damper at its end, which limits the rate at which the lanyard pays out.

Simultaneously, the 20-pound lanyard force is transmitted around an outboard pulley and back to the inboard structure, thereby producing a force of 40 pounds (178 newtons) across the stowed outboard mast. The force holds the outboard mast closed until the inboard mast completes deployment. Then the outboard mast is freed to begin deployment by its own stored energy, producing a 10-pound (45-newton) load on the lanyard.

Springs initiate deployment at the inboard end of the longitudinal members (longerons) of each mast. The springs produce a uniform torque through the first 45° of longeron uncoiling and guarantee that the erection sequence will begin as shown in the figure.

The batten members are 14 percent smaller in diameter in the first and second batten frames on the inboard end of each mast. This provision ensures that the base of the mast will lock up into a fully erect structure before the remaining stowed portions of the mast begin to deploy.

At the completion of deployment, a large transient load is applied to the lanyard from the final release of stored energy as the longerons rapidly rotate into their fully deployed state. The peakload can be as great as 220 pounds (980 newtons) and could break the lanyard. To prevent a break, the viscous damper is attached to the baseplate by springs. When the spring force is exceeded by the peak deployment force, the body of the rotary damper rotates, paying out additional lanyard and greatly reducing the lanyard load.

The controlled deployment sequence allows a boom 27 feet (8.2 meters) long to be uncoiled from a canister only 2 feet (0.61 meter) high. Possible applications include antennas and other lightweight structures that are rapidly erected in the field.

This work was done by Douglas T. Packard of Caltech and Max D. Benton and Robert F. Crawford of AEC-ABLE Corp. for **NASA's Jet Propulsion Laboratory.** *For further information, Circle 36 on the TSP Request Card.*
NPO-15418

Eliminating Wind-Tunnel Flow Breakdown

Floor nozzle ensures more realistic airflow.

Ames Research Center, Moffett Field, California

Undesirable vortexes near the floor in small wind tunnels are suppressed by a simple device that alters the flow pattern there. Air is injected along the floor and interacts with the backflow from the wind-tunnel model. This results in a smoother, more correct airflow and so to more-reliable wind-tunnel data.

Models of high-lift aircraft are difficult to test in small wind tunnels because they create jets of air that disturb airflow in unpredictable ways. A jet of air emerging from an aircraft model strikes the tunnel floor and spreads out forward (against the main airflow) and aft (see figure, left). The forward-moving part of the jet forms a vortex that disrupts the main flow, causing the phenomenon known as tunnel flow breakdown.

However, if air is blown through a nozzle on the tunnel floor into the forward-spreading jet, the vortex is prevented from forming (see figure, right). Instead, the blowing jet creates a mixing region that hardly interferes with the flow at the model. The model experiences better lift, and test data correlate well with data from large tunnels after standard corrections are applied.

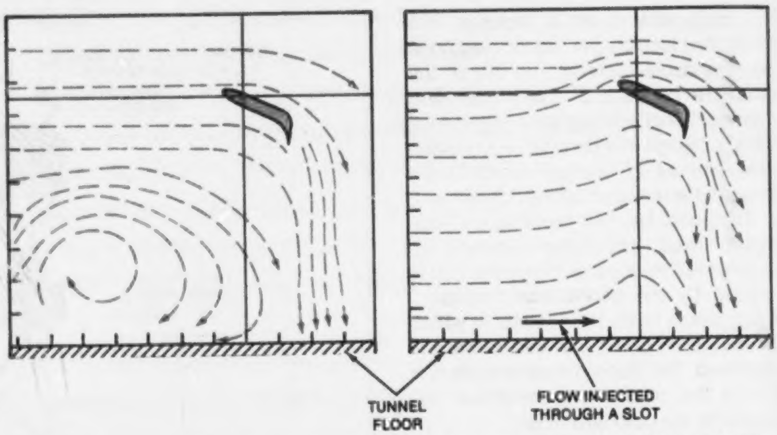

A Vortex Is Suppressed by a Blowing Jet from a floor nozzle. Without the floor jet (left), the vortex disturbs the main airflow around an aerodynamic model. With the floor jet (right), turbulent air is blown downstream. The flow vectors are plotted from laser velocimeter measurements.

The floor jets are easy to use. At the start of a test, the appropriate floor-jet airflow is set up with a valve. The test is then run without further adjustment of airflow.

This work was done by James E. Hackett of Lockheed-Georgia Co. for **Ames Research Center.** *No further documentation is available.*
ARC-11338

Vibration Analysis Reduces Computer Time

Calculation cost is reduced without loss of accuracy.

Marshall Space Flight Center, Alabama

An improved calculation method promises to reduce computer time by a factor of 10 for vibration analysis of complex structures. The method was originally developed to predict the mechanical response of a spacecraft to maneuvers in various cases in which the same booster is used with different payloads (see figure). Many nonaerospace applications are possible whenever major components of a system remain the same while some are varied: These include the design of vehicles and the design or modification of floors, walls, and structural modules.

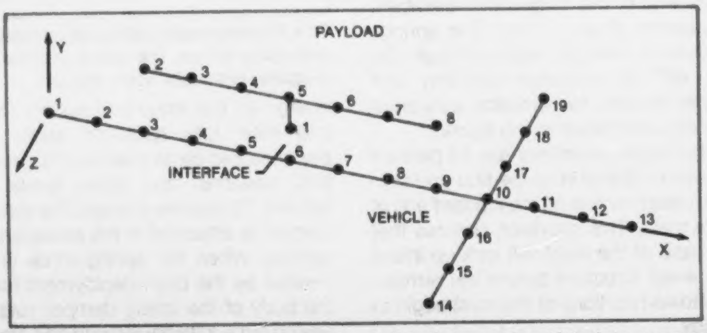

A Representative Analysis separates payload, interface, and vehicle into segmented finite elements. Values of acceleration, velocity, and displacement calculated by the new method and the conventional method differed by as little as a few parts per million.

The method is more exact than conventional normal-mode methods in that it involves no initial approximations or assumptions. An adaptation of the Newmark-Chan-Beta numerical integration technique is directly applied to the coupled system equations, and thus the expensive solution of a system eigenvalue problem is avoided. In the Newmark-Chan-Beta technique, the step size can be based on the cutoff frequency associated with the forcing function regardless of the highest system frequency — a valuable feature since the highest system frequency is usually not known in advance.

Several improvements over conventional techniques and cost-saving features were introduced in the new method. For an indeterminate interface, it is not necessary to express the interface displacements in terms of accelerations and forces. Several simplifications were made in the preliminary calculations that lead to more efficient and convenient calculation of loads.

The method is readily adaptable to short cuts. For example, if a solution of a response and load problem is already available and design changes are made in the payload, it is possible to develop a criterion to determine whether the loads will change significantly.

This work was done by Remi C. Engels of Martin Marietta Aerospace for **Marshall Space Flight Center.** *For further information, Circle 37 on the TSP Request Card.*
MFS-25711

Optical Temperature Sensor Has Digital Output

Device uses a Fabry-Perot multiple-beam fringe sensor.

Lewis Research Center, Cleveland, Ohio

A new instrument* from the world of fiber optics can measure temperatures reliably and accurately. A remote light source feeds light into an optical fiber or cable. The measurement end of the fiber is attached to a Fabry-Perot sensor, which consists of a small spacing that varies with temperature. This spacing is controlled by a temperature-sensitive material. A second output fiber transmits the light passing through this "Fabry-Perot" gap to a photodetection unit and finally to a decoder, before the output is routed to the utilization means.

The gap widens as temperature increases. With this increase in temperature is an increase in the number of spectral bands passing to the receiver. The count of the number of bands passed to the decoder is translated into temperature changes.

A number of advantages accrue to this optical system. Both the temperature sensor and the optical lines are free of all electrical and electromagnetic effects and interference. Variation in the spacer can be made sensitive to other physical quantities, such as pressure. The sensing element itself can be made quite small, enhancing its use in confined areas.

*NOTE: This new instrument is a prototype that is still being further developed; therefore, its accuracy and repeatability have not been determined.

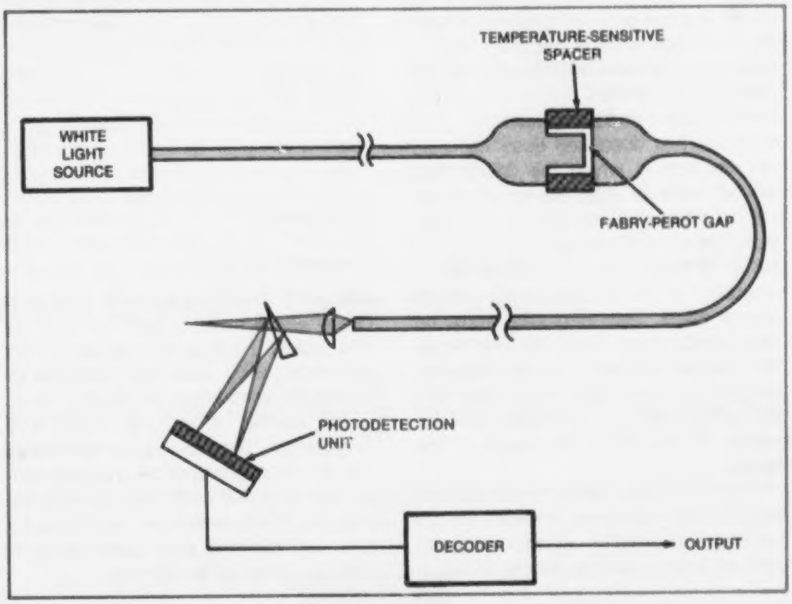

The **Fiber-Optics Temperature Sensor** is free of electromagnetic interference. The sensing element can be made quite small, enhancing its use in confined areas.

This work was done by K. A. James, W. H. Quick, and V. H. Strahan of Rockwell International Corp. for **Lewis Research Center.** *Further information may be found in NASA CR-159519 [N79-27975/NSP], "Analysis and Preliminary Design of Optical Sensors for Propulsion Control" [$10.50]. A copy may be purchased [prepayment required] from the National Technical Information Service, Springfield, Virginia 22161.*

Inquiries concerning rights for the commercial use of this invention should be addressed to the Patent Counsel, Lewis Research Center [see page A5]. Refer to LEW-13413.

Radionuclide Counting Technique Measures Wind Velocity

The change in position of a radioactive source translates into wind-velocity measurement.

Langley Research Center, Hampton, Virginia

A proposed technique for measuring wind velocity is based on the inverse-square-law variation of radioactive counting rates. In the proposal, a radioactive source is deposited on the bottom of a light, hollow sphere, such as a plastic table-tennis ball, and suspended by a flexible wire over a radiation counter. The ball can be punctured with symmetrically distributed holes or otherwise roughened for aerodynamic stability.

If the source position is changed because of wind drag on the ball, the solid angle subtended by the counter decreases, and the counting rate is reduced. A graph of counting rate as a function of source position would be used to determine the source position and the wind drag on the ball.

The single-source/single-detector anemometer just described does not yield the direction in which the source has moved, however. Also, the counting rate will not change if the source is moved along the circumference of a circle, the center of which lies on the center of the projection of the counter window on the source plane. This ambiguity would be removed by using three coplanar radiation counters located at equal distances along the circumference of a circle with the undisplaced source hanging over the center of the circle, as shown in the figure.

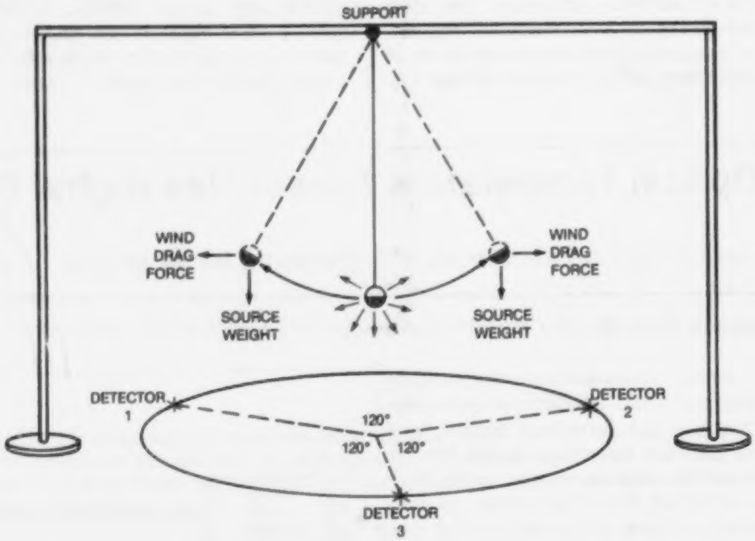

A **Radioactive Source** suspended over three detectors yields both windspeed and wind direction. The concept has been tested using a weak Bismuth 207 source and three Geiger-Müller counters.

An anemometer based on this concept would be self-contained, portable, yet not too fragile. It could be used for extended periods of time, even at remote, inhospitable, and inaccessible sites. The proposed anemometer would be accurate and would have good frequency response (≤1 kHz). Calibration would be affected only by changes in humidity. Thus, in fair weather, it would be stable over long periods. The only requirement is that the radiation detectors be checked periodically to make sure they are working properly. The anemometer would require little maintenance and could measure wind velocities up to 100 m/s.

This work was done by Jag J. Singh of **Langley Research Center,** *G. S. Khandelwal of Old Dominion University, and Gerald H. Mall of Computer Sciences Corp. Further information may be found in NASA TM-83202 [N82-12419/NSP], "A Radionuclide Counting Technique for Measuring Wind Velocity" [$6]. A copy may be purchased [prepayment required] from the National Technical Information Service, Springfield, Virginia 22161.*
LAR-12971

Microwave Ice-Accretion Measurement Instrument (MIAMI)

Microwaves detect icing on aircraft surfaces.

Lewis Research Center, Cleveland, Ohio

An instrument can be used on operational aircraft to warn the pilot of the onset of dangerous ice buildup or as a research tool for use in studying aircraft icing phenomena and in cloud research. Other ice-detection instruments use probes that project from the surface on which ice will collect, thus creating the problem of having to infer how much ice is really on the surface of interest. This is particularly troublesome when the surface of interest is an aircraft surface since the water-droplet catch efficiencies will be different for the ice-detector probe and the aircraft surface. The MIAMI is embedded in the surface to be monitored and conforms to the surface contour. It automatically measures the ice forming on the surface of interest. The MIAMI is the only instrument that measures actual ice thickness and accretion rate in addition to giving an icing-onset warning.

The MIAMI detects the onset of icing on a surface (e.g., aircraft wing), continuously monitors ice thickness, and displays ice thickness and accretion rate. A small, 1.4- by 0.4- by 0.2 inch (35.5- by 10.2- by 5.08-mm), microwave waveguide is implanted just below the surface to be monitored. One or more waveguides may be mounted on different components of the aircraft. A microprocessor monitors the resonant frequency of the waveguide(s). As ice forms on the surface of the waveguide, it causes the waveguide resonant frequency to decrease. The frequency shift is measured by the microprocessor and converted to a dc voltage that is proportional to the ice thickness. The microprocessor also computes the change in ice thickness with respect to time to get the ice-accretion rate. The ice thickness and accretion rates are displayed on digital panel meters.

The theoretical basis for the development of the MIAMI is that a resonant surface waveguide is tuned by the application of a substance (such as ice) with approximately the same dielectric constant as the waveguide material. The resonant frequency of the transducer is very sensitive to the thickness of the ice accreting on top of it. Ice layers of approximately 0.005 to 0.100 inch (0.13 to 2.5 mm) are capable of being measured. The transducer and its associated microprocessor convert the ice thickness to a dc voltage that varies in time in a manner proportional to the ice thickness. The time derivative of this voltage is proportionate to the icing severity (accretion rate) and is continuously being computed and displayed by the microprocessor either as a severity level ("TRACE," "LIGHT," "MODERATE," or "HEAVY") or numerically in inches or centimeters per minute.

The effect of ice on the transducer is different from other substances, such as oil, grease, dirt, insects, or other contaminants. The microprocessor is programed to recognize the difference between ice and other substances so that valid icing signals are generated only when ice forms. Water droplets that may form in the boundary layer are neglected by the system. Should a contaminant or foreign body other than ice adhere to the surface of the MIAMI, a continuous tone will be generated providing a fail-safe indication of its operating ability until the foreign object is removed.

Because no probe projects into the airspace, the transducer may be mounted anywhere on the aircraft without interfering with the aerodynamic properties of the aircraft. Also, since no probe exists, there is no opportunity to damage it or break it off or have it ingested by the engine.

If desired, the MIAMI transducer may be equipped with an electrothermal deicer to remove existing ice. With the MIAMI, ice removal is not necessary until the ice thickness exceeds its dynamic range [0.125 inch (3.2 mm)]. Deicing may be programed to occur repetitively in a manner analogous to magnetostrictive transducers or not to occur until the transducer approaches the limit of its dynamic range, thereby saving aircraft energy. The MIAMI will provide a complete history of ice thickness, including the loss of ice by intentional deicing or natural causes.

This work was done by Bertram Magenheim of Ideal Research, Inc., for **Lewis Research Center.** *For further information, Circle 38 on the TSP Request Card.*
LEW-13784

Minimizing Vibrations While Orienting Large Structures

Control algorithm times thrustor pulses to minimize vibrations.

Marshall Space Flight Center, Alabama

Structural vibrations and dynamic loads have been theoretically analyzed for their effects on the pointing and sluing of a large antenna (100 meters in diameter) deployed from the Space Shuttle at the end of a 100-m-long mast. The analysis resulted in a control algorithm that insures pointing accuracy while minimizing vibrations of the long flexible mast. The approach is applicable to terrestrial antennas or other large lightweight structures.

To point the antenna in a particular direction, the Space Shuttle is maneuvered into the appropriate orientation by its pitch, roll, and yaw thrustors. This involves a problem in vibration and attitude control analogous to that of carrying a bowl of soup: One has to move carefully to avoid spills.

(continued on next page)

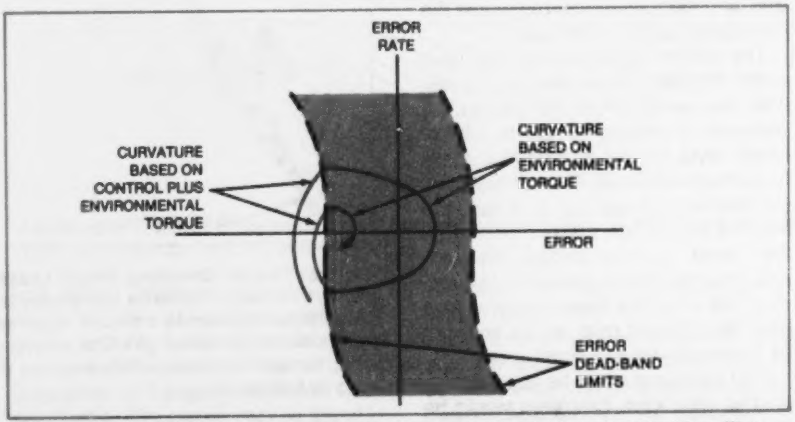
ERROR RATE
CURVATURE BASED ON CONTROL PLUS ENVIRONMENTAL TORQUE
CURVATURE BASED ON ENVIRONMENTAL TORQUE
ERROR
ERROR DEAD-BAND LIMITS

Attitude Error and Error Rate are minimized by a properly-designed control law. The control thrustor returns the attitude to a point within the control dead band whenever the attitude error or error rate strays outside. Within the dead band, the attitude drifts under environmental torque. The leftward thrustor fires when the system phase point is to the right of the error dead band. The opposite is the case for the rightward thrustor.

Similarly, the Space Shuttle or other platform carrying a large antenna on the end of a flexible mast must be moved carefully to avoid setting up oscillations in the mast. Therefore step-by-step plans (more specifically, the turn-on and turn-off times for the thrustor pulses) must be devised for each maneuver, and the mast must be designed to conform to the characteristics of the thrustors.

The analysis resulted in a combined attitude-and-vibration-control law for the attitude-control vernier thrustors. The control law is a function of the calculated vibration modes of the structure, and of the response of the system to environmental torques (gravity gradient, aerodynamic, and solar radiation). The system response to a single control pulse is computed by numerically integrating the equations of motion. The performance of a representative system is illustrated in the figure.

This work was done by Fred Austin of Grumman Aerospace Corp. for **Marshall Space Flight Center.** *For further information, Circle 39 on the TSP Request Card.*
MFS-25439

Locating Small Leaks in Large Structures

"Dead" needle pinpoints small leaks.

Lyndon B. Johnson Space Center, Houston, Texas

A "dead" needle technique pinpoints the exact locations of very small leaks in plumbing and vacuum systems. The new technique confines helium exposure to a small region rather than flooding the entire leak area with helium gas.

In conventional leak detection, helium gas is usually fed to the vicinity of the leak under low pressure, while a mass-spectrometer leak detector monitors the interior of the system for the presence of helium gas. While this method indicates whether or not a leak is present and notes the approximate location of the leak, it usually does not precisely pinpoint the leak. The helium gas floods too wide an area around the leak to enable the operator to determine the leak position with certainty. With the new technique the helium source is not pressurized, and the gas is localized to just the immediate vicinity of the leak.

The test tool uses a fine-control valve and a hypodermic needle (see figure). After the needle is filled with helium, the pressure is allowed to fall to atmospheric level, so that no helium actually flows from the needle if the air is still. As the needle is brought up to a leak, the leak-induced airflow draws helium from the "dead" needle, through the leak, and into the helium detector. This occurs only when the needle is very close (less than about 1 mm), so the leak can be located to within a small area.

This technique could be applied in industrial situations. Examples would be nuclear-powerplant plumbing, valve-and-pump bodies, vacuum systems, or pressure vessels.

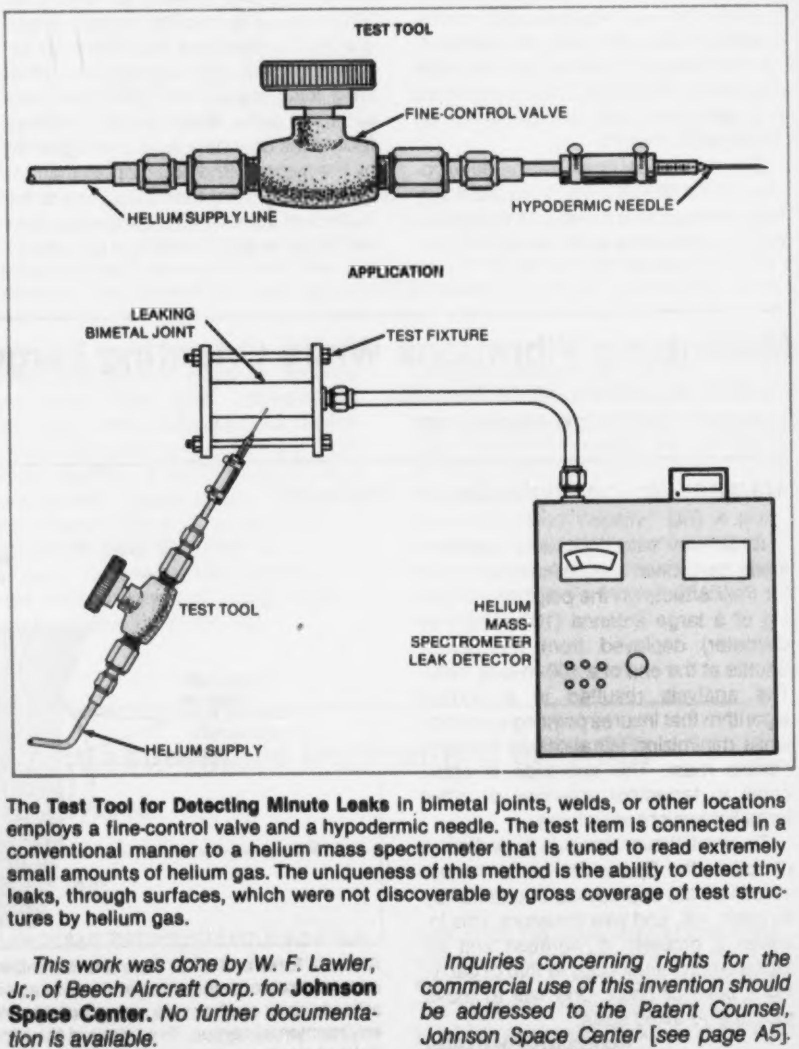

The Test Tool for Detecting Minute Leaks in bimetal joints, welds, or other locations employs a fine-control valve and a hypodermic needle. The test item is connected in a conventional manner to a helium mass spectrometer that is tuned to read extremely small amounts of helium gas. The uniqueness of this method is the ability to detect tiny leaks, through surfaces, which were not discoverable by gross coverage of test structures by helium gas.

This work was done by W. F. Lawler, Jr., of Beech Aircraft Corp. for **Johnson Space Center.** *No further documentation is available.*

Inquiries concerning rights for the commercial use of this invention should be addressed to the Patent Counsel, Johnson Space Center [see page A5]. Refer to MSC-20327.

Acoustic Ground-Impedance Meter

Portable device is based on the Helmholtz-resonator principle.

Langley Research Center, Hampton, Virginia

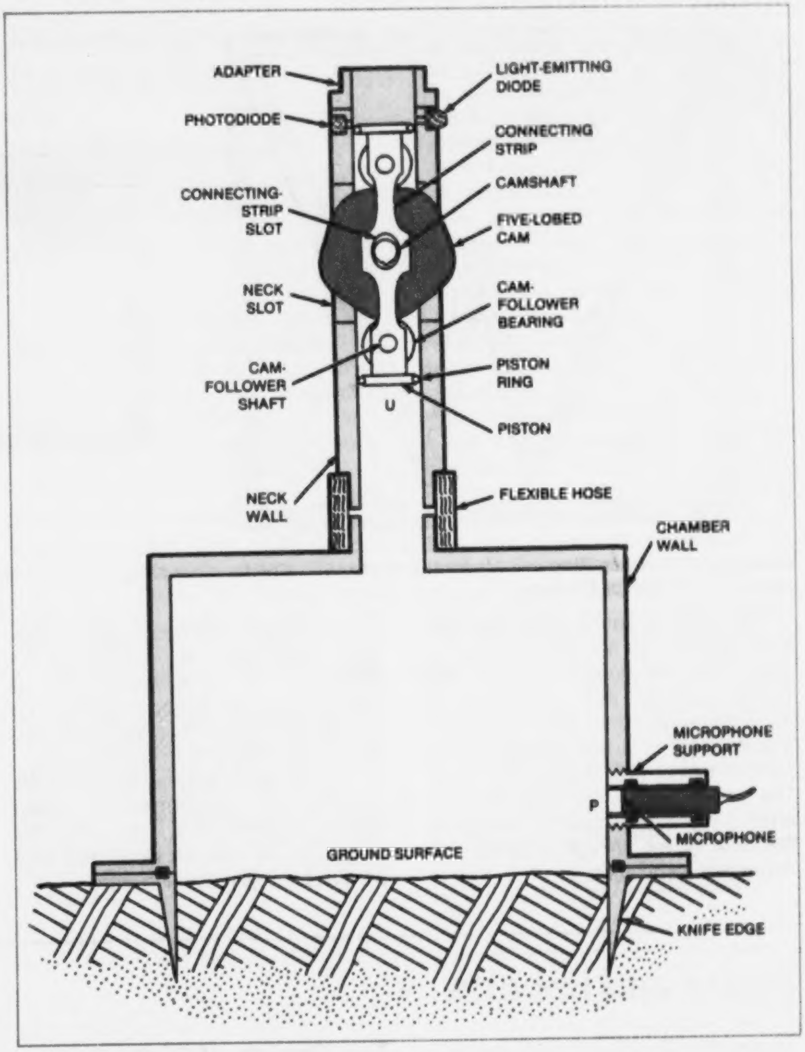

A Helmholtz Chamber is sealed to the test surface by a sharp knife edge. The resonator is 0.220 m in diameter by 0.152 m in height.

A Helmholtz resonator is used in a compact, portable meter that measures the acoustic impedance of the ground or other surfaces. The Earth's surface is the subject of increasing acoustical investigations because of its importance in aircraft noise prediction and measurement.

Constructed of heavy-walled stainless steel but open at the bottom, the resonator is positioned over a surface having unknown impedance. The sound source, a cam-driven piston of known stroke and thus known volume velocity, is located in the resonator neck. The cam speed is variable up to a maximum of 3,600 rpm.

The sound pressure at the test surface is measured by a microphone flush-mounted with the wall of the chamber. An optical monitor of the piston displacement permits measurement of the phase angle between the volume velocity and the sound pressure, from which the real and imaginary parts of the impedance are evaluated. Measurements using a 5-lobed cam can be made up to 300 Hz; these can be extended to nearly 1,000 Hz by a 15-lobed cam.

Previous methods for measuring the acoustic impedance of the ground, all having various unsatisfactory features, are organized into the three basic categories of impedance tube, free field, and direct sound-pressure/volume-velocity measurements. The acoustic ground-impedance meter utilizes direct pressure/volume-velocity measurement, but avoids the major difficulty in the measurement of volume velocity found with other such methods in that the volume velocity is defined by the known stroke of a cam-driven piston.

The acoustic ground-impedance meter offers several advantages. It is compact and portable and can be set up at any test site, irrespective of landscape features, weather, or other environmental conditions. Its speed of operation makes it well suited for use in conjunction with other acoustic measurements, such as aircraft noise measurements; and its operation is simple: At each frequency the acoustic impedance is evaluated from the measurement of one sound pressure and one phase angle for the test surface and from similar data for a calibration plate.

This work was done by Allan J. Zuckerwar of **Langley Research Center.** *Further information may be found in NASA TM-83227 [N82-17476/NSP], "Acoustic Ground Impedance Meter" [$6]. A copy may be purchased [prepayment required] from the National Technical Information Service, Springfield, Virginia 22161.*

This invention is owned by NASA, and a patent application has been filed. Inquiries concerning nonexclusive or exclusive license for its commercial development should be addressed to the Patent Counsel, Langley Research Center [see page A5]. Refer to LAR-12995.

Retaining Ring Fastener for Solar Panels

A collapsible linkage enables rapid installation and removal of panels.

NASA's Jet Propulsion Laboratory, Pasadena, California

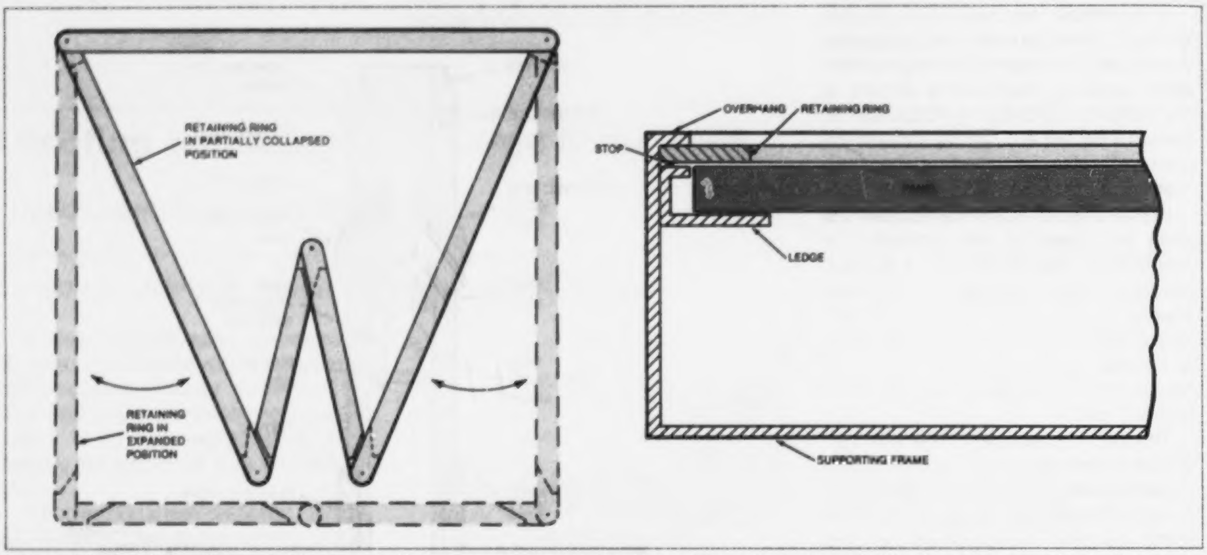
RETAINING RING IN PARTIALLY COLLAPSED POSITION
RETAINING RING IN EXPANDED POSITION
OVERHANG
RETAINING RING
STOP
PANEL
LEDGE
SUPPORTING FRAME

Collapsible Retaining Ring unfolds from a W-shape to a rectangular shape. The unfolded ring holds the solar panel in the frame as shown at the right of the figure.

A simple articulating linkage secures solar panels into a supporting framework. The five-element linkage (see figure) collapses into a W-shape for easy placement into the framework, then expands to form a rectangle of the same dimensions as those of the panel. The result is a large retaining ring around the outer edges of the panel. Removal of the linkage is simply the reverse of installation.

Solar panels mounted on angled supports must often be installed or removed quickly. Conventional fastening methods, such as bolting and unbolting, can be laborious, time consuming, and may require more than one person.

The new quick fastener simplifies the removal and replacement of panels during maintenance. The fastener could also be used on removable wall panels, photographs, and signs.

This work was done by Abraham H. Wilson of Caltech for **NASA's Jet Propulsion Laboratory.** *For further information, Circle 40 on the TSP Request Card.*

Inquiries concerning rights for the commercial use of this invention should be addressed to the Patent Counsel, NASA Resident Office-JPL [see page A5]. Refer to NPO-15369.

Books and Reports

These reports, studies, and handbooks are available from NASA as Technical Support Packages (TSP's) when a Request Card number is cited; otherwise they are available from the National Technical Information Service.

The Design of Lightning Protection

Engineering study could guide the design and monitoring of lightning protection.

Severe environmental conditions, including hurricane-force winds and a corrosive seacoast atmosphere, as well as the need for a 10-year system lifetime were taken into account when refitting and transferring an existing lightning protection system to the Space Shuttle service and access tower. Many components of the system were salvaged from a system used to protect the Apollo-Soyuz mobile launcher.

Engineering design studies for this project have been collected in a 150-page report. It contains a wealth of information both on the design of lightning protection systems and on instrumentation for monitoring the current waveforms of lightning strokes. Also included are the results of examinations of the components of the earlier system that had successfully sustained a direct lightning strike.

Basically, the lightning protection system consists of a 1/2-inch (12.7-mm) stainless-steel wire-rope catenary cable strung over the launchsite in a broad inverted V. At the apex 390 ft (119 m) above ground, the cable is supported by a 65-ft (20-m) fiberglass insulating mast that is mounted atop a hammerhead crane. The cable is anchored at points 1,000 ft (305 m) on either side of the tower and is stretched to clear all grounded objects by at least 50 ft (15 m). The cable is grounded at each end through current coils, which are part of the lightning current-monitoring system.

The lightning current-monitoring system is designed to monitor the first 100 μs of each ligthning stroke; the current range is 2 to 200 kA. Current is monitored via the voltage across the coils at each end of the cable. The rate of change of current is monitored and integrated to obtain the current. To protect the event recorders that monitor the lightning strokes, the signals from the transient recorder are transmitted optically to the data lines.

Various other structural and safety considerations were studied. Loads from hurricane-force winds impose requirements more severe than those due to launch conditions.

Floodlighting of the mast was selected as the simplest economical way to provide aircraft safety warning. The report also describes the testing of ablative coatings used to protect the mast from repeated exposure to the heating effects of Space Shuttle launches.

This work was done by Planning Research Corp. for **Kennedy Space Center.** *Further information may be found in NASA TR-1530 [N81-31277/NSP], "Lightning Protection System for Space Shuttle" [$15]. A copy may be purchased [prepayment required] from the National Technical Information Service, Springfield, Virginia 22161.*
KSC-11224

Measuring Contours of Coal-Seam Cuts

Microprocessor-based instrument integrates small changes in angle and distance.

A final report describes work on an automated system for measuring the contour of a coal face as it is mined by a longwall shearer. [See "Transducer System Traces Mine-Face Curve," (MFS-25289), p. 424, [*NASA Tech Briefs*, Vol. 6, No. 4 (Spring/Summer 1982).]

Angle transducers measure the angle between track sections as the longwall shearer proceeds along the coal face. A distance transducer functions in conjunction with the angle transducers to obtain relative angles at known positions. When a cut is complete, the accumulated data are stored on cassette tape, and the track profile is computed and displayed. The angle and distance transducers are intrinsically safe in the potentially hazardous environment of a coal mine and therefore need no special packaging . The data storge and reduction electronics are not intrinsically safe but are housed in an explosionproof enclosure.

The angle transducers are brushless resolvers in a support structure called the angle cart. The transducers are directly connected to angle-measuring shoes. The angle between track sections is measured differentially by the two resolvers, which are attached to a common reference surface.

Distance is measured by counting pulses that originate from an optical encoder. The encoder is in a support structure called the distance cart. A five-point star-wheel-type gear in the distance cart makes contact with the track and rotates one-fifth of a revolution for each 126 mm of forward travel. Gears transmit the star-wheel rotation to the encoder. The reference point from which distance is measured is established by the simultaneous activation of limit switches and the encoder zero pulse. Once the zero reference point is established, absolute distance is measured by an up/down counter, which accumulates pulses from the encoder as the shearer moves along the face.

Yet another transducer — for roll measurement — is contained within the explosionproof enclosure. The transducer determines the deviation of the face from vertical. The transducer produces an electrical signal proportional to the angular displacement of a pendulum submerged in a damping fluid.

A microprocessor in the explosionproof enclosure calculates the cut surface contour from the trigonometric relations among track angles, distance, and roll measurements. The data reduction process for a 600-ft. (183-m) track takes about 2 minutes.

This work was done by Benton Corp. for **Marshall Space Flight Center.** *To obtain a copy of the report, Circle 41 on the TSP Request Card.*
MFS-25734

Computer Programs

These programs may be obtained at very reasonable cost from COSMIC, a facility sponsored by NASA to make new programs available to the public. For information on program price, size, and availability, circle the reference letter on the COSMIC Request Card in this issue.

Flow Distribution in Hydraulic Systems

Program solves fixed or variable flow problems for series, parallel, or series/parallel systems.

The General Flow Distribution Program analyzes pressure drops and flow distribution in closed and open hydraulic systems. It analyzes a system on the basis of incompressible flow even though the system may contain either compressible or incompressible fluid. The program has been used to analyze Space Shuttle orbiter hydraulic systems used for environmental control and life support. The General Flow Distribution Program solves fixed or variable flow problems for series, parallel, or series/parallel systems.

A flow system is represented by a nodal network with elements of flow resistance. Either a closed network with

(continued on next page)

pumps and fans or an open network with a known total fixed flow rate may be analyzed. The adjustment of variables is permitted through the use of user-supplied routines.

The analytical method is generally based on the successive-approximation method. Flow across a resistance, which may be either a duct, tube, or a black box with known characteristics, is calculated using the Bernoulli pressure-drop equation. Starting with assumed pressures at active nodes, the program iteratively corrects the pressures and flows until pressure and flow balance tests are satisfied. The balanced pressure drops and flows computed are output as analysis results.

This program is written in FORTRAN V for batch execution and has been implemented on a CDC CYBER 170-series computer. As currently dimensioned to accommodate a network of up to 500 nodes and 1,000 line elements, the program has a central memory requirement of approximately 77K (octal) of 60-bit words. The program was developed in 1980.

This program was written by Son N. Nguyen of Rockwell International Corp. for **Johnson Space Center.** *For further information, Circle C on the COSMIC Request Card.*
MSC-20306

Structural Optimization

An interface between SPAR structural analysis and CONMIN optimization

The Programming Structural Synthesis System (PROSSS) provides structural synthesis capability by combining the SPAR and CONMIN computer programs with a set of interface procedures. SPAR is a large general-purpose finite-element structural-analysis program, and CONMIN is a large general-purpose optimization program. The user supplies two small problem-dependent programs to define the design variables, constraints, and the objective function. Unlike many other structural-optimization programs, the design variables, constraints, and the objective function can be represented in PROSSS by any choice of quantities, or combination of quantities, that form input and output of structural analysis. This allows the user to solve practical optimization problems formulated in many different ways.

Execution of the PROSSS analysis/optimization process results in a set of optimum design variables and a minimized objective function subject to a set of constraints. Examples of the applications are (a) minimum-mass design with cross-sectional areas as variables and stress constraints, or (b) the first natural frequency as the objective function with overall shape design variables and stress and buckling constraints.

PROSSS is intended to be used in the following basic ways:

- As a research tool for developing optimization techniques that will interface with an efficient analysis program,
- As a research tool for testing new analysis techniques that will interface with an efficient optimization program, and
- As an application tool for a wide range of problems.

With PROSSS, the analysis and optimization programs are executed repeatedly in a loop until the process is stopped by a user-defined termination criterion. This part of the system is referred to as the repeatable part of PROSSS. However, some of the analysis, such as model definition, need only be done one time and can be saved for future use; these parts are performed outside of the loop and are referred to as the nonrepeatable part of PROSSS. Five options organize optimization procedures by combining nonlinear or piecewise linear programing methods with analytic or finite-difference gradients.

The analysis is always performed on the mainframe, a CDC 6000-series computer, because of the speed on the mainframe CPU. The end processor is also run on the mainframe to reduce the large amount of data generated by the analysis to the small amount of data required by the optimizer. The optimizer may be run on either the mainframe or the minicomputer, a PRIME 750 computer. The minicomputer offers the advantage of virtual memory; for many applications the optimizer requires a significant memory allocation. The primary difference in implementing PROSSS all on the CDC computer and in "distributing" part of PROSSS to the PRIME computer is the method of controlling the flow of the options.

PROSSS is written in FORTRAN IV for batch execution and has been implemented on a CDC 6000-series computer and a PRIME 750 computer. The implementation of PROSSS all on the CDC computer requires approximately 100K (octal) of 60-bit words. The PROSSS user must have access to the CDC version of SPAR (available from COSMIC). PROSSS was developed in 1981.

This program was written by James L. Rogers, Jr., and Jaroslaw Sobieszczanski-Sobieski of **Langley Research Center,** *Rama B. Bhat of George Washington University, and A. R. Dovi and K. M. Riley of Kentron International, Inc. For further information, Circle D on the COSMIC Request Card.*
LAR-13010

Structural-Vibration-Response Data Analysis

Modal frequencies and dampings are obtained from free-decay records.

One area in dynamic testing that continues to be of interest is the selection of a proper anlaylsis method for determining structural parameters from the measured data. A computer program was developed as a structural-vibration-response data analysis tool for use in the dynamic testing of the Space Shuttle.

The program provides a fast and efficient time-domain least-squares curve-fitting procedure for reducing transient response data to obtain structural modal frequencies and dampings from free-decay records. The procedure simultaneously identifies the frequencies, damping values, and participaton factors for noisy multiple-response records. The computer program and the methodology it is based on can be applied to the analysis of transient response data for a wide range of structures and might also be applied to such other areas as the analysis of seismograms.

This program is written in FORTRAN IV for batch execution and has been implemented on an IBM 370-series computer with a central memory requirement of approximately 970K of 8-bit bytes. The program was developed in 1981.

This program was written by William R. Smith, Richard N. Hechenlaible, and Ramon C. Perez of Rockwell International Corp. for **Johnson Space Center.** *For further information, Circle E on the COSMIC Request Card.*
MSC-20182

Costs and Benefits of Advanced Aeronautical Technology

Programs determine the advantages and disadvantages of advanced technology applied to civil aircraft.

Programs available from COSMIC can be used to evaluate the economic feasibility of applying advanced aeronautical technology to civil aircraft of the future. The programs are composed of three major models:

- The Fleet Accounting Module,
- The Airframe Manufacturer Module,
- The Air Carrier Module.

The Fleet Accounting Module estimates the number of new aircraft required as a function of time to meet demand. This estimate is based primarily upon the expected retirement age of existing aircraft and the expected change in passenger-miles demand. Fuel consumption estimates are also generated by this module.

The Airframe Manufacturer Module analyzes the feasibility of manufacturing the new aircraft. This module includes logic for production scheduling and for estimating manufacturing costs. For a series of aircraft selling prices, cash flow is analyzed, and rates of return on investment are calculated.

The Air Carrier Module is a tool for analyzing the financial feasibility of an airline purchasing and operating the new aircraft. This module includes a methodology for computing direct and indirect operating costs, performing cash-flow analyses, and estimating the internal rates of return on investment for a set of aircraft purchase prices.

Input to the Fleet Accounting Module includes data describing growth rate of revenue passenger miles and flight load factors. Descriptions of currently operating aircraft are entered in terms of the year in which the aircraft became operational, seating capacity, fuel consumption, and normal retirement age. The type, number, and age of aircraft currently in operation are entered to complete the description. Similar data are required for the new aircraft that are potential replacements. The module output includes statistics describing the projected fleet composition and activity.

The input to the Airframe Manufacturer Module includes a detailed description of the manufacturing requirement for the new aircraft and the manufacturing cost data. The output includes data describing the manufacturers, their production capacity, the production scheduling, and selected cost parameters.

The input to the Air Carrier Module includes data on the carrier operations and cost factors. The output includes computed direct and indirect cost, as well as various statistics and parameters computed in the financial analysis.

The models are written in FORTRAN IV and COMPASS for batch execution and have been implemented on a CDC 7600 computer with a central memory requirement of approximately 154K (octal) of 60-bit words in small core memory and 144K (octal) of 60-bit words in large core memory. Plotted output is generated for a ZETA 230 plotting system. The models were developed in 1979.

This program was documented by J. C. Bobick, R. L. Braun, and R. E. Denny of SRI International for **Ames Research Center.** *For further information, Circle F on the COSMIC Request Card.*
ARC-11382

Loads and Pressures on Axisymmetric Bodies with Cruciform Fins

Program computes forces and moments on supersonic configurations experiencing pitch and roll.

The NSWCDM computer program calculates the aerodynamic loading and pressure distributions on supersonic configurations consisting of axisymmetric bodies with cruciform or planar canard and tail fins. This versatile program allows for the configuration to be pitched and rolled, and the fins may be deflected. The tail fins may be interdigitated with respect to the foward fins. Fins may have arbitrary planform and thickness but must be planar. The load calculations provide aerodynamic forces and moments acting on the entire configuration.

NSWCDM treats the body and lifting surfaces and performs vortex tracking along the complete configuration in a single application. The theoretical approach is based on representing the configuration components by three-dimensional singularities associated with supersonic, linear flow theory.

The body is modeled by a distribution of supersonic line sources, sinks, and doublets along the centerline. Constant u-velocity panels are laid out over the fins. Interference-containing constant u-velocity panels are placed around the body over a length at least equal to the fin root chord to account for finbody interference. Forebody vortex shedding is modeled by two potential flow vortexes with strengths and positions obtained from an analytical/empirical approach. Canard fin trailing-edge vorticity is calculated and tracked along the afterbody and tail with or without the body nose vortexes. The effects of the body nose and canard vortexes are included in the pressure distributions, and loads are computed for the body and fins. Afterbody vortexes, as well as leading and side-edge vortexes, are not accounted for.

Input to NSWCDM includes configuration geometry and modeling parameters, free-stream and body orientation parameters, and program control parameters. Output from the program includes intermediate and final results used in obtaining the aerodynamic loads and pressure distributions.

NSWCDM is written in FORTRAN IV for batch execution and has been implemented on a CDC CYBER 170-series computer with a central memory requirement of approximately 175K (octal) of 60-bit words. NSWCDM was developed in 1979.

This program was written by M. F. E. Dillenius and C. A. Smith of Nielsen Engineering & Research, Inc., for **Langley Research Center.** *For further information, Circle G on the COSMIC Request Card.*
LAR-12936

Vertical Profiles for Turbojet-Powered Aircraft

Optimum profile minimizes operating cost.

The OPTIM computer program generates optimum vertical profiles for turbojet-powered aircraft. Specifically, OPTIM generates a profile of altitude, airspeed, and flightpath angle as a function of the range between a given set of

(continued on next page)

origin and destination points for particular models of transport aircraft. The profile may be optimized in the sense of minimizing fuel or time or in minimizing the direct operating cost expressed as a combination of fuel and time.

Inputs to the program include the vertical wind profile, the aircraft takeoff weight, and the aircraft engine and aerodynamic characteristics. The optimum vertical flight profile is generated by calculating the airspeed and thrust required to minimize the Hamiltonian at specific energy increments.

OPTIM is written in FORTRAN IV for batch execution and has been implemented on a CDC 6000-series computer with a central memory requirement of approximately 140K (octal) of 60-bit words. The OPTIM program was released in 1981.

This program was written by John A. Sorensen and Mark H. Waters of Analytical Mechanics Associates, Inc., for **Langley Research Center.** *For further information, Circle H on the COSMIC Request Card.*
LAR-12940

Supersonic-Wing Nonlinear Aerodynamics

Predictions of wing overall force and moment coefficients are improved.

The Supersonic Wing Nonlinear Aerodynamics computer program, LTSTAR, estimates the nonlinear aerodynamics characteristics of a wing at supersonic speeds. This corrected linearized-theory method accounts for nonlinearities in the variation of basic pressure loadings with local surface slopes, predicts the degree of attainment of theoretical leading-edge thrust forces, and estimates detached leading-edge vortex loadings that result when the theoretical thrust forces are not fully realized.

The comparison of LTSTAR computations with experimental results show significant improvements in detailed wing-pressure distributions, particularly for large angles of attack and for regions of the wing where the flow is highly three-dimensional. The program provides generally improved predictions of the wing overall force and moment coefficients. LTSTAR could be useful in design studies aimed at aerodynamic performance optimization and in providing more-realistic tradeoff information for the selection of wing planform geometry and airfoil section parameters.

Input to the LTSTAR program includes wing planform data, free-stream conditions, wing camber, wing thickness, scaling options, and output options. The program output includes pressure coefficients along each chord, section normal and axial force coefficients, and the spanwise distribution of section force coefficients. With the chordwise distributions and section coefficients at each angle of attack, three sets of polars are output. The first set is for linearized theory with and without full leading-edge thrust, the second set includes nonlinear corrections, and the third includes estimates of attainable leading-edge thrust and vortex increments along with the nonlinear corrections.

The LTSTAR program is written in FORTRAN IV for batch execution and has been implemented on a CDC CYBER 170-series computer with a central memory requirement of approximately 150K (octal) of 60-bit words. The LTSTAR program was developed in 1980.

This program was written by Harry W. Carlson and Robert J. Mack of **Langley Research Center.** *For further information, Circle J on the COSMIC Request Card.*
LAR-12788

Flexible Aircraft Takeoff and Landing Analysis

Program includes maneuver logic and autopilots for glide slope, flare, landing, and takeoff.

The Flexible Aircraft Takeoff and Landing Analysis program, FATOLA, simulates aircraft takeoff and landing dynamics. FATOLA represents an airplane either as a rigid body with six degrees of freedom or as a flexible body with multiple degrees of freedom. The airframe flexibility is represented by the superposition of up to 20 free vibration modes on the rigid-body motions. The analysis includes maneuver logic and autopilots programed to control the aircraft during glide slope, flare, landing, and takeoff. The program is modular so that the performance of the aircraft in flight and during landing and ground maneuvers can be studied separately or in combination.

Nine effects are simulated in FATOLA:

1. Flexible aircraft control and performance during glide slope, flare, landing roll, and takeoff roll in the presence of changing winds, engine failures, brake failures, control-system failures, strut failures, and restrictions due to runway length, control variable limits, and timelags;
2. Landing-gear loads and dynamics for up to five gears;
3. Single and multiple engines (maximum of four), including selective engine reversing and failure;
4. Drag chute and spoiler effects;
5. Wheel braking (including skid control) and selective brake failure;
6. Ground effect aerodynamics;
7. Aircraft-carrier operations;
8. Inclined runways and runway perturbations; and
9. Flexible or rigid airframes.

Input to FATOLA includes data that describe runway roughness, vehicle geometry, flexibility and aerodynamic characteristics, landing gear(s), propulsion, and initial conditions, such as attitude, attitude-change rates, and velocities. The program time-integrates the equations of motion and outputs comprehensive information on the airframe, state-of-maneuver logic, autopilots, control response, and aircraft loads from impact, runway rollout, and ground operations. Flexible-body and total (elastic plus rigid-body) displacements, velocities, and accelerations are also output in the flexible-body option for up to 20 points on the aircraft.

The FATOLA program is written in FORTRAN IV for batch execution and has been implemented on a CDC 6000-series computer with an overlaid central memory requirement of approximately 115K (octal) of 60-bit words. FATOLA was developed in 1975 and last updated in 1978.

This program was written by Huey D. Carden and John R. McGehee of **Langley Research Center.** *For further information, Circle K on the COSMIC Request Card.*
LAR-12992

Machinery

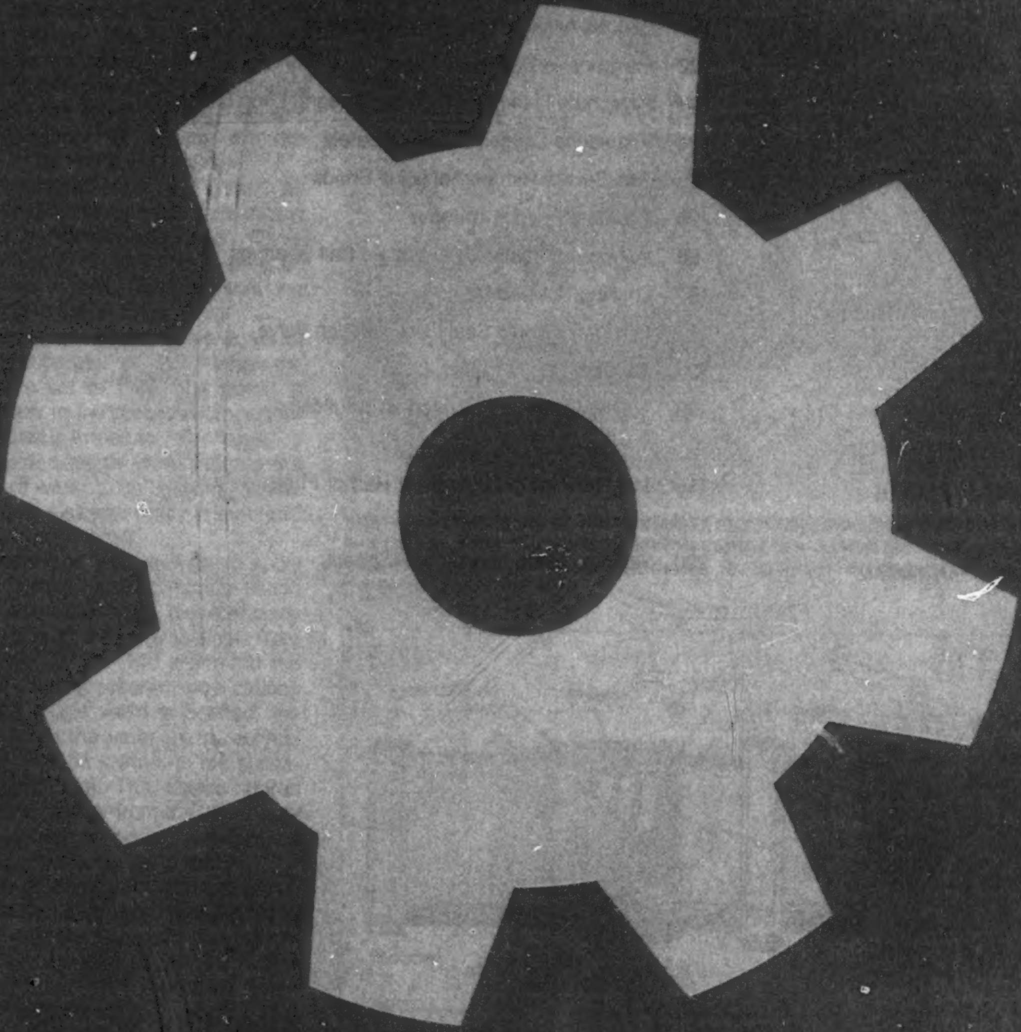

Hardware, Techniques, and Processes

189 Device Stores and Discharges Metered Fluid
190 Quick-Disconnect Fastener
190 Six-Axis Electrical-Discharge Machine
191 Padded Allen Wrench Grips Fastener
192 Inexpensive Bolt-Load Gage
193 Parachute Line Hook Includes Integral Loop Expander
194 Regulating Oxygen Pressure Safely
195 Tool Severs Hidden Adhesive Bonds
196 Coulomb Friction Damper
196 Inserts Automatically Lubricate Ball Bearings
197 Locking Nut and Bolt
197 Ferrofluid Would Seal Linear-Motion Valve
198 Portable Pipe Wrapper
199 Tubing Cutter Is Activated Hydraulically

Books and Reports

199 Light, Compact Pumper for Harbor Fires

Computer Programs

200 Rotating-Machinery Critical Speeds

Device Stores and Discharges Metered Fluid

A portable device accepts, stores, and discharges a preset amount of fluid.

Lyndon B. Johnson Space Center, Houston, Texas

A hand-held container accepts a measured amount of liquid from a pressurized supply. The supply pressure drives a spring-loaded piston that stores enough mechanical energy to discharge the measured liquid into another container. An operator triggers the discharge by turning a valve handle.

The container, shown in Figure 1, attaches to a water (or other fluid) supply through a "quick-disconnect" fitting. The desired amount of fluid is selected by turning a collar that controls the length of the piston travel.

A three-way selector valve is set at "fill," "discharge," or "off." When the selector is set to "fill," the piston is forced back to the preset volume. After the selector is turned to "discharge," a spring-loaded toggle valve triggers the delivery of water to its final destination. The device is stored safely in the "off" position when it is full.

The spring is long enough to apply nearly constant force against the piston over its operating range. It compresses under the liquid pressure available from the source [20 psi (140 kN/m^2) in the case of the spacecraft application]. Once the toggle valve is opened, the spring delivers the water at a lower pressure [15 psi (103 kN/m^2) in the spacecraft application]. The device stores mechanical energy from the water supply in the coiled spring and releases the energy by displacing the water.

The liquid comes into contact with a rolling rubber diaphragm (see Figure 2) but not with the piston. If the fluid is water, this feature keeps the water sterile until use and prevents corrosion of the metallic parts.

The original application of the container was to rehydrate sterilized prepackaged food in the zero-gravity environment of space vehicles. Its possible terrestrial applications include the dispensing of toxic fluids or the metering of fluids for household, commercial, or laboratory uses.

This work was done by Sonnie L. Hooper and Drel Setzer of Pan American World Airways, Inc., for **Johnson Space Center.** *For further information, Circle 42 on the TSP Request Card.*

This invention is owned by NASA, and a patent application has been filed. Inquiries concerning nonexclusive or exclusive license for its commercial development should be addressed to the Patent Counsel, Johnson Space Center [see page A5]. Refer to MSC-20275.

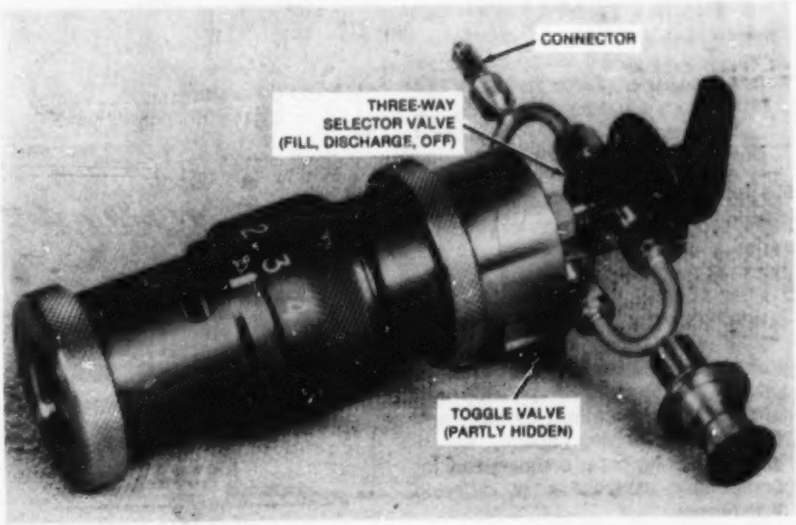
CONNECTOR
THREE-WAY SELECTOR VALVE (FILL, DISCHARGE, OFF)
TOGGLE VALVE (PARTLY HIDDEN)

Figure 1. This **Metering Container** stores a preselected amount of fluid from a pressurized source. The amount is selected [in this case, 2 to 4 ounces (60 to 120 ml)] by turning a calibrated collar on the body of the device. The window in the body permits observation of the amount of stored fluid.

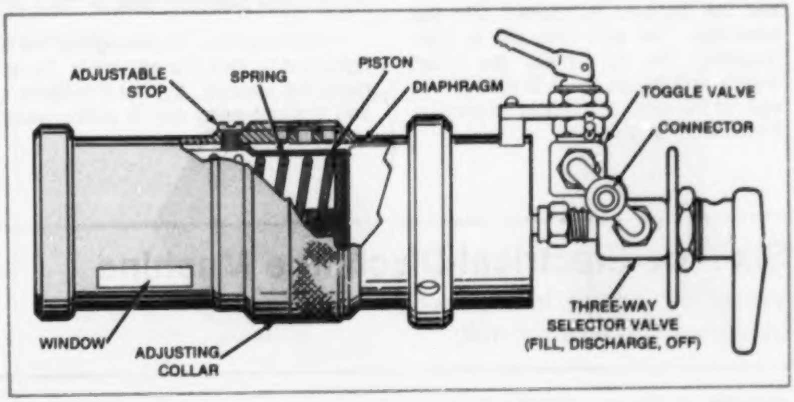

Figure 2. A **Spring and Adjustable Collar** determine the amount of fluid captured in the container. The required spring characteristics depend on the pressure and flow properties of the fluid.

Quick-Disconnect Fastener

A proposed fastener would have good shear- and moment-load-carrying capacity.

Langley Research Center, Hampton, Virginia

A proposed quick-disconnect fastener for two or more parts resists shear loads and torque. It would center the parts to be joined, clamp them, and then tighten them into a single unit. Potential applications for the removable fastener include holding parts for welding, brazing, soldering, riveting, and gluing. Other possible uses would be for attaching removable panels and panels with poor access on one side and for plugging leaks in pressure vessels.

The fastener consists of a spring-loaded hexagonal actuating pin, six springy collet fingers, and a hexagonal-nut locking collar. The collet fingers clamp the fastener in position and should give excellent shear- and moment-load-carrying capacity. An adjustable locking collar compensates for component assemblies of differing thicknesses.

The figure shows the fastener before and after locking. Holes are first drilled in the parts to accept the fastener. With the spring-loaded actuating pin retracted, the six fingers remain together, and the fastener is inserted into the assembly. The actuating pin is then released. The pin enters the collet fingers and forces them to spread out against the sides of the hole, anchoring the fastener in place.

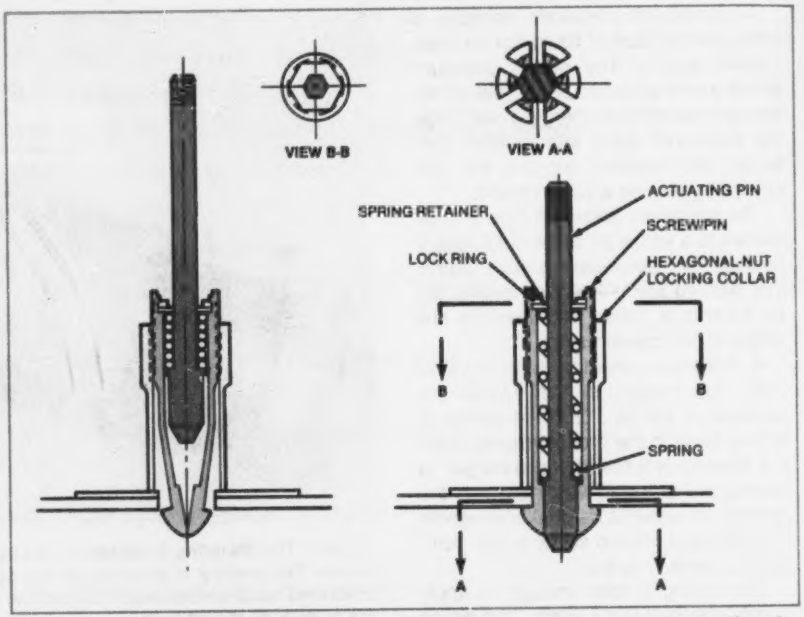

The **Collet Fingers** remain together (left) until forced apart by the hexagonal actuating pin (right). In the proposed fastener, there are six fingers and a hexagonal shank.

In the final step, the hexagonal nut is tightened to lock the assembly. To remove the fastener, the nut is loosened, and the actuating pin is pulled away from the collet fingers.

This work was done by Louis W. Palmer and Jack A. Billyard of Rockwell International Corp. for **Langley Research Center.** *No further documentation is available.*
LAR-12895

Six-Axis Electrical-Discharge Machine

Versatile machine tool is made by converting a radial drill.

Marshall Space Flight Center, Alabama

An electrical-discharge machine (EDM) of unusual versatility has been made by the conversion of a radial drill. The drilling head is replaced by a ram that holds and positions the electrode. A tank and recirculation system for the coolant are added.

A conventional radial drill, used for machining in the tool-and-die industry, has a spindlehead that moves the drill in the z-direction and a worktable that moves the workpiece in the x- and y-directions. The EDM, however, has six independent motions:

1. X-axis motion provided by the radial-drill crossarm and mounting table;
2. Y-axis motion provided by the mounting table;
3. Z-axis motion provided by the ram;
4. Angle motion, as shown in the figure;
5. Arc motion provided by the radial arm; and
6. Rotation of the spindle quill.

Use of the six axes of motion allows full exploitation of the principle of electrical-discharge machining. The mechanical versatility also simplifies the positioning of work fixtures, thus reducing setup time and costs.

Many of the features of the machine may be seen in the figure. The large size of the EDM is apparent: The ram has a traverse of 36 inches (91 cm), and the table working surface is 44 by 44 inches (112 by 112 cm). The dielectric tank is 50 by 50 by 50 inches (127 by 127 by 127 cm). One side of the tank can be removed (as in the photograph) to facilitate installation, inspection, or removal of the workpiece and the electrode.

The capabilities of the machine were demonstrated in performance tests that included an overcut test, a through-hole test, a cavity test, and a small-hole test. All of these required precise machining in steel, using either copper or graphite as the electrode.

This work was done by A. R. Werner of Rockwell International Corp. for **Marshall Space Flight Center.** *For further information, Circle 43 on the TSP Request Card.*
MFS-19695

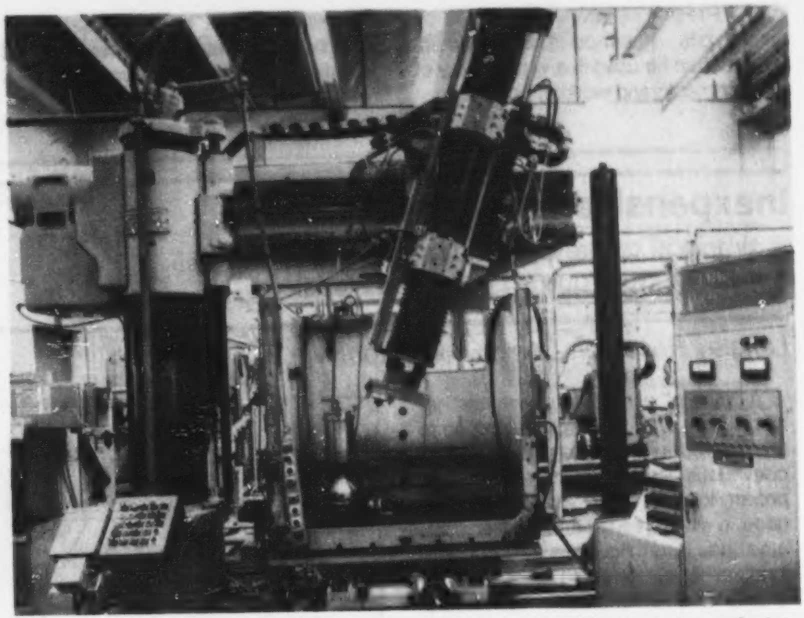

This **Electrical-Discharge Machine** (EDM) has drastically reduced the cost of manufacturing, and new applications for it are constantly being found.

Padded Allen Wrench Grips Fastener

Screws can be inserted in hard-to-reach places.

Marshall Space Flight Center, Alabama

The addition of a PTFE pressure pad increases the utility of a hexagonal socket wrench. The pad presses against opposing inside socket walls, causing a frictional force that retains a socket-head screw against gravitational and handling forces. Developed for spacecraft repairs, the tool is useful wherever there is a possibility of losing the screw due to awkward working conditions or wherever a tight clearance prevents the insertion or removal of the screw by hand.

The modified wrench (see figure) is easy to construct. A hole is drilled through a pair of flats near the end of a basic hexagonal wrench. A tight-fitting PTFE rod is pressed into the hole, then machined until it protrudes by the desired distance.

Unlike magnetic tools, the new device works with socket-head capscrews of both nonferrous and ferrous materials.

(continued on next page)

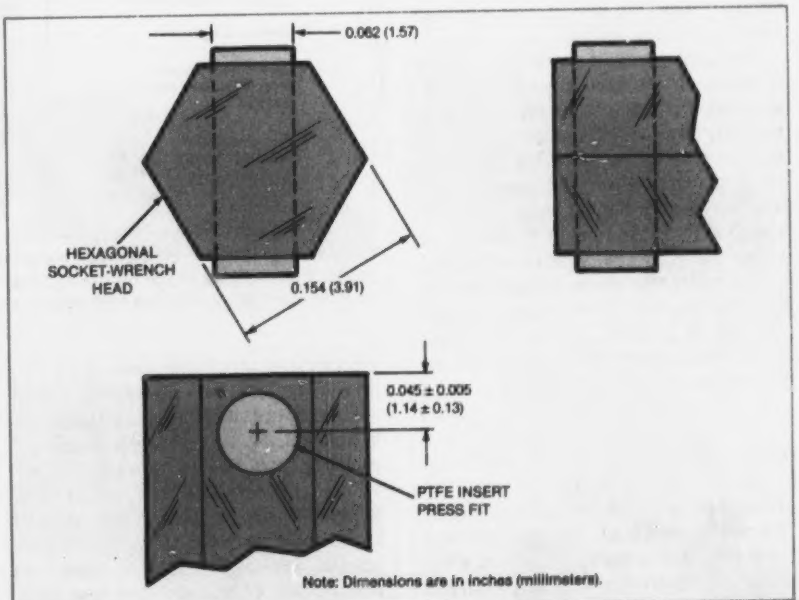

Note: Dimensions are in inches (millimeters).

A PTFE Pad is inserted in a hole near the end of a basic hexagonal socket wrench (allen wrench). The concept is not limited to one wrench size: Dimensions are shown for example only.

Since PTFE is relatively unaffected by gases, oils, or temperature extremes, the tool can be used in a wide variety of environments and working conditions.

This work was done by Michael K. Salisbury of **Marshall Space Flight Center.** *No further documentation is available.*

Inquiries concerning rights for the commercial use of this invention should be addressed to the Patent Counsel, Marshall Space Flight Center [see page A5]. Refer to MFS-25739.

Inexpensive Bolt-Load Gage

A simple screw-and-washer strain gage indicates the optimum torque on bolts and studs.

Langley Research Center, Hampton, Virginia

A "built-in" gage determines whether a large bolt or stud has been torqued to the desired load and also provides for continuous inspection to ensure that proper load is being maintained. The gage, a simple screw-and-washer combination (see figure), detects the longitudinal stress/strain on the bolt; it requires no electronic or sonic test equipment.

The strain gage is based on setting and maintaining a maximum longitudinal "stretch" that the bolt or stud should have under the desired load or stress. This "stretch" can be either calculated or determined by calibration.

The gage screw is fed through a cruciform washer and installed in a drilled hole through the centerline of the bolt or stud. The precise bolt "stretch" length is set between the washer and screwhead by a feeler gage or other simple measuring device, and a jamnut locks in the gap setting.

The gage screw is made of the same material as the bolt to avoid thermal-expansion problems. When the bolt is properly stressed, the gage screwhead clamps the washer and prevents it from rotating, indicating that proper tightening has been achieved. Subsequent inspections require only an attempt to rotate the washer by hand or with a tool.

The cruciform shape makes it easy to grip the washer. If the washer is tight, the bolt is properly loaded. The gage screw may be longer than the bolt, as shown, or the gage screw length may be shorter than the bolt, such that sufficient stretch is measured to ensure that tolerances do not adversely affect accuracy.

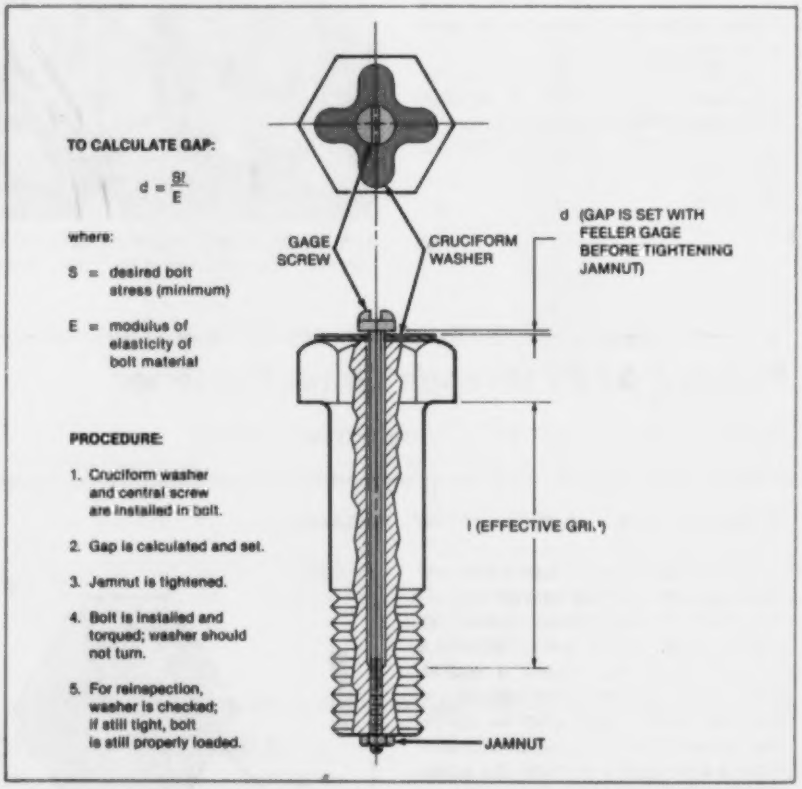

TO CALCULATE GAP:

$$d = \frac{Sl}{E}$$

where:

S = desired bolt stress (minimum)

E = modulus of elasticity of bolt material

PROCEDURE:

1. Cruciform washer and central screw are installed in bolt.
2. Gap is calculated and set.
3. Jamnut is tightened.
4. Bolt is installed and torqued; washer should not turn.
5. For reinspection, washer is checked; if still tight, bolt is still properly loaded.

A **Screw-and-Washer Strain Gage** placed through the center of a bolt or stud indicates proper bolt load for initial tightening and for continuous, easy bolt-load inspection. No special tools or electronics test equipment are needed.

Other methods depend primarily on measurement of the torque imposed on the nut or bolthead. The relation of a torque value to a bolt load involves a frictional coefficient that may vary from bolt to bolt, depending on thread surface smoothness and the degree of lubrication. Therefore, the calculated torque value may not yield the desired bolt load. In addition, the stress/strain condition of a bolt or stud may be measured by advanced sonic/electronic equipment. Sonic measurement techniques are still in the developmental stage and require special, relatively expensive equipment and trained operators. This new technique requires neither.

This work was done by Moses J. Long of **Langley Research Center.** *No further documentation is available.*

This invention is owned by NASA, and a patent application has been filed. Inquiries concerning nonexclusive or exclusive license for its commercial development should be addressed to the Patent Counsel, Langley Research Center [see page A5]. Refer to LAR-12774.

Parachute Line Hook Includes Integral Loop Expander

Parachute packing is simplified with a modified line hook.

Langley Research Center, Hampton, Virginia

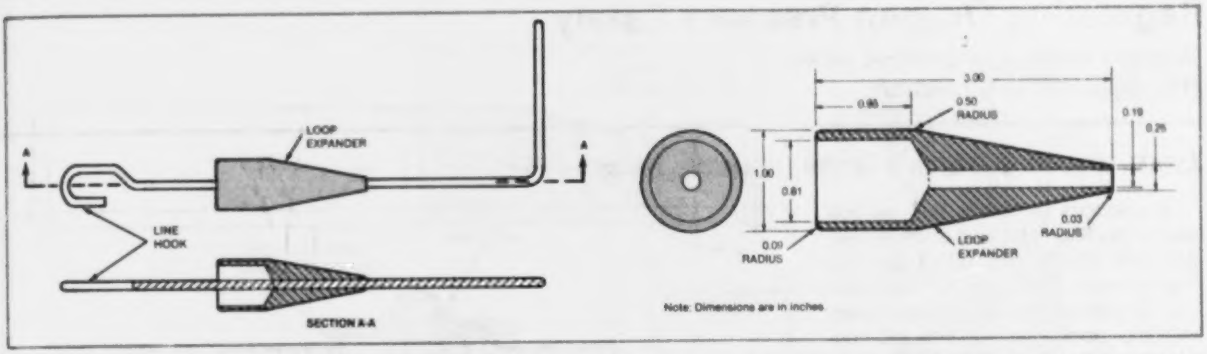

Figure 1. The **Parachute Line Hook** includes a tapered brass fitting that expands locking loops on the parachute bag so that the parachute lines can be pulled through them.

Using a modified line hook developed at Langley Research Center, one person now packs parachutes for test recovery vehicles faster than it previously took a two-person team. The new line hook includes an expander that opens up two locking loops so that the parachute lines can be pulled through them. In the old method, one person operated the line hook while the other person expanded the loops by hand.

The parachutes are packed at high pressure because they have to be compressed into the limited space available in the test vehicles. The pressure creates a large force on the parachute locking flaps.

Two flaps at the mouth of the parachute bag are joined together to lock the parachute in the bag. One flap has two square holes through which two locking loops from the second flap fit. Once the loops from the second flap are pulled through the holes in the first flap, the parachute lines are looped together and pulled through the two loops by using the line hook.

The modified line hook with the loop expander holds the first flap down while expanding the loop and also allows the parachute lines to be pulled through in a one-step operation. The tapered brass piece on the line hook, shown in Figure 1, allows the loop to slide over it, thus expanding the loop. As the line hook is pulled, the loop slides off the expander and over the lines. Once the lines are

(continued on next page)

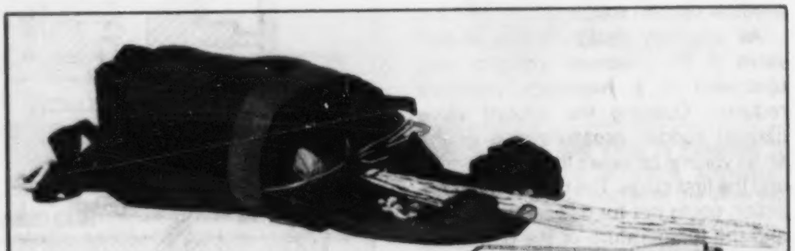

Figure 2. This **Five-Photo Sequence** shows the tapered fitting expanding the loops as the line hook pulls the lines through.

threaded through the loops, the line hook is unlocked, and the packing operation is complete. The photographs in Figure 2 show the parachute lines being pulled through the locking loops.

This work was done by Gary B. Bayless of **Langley Research Center.** *No further documentation is available.*

This invention is owned by NASA, and a patent application has been filed. Inquiries concerning nonexclusive or exclusive license for its commercial development should be addressed to the Patent Counsel, Langley Research Center [see page A5]. Refer to LAR-12875.

Regulating Oxygen Pressure Safely

Sudden heating is avoided when the regulator is turned on.

Lyndon B. Johnson Space Center, Houston, Texas

A pressure regulator for oxygen allows gas flow to be shut off on its low-pressure (outlet) side rather than its high-pressure (inlet) side. The regulator thus avoids the fire hazard associated with the rapid pressurization and consequent adiabatic heating of oxygen on the input side when the regulator is turned on. The new regulator can reduce the danger of fire in aircraft and in medical oxygen supplies.

As originally designed, the shutoff valve of the pressure regulator was upstream of a two-stage pressure reducer. Opening the shutoff valve caused sudden pressurization of the small volume between the shutoff valve and the first stage. The heat of pressurization could not be dissipated rapidly, and the temperature of the gas in the small volume soared to potentially dangerous levels.

In the new version of the regulator (see figure), the shutoff valve is eliminated from the supply side, and its function is transferred to a lift rod. With the lift rod in the up (off) position, the regulator valve stem floats freely, and the inlet pressure holds the valve ball against the regulator valve seat.

However, when the lift rod is pushed down to a position that frees the pressure-sensing bellows plate, the plate can move against the valve stem in response to outlet pressure. The device then functions as a normal regulator. When the regulator is turned on, the oxygen flows suddenly into a large volume instead of a small one: There is no rapid buildup of pressure and temperature.

This work was done by Charles Simons of United Technologies Corp. and Lawrence Gill of Carlton Controls for **Johnson Space Center.** *No further documentation is available.*
MSC-20300

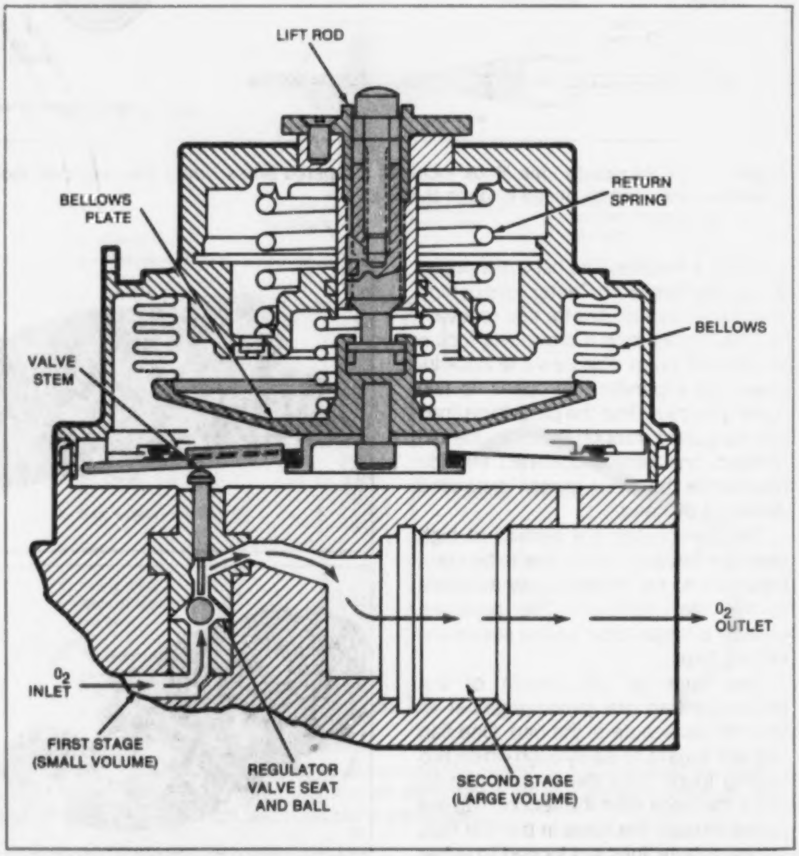
LIFT ROD
BELLOWS PLATE
RETURN SPRING
BELLOWS
VALVE STEM
O_2 OUTLET
O_2 INLET
FIRST STAGE (SMALL VOLUME)
REGULATOR VALVE SEAT AND BALL
SECOND STAGE (LARGE VOLUME)

In the Modified Pressure Regulator (shown here in simplified form), the initial rush of oxygen occurs in the second stage rather than in the first stage of pressure reduction. The large volume of the second stage prevents excessive heating of the gas. The high-pressure source can remain on, and the first stage can remain pressurized at all times.

Tool Severs Hidden Adhesive Bonds

It reaches deep into narrow crevices without damaging adjacent surfaces.

Lyndon B. Johnson Space Center, Houston, Texas

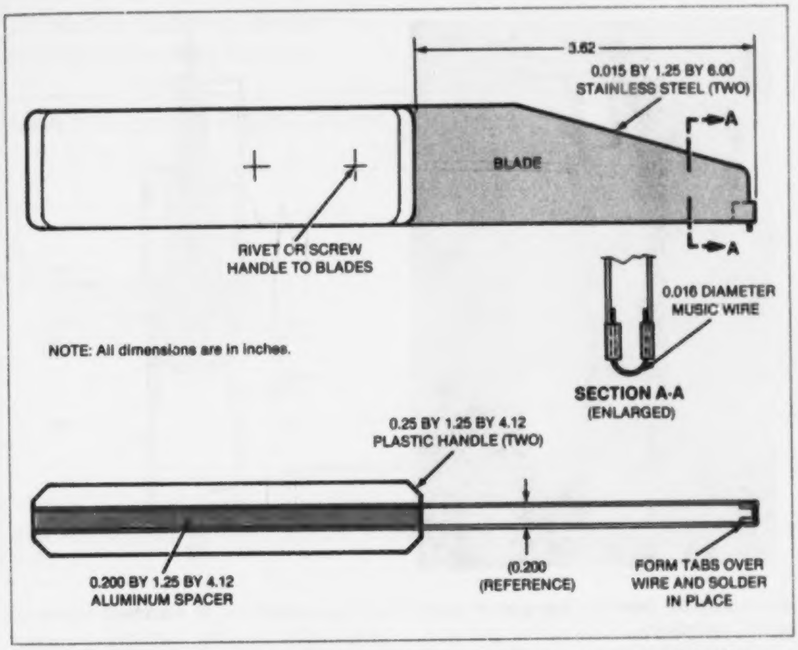
3.62
0.015 BY 1.25 BY 6.00
STAINLESS STEEL (TWO)
A
BLADE
A
RIVET OR SCREW
HANDLE TO BLADES
0.016 DIAMETER
MUSIC WIRE
NOTE: All dimensions are in inches.
SECTION A-A
(ENLARGED)
0.25 BY 1.25 BY 4.12
PLASTIC HANDLE (TWO)
0.200 BY 1.25 BY 4.12
ALUMINUM SPACER
(0.200
(REFERENCE)
FORM TABS OVER
WIRE AND SOLDER
IN PLACE

Figure 1. **Two Parallel Blades,** sandwiched between an aluminum spacer and plastic, support the cutting wire. The wire is crimped to the blades, and the handle is held together by either rivets or screws.

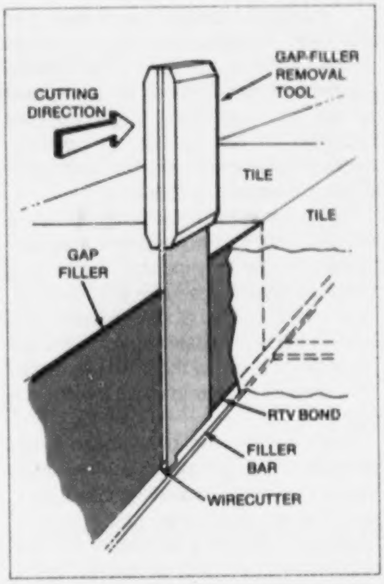
CUTTING
DIRECTION
GAP-FILLER
REMOVAL
TOOL
TILE
TILE
GAP
FILLER
RTV BOND
FILLER
BAR
WIRECUTTER

Figure 2. The **Gap Filler Is Removed** by undercutting the adhesive alternately from one end and then from the other end of the filler.

A new tool enters a narrow gap between fragile materials and removes an adhesively bonded filler without damage to the adjacent surfaces. It reaches deep into narrow crevices to reach hidden bond lines. The tool was originally developed to remove ceramic filler from between the Space Shuttle surface-insulation tiles.

The tool (see Figure 1) has two blades that support a short length of music wire, 0.016 in. (0.4 mm) in diameter. A set of tools with blades spaced at different widths would fit a range of gaps. In the Space Shuttle application, only the length of music wire is used to sever the adhesive bonds; the blades do not actually do any cutting.

As shown in Figure 2, the tool is inserted over the filler to be removed with the two blades straddling the filler. Any adhesive bonds between the filler and adjacent walls are broken by a sharpened spatula before the tool is inserted.

The wire is inserted down to the bond line and pulled with a slight downward pressure along the gap filler, stopping about 2 in. (5 cm) from the end. The path of the tool is then reversed, and the tool is removed at the same place it entered. The tool is then reinserted at the opposite end of the gap filler, and the last remaining bond is severed. The gap filler can then be removed.

This work was done by Andrew R. Keir and Xavier A. Dominguez of Rockwell International Corp. for **Johnson Space Center.** *No further documentation is available.*
MSC-20198

High-Production Silicon-Ingot Slicer

A new ingot slicer comprised of stacks of up to 250 rotating, ganged blades promises to increase wafer production, to improve silicon wafer yield, and to cut manufacturing costs. The rotating ingots are fed into the circular cutters.
(See page 216.)

Explosive Joining for Nuclear-Reactor Repair

A remote ribbon explosive yields a joint with double the parent metal strength. For reactor repair, a 30-grain/foot (0.63-gram/cm) ribbon drives a machined adapter flange into a bellows. This joining technique is useful in remote, dangerous, and inaccessible areas.
(See page 211.)

Boom Deploys With Controlled Energy Release

A self-deploying boom stows in a canister and stores its own erecting energy in coiled, fiberglass springs. The erected boom members form a lattice structure stiffened by diagonal members. Applications include lightweight field-erectable structures.
(See page 175.)

Coulomb Friction Damper

A linear friction damper is effective at low velocities.

Lyndon B. Johnson Space Center, Houston, Texas

A standard hydraulic shock absorber has been modified to form a coulomb (linear friction) damper. The device damps very small velocities and is well suited for use with large masses mounted on soft springs. In contrast, hydraulic dampers can be ineffective when the velocity is reduced.

As shown in the figure, the piston of a conventional hydraulic shock absorber is replaced by a cylindrical friction pad that rubs against the inner cylinder wall. The lateral force of the friction pad against the wall is determined by the adjustment of a spring that presses axially on a conical wedge to force the friction pad outward.

The coulomb friction damper is applicable in situations requiring large damping of small oscillating velocities. It contains no liquid that could leak or freeze and heaters, necessary for low-temperature operation of fluid dampers, are not needed. Performance is relatively insensitive to temperature and to cycle frequency. The damping force is easily adjusted for different loads. These dampers are therefore more reliable than fluid dampers and also more economical to build and to maintain.

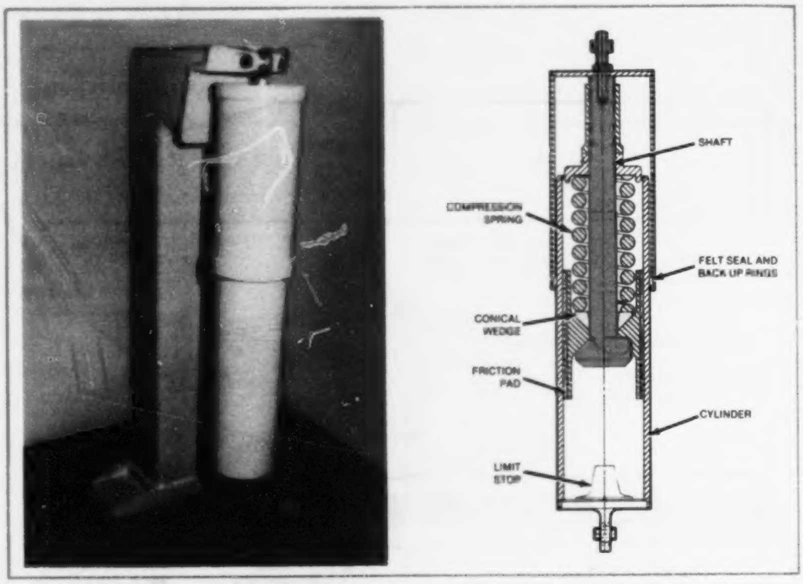

The **Coulomb Friction Damper** is constructed by modifying a standard hydraulic shock absorber.

This work was done by Walter T. Appleberry of Rockwell International Corp. for **Johnson Space Center.** *For further information, Circle 44 on the TSP Request Card.*
MSC-20179

Inserts Automatically Lubricate Ball Bearings

Small inserts in the ball pockets provide a steady supply of lubricant.

Marshall Space Flight Center, Alabama

Inserts on the ball-separator ring of ball bearings will provide a continuous film of lubricant on the ball surfaces. Developed for hard-to-lubricate turbopumps for cryogenic liquids, the yet-to-be-tested technique could be utilized on equipment for which maintenance is often poor and lubrication interval is uncertain — household appliances, automobiles, and marine engines, for example.

The inserts are made from a material high in molybdenum disulfide and poly(tetrafluoroethylene) content — both solid lubricating agents. The ball pockets in a separator are elongated in the circumferential direction by machining. An insert is then snapped into elongations on two adjacent pockets, bearing against the inside surface of the separator (see figure). Lips on the insert hook over the outside surface of the separator, thereby holding the insert in place. When all inserts are in position

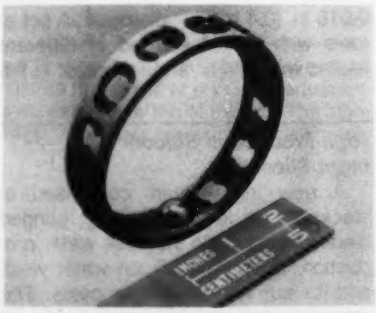

Ball Bearings Are Lubricated by small inserts of a material rich in molybdenum disulfide and poly(tetrafluoroethylene). The inserts can be machined or molded.

on the separator, all ball pockets are circular.

In operation, the balls rub against the inserts as they turn. They thus pick up a film of lubricant, which they transfer to the bearing races.

This work was done by J. A. Hager of Rockwell International Corp. for **Marshall Space Flight Center.** *No further documentation is available.*
MFS-19727

Locking Nut and Bolt

Threaded fastener resists strong loosening forces.

Marshall Space Flight Center, Alabama

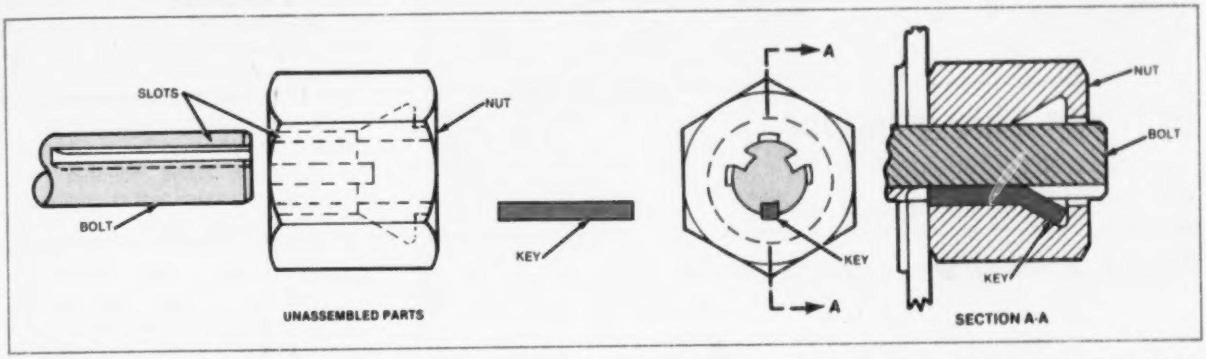

Bolt, Nut, and Key are joined together so that the key occupies alined slots in bolt and nut and prevents the nut from rotating off the bolt.

A new threaded fastener locks parts securely together despite large loosening torques, even under conditions of high temperature and vibration. The positive locking action is suitable for use where conventional fasteners tend to work loose — for example, on high-speed rotating machinery.

The fastener consists of a bolt, a key, and a nut containing an inner annulus (see figure). Longitudinal slots are machined in the external surface of the bolt and in the internal surface of the nut.

In installation, the nut is screwed on the bolt and tightened to the required torque. The nut is rotated farther until one of its slots is alined with the nearest slot in the bolt. Three slots in the bolt and four in the nut allow for easy alinement. The key is inserted in the alined slots and bent into the nut annulus. The bolt and nut are then locked together by the key — one cannot move in relation to the other. The assembly can be separated only by cutting away the nut.

This work was done by Ray Bishop of Rockwell International Corp. for **Marshall Space Flight Center.** *No further documentation is available.*
MFS-19687

Ferrofluid Would Seal Linear-Motion Valve

A magnetic fluid would seal against pressure or vacuum.

Lyndon B. Johnson Space Center, Houston, Texas

A proposed valve would employ a ferrofluid to make a tight seal. The seal would require no precisely machined parts, and hand lapping of valve seats would be unnecessary. [Ferrofluids have low vapor pressure — about 1×10^{-8} torr (10^{-6} N/m^2). They can therefore be used in low and moderate vacuum.]

The valve consists of a hollow shaft with magnetically soft sheaths that can slide through a ring magnet with annular pole pieces (see figure). In its open position, the shaft carries gas, liquid, or vacuum through its hollow core. In its closed position, both ports on the shaft are on the same side of the wall, so that the hole in the wall is sealed.

A ferrofluid — a magnetic liquid — is held in place around the shaft by the ring magnet. The ferrofluid fills the void between the shaft and the pole piece in the chamber wall, providing a tight seal against vacuum or high pressure. The shaft should be made of a nonmagnetic material so that it does not continually wipe away ferrofluid as it is opened and

(continued on next page)

closed. An inexpensive molded plastic should serve well.

More than one ferrofluid seal can be used on a shaft. It can then be used as a multiple-position switching valve in a plumbing system.

This work was done by Joseph A. Chandler of **Johnson Space Center.** *For further information, Circle 45 on the TSP Request Card.*

Inquiries concerning rights for the commercial use of this invention should be addressed to the Patent Counsel, Johnson Space Center [see page A5]. Refer to MSC-20148.

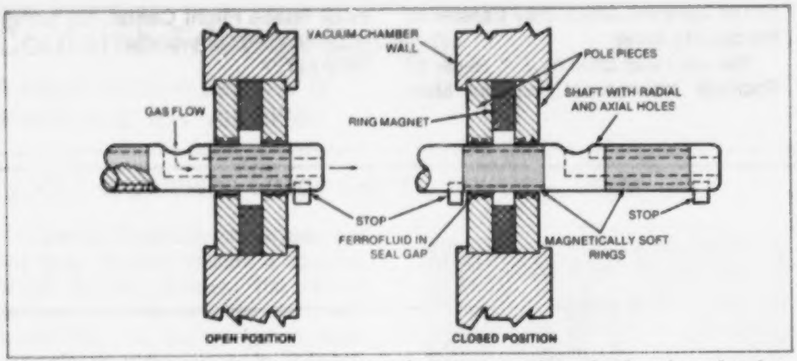

Magnetic Fluid Fills the Gap between a shaft and an annular pole piece in a chamber wall. A precise shaft fit is not necessary.

Portable Pipe Wrapper

Device controls tension and wrap angle.

John F. Kennedy Space Center, Florida

A new tool applies fragile layered insulation to cryogenic tubing. It has been used routinely to apply two layers of fiberglass and one of aluminum foil on pipe used as the inner line in vacuum jacketed cryogenic plumbing. Applying the layers one at a time by hand had proved to be too delicate and time consuming a task: The insulation tended to tear when handled with gloves (required to avoid contamination), and the layers were difficult to apply uniformly.

The new portable pipe wrapper (see figure) has three freely revolving drums that hold the wrapping material. They are mounted on a four-wheeled cart that is pushed along the pipe as wrapping proceeds. The pipe is held in a turntable that turns like a lathe. As the pipe turns, it pulls the wrappings off the rolls and onto the pipe in tight, even layers. An adjustable arm on the wrapper controls the angle of wrap. There is no handling of the wrapping material except at the start and end of the wrap.

The wrapper is easy to use and is made from inexpensive, readily available parts. It can be wheeled to whatever location is convenient for wrapping the pipe. The wrapper should prove useful in applying thermal insulation to hot-water pipes and refrigerant-distribution lines. A similar tool could be used to wrap electrical insulation.

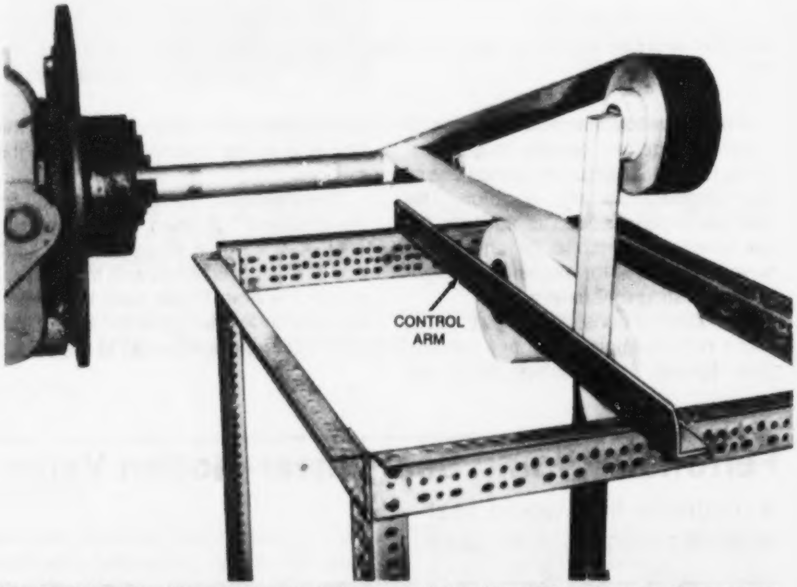

The **Portable Pipe Wrapper** is rolled along parallel to the pipe as the wrappings are applied. The control arm can be adjusted to control the angle of wrap.

This work was done by Gale B. Dennis of Boeing Services International for **Kennedy Space Center.** *No further documentation is available.*
KSC-11244

Tubing Cutter Is Activated Hydraulically

A hydraulic cutter deactivates aircraft ejection seats in rescue operations.

Langley Research Center, Hampton, Virginia

The hydraulically powered tool shown in the figure severs tubing and cable in areas where accessibility is limited. The cutter jaws are attached to one end of a flexible "gooseneck" extension and are closed by a hydraulic piston when the operator squeezes the handle grip. The jaws are released by flipping an on/off lever. The double-jawed cutters cut out a complete section of tubing.

The cutter was originally intended for use by fire/crash crews to deactivate aircraft ejection seats during rescue operations. In that application, the cutter severs the pressure supply lines to the ejector. The cutter has potential as a flight-line tool and can also be useful in automobile and fire rescue work.

A manually-operated cutting tool was utilized prior to use of the hydraulic cutter. The manual tool has long handles, which are necessary to provide sufficient torque to the cutting jaws. The use of both hands is required for operation.

In contrast, the hydraulic tool employs a trigger-grip handle that can be operated easily with one hand. Its gooseneck frame is flexible and can be manipulated so that tubing can be cut in a cramped location.

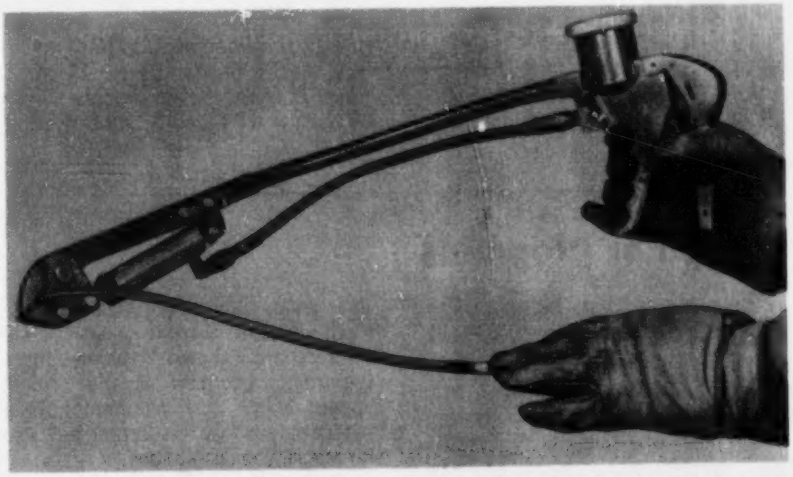

The **Hydraulically-Actuated Tubing Cutter** severs the tubing when the operator squeezes the handle grip. The "gooseneck" extension enables the cutter to be used in areas where accessibility is limited.

This work was done by Dwight G. McSmith and James I. Richardson of **Langley Research Center.** *No further documentation is available.*
LAR-12786

Books and Reports

These reports, studies, and handbooks are available from NASA as Technical Support Packages (TSP's) when a Request Card number is cited; otherwise they are available from the National Technical Information Service.

Light, Compact Pumper for Harbor Fires

Aerospace technology is utilized in a transportable, powerful unit.

A recent report describes the development of a new transportable water-pumping unit for firefighting. The compact, self-contained unit provides fire protection at coastal and inland ports and is lighter than a standard firetruck pumper of the same capacity. [The same report was made available to readers requesting further information on "Mobile Firefighting Module," the technology illustrated on the cover of *NASA Tech Briefs*, Vol. 6, No. 3, Fall/Winter 1981.]

A prototype model has been delivered to the U.S. Coast Guard, and an improved model has been delivered to the U.S. Maritime Administration. Incorporating aerospace technology and materials, the unit is a skid-mounted gas turbine and pump that delivers up to 2,500 gal/min (9,500 liters/min) of water at a discharge pressure of 150 lb/in.^{2} (1 MPa). The water source can be any open stretch of freshwater or saltwater or a high-capacity fire hydrant. The unit primes itself and can draft water to a height up to 20 feet (6.1 meters) above the sea or river surface. It can operate for 4 hours at maximum flow without refueling. It measures 4 by 5.4 by 6.8 feet (1.22 by 1.65 by 2.07 meters) and weighs 1,600 lb (726 kg) dry.

When the unit is delivered at a fire site, an operator drops the suction hose into the water and pushes the start button. The starter/generator spins the engine to 15 percent rated speed, at which point ignition occurs. The engine accelerates to 60 percent speed. The operator pushes the prime button, and the unit automatically primes itself. Atmospheric pressure on the river or sea surface forces water up the suction hose. The unit begins pumping water through the discharge hose and water cannons.

The operator can then set the discharge pressure, and the unit controller will automatically maintain that level. Thus, if a discharge line valve is

(continued on next page)

opened or closed, the controller will change the engine power to maintain the original pressure setting. Alternatively, the operator can manually set the speed.

The primary structural element is the fuel tank, which contains longitudinal stiffeners that also serve as forklift tunnels. Each corner of the tank holds a shock-mounted skid. The engine and pump are integrally mounted on a lightweight frame that is bolted to the fuel tank. A firewall separates the engine combustion chamber from the pump. The engine gearbox, fuel control, starter/generator, exhaust ducts, primer, oil cooler, air eductor, oil pump, pump discharge line, and check valve are in the combustion-chamber section. The engine compressor, inlet filters, pump shock mounts, oil reservoirs, battery, and emergency internal-fire-extinguisher bottle are in the pump section.

The unit can be operated from a riverbank, light truck, trailer, dock, barge, or boat. It can be transported by truck, trailer, boat, forklift, or helicopter. It can be used to fight fires in harbors, cities, forests, refineries, chemical plants, and offshore drilling platforms. Other possible applications include cleaning up oilspills, pumping out ships, and flood-control pumping.

This work was done by Ralph A. Burns of **Marshall Space Flight Center.** *To obtain a copy of the report, Circle 46 on the TSP Request Card.*

Inquiries concerning rights for the commercial use of the invention described in the report should be addressed to the Patent Counsel, Marshall Space Flight Center [see page A5]. Refer to MFS-25784.

Computer Programs

These programs may be obtained at very reasonable cost from COSMIC, a facility sponsored by NASA to make new programs available to the public. For information on program price, size, and availability, circle the reference letter on the COSMIC Request Card in this issue.

Rotating-Machinery Critical Speeds

Solutions are obtained assuming motion in one plane.

A computer program available from COSMIC provides quick, efficient, and accurate results in support of preliminary and proposed rotating-machinery designs. Advanced rotating-machinery design is an iterative process in the early stages of development. With the higher-operating-speed requirements of these flexible rotor designs, the rotor dynamic analysis becomes more important. Location of the critical speeds is not only important from a resonant-response standpoint but also for stability considerations.

To support the designer in the iterative, conceptual design phase, the critical speeds and mode shapes must be accurately calculated. With the complexity of modern rotors, an accurate hand calculation is not practical, and a full finite-element model analysis can be expensive and time consuming. This new program provides timely, critical-speed calculations to support preliminary rotating-machinery designs.

The analysis develops a model from data files that represents the stiffness and mass properties of the rotating assembly. The critical-speeds problem is solved by assuming motion in one plane. Each joint has a translational and rotational degree of freedom; no axial motion is assumed. Bearings are modeled as radial linear springs to ground, and a moment spring may also be added. Typically, critical speeds are calculated by a parametric study that includes gyroscopic motion effects for a wide range of bearing stiffnesses. Output includes plots of rotor modes at critical speeds and of critical speed versus bearing stiffness.

This program is written in FORTRAN V for batch execution and has been implemented on a UNIVAC 1100-series computer with a central memory requirement of approximately 40K of 32-bit words. Plotted output is generated for the Tektronix 4014 graphics terminal. This program was developed in 1980.

This program was written by R. F. Beatty, A. L. Mowers, and E. Mogil of Rockwell International Corp. for **Marshall Space Flight Center.** *For further information, Circle L on the COSMIC Request Card.*
MFS-19669

Fabrication Technology

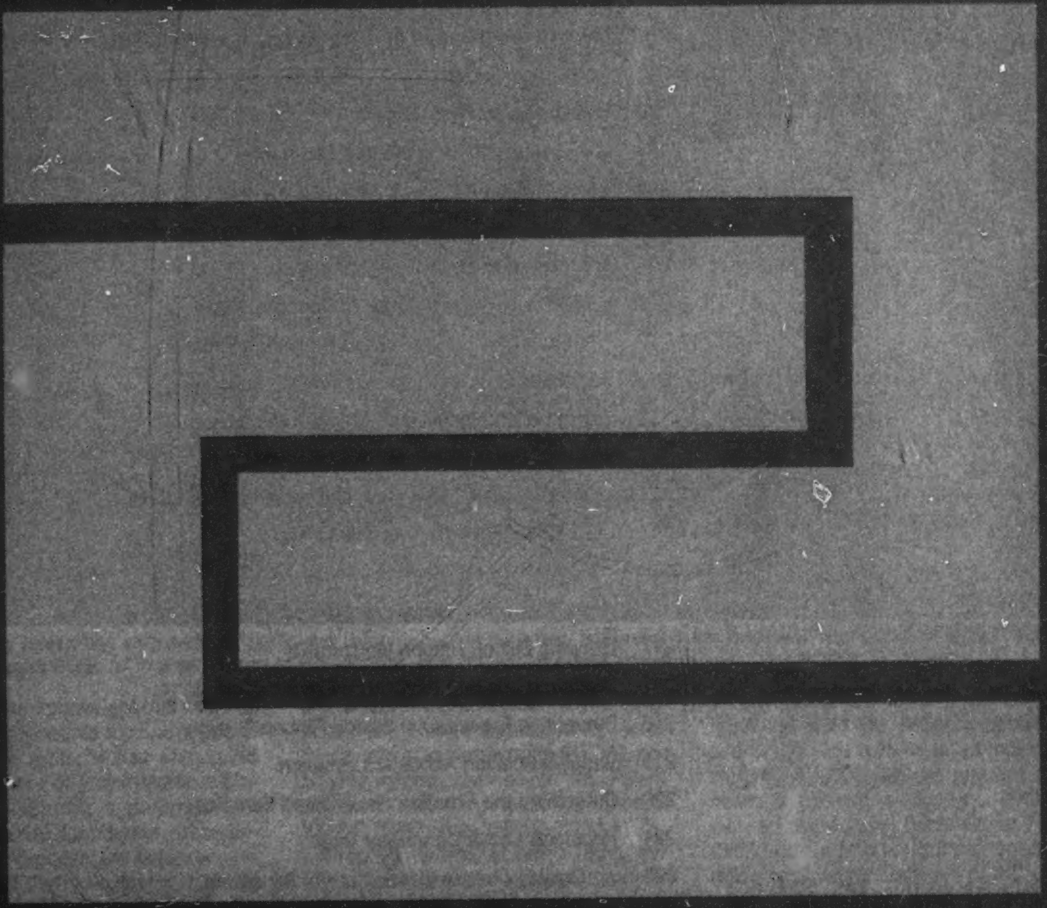

Hardware, Techniques, and Processes

203 Process Yields Strong, Void-Free Laminates
204 Fabrication of a Precise Microwave Reflector
204 Curing of Furfuryl Alcohol-Impregnated Parts
205 High-Temperature Filler for Tile Gaps
206 Pressure Assist Makes Coating More Reliable
206 Multiple-Panel Cylindrical Solar Concentrator
207 Conductive-Tape Substrate for Electroforming
208 Plastic-Sealed Hybrid Power-Circuit Package
209 Low-Cost Electrically-Heated Glass Panels
209 Process Sprays Uniform Plasma Coatings
210 Acoustic Methods Remove Bubbles From Liquids
211 Improved Gloves for Firefighters
211 Explosive Joining for Nuclear-Reactor Repair
212 Electrical Conduit Distributes Weld Gas Evenly
213 Replaceable Sleeve Protects Welder Coil
213 Transport and Installation of Fibrous Insulation
214 InGaAsP CW Lasers on (110) InP Substrates
214 Chemical Vapor Deposition of Germanium on Silicon
215 CLEFT Process for GaAs Solar Cells
215 Wipe Melt for InP Seed Substrate
216 High-Production Silicon-Ingot Slicer
217 Growing Silicon Ribbon Horizontally
217 Meniscus Imaging for Crystal-Growth Control
218 Preventing Freezeup in Silicon Ribbon Growth
219 Variable-Position Acoustic Levitation
220 Controlling the Rotation of Levitated Samples
221 Repairing Loose Connector Pins
222 Jig Quickly Checks Connector-Pin Alinement

Books and Reports

222 Electroforming for High-Performance Products
223 Heat Flow in Horizontal Ribbon Growth
223 Improving Surface Strength of Insulating Tiles

Computer Programs

224 Standard Transistor Arrays
224 Tile-Failure Analysis

Process Yields Strong, Void-Free Laminates

An accurate, reproducible fabrication process
produces composites of consistent quality.

Langley Research Center, Hampton, Virginia

The **Laminate Assembly,** with vacuum ports and thermocouples installed, is placed in an autoclave and cured at 332° C (630° F) maximum temperature, 30 inches (76 cm) of Hg vacuum, and 200 ksi (1.4 GPa) pressure.

The need for lightweight materials as structural components for future space transportation systems has stimulated the development of a systematic method for manufacturing a polyimide/graphite composite. Laminates manufactured by this process are void-free, exhibit excellent thermo-oxidative stability up to 315° C (600° F), and are 40 percent lighter than aluminum. The mechanical properties of this material at 23° C (73° F) include ultimate tensile strength of 200 ksi (1.4 GPa), flexural strength of 250 ksi (1.7 GPa), and interlaminar shear strength of 12 to 15 ksi (0.08 to 1.0 GPa).The process is precise and repeatable. It is ideally suited for researchers and small-lot producers of composite materials.

The composite material consists of an LARC-160 polyimide resin matrix reinforced with graphite fibers. The resin system is formulated to a molecular weight of 1,600 with ethyl alcohol as the solvent. Other monomers in the resin are 5-norborene-2, 3-dicarboxylic anhydride (NA), 3,3′,4,4′-benzophenonetetracarboxylic acid dianhydride (BTDA), and polymethylene polyphenylamine. Polymerization occurs in situ in the range of 273° C (525° F) to 329° C (625° F).

Prepreg material of LARC-160/graphite for laminates is produced on a drum winding machine. The prepreg is cut to the desired size and fiber direction and stacked for "B"-stage consolidation after which the "B"-staged laminate is cured and evaluated for material integrity. Tack and drape are controlled by carefully drying to remove volatiles. The ratio of graphite to resin in the final cured laminate can be precisely controlled by resin-formulation and prepregging-parameter adjustments. The optimum parameters are fiber weight percent,51; resin solids weight percent,44; and volatiles weight percent,5. The prepreg material is stored in polyethylene bags at 17.78° C (0° F) — an environment in which it maintains an indefinite shelf life. Prepreg containing LARC-160 with a formulated molecular weight of 1,600 and 60 percent resin solids by weight produces a laminate with an average ply thickness of 7 mils (0.003 cm), a fiber weight percent of 60, and a resin weight percent of 40.

Laminates (see photograph) are made with temperature pressure cycles that include a "B"-staging at 232° C (450° F) and 28 inches (71 cm) of Hg vacuum, a cure cycle at 332° C (630° F) and 30 inches (76 cm) of Hg vacuum, and cooling to 65.6° C (150° F) or less before releasing vacuum.

This work was done by Leland E. Bryant, Edward W. Covington III, Walter J. Dale, E. Thomas Hall, Jr., James E. Justice, Edward C. Taylor, and Maywood L. Wilson of **Langley Research Center.** *For further information, Circle 47 on the TSP Request Card.*
LAR-12982

Fabrication of a Precise Microwave Reflector

Machined reflector elements are assembled on graphite/epoxy supports.

NASA's Jet Propulsion Laboratory, Pasadena, California

A new antenna reflector integrates several fabrication techniques of optical and composite constraining materials. One of the most critical components in a new radiometer, the reflector must have a precise spherical configuration and must be thermally stable over a very wide temperature range.

The reflector is composed of machined aluminum reflector tiles attached to a graphite/epoxy structure with aluminum flexures (see figure). To obtain sufficient efficiency at the 200-GHz operating frequency, a surface accuracy of ±0.5 mil (0.0127 mm) from a 6-m-radius best-fit sphere is necessary. The tiles, which are about 5¼-by-5¼-by-¼-inch (13.3-by-13.3-by-0.6-cm) squares, are edge-clamped in aluminum surrounds and fly-cut to the desired spherical configuration. Then they are polished to a specular surface with an optical finish of 4 to 10 interference fringes.

The tiles are held by wax on a large aluminum tooling piece of 6-m spherical radius and maintained in that configuration until bonded to graphite/epoxy composite structure. The assembled structure is covered with an electroless copper and nickel flash coat and then sealed with a eutectic metal.

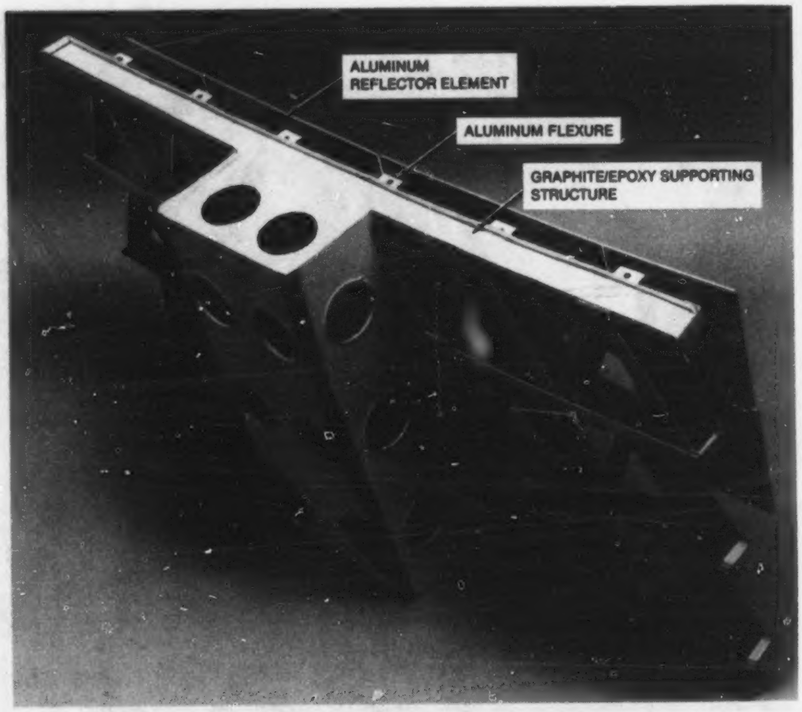
ALUMINUM REFLECTOR ELEMENT
ALUMINUM FLEXURE
GRAPHITE/EPOXY SUPPORTING STRUCTURE

Aluminum Reflector Tiles are supported by a network of beams. Excepting the fasteners, the support structure is composed of lightweight graphite/epoxy composite.

The fabricated optical figure is evaluated by using the specular reflective surface of the tiles to perform a Ronchi test. Distortion is measured in a vacuum chamber. Heat and cold are applied during the tests.

This work was done by Jerome L. Bauer and Eugene W. Noller, of Caltech for **NASA's Jet Propulsion Laboratory.** *For further information, Circle 48 on the TSP Request Card.*
NPO-15377

Curing of Furfuryl Alcohol-Impregnated Parts

A longer cure and improved quality control prevent delaminations.

Lyndon B. Johnson Space Center, Houston, Texas

A delamination problem in reinforced carbon/carbon parts impregnated with oxalic acid-catalyzed furfuryl alcohol is overcome by instituting two additional quality-control tests on the alcohol and by changing the curing conditions. The delamination had occurred following autoclave curing of the catalyzed furfuryl alcohol.

It had been assumed that monitoring alcohol viscosity would suffice as a quality-control check, but from time to time, the impregnating solution developed a froth that interfered with the impregnating process, even though viscosity was proper.

Differential scanning calorimetric (DSC) tests show a rapid, sharp exotherm at 293° F (145° C) as well as a broad exotherm extending beyond 400° F (204° C). It was concluded that the previous 1-hour cure at 290° F (143° C) was insufficient and that postcuring to 400° F at ambient pressure could also release moisture (as a byproduct of the curing reacton), causing delamination in thick regions of the parts being fabricated.

As a result of the investigation, the added alcohol quality-control tests are as follows:

- Alcohol in production use is tested weekly for water content. Water content must remain below 9.5 percent.
- DSC tests used to check the exothermic reaction characteristics of the impregnating solution. The exotherm must be strong.

The revised curing cycle calls for at least 2 hours at 300° ± 10° F (149° ± 6° C) followed by cooling to 175° F (80° C) under autoclave pressure. The extended cure drives the slower reaction nearer to completion. Since instituting these changes, no part delaminations have occurred.

This work was done by James W. Lawton and Thomas H. Brayden of Vought Corp. for **Johnson Space Center.** *No further documentation is available.*

Inquiries concerning rights for the commercial use of this invention should be addressed to the Patent Counsel, Johnson Space Center [see page A5]. Refer to MSC-20224.

High-Temperature Filler for Tile Gaps

Procedure using ceramic fabric can be used in kilns and furnaces.

Lyndon B. Johnson Space Center, Houston, Texas

Gaps between ceramic tiles can be filled with ceramic-coated fabric that withstands temperatures as high as 2,400° F (1,300° C). The caulking procedure with this material supplements existing gap fillers between surface insulation tiles on the Space Shuttle; it saves time by permitting the repair of fillings already in place, without the need to remove, rework, or replace them. High-temperature liners in kilns, furnaces, and other applications of heat-resistant insulation can also be caulked by this technique.

The ceramic fabric used for the gap-filler shim has a thickness of either 0.012 or 0.040 inch (0.3 or 1.0 mm). It is mounted in a metal frame and sprayed with colloidal silica, then sprayed with ceramic coating, and dried. It is then cut to size for the gap and inserted in place. Finally, it is bonded in place with a room-temperature-vulcanizing (RTV) adhesive, as indicated in the figure.

These gap fillers maintain the required pressure against the sidewalls of the tiles, are flexible, and can withstand airloads and high-temperature exposure for repeated missions.

This work was done by Jack W. Holt and David S. Wang of Rockwell International Corp. for **Johnson Space Center.** *For further information, Circle 49 on the TSP Request Card.*
MSC-20137

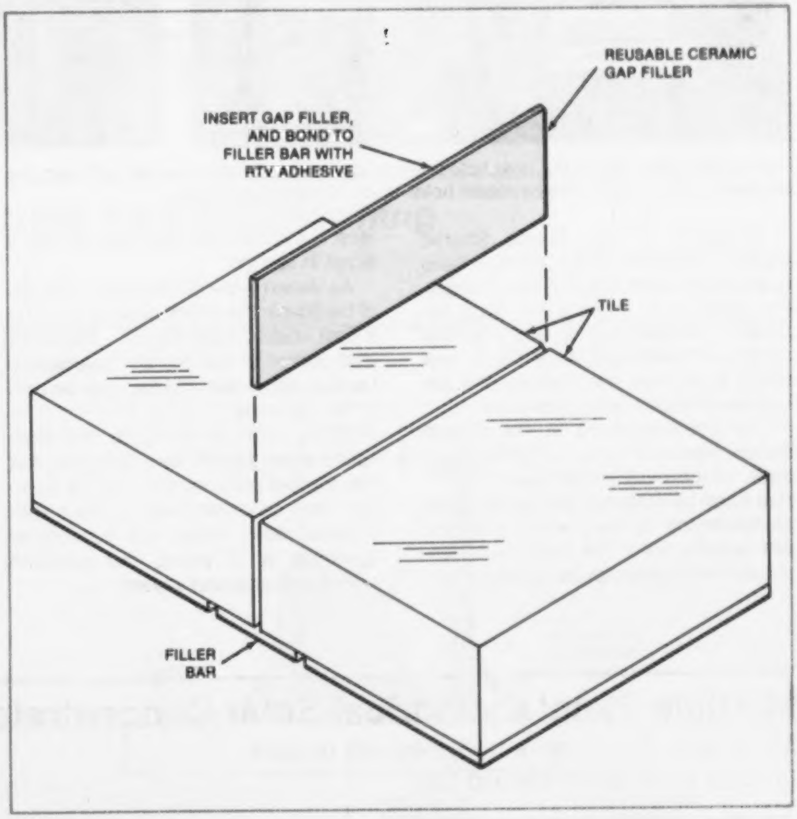
REUSABLE CERAMIC GAP FILLER
INSERT GAP FILLER, AND BOND TO FILLER BAR WITH RTV ADHESIVE
TILE
FILLER BAR

The **High-Temperature Gap Filler** is reusable. It is made of fabric coated with a ceramic slurry and bonded in place with room-temperature-vulcanized adhesive.

Pressure Assist Makes Coating More Reliable

Pressurization forces silicone resin into
the pores of an anodized surface.

Lyndon B. Johnson Space Center, Houston, Texas

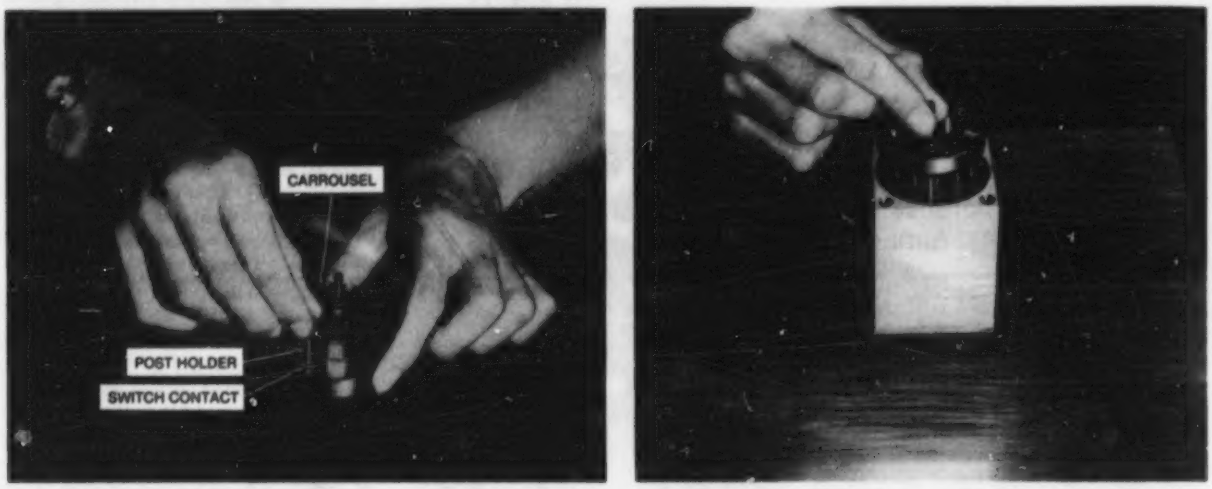

These **Two Views** show the post holder being inserted into the carrousel (left) and the post-holder assembly being inserted into the pressure vessel (right). The carrousel holds up to 12 switch contacts.

Designers of the Space Shuttle S-band communications system have found a new use for an old idea — applying pressure to improve the bond between a viscous coating and a porous surface. In the Shuttle hardware, its new use is to increase the reliability of resin-coated anodized switch contacts.

The contacts used in the S-band switch assembly have a nickel-plated base, which must remain resin-free so that it can be soldered, and an anodized aluminum top contact, which is coated with silicone resin. The resin must completely fill the pores of the anodized surface. If not, the resin can flake off after it is put in service.

As shown in the photograph at the left of the figure, the switch contact is held in a post holder, such that only the anodized portion of the contact is exposed. Up to a dozen post holders can be held in the carrousel.

At the right of the figure, the post-holder assembly is shown being inserted into the pressure vessel. Prior to insertion, the carrousel well is filled with silicone resin. When the post-holder assembly is in place, the pressure vessel is closed and sealed.

The vessel is then evacuated to 25 inches (63.5 cm) of mercury for 3 to 5 minutes. Dry nitrogen gas is applied at 160 psi (1.10×10^6 MPa) for 3 to 5 minutes through a top fitting. After pressure is released, the carrousel is removed. The contacts are removed, and any excess coating is wicked off. The coating is cured, and subsequent coatings are hand-dipped and wiped.

This work was done by A. Warren Berg of Teledyne Microwave for **Johnson Space Center.** *No further documentation is available.*
MSC-20210

Multiple-Panel Cylindrical Solar Concentrator

Multipanel trough reflector does not require
precise orientation toward Sun.

NASA's Jet Propulsion Laboratory, Pasadena, California

A solar concentrator composed of many flat-plate mirrors is efficient even when pointing away from the Sun by as much as 5°. Its concentration ratio is 10 or more with a relatively-small reflector area.

The concentrator is designed to backlight an array of photovoltaic cells; that is, to illuminate solar cells pointing toward the concentrator rather than toward the Sun (see figure). Unlike ordinary backlit concentrators, which employ parabolically curved reflectors, the multiple-flat-plate concentrator does not dramatically lose its effectiveness when it is slightly out of alinement with the Sun.

The plates are arranged in a trough, the cross section of which approximates a parabola. The angles between plates, the width of the plates, and the distance from the solar-cell array to the plate are determined from equations that relate these quantities, the solar-array width, the pointing accuracy, and the concentration ratio. For example, for a pointing accuracy of 1° and a concentration ratio of 16, the area ratio (concentrator area to solar-array area) varies from 31 to 28.39 as the H/L ratio (array width to array/concentrator separation) is varied from 9 to 14.

The multiple-flat-plate concentrator was originally developed for use in power sources on spacecraft. For terrestrial applications, the multiple-flat-plate design offers potential cost reduction and ease of fabrication.

This work was done by Edwin M. Brown of Hughes Aircraft Co. for **NASA's Jet Propulsion Laboratory.** *For further information, Circle 50 on the TSP Request Card.*
NPO-15627

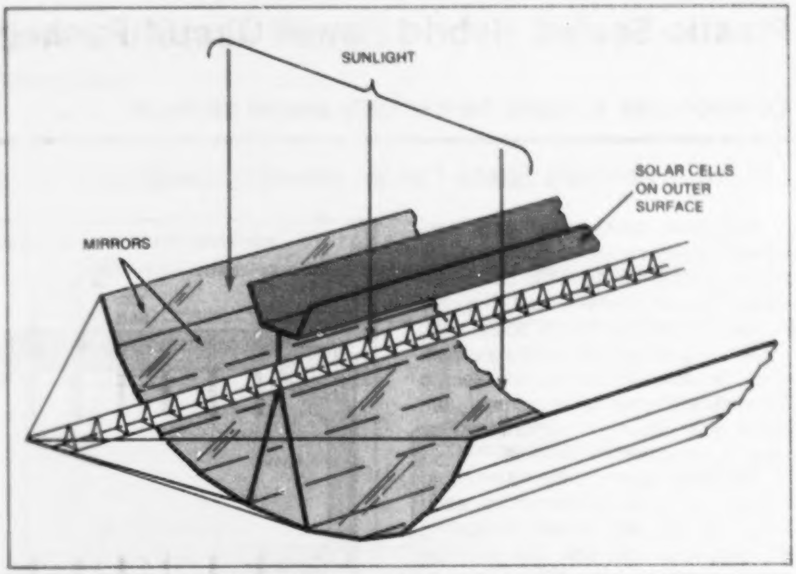

A **Trough Composed of Many Panels** concentrates the Sun's energy on solar cells, even when the trough is not pointed directly at the Sun. It can tolerate a deviation as great as 5° from the direction of the Sun.

Conductive-Tape Substrate for Electroforming

Metal tape has many uses in electroplating.

Marshall Space Flight Center, Alabama

Conductive tape is a versatile substrate for the electroforming of odd-shaped parts. Aluminum-foil tape has been used both as an electrical connection between two metal parts and as a substrate for electroforming a strong mechanical bond between the two parts (see figure). By using a double layer of tape adhesive-to-adhesive, electrical continuity can be established whether or not the tape available has a conductive adhesive.

Copper and aluminum conductive tapes are available commercially. When high dimensional precision is not required, such tape can serve as an electrical conductor, as a fastener, and as a rigid surface on which to electroplate. The tape can be quickly fashioned into the desired shapes with ordinary scissors.

Other uses of such tapes include:

- Taping a wire to a part to be plated, thus avoiding the need for a special clamp or fixture, and
- Using the mechanical strength of the tape to support a part during plating.

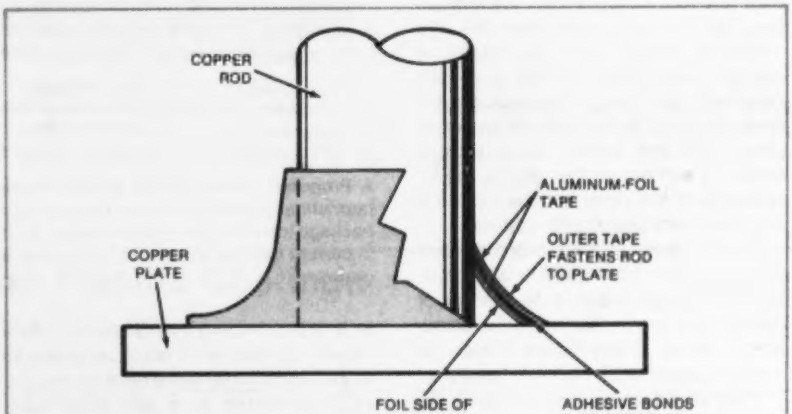
COPPER ROD
ALUMINUM-FOIL TAPE
OUTER TAPE FASTENS ROD TO PLATE
COPPER PLATE
FOIL SIDE OF INNER TAPE CONNECTS ROD AND PLATE ELECTRICALLY
ADHESIVE BONDS TAPE TOGETHER

An **Electroformed Joint** was made by electroplating a thick layer of metal on top of a double layer of aluminum-foil adhesive tape. During the plating the tape connected the rod and plate both electrically and mechanically.

This work was done by M. L. Cassidenti of Rockwell International Corp. for **Marshall Space Flight Center.** *No further documentation is available.*
MFS-19715

Plastic-Sealed Hybrid Power-Circuit Package

Concept uses a plastic hermetically sealed package.

Lyndon B. Johnson Space Center, Houston, Texas

A proposed design for a hybrid high-voltage power-circuit package uses a molded plastic for hermetic sealing instead of a glass-to-metal seal. The new package would be used to house high-voltage regulators and solid-state switches for applications in aircraft, electric automobiles, industrial equipment, satellites, solar-cell arrays, and other equipment in extreme environments.

The design shown in the figure could house four semiconductor chips, each 0.25 inch (6.4 mm) square, dissipating 40 watts to a heat sink. The package could operate at up to 1,000 Vdc in air or vacuum at temperatures from that of liquid nitrogen up to 500° F (260° C). By modifying the package size, the design could be adapted for higher or lower power dissipation or to accommodate entire hybrid circuit chip assemblies comprising transistors, diodes, resistors, or thryristors.

The package consists of a copper heat-sink base, a plastic ring frame, and a cover plate. Gold-plated copper wire leads are molded into the sidewalls of the ring frame for stability and hermetic sealing. The ring frame is attached to the heat sink with pins. The pins are molded into the heat-sink base when the ring frame is molded onto it, forming a hermetic seal. After the hybrid circuits have been mounted in the package, the package cover is hermetically sealed in place with soft solder. To provide a soldering surface on the plastic, the inside edge of the cover and the top of the ring frame are plated with copper.

The 90° bend in the molded-in leads prevents them from rotating and causing the package to leak under thermal or mechanical shock. Such shocks sometimes cause conventional metal- or ceramic-cased assemblies to fracture.

The molded plastic has been selected for its excellent dimensional stability, resistance to heat and radiation, and good mechanical strength. At 70° F (21° C) it absorbs or releases no more than 0.22 percent water with no chemical or dimensional changes.

The wire leads point away from the package base to allow direct connection to a printed-wiring board. As an alternative, harness wires could be soldered to the leads if they were bent into hooks as is sometimes done with relay headers. For printed-circuit-board mounting, the threaded attachment inserts in the corners could be deleted and the wire leads pointed in the direction of the package base. For good heat transfer, the package base could be attached to the heat sink with heat-conducting epoxy.

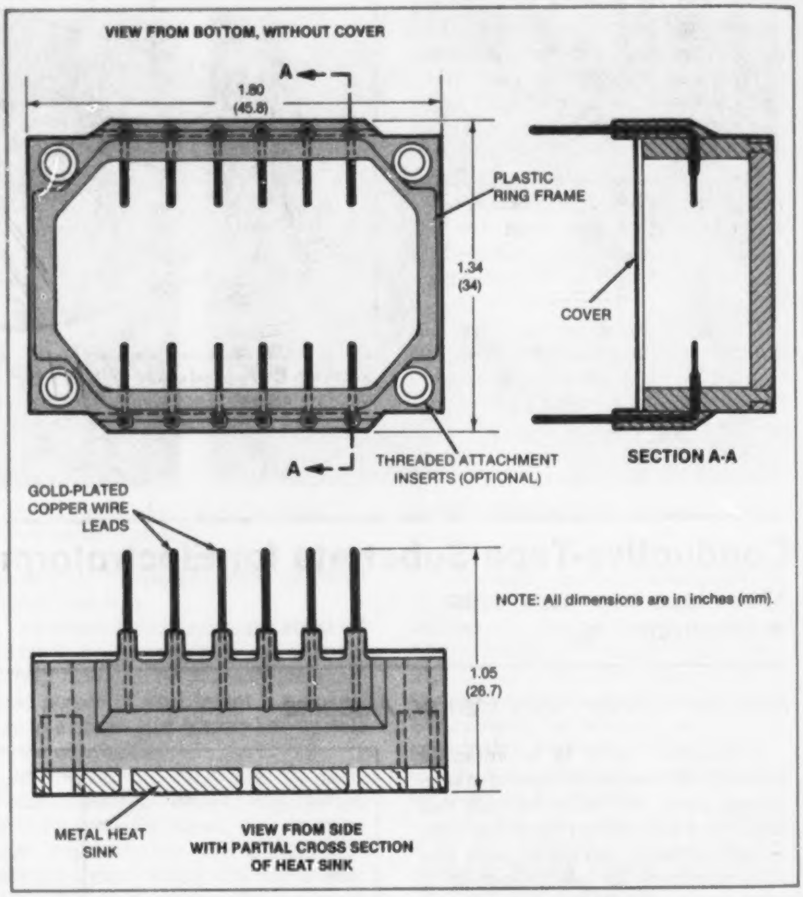
VIEW FROM BOTTOM, WITHOUT COVER
A
1.80
(45.8)
PLASTIC RING FRAME
1.34
(34)
COVER
A
THREADED ATTACHMENT INSERTS (OPTIONAL)
SECTION A-A
GOLD-PLATED COPPER WIRE LEADS
NOTE: All dimensions are in inches (mm).
1.05
(26.7)
METAL HEAT SINK
VIEW FROM SIDE WITH PARTIAL CROSS SECTION OF HEAT SINK

A Proposed Power Hybrid Circuit Package constructed mainly of molded plastic is hermetically sealed without the use of costly metal-to-glass seals. The mass of the package including the copper base is 31.75 grams. An equivalent glass-to-metal package in current use has a mass of 78.9 grams, while an all-copper package has a mass of 86.2 grams.

This work was done by Wilson N. Miller and Ormal E. Gray of Rockwell International Corp. for **Johnson Space Center.** *For further information, Circle 51 on the TSP Request Card.*

This invention is owned by NASA, and a patent application has been filed. Inquiries concerning nonexclusive or exclusive license for its commercial development should be addressed to the Patent Counsel, Johnson Space Center [see page A5]. Refer to MSC-20181.

Low-Cost Electrically-Heated Glass Panels

Simple process converts reflective glass
into electrically heated panels.

NASA's Jet Propulsion Laboratory, Pasadena, California

An inexpensive process converts architectural reflective-coated glass into electrically heated panels. The technique utilizes the reflective layer as a heating element and saves the production costs of applying or embedding heating elements in ordinary glass. The resulting panels have many applications, including automobile windows, home-heating panels, temperature-controlled windows or containers, and food-warming trays. The glass can be maintained indefinitely at temperatures in excess of 100° C.

Architectural reflective glass is usually made by coating clear glass with a metallic film that in turn is covered by a thin protective film. In the conversion process, an electric potential applied between two places on the film surface (see figure) breaks down the high-resistance outer protective layer and brings the reflective film into electrical contact with electrodes on the surface. The reflective film can then be used as a resistance heating element while the protective layer still insulates it from the environment.

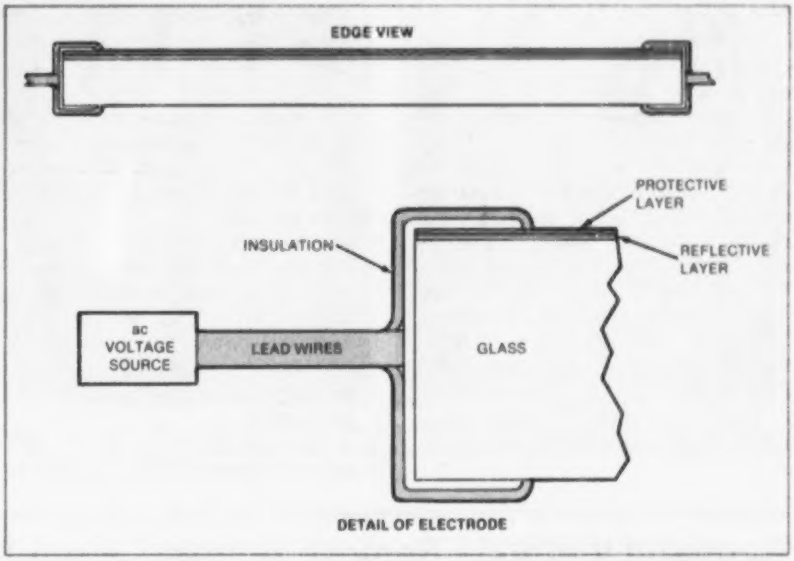

A **Simple Process** converts architectural reflective glass to electrically heated panels. Such glass is usually made by coating clear glass with a metallic film that in turn is covered by a thin protective film. Applying an ac voltage across the protective film causes it to break down, bringing the metallic reflective film in contact with external electrodes.

Metallic or conductive-paint electrode strips are applied to the reflective side and/or the edge of the glass. After curing, an ac variable voltage source is connected across the electrodes. Breakdown of the protective layer commences with the application of a few volts and is completed at about 40 volts, when sparking between the electrode and the reflective film can be seen from the underside of the glass. After this, the heating panel can be operated stably at any voltage from zero to about 100 volts. The application of higher voltages or immersion in water during operation will cause irreversible breakdown of the resistive film. Therefore, for some applications, the panels must be waterproofed or sandwiched with clear glass.

This work was done by Paul J. Shlichta and Bruce A. Nerad of **NASA's Jet Propulsion Laboratory.** *For further information, Circle 52 on the TSP Request Card.*
NPO-15753

Process Sprays Uniform Plasma Coatings

Multicomponent plasma coatings are applied
without the segregation of components.

Lewis Research Center, Cleveland, Ohio

A composite-powder processing procedure has been developed along with plasma-spray parameters to achieve homogeneous, well-bonded, low-porosity, self-lubricating coatings. The purpose was to improve the compositional uniformity of the sprayed coating and to obtain a process that could be used by vendor organizations in preparing and applying these powders and coatings. The coating was NASA-developed lubricant PS 106, which has the nominal composition by weight of 35 silver, 35 Nichrome, and 30 calcium fluoride.

Previous methods for plasma-spray application of multicomponent coatings had been simply to premix powders of the various components and to place them in a hopper from which they were fed to the plasma torch and sprayed onto the surface to be coated. Another ap-

(continued on next page)

proach had been to supply the different powders separately to the torch by means of a multifeed system. Mixing occurred in the torch.

The disadvantages of the prior methods are as follows: (1) Premixed powders of components with different densities tended to segregate when the powders were vibrated, when they flowed through the powder feedlines, and when they were sprayed. The fact that powders manufactured for plasma spraying are designed for easy flow and that often all the component powders are of about the same particle-size range only aggravated the segregation problem. (2) Using separate feeds for the various components tended to seriously complicate the entire system, especially when more than two powder components were involved. Also the feed rates of powders were difficult to control accurately over a period of time; therefore coating compositions were difficult to control by this approach.

It appeared feasible to reduce segregation of such powders by using variations in particle size or by the use of suitable binders. Mixtures of particle sizes promote agglomeration, and small particles may adhere to larger ones, creating a pseudocomposite particle. Such a "particle" might remain essentially intact during the plasma-spraying process. Alternately, binders would be used to improve the between-particle strength of such particle aggregations. The object was to introduce sufficient binder to the particle-connecting necks to achieve maximum strength.

There were two significant steps that minimized powder segregation and permitted the coating to be plasma-sprayed onto a surface without segregation of the components:

1. Very fine (typically 5-micrometer) particle-size powders of selected components were mixed dry with coarser particles (typically 50 to 150 micrometers) of the other components. The very fine particles tended to adhere to the large particles and thus to reduce segregation.
2. A small percentage (2 to 6 weight percent) of monoaluminum phosphate (MAP) aqueous concentrate was added to the powder along with sufficient additional water to form a stirrable slurry. Upon drying, the powder was in the form of a cake in which the particles were loosely held together with the MAP acting as a binder. The powder cake was then broken and passed through a sieve. The sieved powders consisted of multicomponent aggregate particles. The aggregate particles readily flowed through the plasma-spray system and were sprayed with little or no tendency to segregate into the various components.

This work was done by H. E. Sliney and T. P. Jacobson of **Lewis Research Center** *and G. C. Walther and H. H. Nakamura of the IIT Research Institute. Further information may be found in NASA CR-3163 [N79-28315/NSP], "Program for Plasma-Sprayed Self-Lubricating Coatings" [$10.50]. A copy may be purchased [prepayment required] from the National Technical Information Service, Springfield, Virginia 22161.*
LEW-13237

Acoustic Methods Remove Bubbles From Liquids

Sonic oscillation increases the surface area of bubbles and causes them to dissipate.

NASA's Jet Propulsion Laboratory, Pasadena, California

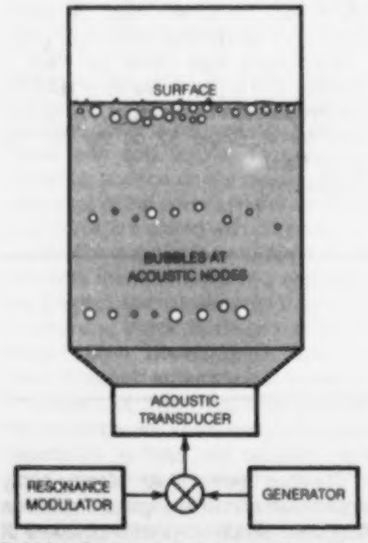

Bubbles Coalesce at the acoustic nodes, which correspond to the succession of resonant frequencies excited in the acoustic resonance chamber, and move to the surface where they break up and dissipate.

Two acoustic methods can be applied to molten glass or other viscous liquids to remove bubbles. Bubbles are either absorbed or brought to the surface by applying a high-intensity sonic field at a resonant frequency. In one method, a swept frequency resonant to bubbles of various sizes is used; and in the second, several resonant modes in an acoustic chamber are applied. The methods could be applied to the production of molds and optical-quality glass.

The first method reshapes the bubbles at their resonant frequency to increase their exposed surfaces to new areas of the liquid and to induce liquid circulation around the bubbles, thus encouraging molecular absorption. The intensity of the acoustic waves, which may be above 160 dB, depends on the density of the fluid.

In the second method (see figure), the liquid is placed in an acoustic resonance chamber. A succession of resonant modes of the chamber is applied, from the higher order modes down to the fundamental. At each frequency, the bubbles migrate to the oscillation nodes; as the frequency is decreased, the number of nodes decreases, and the bubbles tend to coalesce. Eventually they are moved to the liquid/gas interface.

This work was done by Eugene Trinh, Daniel D. Elleman, and Taylor G. Wang of Caltech for **NASA's Jet Propulsion Laboratory.** *For further information, Circle 53 on the TSP Request Card.*
NPO-15334

Improved Gloves for Firefighters

New materials and constructions
give better protection.

Lyndon B. Johnson Space Center, Houston, Texas

New firefighter's gloves are more flexible and more comfortable than previous designs. Since some firefighters prefer gloves made of composite materials while others prefer dip-coated gloves, both types were developed (see figure). The new gloves may also find uses in foundries, steelmills, and other plants where they can be substituted for asbestos gloves.

An aramid fabric was selected as the material for the outer shell of the composite glove because it is strong and resistant to flame and heat. It is also flexible, dries rapidly, and retains its flexibility after repeated wetting and drying. The palm side is a durable tightly woven twill. The back of the shell is a knit.

For the liner, aramid felt was selected because it is puncture-resistant and thermally insulating. A neoprene film 4 to 5 mils (0.10 to 0.13 millimeter) thick on the palm side of the liner helps to prevent the rapid conduction of heat; the film is flexible and flame-retardant.

Wristlets 4 inches (10 centimeters) long protect the wearer's wrists. A felt patch increases the protection on the palm side of the wristlet.

For the dip-coated glove, the shell is coated with a yellow, flame-retardant neoprene layer. A friction layer on the palm side improves the wearer's grip. The yellow dip coating shields against radiant heat better than a dark-colored coating.

The wristlet for the dip-coated glove consists of an aramid knit outer layer and a knit cotton underlayer. The underlayer prevents penetration of the dip coating, which extends a short distance up the wristlet from the hand. A patch of aramid felt gives additional protection to the palm side of the wrist.

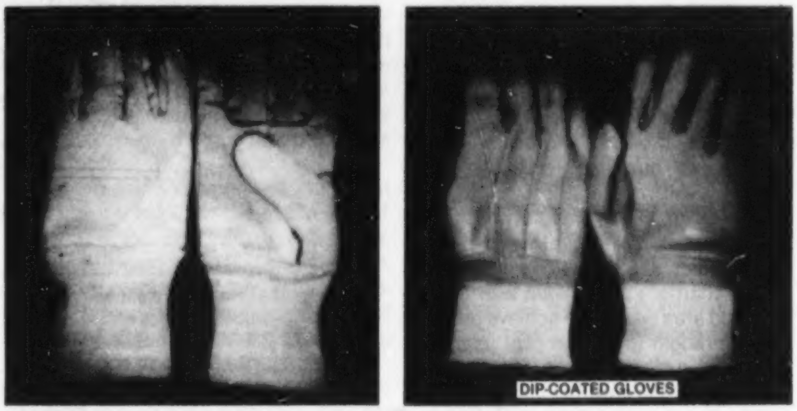

Two Versions of New Firefighter's Gloves accommodate individual preference. The palm of the glove outer shell is a twill, and the back is a knit. A friction layer on the palm side of the dip-coated glove improves the wearer's grip.

Both types of gloves were tested for conformance to standards of the National Institute for Occupational Safety and Health (NIOSH). Both met the cut-resistance criterion — that is, they sustained no cuts with a 16-pound (71-newton) load on a test blade. Puncture tests were conducted on the palm side of the gloves. Both types provided almost double the recommended 13.2-pound (59-newton) puncture resistance.

The standards state that a glove should protect against the injury-threshold temperature for 5 seconds. The composite glove exceeded the threshold after 4.6 seconds. The dipped glove maintained a temperature well below threshold for 5 seconds.

This work was done by Richard P. Tschirch, Kenneth R. Sidman, and Irving J. Arons of Arthur D. Little, Inc., for **Johnson Space Center.** *Further information may be found in NASA CR-167572 [N82-77571/NSP], "Development of Improved Firefighters' Gloves" [$9]. A copy may be purchased [prepayment required] from the National Technical Information Service, Springfield, Virginia 22161.*

This invention is owned by NASA, and a patent application has been filed. Inquiries concerning nonexclusive or exclusive license for its commercial development should be addressed to the Patent Counsel, Johnson Space Center [see page A5]. Refer to MSC-20261.

Explosive Joining for Nuclear-Reactor Repair

A ribbon charge yields a joint with
double the parent metal strength.

Langley Research Center, Hampton, Virginia

High radiation levels and crowded workspaces complicate the repair and replacement of fuel channels in nuclear reactors. Using an explosive joining technique demonstrated at Langley Research Center, however, the repairs are made remotely, resulting in a joint that is double the strength of the parent metal.

In the initial assembly of the reactor, each fuel channel (a total of 390) is manually fusion-welded to a bellows assembly (Figure 1) on the reactor face

(continued on next page)

through a thin-walled low-carbon-steel adapter flange. To remove each fuel channel, the fusion weld is severed, the fuel-channel plumbing disconnected, and the fuel channel disconnected from the end-plate fitting on the opposite reactor face. A new fuel-channel assembly with adapter must be inserted into the bellows assembly and reinstalled.

In the explosive joining technique, the adapter flange from the fuel channel is machined to incorporate a V-notch interface, shown in Figure 2. The ribbon explosive, ½ inch (1.3 cm) in width, drives the V-notched wall of the adapter into the bellows assembly, producing an atomic-level metallurgical bond. A 0.030-inch (0.08-cm) wall thickness for the adapter flange, driven by a 30-grain/foot (0.63-gram/cm) explosive ribbon charge, yields a joint with twice the bond area needed to achieve parent metal strength (a 200-percent joint). A machine surface of 64 rms yields 200-percent-strength joints, but a 32-rms finish is needed to achieve a hermetic seal. Degreasing is necessary; wet wiping with standard no-deposit solvents, such as alcohol or Freon, is sufficient.

An acceptable but considerably weaker joint is made without the anvil-ring supporting structure. The anvil ring prevents tube distortion, allowing more of the explosive energy to be utilized. An acceptable but weaker joint was created with a fuel-channel adapter flange undersized in diameter by 0.060 inch (0.15 cm). The joint is unaffected by heat loads from the reactor as demonstrated by 100 thermal shocks from 570° F (300° C) to ambient.

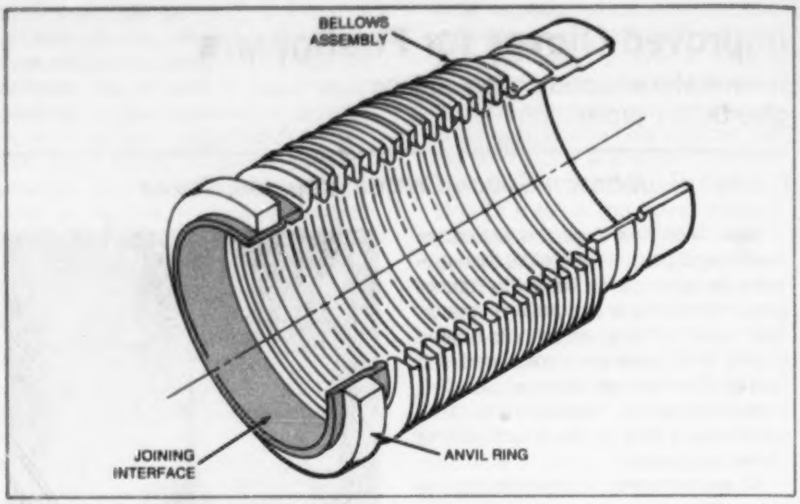

Figure 1. The **Reactor Bellows Assembly**, approximately 8 inches (20.3 cm) inside diameter, includes interface to fuel-channel adapter flange.

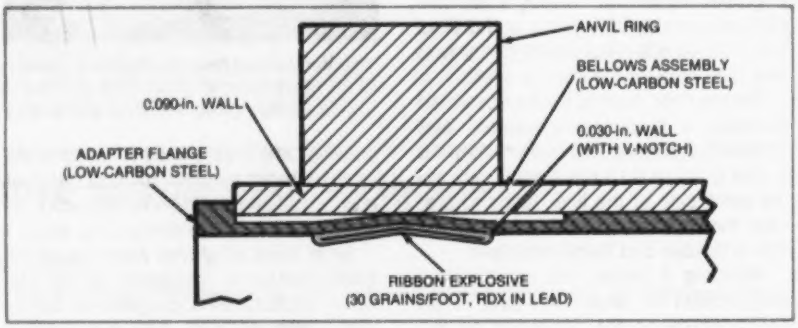
ANVIL RING
BELLOWS ASSEMBLY (LOW-CARBON STEEL)
0.090-in. WALL
0.030-in. WALL (WITH V-NOTCH)
ADAPTER FLANGE (LOW-CARBON STEEL)
RIBBON EXPLOSIVE (30 GRAINS/FOOT, RDX IN LEAD)

Figure 2. A **Ribbon Explosive** drives V-notched adapter flange into the bellows assembly.

This work was done by Laurence J. Bement of **Langley Research Center** *and James W. Bailey of Kentron International. For further information, Circle 54 on the TSP Request Card.*
LAR-12996

Electrical Conduit Distributes Weld Gas Evenly

Flexible conduit with small holes provides even weld-gas coverage.

Marshall Space Flight Center, Alabama

A purge-gas distributor, made from flexible electrical conduit by drilling small holes along its length, provides even gas flow for welding. The previous method was to drill a rigid tube.

The drilled flexible conduit is inserted into the part being welded and lightly pressurized with the purge gas. The escape holes plus the flexible joints in the conduit distribute the purge gas evenly throughout the interior of the part being welded.

The flexible conduit adjusts to accommodate almost any shape. It can be used for gas coverage in other applications that previously needed formed and drilled solid tubing.

This work was done by D. P. Ambrisco of Rockwell International Corp. for **Marshall Space Flight Center.** *No further documentation is available.*
MFS-19665

Replaceable Sleeve Protects Welder Coil

With a carbon insert, deflection coils last longer and are easier to maintain.

Lyndon B. Johnson Space Center, Houston, Texas

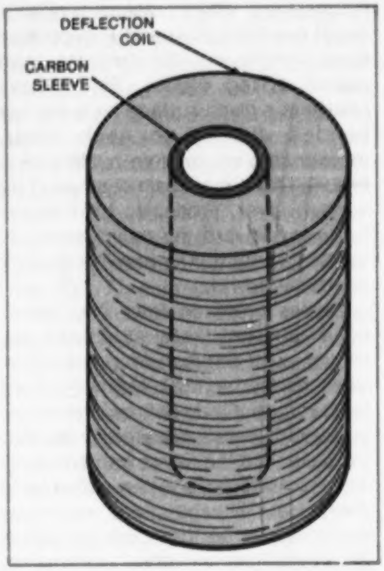

A **Carbon Sleeve** accepts metal-vapor deposits, thereby protecting the electron-beam deflection coil. It is machined from carbon rod 1.500 inches (3.810 cm) in diameter to a length of 1.343 inches (34.11 mm), an inside diameter of 1.000 inch (25.40 mm), and an outside diameter of 1.260 inches (32.00 mm).

A new replaceable carbon insert for the deflection coil in an electron-beam welder promises to decrease maintenance costs. Inserts made from materials other than carbon (not yet tried) may be less expensive, thus reducing costs even further.

During electron-beam welding, metal vapors condense on the inside wall of the deflection coil through which the electron beam passes. A metal film builds up gradually. If the metal is magnetic, it interferes with the operation of the deflection coil, and the beam does not respond to commands as it should.

The usual maintenance practice has been to overhaul the deflection coil regularly, cleaning metal film from the inside wall and recoating it with a protective layer of colloidal graphite. After several such cleanings, the colloidal graphite no longer adheres, and the deflection coil has to be discarded.

The new insert is a cylindrical sleeve machined from carbon rod. The diameter is carefully controlled to assure a snug fit in the deflection coil. Since carbon is nonmagnetic, the sleeve does not interfere with coil operation.

The sleeve is much easier to clean than are conventional protective coatings. Metal deposits are brushed away, and the sleeve is then returned to service.

The carbon sleeve is in regular production use. It reduces welder downtime for coil cleaning and extends the useful life of deflection coils.

This work was done by William L. Baker and Clifton E. Simpson of General Dynamics Corp. for **Johnson Space Center.** *No further documentation is available.*
MSC-20236

Transport and Installation of Fibrous Insulation

Two methods preserve the fiber orientation before and during installation.

Lyndon B. Johnson Space Center, Houston, Texas

Two new techniques simplify the transport and installation of oriented-fiber thermal insulation. Other applications involving oriented fibers or loose fillings might also be able to utilize the methods.

It is necessary to fill spaces around the Space Shuttle reaction-control thrustors with insulation fibers in specific orientations. Each thrustor has to be wrapped with fibers able to withstand 2,500° F (1,370° C) and having the proper density so that the temperatures of thrustor components can be kept within safe limits.

In one installation method, layers of uncured phenolic-impregnated batting in various shapes are wound around a mold and then compressed to the required density by a mandrel. The mold and insulation are then heated to 425° F (218° C) to cure and evaporate part of the binder. The insulation has the minimum practical binder content — 4-1/2 percent, just enough to prevent the parts from breaking up in transit. The rest of the binder is volatilized after installation, when the thrustor is heated to 600° F (316° C) for 48 hours.

The second method uses no resin. Instead, the insulation is compressed in a mold and saturated with water. The wet insulation is then frozen in the shipping container. After the frozen insulation is installed around the thrustor, it is heated until the water is driven off.

This work was done by Sieg Borck, Frederick L. Falconer, and Raymond V. Loustau of The Marquardt Co. for **Johnson Space Center.** *No further documentation is available.*
MSC-20074

InGaAsP CW Lasers on (110) InP Substrates

Threshold current densities are below 1,000 A/cm^2 at room temperature.

Langley Research Center, Hampton, Virginia

Quality InGaAsP/InP CW laser structures have been grown by conventional liquid-phase epitaxy on (110) InP substrates without using special growth procedures. The low broad-area current densities and 1.3-μm CW operation at room temperature indicate that InP/InGaAsP/InP laser structures with characteristics comparable to present state-of-the-art structures can be grown on the (110) InP substrates.

Previous studies of liquid-phase epitaxy of InGaAsP alloy on (110) surfaces of III-V semiconductor substrates had shown layers containing nonwetting defects and terracing. High-quality layers could be grown only after dissolving the substrate surface to a depth of 50 to 100 μm and then growing a buffer layer of approximately 20 μm.

InP wafers having (100) and (110) surfaces with similar doping and similar etch-pit densities were chemimechanically polished, etched, and rinsed. Scanning electron microscopy of the two surfaces showed that the (110) surface had fewer defects.

Double-heterojunction laser structures were grown using liquid-phase epitaxy supercooling with a horizontal sliding boat. Stained cross sections of the samples were examined in an optical microscope. The (110) surfaces were comparable to or slightly better than the (100) surfaces in physical appearance, including layer thickness and interface planarity.

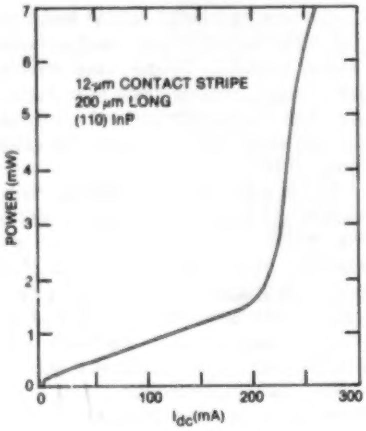

The **Power/Current Characteristic** of an oxide-stripe laser device at room temperature shows a threshold current of about 220 mA for continuous-wave operation.

Improved surface quality and grown-layer morphology are attributable to the nearly-perfect surface stoichiometry of the (110) surface [not available on (100) substrates], which makes available equal numbers of In and P deposition sites. Atoms in (110) surfaces form planar zigzag chains. Since these chains in a given surface layer are not bonded directly to each other, independent single-atom nucleation is required for every chain in a new (110) surface layer, producing an inherent tendency toward the maintenance of surface planarity. This may improve the interface growth.

Diodes prepared from the double-heterojunction laser structures exhibited pulsed threshold current densities as low as 970 A/cm^2 at room temperature. Oxide-defined stripe-contact lasers were fabricated by depositing SiO$_2$ onto the p-type cap and etching 12-μm-wide stripes perpendicular to the (110) cleavage plane, which is perpendicular to the substrate plane. Stripe devices exhibited continuous-wave thresholds as low as 150 mA at room temperature (see figure).

This work was done by Frank Z. Hawrylo of RCA Corp. for **Langley Research Center.** *For further information, Circle 55 on the TSP Request Card.*
LAR-12840

Chemical Vapor Deposition of Germanium on Silicon

Interface stresses are reduced during both growth and cooling periods.

NASA's Jet Propulsion Laboratory, Pasadena, California

Experimental work has shown that chemical vapor deposition (CVD) by pyrolysis of gaseous germanium tetrahydride provides epitaxial layers of germanium on silicon. The relatively low temperature of the CVD process (500° to 900° C) reduces stresses that occur at the layer/substrate interface during growth and cooling. These stresses are created by the mismatch, between the mechanical, thermal, and crystallographic properties of germanium and silicon. The process is under development; when refined, it could be used for fabricating germainium-on-silicon photovoltaic surfaces of the preferred orientation toward Ge (111).

The chemical-vapor-deposition system consists of a vertical quartz reactor, an RF induction heater, and feedlines. Phosphorus-doped (111) silicon is degreased and chemically etched before being placed in the reactor. In the reactor, gaseous germanium tetrahydride (GeH$_4$), which is diluted to 5 percent by helium gas, decomposes into germanium and deposits on the silicon.

To explore the effect of temperature on the deposits, a series of several 30-minute depositions was made on different samples using the same carrier-gas flow rate and GeH$_4$-in-He concentration; the temperatures ranged from 537° to 897° C. From a crystallographic view, the quality of the low-growth-temperature (537° C) deposits is the same as that of the medium (737° C) and high-temperature-growth (897° C deposits.

This work was done by Herzl Aharoni of Caltech for **NASA's Jet Propulsion Laboratory.** *For further information, Circle 56 on the TSP Request Card.*
NPO-15565

CLEFT Process for GaAs Solar Cells

Ultrathin solar cells are repeatedly grown on the same substrate.

Lewis Research Center, Cleveland, Ohio

Basically the CLEFT (cleavage of lateral epitaxial films for transfer) process involves growing an ultrathin gallium arsenide (GaAs solar cell on a much thicker layer of the same material. The growth method is such that the completed solar cell is easily separated by cleaving from the much thicker substrate. The resulting 10-micrometer-thick cell is 90 percent thinner and 77 percent lighter than the thinnest silicon solar cell. Furthermore, the thick substrate is reusable in making additional cells, which reduces cell material cost.

The greatly-reduced material usage in the CLEFT process results in material costs for GaAs cells that are comparable to the costs for silicon cells currently used in space. Since GaAs cells are more efficient (18 percent) than silicon cells (14 percent) and also more radiation-resistant, the process will make GaAs cells more practical for space applications, as well as for uses here on Earth.

The CLEFT process allows a drastic reduction in the usage of GaAs. This is important both as a method of reducing costs of these cells and reducing the usage of comparatively rare material. The reduction in material usage does

The CLEFT process is a peeled-film technique. The basic idea of peeled-film technology is to grow a thin single-crystal epilayer on a single-crystal mold, to separate the epilayer from the mold, and then to use the mold again.

As a demonstration that the CLEFT process can be used to prepare multiple GaAs films, four CLEFT cycles using the same single-crystal GaAs substrate have been carried out. Four successive films of excellent quality were obtained, with thicknesses of 5, 10, 10, and 8 micrometers, respectively. The area of each film is about 4 cm^2. The films prepared and separated in this manner have been shown by Hall measurements to be comparable in quality to conventional single-crystal chemical-vapor-deposition (CVD) layers.

not result in significant degradation in the high efficiency of GaAs cells, which is the major advantage over Si cells. It is expected that CLEFT cells, when fully developed, will achieve conversion efficiencies as high as 20 percent with GaAs layers only 5 micrometers thick.

If this goal can be achieved, the cost of GaAs material will no longer be the major obstacle for this material system. Furthermore, there should be enough Ga available for large-scale deployment of GaAs cells.

This work was done by John C. C. Fan, Carl O. Bozler, and Robert W. McClelland of the Massacusetts Institute of Technology for **Lewis Research Center.** *Further information may be found in "Thin-Film GaAs Solar Cells," Proceedings of the 15th IEEE Photovoltaic Specialists Conference, June 1981, pp. 666-672.*

Inquiries concerning rights for the commercial use of this invention should be addressed to the Patent Counsel, Lewis Research Center [see page A5]. Refer to LEW-13912.

Wipe Melt for InP Seed Substrate

A new combination of elements leaves a smooth high-luster surface.

Langley Research Center, Hampton, Virginia

Indium phosphide (InP) semiconductor substrates used as seed wafers for liquid-phase epitaxy growth tend to lose excessive amounts of phosphorus from the surface during the melt-homogenization portion of the growth cycle. The erosion of the surface due to dissociation results in holes, cracks, indium (metal) spheres, and other unwanted artifacts.

Methods previously used to eliminate or lessen the surface erosion include an InP cover wafer (used as a phosphorus source) and wipe melts of various elemental combinations. (A wipe melt is a liquid solution used to etch back or remove an acceptable amount of the surface and substrate material from the seed wafer. The etch is done at a predetermined temperature during the growth cycle before the substrate enters the semiconductor-layer growth solution.) Although somewhat acceptable, these methods have tended to be inconsistent.

A new four-element wipe melt containing indium (In), gallium (Ga), arsenic (As), and phosphorus (P) has consistently produced an acceptable morphology. The approximate proportion of each element is 94.58 percent In, 4.49 percent As, 0.73 percent Ga, and 0.2 percent P. The weights of the components used in the wipe melt are: 4.4657 g In, 13.2 mg InP, 306.5 mg InAs, and 45.1 mg GaAs.

The seed substrate is pulled under the InGaAsP wipe melt at a temperature of 650° C for approximately 15 to 60 seconds. At 650° C the melt is undersaturated with phosphorus, resulting in controlled dissolution of InP from the seed wafer surface. After pullthrough and meltback, the surface has a high smoothness and luster without the meniscus lines, exaggerated erosion, pits, and pearls that are characteristic of other wipe melts. In addition, the layer-to-substrate interface structure is more planar and of better quality.

This work was done by Frank Z. Hawrylo of RCA Corp. for **Langley Research Center.** *No further documentation is available.*
LAR-12912

High-Production Silicon-Ingot Slicer

Spinning ingots would be cut in balanced pairs.

NASA's Jet Propulsion Laboratory, Pasadena, California

A new concept for slicing silicon ingots into wafers promises to increase production rates and to improve yields of good wafers, thereby reducing the cost of manufacturing silicon solar cells. In the proposed wafer slicer, a stack of ganged blades cuts a group of silicon ingots simultaneously. The blades cut horizontally while the ingots rotate about their vertical axes. Rotation of the ingots increases the net cutting speed and reduces by half the depth to which a blade must penetrate an ingot to sever a wafer. As a result, the production of wafers for a given run is higher, even for moderate or low blade-rotation speeds and feed rates. Lower speeds and rates should produce fewer broken wafers.

Either inside-diameter or outside-diameter blades may be used (Figure 1). Pairs of ingots are positioned symmetrically around the cutting edge. The opposing-pair arrangement helps to balance the forces on the blade, thereby reducing vibration, improving wafer quality, and further reducing wafer breakage. Four, six, eight, or more ingots may be cut simultaneously, provided that the number is made up of opposed pairs.

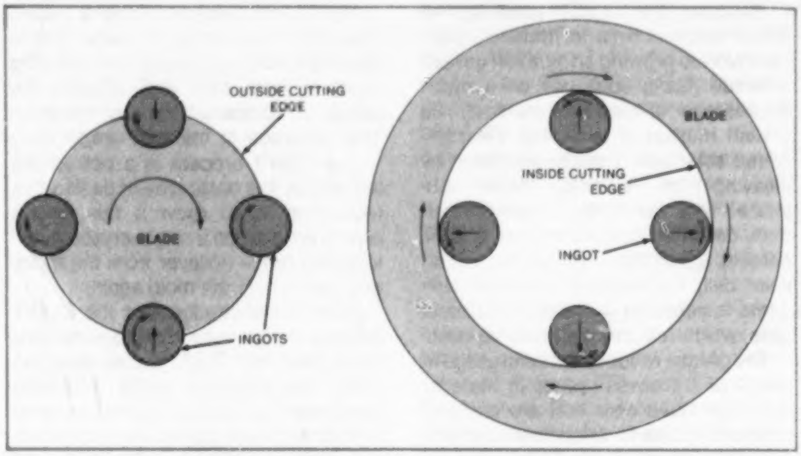

Figure 1. **As They are Rotated,** ingots are fed against the cutting edge of a blade. The cutting edge may be on either the inside or outside circumference of the blade.

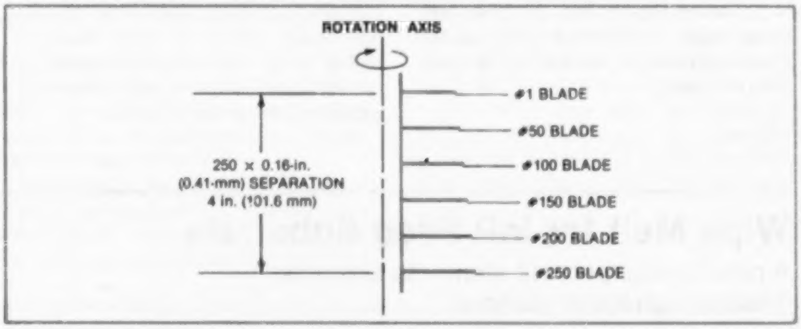

Figure 2. **Blade Edges are Staggered** so that final severance proceeds in rapid succession rather than all at once. Blades shown here are part of a 250-blade stack. Each edge is displaced 0.004 inch (0.1 mm) from the blade below it, for a total displacement of 1 inch (25.4 mm) between the topmost and bottommost edges.

The ingots are fed radially toward the center of rotation of the blade if cutting is done on the outside circumference of the blade and radially away from the center if cutting is done on an inside circumference. The rotation of the ingots about their vertical axes should be in the same sense as that of the cutting blade for outside cutting and in the opposite sense for inside cutting.

The rotation greatly reduces the cutting contact area. Since the contact pressure for effective cutting remains essentially unchanged, the reduced area makes it possible to slice a large number of wafers simultaneously without imposing excessive loads on the machine. Similarly, the thrust applied to each ingot is not unduly large, and bending of the ingots — which are supported only by their upper ends — is reduced.

A further advantage of ingot rotation is that it aids in the removal of debris. Silicon chips and abrasive particles quickly slide off the spinning wafer surface. A potential source of wafer damage and blade wear is thus eliminated, and the flow of coolant over the cut is promoted.

The stacked blades must handle the cut wafers properly to avoid damage. The wafers should leave each ingot from the bottom first in an upward progression. Therefore each blade should have a slightly different diameter from that of its neighbors (Figure 2). If slicing is done by the outside edge of the blade, the diameter of the lowest blade must be slightly larger than that of the blade immediately above it, and so on up the stack. If cutting is done on the inside edge, the cutting hole in the lowest blade must be slightly smaller than the cutting hole in the blade just above it.

The small cutting contact area, the slow feed rate, and the relatively-low rotational speed of the blades may mean that slicing an individual wafer takes a longer time with the new concept. However, the longer time is more than compensated by the large number of ingots that can be cut simultaneously.

This work was done by Yu Shen Kuo of Caltech for **NASA's Jet Propulsion Laboratory.** *For further information, Circle 57 on the TSP Request Card.*
NPO-15483

Growing Silicon Ribbon Horizontally

A faster growth rate is just one
advantage over vertical drawing.

NASA's Jet Propulsion Laboratory, Pasadena, California

Horizontal growth of silicon ribbon offers several advantages over vertical growth. It woud be faster — possibly 1 to 2 centimeters per second — and could be done without using drawing dies, a source of contamination in vertical growth. The horizontal process would naturally create a doping profile (decreasing dopant concentration toward the top surface), and it lends itself to continuous removal of impurities from the silicon melt.

In the proposed horizontal-growth process, a seed crystal is introduced into a crucible of molten silicon and withdrawn horizontally, carrying with it a continuous ribbon of newly-solidified single-crystal silicon (see figure). A long-term goal is to pull ribbons 3 1/2 to 7 mils (0.09 to 0.18 millimeter) in thickness at rates of 1 to 2 centimeters per second. Such a high growth rate is possible because the horizontal orientation offers a relatively large area for the rejection of heat by radiation, forced or natural atmospheric convection, and by conduction and convection from the solidifying ribbon to the liquid below it. In contrast, the heat-rejection area available for vertical growth is merely the cross-sectional area of the ribbon.

The meniscus under the moving ribbon at the crucible will leak slightly under certain conditions. If the leakage is carefully controlled, such spillover can be turned to advantage: It removes the impurity-laden top layer of the melt, preventing impurities from building up. The spilled silicon can be purified and recyled.

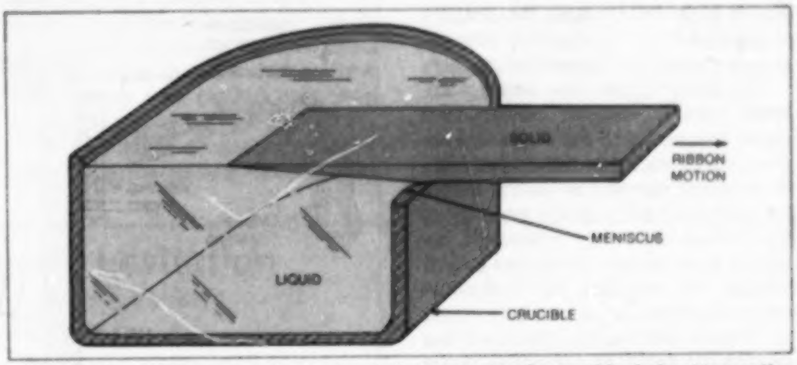

A Solid Ribbon of Silicon is pulled horizontally over the lip of a crucible. As heat leaves the silicon by radiation, conduction, and convection, the surface layer solidifies from the liquid.

The combined effects of thermal diffusion in the solidifying ribbon and the convection induced in the melt by the horizontal ribbon motion result in a dopant-concentration gradient near the surface. As a result, the top (first-to-grow) surface of the ribbon contains a minimum dopant concentration. The dopant density increases with distance below the top surface, reaching a maximum at the bottom (last-to-grow) surface of the ribbon. The low/high-dopant distribution provides a built-in back-surface field — a desirable feature because it makes solar cells more efficient. The top, low-doped ribbon surface is used as the top of a solar cell. The lightly doped region forms a collecting junction that places the material with the highest recombination lifetime in the region of greatest solar-energy absorption. The heavily-doped bottom surface reduces the series resistance of the cell.

To establish the ultimate horizontal-drawing rates for high-quality silicon ribbon, seeded-growth behavior will have to be studied. The rate of surface growth at the leading edge appears to be the factor limiting the drawing rate. A variable-flow jet of helium or argon gas at the leading growth edge may help; the jet will cool the solidifying ribbon more rapidly, thus allowing it to be pulled more quickly.

[For a related article, see "Technique for Crystal-Ribbon Growth" (NPO-15177) on page 93 of *NASA Tech Briefs*, Vol. 7, No. 1.]

This work was done by John A. Zoutendyk of Caltech for **NASA's Jet Propulsion Laboratory.** *For further information, Circle 58 on the TSP Request Card.*
NPO-14977

Meniscus Imaging for Crystal-Growth Control

Anamorphic imaging and adjustable contrast
help to monitor growth conditions.

NASA's Jet Propulsion Laboratory, Pasadena, California

Silicon crystal growth is monitored by a new video system that reduces operator stress and improves the conditions for observation and control of the growing process. The system optics produce greater magnification vertically than horizontally, so the entire meniscus and melt is viewed with high resolution in both the width and height dimensions.

The monitoring system can be used for many different crystal-growth processes and in particular for the capillary-die process illustrated in the figure. Here

(continued on next page)

a silicon ribbon crystal is grown for use in solar cells. The size of the ribbon is affected by the pulling speed and growth-interface temperature.

The enhanced anamorphic meniscus image is displayed on a screen along with control data so that the growth process is observed by the operator with a minimum of fatigue and reaction time. The operator manipulates the circuitry to produce the desired control voltages in response to the displayed information.

The operator can also select automatic control: Voltages derived from digital processing of the image are applied to a servocontrol system that regulates heater currents or pulling speed. For example, the average intensity of the enhanced-contrast processed image is automatically computed over a window that includes the crystal/meniscus interface. As the interface moves up or down, the average intensity in the window increases or decreases above or below a reference intensity level that corresponds to the desired position. The difference between the average and reference levels produces an error signal that is used to alter the pulling rate or heater current.

This work was done by Emanual M. Sachs of Mobil Tyco Solar Energy Corp. for **NASA's Jet Propulsion Laboratory.** *For further information, Circle 59 on the TSP Request Card.*
NPO-15349

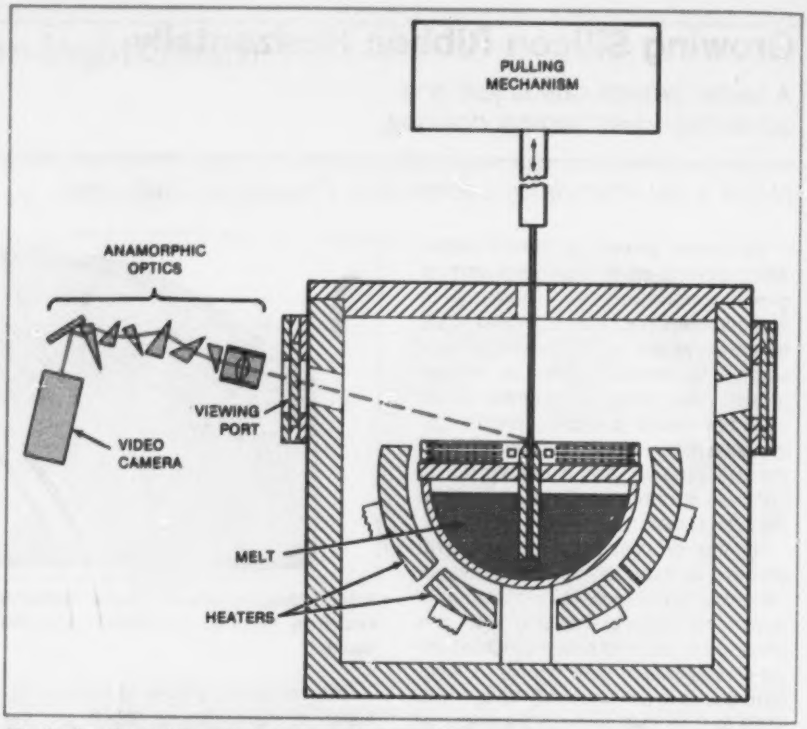

Monitoring Crystal Growth is easier and more effective with this video imaging and control system than with earlier systems employing microscopes and separate control electronics. The camera produces an image on a display screen, and operator-directed circuits for measurement and control adjust crystal-growth parameters.

Preventing Freezeup in Silicon Ribbon Growth

Profiled heat extractor prevents ribbon ends from solidifying prematurely.

NASA's Jet Propulsion Laboratory, Pasadena, California

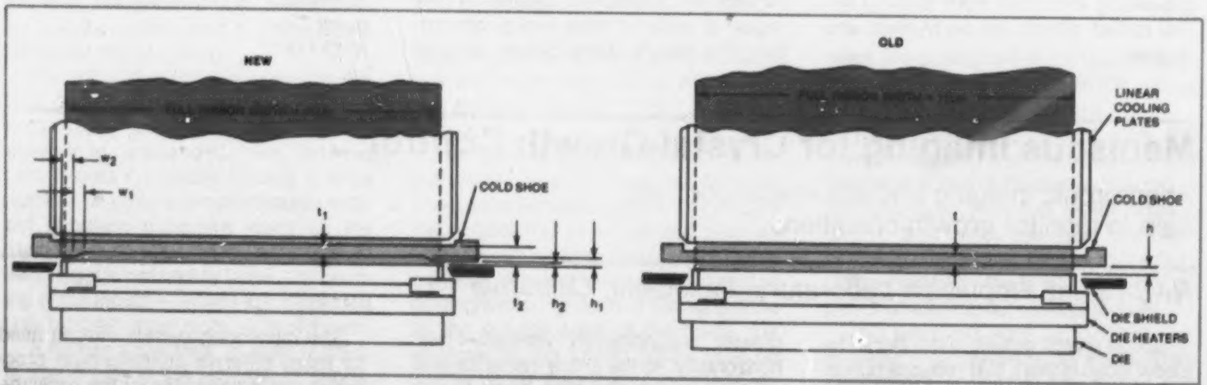

Dimensions of New Cold Shoe are chosen to yield a nearly-zero lateral temperature gradient. New dimensions in centimeters are $h_1 = 0.16$, $h_2 = 0.08$, $t_1 = 0.21$, $t_2 = 0.28$, $w_1 = 0.75$, and $w_2 = 0.39$.

A carefully-shaped heat conductor helps to control the thermal gradients that are crucial to the growth of single-crystal silicon sheets for solar cells. The ends of the die through which the silicon sheet is drawn as a ribbon from molten silicon must be held at a temperature only slightly above the solidification point of silicon. In older systems with poor temperature-gradient control operating near the freezing point, the ribbon often solidifies prematurely, freezing to the die at its ends. The ribbon breaks and must be restarted.

Now, however, a "cold shoe" with contours that are specially shaped promises to solve the freezing problem. The cold shoe, which extracts heat from the ribbon as it emerges from the die (see figure) thus affords a further means of controlling the die-top temperature, in addition to the active control provided by die heaters and the passive control provided by the shape of the die itself. Whereas in previously-designed cold shoes, the distance h between the die top and the cold shoe and the height t of the flat face of the cold shoe are constant, in the new profiled cold shoe, these dimensions are variable.

With the profile dimensions indicated in the figure, the lateral temperature gradient in the ribbon disappeared, and the tendency of the emerging ribbon to freeze prematurely — at its ends before its center — therefore disappeared too. The ribbon grew smoothly at a rate of 3 cm per minute with a uniformly high meniscus across its width and well-developed stable ends.

This work was done by Brian Mackintosh of Mobil Tyco Solar Energy Corp. for **NASA's Jet Propulsion Laboratory.** *For further information, Circle 60 on the TSP Request Card.*
NPO-15294

Variable-Position Acoustic Levitation

Pressure amplitudes and frequencies are varied to change the equilibrium position.

NASA's Jet Propulsion Laboratory, Pasadena, California

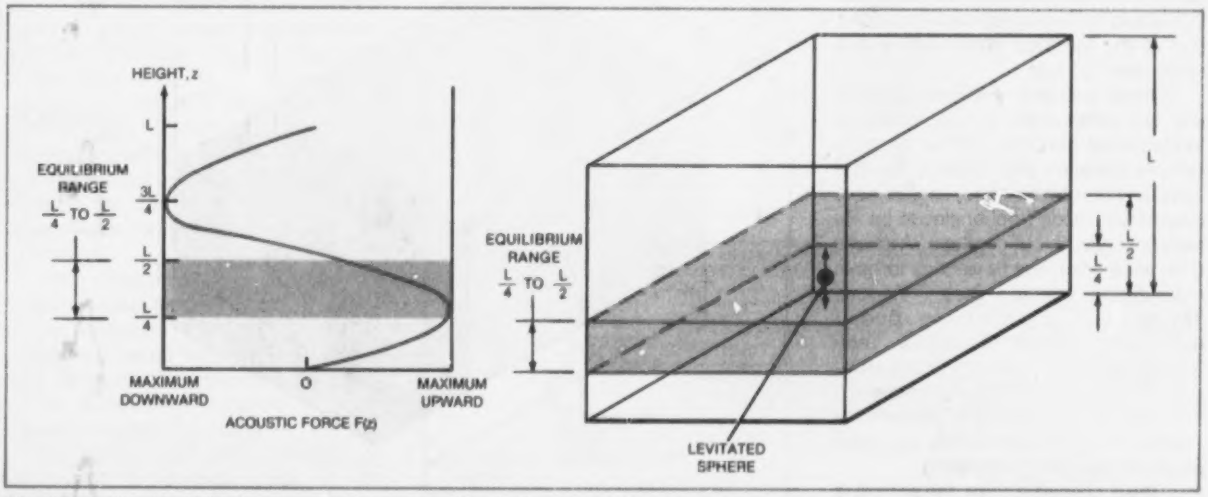

The **Sphere Can Be Raised or Lowered** to any position in the range L/4 to L/2 when the acoustic chamber is excited at its fundamental resonance frequency. When the chamber is excited at harmonics of the fundamental, additional variable-position zones are created.

A method of acoustic levitation supports objects at positions other than the acoustic nodes. Acoustic force is varied so that it balances gravitational (or other) force, thereby maintaining an object at any position within an equilibrium range. When the acoustic frequency is the fundamental resonance of the acoustic chamber, the equilibrium range is one-fourth of the chamber length (see figure).

The levitation method is applicable to containerless processing. In a levitation furnace, for example, it could be used to manipulate specimens without contacting them, perhaps moving them through a temperature gradient.

The acoustic levitation depends upon the sample height, z, and chamber vertical length, L, according to a function that is proportional to $\sin(2\pi Nz/L)$, where N = the order of the harmonic of the fundamental chamber frequency. In the fundamental mode ($N = 1$), the maximum upward acoustic force occurs at $z = L/4$. Above this height, the lifting force decreases with increasing height (as with an object supported by a spring). When this maximum force is greater than or equal to the opposing force (gravity), a sample will levitate at or above the L/4 position. Thus, L/4 is the minimum height at which an object can be supported in equilibrium. Above L/2, the force of gravity acts on the specimen in the same direction as the acoustic force, and further levitation is resisted.

A specimen is placed in an acoustic chamber excited at its fundamental mode. The acoustic amplitude (and thus the acoustic force) is increased until it is

(continued on next page)

just sufficient to hold the specimen at a height of L/4. The acoustic amplitude is increased further until the sample rises to the desired position, anywhere between L/4 and L/2. Given the densities of the sample and gas medium, the equilibrium position between these two points can be determined from the acoustic pressure. There are additional regions of equilibrium if the chamber is excited by harmonics of the fundamental frequency.

A variable force such as an electrostatic force can be substituted for gravity and used to vary the position of a levitated specimen. If the variable force can be both positive and negative, the zones of equilibrium will be extended to twice their size in a unidirectional field and will become continuous.

Such objects as table-tennis balls, hollow plastic spheres, and balsa-wood spheres have been levitated in the laboratory by the new method.

This work was done by Martin B. Barmatz, James D. Stoneburner, Nathan Jacobi, and Taylor G. Wang of Caltech for **NASA's Jet Propulsion Laboratory.** *For further information, Circle 61 on the TSP Request Card.*
NPO-15559

Controlling the Rotation of Levitated Samples

Levitation and rotation modes are separated.

NASA's Jet Propulsion Laboratory, Pasadena, California

In a proposed acoustic levitation system, the separate excitation of different acoustic modes would independently levitate and control the rotation of the sample. Three independent axes of rotation would be available, leading to rotation of the levitated object about any other selected axis.

Existing acoustic levitation systems use two degenerate (equal-frequency) fundamental acoustic modes for both sample levitation and rotation. Sample stability (nonrotation state) requires the degenerate mode frequencies to be exactly inphase or out-of-phase. A phase difference gives rise to viscous torques that cause rotation [see "Viscous Torques on a Levitating Body" (NPO-15413), page 56, *NASA Tech Briefs*, Vol. 6, No. 1 (Spring 1981)]. However, these systems are not efficient if the intent is to control or to prevent the rotation of the sample during high-temperature materials processing.

In the proposed system, the sample is levitated by using nondegenerate fundamental frequencies that do not cause rotation. Rotation is introduced either by adjusting the chamber dimensions to produce higher-frequency degenerate normal modes or by exciting degenerate normal modes in a chamber with specific length ratios.

As an example, consider the rectangular chamber of the figure, with sides of length l_x, l_y, and l_z. The frequency of the n_x, n_y, n_z mode is given by

$$f_{n_x n_y n_z} = \frac{c}{2}\left[\left(\frac{n_x}{l_x}\right)^2 + \left(\frac{n_y}{l_y}\right)^2 + \left(\frac{n_z}{l_z}\right)^2\right]^{1/2}$$

where c = the speed of sound.

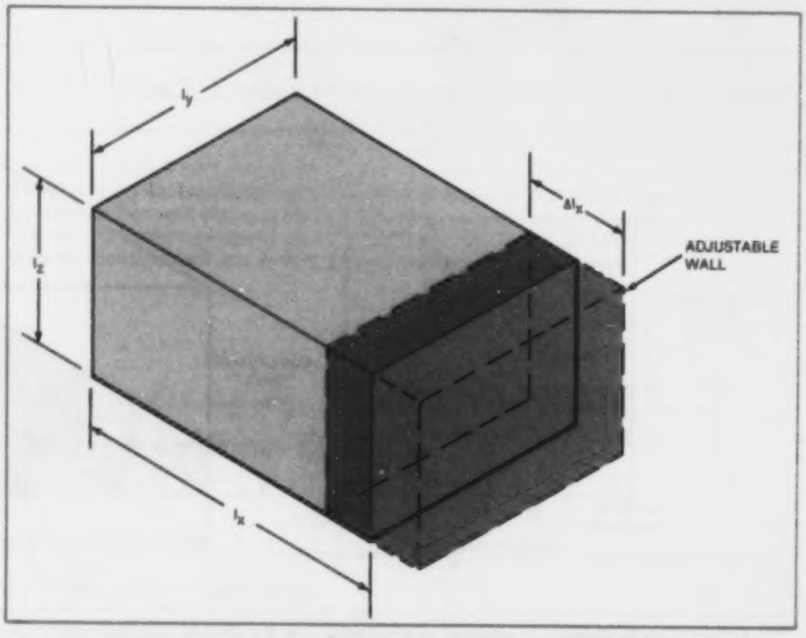

A Rectangular Chamber With at Least One Movable Wall exhibits different acoustic normal modes, depending upon the chosen wall position. The manner of selecting modes and frequencies is analogous to that of tunable waveguides or musical instruments.

If $l_y/l_x = 5/3$ and $l_z/l_y = 5/7$, then there are three pairs of degenerate normal modes; namely, $f_{300} = f_{050}$, $f_{700} = f_{005}$, and $f_{070} = f_{003}$. These mode pairs produce torques about the z, y, and x axes, respectively. The torques depend on the amplitudes and relative phases of the two modes in the pairs.

The net acoustic torque on a levitated object equals the vector sum of the acoustic torques applied by the mode pairs. If the three degenerate mode pairs are excited as in the above example, the sample will rotate about an axis alined with the net torque, with a rotational speed dependent on the magnitude of that torque. While the concept is most easily visualized for a chamber of rectangular cross section, it is applicable to any of the common shapes employed for levitation chambers and for which the normal modes are known.

The port through which a mode is excited must be positioned so as to feed energy maximally to that mode while minimizing the coupling to the other mode of the same frequency. The position selected should simultaneously be an excitation node (pressure antinode) for the normal mode desired and an excitation antinode (pressure node) for the corresponding degenerate mode that one is trying not to excite.

This work was done by Martin B. Barmatz of Caltech for **NASA's Jet Propulsion Laboratory.** *For further information, Circle 62 on the TSP Request Card.*
NPO-15522

Repairing Loose Connector Pins

Pins can be glued in place if a spring finger fails.

Lyndon B. Johnson Space Center, Houston, Texas

The electrical serviceability of a damaged connector can sometimes be restored by bonding loose contacts to the connector insert with an adhesive. The procedure eliminates the time-consuming operations of completely removing and replacing the faulty electrical connector and then testing the affected wiring.

A multipin connector (shown in Figure 1) that has removable contacts is widely used in large, integrated electronic systems because it simplifies the assembly of complex harnesses. Each removable contact is held in place by spring fingers that rest behind a shouldered section of the pin. Because the fingers are integral with the plastic insert of the connector, there is no way to replace or repair them if they become damaged.

In the repair procedure, a hypodermic needle is used (see Figure 2) to apply an epoxy adhesive in and behind the cavity containing the damaged locking finger. The damaged connector does not have to be demated or removed from the harness to apply the epoxy.

The epoxy used (Hysol EA956, or equivalent) is relatively thick: It will neither flow past the pin to the front face of the connector to contaminate the contact, nor will it flow from the repair site after the needle is removed. The epoxy fills the space around the base of the contact to anchor it in position, resulting in a permanent repair.

This work was done by William T. Dean III and Eugene J. Stringer of Rockwell International Corp. for **Johnson Space Center.** *No further documentation is available.*
MSC-20374

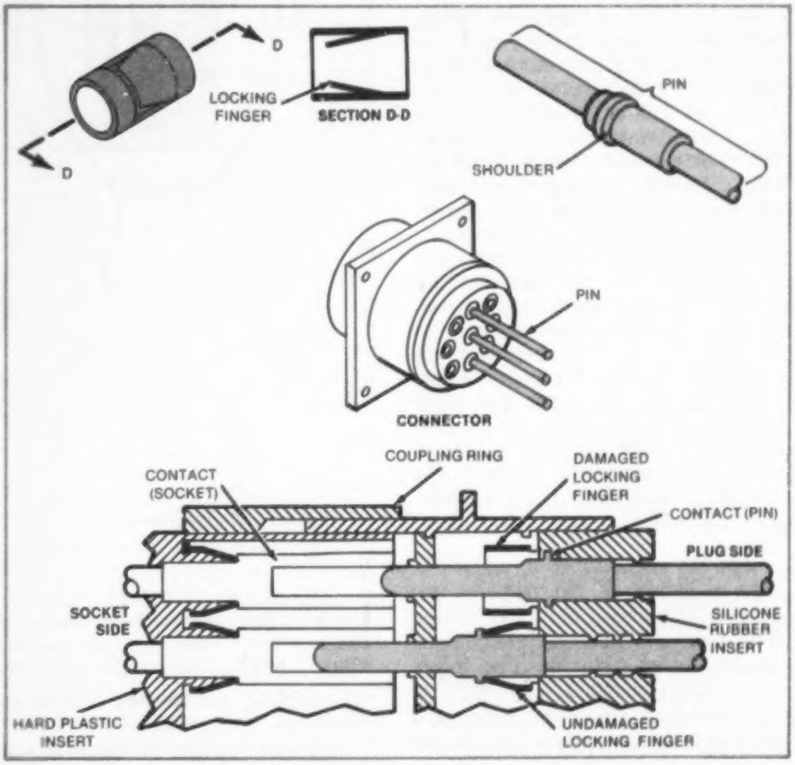

Figure 1. In this **Electrical Connector** (above) a contact pin is inserted and pushed into a spring-locking device to retain it in a secured position. In the two mated connectors (below) both contacts on the socket side are locked in by good locking devices. On the plug side, one pin contact is locked in by a good locking device, while the other pin contact is pushed from its position because of a damaged locking device.

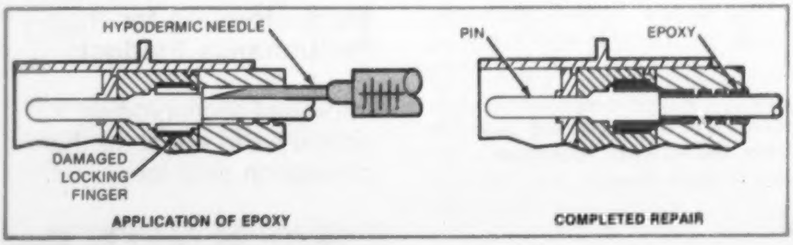

Figure 2. The **Displaced Contact** has been pushed back into its cavity, and a cured epoxy retains it in a secured position. Any number of contacts within the same connector can be repaired the same way.

Jig Quickly Checks Connector-Pin Alinement

Special jig reduces test time from hours to minutes.

Lyndon B. Johnson Space Center, Houston, Texas

A test jig checks whether the pins of a connector are within location tolerance. The jig greatly reduces test time. For a 250-pin connector, for example, a test that takes only 5 minutes with the jig requires 4 hours with a toolmaker's microscope — the conventional way of checking pin location.

The jig is a metal plate that makes electrical contact with out-of-tolerance pins but not with pins that are within tolerance. Parallel longitudinal slots are cut on one side of the aluminum plate, and parallel transverse slots are cut on the other side (see figure). Since the slots are cut through slightly more than half the thickness of the plate, their intersections form rectangular holes.

In a test, the operator inserts the pins of a connector into the holes while the connector body is located by dowels on the plate. If a pin is misalined, it touches the side of a hole. The operator scans the tips of the pins one by one with a stylus. A pin touching the plate establishes electrical continuity from the stylus through the plate to a buzzer or lamp, which provides a signal to the operator. The operator notes the location of misalined pins for later correction.

Jigs can be designed to accommodate a variety of pin patterns and shapes. With chemical milling or laser drilling, extremely-precise hole patterns can be created in stainless-steel sheets only 0.010 to 0.020 inch (0.25 to 0.51 mm) thick. Such templates could be mounted in general-purpose fixtures for checking pin alinement to close tolerances.

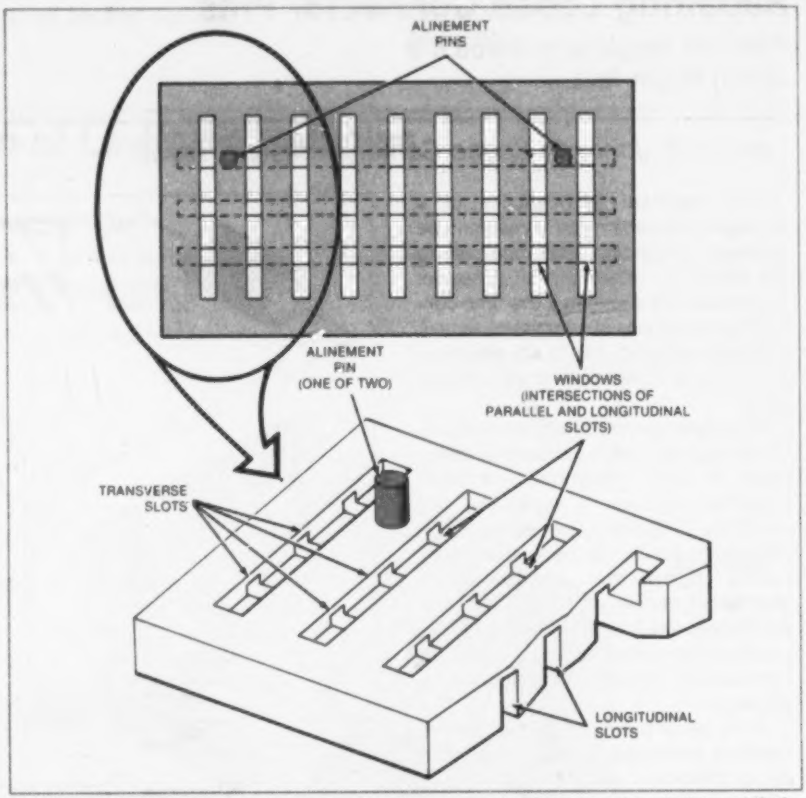
ALINEMENT PINS
ALINEMENT PIN (ONE OF TWO)
WINDOWS (INTERSECTIONS OF PARALLEL AND LONGITUDINAL SLOTS)
TRANSVERSE SLOTS
LONGITUDINAL SLOTS

Machined Slots on opposite faces of a plate form a matrix of rectangular windows at their intersections. If a connector pin is out of alinement, it makes electrical contact with the side of a window, thus triggering an indicator.

This work was done by William M. Hall and Thomas P. Papac of Hughes Aircraft Co. for **Johnson Space Center.** *For further information, Circle 63 on the TSP Request Card.*
MSC-20237

Books and Reports

These reports, studies, and handbooks are available from NASA as Technical Support Packages (TSP's) when a Request Card number is cited; otherwise they are available from the National Technical Information Service.

Electroforming for High-Performance Products

Improved technologies simplify and enhance the deposition process.

Electroforming involves the electrolytic deposition of a metal (primarily copper or nickel) on a conductive substrate material. This technique is especially well suited to the forming of certain complex and highly detailed parts. Parts fabricated in this way are used in a variety of applications ranging from rocket engines to phonograph records. Although the basic process is widely used, there is only a limited amount of high-technology experience. This severely limits the potential since high-technology experience is required to utilize electroforming in producing hardware meeting stringent service requirements. The ability to predict and reproduce physical and mechanical properties uniformly is of prime importance. Processes and procedures are, for the most part, proprietary information with the producers. As a result, the product of one electroformer will frequently differ from that of another with respect to mechanical properties, deposit quality, bond strengths, and the like.

A NASA-funded contractor report describes the development of processes and procedures for the preparation of specifications for electroforming nickel and copper outer shells on cooled rocket thrust-chamber liners. These specifications represent a merging of technical contributions from many sources into a guide for producers of electroformed, high-performance products. This report provides a basic document with which the electroformer can evaluate his product. Improved technologies are reported that simplify and enhance the deposition process. Raw materials, conducting solutions, and deposition rates are evaluated.

The data generated from this investigation will remove many of the questions and uncertainties associated with the electroforming process. Utilization of these results should expand the potential for electroformed products.

This work was done by Glenn A. Malone of Bell Aerospace Co. for **Lewis Research Center.** *Further information, may be found in NASA CR-134959 [N76-20481/NSP], "Final Report Investigation of Electroforming Techniques" [$13.50]. A copy may be purchased [prepayment required] from the National Technical Information Service, Springfield, Virginia 22161.*
LEW-12719

Heat Flow in Horizontal Ribbon Growth

A theoretical analysis focuses on conditions required for stable growth.

A recent theoretical study reveals some important effects of heat flow in horizontal ribbon growth. Particular attention is paid to the heat flow due to a laminar convection current in the melt induced by the horizontal motion of a ribbon-shaped semiconductor crystal being pulled from the melt.

Horizontal growth allows higher "pull" rates than do vertical growth techniques. This is because of the favorable ratio of the large ribbon area available for heat removal to the small cross-sectional area of the ribbon.

Both the motionally-induced and natural (thermally-induced) convection currents in the melt cause a thermal boundary layer to form adjacent to the liquid/solid interface. This causes a nonuniform heat flow from the melt.

Treatment of the combined effects of both natural and induced convection is complex and would have to be done by numerical computation. However, careful control of melt temperature by judicious design of the melt crucible and its heating can minimize the effects of natural convection. Therefore, in this investigation, only the effects due to the motionally-induced convection current are considered.

A series of different modes of ribbon cooling was analyzed to determine the relationships between ribbon thickness, pull rate, melt temperature, and cooling of the ribbon. For each mode the conditions for which ribbon pull would be stable have been investigated.

Under some conditions ribbon thickness is unstable, tending toward zero thickness: a condition that results in ribbon pullout. This occurs if too little active (forced convective) cooling is provided at the thin tip of the ribbon or where there is too little passive cooling of the rest of the ribbon surface.

With such mixed cooling, the ribbon may increase in thickness in the actively cooled region only to remelt partially in the passively cooled region if heat flow from the melt exceeds passive heat loss. The analysis was done for silicon, but it could be redone for other semiconductors by substituting their physical properties for those of silicon.

This work was done by John A. Zoutendyk of Caltech for **NASA's Jet Propulsion Laboratory.** *To obtain a copy of the study, Circle 64 on the TSP Request Card.*
NPO-14979

Improving Surface Strength of Insulating Tiles

A preglaze densification treatment helps tiles resist impact damage.

A procedure for improving tile resistance to impact damage is described in a new report on tile densification. The tile technology was originally described in " 'Densified' Tiles Form Stronger Bonds" (MSC-18741), *NASA Tech Briefs*, Vol. 5, No. 4 (Winter 1980), page 495.

Developed for the Space Shuttle reusable surface insulation, the procedure has potential application when space restrictions necessitate thin layers of insulation with low thermal conductivity. Examples are in advanced heat engines, such as the adiabatic diesel and the automotive gas turbine, as well as in fast-heating high-temperature ovens.

The fused-silica base material for the tiles is formed from high-purity silica fibers (2 to 4 microns in diameter) and a high-purity binder. After firing, the mixture provides a low-strength machinable material having low thermal conductivity, high-temperature resistance, and low thermal expansion. The first step in densifying the machined silica tile surfaces is to mask the tile so that only the surfaces to be treated are exposed. A measured amount of isopropyl alcohol is brushed on to aid in wetting the surfaces. The tile is immediately submerged in a silica slurry for 3 minutes.

The tile is removed from the slurry, and the residue remaining on the tile is brushed into its exposed surfaces. Additional slurry is applied until it starts to build up on the surface. The excess is gently removed by wiping, and further slurry is added, with a total of three brushing and wiping operations. A final brushing operation works the fused-silica aggregate into the surface so that it fills the voids sufficiently to provide a hard surface when the material has dried.

The slurry mix contains approximately 55 percent by weight colloidal silica, 45 percent by weight silica slip (irregularly-shaped particulate silica), and 0.12 percent by weight boron silicide for color. The slurry mix is continuously roll-mixed to keep the silica particles in suspension until they are applied to the tile.

The densification process increases the thermal conductivity of the surface layer but does not seriously affect the effective overall thermal conductivity. For a tile 2 inches (5.1 cm) thick, the overall conductivity is increased by about 4 percent.

This work was done by Jack W. Holt and Laurence W. Smiser of Rockwell International Corp. for **Johnson Space Center.** *To obtain a copy of the report, "Surface Densification of High-Porosity Silica Insulation," Circle 65 on the TSP Request Card.*
MSC-20063

Computer Programs

These programs may be obtained at very reasonable cost from COSMIC, a facility sponsored by NASA to make new programs available to the public. For information on program price, size, and availability, circle the reference letter on the COSMIC Request Card in this issue.

Standard Transistor Arrays

Random-logic integrated MOS digital circuits are generated.

Connections between the transistors in a gate, and connections between gates, occur with such frequency that good physical solutions may be extremely complex. Achieving a good physical solution is especially important in the design of digital large-scale-integration (LSI) circuitry.

The Standard Transistor Array (STAR) design system is a semicustom approach to generating random-logic integrated MOS digital circuits. The primary program in the STAR system is CAPSTAR, the STAR Cell Arrangement Program. CAPSTAR is augmented by an automatic routing program, a display program, and a library of logic cells.

Input to CAPSTAR consists of a description of circuit cells and interconnections. This circuit description is used to form a near-optimum, one-dimensional placement of the cells, which is then "folded" onto STAR to form a two-dimensional layout. By the use of various folding strategies, a number of different layouts are formed. The best of these are selected and are improved by a single interchange technique. The best improved layout is determined, and pads are added to generate the final layout. The placements generated are near-optimum with respect to horizontal and vertical channel usage and the number of nets that can be linearly routed.

STAR includes two programs developed to provide for the simulation of logic circuits and for the generation of test sequences for logic circuits. SIMLOG is a gate-level, logic-simulation program that is based on a three-valued logic model and on a unit-delay timing model. Both combinational and sequential circuits can be handled. Logic elements available for use include NAND gates, NOR gates, unit-delay elements, and edge-triggered D flip-flops. The simulated circuit may also contain single or multiple stuck-type faults. TESTGN is a test-sequence generation program for use with circuits being simulated by SIMLOG. The program can generate tests for unspecified faults or for specified single stuck-type faults.

The programs in STAR are written in BASIC and FORTRAN IV for batch execution and have been implemented on a Xerox Sigma V, with the largest program having a central memory requirement of approximately 128K of 32-bit words. The programs were developed in 1979.

This program was written by G. W. Cox and B. D. Carroll of Auburn University and E. R. Pitts and R. A. Wright of M & S Computing for **Marshall Space Flight Center.** *For further information, Circle P on the COSMIC Request Card.*

MFS-25327

Tile-Failure Analysis

Probability model assesses failure risk of systems with widely-varying loads and material strength.

The Tile Failure Probability Model (TFPM) program was originally developed to quantitatively assess the risk of tile loss of a thermal-protection tile from the Space Shuttle orbiter. TFPM is fairly specific to the orbiter, but the basic technique might be applied in other structural design situations where the anticipated loads and material strength have significantly variable probability distributions.

The model generates probability distributions of the tensile loads acting on a given tile during a mission and combines these with tile material-strength probability distributions to compute the probability of a tile tensile failure during the mission. This probability approach to failure analysis is required because the strength of the system, which consists of the ceramic tile material, strain isolator pad, and room-temperature-vulcanizing bond, exhibits wide variation even for similar sets of material.

The TFPM is written in FORTRAN IV and Assembler for batch execution and has been implemented on an IBM 370-series computer with a central memory requirement of approximately 800K of 8-bit bytes. The program was developed in 1980.

This program was written by Eugene A. O'Hern and Kenneth E. Ryan of Rockwell International Corp. for **Johnson Space Center.** *For further information, Circle Q on the COSMIC Request Card.*

MSC-20139

Mathematics and Information Sciences

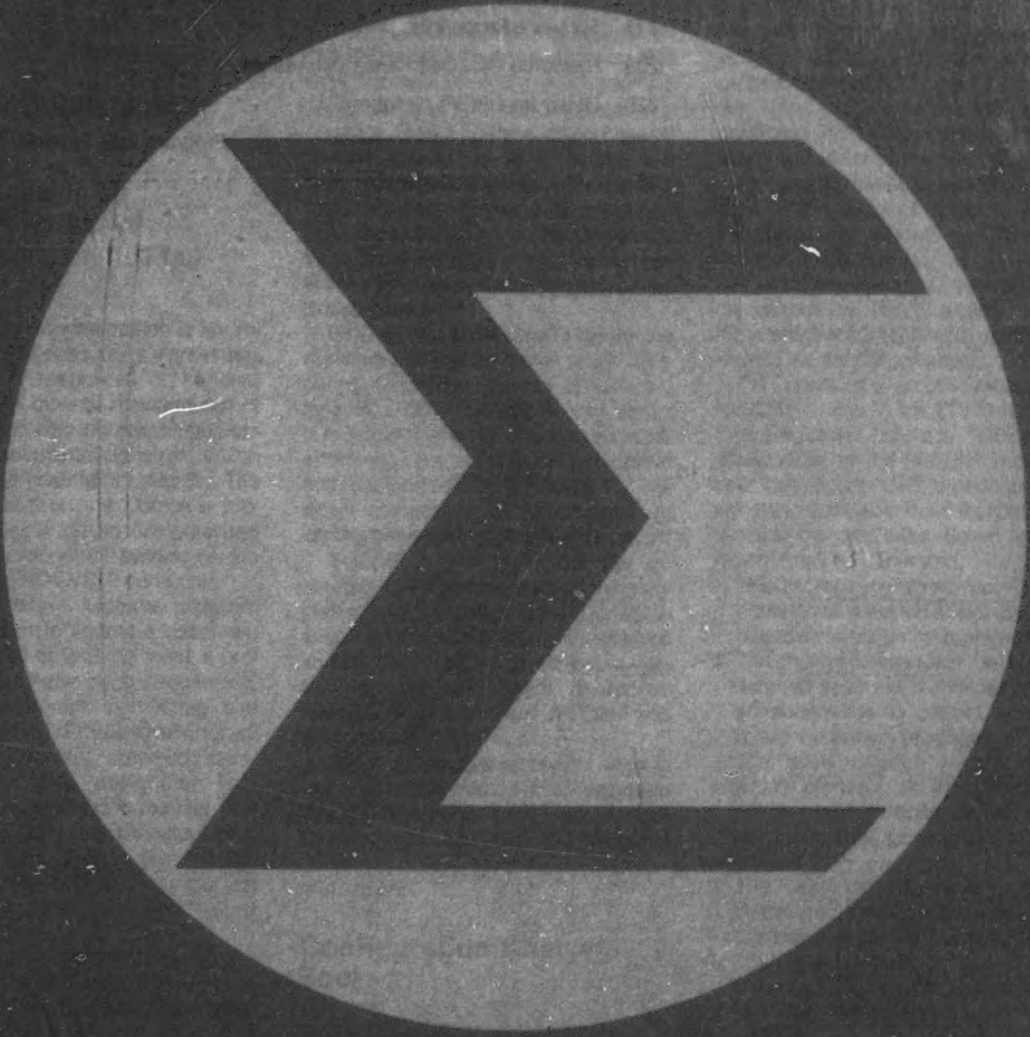

Computer Programs

227 Document Update and Compare

227 Text File Comparator

227 Configuration Analysis Tool

228 Software Repository

228 Resource Escalation and Cost Analysis

228 Driver for DISSPLA Plotter

229 Interactive Data-Collection and Display Program with Debugging

229 NAMELIST Preprocessor

Computer Programs

These programs may be obtained at very reasonable cost from COSMIC, a facility sponsored by NASA to make new programs available to the public. For information on program price, size, and availability, circle the reference letter on the COSMIC Request Card in this issue.

Document Update and Compare

Documents can be modified and lists of modifications printed out.

Maintaining documentation is an important task that can require a great deal of time and resources if handled manually. The manual maintenance of documentation also increases the probability of documentation error, which can decrease document reliability. The Document Update and Compare programs provide a simple computerized document-maintenance system on the Data General NOVA 840 computer.

The Document Update program allows the user to update a document either by batch or terminal input. It provides for automatic page sequencing, automatic paragraph numbering and renumbering (up to three levels) for insertions and deletions, automatic carry forward of station designator, and selectable headers and formatting. The updated document may be output on a line printer with off-page (outside the standard 8-1/2 by 11 area) printing of line numbers for reference and future editing purposes.

The Compare program compares two versions of a document. It prints a listing, by line number, of all insertions, deletions, and changes.

These programs are written in FORTRAN V for batch or interactive execution and have been implemented on a Data General NOVA 840 computer under RDOS with a central memory requirement of approximately 32K words. The programs were developed in 1981.

This program was written by Charles F. Knoch, Dolores C. Caldwell, and David L. Caldwell of Rockwell International Corp. for **Johnson Space Center.** *For further information, Circle R on the COSMIC Request Card.*
MSC-20349

Text File Comparator

Program compares two files and lists their differences.

The File Comparator program, IFCOMP, is a text file comparator for IBM OS/VS-compatible systems. IFCOMP accepts as input two text files and produces a listing of their differences in pseudo-update form. All differences are reported as lines that should be deleted, replaced, inserted, or moved in the first input file to transform it into the second input file. A summary, listing the number of lines involved in each type of change, is also produced.

IFCOMP has provisions to ignore line numbers and trailing blanks when comparing files with records of different lengths. IFCOMP should be very useful in monitoring changes made to software at the source code level. When used in this manner, IFCOMP allows for the direct comparison of source code to identify changes in a consistent manner.

IFCOMP is written in XPL (an extended PLI language for which the compiler executables are supplied) for batch execution and has been implemented on an IBM 370-series computer with a central memory requirement of approximately 46K of 8-bit bytes. IFCOMP was developed in 1979.

This program was written by Reed S. Kotler of Intermetrics, Inc. for **Johnson Space Center.** *For further information, Circle S on the COSMIC Request Card.*
MSC-20276

Configuration Analysis Tool

An interactive program for storing information and generating reports on project configuration management

The Configuration Analysis Tool (CAT), developed for the NASA Goddard Space Flight Center Mission Support Computing and Analysis Division, is an information storage and report generation system for the aid of configuration management activities. Configuration management is a discipline composed of many techniques selected to track and direct the evolution of complex systems. CAT is an interactive program that accepts, organizes, and stores information pertinent to specific phases of a project. In particular, CAT works with information concerning the design, development, testing, and maintenance of project software. During a CAT interactive data input session, the user is prompted for information and is provided with informative and diagnostic messages to ensure rapid and complete data entry. Various project history reports are generated by CAT in response to user queries.

All data needed by CAT reside in a single project file. This is a direct-access file in which a doubly-linked list structure is used for data organization.

CAT operates in an EDIT mode and a REPORT mode. In the EDIT mode, authorized users can add, change, or delete data. In the REPORT mode the user can request CAT to generate project history reports from the data currently in the data base. Seven types of reports may be generated:

1. The discrepancy history report, which contains all reported errors and associated information for a project;
2. The change history report, which contains all reported modifications and enhancements to correct or to improve the project programs;
3. The documentation history report, which contains all the information concerning the disposition and status of documents generated within a project;
4. The test history report, which contains information concerning what has been tested and the test results;
5. The resource history report, which contains task member assignments;
6. The milestone history report, which includes current milestone information; and
7. The data set status history report, which contains the status and location of the project data sets and associated information.

With these reports the configuration analyst should be better able to track and direct the ongoing progress of complex software projects.

CAT is written in FORTRAN IV Plus and Assembler for interactive execution and has been implemented on a DEC PDP-11/70 computer under RSX-11M

(continued on next page)

with a central memory requirement of approximately 26K of 16-bit words. It was developed in 1980.

This program was written by Phillip D. Merwarth of **Goddard Space Flight Center.** *For further information, Circle T on the COSMIC Request Card.*
GSC-12710

Software Repository

Interactive library system aids in locating available software.

In many large organizations, software development is duplicated from one group to another due to the lack of a formalized system for storing and making available information on internally available software. The Common Software Module Repository (CSMR) system provides such a formalized system.

CSMR is basically a computerized library system with high product and service visibility to potential users. The online capabilities of the system allow both the librarian and the user to interact with the library. The librarian is responsible for maintaining the information in the CSMR library. The user may search the library to locate software modules that might meet his or her current needs.

Associated with each library entry are four files of data. The first three files contain the program abstract, the program prolog, and the program software characteristics. The fourth file contains the program source code. The abstract is intended for use as a quick-look query into the primary function of the library entry. In addition, the abstract contains an assigned library catalog number, the title of the software product, category information, the author, references, the date the software was entered into the library, the date of the last software update, the software support person, the target computer, and the source code language.

The prolog is a more specific description of the module in such terms as module function, the method in which the module accomplished its function, module usage, and module interface requirements. The software characteristics include information concerning the operational efficiency of the software, such as storage and memory requirements, run-time estimates, and software metrics. The CSMR system is designed so that all of this information and the software source code may be readily entered and maintained in the CSMR library.

The CSMR system gives the user an easy method of searching the library for software. The user interactively narrows the number of library entries to be examined by responding to CSMR-generated prompts. Once the selection of entries has been reduced to those that satisfy specific requests, the user may examine the abstract, prolog, characteristics, and source code of each. The users may then select one or more entries for use in their software project.

The CSMR system is written in FORTRAN IV-Plus and Assembler for interactive execution and has been implemented on a DEC PDP-11/70 computer under RSX-11M with an overlaid central memory requirement of approximately 28K of 16-bit words. The CSMR system was developed in 1979.

This program was written by Phillip Merwarth of **Goddard Space Flight Center.** *For further information, Circle U on the COSMIC Request Card.*
GSC-12735

Resource Escalation and Cost Analysis

Cost for projects with hierarchical elements is calculated and spread over time.

The Resource Escalation and Cost Analysis Program (RECAP) is a cost compilation program for any project organized in a work breakdown structure (WBS) format. In a WBS format, activities are broken down and organized by level, so that each activity at a high level includes those activities at a lower level. This permits the organization of activities into classes and subclasses.

RECAP can handle up to 1,000 WBS activities and 4 levels with up to 99 classes of activities within a level. RECAP computes the cost of each activity directly, based on one of six cost equations, or indirectly as a function of the cost of some other activity or activities.

RECAP computes the costs of WBS items and distributes those costs over a span of up to 60 user-defined intervals. Costs for each activity may be spread over time according to a standard function with any one of six spread algorithms. The distributed cost for each activity may be summed into a more general activity to yield distributed cost for each activity class.

In addition to escalating cost due to anticipated inflation, RECAP allows the user to assign a fiscal base period to the input costs. Costs may then be escalated for any inflation known or anticipated to have occurred between the time that the project cost was initially calculated and the period in which escalation is to begin.

Input to RECAP consists of program directive records and task records. The program directive records provide information required by the program and specify the processing option to be exercised in a given run. The task records provide information relevant to each task, including information required for cost computation and distribution. Reports generated by RECAP include a summary report, a summary report with escalated output, and line item reports. RECAP can also generate x-y plots of selected costs versus time.

RECAP is written in FORTRAN IV for batch execution and has been implemented on a CDC CYBER 170-series computer with an overlaid central memory requirement of approximately 78K (octal) of 60-bit words. The program was developed in 1981.

This program was written by Darrell A. Wood of **Langley Research Center.** *For further information, Circle V on the COSMIC Request Card.*
LAR-13018

Driver for DISSPLA Plotter

A driver for plotter, microfilm, microfiche, and terminal graphics

DISPLOT is a generalized outside driver for the commercially-available DISSPLA (Display Integrated Software System and Plotting Language) plotting system. The DISPLOT program provides the user with a simple-to-use graphics capability with a great deal of application flexibility. DISPLOT is independent of whatever program generates the data to be plotted.

DISPLOT may be used for the generation of plotter, microfilm, microfiche, and terminal plots. The user has complete control of plot titling, axis labeling, and general annotation. Plots using Cartesian, logarithmic, polar, and map projection scales are readily generated. DISPLOT also allows for the manipulation of the data to be plotted prior to plot generation.

DISPLOT offers flexibility while utilizing simple input because of its design as a DISSPLA driver with a data buffer. With the data buffer, multiple variables can be loaded at one time, which increases the speed of the program. The program also allows the user to manipulate the input data before plotting them. The user controls the flow of the DISPLOT program through economical NAMELIST inputs.

DISPLOT is written in FORTRAN V and Assembler for batch execution and has been implemented on a UNIVAC 1100-series computer with a central memory requirement of approximately 93K of 36-bit words. DISPLOT was developed in 1981.

This program was written by Mark L. Baldwin of McDonnell Douglas Corp. for **Johnson Space Center.** *For further information, Circle W on the COSMIC Request Card.*
MSC-20290

Interactive Data-Collection and Display Program with Debugging

It aids designers when time and hardware constraints make scaled-integer arithmetic necessary.

To be cost-effective and to improve reliability, the number of parts in digital systems designed for ruggedized applications is usually cut to a minimum. Such reductions, along with requirements for increased computing speed, demand assembly or machine language techniques that use scaled-integer arithmetic calculations. Implementing such techniques is difficult, and locating errors within such assembly language programs is extremely difficult, increasing the time and effort required to get the programs up and running.

The INFORM program is designed to aid the assembly language programers of SEL 810B computers in working with scaled-integer applications. INFORM was developed to meet the needs of engineers designing real-time digital controls using the SEL 810B where time and hardware constraints make the use of integer arithmetic and scaled integers necessary. In addition to producing displays of quasi-steady-state values, INFORM provides an interactive mode for debugging programs, for making program patches, and for modifying the displays. The package includes auxiliary routines that add dynamic data acquisition and high-speed dynamic display to the INFORM capabilities.

The INFORM package is written in Assembler for interactive execution and has been implemented on an SEL 810B computer with a central memory requirement of approximately 5K of 16-bit words. The INFORM program was developed in 1980.

This program was written by David S. Cwynar of **Lewis Research Center.** *For further information, Circle X on the COSMIC Request Card.*
LEW-13530

NAMELIST Preprocessor

FORTRAN code is modified for use with the F4P compiler.

The NAMELIST Preprocessor Program, NPP, provides the DEC PDP-11/70 with capabilities identical to the IBM FORTRAN IV NAMELIST feature. The preprocessor modifies the FORTRAN code that contains NAMELIST statements acceptable to the IBM FORTRAN IV compiler to generate an equivalent code that is acceptable to the PDP-11 FORTRAN IV-Plus (F4P) compiler.

NAMELIST provides the FORTRAN programer with additional, flexible input and output capabilities. This feature is particularly useful in the area of data input because NAMELIST data are input in the form of the variable symbolic name being set equal to a constant value, similar to a standard FORTRAN statement. This allows the user to review input data readily and relieves the user from having to place data in certain columns and formats as required in formatted READ statements.

NPP software consists of two parts: the NAMELIST preprocessor and the NAMELIST library routines. The preprocessor modifies the FORTRAN code containing NAMELIST statements into a FORTRAN code acceptable to the PDP-11 F4P compiler. The NAMELIST library routines, which must be included in tasks containing the NAMELIST preprocessor code, are the run-time routines called by the inserted preprocessor code. The FORTRAN programer should find it easy and efficient to incorporate the NAMELIST feature into many applications.

The NPP software system is written in FORTRAN IV-Plus and Assembler code for batch exectuion and has been implemented on a DEC PDP-11/70 under RSX-11M with a central memory requirement of approximately 32K of 16-bit words. The NPP software system was developed in 1978.

This program was written by Phillip D. Merwarth of **Goddard Space Flight Center.** *For further information, Circle Y on the COSMIC Request Card.*
GSC-12704

[illegible]

[illegible]

[illegible]

[illegible]

[illegible]

[illegible]

[illegible]

SUBJECT INDEX

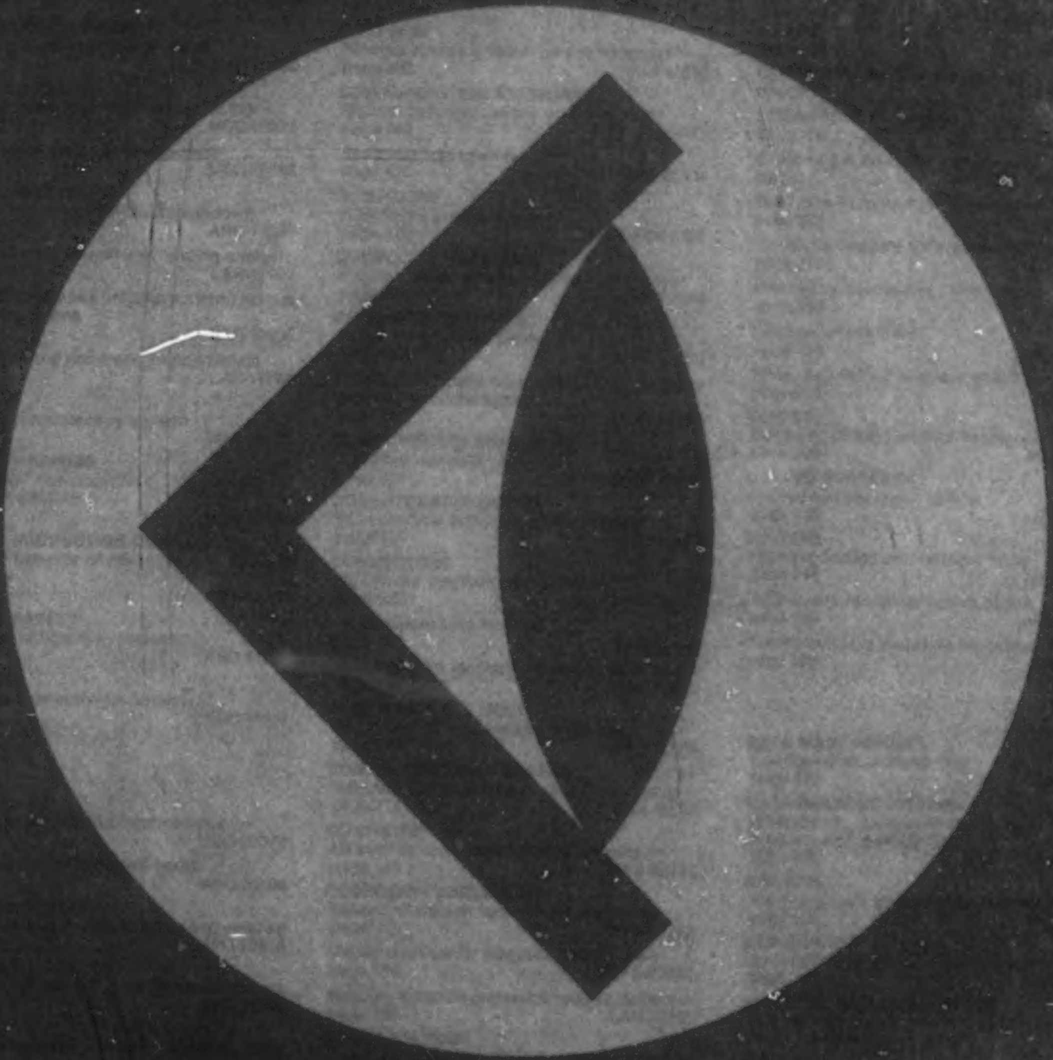

ABERRATION
Curved-surface beam splitter
page 145 GSC-12683
ACOUSTIC EXCITATION
Acoustic methods remove bubbles from liquids
page 210 NPO-15334
ACOUSTIC LEVITATION
Controlling the rotation of levitated samples
page 220 NPO-15522
Variable-position acoustic levitation
page 219 NPO-15559
ACOUSTIC MEASUREMENT
Acoustic ground-impedance meter
page 181 LAR-12995
ADHESIVE BONDING
Repairing loose electrical-connector pins
page 221 MSC-20374
Tool severs hidden adhesive bonds
page 195 MSC-20198
AERODYNAMIC LOADS
Eliminating wind-tunnel flow breakdown
page 176 ARC-11338
Flexible aircraft takeoff and landing analysis
page 186 LAR-12992
Loads and pressures on axisymmetric bodies with cruciform fins
page 185 LAR-12936
Supersonic-wing nonlinear aerodynamics
page 186 LAR-12788
AEROSOLS
Holographic microscopy system
page 147 MFS-25673
AIRCRAFT HAZARDS
Microwave ice-accretion measurement instrument (MIAMI)
page 178 LEW-13784
AIRCRAFT PRODUCTION COSTS
Costs and benefits of advanced aeronautical technology
page 185 ARC-11382
AIRCRAFT SAFETY
The design of lightning protection
page 182 KSC-11224
ALIGNMENT
Jig checks connector-pin alinement
page 222 MSC-20237

BONDING
Repairing loose electrical-connector pins
page 221 MSC-20374
Tool severs hidden adhesive bonds
page 195 MSC-20198
BOOMS (EQUIPMENT)
Boom deploys with controlled energy release
page 175 NPO-15418
BREADBOARD MODELS
Hardware fault simulator for microprocessors
page 140 NPO-15080
BUBBLES
Acoustic methods remove bubbles from liquids
page 210 NPO-15334
BUDGETING
Costs and benefits of advanced aeronautical technology
page 185 ARC-11382

CERAMIC COATINGS
High-temperature filler for tile gaps
page 205 MSC-20137
Improving surface strength of insulating tiles
page 223 MSC-20063
CHARGE EFFICIENCY
Improved method for charging Ni/Cd cells
page 133 GSC-12779
CHEMICAL REACTION CONTROL
Meniscus imaging for crystal-growth control
page 217 NPO-15349
CIRCUIT BOARDS
Terminal strip facilitates printed-circuit board
page 134 GSC-12748
COAL
Measuring contours of coal-seam cuts
page 183 MFS-25734
COAL LIQUEFACTION
Viscosity depressants for coal liquefaction
page 167 NPO-15174
COATINGS
Process sprays uniform plasma coatings
page 209 LEW-13237
COMMUNICATION NETWORKS
Shuttle communications blackout study
page 142 MSC-20141
Space-platform technology
page 141 MFS-25704
COMPILERS
NAMELIST preprocessor
page 229 GSC-12704
COMPOSITE MATERIALS
Process yields strong, void-free laminates
page 203 LAR-12982
COMPUTER GRAPHICS
Driver for DISSPLA plotter
page 228 MSC-20290
Interactive data-collection and display program with debugging
page 229 LEW-13530
COMPUTERIZED SIMULATOR
Standard transistor arrays
page 224 MFS-25327
CONCATENATED CODES
VLSI modular error-correction encoder
page 130 NPO-15470
CONNECTORS
Jig checks connector-pin alinement
page 222 MSC-20237
Quick-disconnect fastener
page 190 LAR-12895
Terminal strip facilitates printed-circuit board
page 134 GSC-12748
CONTAINERLESS MELTS
Variable-position acoustic levitation
page 219 NPO-15559
CONTINUOUS WAVE LASERS
InGaAsP CW lasers on (110) InP substrates
page 214 LAR-12840
CONTOURS
Measuring contours of coal-seam cuts
page 183 MFS-25734
CORROSION PREVENTION
Heated aluminum tanks resist corrosion
page 157 MFS-25780
Milder solution for stress-corrosion tests
page 156 MFS-25792
Vacuum ampoule isolates corrosive materials
page 158 LAR-12898
COST ANALYSIS
Costs and benefits of advanced aeronautical technology
page 185 ARC-11382
Resource escalation and cost analysis
page 228 LAR-13018
COUPLINGS
Tangleproof rotary electrical coupling
page 129 MFS-25174
CRITICAL VELOCITY
Rotating-machinery critical speeds
page 200 MFS-19669
CROSSLINKING
Estimating the degree of crosslinking in rubber
page 165 NPO-15590
High-performance matrix resins
page 159 LEW-13864
CRUCIBLES
Silicon-delivery tube
page 156 NPO-15637
CRUCIFORM WINGS
Loads and pressures on axisymmetric bodies with cruciform fins
page 185 LAR-12936
CRYOGENIC EQUIPMENT
Solid-state circuits for cryogenic operation
page 133 NPO-15255
CRYSTAL GROWTH
Chemical vapor deposition of germanium on silicon
page 214 NPO-15565
CLEFT vapor for GaAs solar cells
page 215 LEW-13912
Efficient silicon reactor
page 155 NPO-15636
Growing silicon ribbon horizontally
page 217 NPO-14977
Heat flow in horizontal ribbon growth
page 223 NPO-14979
Mensicus imaging for crystal-growth control
page 217 NPO-15349
Preventing freezeup in silicon ribbon growth
page 218 NPO-15294
Silicon-delivery tube
page 156 NPO-15637
Wipe melt for InP seed substrate
page 215 LAR-12912
CURING
Curing of furfuryl alcohol-impregnated parts
page 204 MSC-20224
CURVED SURFACES
Curved-surface beam splitter
page 145 GSC-12683
CUTTERS
High-production silicon-ingot slicer
page 216 NPO-15483
Tool severs hidden adhesive bonds
page 195 MSC-20198
Tubing cutter is activated hydraulically
page 199 LAR-12786

DATA MANAGEMENT
Configuration analysis tool
page 227 GSC-12710
DATA READOUT SYSTEMS
Interactive data-collection and display program with debugging
page 229 LEW-13530
DEFECTS
Hardware fault simulator for microprocessors
page 140 NPO-15080
DEPLOYMENT
Boom deploys with controlled energy release
page 175 NPO-15418
DIRECT POWER GENERATORS
Simplified design calculations for thermoelectric generators
page 149 NPO-15286
DISCONNECT DEVICES
Quick-disconnect fastener
page 190 LAR-12895
DISPENSERS
Device stores and discharges metered fluid
page 189 MSC-20275
DISPLAY DEVICES
Driver for DISSPLA plotter
page 228 MSC-20290
DOCUMENTATION
Document update and compare
page 227 MSC-20349
DRILLS
Six-axis electrical-discharge machine
page 190 MFS-19695

EARTH SURFACE
Acoustic ground-impedance meter
page 181 LAR-12995

ELECTRODEPOSITION
Electroforming for high-performance products
page 222 LEW-12719

ELECTRIC BATTERIES
Improved method for charging NiCd cells
page 130 GSC-12779

Large electrochemical storage cells
page 151 NPO-15185

ELECTRIC COILS
Replaceable sleeve protects welder coils
page 213 MSC-20238

ELECTRIC CONNECTORS
Jig checks connector-pin alinement
page 222 MSC-20237

Repairing loose electrical-connector pins
page 221 MSC-20374

Tangleproof rotary electrical coupling
page 129 MFS-25174

ELECTRIC WIRE
Phase-sensing guidance for wire-following vehicles
page 39 NPO-15341

ELECTROCHEMICAL CELLS
Large electrochemical storage cells
page 151 NPO-15185

ELECTROCHEMICAL MACHINING
Six-axis electrical-discharge machine
page 190 MFS-19695

Terminal strip facilitates printed-circuit board
page 134 GSC-12748

FASTENERS
Locking nut and bolt
page 197 MFS-19687

Padded allen wrench grips fastener
page 191 MFS-25739

Quick-disconnect fastener
page 190 LAR-12895

Retaining-ring fastener for solar panels
page 182 NPO-15369

FERROFLUIDS
Ferrofluid seals linear-motion valve
page 197 MSC-20148

FIBER OPTICS
Optical temperature sensor has digital output
page 177 LEW-13413

FIBER-REINFORCED COMPOSITES
A solvent-resistant, thermoplastic poly(imidesulfone)
page 159 LAR-12858

Process yields strong, void-free laminates
page 203 LAR-12982

FIBERS
Transport and installation of fibrous insulation
page 213 MSC-20074

FILE MAINTENANCE (COMPUTERS)
Document update and compare
page 227 MSC-20349

FIRE FIGHTING
Improved gloves for firefighters
page 211 MSC-20261

Light, compact pumper for harbor fires
page 199 MFS-25784

FLOW DISTRIBUTION
Eliminating wind-tunnel flow breakdown
page 176 ARC-11338

Flow distribution in hydraulic systems
page 183 MSC-20306

FLOW MEASUREMENT
Device stores and discharges metered fluid
page 189 MSC-20275

FLUIDIZED BED PROCESSORS
Improved fluidized bed gas injector
page 166 NPO-15572

FLUORIDES
Sodium spray would speed silicon production
page 162 NPO-15246

Two-temperature-zone silicon reactor
page 163 NPO-15368

FLYING EJECTION SEATS
Tubing cutter is activated hydraulically
page 199 LAR-12786

FOILS (METALS)
Conductive-tape substrate for electroforming
page 207 MFS-19715

FOLDING STRUCTURES
Boom deploys with controlled energy release
page 175 NPO-15418

Parachute line hook includes integral loop expander
page 193 LAR-12875

FRICTION REDUCTION
Coulomb friction damper
page 196 MSC-20179

FRICTIONLESS ENVIRONMENT
Controlling the rotation of levitated samples
page 220 NPO-15522

Variable-position acoustic levitation
page 219 NPO-15559

FURFURYL ALCOHOL
Curing of furfuryl alcohol-impregnated parts
page 204 MSC-20224

GALLIUM ARSENIDES
CLEFT process for GaAs solar cells
page 215 LEW-13912

GALLIUM ARSENIDE LASERS
InGaAsP CW lasers on (110) InP substrates
page 214 LAR-12840

GAS DETECTORS
Locating small leaks in large structures
page 180 MSC-20327

GAS INJECTION
Improved fluidized bed gas injector
page 166 NPO-15572

GAS WELDING
Electrical conduit distributes weld gas evenly
page 212 MFS-19665

GERMANIUM COMPOUNDS
Chemical vapor deposition of germanium on silicon
page 214 NPO-15565

GLASS
Acoustic methods remove bubbles from liquids
page 210 NPO-15334

Designing glass panels for economy and reliability
page 161 NPO-15252

Low-cost, electrically-heated glass panels
page 209 NPO-15753

Thermal-gradient fining of glass
page 160 MFS-25757

GLOVES
Improved gloves for firefighters
page 211 MSC-20261

GRAPHITE-POLYIMIDE COMPOSITES
Process yields strong, void-free laminates
page 203 LAR-12982

GUAYULE
Tissue-culture method of cloning rubber plants
page 171 NPO-15756

GUIDANCE SENSORS
Phase-sensing guidance for wire-following vehicles
page 139 NPO-15341

HERMETIC SEALS
Ferrofluid seals linear-motion valve
page 197 MSC-20148

HIGH VOLTAGES
Plastic-sealed hybrid power-circuit package
page 208 MSC-20181

HIGH-PRESSURE OXYGEN
Regulating oxygen pressure safely
page 194 MSC-20300

HOLDERS
Retaining-ring fastener for solar panels
page 182 NPO-15369

HOLOGRAMMETRY
Holographic microscopy system
page 147 MFS-25673

HYBRID CIRCUITS
Plastic-sealed hybrid power-circuit package
page 208 MSC-20181

HYDRAULIC EQUIPMENT
Flow distribution in hydraulic systems
page 183 MSC-20306

Tubing cutter is activated hydraulically
page 199 LAR-12786

HYDROCARBONS
Viscosity depressants for coal liquefaction
page 167 NPO-15174

HYDROLYSIS
Development of silane hydrolysate binder for thermal-control coatings
page 168 MFS-25749

ICE FORMATION
Microwave ice-accretion measurement instrument (MIAMI)
page 178 LEW-13784

IMPACT STRENGTH
Improving surface strength of insulating tiles
page 223 MSC-20063

INDIUM PHOSPHIDES
Wipe melt for InP seed substrate
page 215 LAR-12912

INDUSTRIAL WASTES
Membranes remove metal ions from industrial liquids
page 167 LEW-13853

INFORMATION RETRIEVAL
Software repository
page 228 GSC-12735

INJECTORS
Improved fluidized bed gas injector
page 166 NPO-15572

INSOLATION
Estimating insolation incident on tilted surfaces
page 151 MFS-25501

INSULATION
Transport and installation of fibrous insulation
page 213 MSC-20074

INTEGRATED CIRCUITS
Microprogramed sequencer for tunable RF oscillator
page 128 LAR-12903

INVERTERS
Milliwatt dc/dc inverter
page 132 NPO-15157

ION DISTRIBUTION
Ion mass/velocity/charge spectrometer
page 148 NPO-15423

JET AIRCRAFT
Vertical profiles for turbojet-powered aircraft
page 185 LAR-12940

JIGS
Jig checks connector-pin alinement
page 222 MSC-20237

LAMINATES
Process yields strong, void-free laminates
page 203 LAR-12982

LASERS
InGaAsP CW lasers on (110) InP substrates
page 214 LAR-12840

LEADING EDGE THRUST
Supersonic-wing nonlinear aerodynamics
page 188 LAR-12788

LEAKAGE
Locating small leaks in large structures
page 180 MSC-20327

LEVITATION
Controlling the rotation of levitated samples
page 220 NPO-15522

Variable-position acoustic levitation
page 219 NPO-15559

LIBRARIES
Software repository
page 228 GSC-12735

LIFE CYCLE COSTS
Costs and benefits of advanced aeronautical technology
page 185 ARC-11382

LIGHTNING
The design of lightning protection
page 182 KSC-11224

LINKAGES
Retaining-ring fastener for solar panels
page 182 NPO-15369

LIQUID HELIUM
Solid-state circuits for cryogenic operation
page 133 NPO-15255

LIQUID SODIUM
Sodium spray would speed silicon production
page 162 NPO-15246

LIQUID WASTES
Membranes remove metal ions from industrial liquids
page 167 LEW-13853

LIQUID-VAPOR INTERFACES
Acoustic methods remove bubbles from liquids
page 210 NPO-15334

LOADS (FORCES)
Structural-vibration-response data analysis
page 184 MSC-20182

Vibration-analysis method reduces computer time
page 176 MFS-25711

LOGIC CIRCUITS
Standard transistor arrays
page 224 MFS-25327

LOW GRAVITY MANUFACTURING
Thermal-gradient fining of glass
page 160 MFS-25757

LUBRICATION
Inserts automatically lubricate ball bearings
page 196 MFS-19727

MACHINE ORIENTED LANGUAGES
Interactive data-collection and display program with debugging
page 229 LEW-13530

MACHINE TOOLS
Six-axis electrical-discharge machine
page 190 MFS-19695

MAGNETIC RECORDING
Transport control for high-density digital recorder
page 138 GSC-12727

MAINTENANCE
Explosive joining for nuclear-reactor repair
page 211 LAR-12996

Inserts automatically lubricate ball bearings
page 196 MFS-19727

Repairing loose electrical-connector pins
page 221 MSC-20374

MANAGEMENT INFORMATION SYSTEMS
Life sciences MIS
page 171 MSC-20238

Software repository
page 228 GSC-12735

MANEUVERABILITY
Flexible aircraft takeoff and landing analysis
page 186 LAR-12992

MASS SPECTROMETERS
Ion mass/velocity/charge spectrometer
page 148 NPO-15423

MATERIALS RECOVERY
Membranes remove metal ions from industrial liquids
page 167 LEW-13853

MELTS (CRYSTAL GROWTH)
Efficient silicon reactor
page 155 NPO-15636

Growing silicon ribbon horizontally
page 217 NPO-14977

Heat flow in horizontal ribbon growth
page 223 NPO-14979

Short shot tower for silicon
page 164 NPO-15607

Wipe melt for InP seed substrate
page 215 LAR-12912

MEMBRANES
Membranes remove metal ions from industrial liquids
page 167 LEW-13853

METAL COATINGS
Development of silane hydrolysate binder for thermal-control coatings
page 168 MFS-25749

METAL JOINTS
Explosive joining for nuclear-reactor repair
page 211 LAR-12996

MICROPROCESSORS
Hardware fault simulator for microprocessors
page 140 NPO-15080

MICROSCOPY
Holographic microscopy system
page 147 MFS-25673

MICROWAVE EQUIPMENT
Fabrication of precise microwave reflector
page 204 NPO-15377

Microwave ice-accretion measurement instrument (MIAMI)
page 178 LEW-13784

Using SAW resonators in RF oscillators
page 131 ARC-11390

MOISTURE
Heated aluminum tanks resist corrosion
page 157 MFS-25760

NICKEL CADMIUM BATTERIES
Improved method for charging Ni/Cd cells
page 133 GSC-12779

NOISE MEASUREMENT
Acoustic ground-impedance meter
page 181 LAR-12995

NUCLEAR REACTORS
Explosive joining for nuclear-reactor repair
page 211 LAR-12996

NUMERICAL ANALYSIS
Interactive data-collection and display program with debugging
page 229 LEW-13530

NUTS (FASTENERS)
Locking nut and bolt
page 197 MFS-19687

OPERATING COSTS
Vertical profiles for turbojet-powered aircraft
page 185 LAR-12940

OPTICAL EQUIPMENT
Curved-surface beam splitter
page 145 GSC-12683

Holographic microscopy system
page 147 MFS-25673

Meniscus imaging for crystal-growth control
page 217 MFS-15349

Optical sensor for robotics
page 146 MFS-25713

Optical temperature sensor has digital output
page 177 LEW-13413

Video target tracking and ranging system
page 137 MSC-20098

OSCILLATION DAMPERS
Coulomb friction damper
page 196 MSC-20179

OSCILLATORS
Microprogramed sequencer for tunable RF oscillator
page 128 LAR-12903

OXYGEN
Regulating oxygen pressure safely
page 194 MSC-20300

PANELS
Designing glass panels for economy and reliability
page 161 NPO-15252

Low-cost, electrically-heated glass panels
page 209 NPO-15753

Multiple-panel cylindrical solar concentrator
page 206 NPO-15627

PARACHUTES
Parachute line hook includes integral loop expander
page 193 LAR-12875

PELLETS
Casting silicon pellets from powder
page 163 NPO-15272

Short shot tower for silicon
page 164 NPO-15607

PHASE CONTROL
Control system damps vibrations
page 141 NPO-15002

Transport control for high-density digital recorder
page 138 GSC-12727

PHASE MATCHING
Phase-sensing guidance for wire-following vehicles
page 139 NPO-15341

PHOTO MICROGRAPHY
Holographic microscopy system
page 147 MFS-25673

PINHOLES
Locating small leaks in large structures
page 180 MSC-20327

PINS
Jig checks connector-pin alinement
page 222 MSC-20237

PIPES (TUBES)
Portable pipe wrapper
page 198 KSC-11244

Tubing cutter is activated hydraulically
page 199 LAR-12786

PITTING
Milder solution for stress-corrosion tests
page 156 MFS-25792

PLANTS (BOTANY)
Tissue-culture method of cloning rubber plants
page 171 NPO-15756

PLASMA INTERACTIONS
Ion mass/velocity/charge spectrometer
page 148 NPO-15423

Shuttle communications blackout study
page 142 MSC-20141

PLASMA SPRAYING
Process sprays uniform plasma coatings
page 209 LEW-13237

PLASTICS
Plastic-sealed hybrid power-circuit package
page 208 MSC-20181

PLOTTERS
Driver for DISSPLA plotter
page 228 MSC-20290

POINTING CONTROL SYSTEMS
Minimizing vibrations while orienting large structures
page 179 MFS-25439

POLLUTANTS
Membranes remove metal ions from industrial liquids
page 167 LEW-13853

POLYIMIDES
A solvent-resistant, thermoplastic poly(imidesulfone)
page 159 LAR-12858
High-performance matrix resins
page 159 LEW-13864

PORTABLE EQUIPMENT
Light, compact pumper for harbor fires
page 199 MFS-25784
Portable pipe wrapper
page 198 KSC-11244

POSITIONING
TRISCAN antenna-positioning algorithm
page 148 NPO-15577

POWDER (PARTICLES)
Casting silicon pellets from powder
page 163 NPO-15272
Process sprays uniform plasma coatings
page 209 LEW-13237

POWER SUPPLY CIRCUITS
Voltage regulator for a dc-to-dc converter
page 127 NPO-15208

PRESSURE
Pressure assist makes coating more reliable
page 206 MSC-20210

PRESSURE REGULATORS
Regulating oxygen pressure safely
page 194 MSC-20300

PRINTED CIRCUITS
Terminal strip facilitates printed-circuit board changes
page 134 GSC-12748

PRODUCT DEVELOPMENT
Designing glass panels for economy and reliability
page 161 NPO-15252

PROJECT MANAGEMENT
Configuration analysis tool
page 227 GSC-12710
Life sciences MIS
page 171 MSC-20238

PROTECTIVE CLOTHING
Improved gloves for firefighters
page 211 MSC-20261

PURGING
Electrical conduit distributes weld gas evenly
page 212 MFS-19665

PURIFICATION
Efficient silicon reactor
page 155 NPO-15636
Growing silicon ribbon horizontally
page 217 NPO-14977
Processor generates and extracts silicon
page 161 NPO-15582
Two-temperature-zone silicon reactor
page 163 NPO-15368

QUALITY CONTROL
Hardware fault simulator for microprocessors
page 140 NPO-15060

RADAR ANTENNAS
TRISCAN antenna-positioning algorithm
page 148 NPO-15577
Fabrication of precise microwave reflector
page 204 NPO-15377

RADIATION COUNTERS
Radionuclide counting technique measures wind velocity
page 178 LAR-12971

RADIO DIRECTION FINDERS
TRISCAN antenna-positioning algorithm
page 148 NPO-15577

RADIO FREQUENCIES
Microprogramed sequencer for tunable RF oscillator
page 128 LAR-12903
Shuttle communications blackout study
page 142 MSC-20141

RANGE AND RANGE RATE TRACKING
Video target tracking and ranging system
page 137 MSC-20098

RECORDS
Document update and compare
page 227 MSC-20349

RECOVERY PARACHUTES
Parachute line hook includes integral loop expander
page 193 LAR-12875

RECRYSTALLIZATION
Chemical vapor deposition of germanium on silicon
page 214 NPO-15565

REDUCTION (CHEMISTRY)
Processor generates and extracts silicon
page 161 NPO-15582
Two-temperature-zone silicon reactor
page 163 NPO-15368

REFLECTANCE
Low-cost, electrically-heated glass panels
page 209 NPO-15753

REINFORCED PLASTICS
A solvent-resistant, thermoplastic poly(imidesulfone)
page 159 LAR-12858

REINFORCEMENT (STRUCTURES)
High-temperature filler for tile gaps
page 205 MSC-20137

REMOTE CONTROL
Phase-sensing guidance for wire-following vehicles
page 139 NPO-15341

REPORT GENERATORS
Configuration analysis tool
page 227 GSC-12710
Text file comparator
page 227 MSC-20276

RESCUE OPERATIONS
Tubing cutter is activated hydraulically
page 199 LAR-12786

RESIN BONDING
Pressure assist makes coating more reliable
page 206 MSC-20210

RESIN MATRIX COMPOSITES
High-performance matrix resins
page 159 LEW-13864

RESISTANCE HEATING
Low cost, electrically-heated glass panels
page 209 NPO-15753

RESONATORS
Using SAW resonators in RF oscillators
page 131 ARC-11390

RESOURCES MANAGEMENT
Resource escalation and cost analysis
page 226 LAR-13018

ROTATING BODIES
Tangleproof rotary electrical coupling
page 129 MFS-25174

ROTORS
Rotating-machinery critical speeds
page 200 MFS-19669

RUBBER
Estimating the degree of crosslinking in rubber
page 165 NPO-15590
Tissue-culture method of cloning rubber plants
page 171 NPO-15756

SAFETY DEVICES
Regulating oxygen pressure safely
page 194 MSC-20300

SATELLITE-BORNE INSTRUMENTS
Space-platform technology
page 141 MFS-25704

SCREWS
Inexpensive bolt-load gage
page 192 LAR-12774

SEALS (STOPPERS)
Ferrofluid seals linear-motion valve
page 197 MSC-20148

SEMICONDUCTOR DEVICES
Solid-state circuits for cryogenic operation
page 133 NPO-15255

SEMICONDUCTOR LASERS
InGaAsP CW lasers on (110) InP substrates
page 214 LAR-12840

SEMICONDUCTOR MATERIALS
Wipe melt for InP seed substrate
page 215 LAR-12912

SERVOCONTROL
Transport control for high-density digital recorder
page 138 GSC-12727

SHAFTS (MACHINE ELEMENTS)
Inserts automatically lubricate ball bearings
page 196 MFS-19727

SHEARS
Tool severs hidden adhesive bonds
page 195 MSC-20198

SHOCK ABSORBERS
Coulomb friction damper
page 196 MSC-20179

SILICON
Casting silicon pellets from powder
page 163 NPO-15272
Efficient silicon reactor
page 155 NPO-15636
Growing silicon ribbon horizontally
page 217 NPO-14977
Heat flow in horizontal ribbon growth
page 223 NPO-14979
High-production silicon-ingot slicer
page 216 NPO-15483
Meniscus imaging for crystal-growth control
page 217 NPO-15349
Preventing freezeup in silicon ribbon growth
page 218 NPO-15294
Processor generates and extracts silicon
page 161 NPO-15582
Short shot tower for silicon
page 164 NPO-15607
Silicon-delivery tube
page 156 NPO-15637
Sodium spray would speed silicon production
page 162 NPO-15246
Two-temperature-zone silicon reactor
page 163 NPO-15368

SINGLE CRYSTALS
Heat flow in horizontal ribbon growth
page 223 NPO-14979
Preventing freezeup in silicon ribbon growth
page 218 NPO-15294

SIZING MATERIALS
High-temperature filler for tile gaps
page 205 MSC-20137

SOLAR ARRAYS
Designing glass panels for economy and reliability
page 161 NPO-15252

SOLAR CELLS
CLEFT process for GaAs solar cells
page 215 LEW-13912

Multiple-panel cylindrical solar concentrator
page 206 NPO-15627

SOLAR COLLECTORS
Estimating insolation incident on tilted surfaces
page 151 MFS-25501

Multiple-panel cylindrical solar concentrator
page 206 NPO-15627

Retaining-ring fastener for solar panels
page 182 NPO-15369

SOLAR ENERGY CONVERSION
Evaluating energy conversion efficiency
page 150 LAR-12948

SOLAR WIND
Ion mass/velocity/charge spectrometer
page 148 NPO-15423

SOLIDIFICATION
Short shot tower for silicon
page 164 NPO-15607

SOUND PRESSURE
Acoustic ground-impedance meter
page 181 LAR-12995

SOUND WAVES
Acoustic methods remove bubbles from liquids
page 210 NPO-15334

SPACECRAFT DOCKING
Optical sensor for robotics
page 146 MFS-25713

SPARK MACHINING
Six-axis electrical-discharge machine
page 190 MFS-19695

SPECTRAL BANDS
Optical temperature sensor has digital output
page 177 LEW-13413

SPIRAL WRAPPING
Portable pipe wrapper
page 196 KSC-11244

SPRAYED COATINGS
Process sprays uniform plasma coatings
page 209 LEW-13237

STABILIZED PLATFORMS
Space-platform technology
page 141 MFS-25704

STORAGE BATTERIES
Large electrochemical storage cells
page 151 NPO-15185

STORAGE TANKS
Heated aluminum tanks resist corrosion
page 157 MFS-25780

STRAIN GAGES
Inexpensive bolt-load gage
page 192 LAR-12774

STRUCTURAL ANALYSIS
Structural optimization
page 184 LAR-13010

STRUCTURAL FAILURE
Tile-failure analysis
page 224 MSC-20139

STRUCTURAL MEMBERS
Retaining-ring fastener for solar panels
page 182 NPO-15369

STRUCTURAL VIBRATION
Structural-vibration-response data analysis
page 184 MSC-20182

Vibration-analysis method reduces computer time
page 176 MFS-25711

STUDS
Inexpensive bolt-load gage
page 192 LAR-12774

SUBSTRATES
Chemical vapor deposition of germanium on silicon
page 214 NPO-15565

Conductive-tape substrate for electroforming
page 207 MFS-19715

InGaAsP CW lasers on (110) InP substrates
page 214 LAR-12840

SURFACE ACOUSTIC WAVE DEVICES
Using SAW resonators in RF oscillators
page 131 ARC-11390

SURFACE VEHICLES
Phase-sensing guidance for wire-following vehicles
page 139 NPO-15341

SWIVELING CIRCUITS
Milliwatt dc/dc inverter
page 132 NPO-15157

SYNCHRONIZED OSCILLATORS
Transport control for high-density digital recorder
page 136 GSC-12727

SYNTHESIS (CHEMISTRY)
Two-temperature-zone silicon reactor
page 163 NPO-15368

TANKS
Heated aluminum tanks resist corrosion
page 157 MFS-25780

TARGETS
Video target tracking and ranging system
page 137 MSC-20098

TEMPERATURE CONTROL
Preventing freezeup in silicon ribbon growth
page 218 NPO-15294

TEMPERATURE GRADIENTS
Thermal-gradient fining of glass
page 160 MFS-25757

TEMPERATURE SENSORS
Optical temperature sensor has digital output
page 177 LEW-13413

TENSILE STRESS
Tile-failure analysis
page 224 MSC-20139

TEST CHAMBERS
Controlling the rotation of levitated samples
page 220 NPO-15522

THERMAL CONTROL COATINGS
Development of silane hydrolysate binder for thermal-control coatings
page 168 MFS-25749

THERMAL INSULATION
Improving surface strength of insulating tiles
page 223 MSC-20063

Portable pipe wrapper
page 198 KSC-11244

Transport and installation of fibrous insulation
page 213 MSC-20074

THERMAL STRESS
Tile-failure analysis
page 224 MSC-20139

THERMOELECTRIC GENERATORS
Simplified design calculations for thermoelectric generators
page 149 NPO-15286

THERMOPHYSICAL PROPERTIES
Vacuum ampoule isolates corrosive materials
page 158 LAR-12898

THERMOPLASTIC RESINS
A solvent-resistant, thermoplastic poly(imidesulfone)
page 159 LAR-12858

THREADS
Locking nut and bolt
page 197 MFS-19687

THRUST CONTROL
Minimizing vibrations while orienting large structures
page 179 MFS-25439

THUNDERSTORMS
The design of lightning protection
page 182 KSC-11224

TILES
High-temperature filler for tile gaps
page 205 MSC-20137

Improving surface strength of insulating tiles
page 223 MSC-20063

Tile-failure analysis
page 224 MSC-20139

TITANIUM OXIDES
Development of silane hydrolysate binder for thermal-control coatings
page 168 MFS-25749

TOOLS
Padded allen wrench grips fastener
page 191 MFS-25739

Tool severs hidden adhesive bonds
page 195 MSC-20198

TORQUE
Inexpensive bolt-load gage
page 192 LAR-12774

TRACKING (POSITION)
Video target tracking and ranging system
page 137 MSC-20098

TRANSFORMERS
Voltage regulator for a dc-to-dc converter
page 127 NPO-15208

TRANSISTOR CIRCUITS
Standard transistor arrays
page 224 MFS-25327

TRANSMITTER RECEIVERS
Optical sensor for robotics
page 146 MFS-25713

TUNING
Microprogramed sequencer for tunable RF oscillator
page 128 LAR-12903

TURBINE PUMPS
Light, compact pumper for harbor fires
page 199 MFS-25784

VACUUM SYSTEMS
Locating small leaks in large structures
page 180 MSC-20327

Vacuum ampoule isolates corrosive materials
page 158 LAR-12898

VALVES
Ferrofluid seals linear-motion valve
page 197 MSC-20148

VAPOR PHASE EPITAXY
Chemical vapor deposition of germanium on silicon
page 214 NPO-15565

VEGETATION GROWTH
Tissue-culture method of cloning rubber plants
page 171 NPO-15756

VIBRATION ANALYSIS
Vibration-analysis method reduces computer time
page 176 MFS-25711

VIBRATION DAMPING
Control system damps vibrations
page 141 NPO-15002

Coulomb friction damper
page 196 MSC-20179

Minimizing vibrations while orienting large structures
page 179 MFS-25439

Structural-vibration-response data analysis
page 184 MSC-20182

VISCO-ELASTICITY
Estimating the degree of crosslinking in rubber
page 165 NPO-15590

VISCOSITY
Viscosity depressants for coal liquefaction
page 167 NPO-15174

VOLTAGE CONVERTERS (DC TO DC)
Voltage regulator for a dc-to-dc converter
page 127 NPO-15208

VULCANIZING
Estimating the degree of crosslinking in rubber
page 165 NPO-15590

WAFERS
High-production silicon-ingot slicer
page 216 NPO-15483

WELDING
Electrical conduit distributes weld gas evenly
page 212 MFS-19665

Replaceable sleeve protects welder coil
page 213 MSC-20236

WIND TUNNEL NOZZLES
Eliminating wind-tunnel flow breakdown
page 176 ARC-11336

WIND VELOCITY MEASUREMENT
Radionuclide counting technique measures wind velocity
page 178 LAR-12971

WINDOWS (APERTURES)
Designing glass panels for economy and reliability
page 161 NPO-15252

WING LOADING
Supersonic-wing nonlinear aerodynamics
page 186 LAR-12766

WIRING
Repairing loose electrical-connector pins
page 221 MSC-20374

WORD PROCESSING
Text file comparator
page 227 MSC-20276

WRENCHES
Padded allen wrench grips fastener
page 191 MFS-25739

[illegible]

[illegible]

[illegible]

National Aeronautics and
Space Administration

Washington, D.C.
20546

Official Business
Penalty for Private Use: $300

NO POSTAGE
NECESSARY
IF MAILED
IN THE
UNITED STATES

BUSINESS REPLY MAIL

FIRST CLASS PERMIT NO. 12028 WASHINGTON, D.C.

POSTAGE WILL BE PAID BY NASA

Manager, Technology Transfer Division
P.O. Box 8757
Baltimore/Washington International Airport, MD 21240

National Aeronautics and
Space Administration

Washington, D.C.
20546

Official Business
Penalty for Private Use: $300

NO POSTAGE
NECESSARY
IF MAILED
IN THE
UNITED STATES

BUSINESS REPLY MAIL

FIRST CLASS PERMIT NO. 12028 WASHINGTON, D.C.

POSTAGE WILL BE PAID BY NASA

Manager, Technology Transfer Division
P.O. Box 8757
Baltimore/Washington International Airport, MD 21240

National Aeronautics and
Space Administration

Washington, D.C.
20546

Official Business
Penalty for Private Use: $300

NO POSTAGE
NECESSARY
IF MAILED
IN THE
UNITED STATES

BUSINESS REPLY MAIL

FIRST CLASS PERMIT NO. 12028 WASHINGTON, D.C.

POSTAGE WILL BE PAID BY NASA

Manager, Technology Transfer Division
P.O. Box 8757
Baltimore/Washington International Airport, MD 21240

TECH BRIEFS SUBSCRIPTIONS

WINTER
1982

☐ Please place me on the subscription list for NASA Tech Briefs (issued quarterly).

☐ I wish to change the delivery address for my current subscription. The identification number at the top right of my current mailing label is T__________.

1. Please check any of the following that describe your organization:
   - ☐ Federal Government
   - ☐ State Government
   - ☐ Municipal Government
   - ☐ University/College
   - ☐ Secondary School
   - ☐ Trade/Vocational School
   - ☐ Manufacturing
   - ☐ Sales
   - ☐ Research
   - ☐ Consulting
   - ☐ Medicine
   - ☐ Professional Society
   - ☐ News Media
   - ☐ Information Sciences/Library
2. Please check the number of employees in your organization: ☐ Under 25 ☐ 25-100 ☐ 100-500 ☐ Over 500
3. Please indicate if your position is one of the following: ☐ Owner or Chief Executive Officer ☐ Administrator/Manager ☐ Scientist ☐ Engineer ☐ Other __________

[PLEASE PRINT]

NAME __________ TITLE __________

COMPANY & STREET ADDRESS __________ PHONE __________

CITY __________ STATE __________ ZIP __________

TECH BRIEFS SUBSCRIPTIONS

WINTER
1982

☐ Please place me on the subscription list for NASA Tech Briefs (issued quarterly).

☐ I wish to change the delivery address for my current subscription. The identification number at the top right of my current mailing label is T__________.

1. Please check any of the following that describe your organization:
   - ☐ Federal Government
   - ☐ State Government
   - ☐ Municipal Government
   - ☐ University/College
   - ☐ Secondary School
   - ☐ Trade/Vocational School
   - ☐ Manufacturing
   - ☐ Sales
   - ☐ Research
   - ☐ Consulting
   - ☐ Medicine
   - ☐ Professional Society
   - ☐ News Media
   - ☐ Information Sciences/Library
2. Please check the number of employees in your organization: ☐ Under 25 ☐ 25-100 ☐ 100-500 ☐ Over 500
3. Please indicate if your position is one of the following: ☐ Owner or Chief Executive Officer ☐ Administrator/Manager ☐ Scientist ☐ Engineer ☐ Other __________

[PLEASE PRINT]

NAME __________ TITLE __________

COMPANY & STREET ADDRESS __________ PHONE __________

CITY __________ STATE __________ ZIP __________

FEEDBACK — YOUR COMMENTS

WINTER
1982

WE NEED YOUR HELP!

Our ultimate goal is to provide you with solutions to your day-to-day technical problems. Are we meeting that goal? Tell us how Tech Briefs has helped you, or how it can be made more useful. We are especially interested in brief descriptions of specific instances where Tech Briefs has either helped you solve a problem or been applied to your product line.

____

____

____

____

If you need more space, write us a letter at the address on the front of this card.

[PLEASE PRINT]

NAME __________ TITLE __________

COMPANY & STREET ADDRESS __________ PHONE __________

CITY __________ STATE __________ ZIP __________

TSP REQUESTS

Please send me the Technical Support Package (TSP)
for the Tech Brief articles circled below:

WINTER
1982

☐ I would like information about NASA's Industrial Applications Centers and other NASA TU services.

I am requesting these TSP's for:
☐ Current Awareness
☐ Product Development
☐ Other ____________________
☐ Process Improvement
☐ Problem Solving

Approximately how many TSP's have you requested from NASA in the last five years?
☐ 0 to 10 ☐ 11 to 25 ☐ over 25

— [PLEASE PRINT] —

NAME ____________________

TITLE ____________________

COMPANY & STREET ADDRESS ____________________ PHONE ____________

CITY ____________ STATE ______ ZIP ______

1	2	3	4	5	6	7	8	9	10	11	12	13	14	15
16	17	18	19	20	21	22	23	24	25	26	27	28	29	30
31	32	33	34	35	36	37	38	39	40	41	42	43	44	45
46	47	48	49	50	51	52	53	54	55	56	57	58	59	60
61	62	63	64	65	66	67								

TSP REQUESTS

Please send me the Technical Support Package (TSP)
for the Tech Brief articles circled below:

WINTER
1982

☐ I would like information about NASA's Industrial Applications Centers and other NASA TU services.

I am requesting these TSP's for:
☐ Current Awareness
☐ Product Development
☐ Other ____________________
☐ Process Improvement
☐ Problem Solving

Approximately how many TSP's have you requested from NASA in the last five years?
☐ 0 to 10 ☐ 11 to 25 ☐ over 25

— [PLEASE PRINT] —

NAME ____________________

TITLE ____________________

COMPANY & STREET ADDRESS ____________________ PHONE ____________

CITY ____________ STATE ______ ZIP ______

1	2	3	4	5	6	7	8	9	10	11	12	13	14	15
16	17	18	19	20	21	22	23	24	25	26	27	28	29	30
31	32	33	34	35	36	37	38	39	40	41	42	43	44	45
46	47	48	49	50	51	52	53	54	55	56	57	58	59	60
61	62	63	64	65	66	67								

COSMIC REQUESTS

I would like price and availability information about the computer program(s) circled below.

WINTER
1982

A B C D E F G H J K L M N P Q R S T U V W X Y

— [PLEASE PRINT] —

NAME ____________________

TITLE ____________________

COMPANY & STREET ADDRESS ____________________

CITY ____________ STATE ______ ZIP ______

Please send me further information about software and services available from COSMIC. I am particularly interested in programs in the following areas:

____

____

____

____

National Aeronautics and
Space Administration

Washington, D.C.
20546

Official Business
Penalty for Private Use $300

NO POSTAGE
NECESSARY
IF MAILED
IN THE
UNITED STATES

BUSINESS REPLY MAIL

FIRST CLASS PERMIT NO. 12028 WASHINGTON, D.C.

POSTAGE WILL BE PAID BY NASA

Manager, Technology Transfer Division
P.O. Box 8757
Baltimore/Washington International Airport, MD 21240

NASA

National Aeronautics and
Space Administration

Washington, D.C.
20546

Official Business
Penalty for Private Use $300

NO POSTAGE
NECESSARY
IF MAILED
IN THE
UNITED STATES

BUSINESS REPLY MAIL

FIRST CLASS PERMIT NO. 12028 WASHINGTON, D.C.

POSTAGE WILL BE PAID BY NASA

Manager, Technology Transfer Division
P.O. Box 8757
Baltimore/Washington International Airport, MD 21240

NASA

National Aeronautics and
Space Administration

Washington, D.C.
20546

Official Business
Penalty for Private Use $300

NO POSTAGE
NECESSARY
IF MAILED
IN THE
UNITED STATES

BUSINESS REPLY MAIL

FIRST CLASS PERMIT NO. 12028 WASHINGTON, D.C.

POSTAGE WILL BE PAID BY NASA

COSMIC
Computer Software Management and Information Center
Suite 112, Barrow Hall
Athens, GA 30602

NASA

National Aeronautics and
Space Administration

Washington, D.C.
20546

Official Business
Penalty for Private Use $300

25
25th Anniversary
1958-1983

THIRD-CLASS BULK

THIRD-CLASS BULK RATE
POSTAGE & FEES PAID
NASA
WASHINGTON, D.C.
PERMIT No. G27

NASA

Xenon lamps used for nighttime illumination of launchsites at Kennedy Space Center have found many commercial spinoffs. Among them are 12,000-watt movie-projector lamps used in theaters worldwide. [See the bottom of page A1.]